Year: 2023

Study of white automobile paint of same manufacturer

Lei Lei

UNIL | Université de Lausanne
Faculté de droit,
des sciences criminelles
et d'administration publique

Study of white automobile paint of same manufacturer

Thèse de doctorat

Présentée à la

Faculté de droit, des sciences criminelles et d'administration publique,

École des Sciences Criminelles

de l'Université de Lausanne par

Lei Lei

Jury:

Prof. Geneviève Massonnet, directrice de thèse (Université de Lausanne)

Prof. Yuanfeng Wang, experte externe (China University of Political Science and Law)

Prof. Cyril Muehlethaler, expert externe (Université de Québec Trois-Rivières)

Prof. Andy Bécue, expert interne (Université de Lausanne)

Sous la présidence du Prof. Christophe Champod (Université de Lausanne)

Lausanne 2023

Study of white automobile paint of same manufacturer

Thèse de doctorat

Présentée à la

Faculté de droit, des sciences criminelles et d'administration publique,

École des Sciences Criminelles

de l'Université de Lausanne par

Lei Lei

Jury:

Prof. Geneviève Massonnet, directrice de thèse (Université de Lausanne)

Prof. Yuanfeng Wang, experte externe (China University of Political Science and Law)

Prof. Cyril Muehlethaler, expert externe (Université de Québec Trois-Rivières)

Prof. Andy Bécue, expert interne (Université de Lausanne)

Sous la présidence du Prof. Christophe Champod (Université de Lausanne)

Lausanne 2023

UNIL | Université de Lausanne
Ecole des sciences criminelles
bâtiment Batochime
CH-1015 Lausanne

IMPRIMATUR

A l'issue de la soutenance de thèse, le Jury autorise l'impression de la thèse de Madame Lei LEI, candidate au doctorat en science forensique, intitulée :

« **Study of White Automobile Paint of same Manufacturer** »

Professeur Christophe Champod
Président du jury

Lausanne, le 17 octobre 2023

Acknowledgement

This thesis is the culmination of the efforts of numerous individuals who have made contributions, both directly and indirectly, to this project. They have been a pillar of support throughout my six-year journey, and I am profoundly thankful to each and every one of them.

First and foremost, I would like to convey my deepest gratitude to my PhD supervisor, Prof. Geneviève Massonnet, for her unwavering support, guidance, and mentorship during my doctoral journey. I am extremely thankful for the invaluable opportunities she has provided me; these experiences have been truly precious. I couldn't have asked for a better PhD supervisor.

I want to express my appreciation to my thesis committee members: Professor Christophe Champod, the Director of the School of Criminal Justice and the President of the jury, as well as Prof. Yuanfeng Wang from CUPL (China), Prof. Cyril Muehlethaler from UQTS (Canada), and Prof. Andy Bécue from Unil (Lausanne). Their willingness to evaluate my work and provide valuable insights has been instrumental. Their questions and suggestions have challenged me to think more deeply about my research and have significantly enhanced the quality of this dissertation.

I am deeply grateful for the opportunity to collaborate with an exceptional team of individuals who have made this journey enjoyable. Thanks to the current members of the Microtraces group, Yu Chen Lim-Hitchings and Virginie Favre, for their unwavering support and the wonderful moments we've shared. My gratitude also extends to the former team members: Dr. Danny Lambert, whose generosity in sharing knowledge and experience greatly contributed to the success of this research; Valentina Cammarota, for her support and guidance during my early days in this academic environment; André Marolf, Michael Schnegg, and Céline Burnier, for affording me the opportunity to work with and learn from them.

I extend my gratitude to all my friends and colleagues at ESC. While It is impractical to list everyone individually, I want to emphasize that the treasured moments we've shared, their kindness, and the invaluable support I've received remain deeply etched in my memory. Their presence has made me feel like a welcomed part of the group, never a complete outsider.

I want to express my gratitude to Prof. Yuanfeng Wang. Her influence on my journey has been profound, and I greatly appreciate her role in building my self-confidence. Her mentorship has been a critical factor in my academic and professional development.

I also want to express my thanks to all the police officers I had the privilege of meeting in China. Their selfless assistance during my sample collection was invaluable, and without their support, I would not have been able to successfully complete my project.

Thanks to Chuankai Wang and Julia Wild who have been involved in the master project linked to this research. I really appreciate their hard work and great contribution to this research.

I count myself incredibly fortunate to have a circle of friends who have stood by me throughout this challenging journey. Their companionship has created unforgettable memories. My heartfelt gratitude goes out to the following friends: Yanmei Duan, your unwavering encouragement and support were instrumental in helping me complete my thesis; Xi Fan, your brilliant ideas have broadened my horizons in profound ways; Xu Huang, you are not only my closest friend but also my family; Ke Hu, thank you for being a patient and empathetic listener, offering your unwavering support no matter how trivial the matter. I also want to express my thanks to Shuyue Wang, Yanghaoyue Xiong, Ruitong Zhou, Yao Zhou, Rui Lei, Celina Zhang, Li Yuan, Yue Li, Marrisa Kooperman, Alisa Lim-Hitchings, Sofie Huisman, and Malou DenHarder for the wonderful travel and game moments we've shared together. To my fellow members of the Swiss Massive Alcoholic Road Trip (SMART), Natalia Pawlowska, Natalie Kummer, and Amanda Frick, I am profoundly grateful for orchestrating and successfully completing this exceptional journey with me. Our expedition through all 26 cantons of Switzerland is an accomplishment I will carry with pride throughout my lifetime.

Last but certainly not least, I dedicate this achievement to my parents. Their unwavering love, support, and the sacrifices they have made are the bedrock upon which my academic journey stands. I am profoundly grateful for their boundless love and support.

Abstract

In forensic science, paint is one of the most common types of trace evidence. It can offer vital insights during the investigation of traffic accidents, especially hit-and-run incidents. Because paint originates from mass production, it often exhibits significant similarity across different samples, resulting in considerable uncertainty regarding this type of evidence. The evaluation of physical and chemical characteristics through instrumental analysis is essential in determining the rarity and significance of paint evidence. Nevertheless, there is a lack of comprehensive studies on recent variations in mass-produced automotive paints. This thesis aims to fill this gap by examining the most representative manufacturers and colors of automotive paint through microscopy, Fourier transform infrared spectroscopy (FTIR), Raman spectroscopy, and pyrolysis gas chromatography-mass spectrometry (Py-GC/MS). The research uses statistical tools (chemometrics) to evaluate the analytical data and identify variations in paint production, thereby providing forensic scientists with improved frameworks for interpreting paint evidence.

The study collected 62 white automotive paint samples, with 135 subsamples, from Volkswagen vehicles produced by two Chinese manufacturers. All samples underwent a thorough analytical sequence using the aforementioned techniques. The discriminating power of each technique, individually and in combination, was calculated. It reveals that the intra-sample and inter-sample variability in this sample set was relatively high. This study also examined the necessity of analyzing all layers, revealing that analyzing the primer with FTIR and the clearcoat with Raman spectroscopy yields highly effective discriminatory results.

Through the defined analytical sequence, an impressive discriminative power of 99.6% was achieved for this sample set, with only seven pairs of samples remaining undifferentiated. The study thoroughly investigated the undifferentiated sample pairs, the correlation between paint characteristics and sample origin (make, model, assembly plant), and the sample variability related to topcoat color, production year, batch variation, and geographic variation using the integrated data.

The comprehensive analysis and comparisons conducted in this research provide a solid foundation for future forensic investigations involving automotive paint.

Table of Contents

Abbreviations & Acronyms

ACR	Acrylic
ACR ALK	Acrylic alkyd
ACR MEL	Acrylic melamine
ACR URE	Acrylic urethane
ALK IPH	Isophthalic alkyd
ALK MEL	Alkyd melamine
ALK OPH	Orthophthalic alkyd
ALK TER	Terephthalic alkyd
ALK U	Alkyd-urea
ASTM	American Society for Testing and Materials
ATR	Attenuated total reflection
BEID	Singapore Police Force's Bomb & Explosive Investigation Division
BKA	Bundeskriminalamt, Central National Laboratory, Wiesbaden, Germany
BSE	Backscattered Electrons
BZG	Benzonguanamine
CAAM	China Association of Automobile Manufacturers
CCD	Charge-Coupled Device
CCSWA	Common Components and Specific Weights Analysis
CYA NIT	Acrylonitrile $N \equiv C$
DP	Discriminating Power
DTGS	Deuterated Triglycine Sulphate
ENFSI	European Network of Forensic Science Institutes
EPGT	European Paint, Glass & Taggants Expert Working Group
EPY	Epoxy
ES	Emission Spectrometry
EUCAP	European Collection of Automotive Paint
FBI	Federal Bureau of Investigation
FCPL	Forensic Chemistry and Physics Laboratory
FSO	Federal Statistic Office

FTIR	Fourier Transform Infrared Spectroscopy
HALS	hindered amine light stabilizer
HCA	Hierarchical Clusters Analysis
IR	Infrared
LDA	Linear Discriminant Analysis
MCT	Mercury–Cadmium–Telluride
MEL	Melamine
MSP	Microspectrophotometry
NCL	Nitrocellulose
NIST	National Institute of Standards & Technology
OEM	Original Equipment Manufacturer
PBD	Polybutadiene
PCA	Principal Component Analysis
PDQ	Paint Data Query
PLM	Polarized Light Microscopy
PLS-DA	Partial Least Squares Discriminant Analysis
POL	Crossed polarized light
POL MEL	Polyester-melamine
PUR	Polyurethane
PY-GC/MS	Pyrolysis Gas Chromatography Mass Spectrometry
Raman	Raman spectroscopy
RCMP	Royal Canadian Mounted Police
RMS	Root Mean Square
ROC	Receiver operating characteristic
SE	Secondary Electrons
SEM/EDX	Scanning Electron Microscopy with Energy Dispersive X-Ray Spectroscopy
SIMCA	Soft Modeling of Class Analogy
SNR	Signal-to-Noise Ratio
STY	Styrene
SVMDA	Support Vector Machine Discriminant Analysis
SWGMAT	Scientific Working Group for Materials Analysis
TLC	Thin Layer Chromatography

UNIL	University of Lausanne
UVA	Ultraviolet absorbers
UV-VIS	Ultraviolet–Visible
VIN	Vehicle Identification Number
VOC	Volatile Organic Compound
VPD	Vehicle Paint Database
VW	Volkswagen

1. Introduction

1.1.   Forensic research context

Many objects encountered in daily life, such as tools, buildings, automobiles, are covered with paints. These paints can be transferred in criminal activities, which makes paint evidence one of the most common types of trace evidence in forensic science. Among them, automotive paint is the largest category and is used to provide valuable information that helps with investigation of traffic accidents, such as hit and run cases. When used as evidence, the rarity of physical and chemical characteristics revealed by instrumental analysis of paint should be evaluated. Comprehensive studies have been conducted to obtain information that could assist with the interpretation of paint evidence. Most of the published research is based on paint samples collected from random manufacturers and colors when the aim concerns paint differentiation. However, automobile paints are mass-produced products, to what extent can the paints be differentiated and the significance of non-differentiation when analyzing this kind of mass products are also important issues in forensic practice. In fact, batch variation is one of the key figures that need to be considered when it comes to paint frequency interpretation. The only systematic study that focused on this topic was published in 1998 (Stoecklein and Palenik,1998). The authors tried to provide the answer to the questions such as '*in how many vehicles produced by one manufacturer and painted in the same color, can the paint be distinguished*' and '*how many examinations must be carried out before two samples can be said to be non-differentiated*'. Since then, paint application technology has developed and improved significantly. Similar research which focuses on the discrimination of paints from the same manufacturer and color, however, is scarcely found in literature. Nowadays, forensic casework relies more and more on paint databases. Databases can indeed provide information that could help with the interpretation of paint evidence. However, our in-depth understanding of mass-produced paint should also be updated from systematic study of paint of same manufacturer and color. The present research derives from this need and strives towards a deeper understanding of more recent paint variation in manufactured automotive paint.

This thesis aims to analyze the most representative manufacturer and color of automotive paint using several common analytical techniques, namely microscopy, Fourier transform infrared spectroscopy (FTIR), Raman spectroscopy (Raman), and pyrolysis gas chromatography mass spectrometry (Py-GC/MS). The acquired analytical results will be evaluated from the perspective of discrimination of batch production with the aid of statistical tools (chemometrics). In-depth information about automotive paint batch differences will be discussed to aid forensic scientists with their interpretation of the strength of paint evidence.

1.2. Structure of the manuscript

This research will be presented and summarized in a total of 12 chapters, structured in a logical order from theory to practice. Each chapter will cover specific aspects of the research and contribute to the overall understanding of automotive paint analysis.

Chapter 2 will provide a brief introduction to automotive paint, focusing on the coating system (layer sequence) and composition. This chapter will establish the foundational knowledge necessary for understanding the subsequent chapters.

Chapter 3 will discuss the current status of forensic automobile paint analysis, exploring various aspects related to the methods commonly used in paint analysis. It will highlight the working principles of each instrument and provide a comprehensive literature review of their applications in forensic analysis of automotive paint.

Chapter 4 will present a detailed elaboration of the aims, objectives, and methodologies of this study. It will discuss the gaps and limitations in existing research and outline the additional information expected to be obtained from this research.

Starting from Chapter 5, the focus will shift to the practical part of the thesis. This chapter will provide detailed information on the selection, collection, and constitution of the paint samples, setting the stage for the subsequent experimental chapters.

Chapters 6 to 10 will present the experimental aspects of the research. Chapter 6 will focus on the optimization and standardization of the sample preparation method and experimental parameters of each technique involved in this thesis. Chapters 7, 8, 9, and 10 will cover the specific analysis techniques used in this study, namely microscopy, FTIR spectroscopy, Raman spectroscopy, and Py-GC/MS. Each chapter will delve into the respective method, including experimental results, and any necessary discussions.

Chapter 11 will provide a comprehensive discussion of the combined results obtained from all the analysis methods employed in this study. It will offer in-depth insights into the characteristics and properties of automotive paint based on the findings.

Finally, Chapter 12 will serve as the conclusion of the thesis, summarizing the key findings, discussing their implications, and providing a concise summary of the overall research.

By organizing the thesis in this manner, the research progresses logically from theoretical foundations to practical experimentation and analysis, ensuring a comprehensive and coherent exploration of automotive paint analysis.

2. Automobile paint

As defined in "Standard Terminology for Paint, Related Coatings, Materials, and Applications" which is published by American Society for Testing and Materials (ASTM), paint is known as '*a pigmented coating which is converted to a solid, protective, decorative, or combination thereof, film after application*' (ASTM-D16-19). In forensic case work, three categories of paint evidence are normally confronted, i.e., automobile paint, household paint and art paint (Muehlethaler *et al.*,2013). Automobile paint is the most common type and can be transferred to another object during a collision and/or left on a crime scene or on victims' clothes in hit-and-run cases. In order to achieve the forensic objective of paint discrimination, it is first necessary to understand the constitution and composition of automotive paint. The systematic introduction of the technology and the paint materials used in automotive coating processes are available from the following books (Lambourne and Strivens,1999; Streitberger and Dössel,2008). A brief summary will be provided here.

2.1.   Paint coating system (OEM)

In today's automobile manufacturing industry, the car body itself is made of various metals or plastics. In order to protect the metal body from corrosion due to direct exposure to the air and provide an appealing look, the car body is usually applied with paint coatings. The development of science and technology has changed the coating process from the initial hand-painting and air-drying procedure, requiring several weeks to a worldwide standardized process that takes only hours. Automobile paint should provide durable protection and aesthetic appeal. In order to meet the above demands, the standardized coating process is designed to be able to apply several layers of coatings that have different functions on the car body. The original coating system which is generated from this standardized coating line is referred to as an original equipment manufacturer (OEM) system. At present, a standard OEM coating system produces 4 to 5 layers of paint with a total thickness of 100-140 µm, from the inside to the outside, including pretreatment, cathodic electrodeposition primer, primer surfacer, basecoat and clear coat (see *Figure 1*).
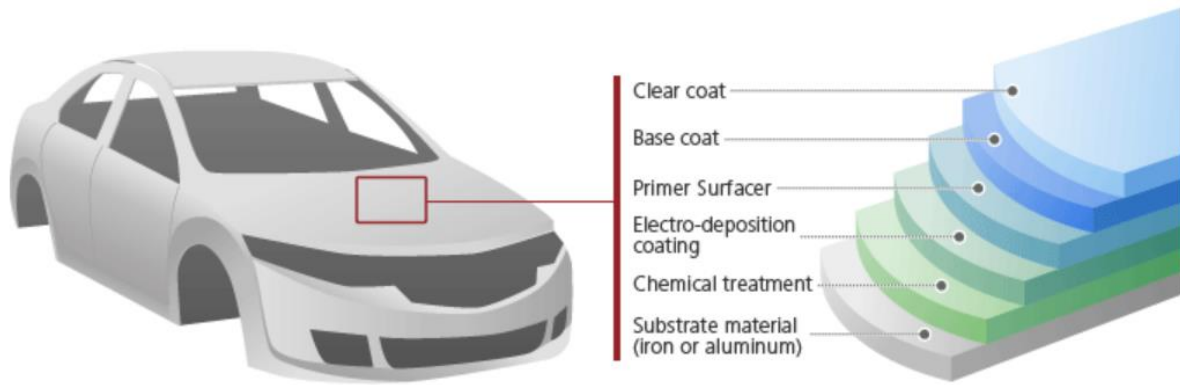
Figure 1. Schematic of an OEM coating system
(https://www.shintoacs.com/english/products/index.html)

2.1.1. Pretreatment

Currently, most car bodies worldwide are produced from either zinc-coated steel, aluminum sheets or coils. The surface would normally contain some contaminations materials like oils and lubricants resulting from the body assembly process. Metal surfaces easily rust or corrode due to their impurities and a humid environment. Since paint films lack adhesion to bare metal, corrosion would easily take place if paints were to be directly applied onto untreated metal surfaces. Removing these contaminants provides corrosion protection for the metal substrate and improves paint adhesion so that the subsequent primer could be better adhered to the car body. The substrate surface would be first pretreated under a process called 'degreasing' to remove all the contaminants followed by a zinc phosphating process. During the zinc phosphating process, a reaction between the metal and zinc phosphate solutions would initially occur forming a thin, phosphate crystal coating with the thickness between 1 and 3 μm on the metal surface. This step is the standard process for pretreating car bodies.

Puomi *et al* has reported on a new development in which they replaced the zinc phosphating and E-coating system (will be introduced in next section) with one epoxy-acrylate primer system (Puomi *et al.*,2008). Since virtually no pretreatment is needed before primer coating, the proposed technology simplified the traditional automotive finishing process.

2.1.2. Cathodic electrodeposition primer

After the pretreatment process, the body-in-white would be then coated with a primer, undergoing the electrocoating (E-coating) process. The electrocoating process is to immerse the conductive substrate, i.e., body-in-white in a tank filled with the electrocoat as the cathode and set up a corresponding anode in the tank. After the direct current is connected

for some period, a uniform and dense paint film (insoluble in water) will be deposited on the surface of the object, known as the cathodic electrodeposition primer. The ideal thickness of this coating is around 20-22 µm. The paint film usually results in a grey/black color and has a characteristic bubble-type structure morphology due to the hydrogen and oxygen gases developed during the process. The cathodic electrodeposition primer, which is considered as a layer directly adhered to body-in-white, plays a critical role of corrosion prevention and improved paint adhesion.

2.1.3. Primer surfacer

The primer surfacer, often termed surfacer, is referred to as middle coat, playing an important role in connecting the upper and lower coatings. The primer surfacer 'fills' the holes and lines on the rough surface to make a flat and smooth surface, thus producing good bonding/adhesion between the upper and lower coatings. It also fulfils the requirement of stone chip resistance and climatic protection. The flatness and smoothness of the coating can effectively hide the imperfections of the body-in-white and increase the fullness and clarity of the topcoat. The application of this coating is often not standardized due to the complex requirements.

2.1.4. Basecoat (color coat)

The basecoat, also termed color coat, is the layer applied over the primer surfacer that can be seen from the outside, determining the color of vehicles. Pigments are the key components that are present in the basecoat responsible for basic solid colors. Particles such as metallic and mica flakes can also be added to produce effect color, hence increasing the richness of colors. The presence or absence of the effect flakes distinguishes basecoat into two types: solid or effect. The basecoat provides the function of aesthetic appearance and durability to the car. Since color is the appealing factor to the customer, manufacturers tend to use a variety of pigments or different combinations of pigments to give their products an attractive appearance. The characteristics of basecoat can be regarded as the discriminating feature for vehicles from different manufacturers, models and production years.

With regards to the color popularity, according to annual automotive color popularity and trend data published by world's leading coating suppliers (such as BAFS and PPG), white retained the leading spot as the most popular car color not only regionally but also globally (see *Figure 2*).

Figure 2. Regional and Global color trend popularity in 2019
(https://news.ppg.com/2019automotivecolor/)

2.1.5. Clear coat

The clear coat is the outermost layer of the coating system, a transparent paint layer that one can touch directly. Its function is to protect the colored basecoat, preventing the whole paint system from stone chips, scratches, ultraviolet radiation, weather and temperature changes and any other damage from the outside world.

2.2.   New trends for coating application

In a standard OEM coating process, each functional coating is applied step by step. In between steps, the oven-baking process is necessary in order for the coatings to be cured or dried, thus forming a hard film before applying the subsequent coating (see *Figure 3*).
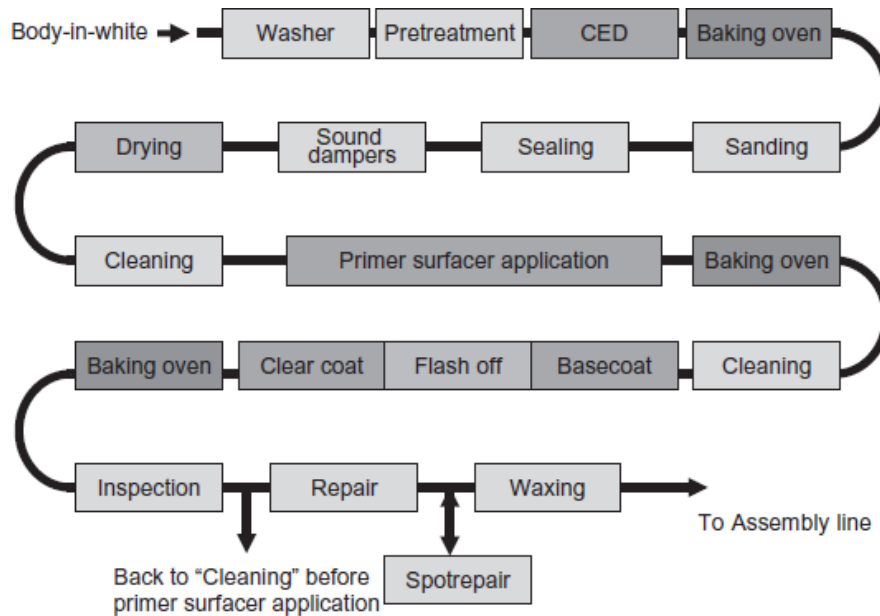
Figure 3. Standard coating process for OEM paint system (Streitberger and Dössel,2008)

In recent years, driven by energy and cost saving, several integrated paint processes were developed. The first compact process is to reduce the baking step, i.e., to conduct a wet-on-wet-on-wet application for primer, basecoat and clear coat. Only one baking process would take place after the coatings mentioned above are applied. This is known as 'the 3-wet process' or the 'wet-on-wet-on-wet process' (see *Figure 4*). This process may result in a reduction in the number of paint layers, less distinct boundaries between layers, and an increase in the thickness of the paint layers.
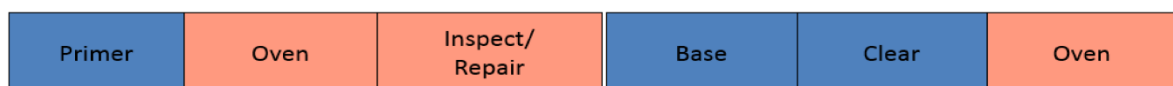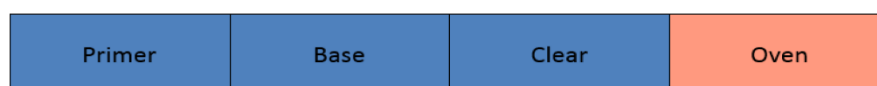
Figure 4. Wet-on-wet-on-wet processes of the primer coat(Akafuah et al.,2016)

Another consolidated process is called the 'primerless coating process', which eliminates the use of primer surfacer by applying two layers of basecoat and enhancing their properties (see *Figure 5*). In this system, the first basecoat layer serves as primer to meet the requirement of anti-chip and durability. The second basecoat will remain as a classic color layer to provide color and additional durability. Both layers are applied wet-on-wet without a heated flash-off zone in between(PPG).
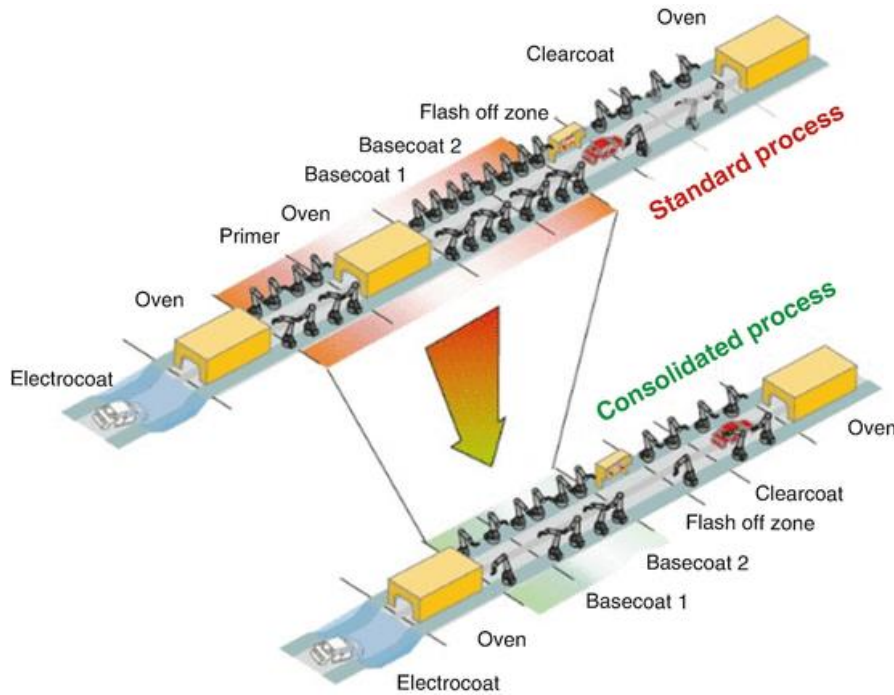
Figure 5. Primerless coating process(Moore,2017)

The advantages of these compact processes are that they are more eco-friendly as they reduce the emission of CO_2 and volatile organic compounds (VOC) as well as overall energy consumption. This process, however, increases the risk of chemical component penetration at the interface of each of the two wet layers resulting in an inhomogeneous performance for each layer.

2.3.   Paint system on plastic parts

The utilization of plastic materials on the car body has been increasing since the 1970s. They are often used as exterior components such as bumpers, 'spoilers' and 'wrap-arounds' (Ansdell,1999). Plastic bodies, on one hand, have the advantage of weight-saving, style and better resistance but, on the other hand, bring coating difficulties such as poor adhesion, baking limitation and color match problems. Due to the property of heat distortion, only a few heat-resistance plastics can pass through the entire painting process together with the

metal body. Most of the plastic substrates are painted by suppliers or in a separate coating line at the automotive manufacturer (Wilke and Jacob,2008). This results in a high probability of paint layer diversity. The layer sequence or the composition of paint on plastic substrates and of paint on metal bodies from the same car may vary greatly.

2.4.   Refinishing system

Defects may occur in every step of painting process. This leads to a situation where most of the new cars will have to be repaired at least once before delivery to customers (Dössel,2008). Detected defects or damages are removed by sanding or polishing and an additional coating step for this segment or even the whole car is then required. This may cause unusual layer structure of paint.

While brought into use, car paint provides adequate protection for the car body. However, it also suffers from various damages such as aging and peeling caused by climatic factor, stone chip attacks, scratching, and even major damage caused by a car collision. For protective and aesthetic reasons, these damages must be repaired. Furthermore, when some OEM paints cannot provide customers with a wealth of color choices, they may tend to design their own paint colors. The need for maintenance and customization of paint on a car body is what ultimately led to the establishment of the refinishing industry. Repainting services might be provided by refinishing department of original carmaker, automobile repair shops, or even small local workshops. Different repainting requirements and various service suppliers make the refinishing coating system and chemical composition diverse. Unlike the OEM coating system, there is no standardized layer sequence for a refinishing paint system. The whole OEM system can be eliminated if damage causes the entire coating to peel. A thick primer might be used to fill the deformations caused by stone chip attack or collision to form a flat surface. Topcoats (basecoat and clear coat) are the most common additional layers added to OEM coating system. These specific layer sequence and variety in chemical composition make refinishing paint more distinguishable than OEM paint.

2.5.   Composition of automobile paint

Automobile paint is different from other paints because it is always exposed to nature and is subject to seasonal changes. In order to protect the car body for as long as possible, the performance requirements of coatings are extremely high. As previously mentioned, automobile paint should not only have good mechanical properties, and high durability, but also good adhesion, high hardness, strong scratch resistance, excellent weather resistance and superior resistance to all kinds of pollutants such as gasoline, alcohols, acids, alkalis, salt spray, not to mention satisfying the demand for aesthetics such as attractive color, gloss continuity and so on. All these performances have special requirements for the chemical composition of paint. For automobile paint, there are usually four components: the binders

or resins, pigments and extenders, solvents and additives (Lambourne and Strivens,1999). The detailed explanation of each component can be found in the following books or book chapters (Lambourne and Strivens,1999; Caddy,2001; Ryland and Suzuki,2011). Only a brief introduction will be given next.

2.5.1. Binders

A binder is the substance that holds or draws other materials together to form a cohesive whole mechanically, and chemically, by adhesion. In automobile coating systems, resin plays the role as a binder to be the polymeric substance that provides support medium for pigments, extenders and additives, forming a hard film after curing (Saferstein,2018). The polymers that are used for paint binders include acrylics, alkyds, polyesters, urethanes, amino resins, epoxies, vinyls, cellulosics, and silicones (Ryland and Suzuki,2011). The physical properties of the paint such as hardness, flexibility, durability, acid and alkali resistance are determined by the binder or resin (Bender,2013). Incidentally, the binder type is the most significant characteristic in forensic paint examination.

2.5.2. Solvents

Resin is a solid or highly viscous substance. When used as a coating material, it needs to be diluted in solvents so that the solution could be easily coated onto the car body, either by dipping or by spraying. This makes the solvent an essential component of automobile paint. Solvents used as diluents can be either organic solvents (solvent-borne paint) or aqueous (waterborne paint). Solvent choice is determined by both the resin system and by the method of application (Caddy,2001). However, waterborne paint is becoming the better choice for more and more manufacturers when considering environmental impact since organic solvents are considered as volatile organic compounds (VOCs) that are harmful to environment and regulated by countries. As a result of volatility during application, solvents are almost impossible to be detected during examination.

2.5.3. Pigments and extenders

Pigments are fine colored powder-like substances that are generally insoluble but can be evenly dispersed in water or resin, providing opacity, color and protection to paint as well as concealing properties. They can be organic or inorganic and they can enhance the permeability, durability, weather resistance, abrasion resistance and anti-aging properties of paint films. The physical shape, size and refractive index of pigment particles must be optimal to scatter light so as to provide opacity. The choice of pigments depends on the effect carmakers want to achieve. Organic pigments can provide brighter and more attractive colors,

while inorganic pigments can provide black and white as well as additional properties such as lightfastness, heat stability and UV absorption (Caddy,2001). Effect pigments are now widely applied in the coating industry. These pigments contain effect particles such as mica and metallic flakes that provide a pearlescent or flashy appearance (see *Figure 6*).
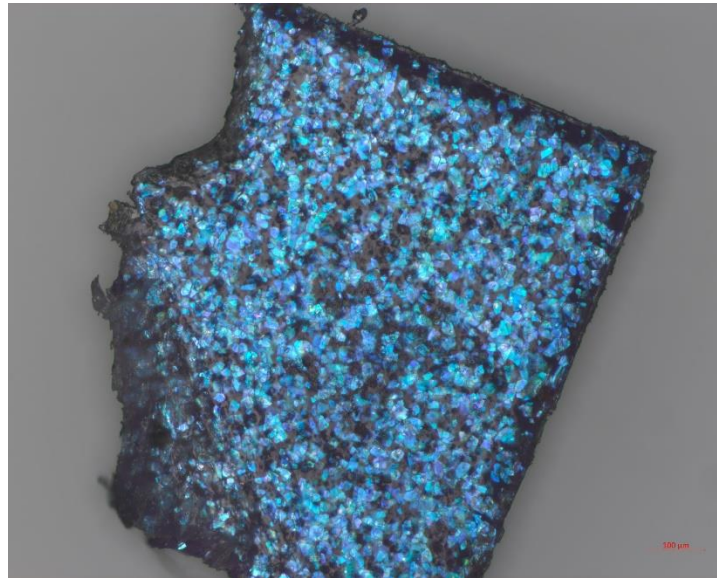
Figure 6. The effect particles present in the automotive coat.

Extender pigments, also termed extenders or fillers, do not have concealing power and tinting power. They cannot scatter light, nor can they add color to the paint. The main role of extenders is to increase volume and reduce costs since they are less expensive than pigments. The extender pigments can also improve the physical and chemical properties of the paint such as film thickness, gloss, viscosity, paint film structure, strength and durability. Some extender pigments have low density and good suspension power, which can help with pigment dispersion and prevent the precipitation of dense pigments, thus allowing a homogeneous appearance. Common extenders used in paints include calcium carbonate (calcite), magnesium silicate (talc), potassium aluminum silicate (mica), barium sulfate (barytes), kaolin (clay), and silicon dioxide (quartz) (Ryland and Suzuki,2011).

2.5.4. Additives

The formulation of paint film is a very complex process. It not only depends on the properties of the film-forming substance, i.e., the binder itself, but it is sometimes necessary to add chemicals to achieve certain reactions or enhance a desired property of car paint. Additives are the small amounts of substance added to the paint to provide the best properties and appearance. The types of additives vary with the purpose and location of use, including corrosion inhibitors, catalysts, ultraviolet absorbers (UVA), hindered amine light stabilizer (HALS), anti-mold components, plasticizers, pigment dispersion additives, etc.

3. Forensic analysis of automobile paint

3.1.　　　Introduction

Automobile paint traces are usually recovered from damaged cars, motorcycles, bicycles, human bodies, clothes of a victim and/or other items that have been left on the crime scene. The purpose of forensic paint analysis is to find the original sources of these 'unknown' traces, or in other words, to link these questioned traces to a specific vehicle. The strategies used in each case depend on the availability of the reference samples which were normally seized from a suspect vehicle. If a reference sample is available, the two samples should be analyzed by different analytical techniques and compared based on their physical and chemical characteristics to determine if they might have common source. If the reference sample is missing, then the profile of the unknown sample needs to be characterized and compared across relevant databases in order to get identifying information that could help with the investigation. Comparative analysis will be conducted after a suspected item is seized. Therefore, depending on the presence or absence of the known samples, a bifurcate analytical scheme is generated, which is illustrated in *Figure 7*.
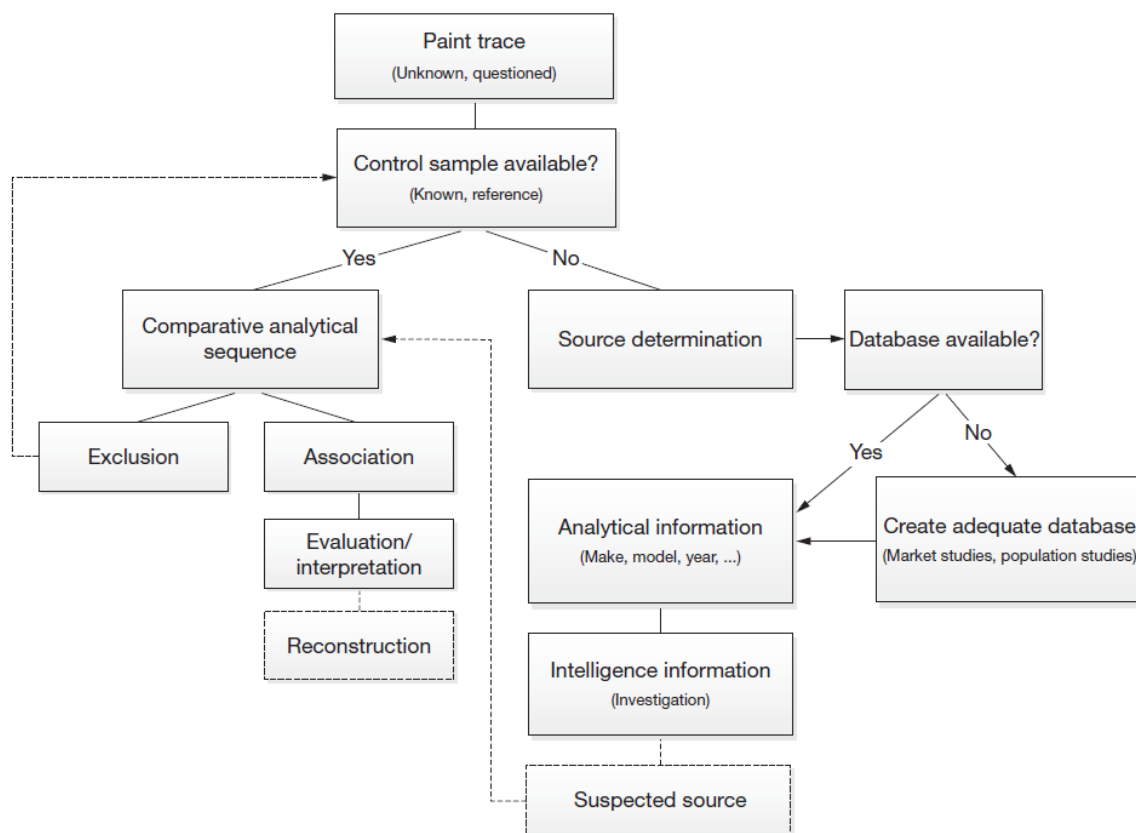
Figure 7. Flowchart of forensic paint analysis (Muehlethaler et al.,2013)

Since paint analysis results are served as evidence in the court, it has to be scientific, robust, logical and transparent. The analysis sequence must be conducted using validated methods and consistent approaches. Thus, guidelines have been established to provide a framework. In the U.S, the Scientific Working Group for Materials Analysis (SWGMAT) and the American Society for Testing and Materials (ASTM) have been publishing standard guides concerning all aspects of paint analysis and comparison (ASTM-E1610-18 ; SWGMAT,1999). These guides are intended to provide a reasonable reference for all the individuals conducting forensic paint analyses. In Europe, the European Paint, Glass & Taggants Expert Working Group (EPGT) of European Network of Forensic Science Institutes (ENFSI) has similarly developed a set of guidelines to provide recommendations for the forensic examination of paint (EPGT,2022).

In these guidelines, optical microscopy examination, FTIR, Raman, SEM/EDX and Py-GC/MS are the recommended techniques and likewise the most widely used techniques in forensic paint examination (Duarte *et al.*,2020). As they are the chosen methods for this study, the theory and their application in forensic automobile paint analysis will be amply discussed in the following sub-chapters. The choice of analytical methods and sequence are significant and will also be discussed in this chapter.

3.2. Forensic paint databases

3.2.1. Automotive paint databases

In the case where only paint traces are available, being able to obtain investigative information is significant. For instance, in a hit-and-run accident, investigators rely on the automobile paint fragments left on the victim to provide information regarding the potential source, such as manufacturer, color, model and production years. This achievement is established on the presence of an adequate database containing extensive data so that the questioned sample may be compared to it. The more exhaustive one database is, the greater the role the database can play. Based on this fact, various paint databases have been established since the 1970's. However, one single institute can never achieve the establishment of a comprehensive database, it requires collaboration. As a result, two international-scale databases for automobile paint were developed in North America and the other in Europe.

Since 1970's, the Royal Canadian Mounted Police (RCMP) Forensic Laboratories have been systematically gathering physical and chemical information on automotive paint. They have subsequently generated a database containing optical features, infrared spectra and all related sample information, known as Paint Data Query (PDQ). This database contains information related to automobile layer sequence, color description, manufacturer, location of assembly plant, year of production, model, topcoat color code, vehicle identification number(VIN) and substrate (Buckle *et al.*,1997). As for the chemical composition of each layer, they are recorded by means of functional groups, chemical types and crystalline structures

(i.e., extenders) from which can be identified from IR spectra. Spectra of an unknown sample can be searched and compared in the database generating a 'hit list', which includes manufacturer, model, production year and assembly plant. The 'hit list' is a list of vehicles that are similar to the unknown sample in terms of layer sequence and chemistry composition. This obtained information could thus help identify the source of the unknown sample (Wright,2010; Wright,2012). Since its establishment, maintenance and development of databases have not stopped. Partner laboratories continuously expanded the databases adding approximately 500 samples to PDQ annually (Bradley *et al.,*2007). Nowadays, the PDQ contains over 21000 samples in the database and is used in as many as 24 countries (Hodgins,2016). Techniques behind the database and its search algorithms were simultaneously updated (Lavine *et al.,*2014a). This makes PDQ one of the most significant international automotive paint databases.

In Europe, the European Collection of Automotive Paints (EUCAP) databases were built up by the EPGT in 1995. At the same time, EPGT started to cooperate with the RCMP and the FBI by means of sample and data exchange. Currently, the EUCAP databases are maintained by and contributed to most laboratories in Europe. It offers the possibility of identification or characterization of unknown paint samples encountered in casework. Similar to the PDQ, EUCAP databases also contain paint layer information, color, car make, model, production year as well as chemical component revealed by infrared spectra. EUCAP databases have over 60000 IR spectra from almost 24000 paint samples. Additionally, Raman spectra libraries for organic and inorganic dyes and pigments are also generated and can be used to identify existing pigments and extenders in the automobile paint topcoat. EUCAP can be accessed by not only ENFSI members but also by non-European countries such as the U.S, Canada, Singapore, and so on. This makes EUCAP also one of the most significant international automotive paint databases.

The establishment of databases stems from the need to solve difficulties encountered during the comparison and interpretation of casework. Driven by this need, several countries, such as Japan, Singapore, and Australia, have also established their own local automotive paint databases. In Singapore, the Forensic Chemistry and Physics Laboratory (FCPL) of Health Sciences Authority and Singapore Police Force's Bomb & Explosive Investigation Division (BEID) started a collaborative project in 2008. Since then, they have collected over 2500 automotive paint samples from the streets and establish a Vehicle Paint Database(VPD) for physical, microscopic and chemical examinations (Soong *et al.,*2020). In fact, most forensic laboratories would have several small local databases, which often are associated with specific cases.

The existence of automotive paint database makes it possible to correlate the chemistry of the automotive paint with a particular vehicle make and model within a limited production year range (Lavine *et al.,*2016b).

3.2.2. Other paint databases

As automobile paints are not the only type of paint traces that can be found in casework, databases for tool paints, architectural paints and spray paints were also created. In EPGT, databases containing thousands of spray paint IR spectra, hundreds of tool paint IR spectra as well as several architectural paint IR spectra are also established and continuously updated.

3.3. Analytical sequence of automobile paint

Since automobile paint is a multilayered mixture, analytical techniques should be chosen to provide a comprehensive examination protocol. The sequence should follow the principle from general to specific, from physical to chemical characteristics. Considering the limited quantity of samples, the non-destructive methods should be prior to those that are destructive or require more sample preparation (ASTM-E1610-18). When determining which techniques should be applied using which sequence, the case requirement, the sample condition, the instrument available in a laboratory, the available time, and the cost should be taken into consideration. Before starting any analysis, a pre-assessment should be conducted to predict the potential value that the examination may provide and to determine the analytical strategy (Muehlethaler *et al.*,2013). An analytical sequence has been defined based on the above principles, as illustrated in *Figure 8*. The methods mentioned in the figure will be amply discussed in the following subchapters.
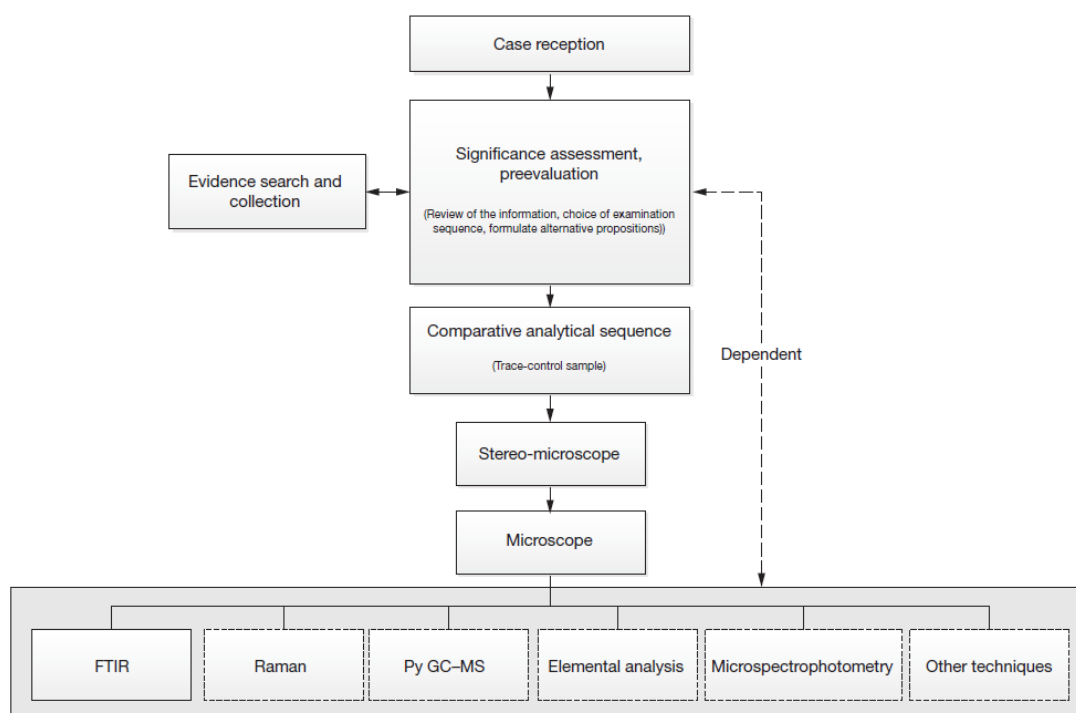
Figure 8. A general analytical sequence that can be applied for automobile paint analysis (Muehlethaler et al.,2013).

3.4.   Microscopy

No matter the condition of a sample or which analytical strategy is adopted afterwards, the first step in forensic analysis of automotive paint remains visual evaluation and description (ASTM-E1610-18 ; SWGMAT,1999). Since paint samples are often small in size and of a limited quantity, this step is usually accomplished using a stereomicroscope. Once general properties such as size, shape, surface features, and color of a sample are documented, observation and comparison of further distinctive physical properties of a paint system using a microscope is the next key step. The color, texture, morphology, gloss, pigment appearance, effect pigment size and distribution, anomalies, layer structure and relative layer thickness are all important features for an automotive paint system (ASTM-E1610-18 ; Buzzini and Stoecklein,2005; Muehlethaler *et al.*,2013). Many studies have shown that automotive paint can be well distinguished using only microscopy comparison (Gothard,1976; Ryland and Kopec,1979; Edmondstone *et al.*,2004; Reynolds *et al.*,2018; Kruglak *et al.*,2019). Among these features, the number, sequence and type of layers are the most distinctive points (Gothard,1976; Ryland and Kopec,1979; Edmondstone *et al.*,2004). The examination of layer structure is also able to differentiate an OEM paint from refinishing paint, which requires an accurate examination by obtaining a cross-section of paint either using a scalpel /razor blade or a microtome (ASTM-E1610-18).

The characteristic features of automotive paint can be revealed by various illumination techniques. Without sample preparation, paint flakes can be placed directly on a microscope slide and observed with incident light. This permits the observation of color, size, shape, effect flakes and surface properties (Buzzini and Stoecklein,2005).Transmitted light has been proven to be the most valuable for paint thin section, with a discriminating power (DP) over 95% for colored paints (Allen,1992a). Both bright field and dark field illumination should be applied for the most complete examination (Caddy,2001). *Figure 9* presents a good example which shows that dark field illumination allows the color difference of primer surfacer and primer where they could not be differentiated in bright field. Polarized light microscopy (PLM) (both plan-polarized light and double polarization) and fluorescence microscopy are necessary techniques for the examination of pigments and extenders used in paint since these compounds may show special polarization or fluorescence colors (Hamer,1982; Hopen and Davis,2009).
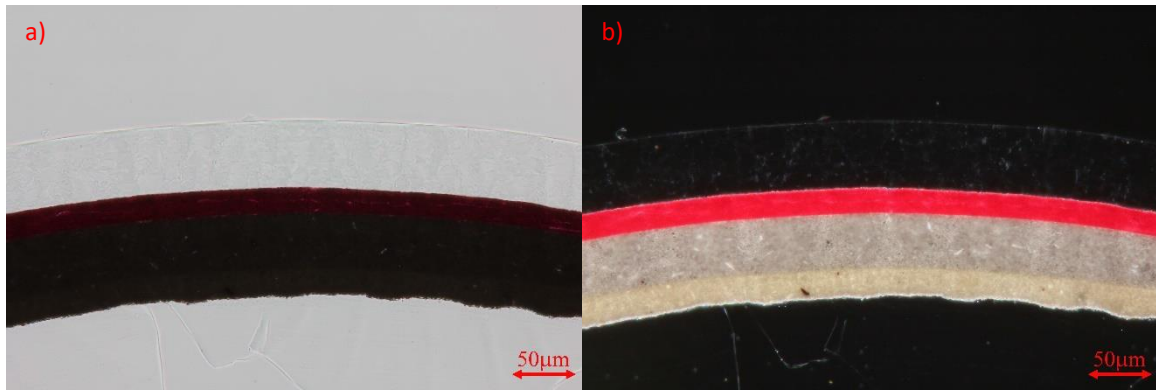
Figure 9. Microscopic examination of the cross-section (5 µm) of a red automobile paint in a) transmitted light bright field, b) transmitted light dark field.

Discriminating power is defined as "the probability of discriminating two distinct samples selected at random from the population of interest"(Smalldon and Moffat,1973). It was developed to assess whether one attribute of a sample is more discriminating than others so that making it worthy of being measured. Now it serves more as a key parameter to evaluate whether a method is a good choice to discriminate certain samples.

Several studies have shown that microscopy in general provide high discriminating power for automotive paint examination. A summary of these existing published data is provided in *Table 1*. The year of publications, the total number of samples, the techniques used, and their DPs are listed.

Table 1. Summary of the automotive paint studies conducted using microscopic techniques.

Authors, Year of publication	Country	Total number of samples (N)	Techniques	DP (Number of non-differentiated pairs)
Gothard,1976	Australia	500	Varied lighting conditions	0.9999 (5)*
Ryland and Kopec,1979	US	200	Varied lighting conditions	0.9993 (13)
Massonnet,1996	Switzerland	124 (only metallic grey)	Transmitted light bright field	0.9205 (606)
			Transmitted light dark field	0.9498(383)
			Reflected light bright field	0.9041 (731)
			Reflected light dark field	0.918 (625)
			Polarized light	0.9039 (733)
			Fluorescence light (UV filter)	0.9018 (749)
			Fluorescence light (purple filter)	0.8734 (965)
			Fluorescence light (blue filter)	0.877 (938)
			Fluorescence light (green filter)	0.8408 (1214)
Edmondstone *et al*.,2004	Canada	260	Reflected light	0.999 (35)
Reynolds *et al*.,2018	US	231	Transmitted light	0.9997 (7)
Kruglak *et al*.,2019	US	200	Transmitted light bright field and polarized light	0.9999 (1)
Soong *et al*.,2020	Singapore	256	Reflected light (stereomicroscope)	0.9986 (65)

* Chemical tests were also conducted to the samples and counted for microscopic differentiation.

From the published studies, it is known that when the sample set involves one single color, the DP is less than those containing various colors. In general, the more layers of paint present in a paint chip, the less likely it is for one to randomly encounter another source of paint with the same characteristics (layer sequence and layer components) (SWGMAT,2011). In order to achieve a comprehensive optical examination, it is recommended to combine all the aforementioned techniques.

3.5.   FTIR

After physical and optical examination, the following step of automobile paint examination should be the characterization and comparison of their chemical features. Vibrational spectroscopy can be used to determine the molecular structure of materials non-destructively, and is currently the preferred choice as a first-pass analytical technique in forensic science (Chalmers *et al.*,2012c). Among these, IR spectroscopy is the most common and powerful technique for identifying and comparing automotive paint by determining chemical components such as binders, pigments or additives (ASTM-E1610-18 ; Ryland *et al.*,2001; Ryland *et al.*,2006; Duarte *et al.*,2020; EPGT(EPG-GDL-002),2022). Since paint samples encountered in casework are often limited in quantity, a Fourier transform infrared (FTIR) spectrometer with microscope accessory is essentially used for adequate characterization (ASTM-E2937-18 ; MacDougall *et al.*,2001; Muehlethaler *et al.*,2013).

3.5.1. FTIR spectroscopy principles

More detailed theoretical principles of FTIR have been well documented in the following references (Darlene and Brezinski,1991; Humecki,1995; MacDougall *et al.*,2001; Chalmers and Griffiths,2002; Griffiths and De Haseth,2007; Chalmers *et al.*,2012a). This section provides a basic introduction of relevant principles and instrumentation.

When light in the range of IR radiation passes though or is reflected off a sample, some radiation may be absorbed. The intensity and the frequency of absorption is a result of the molecular structure of the sample as well as the vibrational mode of the molecules, which is characteristic for a specific functional group (Griffiths and De Haseth,2007). Thus, a vibrational spectrum can be generated, where the x-axis represents the frequency of absorption in units of wavenumber (cm^{-1}), the   y-axis represents the absorbance or percentage transmission of IR radiation (MacDougall *et al.*,2001). A typical IR spectrum is in the wavenumber range of 4000-400 cm^{-1}, known as mid-infrared, encompassing chemical information that is particularly relevant to the forensic scientist. The range of 1500-400 cm^{-1} is often referred to as the 'fingerprint' region of an IR spectrum since it usually contains a large number of peaks that may be unique and used to distinguish between compounds (Chalmers *et al.*,2012a). The IR spectra of binders or resins used in paint contain many sharp bands in the range of 3600-500 cm^{-1}, whereas inorganic compounds such as inorganic

pigments and extenders often present bands in the region of 1500-200cm^{-1} (MacDougall *et al.*,2001). Since the individual peaks present in IR spectra are associated with unique compounds, the spectra can be interpreted to identify the functional groups and further compared to a library database of reference spectra (Chalmers *et al.*,2012a).

3.5.1.1. FTIR instrumentation

A typical FTIR spectrometer contains an infrared source, an interferometer and detectors. When it comes to the analysis of samples of a limited quantity, the FTIR spectrometer is usually coupled with an IR microscope accessory.

The most common infrared source used in FTIR spectrometers is the Globar (Chalmers and Griffiths,2002; Griffiths and De Haseth,2007). It is a resistively heated silicon carbide rod that is electrically heated to 1200 °C (or ~1400K), which is high enough to emit continuous mid-infrared radiation.

The interferometer consists of a beamsplitter and two mirrors that are perpendicular to each other – one stationary and one moving (see *Figure 10*). After the IR radiation is emitted from the infrared source, it reaches the interferometer and is split into two parts by the beamsplitter. These two parts are then directed to the fixed and moving mirrors, respectively. The two beams interfere with each other and recombine at the plane of beamsplitter. The recombined beams then pass though the sample, interact with samples, and finally reach the detector. The interference patterns can be converted to infrared spectra by a Fourier transform (MacDougall *et al.*,2001).
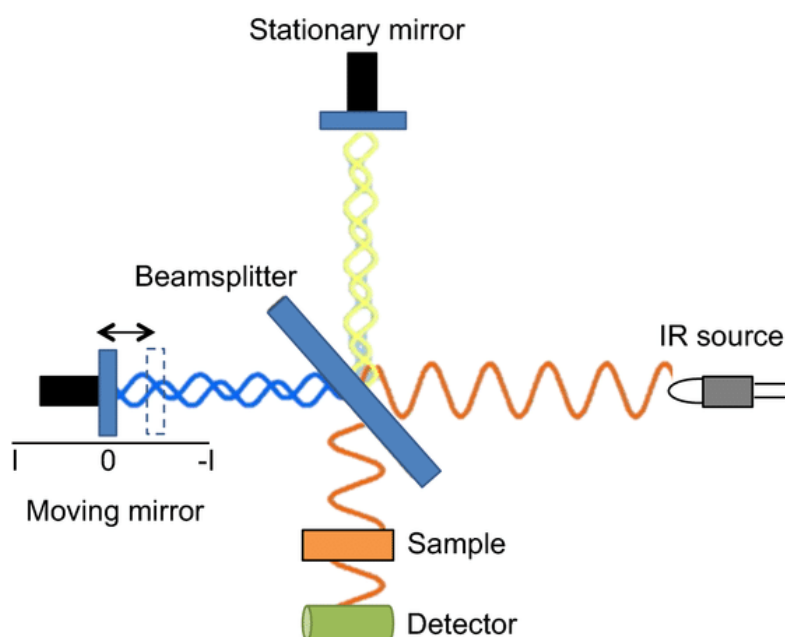
Figure 10. A schematic of an interference in FTIR spectrometer (Campanella et al.,2021)

The two most common infrared detectors used in mid-FTIR spectroscopy are the deuterated triglycine sulphate (DTGS) detector, which is a thermal detector, and the mercury–cadmium–telluride (MCT) detector, which is a quantum detector. The MCT detector has higher sensitivity and speed of response than the DTGS detector, so it is the most commonly used detector when FTIR is coupled with microscope. However, the drawbacks of the MCT detector are that it must be cooled by liquid nitrogen to achieve its best sensitivity. Additionally, it has a narrower spectral range than the DTGS detector where the spectra are cut off at 600 cm^{-1}. This results in the limitation of obtaining inorganic information from the sample (Kirkbride,2015).

The microscope coupled with FTIR spectrometer use special Cassegrain optics. The beam from the interferometer is firstly focused by the Cassegrain condenser onto the sample, then collected by the Cassegrain objective after passing through the sample, and finally focused onto the MCT detector (Griffiths and De Haseth,2007). In the microscope, the glass lens is replaced by metal-coated lens in order to avoid IR radiation absorption. The sample to be analyzed is mounted on the stage and the analysis region is selected by variable apertures. The aperture size can be adjusted and adapted to the size of a paint layer with a minimum diameter of 10 μm (EPGT(EPG-GDL-002),2022). The optical bench of the microscope is often adapted to the spectrometer so that the whole system becomes FTIR microspectrometry, thus being able to measure samples in both transmission and reflective mode. However, the transmission mode is more preferred due to the spectral distortion and mathematical corrections in the reflectance spectra (Ryland,1995; MacDougall *et al.*,2001).

3.5.1.2. Sampling techniques

A large variety of sampling techniques are available for paint analysis, including transmission, reflection, attenuated total reflection(ATR), and various microsamping methods (MacDougall *et al.*,2001). The detailed explanation for these methods can be found in the references mentioned at the beginning of this chapter (page 18). In this section, only the sampling techniques involved in transmission FTIR microspectroscopy will be discussed.

The diamond anvil cell (high pressure or low-pressure) is one of the recommended sampling techniques for transmission measurements in the field of forensic paint analysis. It has been proven by Tweed *et al.* in 1974 to be a reliable sampling method for sample preparation (Tweed *et al.*,1974). This has also been confirmed by several subsequent published studies and recommended by guidelines (ASTM-E2937-18 ; Rodgers *et al.*,1976a; Schiering,1988; Allen,1992b; Cassista and Sandercock,1994; SWGMAT,1999; MacDougall *et al.*,2001; Ryland and Suzuki,2011; EPGT(EPG-GDL-002),2022). The diamond anvil cell consists of two diamond windows (type II), a holder, and a mechanism that helps squeeze the samples. For single-layer paint sample, it can be placed between two diamond windows and flattened by compressing the diamond windows with the fingers. For multilayered samples such as automotive paint, thin cross sections (normally 5 μm) are made using either a microtome or a razor blade. They can be either pressed using a scalpel blade or rolled with an appropriate tool before being

directly positioned onto the support (EPGT(EPG-GDL-002),2022). Once the sample is prepared, it is mounted onto the stage and first observed using the microscope. The region of interest is centered in the field of view and defined by the apertures. The acquired spectrum is a mixture of sample and background. The sample should be moved out of the field of view in order to collect the spectrum of background. The ratio between the two spectra gives the IR spectrum of the sample. The spectra are often plotted as transmission spectra, at 4 cm^{-1} resolution with a spectral range of 4000-650cm^{-1}.

KBr micropellets is another microsampling technique for transmission measurements. KBr (potassium bromide) is the most common alkali halide used in the pellets. Since it is totally transparent to the IR radiation between 4000cm^{-1} – 450 cm^{-1}, it doesn't exhibit absorption in this range. The samples should be deposited on a KBr pellet for measurement. It is now gradually being replaced by the more convenient diamond cell techniques.

3.5.2. Application of IR spectroscopy in the forensic analysis of automotive paint

The use of IR spectroscopy for forensic application began in the 1950's (Chalmers *et al.*,2012c). Years of studies have proved that IR spectroscopy is particularly well suited for the non-destructive identification and classification of binder, pigments and extenders used in automotive paint. Several studies have shown that IR analysis of automotive paint have a high DP of 0.9 to 1.0 (Massonnet and Stoecklein,1999b; Eyring *et al.*,2007). A summary of existing surveys on automotive paints is presented in *Table 2*. The year of publications, the total number of samples, the sampling techniques used, and their DPs are listed. To be noticed, in some population studies, IR spectroscopy was only used to distinguish samples that could not be differentiated by microscopic examination and can significantly reduce the undifferentiated pairs, in other words, add the total discriminating power. These population studies will be fully discussed in the following chapter (see chapter 3.8). Only the surveys that provide the DPs of IR spectroscopy are listed here.

Massonnet carried out a systematic examination on grey metallic automotive paint (Massonnet,1996). Each layer of paint samples was measured and characterized. The discriminating powder with regard to each layer as well as the different combination of layers was well presented. In her study, the most distinction layer for grey metallic paint is the primer surfacer, with the DP of 0.98.

Table 2. Summary of the automotive paint studies conducted using IR spectroscopy.

Authors, Year of publication	Country	Total number of samples (N)	color of the samples	Techniques reported	DP (Number of Non differentiated pairs)
Massonnet, 1996	Switzerland	124	Grey metallic	Sampling: FTIR-Microscope + KBr pellet Detector: narrow band MCT Scan:200 Spectra range: 4000-650 cm^{-1} Resolution: 4 cm^{-1}	0.99829 (11) when considering the entire layers
Massonnet and Stoecklein,1999b	Switzerland	59	27 light red 27 dark red 5 red metallic	Sampling: FTIR-Microscope + diamond anvil cell Detector: broad band MCT Spectra range: 4000-450 cm^{-1} Resolution: 4 cm^{-1}	Light red: 0.94587(19) Dark red: 0.95726 (15) Metallic: 1(0)
Ryland *et al.*, 2001	US	9	Nonmetallic black	See details in the paper	1(0)
Eyring *et al.*,2007	Canada	104	34 red 70 white	Sampling: micro-ATR-FTIR Scan: 512 Resolution: 4 cm^{-1}	Red: 0.99287(4) White: 0.99857(3)
Lambert, 2017	Switzerland	54	Red	Sampling: FTIR-Microscope + diamond anvil cell Detector: MCT Scan: 32 Spectra range: 3600-650 cm^{-1} Resolution: 4 cm^{-1}	0.91964(115)
Kruglak *et al.*,2019	US	26	Red	Sampling: FTIR-Microscope + Diamond anvil cell Scan: 128 Spectra range: 4000-400 cm^{-1} Resolution: 4 cm^{-1}	1(0)

When characterizing the chemical composition of automobile paint, the classification of binder type is always the most vital step. *Table 3* provides a summary of common binder/resin types used in automobile paints and their identifying peaks (Caddy,2001; Buzzini and Stoecklein,2005). A flow chart is created by Ryland to assist binder classification as shown in *Figure 11* (Ryland and Suzuki,2011). The binders used in topcoats and undercoats may be different (Rodgers *et al.*,1976a; Rodgers *et al.*,1976b). Massonnet demonstrated in her thesis after analyzing each layer of grey metallic automotive paint that acrylic resins (often modified by melamine and/or styrene) is the most common type used in OEM clear coats, whereas alkyd resins are mostly found in metallic color coat and primer surfacer (Massonnet,1996). As for primer, the majority resins detected are epoxies based on bisphenol A. Polyurethane as well as nitrocellulose are mostly used in repainted samples. These findings were confirmed by several studied from which the authors conclude acrylic-melamine and polyurethane resins are most likely to be detected in clear coats, whereas epoxies, alkyds and nitrocellulose are mostly found in primers (Maric *et al.*,2012; Bender,2013; Lavine *et al.*,2014b; Houck and Siegel,2015).

Table 3. Identifying peaks of common binder/resin used in automobile paints (MacDougall et al.,2001; Buzzini and Stoecklein,2005).

Binder/Resin	Code	Identifying IR absorption bands（cm−1）							
Acrylic	ACR	1450	1380	1250-1150		1070	840	750	705
Acrylic-melamine	ACR MEL	1550	1480	1370	(1270/1240)	1170	1090	815	
Acrylic-alkyd	ACR ALK	1260	1180	1130	1070				
Acrylic-urethane	ACR URE	1530	1240	1170	1070				
Orthophthalic alkyd	ALK OPH	1450	1380	1270	1130	1070	740	700	
Isophthalic alkyd	ALK IPH	1475	1373	1305	1237	1135	1074	730	
Terephthalic alkyd	ALK TER	1270	1250	1120	1105	1020	815	730	
Alkyd-melamine	ALK MEL	1550	1270	1120	1070	740	700		
Polyester-melamine	POL MEL	1550	1330	1240	815	750	730	705	
Alkyd-urea	ALK U	1650	1540	1270	1120	770	740	705	
benzonguanamine	BZG	1590	1540	825	789	710			
Epoxy	EPY	1610	1510	1240	1180	830			
Melamine	MEL	1550	815						
Nitrocellulose	NCL	1650	1280	840	750				
Polybutadiene	PBD	970	915						
Polyurethane	PUR	1690	1530	1470	1250	1150	770		
epoxy modified		1730	1510						
water based		1690	770						
Styrene	STY	3100-3000	1490	1450	760	700			
Urea	U	1655	1540	1270-1250					

Both organic and inorganic pigments as well as extenders have also been fully explored by FTIR spectroscopy (Harkins *et al.*,1959; Rodgers *et al.*,1976a; Suzuki,1996b; Suzuki and Marshall,1997; Suzuki and Marshall,1998; Suzuki,1999a; Massonnet and Stoecklein,1999b; Suzuki,1999b; Spathis *et al.*,2003; Suzuki and McDermot,2006; Vahur *et al.*,2010; Suzuki,2014a; Suzuki,2014b). *Table 4* presents the IR characteristic absorption bands of common pigments and extenders used in automobile paint (MacDougall *et al.*,2001; Buzzini and Stoecklein,2005; Ryland and Suzuki,2011).

It has been proven that the OEM paint chips can be sourced to a specific make and model of automotive through the classification and comparison of binder types and pigments using FTIR spectroscopy (Rodgers *et al.*,1976c; Audette and Percy,1979; Audette and Percey,1982; Suzuki,1996a; Wright,2010). Maric *et al* demonstrated in a study where 130 clear coats were analyzed using ATR-FTIR that one can correlate the binder and resin type detected from the clear coat to the vehicle origin (Maric *et al.*,2012). Lavine *et al* conducted a study where IR spectra of 1314 cleat coat paint samples in the year range of 2000-2006 from the PDQ database were used to develop a library search filter that can be used to determine the assembly plant and model of an automobile from a clear coat paint (Lavine *et al.*,2015). The color, layer sequence, and chemical composition of the undercoats can be compared to identify the production year and assembly plants (Audette and Percey,1982). However, it is more difficult to differentiate OEM topcoats due to their similar chemistry, especially when only a single topcoat layer exists (Cassista and Sandercock,1994). An attempt was also made

to differentiate paint samples having the same color code but originating from different paint suppliers (Cassista and Sandercock,1994; Stoecklein and Palenik,1998; Eyring *et al.*,2007). Results from Cassista and Sandercork showed that samples with the same binder type could barely be differentiated by FTIR and that further differentiation could be achieved by Py-GC analysis. Stoecklein and Palenik have presented in their study that only very small differences were determinable by FTIR among those samples. Eyring *et al.* concluded that paint samples with the same color code could be differentiated by the comparison of clear coats and primer.
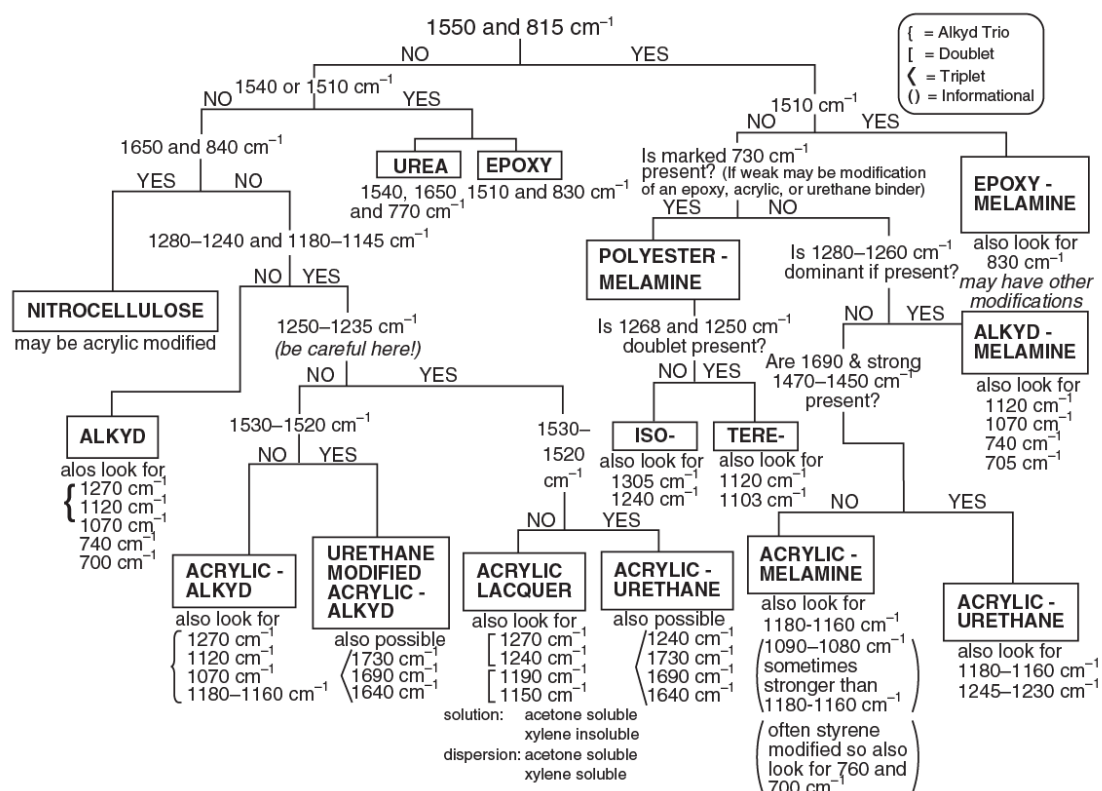
Figure 11. Automotive paint binder classification flow chart based on IR absorption(Ryland and Suzuki,2011).

Comparison and identification of automotive paint may sometimes be problematic when weathering induced changes are involved. Weathering may embrittle coatings, causing gradual loss in gloss (Nichols *et al.*,1999). The mechanism and the performance of weathering of an automotive coating system, has been well investigated from an industrial perspective (Bauer,1997; Nichols *et al.*,1999; Bauer,2000; Perrin *et al.*,2001; Tahmassebi *et al.*,2005; Shi and Croll,2010; Nichols *et al.*,2013; Makki *et al.*,2015; Razin *et al.*,2015). In the field of forensic science, the degradation of binders may cause small decreases or increases in the intensity of absorptions in some regions of the IR spectrum, due to the destruction and generation of various chemical groups during weathering (Hodson and Lander,1987; Perrin *et al.*,2001; Makki *et al.*,2015; Van Der Pal *et al.*,2016; Kumano *et al.*,2019).

Table 4. Identifying peaks of common pigments and extenders used in automobile paints (MacDougall et al.,2001; Buzzini and Stoecklein,2005)

Pigment/extender	Identifying IR absorption peaks （cm⁻¹）							
Calcium carbonate								
aragonite	1445	870	857	712	317			
calcite	1445	870	712	317				
Chromate								
Barium chromate	935	896	860					
Potassium zinc chromate	950	880	805					
Strontium chromate	911	887	875	845				
Chromium oxide	680	634	582	446	417	400		
Iron oxide								
red	560– 530	480– 440	350– 310					
yellow	899	797	606	405	278			
Silicon dioxide								
cristobalite	1090	795	621	485	387	300		
diatomaceous silica	1100	800	480					
quartz	1081	798	779	512	460	397	373	
Titanium dioxide								
rutile	600	410	340					
anatase	600	340						
Zinc phosphate	1120	1080	1020	950	630			
Zinc oxide	1096	888	520	501	401			
Silicate								
Magnesium(talc)	1030	1015	670	465	450	420	390	345
Aluminum(Kaolinite)	1035	1005	940	910	540	470	430	350
Mica	1065	1032	936	834	756	699	535	478	411
Barium sulfate	1175	1080	980	640	610			
Lead carbonate	1412	1047	848	695	683	404		
Lead sulfate	1410	1172	1078	969	687	632	600	428	363
Cobalt aluminate	1102	1035	1012	905	735	652	558	508	239

3.6.   Raman spectroscopy

Raman spectroscopy is another significant vibration spectroscopy which is applied to the study of molecular structure by analyzing the scattering spectra generated from the interaction between a sample and a monochromatic radiation. In the field of forensic analysis, Raman spectrometry is used from the 1990s and is described as the vibrational spectrometry complement of infrared spectrometry (Larkin,2011; Chalmers *et al.*,2012c; Muehlethaler *et al.*,2013; Kirkbride,2015). Since automotive paint usually has a complex mixture of compounds and functional groups, both infrared and Raman spectrometry can provide significant information from different aspects. Compared to IR spectroscopy, Raman is more used for the identification of organic and inorganic pigments as well as extenders. What's more, the pigments in automobile paint present abundant information in the low region of mid-IR spectra, which is beyond the MCT detector range (usually cutoff at 600 cm^{-1}). Therefore, Raman spectrometry is the complementarily effective option for exploring this valuable region for the examination of pigments(Kirkbride,2015). For example, titanium dioxide is a widely used pigment in both undercoats and topcoats of automobile paint. It exists mainly in two forms, anatase and rutile, which show identical peaks at 600 cm^{-1} and 340 cm^{-1} in infrared spectra. They can however be easily discriminated using Raman spectroscopy as rutile presents two large peaks at 448 cm^{-1} and 610 cm^{-1}, while anatase only shows a single high peak at 143 cm^{-1}.

3.6.1. Raman spectroscopy principles

Several comprehensive reviews are available for all aspects of Raman spectroscopy (McCreery,2000; Lewis and Edwards,2001; Koçak,2011; Larkin,2011; Chalmers *et al.*,2012a), so only a brief summary will be provided here.

Raman spectroscopy is based on the Raman effect discovered by Indian scientist Chandrasekhar Raman. Unlike IR absorption spectra, Raman spectra result from the inelastic scattering of monochromatic radiation when it strikes a sample, as illustrated in *Figure 12*. Most of the scattering is elastic, which means the frequency of this part is unchanged, referred to as Rayleigh scattering. However, a small part of photon excites the molecule and impulses it into a virtual energy state. This makes the molecule to be unable to return to its original energy level, consequently, causes energy differences between initial radiation and emitted one, which is mentioned as inelastic scattering or Raman scattering. The final energy state of the molecule is either higher or lower than the initial energy state, which causes the frequency of photon decreasing (Stokes) or increasing (anti-Stokes), respectively (see *Figure 13*). The changes of frequency are then defined as Raman shifts. A Raman spectrum is thus displayed on the x-axis as a Raman shift, which is in the unit of cm^{-1}, the y-axis as the intensity of scattered light.
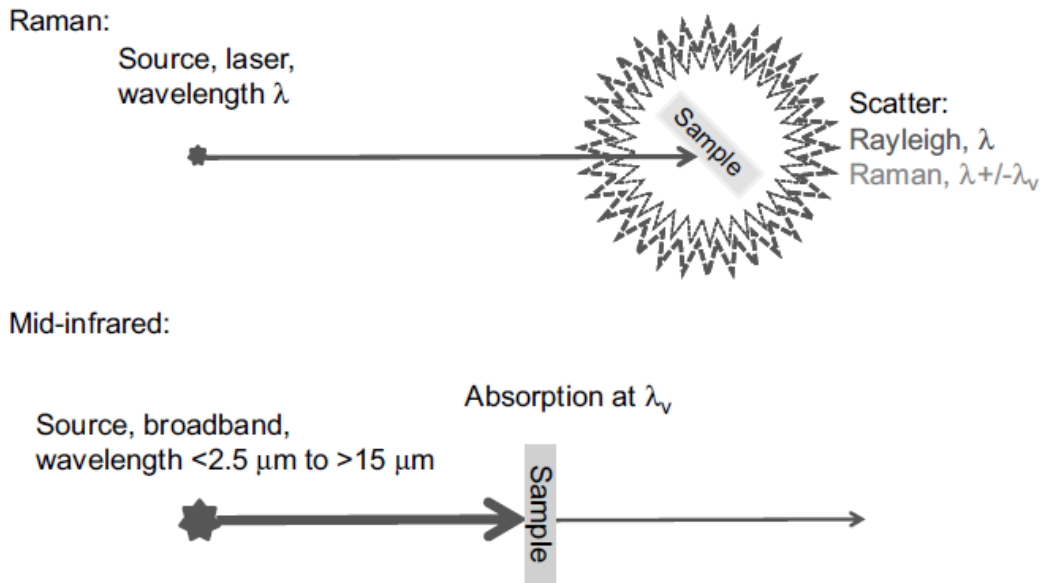
Figure 12. Simplified scheme of Raman scattering and IR absorption (Chalmers et al.,2012b).
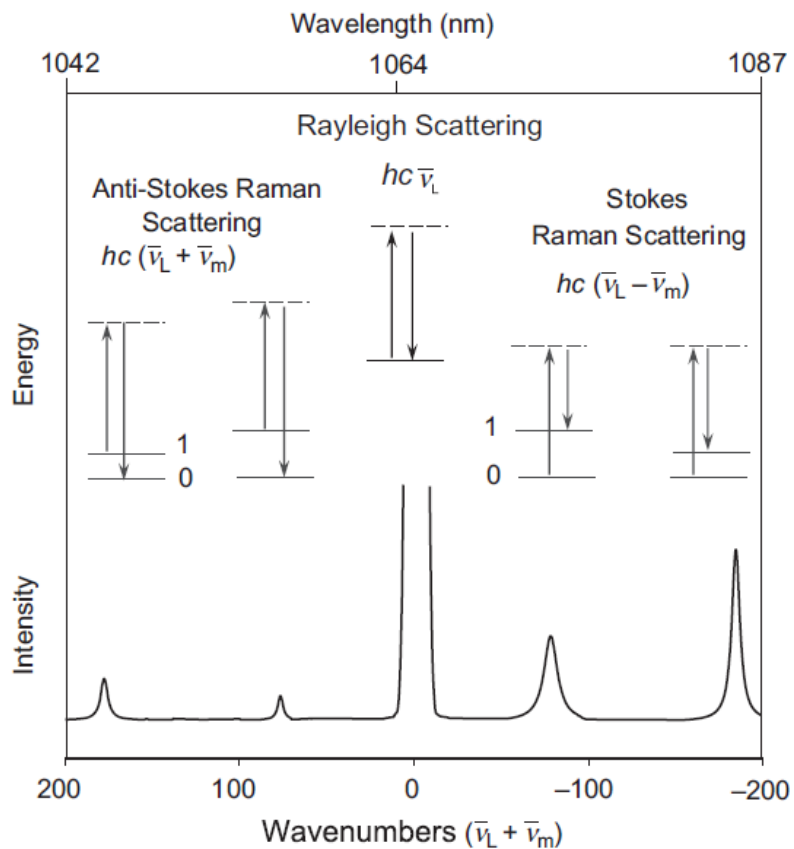
Figure 13. Illustration of Raman scattering (Larkin,2011)

3.6.1.1.   Raman spectroscopy instrumentation

The Raman spectrometers have two types, the dispersive(spectrograph/CCD) and nondispersive (FT-Raman) instruments (McCreery,2000). Only the dispersive Raman spectrometer will be discussed below since It is the most commonly used type and will also be used for this study.

The conventional dispersive Raman spectrometer consists of laser excitation sources, collection optics, dispersive spectrometer, and detectors (see *Figure 14*). The Argon laser at 488 cm^{-1} and 514 cm^{-1}, the He-Ne laser at about 633 cm^{-1} and near-infrared diode laser at about 785 cm^{-1} is the more commonly used laser source. The dispersive spectrometer, which is normally a single spectrograph, is the foundation of a Raman spectrometer. Since the Raman scattered radiation is often very weak and overwhelmingly block by the strong Rayleigh scattered light, the holographic notch or edge filters are introduced in the spectrograph to suppress these stray lights and Rayleigh lines (Chalmers *et al.*,2012a). The filtered radiation then passes through the entrance slit of the spectrograph and dispersed into monochromatic components by the diffraction gratings. The radiation of suitable wavelength is focused onto the exit slit of the spectrograph and finally reaches at the detector (Larkin,2011). Today, most Raman spectrographs use a multi-channel charge-coupled device (CCD) detector to measure simultaneously the intensities of the Raman-shifted wavelengths (Chalmers *et al.*,2012a).
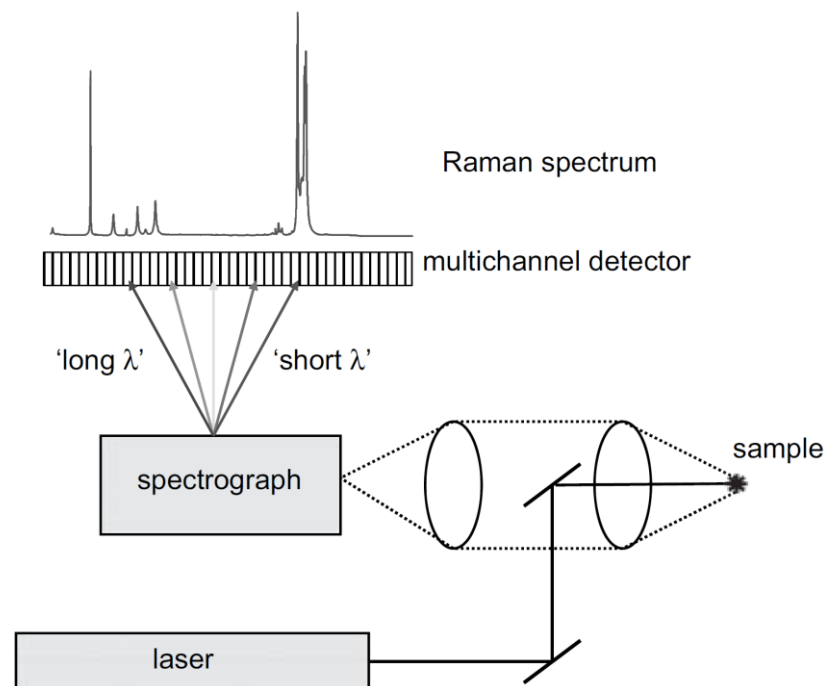
Figure 14. Schematic of a dispersive Raman spectroscopy with a CCD detector (Chalmers et al.,2012a)

3.6.1.2. Raman sampling techniques

Sampling techniques for Raman can be divided into three general categories, namely the conventional sampling, the remote sampling and the Raman microscopy(McCreery,2000). Only Raman microscopy will be discussed since It is the technique that used in this study. The introduction and explanation of the rest sampling techniques can be found in the above-mentioned references.

Raman microscopy has been widely used for analysis of microsamples such as automotive paints. *Figure 15* shows a confocal schematic for a Raman microscope system. The Raman microscopy offers the high lateral spatial resolution, which can be up to 1 μm. This sampling technique requires a minimum of sample handling and preparation (Larkin,2011). Samples can be easily mounted on an x–y–z translation motorized microscope stage and examined visually using a wide range of conventional optical microscopy illuminations (Chalmers *et al.*,2012a). The measurement of the sample can be acquired from a single point on the sample or several points, which is referred to as point-to point mapping. It is also possible to measure the sample in a line or in a selected sample area where spatially resolved spectra are acquired at many points along the line or over the entire area. These methods are categorized broadly as Raman imaging. Based on spectroscopic information such as molecular-specific concentrations, a sample image is usually displayed in either a grey-scale or false-color scale representation (McCreery,2000; Chalmers *et al.*,2012a).
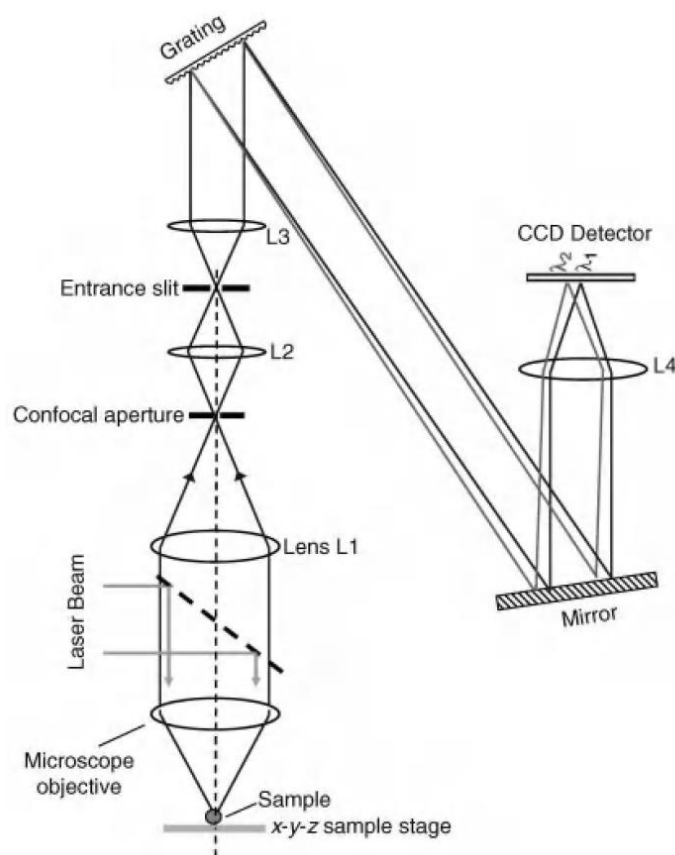
Figure 15. A simplified schematic of a confocal Raman microscope (Chalmers et al.,2012a).

3.6.2. Application of Raman spectroscopy in forensic analysis of automotive paint

The applications of Raman spectroscopy were traditionally in the field of art and archeology to identify pigments used and detect forgeries due to its advantages of non-destructiveness, in-situ possibility and minimal sample preparations (Chaplin *et al.*,2002; Brown and Clark,2004; Edwards *et al.*,2004; Kendix *et al.*,2008; Scherrer *et al.*,2009; Castanys *et al.*,2011; Doménech *et al.*,2011; Fremout and Saverwyns,2012; Otero *et al.*,2014; Carlesi *et al.*,2016). For forensic automotive paint analysis, it has been demonstrated that Raman spectroscopy is rather effective for the comparison and identification of paint binders, pigments and extenders (Kuptsov,1994; Massonnet and Stoecklein,1999; Suzuki and Carrabba,2001). The possible contribution of Raman spectroscopy for the analysis of automotive paint samples as well as the performance when identifying different composition(binder, pigments, extender) in all paint layers were evaluated by De Gelder and coauthors (De Gelder *et al.*,2005). The results showed that Raman spectroscopy can better distinguish organic pigments as well as extenders rather than binder and the basecoat could provide the best spectra to differentiate paint samples. The authors also suggest that Raman spectroscopy should be applied in combination with IR spectroscopy in order to provide better discrimination. This statement is confirmed by several studies in which the authors have used both IR and Raman spectroscopy to differentiate paint samples (Buzzini *et al.*,2006; Zięba-Palus and Borusiewicz,2006).

However, Raman spectroscopy has not become extensively used until the last decade. Due to modern developments, Raman has evolved into a fast vibrational technique and often used in combination with FTIR for the identification of pigments and extenders in automobile paint (Zięba-Palus *et al.*,2011; Zięba-Palus and Trzcińska,2013; Zięba-Palus and Michalska,2014; Suzuki,2014a; Chen *et al.*,2015; Lv *et al.*,2016). Not only that, Maric *et al*. have demonstrated that Raman spectroscopy is potentially more discriminating than IR spectroscopy when characterizing the population of automotive clear coats (Maric *et al.*,2016). This observation is further confirmed in the research conducted by Affadu-Danful *et al*., wherein the authors highlight that combining Raman spectroscopy with pattern recognition methods surpasses FT-IR in identifying and distinguishing automotive clearcoats. Moreover, this approach can also determine a vehicle's make and model, showcasing its potential for advanced automotive analysis (Affadu-Danful *et al.*,2023).

A summary of existing surveys on the performance of Raman spectroscopy for automotive paints comparison is presented in *Table 5*. The year of publications, the total number of samples, the laser used, and their DPs are listed. The DPs provided from these studies have further proved the capabilities of Raman spectroscopy in forensic automotive paint examination.

The measurement variability and the spectral quality have a great influence on the accurate comparison of paint samples as well as library search. Several studies have been performed to evaluate the impact of various factors on the response of measurement variability (Lambert *et al.*,2014; Ferreira *et al.*,2017). Lambert *et al.* have demonstrated that sample preparation was found to affect considerably the spectral variability, so the authors

recommended using polished cross sections for Raman measurements. In the study of Ferreira *et al.*, objective lens, accumulation number, laser mode and wavelength, sample substrate and preparation have demonstrated the greatest influence on the spectral quality, the authors suggested that the 50x objective lens, around 6 accumulation numbers, 'edge' laser mode, and laser power (maximum intensity without burning the sample) allowed a significant improvement of the collected spectra (Ferreira *et al.*,2017). The authors also stated that the 785 nm laser (NIR diode laser) is the best excitation laser source providing information on pigment content. This statement was confirmed by several other studies (Suzuki and Carrabba,2001; Bell *et al.*,2005a; Bell *et al.*,2005b; Bell *et al.*,2005c; Zięba-Palus and Michalska,2014).

Table 5. Summary of the automotive paint studies conducted using Raman.

Authors, Year of publication	Total number of samples (N)	Color of the samples	Laser used	DP (Number of Non differentiated pairs)
Massonnet and Stoecklein,1999c	59	27 light red 27 dark red 5 red metallic	1064 nm	Light red: 0.89459(37) Dark red: 0.96866 (11) Metallic: 0.9(1)
Skenderovska *et al.*, 2008	10	Various color	685nm	1
Zięba-Palus *et al.*, 2011	13	Green	514nm 633nm 785nm	Not provided
Zięba-Palus and Michalska,2014	66	26 blue solid 40 blue metallic	514nm 633nm 785nm	Blue solid:0.97231 (9) Blue metallic: 0.98846(9)
Michalska *et al.*, 2015	55	25 blue solid 30 blue metallic	785nm	Blue solid:0.82333 (53) Blue metallic: 0.91494(37)
Lambert, 2017	54	Red	785nm 488nm	785nm: 0.73026(386) 488: 0.75681(348)

3.7. Py-GC/MS

Py-GC/MS is an analytical method in which the sample is heated to decomposition (pyrolysis) to produce small molecular fragments that are separated by gas chromatography (GC) and detected using mass spectrometry (MS). Although it is a destructive technique, it is powerful in identifying and comparing polymers as well as some additives. This technique has been widely used for the characterization and comparison of forensic evidence since the early 1970s (Challinor,2001). It is considered as an additional technique for confirming or extending the information obtained from vibrational spectroscopy (Wright *et al.*,2020).

3.7.1. Py-GC/MS principles

A conventional Py-GC/MS often consists of the pyrolysis unit coupled with a gas chromatograph and a mass spectrometer (see *Figure 16*). Pyrolysis is the thermal fragmentation of a substance in an inert atmosphere. The pyrolysis products are detected and identified by GC/MS.

The most frequently used pyrolyzers are the pulsed filament type, the Curie-point type, and the furnace type. The filaments pyrolyzer consists of a heated platinum coil that can be continuously heated from 200 °C to 1400 °C, and a quartz tube which is placed in the coil and used to hold the sample. The Curie-point system uses high frequency oscillating currents in coils to inductively heat the metal or alloy wire to its Curie point. The furnace type accomplishes the fragmentation process by introducing the sample into an oven unit. When choosing a pyrolysis system, true final pyrolysis temperatures, rapid temperature-rise-time, low dead volume and ease of sample lading should be all taken into consideration (Challinor,2001).

Once the sample is decomposed into monomer units during the fragmentation process, the small molecular fragments are then introduced into a gas chromatography equipped with silica capillary columns and temperature programming. They are usually detected and identified based on their retention times by a flame ionization detector (FID), the commonly used detection system for the gas chromatograph. Nowadays, a mass spectrometer is the most favored detection system that can achieve the unequivocal identification of some of the pyrolysis products by gas chromatography and the interpretation of the polymer composition of resins in paint.
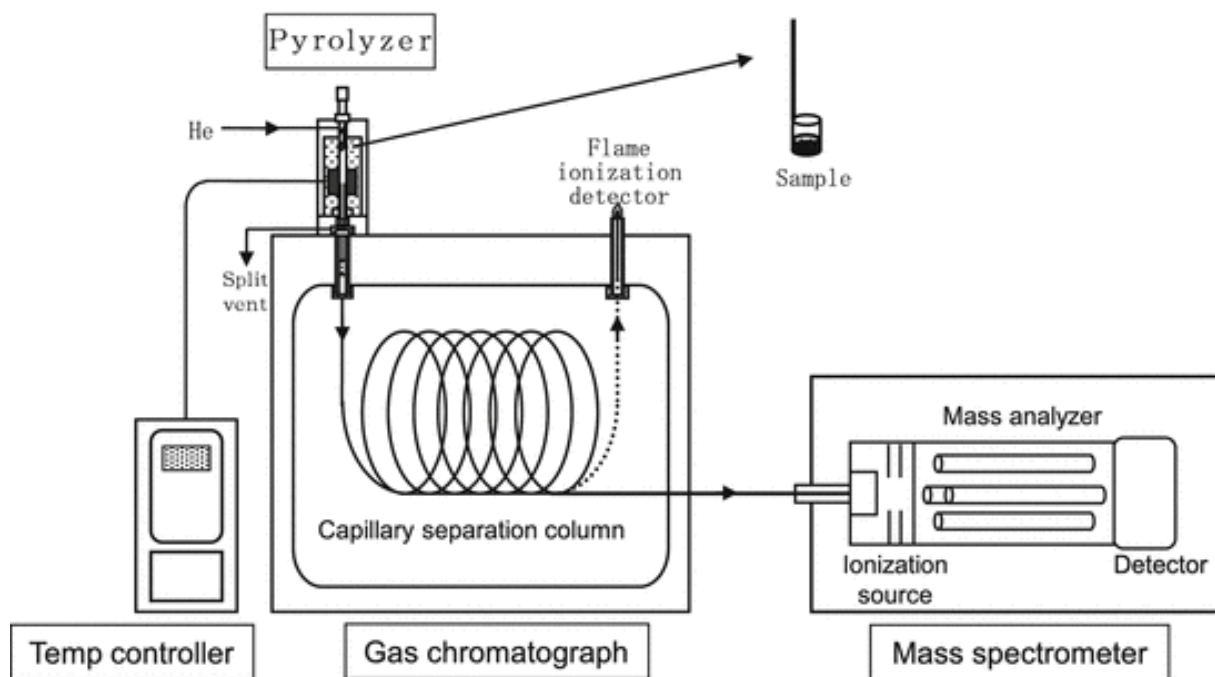
Figure 16. A typical Py-GC/MS system (Tsuge and Ohtani,2014).

3.7.2. Application of Py-GC/MS in forensic analysis of automobile paint

As Py-GC/MS is a widely useful technique in the identification of polymeric materials, a lot of excellent references have been published to provide the Py-GC/MS information about natural and synthetic resins, additives, organic paint binders and pigments. Bonaduce and Andreotti have provided a good reference on the topic of natural organic materials such as proteinaceous materials, polysaccharide gums and drying oils (Bonaduce and Andreotti,2009). Scalarone and Chiantore have summarized the Py-GC/MS characterization information of natural resins such as Terpenoid resins and synthetic polymers such as acrylic, alkyd (Scalarone and Chiantore,2009). Russell *et al.* have collected more than 70 synthetic organic pigments and reported the identification results, possibility and limitations of Py-GC/MS for the identification of pigments in modern works of art(Russell *et al.*,2011). Shin *et al* have compiled the comprehensive pyrolysis data for representative synthetic polymer and the mass spectra of major pyrolyzates, the retention index data on each pyrogram in their data book (Shin *et al.*,2011). Ghelardi *et al.* have analyzed 76 synthetic pigments with Py-GC/MS, 45 of them have never been previously reported (Ghelardi *et al.*,2015).

As for automobile paint, Py-GC has been proved to be a high discriminating technique in the classification and comparison of the composition of the binder used in automobile paint.

33

Stewart showed the ability of Py-GC to distinguish the binder types used by Chrysler, American Motors and Ford Motor automobile manufacturer in 1973 (Stewart,1974). Wheals and Noble also reported that by comparing the reproducible pyrograms obtained from automotive paints, it was able to discriminate paint from vehicles of British manufacturer (British Leyland) and American companies (Ford and Chrysler) due to the fact that the major part of the British production was coated with thermosetting alkyds whereas Ford and Chrysler used thermosetting acrylics (Wheals and Noble,1974). Fukuda analyzed 78 Japanese automobile topcoats (31 white, 31 silver metallic and 16 clearcoat) and discriminated most of the paint by their pyrolysis products (Fukuda,1985). The author also reported that the technique cannot detect inorganic components and should be used together with IR and/or SEM-EDX for the full characterization of paint samples.

Nowadays, Py-GC/MS is more available and widely used in automobile paint analysis since it could provide more reliable results. McMinn *et al.* tested the performance of Py-GC/MS on 39 paints and built a library based on the obtained pyrograms (McMinn *et al.*,1985). The authors presented an encouraging result that it was possible to establish a searchable database based on the composite mass spectra without worrying too much about the standardization of GC conditions. Wampler et al reported that the changes in automotive paint formulation can be well recorded by Py-GC/MS since the degree of crosslinking must be increased in the pyrogram of a high solids content paint, thus differing from that in a traditional high solvent-based paint (Wampler *et al.*,1997). Kochanowski and Morgan presented a preliminary investigation based on Py-GC/MS analysis of 100 automobile paint samples of five different colors(20 each of white, red, black, blue, silver) (Kochanowski and Morgan,2000). The authors firstly conducted designed experiments on two white paint samples to find pyrolysis conditions to maximize the discrimination of samples and set the experiment conditions (250°C initial temperature, 15°C initial ramp rate, 650°C final temperature, and 15s final time). Then, they used multivariate statistical methods for the comparison of obtained pyrograms and good separation of most of the paint groups was shown. Yang *et al.* characterized 54 vehicle topcoats pyrograms using multivariate chemometric analysis and evaluated the capabilities of using averaged mass spectra obtained from pyrograms to assess the group distributions (Yang *et al.*,2015). The study proved that HCA and PCA allow the extraction of chemical information from experimental results for statistical treatments.

In contemporary applications, Py-GC/MS is often applied after FTIR and/or Raman spectroscopy in order to obtain further discrimination. Several studies have demonstrated that paint sample which are undifferentiated by FTIR spectroscopy can be distinguished by Py-GC/MS. Cassista and Sandercock reported that some acrylic lacquers and acrylic enamels which revealed no differences by IR spectroscopy could be easily differentiated using Py-GC (Cassista and Sandercock,1994). MacDougall *et al.* also showed examples in their book chapter that two white acrylic melamine original automotive paints which have very similar IR spectra show different pyrograms (MacDougall *et al.*,2001). Burns and Doolan conducted a pilot project to compare Py-GC/MS results for 75 paint samples (including basecoats ,'solid paint' paints and clear coats) with known FTIR groupings and the result showed that all examined samples could be distinguished including those in the sample FTIR groups (Burns

and Doolan,2005a). The authors further demonstrated the discriminating power of Py–GC/MS by successfully dividing 300 clear coats that were indistinguishable by FTIR into several subgroups (Burns and Doolan,2005b). Plage *et al*. evaluated the differentiation of 25 automotive clear coats which were assigned to 8 different FTIR groupings using Py-GC/MS (Plage *et al.*,2008). Their results showed that only three pairs remained undifferentiated after Py-GC/MS analysis, which provided a DP of 0.99. Zięba-Palus *et al*. applied Py-GC/MS to differentiate 36 styrene acrylic urethane clearcoats that were indistinguishable on the basis of their infrared spectra and elemental composition and used likelihood ratio model to deliver information about the evidential value of the results of Py-GC/MS (Zięba-Palus *et al.*,2008). Similarly, the authors conducted another research to identify the polymer binder in 60 automotive paint samples using both IR and Py-GC/MS and concluded that Py-GC/MS can provide additional information helpful in further characterization and discrimination of paint having similar IR spectra (Zięba-Palus *et al.*,2008a). Moreover, this same group of scientists performed a study to compare the polymer binder of 150 automobile acrylic clearcoat samples using Py-GC/MS and demonstrated that the application of Py-GC/MS can lead either to the complete differentiation or to the split of subclasses (Zięba-Palus *et al.*,2008b). Milczarek *et al*. put their focus on the primer layer of automotive paint and successfully achieved good discrimination between 10 epoxy primer layers that have similar IR spectra using Py-GC/MS (Milczarek *et al.*,2009). The authors also suggested that the epoxy paints should better be analyzed after derivatization process since it increases the number and amount of the pyrolysis products.

One of the main issues concerned in Py-GC/MS analysis of automobile paint is its reproducibility, a standardized protocol should therefore be established. A summary of Pyrolysis and GC conditions founded in several representative studies is listed in *Table 6*. The variables in the pyrolysis process include temperature-rise-time, pyrolysis temperature, sample mass, carrier gas type, split ratio and flow rate. From the summary, the pyrolysis and GC conditions vary a lot. Generally, a minimum of 10-30 μg of sample are required for Py-GC/MS (Muehlethaler *et al.*,2013; Wright *et al.*,2020). Helium is the most commonly used carrier gas. The ideal size of the column for automobile paint analysis is a capillary column with 30mx 0.25mm ID x0.25 μm film thickness. As for other factors, they need to be standardized according to the involved instrument and sample condition.

Table 6. A summary of pyrolysis and GC conditions used for automobile paint analysis.

Author/year	Sample	Sample mass	Py type	Ramp	Temperature	time	Interface temp	Column	Injector temp	Split ratio	Carrier gas	Flow rate	Temperature program
					Pyrolysis			**GC**					
McMinn et al.,1985	Paint panels	30 µg	CDS Pyroprobe/ quartz tube	off	750 °C	5s	175 °C	Fused silica capillary column 30mx 0.25mm	165 °C	20/1	Helium	0.76 mL/r	Set at 40°C for 3 min, ramped to 250°C at 25°C/min, and held at 250°C for 2 min.
Cassista and Sandercock,1994	Paint panels	20-30 µg	CDS Pyroprobe/ quartz tube	off	980 °C	10s	NA	Fused silica capillary column 30mx 0.25mmID x0.25 µm film thickness	200°C	39/1	Hydrogen	2 mL/min	Set at 0°C for 1 min, ramped to 300°C at 12°C/min, and held at 300°C for 6 min.
Kochanowski and Morgan,2000	Topcoats	less than 100 µg	CDS Pyroprobe/ quartz tube	15 °C/m	650 °C	15s	250 °C	5% phenyl–95% methyl polysiloxane-coated column 30 m × 0.25-mm i.d., 0.25-µm film thickness	250 °C	60/1	Helium	1 mL/min	Set at 50°C for 1min, ramped to 300 °C at 10 °C/min, and held at 300 °C for 10 min
Burns and Doolan,2005	Topcoats	20-70 µg	CDS Pyroprobe/ quartz tube	NA	750 °C	2s	250 °C	30m (i.d. 0.25 mm, film thickness 0.25 µm)	250 °C	20/1	Helium	25 mL/mi	Set at 40°C for 3min, ramped to 280 °C at 10 °C/min, and held at 280 °C for 10 min
Plage et al.,2008	Clear coat	NA	CDS Pyroprobe/ quartz tube	NA	550 °C	20s	250 °C	35% phenyl–65%-dimethyl polysiloxane capillary column 30 m, 0.25 mm, 0.25 µm film thickness	NA	NA	Helium	1.5 mL/m	Set at 40°C for 3 min, ramped to 300°C at 20°C/min.
Zięba-Palus et al.,2008a	Clearcoat	NA	CDS Pyroprobe/ quartz tube	NA	400 °C/ 75	NA	NA	35% phenyl–65%-dimethyl polysiloxane capillary column 30 m, 0.25 mm, 0.25 µm film thickness	NA	NA	Helium	NA	Set at 40°C for 2min, ramped to 300 °C at 10 °C/min, and held at 300 °C for 2 min, ramped to 320 °C at 30 °C/min, and held at 320 °C for 3 min,
Zieba-Palus et al.,2008	Clear coat	50-100 µg	CDS Pyroprobe/ quartz tube	NA	750 °C	20S	NA	35% phenyl–65%-dimethyl polysiloxane capillary column 30 m, 0.25 mm, 0.25 µm film thickness	NA	NA	Helium	NA	Set at 40°C for 2min, ramped to 300 °C at 10 °C/min, and held at 300 °C for 2 min, ramped to 320 °C at 30 °C/min, and held at 320 °C for 3 min,
Zieba-Palus et al.,2008b	Clear coat	50-100 µg	CDS Pyroprobe/ quartz tube	NA	750 °C	10s	NA	35% phenyl–65%-dimethyl polysiloxane capillary column 30 m, 0.25 mm, 0.25 µm film thickness	NA	NA	Helium	NA	Set at 40°C for 2.5min, ramped to 320 °C at 10.5 °C/min, and held at 320 °C for 5 min
Milczarek et al.,2009	Primer	NA	CDS Pyroprobe/ quartz tube	NA	750 °C	NA	NA	35% phenyl–65%-dimethyl polysiloxane capillary column 30 m, 0.25 mm, 0.25 µm film thickness	NA	NA	Helium	NA	Set at 40°C for 2.5min, ramped to 320 °C at 10.5 °C/min, and held at 320 °C for 5 min
Yang et al.,2015	Topcoats	50 µg	Funace type		550°C	NA	NA	An Ultra Alloy-1 metal coated with dimethyl polysiloxane capillary column (30 m, 0.25 mm id, 0.25 mm filmthickness)	300°C	10/1	Helium	1 mL/min	Set at 40°C for 2min, ramped to 130 °C at 12 °C/min, and held at 130 °C for 1 min, ramped to 300 °C at 12 °C/min, and held at 300 °C for 8 min,

3.8. Population studies of automotive paint

In the field of forensic science, automotive paint serves as an important type of evidence. The role of forensic scientist is not only to analyze the paint via different types of analytical instruments, but also to interpret the obtained results and provide the evidential value of paint evidence to the court. Therefore, forensic scientist should be aware of every aspect of paint evidence, including but not limited to the paint composition, the paint layer structure, the paint population information such as the frequency or distribution of automotive manufacturers and colors, the discriminating capabilities of every single technique used and their limitations. More importantly, forensic scientists should be able to evaluate the rarity of physical and chemical features of the analyzed paint, i.e., the evidential value of paint evidence using this information. The population study is the type of study in which a large amount of automotive paint samples is randomly selected and compose a set of reference samples that can be representative of a population of interest. The variations of the different characteristics of the samples are observed or analyzed by analytical techniques so that the frequency information of the commonness of some specific features are obtained. The discrimination capabilities of involved analytical techniques are also verified.

Over the past three decades, several population studies have been conducted in different countries. These studies often involve full examination of microscopical and chemical features of paint layers. A summary of the current existing population studies is presented in *Table 7*. The authors and year of publications, the countries where population studies were conducted, the top three vehicle makes, colors and layer numbers, the technique used, and the total discriminating power are listed in the table.

Table 7. Summary of the automotive paint population studies conducted.

Authors, Year of publication	Country	Total number of samples (N)	Top 3 vehicle makes	Top 3 vehicle colors	Top 3 layer number	Techniques used	DP (Number of Non differentiated pairs)
Gothard,1976	Australia	500	GM Leyland Ford	White Green Blue	3 4 2	Microscopy, chemical tests, IR, Emission spectrometry (ES), Py-GC	0.99998 (2)
Ryland and Kopec,1979	US (Northeastern)	200	GM Ford Chrysler	Brown/gold Green blue	3 2 4	Microscopy, solvent tests IR, ES, SEM-EDX, Py-GC, neutron activation analysis	1.00000(0)
Edmondstone *et al.*,2004	Canada	260	GM Ford Chrysler	Red Blue White	NA	Microscopy, ATR-FTIR	0.99997 (1)
Reynolds *et al.*,2018	US	231	GM Chrysler Ford	Grey/Silver Red/Purple Blue	4 3 5	Microscopy, FTIR, SEM-EDX	0.99992 (2)
Kruglak *et al.*,2019	US (Northeastern)	200	Honda Toyota Nissan	White Silver Grey	4 5 6	Microscopy, Ultraviolet–Visible (UV-VIS) Microspectrophotometry (MSP), FTIR, Raman	1.0000 (0)
Soong *et al.*,2020	Singapore	256	Honda Toyota Hyundai	Black White Grey	4 3 6	Microscopy, FTIR, SEM-EDX	0.99981 (1)

As shown in *Table 7*, the frequency information obtained from the population studies such as make, color and layer number, may have periodical and geographical variations. Forensic scientists should interpret paint evidence based on their specific context. It is therefore important to continuously conduct these population studies and update the dynamic situation of the automotive paint distribution.

It is also shown in *Table 7* that a rather high discriminating power can be achieved with the combination of different analytical methods. **The undifferentiated pairs left in each study are all reported to be vehicles of same make, model and color. Some are even manufactured at the same plant in the same or relevant years.** This result can be explained as automotive paints are mass products. Therefore, to reach the best discrimination of paint, it is recommended to set a standard protocol which includes various analytical techniques for paint examination in laboratories.

3.9.   Color surveys of automotive paint

Automotive paint color is one of the most important features in forensic automotive paint analysis. It is not only the key feature when grouping paint samples in population studies, but also the first considered variable when evaluating the rarity of a paint sample. Although population studies can provide the frequency of color, the assignment of an occurrence frequency to an automotive paint color requires sufficient color distribution data. The need drives the launch of color surveys. These surveys were carried out in the US (Ryland *et al.*,1981), Canada(Buckle *et al.*,1987; Volpé *et al.*,1988; Stone *et al.*,1991), Ireland(McDermott *et al.*,1999), Australia (Jackson *et al.*,2015) and Singapore (Soong *et al.*,2020). Compared to population studies, these color surveys often contain several thousands of samples, which the occurrence of a color is more representative. In the article of Jackson *et al.*, they have made a comparison chart of color surveys that have been conducted in those mentioned countries(Jackson *et al.*,2015). Soong *et al.* have also made a comparison figure of color distribution of these color survey in their recent published article (Soong *et al.*,2020).

From those comparison data, it is noted that blue was the most common color in most of the surveys conducted in Northern America (Canada and US) in 1980's. However, a clear difference of color trend has been noticed since the most common color has become white according to the surveys conducted after 2010 in Australia. Soong *et al.* reported that white is also the most commonly encountered automotive colors in Singapore. This observed color trend corresponds to the distribution of the world's most popular automotive color provided by the industry paint experts such as PPG, BAFS and Axalta. In their regional and global automotive colour popularity/trend reports, white has been reported as worldwidely the most popular color since 2015 (As an example, see *Figure 2* in Chapter 2, page 6).

In Europe, very few color surveys were found. According to the data from EPGT website, among 18486 samples that collected from metal substrates of automotives in the EUCAP

database, grey (24%), blue (20%), red (13%), green (11%), black (8%) and white (7%) are the most common colors.

In Switzerland, the Federal Statistical Office (FSO) has been continuously compiling the data relating to the color of registered vehicles. *Figure 17* illustrates the color distribution of the registered vehicles from 2016 to 2020 according to the data from FSO. Being slightly different from the world trend, grey is the most common color in Switzerland for the last 5 years. Black and white are the second and third most frequently observed colors.
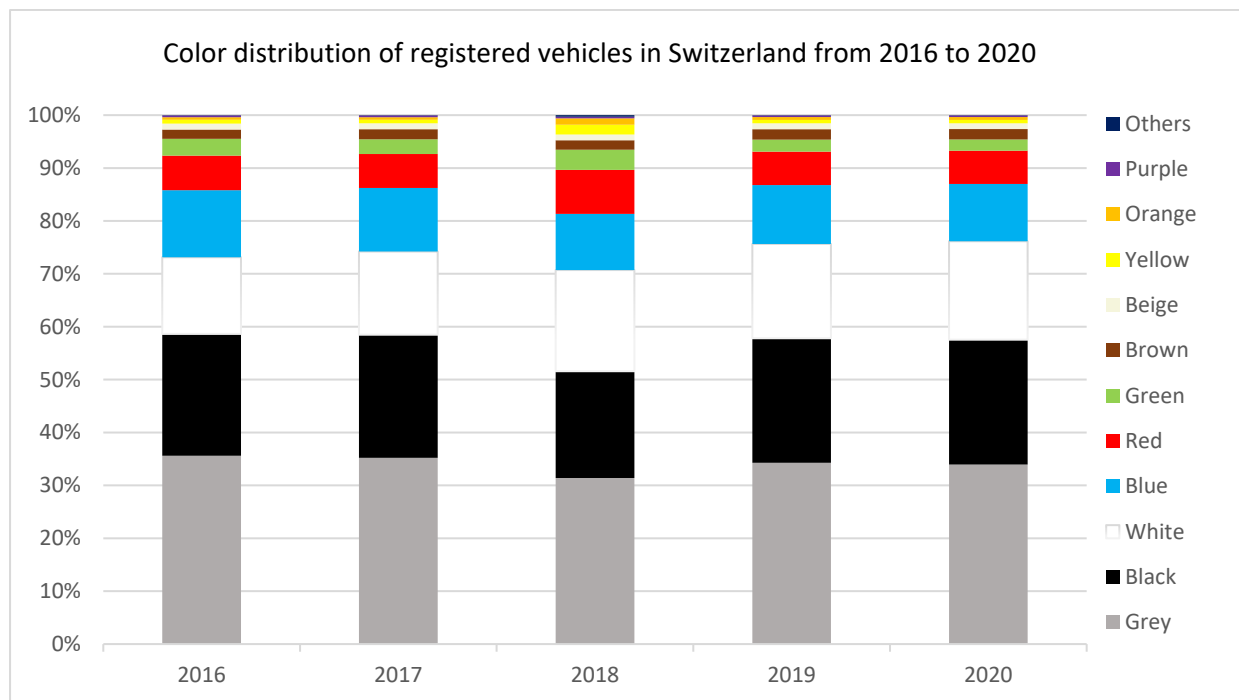
Figure 17. Color distribution of registered vehicles in Switzerland from 2016 to 2020, according to the data provided by the Federal Statistical Office (FSO).

Apart from color frequency information, information on the chemical composition of a certain color of automotive paint is equally important since the rarity of chemical features need to be evaluated as well when interpreting the evidential value. Very few studies that concern only one specific color were published. A summary of these studies is provided in *Table 8*.

Although white is the most common color of automotive paint, little research has been carried out on white automotive paint. White is considered as one of the most difficult colors encountered in forensic paint discrimination since it has little variety of pigment formulation. White pigments are all inorganic pigments. Titanium dioxide (TiO_2) in the form of rutile is the most common white pigment in use (Henson and Jergovich,2001). Its unrivalled opacity and durability make it widely used in paint layers. Most of the white paint studies were carried out in the field of architectural paints. Although the formulation and application of automobile paint and architectural paint is different from each other, they are all composed of resin, pigments and extenders. Worthwhile information about white architectural paint can still be learned and referenced for the forensic analysis of automotive white paint.

Table 8. Summary of studies carried out on automotive paint of a single color.

Color	Authors, Year of publication	Total number of samples (N)	Techniques used	Information provided
Grey	Massonnet,1996	124	Microscopy MSP FTIR	DP of microscopy relating to illuminations DP of MSP DP of FTIR relating to each layer chemical composition detected by FTIR
Red	Massonnet and Stoecklein,1999a, 1999b, 1999c	98 organic pigments 59 red paint samples	Thin Layer Chromatography (TLC) FTIR Raman	DP of single instrument IR and Raman spectra of organic pigments
	Eyring *et al.*,2007	34	ATR-FTIR MSP	Red paint having identical color code can be differentiated by analyzing their clear coat and primer.
	Lambert, 2017	54	Raman	DP of Raman Best laser for red paints
	Kruglak *et al.*,2019	26	Microscopy UV-VIS MSP FTIR Raman	DP of UV-VIS MSP Chemical Composition of each layer
Blue	Zięba-Palus and Michalska,2014	66	Raman	DP of Raman best laser for blue paints
	Michalska *et al.*, 2015	55	Raman	DP of Raman 785 nm laser performance for blue paints
White	Eyring *et al.*,2007	70	ATR-FTIR MSP SEM/EDX	White paint having identical color code can be differentiated by analyzing their clear coat and primer.

Bell *et al.* carried out a study where 39 resin samples used for the manufacture of architectural finishes were analyzed by FTIR and Raman (Bell *et al.*,2005a). They reported that Raman spectroscopy has considerable advantages over the established FT-IR method for the discrimination of resins used for paint manufacture. Furthermore, the authors conducted another study where 51 white architectural paints were analyzed by FTIR and Raman (Bell *et al.*,2005b). They reported that the largest discriminating feature was the type of resin presented in Raman spectra. The authors stressed that rutile was presented in all the samples, no discrimination could be achieved based on that. However, the presence or absence of some inorganic pigment and extenders such as calcium carbonates or dolomite can be the second discriminating feature for white paint analysis. Moreover, by measuring the relative band intensity ratios of some important features after normalizing the spectra to the intensity of the strong rutile band at 610 cm^{-1}, it was possible to provide more discrimination. Stewart *et al.* reported a similar work on the characterization of multilayer samples of white architectural paint (Stewart *et al.*,2012). Their results confirmed that white paint could be differentiated by the overall composition and the relative proportions of some components detected by Raman spectroscopy. Wright *et al.* carried out comparative analyses of 50 single-layer white architectural paints using FTIR, SEM/EDX and Py-GC/MS and reported that the overall discriminating power was 99.35% (Wright *et al.*,2013). With this information, high discrimination of automobile white paint can be expected since paint layer was the additional feature comparing single-layer architectural paint that may lead to more discrimination.

It is noted that all the Raman analysis in the mentioned studies were carried out with a 785 nm diode laser. This is due to the fact that the use of other lasers may produce unacceptable level of fluorescence, while the 785 nm laser provide excellent spectra (Bell *et al.*,2012).

3.10. Chemometrics in forensic automotive paint

Chemometrics is a discipline that uses mathematical and statistical approaches to manipulate and interpret experimental data and derive maximum chemical information from data (Adams,2004). Chemometrics techniques have become a popular approach for the interpretation of the data obtained from instrumental analysis. Unlike traditional subjectively visual comparisons of sample spectra, chemometrics provide an objective manner for the classification and comparison of samples. Chemometrics often have better sensitivity and can minimize subjective bias that may occur during visual comparison. Studies have demonstrated that chemometrics allow for a comparable correct but quicker classification of samples compared to the visual classification (Muehlethaler *et al.*,2011; Muehlethaler *et al.*,2013b; Muehlethaler *et al.*,2014).

Since the instrumental spectra all contain large number of variables, multivariate statistical methods are effective at these spectral data interpretations. Unsupervised methods such as principal component analysis (PCA), hierarchical cluster analysis (HCA) and supervised methods such as Linear Discriminant Analysis (LDA), Soft Independent Modeling of Class Analogy (SIMCA), Partial Least Squares Discriminant Analysis (PLS-DA), and Support Vector Machine Discriminant Analysis (SVMDA) are all powerful statistical methods that have been widely used for the interpretation of automotive paint analysis (Duarte *et al.*,2020). Comprehensive introductions and explanations of these statistical methods can be found in several references (Shaver,2001; Adams,2004; Gemperline,2006; Brereton,2007; Mark and Workman,2007; Brereton,2009; Wehrens,2011; Rencher and Christensen,2012). A brief introduction of the most frequently used methods (PCA, HCA, LDA, SIMCA and CCSWA) will be given below.

Principal Component Analysis. PCA is an exploratory tool to identify patterns and extract key variables from multivariate data. The goal of PCA is to reduce the number of variables while keeping the maximum total variance explained in the first principal components. PCA captures the most variation in a dataset by rotating and projecting the original variables onto a new axis (see *Figure 18*). The axis should convey the maximum variation, known as the first principal component (PC). The procedure is continued to find the second, third axis (often perpendicular to each other) which has most of the remaining variance, until all the principal components have been calculated (Adams,2004). The new coordinates are generated, known as scores, and the new dimensions are linear combinations of the original variables, called loadings, which can reflect the variables in the original data that have a significant weighting on a PC. Thus, the original dataset can by reconstructed by a small number of these PCs, strong patterns and structures can also be revealed (Brereton,2009). Each sample will be represented by the scores on the PCs. By plotting the scores for the first two or three PCs, it is possible to map the sample by individual dots. Samples that have similar scores on PCs would be clustered into groups, which often indicate that these sample have similar chemical compositions. By examining the loadings, it is possible to get the information about which variables have a significant impact on a PC that can lead to the separation and clustering of the samples (Adams,2004).
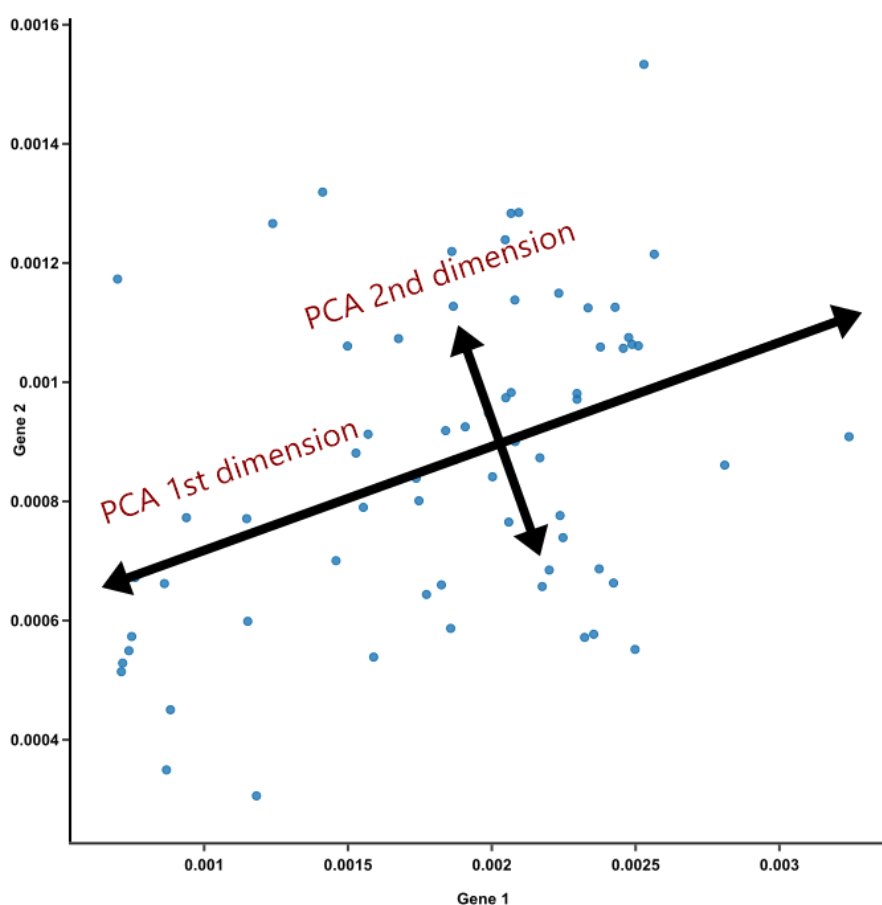
Figure 18. A simplified scheme of the transformation of original data into principal components. (https://blog.bioturing.com/2018/06/14/principal-component-analysis-explained-simply/)

The power of PCA is to provide a direct mapping of multivariate data into a two- or three-dimensional space containing most of the information in the original data so that the classification and interpretation of spectra data can be easily conducted (Wehrens,2011). This advantage makes PCA the most frequently used method in automobile paint analysis (Duarte *et al.*,2020). Almost all the studies would apply PCA to the obtained FTIR or Raman spectra data for the classification and interpretation (Lambert *et al.*,2014; Lavine *et al.*,2014a; Fasasi *et al.*,2015; Lavine *et al.*,2015; Maric *et al.*,2016; Lavine *et al.*,2016a; Lavine *et al.*,2016c; Ferreira *et al.*,2017; Ferreira *et al.*,2017; Lavine *et al.*,2017).

Hierarchical cluster analysis. Cluster analysis is an exploratory, powerful investigative tool, which can aid in determining and identifying the structure or the grouping in the data. It is based on the distances between variates calculated by various distance metrics, the greater the distance between objects the less their similarity. The commonly used distance metrics include the Euclidean distance, the Minkowski distance, the Mahalanobis distance, the Pearson correlation and so on, different clustering results may be obtained using different measures (Adams,2004). It is necessary to try all methods in order to get the most appropriate result (Wehrens,2011). Among these, HCA is the most frequently applied methods in automotive paint analysis and often used in association with PCA and other methods (Fasasi

et al.,2015; Yang *et al.*,2015; Lavine *et al.*,2016a; Lavine *et al.*,2016c; Perera *et al.*,2018; Duarte *et al.*,2020). This is because the data like automobile paint spectra often have a hierarchical structure where groups consist of many sub-groups and this structure can be visualized in a tree-like dendrogram (see *Figure 19*). The y-axis of the dendrogram indicates the 'distance' between different groups, whereas the connections show where the different groups merge into one bigger group. Different algorithms such as single, average, complete linkage, and Ward's method are available for hierarchical methods. It is also necessary to try all the algorithms for the best results.
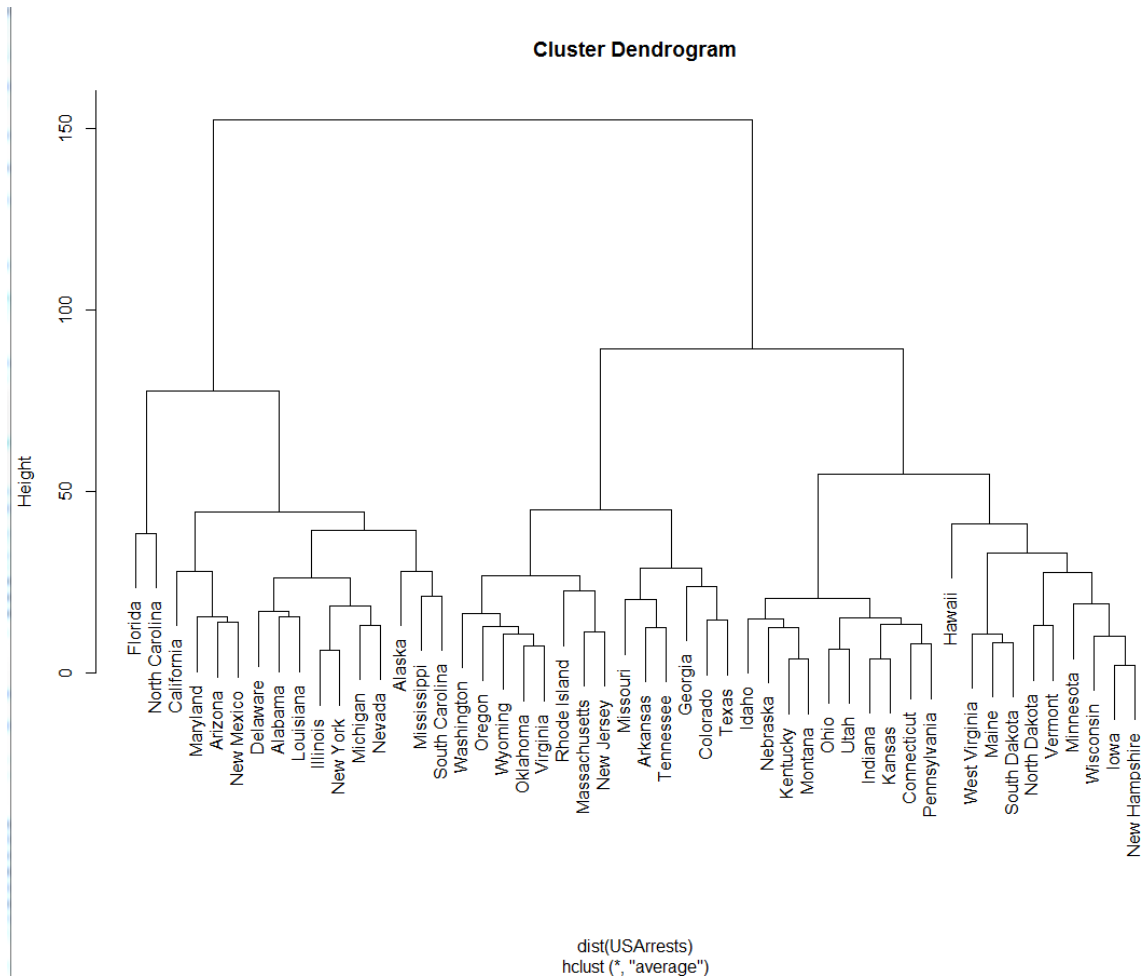
Figure 19. A typical cluster dendrogram (https://stats.stackexchange.com/questions/82326/how-to-interpret-the-dendrogram-of-a-hierarchical-cluster-analysis)

Linear Discriminant Analysis. Discriminant analysis, or referred to as classification or supervised pattern recognition, is a method used to identify and categorize unknown samples based on the information of parent groups obtained from unsupervised pattern recognition (Adams,2004). To apply discriminant analysis, the data set is often divided into two sets, one group contains a suitable amount of data as a training set, the other group serves as validation set. The training set is trained by various parametric or non-parametric algorithms, thus deriving the classification rule or discriminant function. The developed classification rule is then validated by the validation set. LDA is a commonly used classification technique when

the covariance matrices for both groups are known and similar. LDA generates discriminant functions through linear combinations of the original variables, thus providing maximum separation between subgroups (Adams,2004). The validated model is then used to predict the classification of the unknown samples, providing a probability of correct classification. In the analysis of automobile paint, LDA is often applied in combination with PCA for the classification (Kochanowski and Morgan,2000; Lavine *et al.*,2011; Maric *et al.*,2012; Lavine *et al.*,2014a).

Soft Independent Modeling of Class Analogy. SIMCA is another supervised pattern recognition that is based on PCA. In PCA, the data set is structured and classified into several groups, each group is then independently modelled in SIMCA. The developed models are used to classify unknown samples by comparing the residual variance of a sample with the average residual variance of a group (Lavine and Davidson,2006; Brereton,2007). Similar to discriminant analysis, SIMCA develops the models using a training set and the models can be validated by a validation set. The advantage of SIMCA is that It is a 'soft' classification method, which means the unknown sample can be grouped into one group, more than one group or even no group (Lavine and Davidson,2006).

Common Components and Specific Weights Analysis. CCSWA is a multiblock statistical method and used in the case where different sets of data obtained from the same samples need to be combined together (Mazerolles *et al.*,2006). It is considered as an extension of PCA. Each data set (obtained from one analytical technique) can be considered as a block. Similar to PCA, the common components of each block were determined by specific weights that correspond to the variability of the block so that the structure of the considered block can be projected to these representative common components. Like the loadings plots of a PCA, the specific weights associated to the blocks for each common component allow us to visualize the importance of the original variables on the global projection. The information within a block can thus be studied, as well as the relations between different blocks. This technique was first applied to the analysis of food products (Mazerolles *et al.*,2006). Lambert *et al* applied CCSWA to combine the red household paint data obtained from IR and Raman spectroscopy and the results of this study successfully showed patterns groups of the analyzed paints (Lambert *et al.*,2016).

4. Project & Methodologies

4.1.　　Aim of the project

Automobile paint evidence is one of the most common types of trace evidence that could be encountered in forensic case work. In order to get a better understanding of automobile paint composition from a forensic perspective and to provide data that can be used for the evaluation of automobile paint evidence, considerable research has been conducted. Most of these studies either focus on assessing the discriminating power of one particular instrument or combined analytical instruments for characterization and identification of the chemical composition of automobile paints (Duarte *et al.*,2020). Even though automobile paint evidence is well exploited from various aspects, the author finds that there is still much worth exploring and many questions waiting to be answered.

1) Several studies seek to assess the frequency of physical and chemical composition and color of automobile paints so as to provide population data that could be used for determination of evidential value of paint evidence in particular regions (Gothard,1976; Ryland and Kopec,1979; Volpé *et al.*,1988; Stone *et al.*,1991; McDermott *et al.*,1999; Edmondstone *et al.*,2004; Reynolds *et al.*,2018; Kruglak *et al.*,2019; Soong *et al.*,2020). Regardless of whether it is an analytical instrument performance study or a population study, for the purpose of validity and representativeness, the sample sets in these studies must include the greatest diversity. This means that the samples must be collected from different manufacturers and have a large range of colors. In these studies, after using various analytical methods, there are always samples that could not be differentiated. The last remaining indistinguishable samples tend to have a common feature, that is, they are of same color and come from the same make, model and have same or similar production year, e.g., the study by Edmonstone *et al*. and Reynolds *et al*. (Edmondstone *et al.*,2004; Reynolds *et al.*,2018). These common conclusions reached by different authors provide the impression that as long as OEM samples come from same make, model, plant and year, they are non-differentiable. The proposition that "if automotive paints come from the same manufacturer, have same color and model, are produced in the same assembly plant in the same year, they cannot be distinguished", however, still needs to be verified. This leads to the first question: **to what extent OEM-paint from mass-produced vehicles of same color, manufactured by same make, can be differentiated and under what conditions can this be done?**

2) Automotive OEM coating products are now provided by rather few transnational coating suppliers such as PPG, DuPont and BASF, which may lead to a high degree of similarity in paint composition (Kirkbride,2015). However, automobile manufacturers tend to choose their unique coating technology, application process and paint formulation to form brand characteristics as well as to meet customers' needs. Therefore, the diversity of paint

between different manufacturers is expected to be high and detectable. The above-mentioned studies have well demonstrated this statement by means of highly discriminating results. Several studies have also demonstrated that even when only the clear coat is examined, one can correlate the chemical formation to the vehicle origin (Maric *et al.*,2012; Lavine *et al.*,2015). Additionally, if color factors are added into comparison, paint samples can be more easily differentiated. A good example of this can be found in a recent population study including 200 samples of different makes and colors – all of them differentiable using optical examination and instrumental methods (Kruglak *et al.*,2019) .As previously mentioned, due to different coating processes and raw material ratios selected by automotive manufacturers, from a forensic analysis perspective, vehicle make may be the simplest discriminating factor. However, identification factors for automobile paint also include model, production year, assembly plant as well as topcoat color codes (assigned to some specific colors). One study has shown that the assembly plant plays as an anchor for automobile paint samples in the PDQ database (Lavine *et al.*,2014). The author states that "*as the primer and clear coat layer are often unique to the assembly plant where these layers were applied, combining chemical information obtained from the FTIR spectra of the two primer layers and from the clear coat layer makes it possible to rapidly and accurately identify the make and model of the automobile within a limited production year range from the paint system alone*" (Lavine *et al.*,2016b). However, it is still unclear whether or not the assembly paint is the key discriminating feature. If the samples have the same make, model, color and are produced in the same assembly plant but in different years, what conclusions can be drawn? What will the conclusion be if the samples have the same make, model, color and production year but are produced in different plants? In addition, even if there are studies demonstrating that the assembly plant can be identified in a sample set where they all come from the same make within a limited production year, these studies involve only North American manufacturers (Audette and Percey,1982; Lavine *et al.*,2014; Lavine *et al.*,2015; Lavine *et al.*,2016a; Affadu-Danful *et al.*,2023). Although there is regional variation, whether this conclusion can be applied globally or only across North America is yet to be confirmed. Interestingly, research aimed at answering the above questions is rare. This leads to the second question: **which identifying factor (model, topcoat color code, production years, assembly paint) contributes the greatest towards non differentiation of samples?**

3) Paint evidence is regarded as class evidence (i.e., not unique), it possesses class characteristics and can be associated only with a group and never with a single source. This is because automobile coating is applied batch-to-batch to the body-in-white and is considered mass produced. From the perspective of the manufacturer, in order to maintain production quality, the paint composition ratio and coating application for the same vehicle model tend to be consistent. In theory, the same batch of products should have exactly the same chemical composition when leaving the plant. However, according to a presentation given by Stoecklein and Palenik in 1998 (Stoecklein and Palenik,1998), depending on the quality of painting devices and numerous errors that may occur in coating application process, corrective work may be conducted on primer, primer surfacer or topcoats (such as repaint a second topcoat). Moreover, as automotive paint is

multilayer paint, primer/primer surfacer batch changes may occur during the working period of one batch of color paint. Automobile paint may show inhomogeneity or have inconsistent composition and layer structure in or between batches or even in the different parts of same vehicle (despite having a highly consistent appearance in color). The inter-sample and intra-sample variability need to be further explored. This leads to the third question: **what is the degree of inter-sample and intra-sample variability as well as batch variation in automotive paint?**

4) Automobile paint is a multilayer coating system. The layer sequence is the most important characteristic for discrimination. This feature can be examined under an optical microscope all at once if a thin cross section is prepared. However, when it comes to the identification of chemical composition, the examination must be inspected layer by layer using various instruments. It is usually quite time-consuming and not economical if all the layers must be analyzed. Maric *et al.* have conducted several studies demonstrating that excellent differentiation between vehicle manufactures can be achieved by analyzing only the clear coat using FTIR and Raman spectroscopy (Maric *et al.*,2012; Maric *et al.*,2016). Eyring *et al*. have demonstrated that samples that have identical color codes can be mostly distinguished by examining only the clear coat and fully discriminated with additional comparison, without the need to analyze the basecoat (Eyring *et al.*,2007). However, there is still a lack of information to conclude that the basecoat or other layers have less discriminating power. Massonnet dealt with this topic on grey metallic automotive paint (Massonnet,1996), this need to be updated and confirmed with other color of paint. This leads to the fifth question: **which single layer can contribute the greatest distinction and what layer combination examination can provide sufficient evidential value?**

This project derives from the interest and need to study these questions. Thus, the aim of this project is to answer the following questions:

1. To what extent OEM-paint from mass-produced vehicles of same color manufactured by same make, can be differentiated and under what conditions can this be done?
2. Which identifying factor (model, topcoat color code, production years, assembly paint) contributes the greatest towards non differentiation of samples?
3. What is the degree of inter-sample and intra-sample variability as well as batch variation of automotive paint?
4. Which single layer can contribute the greatest distinction and what layer combination examination can provide sufficient evidential value?

This project aims to answer aforementioned questions by analyzing a carefully selected sample set using various methods and applying a reasonable analytical sequence.

4.2.   Methodological work plans

Since the information obtained in this research is ultimately used to serve the deeper understanding of automotive paint and should be representative, the selected samples and analytical methods should be closest to practical conditions. The methodological work plans of this research are as follows:

1) **Select and collect an ideal sample set based on the aim of this study.**

To get profound information about paint composition and focus on the issues mentioned before, the scope of samples should be representative paint from a specific manufacturer and color, but with as many models, production years and plants as possible. The chosen manufacturer and color should be common and popular, the samples involved should be street samples collected from different regions, which can represent the actual situation of samples encountered in real casework. The choice of these limitations will be described in detail in the following chapters.

2) **Design the proper analytical sequence for this study.**

The analytical result is ideal to be obtained by conventional techniques so that the data could be widely used in routine casework. As described in Chapter 3, microscopic techniques, FTIR, Raman spectroscopy, Pyrolysis GC/MS are the most common analytical methods used in paint examination and therefore expected to be applied in this research. The sequence of analysis is expected to be from physical (Microscopic examination) to chemical (FTIR, Raman spectroscopy, Py-GC/MS). These analytical instruments are able to provide information from every aspect.

3) **Optimize the sample preparation and experimental parameters for all instruments involved.**

This research aims to assess the differences in the samples themselves, in other words, to explore inter-sample variability. Consequently, images and spectra obtained from each instrument must be of high quality and reproducible. Intra-sample variability caused by sample preparation variation or instrument errors must be minimized or even eliminated. It is imperative to standardize sample preparation procedure, optimize experimental parameters for each instrument based on some valid protocols and always analyze samples with the same calibrated instrument under same condition.

4) **Characterize physical and chemical features of samples and determine the DP of each instrument from different perspective.**

Each layer of paint is expected to be systematically analyzed by the chosen methods, physical and chemical properties would be compared and grouped. These features should be fully explored in order to provide answers to the proposed questions. Discriminating

power of each instrument or combined methods with regard to different paint features need to be calculated.

5) Process obtained instrumental data with the help of chemometric techniques.

Chemometrics are nowadays popular and powerful techniques for data visualization and comparison objectively. Proper statistical methods will be selected and used to visualize and group data based on the sample information. Visual comparison and statistical results will be cross checked and the discriminating power of both methods will be calculated and compared.

6) Combine all the obtained information and provide answers to the proposed questions.

When all the necessary data are obtained, they need to be combined and interpreted to provide answers to the proposed questions. What conclusions can be drawn from this project and how they can be used will be evaluated.

4.3.   Analytical sequence

Analytical results should be obtained by conventional techniques so that the data could be widely used in routine casework. As described in Chapter 3, microscopic techniques such as FTIR spectroscopy, Raman spectroscopy, and Py-GC/MS, are the most commonly applied analytical methods used in paint examination and have therefore been chosen for this research. A scheme of the analytical sequence in this study is illustrated in *Figure 20*.

Step 1: Microscopy   Color and texture, layer sequence, relative layer thickness
   • All samples including subsamples

Step 2: FTIR spectroscopy   Binder type, pigments and extenders, additives
   • Each layer of all samples including subsamples
   • Generation of a representative sample set

Step 3: Raman spectroscopy   Pigments and extenders
   • Each layer of all representative samples

Step 4: Py-GC/MS   Further information about binder composition
   • The samples that cannot be differentiated by FTIR and Raman spectroscopy

Figure 20. Analytical sequence of this study

5. Sample set selection and collection

5.1.   Sample set selection

Driven from the aim of this research, the idea for sample selection is to restrict sample diversity to one specific manufacturer and color but at the same time achieve the greatest diversity within this scope, i.e., as many models, production years and assembly plants as possible. Within the controllable variables, to which extent automotive paint of same make and color can be distinguished, can be evaluated. The more diverse the samples involved, the better the proposed questions can be answered. Due to the time constraint of this project, it is not possible to involve as many samples as possible. In order to obtain the most representative results, the chosen make and color should be the most common one.

As previously described, white is considered as one of the most difficult colors encountered in forensic paint discrimination due to its little variety of pigment formulation. Differentiating white automotive paint is quite challenging, but it is the perfect choice to inspect to which extent automotive paint is able to be distinguished. What's more, white is also the world-widely most common color in recent 5 years and is reported to be the most common encountered color in several regions. The in-depth information of white automotive paint would be helpful in forensic practice. Thus, white is chosen for this project.

As for the manufacturer, the automotive paints from American manufacturers (such as GM, Ford and Chrysler) have been fully explored by different experts over the past two decades. It is good to focus on some other make. China is currently the country with the largest motor vehicle ownership in the world. According to the data published by Traffic Administration of the Ministry of Public Security of China, by 2017, there are 217 million cars registered in China (Xinhua,2018). Considering the convenience and feasibility of sampling, combined with the author's background, the sampling site is selected in China. Annual car sales data published by China Association of Automobile Manufacturers (CAAM) showed that Volkswagen(VW) has the largest passenger cars population in China (CAAM,2018). Volkswagen has two large joint ventures in China, producing 31 models in 14 assembly plants (FAW-Volkswagen ; SAIC-Volkswagen). This meets the needs of sample diversity within the range perfectly.

Therefore, the sampling target for this research is decided as **white Volkswagen** passenger cars produced in China. The additional advantage of sampling in China is that these samples can also be compared with the white Volkswagen paint samples existing in the EUCAP databases to determine the geographical variations.

5.2.   Sample collection

In June 2018, sixty-two samples were collected from vehicles that were placed in accident vehicle parking lots belonging to traffic police as well as VW service shops in Guangzhou, shanghai, Suzhou, Xuzhou and Beijing.   Each sampling vehicle was photographed and information including manufacturing company, model, year, VIN code, color code and sampling locations was recorded in a standard sampling form (as shown in *Figure 21*). For each vehicle, intact paint chips were collected from three to five positions of the metal substrate (two front doors and front engine block). In the situation where this sampling manner was not allowed, samples were taken from the damaged areas. Before sampling, target locations and tools were cleaned using ethanol. Each sample was then placed individually into a small paper envelope and labeled with a marker.
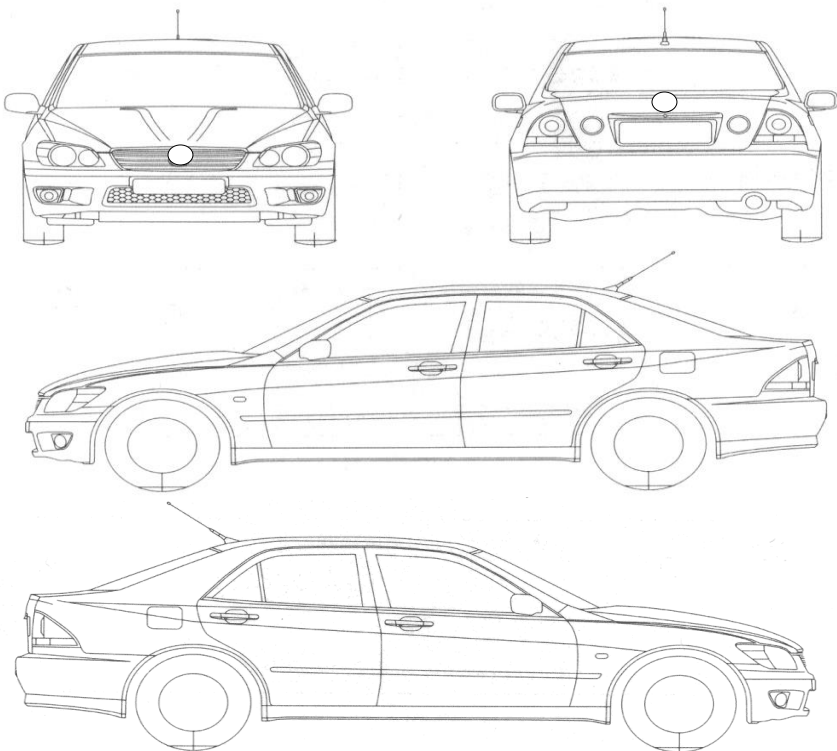
样品编号 Sample No.		品牌 Company		车型 Model	
型号 Type			制造年月 production year		
车辆识别代号 VIN Code					
颜色代码 Paint color Code			颜色 Color	单色 ☐ Solid	金属 ☐ Metallic
采样位置 Picking Psition ☐前部 Front 高度 Height (cm) [　　　] ☐后部 Back 高度 Height(cm) [　　　] ☐左侧 Left 高度 Height(cm) [　　　] ☐右侧 Right 高度 Height(cm) [　　　]					
补充信息 Additional information	Photo/Repaint				

Figure 21. Paint sampling form

5.3.   Sample constitution

After collection, each sample and its corresponding subsamples (paint collected from different locations on a single vehicle) were assigned unique reference numbers, starting with 'W001'. If subsamples were available, they were designated as 'W001_1', 'W001_2', and so on. The associated details, such as manufacturing company, model, production year, color code, color description, and VIN code, were meticulously recorded in *Table 9* Overall, a total of 62 samples, comprising 135 subsamples, were successfully gathered.

As Volkswagen is a German brand, in order to produce their vehicles in Mainland China, it collaborated with two different Chinese state-owned companies, i.e. First Automobile Work Group Corp., Ltd. (FAW) and Shanghai Automotive Industry Corporation Motor Corp., Ltd (SAIC). As a result, the collected samples encompass vehicles from these two different manufacturing companies. Referring to the 'Company' column in *Table 9*, F-VW represents vehicles manufactured by FAW-Volkswagen, while S-VW designates those produced by SAIC-Volkswagen.

Involved models, production years and color codes were sorted and counted. A total of 15 different models were collected (see *Table 10*). These samples are characterized by three distinct color codes: LB9A, LC9A, and LY9H, corresponding respectively to color descriptions of "candy white," "pure white," and "polar white" (as illustrated in *Figure 22*). The samples also cover a wide range of years from 2002 to 2018, the distribution is shown in *Figure 23*.

Table 9. Sample set and relevant information.

Reference number	Company	Model	Production Year m/d/y	Color Code	Color Description	VIN
W001_1	F-VW	Bora	3/13/2002	NA	NA	LFVBA21J923006494
W001_2						
W001_3						
W002_1	F-VW	Sagitar	12/29/2017	LC9A	Pure white	LFV2A21K6H4331566
W002_2						
W002_3						
W003_1	S-VW	Polo	11/2017	NA	NA	LSVG446R8H216340
W003_2						
W003_3						
W004_1	S-VW	Polo	2003	NA	NA	LSVFA49J13200153
W004_2						
W004_3						
W005	F-VW	Jetta	9/24/2014	LB9A	Candy white	LFV2A2BS3E4645928
W006_1	F-VW	New Bora	11/23/2016	LC9A	Pure white	LFV2A215XG3193593
W006_2						
W006_3						
W007_2	S-VW	Santana	6/4/2013	LY9H	Polar white	LSVAB4BR5DN059987
W007_3						
W007_4						
W008_1	F-VW	Jetta	NA	NA	NA	LFVAA11A4Y2013633
W008_2						
W009_1	S-VW	New Lavida	2/2/2015	LY9H	Polar white	LSVNN2188FN023316
W009_2						
W009_3						
W010_1	S-VW	Santana	12/23/2017	LY9H	Polar white	LSVN04BR4HN277660
W010_2						

W010_3						
W011	S-VW	Polo	7/14/2017	LY9H	Polar white	LSVG226R6H2096580
W012_1	S-VW	New Lavida	11/16/2017	LY9H	Polar white	LSVWY418XHN387568
W012_2						
W013_1	F-VW	Jetta	10/19/2010	NA	Polar white	LFV2A11G1A3148822
W013_2						
W013_3						
W013_4						
W014	S-VW	New Lavida	6/1/2017	LY9H	Polar white	LSVNB4185H2097432
W015	S-VW	New Lavida	6/1/2017	LY9H	Polar white	LSVNB4186H2097729
W016	S-VW	New Lavida	6/1/2017	LY9H	Polar white	LSVNB4186H2097606
W017_1	S-VW	Tiguan	8/21/2015	LY9H	Polar white	LSVXZ65N4F2168181
W017_2						
W018	S-VW	New Lavida	12/11/2016	LY9H	Polar white	LSVWF2180G2312727
W019_1	S-VW	Polo	3/9/2017	LY9H	Polar white	LSVG226R7H2040681
W019_2						
W019_3						
W020_1	S-VW	Santana	6/12/2016	LY9H	Polar white	LSVFT2BR8GN118803
W020_2						
W020_3						
W020_4						
W021_1	S-VW	Polo	8/18/2016	LY9H	Polar white	LSVG026R9G212867
W021_2						
W021_3						
W021_4						
W022_1	S-VW	Touran	4/10/2010	LB9A	Candy white	LSVVM41T0A2539599
W022_2						
W022_3						
W023_1	F-VW	Sagitar	12/4/2017	LC9A	Pure white	LFV2A21K4H4304592
W023_2						
W023_3						
W023_4						
W023_5						
W024_1	S-VW	Tiguan	2/4/2012	LB9A	Candy white	LSVUG65N3C2025047
W024_2						
W024_3						
W024_5						
W024_6						
W025_1	S-VW	Polo	11/8/2016	LY9H	Polar white	LSVG066R5G2014107
W025_2						
W025_3						
W025_4						
W025_5						
W026_1	W-VW	Goco	10/25/2012	LC9A	Pure white	WVWB151K7DK006679
W026_2						
W026_3						
W027_1	S-VW	Passat	3/21/2004	NA	Candy white	LSVCG49F442267866
W027_2						
W027_3						
W028_1	S-VW	Passat	7/16/2003	LB9A	Candy white	LSVCC49F432297377
W028_2						
W028_3						
W029	F-VW	Bora	2002	NA	NA	LFVBA21J623008333
W030	S-VW	Tiguan	12/2/2016	LY9H	Polar white	LSVXZ65N1G2217919
W031	S-VW	Tiguan	12/15/2017	LY9H	Polar white	LSVUC60T2H2217052
W032_1	S-VW	Gran Lavida	11/8/2015	LY9H	Polar white	LSVGF6189F2235379
W032_2						
W033_1	S-VW	New Lavida	2/6/2014	LY9H	Polar white	LSVN42185EN024375
W033_2						
W034_1	F-VW	New Bora	7/15/2017	LC9A	Pure white	LFV2A1150H3138257
W034_2						

W035_1	F-VW	New Bora	3/3/2018	LC9A	Pure white	LFV2A2152J3879702
W035_2						
W036	F-VW	Sagitar	11/29/2017	LC9A	Pure white	LFV2A21K4H4299359
W037_1	S-VW	Lavida	1/19/2009	LC9X	DEEP BLACK	LSVAB418892184743
W037_2						
W038	F-VW	Jetta	9/28/2008	NA	ALPINE WHITE	LFV2A11G883147533
W039	S-VW	Polo	11/25/2017	LY9H	Polar white	LSVG446R6H2169534
W040	S-VW	Polo	12/12/2015	LY9H	Polar white	LSVG026R2F2172962
W041_1	S-VW	Santana	10/27/2017	LY9H	Polar white	LSVNY2BR7HN233746
W041_2						
W042_1	S-VW	New Lavida	4/12/2017	LY9H	Polar white	LSVWR2188H2056068
W042_2						
W043	S-VW	Gran Lavida	5/28/2015	LY9H	Polar white	LSVFV618XF2621761
W044_1	S-VW	Passat	6/2/2017	LY9H	Polar white	LSVD78A44HN083814
W044_2						
W045	S-VW	Lamando	2/8/2018	LY9H	Polar white	LSVCL6BM3JN030683
W046_1	S-VW	Passat	10/10/2013	LY9H	Polar white	LSVCH6A49DN183012
W046_2						
W047_1	S-VW	New Lavida	8/12/2017	LY9H	Polar white	LSVWY2180HN336715
W047_2						
W048_1	S-VW	New Lavida	3/8/2018	LY9H	Polar white	LSVWY218XJ2067923
W048_2						
W049	S-VW	New Lavida	10/10/2016	LY9H	Polar white	LSVWA2182G2252867
W050_1	S-VW	Polo	10/29/2012	LY9H	Polar white	LSVFB26R2C2112164
W050_2						
W051_1	S-VW	Lamando	12/25/2017	LY9H	Polar white	LSVCJ2BM5HN145360
W051_2						
W052_1	S-VW	Tiguan	3/7/2017	LY9H	Polar white	LSVUC60T7H2033709
W052_2						
W053_1	S-VW	New Lavida	5/16/2014	LY9H	Polar white	LSVNV4184EN064438
W053_2						
W054	S-VW	New Lavida	11/21/2016	LY9H	Polar white	LSVWL2189G2292728
W055_1	S-VW	Lavida	2/19/2014	LY9H	Polar white	LSVFV6180E2055009
W055_2						
W056	S-VW	New Lavida	12/15/2014	LY9H	Polar white	LSVNU2181EN140611
W057_1	S-VW	New Lavida	5/27/2017	LY9H	Polar white	LSVWT2189HN286900
W057_2						
W058_1	S-VW	Tiguan	4/13/2013	LB9A	Candy white	LSVUL25N9D2063467
W058_2						
W059_1	F-VW	New Bora	12/29/2013	LC9A	Pure white	LFV2A2152D3223097
W059_2						
W060_1	F-VW	Golf	8/21/2012	LB9A	Candy white	LFV3B21K0C3277505
W060_2						
W060_3						
W061	F-VW	Bora	2/26/2003	NA	Candy white	LFVBA11J233010236
W062_1	S-VW	New Lavida	1/1/2018	LY9H	Polar white	LSVWY4186J2010663
W062_2						
W062_3						

54

Table 10. List of model and number of collected samples.

Model	Sample no.
Bora	3
Sagitar	3
Jetta	4
New Bora	4
Golf	1
Polo	9
Santana	4
New Lavida	16
Tiguan	6
Touran	1
Passat	4
Gran Lavida	2
Lavida	2
Lamando	2
Goco	1
Total	62

Table 11. list of plant code and plant location of collected samples (n=61).

Manufacturing company	Plant code	Plant location	Number of samples
W-VW	K	Osnabrück	1
F-VW	3	Changchun	10
	4	Chengdu	4
S-VW	2	Anting	31
	Ni	Nanjing	13
	No	Ningbo	2
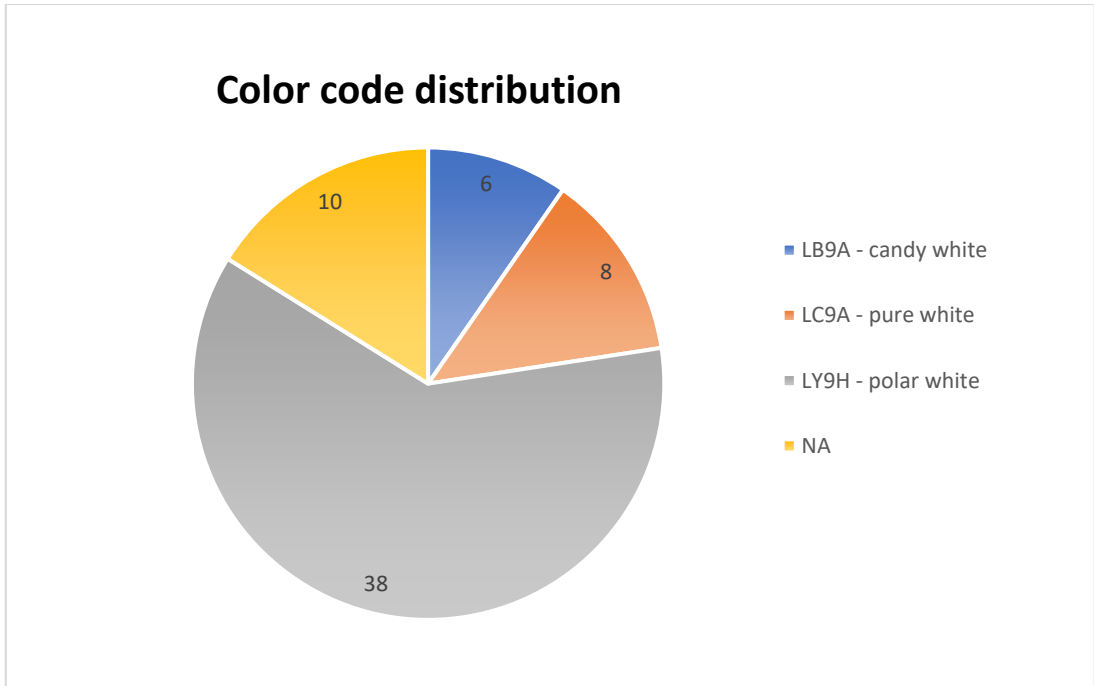
Figure 22. Pie chart of sample distribution based on color code(n=62).
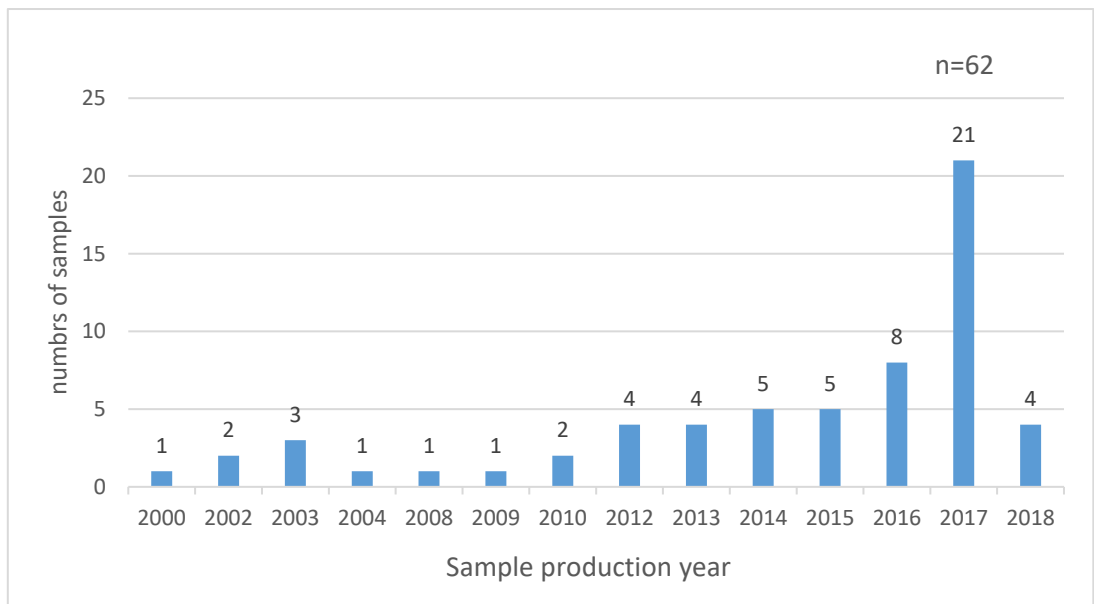
Figure 23. Histogram of sample distribution based on vehicle production year(n=62).

VIN of a vehicle is a unique identifying code consisting of 17 characters. It displays one vehicle's specific features such as the origin of the vehicle, the manufacturer, the production year, the assembly plant. By decoding VIN, known information such as make and production year can be crosschecked and additional information such as assembly plant of the sample can be discovered. After decoding VIN of each sample, it was found that 60 samples were produced in 5 different plants in China and one sample was produced in Germany. The plant code corresponding to each company, the plant location and the number of vehicles produced by each plant were listed in *Table 11* (Wikipedia,2023). To be noticed, due to a recording error and the age of production, the plant information of W008 could not be identified.

The color codes LB9A and LC9A were found in NEXA AUTOCOLOR® vehicle identification plates. Their color and identification information are presented in *Figure 24*. This identification plate could be used to physically compare the colors of paint chips with the same color code.

Figure 24. NEXA AUTOCOLOR® vehicle identification plates with the color code LB9A and LC9A.

6. Optimization and standardization of sample preparation method and experimental parameters

This research aims to assess the differences in the samples themselves, in other words, to explore inter-sample variability. Consequently, images and spectra obtained from each instrument must be of high quality and reproducible. Intra-sample variability caused by sample preparation variation or instrument errors must be minimized or even eliminated. It is imperative to standardize sample preparation procedure, optimize experimental parameters for each instrument based on valid protocols and then adapt these validated parameters and procedure to the whole sample set. Therefore, a selective sub-sample set was generated for the optimization, standardization, and validation of the instrumental settings for this study. The construction of this test sample set is described in chapter 6.1. All the consideration and preliminary results concerning the above aspects with regard to each analytical method will be summarized in chapter 6.2 (microscopy), 6.3 (FTIR), 6.4 (Raman) and 6.5 (Py-GC/MS).

6.1. Selection of test sample set

The select set was deliberately designed to contain specific identifying factor combinations. In this way, the preliminary study can not only be used to optimize and standardize the instrumental parameters, but also to explore whether some characteristics can be associated with any particular factor. Therefore, 15 samples including 3 color codes were selected to be a part of the test sample set, only one sub-sample per vehicle was chosen as a representative for the sample. The complete information of these 15 samples is listed in *Table 12.*

The sample set covers 3 different color codes, containing three types of combinations listed as follows:

- Same model, same assembly plants but different production year
- Same model, same production year but different assembly plants
- Same model, same production year, and same assembly plants

Table 12. Select sample set and relevant information.

Reference number	Model	Production year	Color code	Assembly Plant
W006_1	New Bora	2016	LC9A	Plant Changchun
W034_1	New Bora	2017		Plant Changchun
W035_1	New Bora	2018		Plant Changchun
W023_5	Sagitar	2017		Plant Chengdu
W002_3	Sagitar	2017		Plant Chengdu
W012_1	New Lavida	2017	LY9H	Plant Nanjing
W014	New Lavida	2017		Plant Anting
W018	New Lavida	2016		Plant Anting
W019_2	Polo	2017		Plant Anting
W021_4	Polo	2016		Plant Anting
W020_3	Santana	2016		Plant Nanjing
W005	Jetta	2014	LB9A	Plant Chengdu
W022_3	Touran	2010		Plant Anting
W058_1	Tiguan	2013		Plant Anting
W060_1	Golf	2012		Plant Changchun

6.2. Optimization and standardization of the parameters for optical examination

6.2.1. Sample preparation

Optical examination is always the first step in forensic paint analysis. A thin cross section is the recommended sample format since it can not only provide information as to the color, layer sequence, layer thickness under microscopy, but also be used for IR spectroscopy analysis (ASTM-E1610-18). In this study, a cross section of each sample is made by a microtome and then mounted onto a microscope slide for the examination using different microscopic techniques. The sample preparation procedure used in the author's laboratory is well-established and validated by forensic casework practice and proficiency tests. This procedure is used in this study and as follows:

1) A small size (1 mm x 1 mm) of paint film is picked from each sample and cleaned with ethanol.
2) The paint film is then placed in the mold vertically and then embedded with a standard resin (Technovit 2000 LC Heraeus Kulzer light curing resin). A resin block is mounted onto the mold.
3) The mold containing the sample is cured using the Heraeus Kulzer Technotray CU Curing Light for 15 minutes. An inclusion is then obtained.

4) The inclusion is then mounted onto the Leica RM2265 – Fully Motorized Rotary Microtome using a steel knife and cut into a 5-μm thick cross-section. The rest of the inclusion is kept for Raman analysis (see chapter 6.4).

5) The obtained cross-section is permanently mounted onto a microscope slide using Gurr$^@$ XAM Neutral Medium, improved white (xylene, refractive index: 1.4920-1.4950).

6) Each microscope slide is then labeled with a unique sample number.

6.2.2. Instrumentation

In this study, a Zeiss Axio Imager.Z2m microscope is used for all the optical observations. It is a combined reflected-light/transmitted-light motorized microscope which is also equipped with fluorescence light sources, removable polarizer/analyzer and a Zeiss AxioCam 506 color digital camera, making it a comprehensive instrument that can be used to analyze samples using various techniques. This microscope is associated with software ZEN 2.3 (blue edition) which can conduct all the settings of a microscope as well as image acquisition, processing and analysis. All the microscope settings, camera settings and display settings can be saved, reloaded and applied to subsequent examinations. This allows the sample to be observed and photographed under the same conditions every time.

6.2.3. Color calibration of microscope

Apart from the number of layers, layer sequence, texture of each layer, color is another important feature that needs to be recorded during optical examination. Digital imaging allows samples to be fixed, presented and compared. However, the microscope illumination (source), the quality and stability of digital camera, white balance and monitor display accuracy all have an impact on the color accuracy of digital images(Clymer and Wei,2014). Any slight alteration of these elements may lead to inaccurate color display. In order to achieve the most accurate reproducibility as well as deliver stable performance regardless of changes in microscope and camera settings, it is necessary to perform color calibration.

A color reference card called "Fuji HCT 01F35T" produced by HutchColor, LLC. is used for color calibration. It is a transparent film with many color patches and is of the same size as a microscope slide. It is equipped with a unique reference file that records standard CIE XYZ and CIE L*a*b* values for each patch. Once the set-up of the microscope and the camera are complete, the image of calibration slide is captured. For each patch, the image color space data can be read in Adobe Photoshop and then compared with the reference file. Ideally, the images should have a* and b* values within about ± 1.0 of the reference files. More tolerance is allowed in L* values, e.g. ± 2.0, but all L* errors should be in roughly the same direction (HutchColor,2019). If this is not the case, it indicates an improper setting of the microscope

and camera. All the settings should be calibrated until the captured image color space values match the reference data (HutchColor,2019). In theory, any changes to the settings will affect the color space value of the image, a new calibration slide image needs to be taken for each new calibration. This process is repeated every time the setting is changed. This leads to a cumbersome and repetitive workflow. Therefore, it is necessary to provide a more efficient and practical workflow to minimize the number of additional calibration repeats(Wei *et al.*,2015).

Adobe Photoshop is a well-known image processing software developed by Adobe Inc. Adobe Bridge is an organization tool program developed by Adobe whose function is to manage multimedia files and connect the various applications of Adobe system. Camera Raw software is a plug-in with Adobe Photoshop and adds functionality to Adobe Bridge. It gives these applications the ability to import and process images(AdobePhotoshop). Using these software, images can be calibrated and processed in batches since they provide all the camera and display settings similar to Zeiss Zen software. Once the microscope is set to Kohler illumination, the camera and display settings need to be adjusted to adapt to the condition of sample. Sample images and color calibration slide images are then acquired under the same recorded conditions. The color calibration can be performed in the abovementioned Adobe software all at the same time. In Adobe software, acquired images can be imported in batches. The color space values of several patches on the calibration slide image are first checked and compared with the given reference file. If necessary, image setting such as exposure time, white balance and tone curve are edited until the displayed color space values match the given reference data. All the edit settings are consequently copied and applied to all sample images. In this way, color calibrated images are generated. A workflow modified based on that by Wei *et al.* (Wei *et al.*,2015) ,is shown in *Figure 25*.

As previously mentioned, a big advantage of the involved Zeiss microscope and its supporting software is that all settings can be saved and applied to further experiments. As a result, once the workflow is executed for the first time, the applicable settings can be recorded so that the setting adjustment can be skipped in the following examination by reloading the recorded settings. The acquired calibration slide image can then be reused as a color calibration reference within a reasonable period. It is, of course, ideal to capture an image of the calibration slide during each examination. Thus, all the captured calibration slide images can be compared to see if the settings of microscope are stably applied.

Overall, by performing color calibration on the microscope, any color variance caused by the instrument can be eliminated and color display of sample image is deemed accurate.

On microscope

Set up microscope(kohler) using a sample slide

⬇

Adjust the microscope/camera/display until the image looks good*

⬇

record the settings and capture the images of samples

⬇

Set up color calibration slide

⬇

Capture the image of calibration slide at the recorded settings

On computer with Adobe software

Carry all samples images and color calibration slide image to the computer with Adobe Photoshop and Bridge

⬇

Load all images in Adobe Bridge and open with Camera Raw

⬇

Adjust edit settings of color calibration slide image according to the reference data (given by HCT)

⬇

Copy all the edit settings and apply them to all sample images to generate the color calibrated images

* 'Good' means that the live image should not be overexposed, the white balance is roughly correct, and the color of the sample looks similar to the color observed through the ocular.

Figure 25. Workflow of color calibration.

6.2.4. Preliminary study for the selection and optimization of illuminations

Automobile paint can reveal diverse characteristics under different illuminations. Common illumination types used in forensic analysis of automobile paint include transmitted light (bright field/dark field), incident light (bright field/dark field), polarization, and fluorescence illumination. Due to their variable sensitivity to different samples, these illumination types tend to provide different discriminating power (Massonnet,1996). In this study, going through all the illumination types would be quite time consuming. Furthermore, some of the illumination techniques might not provide much discrimination. Additionally, the choice of magnification often depends on the size of the sample. Generally, it should be large enough to observe detailed features in the paint layer. Therefore, it is necessary to conduct a preliminary study to test the performance of each illumination on the white paint sample and determine the optimum illumination parameters.

The test was conducted on the select sample set described in chapter 6.1. A paint chip of each sample was first placed on a microscope slide and observed using incident light (bright field and dark field). A small paint film, approximately 1mm x 1mm in size, was carved from each paint chip. The 5-μm cross section was obtained by embedding and microtomy. They were prepared and mounted following the procedure described in chapter 6.2.1. The mounted samples were examined using transmitted light (bright field/dark field), polarization, and fluorescence illumination and their DPs were calculated. A standardized analytical strategy as well as the illumination parameters was generated based on the examination results of this sample set.

Paint chip surface examination. The dry mounts of paint chips were first observed with the 10x, 20x and 50x objectives using incident light bright field. The magnification provided by 10x objective was too low to observe the detailed characteristic of paint surface. On the contrary, the magnification of the 50x objective was too high to obtain a focused plane. The 20x objective was found to be the reasonable choice and allowed for the observation of detailed surface characteristics on a relatively well focused plane. The select sample set was then observed with the 20x objective using incident light in bright field (RL BF) and darkfield (RL DF). The color, pigment appearance, surface morphology, and defects were examined and recorded.

Cross section examination. The mounted cross sections were first observed with 10x, 20x and 40x objectives respectively using transmitted light bright field. The magnification provided by 10x objective was too low to observe the detailed characteristic of each layer. On the contrary, the magnification of the 40x objective was too high to observe the complete layer structure in the field of view. The 20x objective was found to be the more reasonable choice permitting the observation of layer structure as well as detailed characteristics in the field of view. The select sample set was then observed with the 20x objective using transmitted light bright field (TL BF)/dark field (TL DF) illumination mode, crossed polarized light (POL) and fluorescence illumination mode. Three fluorescent filters, namely DAPI (excitation:357-371 nm/emission: 397 nm), Alexa Fluor 488 (AF 488, excitation:450-490 nm/emission:515 nm), and Alexa Fluor 546 (AF 546, excitation:510-560 nm/emission: 590 nm), were available for observation with the Zeiss microscope. The layer sequence, color, texture, and morphology of each layer for each illumination type were recorded.

Calculation of discriminating power (DP). Samples were visually compared with each other based on their observed physical features under each illumination. The discriminating power of each illumination technique was calculated and displayed in *Table 13*. It is worth noting that the discrimination of samples under incident light was quite challenging because it was uncertain whether the surface morphological features of the clear coat (such as striae and defects) were essential or accidental. Thus, it was decided that they would not be taken into consideration when differentiating between samples. The differentiation depended mainly on the observed color and texture of the basecoat. Whether the surface morphology was characteristic needed to be further verified by the intra-sample variability examination.

Table 13. Discriminating power of each illumination technique.

Illumination	Undifferentiated pairs	DP (n=15)
RL BF	55	0.476
RL DF	51	0.514
TL BF	16	0.848
TL DF	5	0.952
POL	8	0.924
DAPI	26	0.752
AF 488	55	0.476
AF 546	54	0.486

As presented in *Table 13*, both transmitted light bright field/dark field and crossed polarized light offers promising discrimination in this test. On contrary, incident light bright field/dark field as well the fluorescence illumination could not well distinguish white automotive paint samples. Since incident light could not reveal as many discriminant characteristics as well as other illuminations and introduced additional difficulties in characterization, it was excluded from this study. As for the decision for all the rest illuminations, a detailed discussion is presented in the following section.

Characterization and classification. Based on observations under incident light, all the samples were characterized as white solid paint. This was confirmed under polarized light as no effect pigments were observed in the basecoat with the exception of very few birefringent particles. The layer sequence, relative layer thickness, color, and texture of layer were observed and differentiated under transmitted illumination, both in bright field and dark field. It was found that two samples had repainted basecoats and clear coats on top of their original coatings. In such cases, only the OEM system was considered. In bright field illumination, 16 out of 105 pairs were undifferentiated, giving a DP of 0.848. 5 pairs remained undistinguishable under dark field illumination, providing a higher DP of 0.952 in terms of further discrimination of basecoat texture and primer color. The samples had either a three-layers (clearcoat-basecoat-primer) or a four-layers (clearcoat-basecoat-primer surfacer-primer) structure. The number of samples in these two groups was approximately equal, i.e., 8 three-layer samples and 7 four-layer samples. The classification based on the layer sequence and characteristics observed in bright field and dark field are presented in *Figure 26*. Representative examples for layer structure of each group in dark field illumination mode are presented in *Figure 27*. It is worth noting that the color and texture of the basecoat and the primer surfacer of the four-layers samples were highly similar. Since bright field and dark field illumination were able to reveal significant information pertaining to the physical features of the sample and generated a high DP, they will both be applied to the whole sample set. Dark field illumination, in particular, would be the first choice for characterization and discrimination of paint samples.

Figure 26. Classification of the select sample set using transmitted light bright field and dark field. Red boxes indicate the undifferentiated pairs.

Polarized light provided a DP of 0.924 where 8 pairs could not be differentiated. Polarized light did help with further discrimination; however, it could not provide as much additional information as dark field illumination since the pairs remained undifferentiated. Thus, polarized light will not be considered the first choice for this study. Only the samples that could not be differentiated by dark field illumination would be observed under polarized light for potential further discrimination.

The overall performance of the samples under three fluorescent illuminations was not ideal. Only the primer reacted to fluorescence illumination and all samples exhibited similar fluorescence emission (color). Consequently, the DP of the three fluorescent illuminations were rather low. Surprisingly, it was found that Alexa Fluor 488 fluorescence was capable of further differentiation of the pairs that were not previously distinguishable by dark field illumination. Under Alexa Fluor 488 fluorescence illumination, the undifferentiated pair, W012_1 and W014, exhibited different characteristics, in which the basecoat of W012_1 presented greenish fluorescence, while the one of W014 did not (see *Figure 28*). The same was true for the pair, W021_4 and W058_1 (see *Figure 29*). The samples under Alexa Fluor 546 and DAPI fluorescence revealed similar characteristics but not as obvious as under Alexa Fluor 488. Only the pair of W002_3 and W005 remained undifferentiated under fluorescence illumination. As a result, only Alexa Fluor 488 fluorescence will be applied to the undifferentiated samples, the other two were excluded.
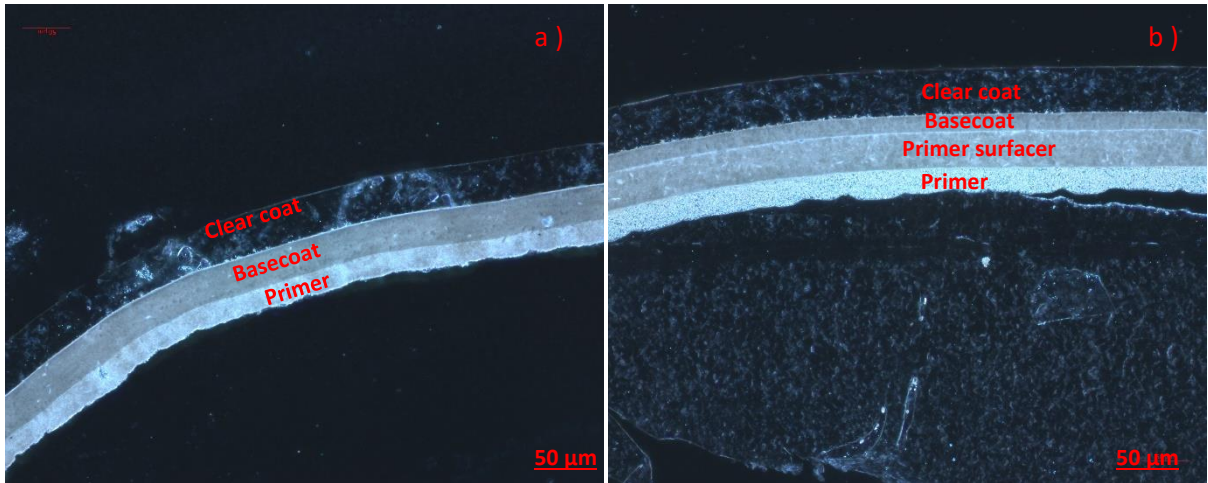
Figure 27. Dark field images of cross-sections of a) Sample W023_5 with three layers, and b) Sample W035_1 with four layers.
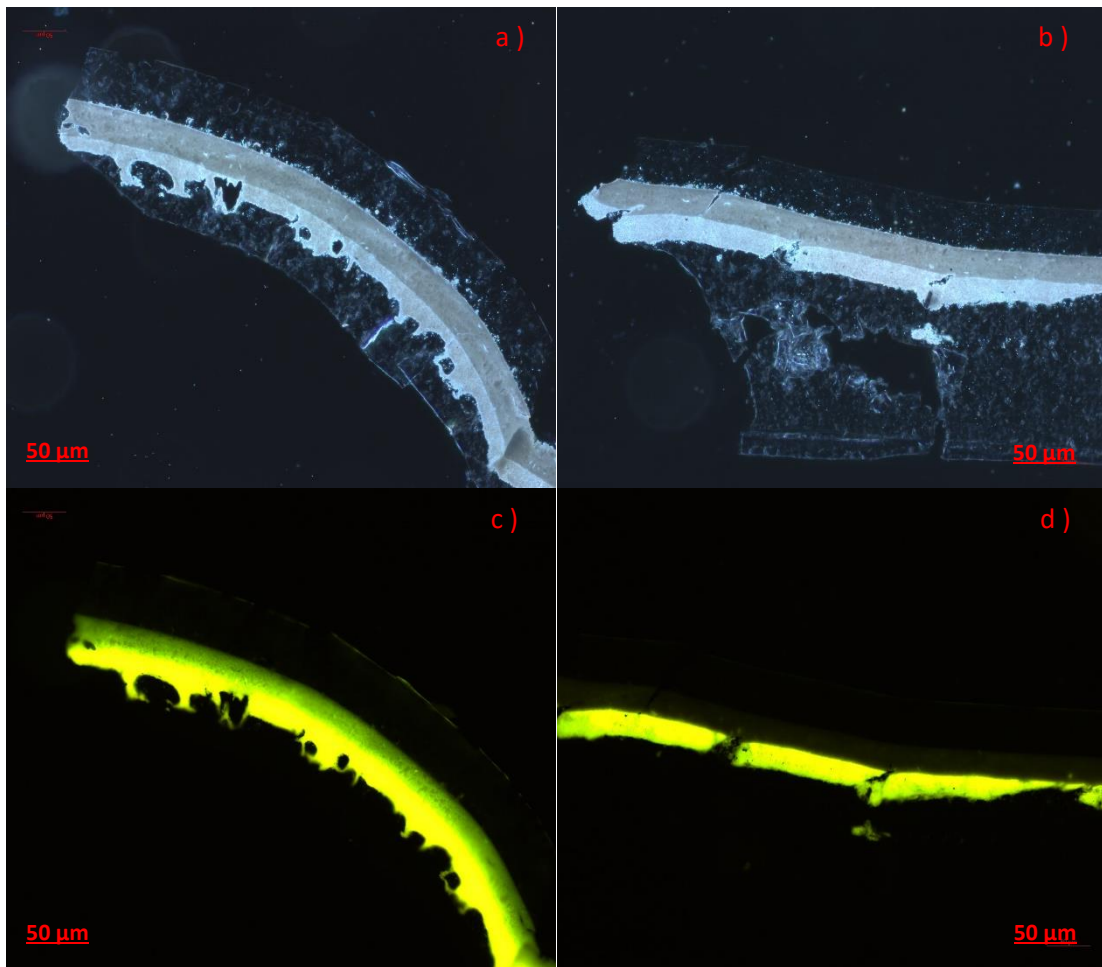
Figure 28. Images of cross-sections of Sample W012_1 and W014 under transmitted light dark field (a and b, respectively) and under Alexa Fluor 488 fluorescence illumination (c and d, respectively).
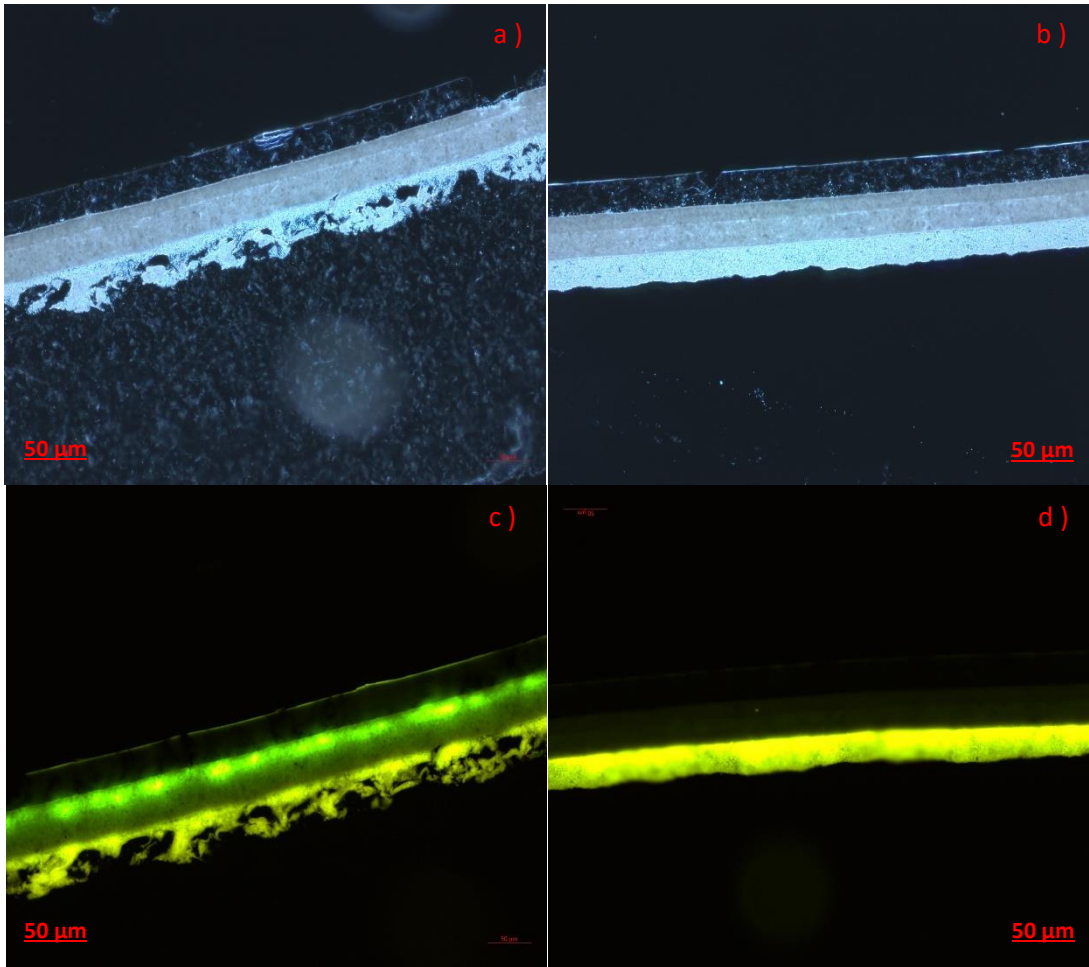
Figure 29. Images of cross-sections of Sample W021_4 and W058_1 under transmitted light dark field (a and b, respectively) and under Alexa Fluor 488 fluorescence illumination (c and d, respectively).
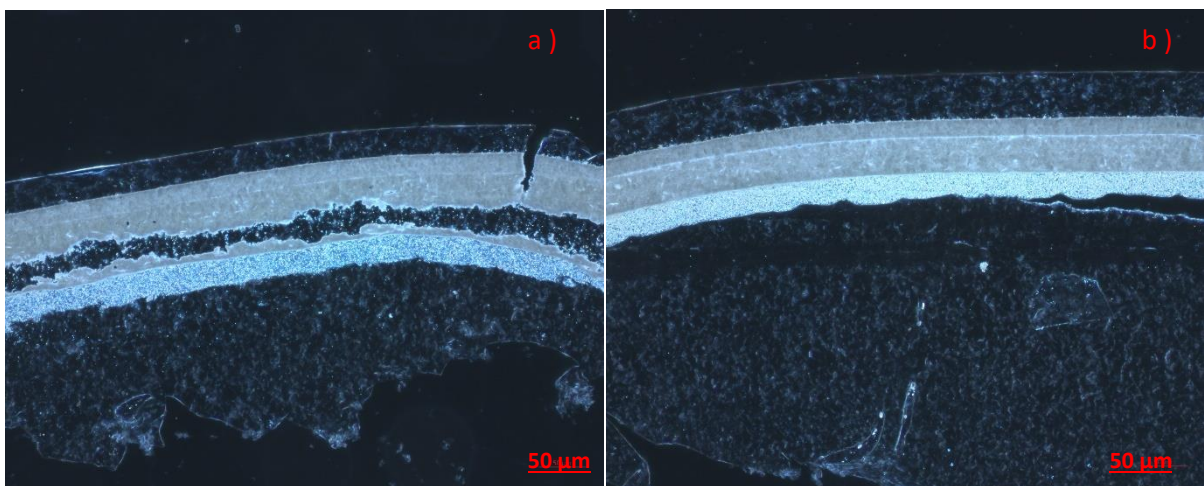
Figure 30. Dark field images of cross-sections of a) Sample W034_1 produced in 2017, and b) Sample W035_1 produced in 2018. They were all Volkswagen NEW BORA produced in the same plant.

Correlation between physical properties and sample origin. Once the optimization and characterization were done, the correlation between physical properties and sample origin was explored. Results showed that the layer sequence of one model would remain the same regardless of whether they were produced in different plants in different years.

However, variation was found in samples of **same model** from **same plant** but **produced in different years**. For example, sample W034_1 and W035_1 originated from two Volkswagen NEW BORA cars produced in 2017 and 2018, respectively. They both had the same color code 'LC9A' and were produced in plant Changchun. Interestingly, variability in the color of the primer and the relative thickness between the clear coat and the basecoat under dark field illumination was observed (see *Figure 30*).

Variability was also found in samples of the **same model and production year** but **produced in different plants**. These samples were W012_1 and W014, two Volkswagen New Lavida produced in plant Nanjing and plant Anting, respectively. They were both produced in 2017 with the color code 'LY9H'. These samples were undifferentiated using transmitted light in bright field and dark field mode. The variation was only observed under Alexa Fluor 488 fluorescence illumination where the basecoat of these two samples showed distinct fluorescence characteristics, as illustrated in *Figure 28*.

Regarding samples originating from the **same model, production year, and assembly plants** (specifically W002_3 and W023_5), they could not be distinguished using microscopic examination.

6.2.5. Standardization of analytical strategy for the whole set

This preliminary study has proved that microscopy is a powerful technique for white automotive paint analysis. The physical properties of each sample including the number of layers, layer sequence, relative layer thickness, color and texture of each layer can be determined. Based on the results discussed in the previous section, the analytical strategy as well as the involved illumination for microscopy was decided as follows. The cross sections of each sample, along with their respective subsamples, will be prepared and mounted using the methodology elucidated in Chapter 6.2.1. Subsequently, these mounted samples will be subjected to observation under transmitted light bright field and dark field illumination, employing a 20x objective. The images of the samples will be captured with the assistance of a color-calibrated microscope. A comparison will then be conducted among the samples, focusing on their layer structure, individual layer color and texture, and the relative thickness of each layer. For the samples with sub-samples, the comparison will first be conducted within the sample subset. For those with subsamples, the intra-sample variability will also be examined. If subsamples have identical physical features, the subsample largest in quantity with the most complete layer structure will be selected to represent this sample. If not, all the different subsamples should be selected and join the whole comparison. Any undifferentiated pairs will be further examined using polarized light and Alexa Fluor 488 fluorescence illumination. The samples will ultimately be organized into groups based on visual comparison, and the discriminating power of each illumination method will be quantified. Additionally, efforts will be made to uncover correlations between physical attributes and identifying factors.

6.3.   Optimization and standardization of the parameters for FTIR analysis

6.3.1. Sample preparation

Automobile paint is often analyzed by FTIR in transmission mode (with the microscope accessory) using cross-section or thin paint smear with or without support (ASTM-E2937-18 ; EPGT(EPG-GDL-002),2022). The cross sections are conventionally cut vertically with respect to paint surface so that a complete layer sequence can be obtained. IR spectra of each layer are then acquired by moving the sample stage until the spot of aperture window is directly onto the desired layer. The aperture size must be adapted with the size of paint layer.

A collaborated project between the University of Lausanne (UNIL) and the Bundeskriminalamt (BKA) was carried out for optimization of inter-laboratory comparability of IR spectra from automotive paint layers in 2018 (Lambert,2018). A strict acquisition procedure including an instrument health check, sample preparation procedure for transmission mode, support selecting (no support, KBr, half diamond cell), and the optimization of measurement parameters was defined. Among these, a horizontal cross section method was introduced, and its effect was studied. This method involves placing the small paint film parallel to the bottom of the mold (rather than perpendicular) when embedding. The cross section obtained from microtome is then a horizontal cross section of each layer. The surface of the section is then large enough to cover the standard spot size of the aperture (normally 50μm×50μm), which can remain steady and allow for a good signal-to-noise ratio (SNR) and good spectra reproducibility.

However, from practical aspect, the sample preparation process proves especially challenging, particularly for those with four layers where the basecoat measures a thin 10-20 μm. The resemblance in color and texture for basecoat and primer surfacer further complicates differentiation within these thin sections. Consequently, assurance about the absence of layer contamination in horizontal cross-sections becomes uncertain. Considering the comparison of performance against the required effort, combined with the complexities and uncertainties linked to horizontal cross-section preparation, their inclusion in FTIR measurements within this thesis is deemed unwarranted. Hence, the conventional method of preparing 5 μm vertical cross-sections was employed. The aperture size must be adapted with the size of paint layer.

The effect of using different supports on spectral performance was studied in aforementioned project. Results showed that the best signal-to-noise ratio was obtained when cross sections were measured without any support. The paint section should ideally be flat to allow for a good spectral contrast and SNR (Chalmers *et al.*,2012b). However, this is not easily achieved when the sample has no support. Thus, a custom-made stage with a size of 75mm x 25mm was specially designed for mounting samples without any support (see *Figure 31*). The stage is a steel sheet containing two lines of eight holes in total with a diameter of 1mm (the top line) and 2mm (the line below). A cross section of the paint sample is placed above the hole,

stretched out and flattened using a drop of methanol. The methanol will evaporate after a while, leaving the section adhered onto the stage. The sample is subsequently placed on the IR microscope stage and analyzed without a support (i.e., there is only air between the sample and the detector). Any empty hole can be used for background acquisition.

Figure 31. A custom-made steel stage for no support sample preparation.

6.3.2. Instrumentation and calibration

In this research, a Thermo iS50 FTIR spectrometer coupled with a Nicolet Continuum FTIR Microscope from Thermo Electron Corp., equipped with a 32x objective and a mercury cadmium telluride detector (MCT/A), is used for all infrared analysis.

Routine health checks for FTIR spectrometers are performed to maintain the stability of the instrument. Calibration of the instrument, however, is always an indispensable step before running experiments. Three standard guideline from ASTM and one from EPGT (ASTM-E1421-99[2015]e1 ; ASTM-E1866-97[2013] ; ASTM-E2937-18 ; EPGT,2022) are used as references for setting up the calibration protocol for FTIR analysis.

Since the MCT detector must be cooled down with liquid nitrogen, the instrument should be allowed 20 minutes to settle after the addition of liquid nitrogen. The signal of the instrument is then checked using the software OMNIC 9.1 and recorded in the instrument's logbook. The calibration will then be executed using a standard matte-finish polystyrene film (NIST SRM1921b certified polystyrene, approximately 38-μm thick, having a 2.5-cm aperture). Two spectra acquired and stored following the last major instrument maintenance are used as references, namely Reference 1 and Reference 2, respectively. Reference 1, in terms of single-beam energy spectrum of an empty beam, is a background acquisition spectrum with no support (only air is in the optical path during acquisition). Reference 2 is a transmittance spectrum of the polystyrene standard. The details are discussed as follows:

1) Energy spectrum test

This test is setup for examination of any changes in energy level. Two background spectra are acquired one after each other and overlaid to detect any differences. If no difference is observed, one of the acquired background spectra is then compared with Reference 1 and used to calculate the energy ratio at 4000/2000 cm^{-1}, 2000/1000 cm^{-1} in the range of 95 to 105 % T. The value is then noted.

2) 100%-line test

This test is performed to check if the noise or baseline is within the accepted range. The 100% transmittance line of the background spectrum displays the ordinate range, which should be between 99-101%. Root mean square (RMS) values in the range of 2000 cm^{-1} to 2200 cm^{-1} should also be recorded.

3) Polystyrene Subtraction Test

A new transmittance spectrum of the polystyrene standard needs to be acquired and then overlaid with Reference 2. The reference spectrum is then subtracted from this new spectrum. The residue is then plotted over a range of −1 to +1 % T and interpreted by checking how much residue is left.

4) Automated Polystyrene check

An automated application programmed by Danny Lambert based on the recommendations of the National Institute of Standards & Technology (NIST) was designed for a health check of the FTIR instrument. This application provides a warning when the frequency scale (x-axis) should be corrected by a specific technician. The material used for this check is certified polystyrene from NIST (SRM1921b). Six IR spectra of the certificated polystyrene should be acquired using the request acquisition parameters. They are then loaded in the application for an automated calibration of the sum as well as the difference between the chosen peak mean and standard deviation. This procedure results in a peak table where a "pass" or "fail" of the test will be indicated (see *Figure 32*).

Spectrum1	Spectrum2	Spectrum3	Spectrum4	Spectrum5	Spectrum6	Peak mean	Peak sd	Peak NIST	Test result	Practical limits
841.73	841.76	841.64	841.74	841.77	841.59	841.71	0.07	842.10	PASS	1.78
906.81	906.77	906.77	906.78	906.79	906.78	906.78	0.02	906.82	PASS	0.99
1028.54	1028.53	1028.55	1028.54	1028.54	1028.52	1028.54	0.01	1028.42	PASS	1.03
1069.34	1069.32	1069.42	1069.33	1069.41	1069.40	1069.37	0.04	1069.27	PASS	1.32
1154.66	1154.69	1154.65	1154.70	1154.66	1154.66	1154.67	0.02	1154.62	PASS	0.99
1583.39	1583.40	1583.40	1583.40	1583.41	1583.40	1583.40	0.01	1583.04	PASS	0.99
1601.39	1601.39	1601.39	1601.40	1601.39	1601.39	1601.39	0.00	1601.38	PASS	0.99
2849.68	2849.68	2849.69	2849.71	2849.81	2849.70	2849.71	0.05	2850.20	PASS	0.99
3001.69	3001.69	3001.67	3001.68	3001.67	3001.66	3001.68	0.01	3001.40	PASS	0.99
3026.01	3026.08	3026.18	3026.12	3026.20	3026.11	3026.12	0.07	3026.44	PASS	0.99
3060.05	3060.01	3060.01	3060.06	3060.01	3060.04	3060.03	0.02	3060.14	PASS	0.99
3082.14	3082.15	3082.14	3082.15	3082.14	3082.14	3082.14	0.01	3082.22	PASS	0.99

Figure 32. A peak table of the automated polystyrene check showing a "pass" test result.

In addition to the utilization of standard calibration materials, an 'in-lab' reference was formulated for the purpose of quality control. The 'in-lab' reference is a sample selected from the sample set, serving as an internal standard throughout the study. This 'in-lab' standard reference was selected from the sample having more than one subsample with a thicker layer. To ensure consistency, a cross section of this reference sample was prepared and mounted permanently on a custom-made steel sheet sample stage. This approach guarantees the unwavering status and orientation of the reference sample. Prior to commencing each sample analysis session, the basecoat of this reference was subjected to measurement using a fixed aperture size of 50 x 15 µm at a random location. The resultant data was then stored, following the calibration procedures that were previously described.

6.3.3. Optimization and standardization of instrumental settings

Since the FTIR instrument and the samples involved in different automobile paint study can never be the same, the instrumental settings from different literature often vary a lot. When samples are measured by FTIR spectrometer equipped with a microscope, the MCT detector is the only choice. Consequently, the spectral range is often in the 650/700 - 4000 cm^{-1} or 400/450 - 4000 cm^{-1} range if It is a broadband MCT detector (Massonnet and Stoecklein,1999b; Ryland *et al.*,2001; Kruglak *et al.*,2019). The objectives and gains are seldom mentioned in the literature. The number of scans are not standardized and vary greatly in literature, e.g. 64 (Beauchaine *et al.*,1988), 128 (Wright,2010; Kruglak *et al.*,2019), 200 (Reynolds *et al.*,2018), 256 (Zięba-Palus and Borusiewicz,2006; Zięba-Palus *et al.*,2011), 512 (Zięba-Palus *et al.*,2008a; Zięba-Palus and Trzcińska,2013). The variable aperture size is often adapted to the layer thickness. A resolution at 4 cm^{-1} is mostly used. From the literature, it is difficult to determine which instrumental settings are ideal for this study.

Thesis of Muehlethaler (Muehlethaler,2015) employed a design of experiment to assess various factors, including resolution, number of scans, sample thickness, paint type, and FTIR measurement window size, with the aim of determining optimal measurement conditions. His findings indicated that among these factors, paint type exhibited the least influence. Consequently, the measurement conditions delineated in his thesis can be readily extended to the samples examined in the current study. In conjunction with the previously referenced investigation, the initially established optimal measurement conditions, which have undergone evaluation, utilization, and recommendation not only within Muehlethaler's thesis but also in the aforementioned project (Lambert,2018) and the ASTM standards and EPGT guidelines, are comprehensively presented in *Table 14.*

These measurement parameters are initially applied to the select sample set to evaluate their efficacy, and subsequently adjusted, if necessary, based on the samples' performance. Each layer of every sample underwent five measurements, each measurement was measured from different locations of the same section. Quality and reproducibility of spectra were the guiding criteria for parameter optimization.

Table 14. Instrumental settings for validation study.

PARAMETERS	CONDITIONS
Instrument	Thermo iS50 FTIR spectrometer
Acquisition Mode	Transmission though FTIR microscope
Detector	MCT/A
Apodization function	Blackmann-Harris
Objective	32x
Spectral Range	650-4000 cm^{-1}
Gain	Automatic
Resolution	4 cm^{-1}
Scans	32
Aperture Size	Depend on the thickness of layer

6.3.3.1.   Spectra quality and reproducibility

The quality of spectra was initially visually inspected, adhering to the criteria outlined in the ASTM standard and EPGT guidelines. The reason for the observed problems and solutions to the problems were investigated. The assessment results were then documented in *Table 15*.

Table 15. Spectra quality criteria and performance within the selected sample set.

PARAMETER	CRITERIA	OBSERVED PROBLEM	CAUSE	SOLUTIONS
Transmission Range	Optimal range: 100% to 10%	1) Baseline exceed 100% 2) Baseline lower than 80%	1) Incorrectly acquired background spectrum 2) Scattered and reflected radiation	1) Recollect background and redo measurement 2) Remount the cross section on the sample stage
Baseline	Stable and flat	Curved baseline	Less flat sample surface	1) Remount the cross section on the sample stage
Noise	Smooth	Noisy baseline	1) too small aperture size 2) low number of scans	1) Enlarge aperture size if possible 2) Increase number of scans

The acquired spectra generally exhibited good quality upon visual inspection. The majority of identified issues stemmed from suboptimal sample preparation and incorrect background spectrum acquisition. These problems can be effectively resolved through sample re-preparation or background spectrum re-acquisition. Conversely, the impact of smaller aperture sizes is inevitable due to the inherent nature of thin paint layers. Additionally, the issue of noise can be mitigated by increasing the number of scans.

The evaluation of reproducibility involved assessing intra-sample and inter-sample variability using Pearson correlation coefficients, a statistical method that calculates the similarity between different spectra. This was carried out on IBM® SPSS® Statistics V.28.0.1.1(14) software. The resulting intra-sample variability within five replicates of each layer for every individual sample was calculated, along with the inter-sample variability for each layer. This information is visualized in *Figure 33.*

Overall, the study's reproducibility yielded positive results, with low levels of intra-sample variability and prominent inter-sample variability. Nevertheless, It is important to acknowledge that certain measurements exhibited notable cases of intra-sample variability. This can be primarily attributed to inconsistent baseline quality, a consequence of insufficient sample preparation. For instance, the significant intra-sample variability observed in the clearcoat can be attributed to this factor. Additionally, noise introduced by employing a small aperture size has contributed to greater intra-sample variability, as evidenced in the basecoat of sample W060.

Addressing these concerns, employing a flatter section surface can effectively mitigate abnormal baselines. Regarding noise reduction, enlarging the aperture size isn't always feasible. Alternatively, augmenting the number of scans serves to minimize background noise in spectra, concurrently enhancing the signal-to-noise ratio.

In the assessment, 32 scans and 64 scans were compared for reproducibility. The outcomes are illustrated in *Figure 34*. The findings indicate that for aperture sizes smaller than 50x15 µm, 64 scans lead to lower intra-variability. Conversely, when the aperture size meets the minimum optimal threshold (1250 µm or 50x25 µm), increasing the number of scans doesn't significantly affect intra-sample variability. Consequently, considering a balance between improving measurements for thinner layers and not excessively prolonging acquisition time, the choice of 64 scans was favored over 32 scans.

The internal standard reference (basecoat) was consistently measured before the commencement of each experiment, enabling the assessment of instrument stability's reproducibility. The lowest level of intra-sample variability was identified across different measurement days, as shown in *Figure 35*. This was also illustrated in *Figure 33* (highlighted in red rectangular) to have a parallel comparison with other intra-sample variability. The predominant source of variability stemmed from random measurement position, resulting in the capture of a more intensity talc peak.

Given the overall homogeneity of the samples and the low intra-sample variability, taking into account the scale of the sample set, it was determined that a minimum of 3 replicates would be suitable. However, in cases where the samples exhibit heterogeneity, it is necessary to increase the number of replicates for a more comprehensive representation.
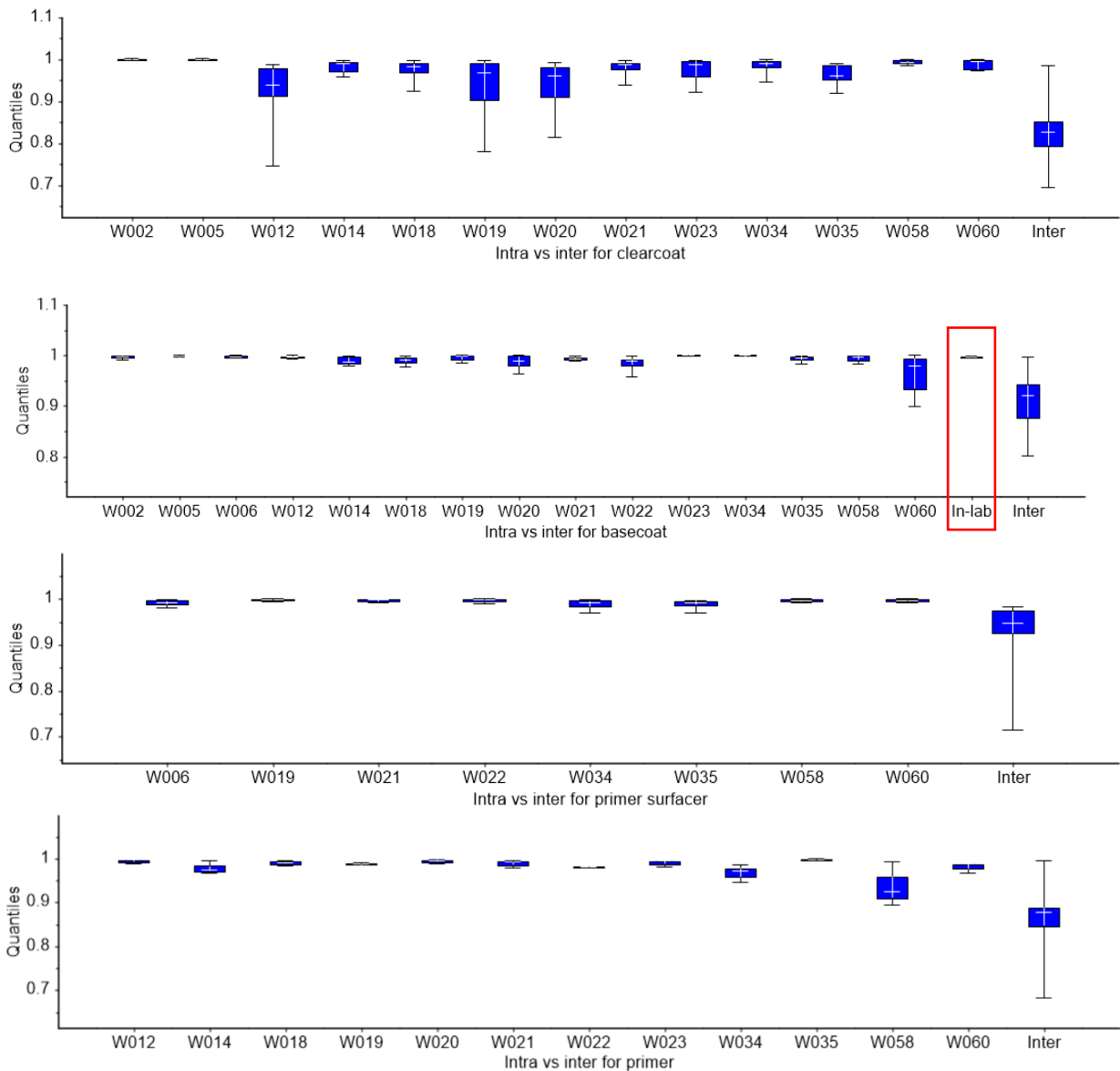
Figure 33. Box plots illustrating the intra-sample and inter-sample variability of each layer within the chosen sample set (calculated by raw spectra).
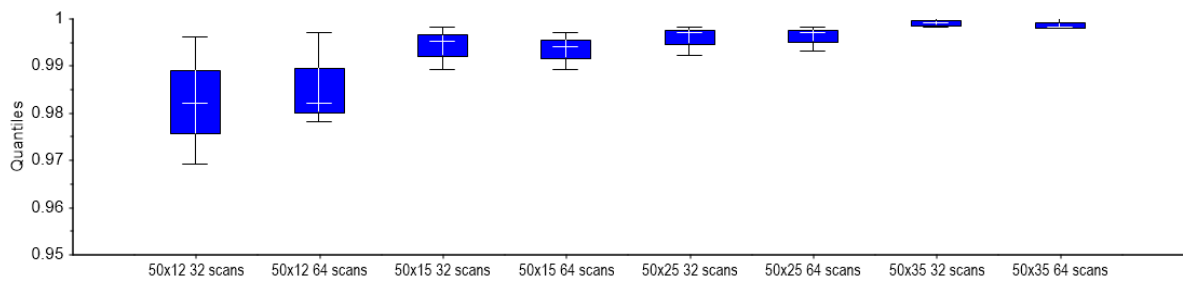
Figure 34. Box plots comparing the intra-sample variability between 32 scans and 64 scans, utilizing varying aperture sizes (aperture size in μm).

Mean:	0.9956
Max:	0.998
Min:	0.993
Std Deviation:	0.00163882
Variance:	2.68573E-06
Q1:	0.9945
Q3:	0.997
Median:	0.996
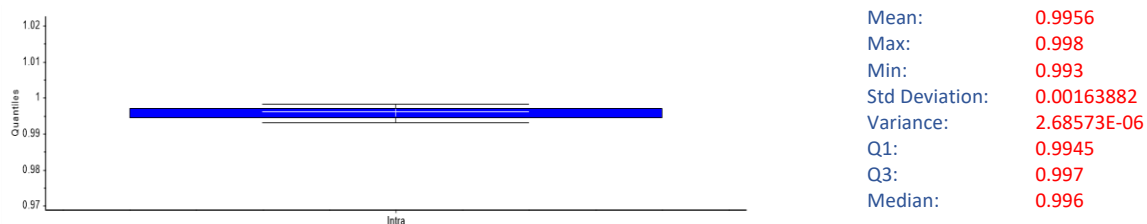
Figure 35. Over time reproducibility check result using internal standard (IR).

6.3.3.2. Pretreatment

Indeed, while obtaining optimal spectrum measurements is the most efficient way to mitigate variability, It is not always achievable due to factors such as sample characteristics, quantities, and potential external contamination. Consequently, post-measurement data pre-processing becomes a crucial step in multivariate processing. Standard normal variate (SNV) and detrending with a polynomial order of 2 (det2) proved to be an effective pretreatment process that enables optimum correction of the scattering effects encountered in the raw spectra and offers many practical advantages for its implementation (Muehlethaler,2015). This pretreatment method was chosen to test its adaptability for this sample set. Samples with layers exhibiting larger intra-variability were selected for the test. The results, presented in *Figure 36*, reveal a substantial reduction in intra-sample variability and an increase in inter-sample variability.
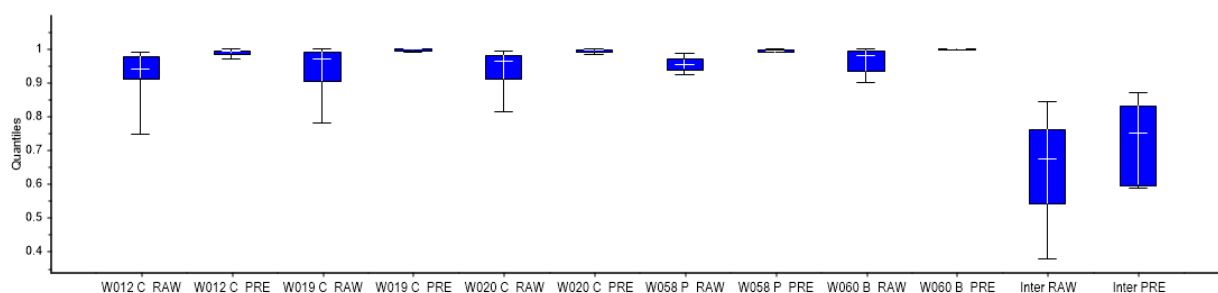
Figure 36. box plot illustrating the comparing the intra- and inter-sample variability between raw data and pretreated data (SNV + Detrending 2).

Principal Component Analysis (PCA) was also performed on both raw spectra and pretreated data to visualize the cluster projection, as shown in *Figure 37*. The application of pretreatment notably clustered similar samples and increased the differentiation between different

samples. In some cases, two samples that were almost indistinguishable (Pearson correlation = 0.99) remained challenging to separate.

Consequently, the SNV with detrending technique demonstrated its effectiveness for this sample set and was chosen as the preferred pretreatment method for raw spectra.
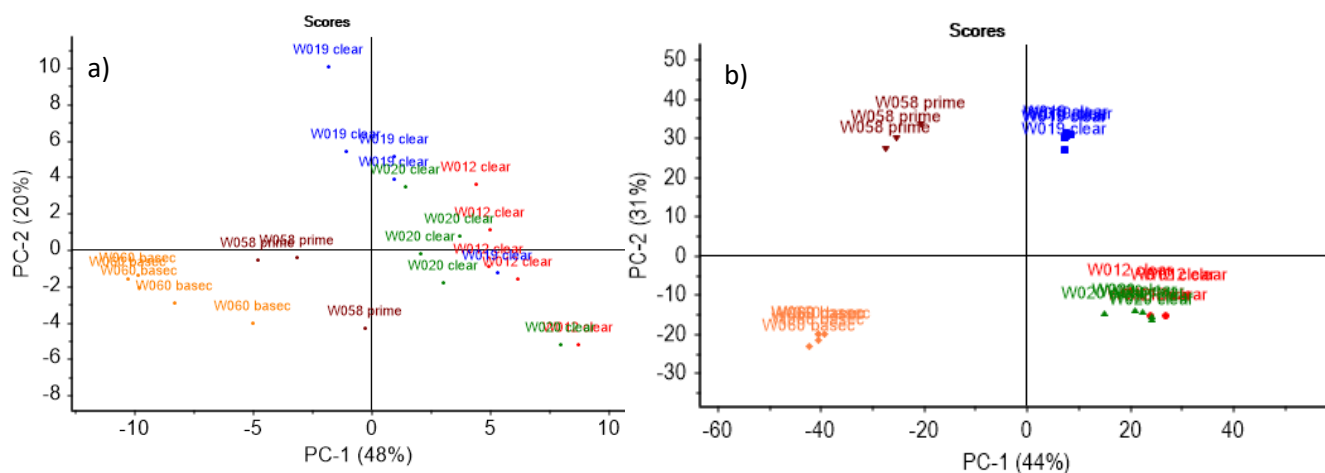
Figure 37. PCA score plot showing the projection of raw spectra (a) and pretreated spectra (b).

6.3.3.3. Statistical Validation

Since the experimental parameters and pretreatment methods have been established, a statistical classification and validation process was conducted using LDA as a single-classification method, as well as SIMCA as a multi-classification method. The clearcoat dataset was chosen for this validation due to its significant intra-sample variability.

Prior to conducting the statistical validation, the acquired spectra underwent a visual quality check, followed by characterization and comparison. It was observed that spectra within the range of 3100-2828 and 1800-680 cm^{-1} exhibited abundant peaks corresponding to various functional groups and compounds. This spectral range was selected for statistical analysis as it encapsulated the complete chemical information of a sample while minimizing irrelevant data.

To streamline the subsequent supervised methods, unsupervised method PCA was initially conducted on the pretreated data to reduce the number of variables. HCA was also conducted for the cluster analysis.

The visual characterization, along with the results obtained from both visual comparison, PCA separation and HCA clustering, are consolidated and presented in *Table 16*.

Table 16. Visual characterization and comparison, PCA and HCA grouping result (n=13).

Chemical class	Visual grouping	PCA	HCA (Complete linkage + correlation)
PUR+STY	W002, W020, W023 W012, W014, W018	W002 W020, W023 W012, W014, W018	W002, W012, W014, W018, W020, W023
PUR	W005	W005	W005
ACR+STY+MEL+PUR	W019 W021 W034 W035, W058, W060	W019 W021 W034 W035, W058, W060	W019 W021 W034 W035, W058, W060
Discriminating power	**88.5%**	**91%**	**77%**

PCA was initially conducted on the complete clearcoat dataset, as depicted in Figure 38. The score plot was generated utilizing the first two principal components (PC), which collectively contribute to 88% and 5% of the overall variance, respectively. This PCA process effectively segregates samples into two primary groups based on the chemical composition of the clearcoat. Notably, the ACR sample group can be further subdivided into two distinct subgroups by considering the second principal component (PC2), which is due to the intensity of melamine peak according to the loading plot of PC2. However, within each initial PCA-defined group, distinguishing between individual samples was challenging due to their minimal differentiation. In response, additional PCA analyses were undertaken on the subsets of samples that exhibited such limited differentiation (as indicated by the dashed line). When samples were found to be randomly dispersed across the entire score plot, they were deemed undifferentiated. For instance, samples like W035, W058, W060, or W20, W23, as well as W012, W014, W018, fell under this category of undifferentiated distribution.

The PCA separation closely mirrors the outcomes obtained through visual comparison. It efficiently visualizes the underlying data structure and groupings in a straightforward and rapid manner. Consequently, PCA was included as a robust alternative that facilitates the process of sample discrimination in further analysis.

In contrast, the results from HCA exhibit diminished discriminative power, and determining a clear separation criterion becomes challenging. Achieving a more reasonable and reliable separation necessitates the generation of a Receiver Operating Characteristic (ROC) curve, which demands a substantial investment of effort. The clustering outcomes, unfortunately, fall short of meeting the desired standards. As a consequence, this analysis will not be implemented in the subsequent stages.
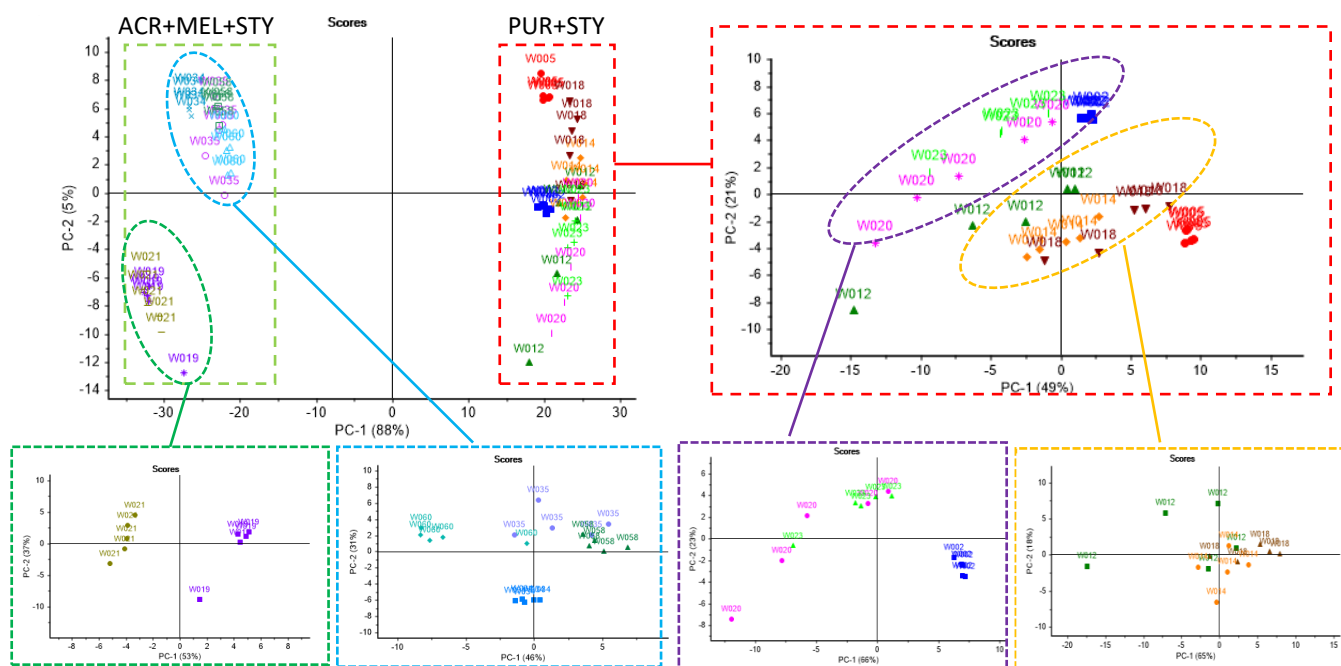
Figure 38. PCA score plot constructed for the IR spectra of the clearcoat, according to the first two principal components (PCs). Subsequent PCA analyses were carried out on specific groups of samples (identified by dashed lines) that initially displayed minimal differentiation.

The validation of the statistical models was performed for each supervised model using an independent validation set. Since the dataset consisted of more variables than samples, PCA scores were employed as the input data for LDA. Moreover, due to the limitation of the available dataset, the maximum number of usable components was confined to 3. SIMCA was also based on the PCA model. From the 5 replicates, a random selection of 3 replicates formed the training set for each method. The remaining 2 replicates constituted the validation set, utilized to assess method performance metrics such as classification accuracy, false positive rate, and false negative rate. The results were presented in *Table 17*.

Both classification methods have yielded generally favorable outcomes, with LDA exhibiting a higher rate of correct classification. It is worth noting that the high number of false positives observed in SIMCA is attributed to the existence of samples that are indistinguishable. In the context of SIMCA, these undifferentiated samples were categorized into multiple classes.

When the samples possess distinct discriminative characteristics, LDA proves effective in achieving accurate classifications or predictions. However, in situations where a significant number of samples are difficult to differentiate, LDA can lead to an increased occurrence of false positives. On the other hand, SIMCA presents an advantage by offering a broader range of potential sources for unknown samples, which proves more practical for forensic paint investigation.

80

Table 17. Performance of two classification methods

PARAMETNER	LDA	SIMCA (5%)
TRUE POSITVE	17	23
FALSE POSITIVE	9	65
FALSE NEGATIVE	9	2
TRUE NAGATIVE	303	247
CORRECT CLASSIFICATION RATE	0.9467	0.7988
MISCLASSIFICATION RATE	0.0533	0.1982
SENSITIVITY	0.6538	0.9200
SPECIFICITY	0.9712	0.7917
FALSE NEGATIVE RATE	0.3462	0.0800
FALSE POSITIVE RATE	0.0288	0.2083
POSITIVE PREDICTIVE POWER	0.6538	0.2614
NEGATIVE PREDICTIVE POWER	0.9712	0.9920
GENERAL DIAGNOSTIC POWER	0.9231	0.9231

6.3.4. Standardization of FTIR analysis protocol of whole sample set

As outlined in the preliminary study, the optimized instrumental parameters produce high-quality spectra that exhibit strong consistency, thereby effectively presenting extensive chemical insights from each sample. The preprocessing techniques facilitate maximal variation between samples and minimal variability within individual samples. Reliable statistical approaches such as PCA and LDA offer substantial support for distinguishing between samples and enabling classification. The validation of the instrumental parameters, preprocessing steps, and statistical model was conducted using LDA and SIMCA, thereby confirming their suitability for implementation. The procedure for IR analysis of the entire sample collection is summarized in *Table 18*.

It is essential to emphasize that while this protocol forms a foundational criterion and should be uniformly applied to all samples, practical scenarios might necessitate adaptability based on the conditions of each sample. In certain instances, modifying multiple factors may be necessary to ensure optimal quality. It is of utmost importance to document any such alterations.

Table 18. Protocol for the IR analysis of the whole sample set in this thesis.

Step 1: Sample preparation		
• Prepare vertical cross sections of 5 µm thickness following the procedure described in chapter 6.2.1		
• Mount the cross section on the custom-made steel stage.		
• Ensure that the surface of the cross section is flat.		

Step 2: IR measurement		
Instrument calibration	Signal check, 100% line test, Polystyrene check	
Instrumental settings	Instrument	Nicolet iS50 FTIR spectrometer
	Acquisition Mode	Transmission though FTIR microscope
	Detector	MCT/A
	Apodization function	Blackmann-Harris
	Objective	32x
	Spectral Range	650-4000 cm^{-1}
	Gain	Automatic
	Resolution	4 cm^{-1}
	Scans	64
	Aperture size	Depend on the thickness of layer
Reproducibility check	Measure the basecoat of internal standard using an aperture size of 50 x 15µm before conducting the experiment	
Replicates	• Begin with a minimum of 3 replicates. • Increasing the number of replicates if significant variability observed.	

Step 3: Spectra quality check		
• Visually inspect the acquired spectra for quality assurance (% transmission, baseline, noise, defects, contaminations).		
• Re-prepare and re-measure the sample if any issues are identified.		

Step 4: Pretreatment	
Methods	SNV+ detrending with a polynomial order of 2
Software	Unscrambler X 10.1 (CAMO software)
Spectra range	3100-2828 and 1800-680 cm^{-1}

Step 5: Visual characterization and Classification	
• Identify functional groups through comparison with literature and available databases.	
• Perform visual comparison and classification based on the presence/absence of peaks or relative intensity.	

Step 6: Statistical discrimination and classification		
Reproducibility Check	Measure intra sample variability of internal standard	
Methods	PCA	• Data structure visualization • Intra sample variability check.
	LDA	• Discrimination • Classification
Software	• IBM® SPSS® Statistics V.28.0.1.1(14) • Unscrambler X 10.1	

Step 7: Validation (Blind test)	
Measurement	5 samples measured by another person using the same protocol
Classification	• PCA projection • LDA or SIMCA prediction
Software	Unscrambler X 10.1

6.4.   Optimization and standardization of the parameters for Raman analysis

6.4.1. Sample preparation

A study by Lambert *et al*. demonstrates that sample preparation method has a significant influence on the variability of Raman measurements (Lambert *et al*.,2014). The authors recommend that automobile paint samples should be polished and then directly analyzed on the surface. Since the inclusions of samples are already prepared for optical examinations, the rest resin blocks are used for Raman measurements. The surface of inclusions (also the transversal surface of paint sample) are polished by PRESI Mecatech – 234 automatic polishing machine using a four-steps procedure which has been programmed into the machine by Lambert (Lambert,2017). Detailed parameters of each polishing step are displayed in *Table 19*. After polishing, the samples are dried under air flow and the surface is cleaned with ethanol.

Table 19. Four-steps procedure and parameters for inclusion polishing

Step	Rotation Speed of Polishing Platen	Rotation Speed of Polishing Head	Force per Specimen	Time	Reflex magnetic pad	Polishing Agents
Step 1	120RPM*	80RPM	0.00daN	15s	P2400 (10μm grit)	Continuous water flow
Step 2	120RPM	80RPM	0.00daN	15s	P4000 (5μm grit)	Continuous water flow
Step 3	120RPM	80RPM	0.50daN	60s	NT3μ	Diamond Suspension Reflex LDM 3μ
Step 4	120RPM	80RPM	0.00daN	120s	NT1μ	Diamond Suspension Reflex LDM 1μ

* RPM: rotations per minute

6.4.2. Instrumentation and calibration

As previously emphasized, in order to minimize variations caused by the instrument, only one Raman instrument is used for acquisition of Raman spectra of the samples throughout this research. The Raman instrument used in this research is the Renishaw Invia Confocal Microscope equipped with various laser sources with operational wavelengths of 488 and 515 nm (Argon, Ar + Laser), 633 nm (Helium and Neon, He-Ne Laser), and 785 nm (Near infrared, diode lasers, NIR Diode Laser).

Systematic errors produced by the instrument nevertheless exist. Hence, calibration procedures should be performed prior to conducting Raman measurements. Calibration of Raman spectroscopy involves mainly two types: the Raman wavenumber shift calibration in

the abscissa dimension and the Raman relative intensity response calibration in the ordinate dimension (Mann and Vickers,2001). Two ASTM standard guides were published based on these topics (ASTM-E1840-96[2014] ; ASTM-E2911-13) and are used as references for calibration.

6.4.2.1. Raman wavenumber shift calibration

Instrument calibration is an important step for maintaining instrument health and the stable output of spectra. Modern Raman Spectrometers are all equipped with an internal standard for quick calibration. The standard is a silicon wafer mounted inside the instrument which will present a peak at 520 cm^{-1}. It is designed for fast calibration that can performed on a daily basis before sample analysis and/or after changing between lasers. However, due to its one single peak, this particular calibration may lack frequency accuracy. A more complex standard is thus required.

The internal standard sample, which is described in chapter 6.3.2 emerges as an ideal choice. This internal standard was prepared using the standard procedure described in the previous section. The basecoat of this reference was measured under the same conditions before running sample analysis. The acquired spectra are then compared with each other to see if wavenumber shift is of a reasonable value (with standard deviations less than 1.0 cm^{-1}). The standard spectra can additionally be useful for monitoring the instrument stability.

6.4.2.2. Correction of Raman relative intensity response function

Raman Relative intensity response calibration is another key point for accuracy of Raman result. The procedure allows for comparison of Raman spectra acquired from differing instruments, excitation, wavelengths, and laboratories. Instrumental response will vary with different machines due to the use of different laser excitation wavelengths, and detector efficiencies. It is also possible to observe variations on the same instrument after a component change or after service work has been performed (ASTM-E2911-13). The ASTM Standard Guide for Relative Intensity Correction of Raman Spectrometers is a comprehensive protocol for this calibration. The following procedure is summarized based on this standard.

The simplest way to check Raman intensity is to compare the peak intensity at 520 cm^{-1} of the silicon reference. Calibration of the Raman intensity (y axis) allows to correct for variations in spectral peak intensities by obtaining a relative luminescence intensity correction curve using NIST SRM standard fluorescent glass. It has a smooth surface on one side and a frosted surface on the other side. The frosted surface is used for calibration. Each glass is equipped with a calibrated certified relative spectral intensity that could be used to produce the corrected curve. Raman shift wavenumbers calibration needs to be accomplished and verified before this calibration. To achieve the best accuracy, the luminescence spectrum of the glass must be acquired over the same Raman range, with the same data point density, and using the

same instrumental parameters as for sample data acquisition. After acquisition, the relative intensity correction curve is obtained by dividing the calculated certified relative spectral intensity by the measured luminescence spectrum of the SRM. The generated curve can be then used for correction of sample measurements by multiplying it by the measured Raman spectrum of the sample.

6.4.3. Preliminary study for the selection and optimization of instrumental settings

Although it is well known that Raman spectroscopy can provide reliable information about pigments as well as extenders used in paint, little research has been conducted on automobile white paint. Studies of white paint are mostly conducted on single or multilayer white architectural paint(Bell *et al.*,2005a; Bell *et al.*,2005b; Bell *et al.*,2012; Stewart *et al.*,2012). These studies have demonstrated the remarkable discriminatory potential of Raman spectroscopic methods in distinguishing between various white paint samples, with the 785 nm diode laser being the preferred choice for white paint analysis. Despite the compositional similarity between white automobile paint and white architectural paint, the efficacy of Raman spectroscopy in discriminating white automobile paint requires validation. Moreover, the experimental parameters for examining white automobile paint necessitate optimization, tailored to the specific instrument.

A preliminary study, conducted as a master project Chuankai Wang, has delved into this subject matter (WANG *et al.*,2019). The project focused solely on the basecoat within the select sample set (n=15). It concluded that the 785 nm laser effectively unveiled optimal sample information within the range of 200 to 2000 cm^{-1} and exhibited strong discriminatory capabilities, achieving an 85.7% discriminating power (15 distinguishable pairs out of 15 samples).

However, the project only employed a single sample for the experimental parameter optimization, which proved inadequate for assessing inter-sample variability stemming from the laser utilization. The possibility of alternative lasers offering significant discrimination while yielding lower-quality spectra remains uncertain. Additionally, whether the 785 nm laser is indeed the most suitable choice for other paint layers has remained unexplored. The study also encountered reproducibility issues that require further investigation. Thus, there arises a necessity to undertake a renewed selection and optimization of instrumental settings using a more extensive sample pool.

Consequently, a total of three samples have been carefully chosen for the purpose of optimization. Within this selection, two types of layer structures are represented – one with three layers and two with four layers. These samples exhibit discernible variations in their clearcoat and basecoat, while also displaying undifferentiated primer surfacers and similar primers, as determined through IR analysis. Following the parameter optimization, a preliminary study was undertaken. This study involved employing the optimized parameters

to the select sample set of 15 samples for adaptability checks, to ensure that the optimized parameters are effectively applied and validated across the broader numbers of samples.

Sample preparation.

The resin block containing each sample was polished using a PRESI Mecatech–234 automatic polishing machine following the four-step procedure listed in *Table 19*.

Optimization of the experimental parameters.

The magnification of the microscope was first tested. Samples were observed using the 5x, 20x, 50x, and 100x objectives. It was found that 5x and 20x magnification were too low to precisely locate the desired measuring point while 100x magnification was too high to see the entire layer sequence as well as to obtain a focused plan. The 50x objective (NA 0.75) met the above requirements and was therefore selected.

Regarding the spectral range, the primary bulk of information pertaining to pigments and extenders was all presented within the lower region. This was confirmed by conducting measurements within both the 200-4000 cm^{-1} range and the 200-2000 cm^{-1} range. Notably, the spectra held minimal valuable insights within the span of 2000-4000 cm^{-1}. Consequently, the decision was made to narrow down the wavenumber range for subsequent measurements to between 200 and 2000 cm^{-1}.

Subsequently, an examination of laser performance was conducted. Raman signals obtained using the 633nm laser were significantly obscured by fluorescence, revealing no meaningful information. Similarly, the 515nm and 488nm lasers yielded only minimal information, accompanied by poor spectral quality. Among all four lasers tested, the 785nm laser emerged as the most suitable choice, not only for the basecoat but also for other layers. It was also found that the limited information garnered from the 515nm and 488nm lasers largely overlapped with the data acquired through the 785nm laser. The information derived from the 515nm laser did not contribute any supplementary value to the characterization or differentiation process. In contrast, the 785nm laser provided the maximum amount of sample information, coupled with excellent spectral quality in general.

In terms of laser power and exposure time, their settings needed to be tailored to the signal response of the samples. Thus, standardization was not feasible. Typically, the exposure time was set at 10 seconds, and the laser power should be gradually increased to its maximum intensity without causing damage to the sample. This approach aimed to achieve a spectrum characterized by an improved signal-to-noise ratio, and thus, good quality.

Once the laser power and exposure time have been optimized but continue to yield a relatively noisy spectrum, the next step involves increasing the number of accumulations. Raman accumulation serves a role similar to the scans in IR analysis. It refers to the process of repeatedly measuring Raman spectra at the same location or under the same conditions and then combining or averaging these spectra to improve the signal-to-noise ratio and obtain a more reliable and accurate Raman spectrum.

Figure 39 illustrates a comparison between Raman spectra obtained from a single measurement and those obtained through 8 accumulations. Notably, the baseline of the 8 accumulations displays a smoother profile in contrast to the single measurement. Furthermore, *Figure 40* provides a boxplot representation of the intra-sample variability assessment. Using 8 accumulations can significantly minimize the intra-sample variability and therefore included in the instrument optimization.
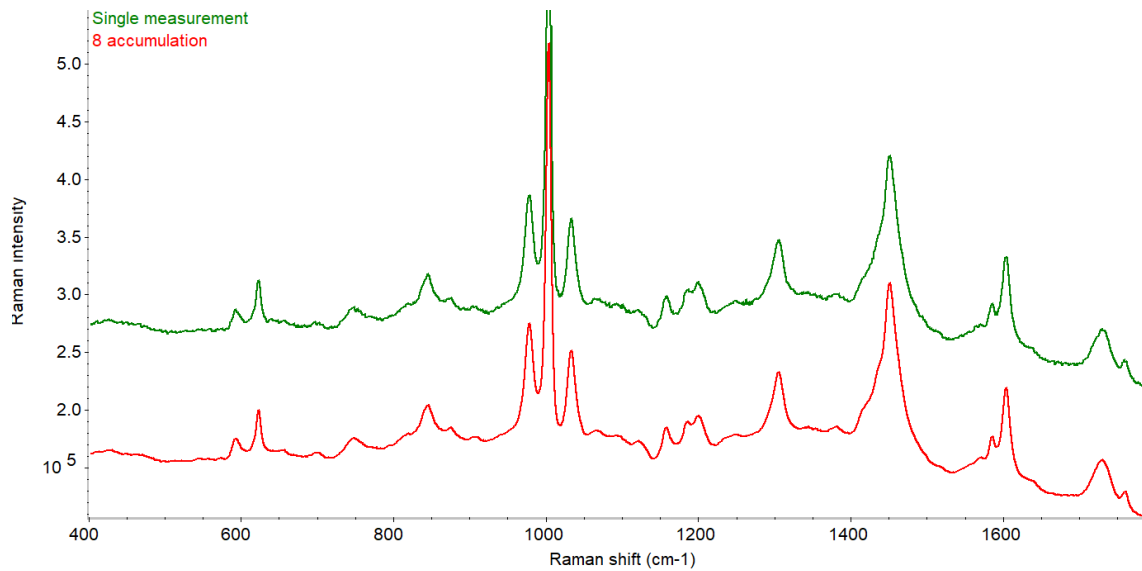
Figure 39. Spectra quality comparison between single measurement (green) and 8 accumulations (red).
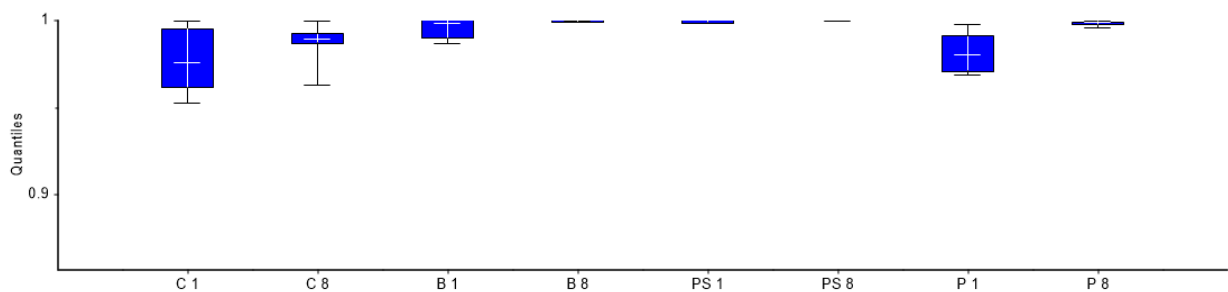
Figure 40. Box plots illustrating the intra-sample of each layer for single measurement and 8 accumulations. C for clearcoat, B for base coat, PS for primer surfacer and P for Primer.

Based on the previous assessments, the optimized parameters for Raman measurement is summarized in *Table 20*.

Table 20. Optimized Raman spectroscopy parameters used in this preliminary study.

Laser	objective	Laser power	Exposure time	Spectra range	Accumulation
785 nm	50x	depends	10s	200-2000 cm^{-1}	8

Subsequently, this configuration was implemented for the chosen sample set to undertake performance evaluation and validation. Given that 1) basecoat had already been extensively studied in the master project; 2) the presence of the primer surfacer was limited to only a subset of the samples; and 3) the primer itself produced spectra of poor quality and limited information, the validation test was conducted on the clearcoat of the selected sample set.

Furthermore, due to the minimal intra-sample variability and the increased acquisition time resulting from the accumulation, the number of replicate measurements was trimmed down to three. More measurement should be taken if heterogeneity is encountered during the measurement.

Following acquisition, all Raman spectra underwent initial correction for cosmic rays, followed by automated baseline correction using Wire 5.5 software. Subsequently, the spectra were imported into Thermo Fisher Scientific Inc.'s software 'OMNIC 9.12.928' for characterization and visual comparison. The preprocessing techniques previously employed for IR spectra were similarly applied to the Raman data to evaluate their applicability.

PCA was carried out for data visualization and to aid in discrimination. Additionally, LDA and SIMCA were utilized for classification and validation purposes.

Visual spectra quality check.

The spectra, on the whole, demonstrated excellent quality and homogeneity across the three replicates. Upon visual inspection, one notable observation was that certain clearcoat samples exhibited peaks associated with titanium dioxide in their spectra. However, cross-referencing with the IR spectra confirmed the absence of titanium dioxide in the clearcoat. This could be attributed to the diagonal embedding of some samples, resulting in the laser penetrating through the transparent clearcoat and detecting the titanium dioxide in the basecoat. This issue, though not entirely avoidable due to the lack of perfectly vertical embedding, fortunately doesn't impact discrimination as there are no informative peaks in that area. Consequently, wavenumbers below 670 cm^{-1} were excluded. Similarly, the range between 1800 and 2000 cm^{-1}, containing no meaningful information, was also excluded. Hence, the wavenumber range of 670-1800 cm^{-1} was selected for further analysis.

Intra and inter sample variability.

Figure 41 depicts the calculation of intra and inter-sample variability using Pearson correlation coefficients, revealing an overall low level of intra-sample variability. Notably, four samples exhibited exceptionally high correlation values almost equal to 1, which prevented their appearance in the general box plot. Conversely, three samples displayed relatively high intra-

sample variability. This deviation was attributed to the presence of baseline variations within these samples. As a remedy, pretreatment procedures are necessary to resolve this issue.
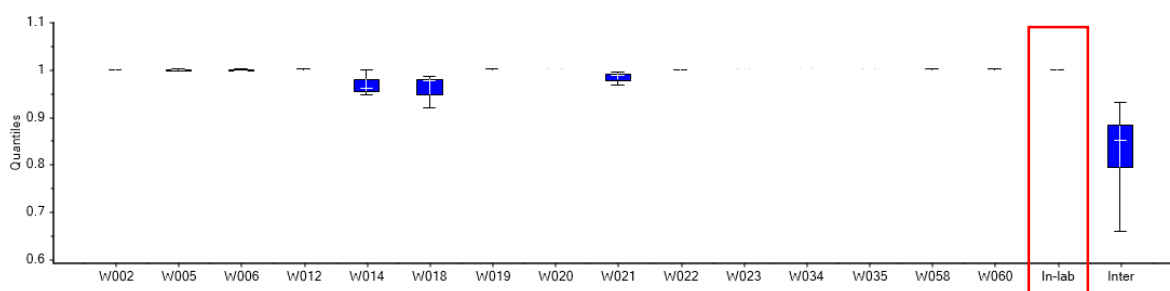
Figure 41. box plot of intra and inter sample variability within clearcoat.

As a part of quality control and reproducibility check, the internal standard reference (basecoat) was consistently measured prior to the beginning of each experiment. This practice served to evaluate the instrument's stability and reproducibility over time. Notably, the most consistent results in terms of intra-sample variability were observed when measurements were taken on different days, as depicted in *Figure 42*. This was also illustrated in *Figure 41* (highlighted in red rectangular) to have a parallel comparison with other intra-sample variability.
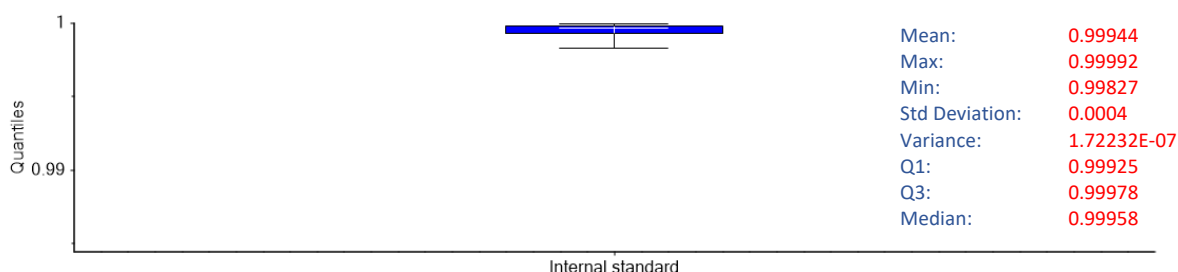
Figure 42. Over time reproducibility check result using internal standard (Raman).

Pretreatment and classification.

Two pretreatment methods, SNV and SNV combined with detrending using a polynomial order of 2 (det2), were assessed based on the PCA score plot. As depicted in *Figure 43*, the PCA score plot generated from SNV-pretreated data exhibited notable separation among different samples. The projections of same samples were closely clustered. Conversely, the addition of det2 did not enhance separation; rather, it seemed to magnify the intra-sample variability to some extent (as shown in dashed line in *Figure 43*). It is noteworthy that the baseline-corrected Raman spectra did not exhibit any discernible nonlinear trends, rendering this type of pretreatment unnecessary for the clearcoat samples. Consequently, solely SNV

pretreatment was chosen as the essential method, and detrending will be implemented only if deemed necessary.
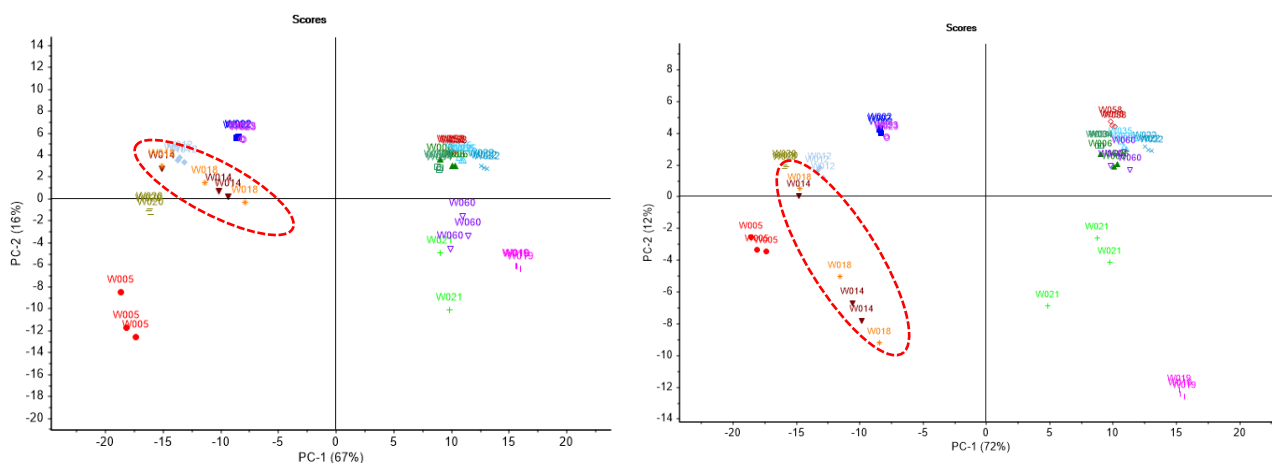
Figure 43. PCA score plots of SNV-pretreated data (a) and SNV+det2-pretreated data (b) according to the first two PCs, which account for around 74% of the total variance.

PCA offers superior discrimination capabilities when contrasted with visual grouping, as shown in *Table 21*. Nevertheless, It is important to note that certain separations observed in the PCA results might be attributed to baseline variations rather than indicative of the actual presence or absence of specific Raman bands. Consequently, It is imperative to validate the outcomes of PCA grouping by closely examining the spectra themselves.

Table 21.Visual grouping and PCA separation of the select sample set (n=15).

GROUP	VISUAL GROUPING	PCA SEPARATION
1	W002, W023	W002, W023
2	W005	W005
3	W012, W020	W012
		W020
4	W014, W018	W014, W018
5	W006	W006
6	W019, W021	W019
		W021
7	W022, W035, W060	W022
		W035
		W060
8	W034	W034
9	W058	W058
DISCRIMINATING POWER (%)	93.3%	98.1%

Statistical validation.

Similar to the approach employed in IR analysis, LDA were conducted based on the foundation of the PCA model to validate the supervised model. Due to the constraint of limited replicates, the application of SIMCA using the training set could not be accomplished. In a similar vein, for each method, a training set was formed by randomly selecting 2 out of the 3 replicates. The remaining replicate was reserved as the validation set, used to evaluate performance metrics of the methods including classification accuracy, false positive rate, and false negative rate. The outcomes of these assessments were then presented in *Table 22*. LDA yielded generally promising results. It is important to note that these outcomes might not be fully representative, but this concern won't affect subsequent blind tests.

Table 22. Performance of LDA

PARAMETNER	LDA
TRUE POSITVE	12
FALSE POSITIVE	3
FALSE NEGATIVE	3
TRUE NAGATIVE	102
CORRECT CLASSIFICATION RATE	0.9500
MISCLASSIFICATION RATE	0.0500
SENSITIVITY	0.8000
SPECIFICITY	0.9714
FALSE NEGATIVE RATE	0.2000
FALSE POSITIVE RATE	0.0286
POSITIVE PREDICTIVE POWER	0.8000
NEGATIVE PREDICTIVE POWER	0.9714
GENERAL DIAGNOSTIC POWER	0.8750

6.4.4. Standardization of Raman analysis protocol

A comprehensive Raman analysis protocol has been formulated, drawing from the preliminary investigation, and is outlined in *Table 23*. Certain adjustments might be made to tailor with sample conditions. Any changes will be documented.

Table 23. Protocol for the Raman analysis of the whole sample set in this thesis.

Step 1: Sample preparation		
• Prepare vertical cross sections of 5 µm thickness following the procedure described in chapter 6.2.1 • Mount the cross section on the custom-made steel stage. • Ensure that the surface of the cross section is flat.		
Step 2: Raman measurement		
Instrument calibration	Wavenumber shift calibration (silicon and internal standard)	
Instrumental settings	Instrument	Renishaw Invia Confocal Microscope
	Laser	785 nm
	Objective	50x
	Spectral Range	200-2000 cm^{-1}
	Exposure time	10s
	Laser power	Adjust according to sample
	Accumulation	8
	Grating	1200m/l
Reproducibility check	Measure the basecoat of internal standard (same standard utilized for IR analysis) before conducting the experiment	
Replicates	• Begin with a minimum of 3 replicates. • Increasing the number of replicates if significant variability observed.	
Step 3: Spectra quality check		
• Visually inspect the acquired spectra for quality assurance (noise, defects, contaminations). • Automate baseline substrate and cosmic ray removal.		
Step 4: Pretreatment		
Methods	SNV, detrending with a polynomial order of 2 if need	
Software	Unscrambler X 10.1 (CAMO software)	
Step 5: Visual characterization and Classification		
• Identify Raman bands through comparison with literature and available databases. • Perform visual comparison and classification based on the presence/absence of peaks or relative intensity of peak.		
Step 6: Statistical discrimination and classification		
Reproducibility Check	Measure intra sample variability of internal standard	
Methods	PCA	• Data structure visualization • Intra sample variability check.
	LDA	• Discrimination • Classification
Software	• IBM® SPSS® Statistics V.28.0.1.1(14) • Unscrambler X 10.1	
Step 7: Validation (Blind test)		
Measurement	5 samples measured by another person using the same protocol	
Classification	• PCA projection • LDA prediction	
Software	Unscrambler X 10.1	

6.5. Optimization and standardization of the parameters for Py-GC/MS

Py-GC/MS have been demonstrated to be capable of providing further discrimination for the samples that cannot be distinguished by FTIR and Raman (Cassista and Sandercock,1994; Challinor,2001; Henson and Jergovich,2001; MacDougall *et al.*,2001; Burns and Doolan,2005a; Eyring *et al.*,2007; Zięba-Palus *et al.*,2008a; Soong *et al.*,2020). In this study, this method is selected as an additional technique for extending the information obtained from vibrational spectroscopy and providing further discrimination. Therefore, the samples involved in this method are those remain undifferentiated after IR and Raman analysis.

However, it is important to note that the reproducibility of Pyrolysis-GC/MS results can be influenced by sample preparation and experimental parameters, especially when dealing with complex paint samples. Therefore, it is necessary to establish a specific protocol that can be adapted to the characteristics of the paint samples used in this study. This protocol should take into account the paint type and optimize the experimental parameters to ensure reliable and reproducible results.

In this study, the optimization and standardization of sample preparation methods and experimental parameters for white automotive paint in Py-GC/MS analysis were conducted through a master project (Wild,2022). The goal was to develop a standardized analysis protocol based on reported parameters found in the literature, which were summarized in Chapter 3.8 (*Table 6*).

This chapter focuses on preparing paint samples for Pyrolysis-GC/MS analysis, discussing both the sample preparation method and the optimization of pyrolysis GC/MS parameters. The optimization process involved varying parameters such as sample mass, pyrolysis temperature, carrier gas type, flow rate, and temperature ramp. By systematically varying these parameters and analyzing the resulting pyrograms, the optimal conditions for white automotive paint analysis were determined.

6.5.1. Sample preparation

According to various guidelines for pyrolysis GC/MS paint analysis (ASTM-E1610-18 ; EPGT,2022), the sample size is an important factor that influences the applicability and reproducibility of the technique. In order to ensure reliable and meaningful results, samples selected for comparison should fall within a ±20% weight range, and efforts should be made to achieve similar volumes and shapes to minimize additional sources of variability. While the recommended sample size in the guidelines is a minimum of 5-10 μg, it should be noted that working with smaller sample sizes can present challenges in terms of sample manipulation and handling. A review of the literature (refer to *Table 6*) reveals that the majority of research studies have utilized sample weights ranging from 30 to 100 μg. Therefore, the sample size involved in this study was decided to be around 30-50 μg. The reproducibility with regards to this sample size was also tested during the optimization process and will be discussed in the following chapter.

6.5.1.1. Preparation for reference standards

The initial investigation of IR analysis in the chosen sample set revealed an indistinguishable basecoat in a subgroup of seven samples. All these samples featured polyurethane as their primary binder. Further differentiation was necessary. During parameter optimization and standardization, reference polyurethane standards were required for comparison and analysis. However, obtaining pure polyurethane standards posed difficulties due to their limited availability. Instead, reference polyurethane paint samples were acquired from local repair shops. Although uncertified and invalidated, these samples provided reference points for analysis. Their FTIR spectra were compared with those of the analyzed samples, resulting in the selection of two closely resembling references: R2 (clearcoat) and R4 (white paint), as illustrated in *Figure 44*.

Creating the reference standards involved applying the wet paint acquired from repair shops onto glass plates, allowing it to dry. The dried paint was then scraped from the glass slide and cut into fragments using a scalpel under a macroscope. Each fragment's weight was measured using an analytical balance, and only chips falling within the predefined weight range of 35 ± 20% μg were chosen for subsequent analysis.

The selected reference chips were positioned at the bottom of the sample cup and inserted into the pyrolyzer's Auto-shot Sampler. To account for potential background signals or contamination, an empty cup was inserted between each sample, acting as a "blank run."

During the optimization of pyrolysis temperature, ten replicates of the reference samples were analyzed on the same day. Additionally, a second sequence involving five replicates was conducted one to two weeks later to assess result reproducibility. This rigorous approach ensured the reliability and consistency of the analysis.
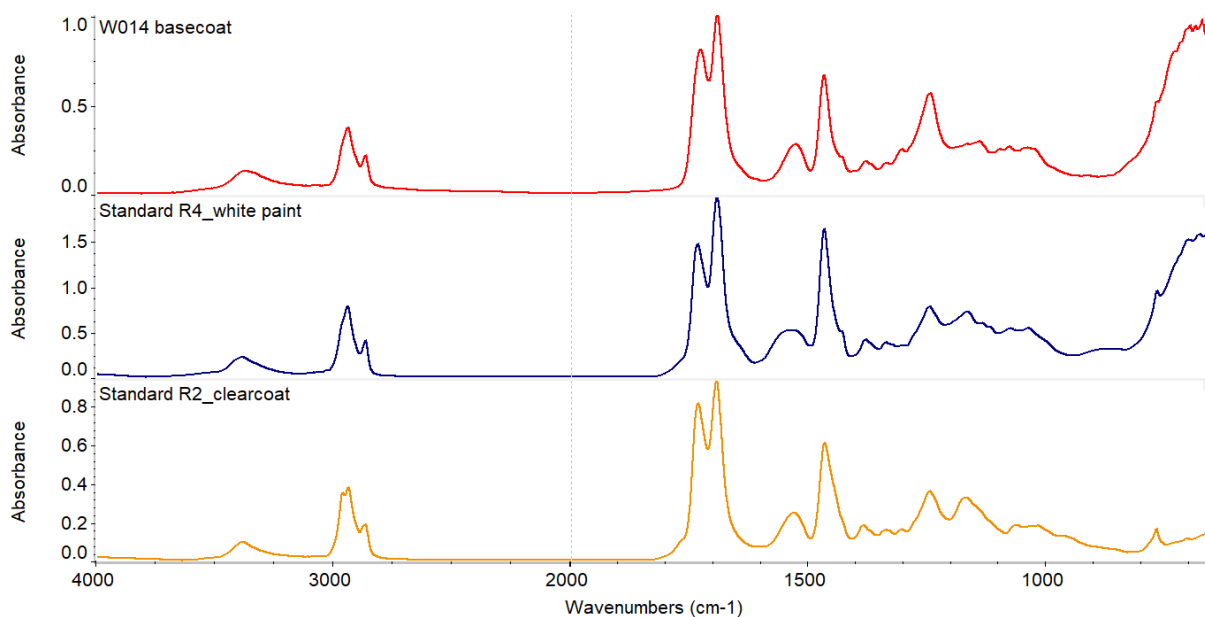
Figure 44. Comparison of IR spectra of Sample W014 (top) that contain polyurethane binder with the reference polyurethane white paint R4 (middle) and polyurethane resin R2 (bottom).

6.5.1.2. Preparation for multi-layer automotive paint

In the case of multi-layer paint analysis, it is crucial to physically isolate the target layer from other layers in order to effectively characterize the binder. Since the particular interest in this study is for the basecoat layer, a protocol for isolating the basecoat layer from the entire sample has been established. This protocol will be discussed in detail, outlining the steps and procedures for achieving the physical separation of the basecoat layer.

In this study, two isolation methods were employed and compared for the purpose of isolating the basecoat layer: vertical cross sections of 20 µm thickness and horizontal sections of 5 µm thickness. The creation of vertical cross section followed the protocol described in chapter 6.2.1, while the creation of horizontal sections followed a similar protocol, but with the paint chips placed horizontally in the resin block during the embedding step.

Given that the samples in this study encompass two types of layer structures, namely OEM3 (a three-layer structure) and OEM4 (a four-layer structure), a sample was chosen from Group OEM3 and another from Group OEM4 to assess the feasibility of preparing both types of samples. The dark field images of vertical cross sections of these two samples and the thickness of basecoat are illustrated in *Figure 45*.
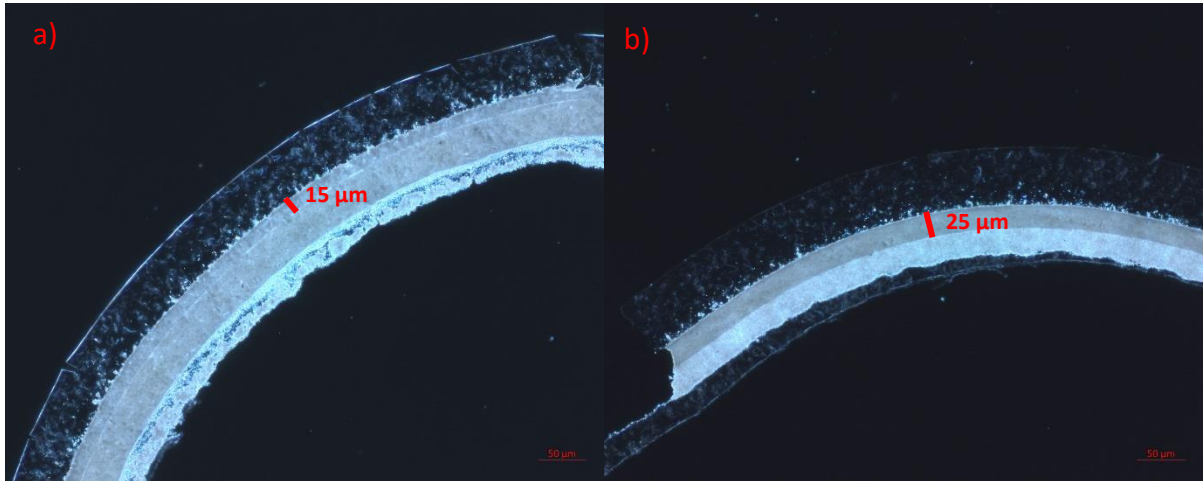
Figure 45. Dark field images of vertical cross sections used for basecoat isolation test: a) Sample W019, displaying an OEM4 structure; b) Sample W062, illustrating an OEM3 structure. The basecoat thickness is indicated on the images.

Preparing the samples poses several challenges that need to be addressed. The first challenge involves having a sufficient amount of paint material available. The initial extent of the basecoat's surface depends on the dimensions and contours of collected paint chips. During the preparation of horizontal sections, if the paint chip is too thin or not perfectly aligned horizontally with the resin block's surface, the amount of basecoat recovered per microtomic slice is reduced (see *Figure 46*). Additionally, depending on the flatness and quality of paint chips, the basecoat's shape within the microtomic slice isn't consistently uniform; it could be rectangular, round, S-shaped, U-shaped, or even contain voids (see *Figure 47*). For practical purposes and to minimize the variability introduced due to the shapes of samples, the basecoat often can't be isolated in strict accordance with its actual shape. Therefore, It is crucial to acknowledge the necessity of ensuring that the basecoat possesses adequate surface area to be uniformly shaped during cutting. However, achieving this in practice to retain a sufficient amount of material for analysis can be challenging.
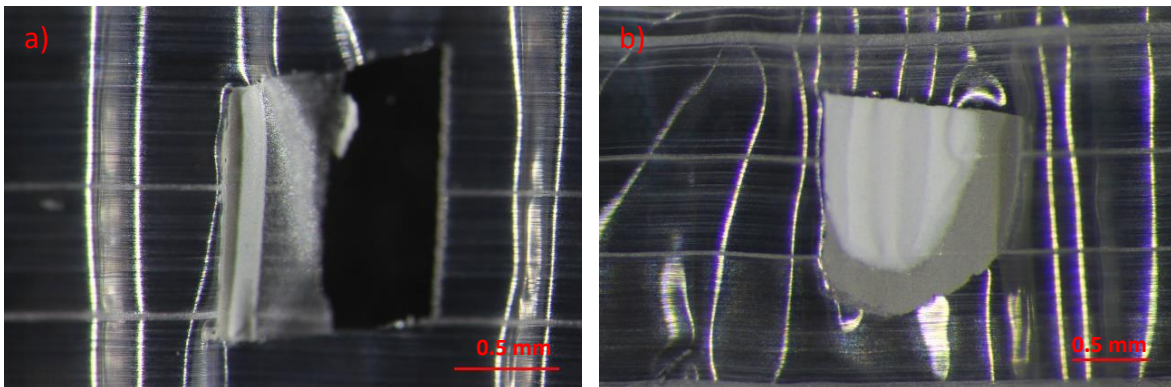
Figure 46. Horizontal sections with a) minimal amount of basecoat and b) significant amount of basecoat.
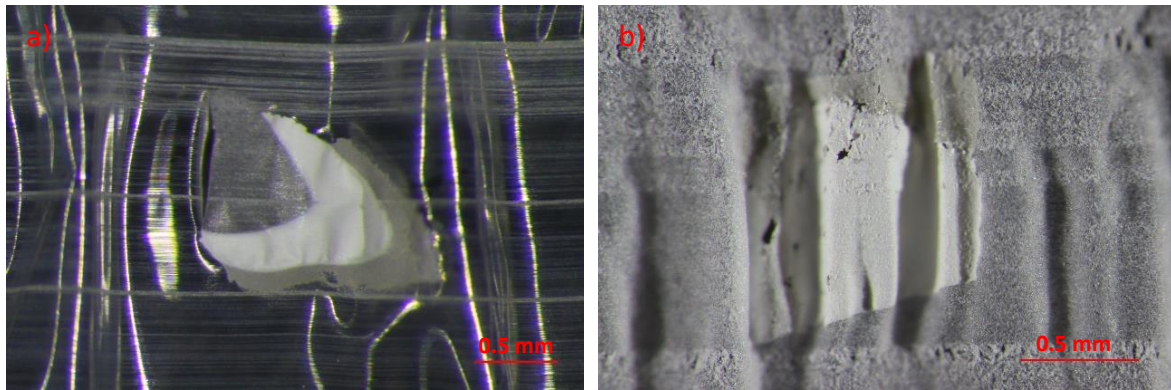
Figure 47. illustration of the shapes and morphologies encountered during the preparation process of the basecoat: a) U-shaped basecoat; b) basecoat with voids.

Another intricate step involves the manual cutting process required to isolate the basecoat. For the vertical cross section of 20 µm thickness, the manipulation area is remarkably small, presenting significant challenges in isolation. This challenge is even more evident for the OEM4 sample. This is due not only to the extremely thin basecoat of the OEM4 sample but also to the minute color contrast between the basecoat and the primer surfacer, as exemplified in *Figure 45a*. When operating under a stereo macroscope, discerning the boundary between these layers becomes exceedingly challenging, rendering the isolation of the basecoat without any cross-contamination from adjacent layers highly uncertain. Similar challenges arise in the case of horizontal sections. Although the manipulation surface area is larger here, the thinness of the basecoat and the striking resemblance in color between the basecoat and primer surfacer pose challenges. It becomes arduous to consistently identify potential layer overlaps. These challenges and the considerable effort required for meticulously isolating the basecoat from OEM4 samples make the task highly demanding and practically unfeasible.

While dealing with the OEM3 sample offers relatively better ease, the same fundamental issue persists, particularly concerning the overlap of the clearcoat with the basecoat, as indicated in *Figure 48*. Extra care needs to be exercised to prevent any potential contamination. Thus, a margin is consistently maintained along the edges of the basecoat, preventing minor mingling between layers or with the resin employed to create the block. Regions with holes are also sidestepped due to the uncertainty concerning potential influences from other layers or the resin of the block.
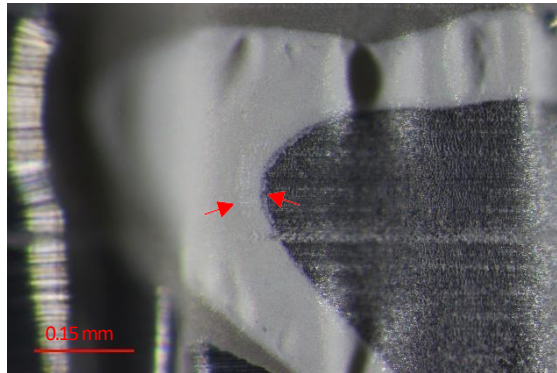
Figure 48. Illustration of basecoat and clearcoat superimposition in horizontal sections.

The obtained prepared samples were analyzed by Py-GC/MS to test the pyrogram quality and reproducibility. By comparing the two methods, it was determined that the preparation method using horizontal sections offered better handling feasibility and resulted in higher quality pyrograms. This was primarily due to the larger surface area available for manipulation and the ability to control the shape of the sections. Additionally, the presence of color differences among the layers facilitated the recognition and isolation of the basecoat layer.

The following steps were followed to isolate the basecoat layer using the preferred method:

1) Select a small size (2 mm x 2 mm) paint from each sample, giving preference to the flattest chips. Clean the paint with ethanol.
2) Place a mold on a flat surface and add several drops of standard resin (Technovit 2000 LC Heraeus Kulzer light curing resin) into the bottom of the mold. Ensure that the resin surface is level. Next, position the mold into the Heraeus Kulzer Technotray CU Curing Light device and allow the resin to cure for 2 minutes. Place the paint chips horizontally on the partially cured resin and fill the mold with additional resin. Finally, mount a resin block onto the mold. Cure the mold containing the sample for 15 minutes.
3) Mount the resin block onto the Leica RM2265 – Fully Motorized Rotary Microtome and cut it into sections that are 5 µm thick. Place the resulting slices onto a microscopic slide in sequential order.
4) Observe and identify the slices that contain the basecoat layer. Select one desired slice containing the basecoat layer and place it onto a microscopic slide. Flatten the slice by adding a few drops of methanol. Using a razor blade, carefully cut out the basecoat layer, ensuring that other layers are not included.
5) Weigh the isolated basecoat layer using an analytical balance (XP2U Ultra Micro Balance, Mettler Toledo).
6) If the weight of the isolated basecoat layer meets the specified criteria, place it into a measuring cup for further analysis.

6.5.2. Instrumentation and calibration

The Py-GC/MS system used in this study consisted of a Single-Shot Pyrolyzer (PY-3030S) equipped with an Auto-Shot Sampler (AS-1020E) from Frontier Lab. The sample cups used with the auto-shot sampler were Eco-Cup LF type from Frontier Lab. The coupled GC/MS system was from Agilent Technologies and included an 8890 GC System (G3540A), an Agilent J&W GC Columns, DB-35MS (30 m, 0.25 mm, 0.25 μm), and a 5977B GC/MSD System (G7077B). The analysis of the pyrograms was performed using the MSD ChemStation Data Analysis Application.

Before running the analysis on the samples, the instrument underwent a self-calibration procedure called Autotune. A tune report was generated from this calibration to evaluate the performance of the 5977 MSD tune. The parameters recorded in the tune report were compared to acceptance criteria. The software included a 'Tune Evaluation' function to check if any results were outside the specified limits.

In addition to the self-calibration procedure, the system was also calibrated using a polystyrene standard. This standard, known as the polystyrene standard sample (P/N: PY1-4908), consisted of a 2.5 mg film of polystyrene with 5wt% mestearate. A solution was prepared by adding 0.5 ml of dichloromethane to the standard, and then further diluted at a ratio of 1:4 with dichloromethane. This standard was used to verify the stability of the instrumentation. The standardized polystyrene analyses were performed every week during the experiment period, and the results were compared with the previous week's analyses to check the peak position (retention time) as well as the relative intensities of certain pyrolyzates. Through visual comparison and statistical processing, it was determined that the variability between the analytical results was minimal, indicating good stability over time.

By conducting these performance checks, the Py-GC/MS system demonstrated sufficient stability to enable comparison of analysis results across different days. The calibration procedures and stability tests performed ensured the reliability and accuracy of the system for the analysis of the paint samples in this study.

6.5.3. Optimization and standardization of the parameters for Py-GC/MS

6.5.3.1. Choices of parameters

The pyrolysis temperature is a crucial parameter in Py-GC/MS analysis as it determines the extent of bond dissociation and the formation of pyrolysis products. For the analysis of polyurethane-based samples, which is the binder used in this sample set, it is important to choose a pyrolysis temperature that ensures complete pyrolysis without causing excessive bond breakage.

The specific type of polyurethane resin used in the samples can influence the temperature required for the dissociation of urethane bonds. Different isocyanates and polyols used in the resin formulation can have varying thermal stability and reactivity. As a result, the pyrolysis temperature needs to be optimized to achieve the desired pyrolysis products for analysis.

In this study, three different pyrolysis temperatures were tested: 450°C, 550°C, and 650°C. These temperatures were selected based on their common usage in the literature and their reported effectiveness in facilitating the dissociation of various types of paint. By testing different pyrolysis temperatures, it becomes possible to identify the optimal temperature that provides complete pyrolysis and the generation of characteristic pyrolysis products specific to polyurethane-based samples.

The pyrolysis time was set at 12 seconds due to the consistency provided by the autosampler, where the time of staying in the pyrolysis part remains the same regardless of the software settings. Additionally, the interface temperature was set at 300°C.

For the gas chromatography part, a commonly used oven program was employed, starting with an initial temperature of 40°C for 3 minutes. A temperature ramp of 10 to 20°C per minute was then applied, increasing the temperature up to 320°C, which was maintained for approximately 10 minutes. The interface temperatures typically ranged from 280°C to 320°C. Furthermore, a 35% diphenyl-/65% dimethylpolysiloxane capillary column with dimensions of 30 m x 0.25 mm x 0.25 µm was selected for the analysis.

Table 24 provides a summary of the experimental parameters tested in this study, including the pyrolysis temperatures, pyrolysis time, interface temperature, oven program, and the mass spectrometry settings.

Table 24. Tested experimental parameters of the Py-GC/MS

Pyrolysis parameters		
	Temperature of pyrolysis [°C]	450/550/650
	Pyrolysis time [s]	12
	Interface [°C]	300
Gas chromatography parameters		
	Initial temperature	40°C for 3 min
	Ramp	10°C/min
	Final temperature	320°C for 10 min
	Injector temperature	280°C
	Split Ratio	50 :1
	Carrier gas	He
	Flow	1 ml/min
	MSD Transfer Line	300°C
	Column type	35% phenyl- 65% dimethyl polysiloxane capillary column (30 m, 0.25 mm, 0.25 μm)
Mass spectrometry parameters		
	Tune Type	EI (Electron Impact)
	Scanning parameters	Weights: 29 - 550 amu Threshold: 30 Scan speed [u/s]: 1.562 Frequency [scans/s]: 2.8
	Electron multiplier voltage (ΔEMV)	0

6.5.3.2. Experimental parameters determination

The analysis results obtained from different pyrolysis temperatures were discussed in detail in the master thesis generated from this project (Wild,2022). The thesis provides a comprehensive discussion on the visual characterization and comparison of pyrograms, highlighting the compounds generated and identified at each temperature along with their corresponding retention times. The reproducibility of the results obtained at each temperature is also examined through visual comparison of pyrograms and statistical analysis. In this section, only a brief summary of the analysis results will be presented.

From the visual comparison of pyrograms, it was observed that the pyrograms obtained at 450°C had a lower number of peaks compared to those obtained at 550°C and 650°C. This is attributed to the lower fragmentation of compounds at the lower temperature. Therefore, the method with a pyrolysis temperature of 450°C was discarded due to its lower number of peaks and lower discrimination potential. On the other hand, the pyrograms obtained at 550°C and 650°C were qualitatively well interpretable and exhibited a sufficient number of peaks for potential discrimination. Both methods were found to be similar in terms of quality, with a slight shift of peaks towards lower retention times for the 650°C method compared to the 550°C method.

In terms of reproducibility, both the 550°C and 650°C methods showed similar results upon visual comparison of pyrograms. However, statistical treatments, such as Principal Component Analysis (PCA) and Hierarchical Cluster Analysis (HCA), favored the 650°C method, which exhibited slightly less variance, particularly between replicas analyzed on different days. This was also supported by the calculated relative standard deviations (RSD) of the component areas, which were often lower for the 650°C method compared to the 550°C method.

Based on these findings, the chosen pyrolysis temperature for the analysis of the samples is 650°C. However, it should be noted that the results at 550°C and 650°C were very close in terms of both quality and reproducibility.

During the analysis process, a recurring issue that arises is the variation in air entry observed in some samples or analysis sequences. This phenomenon is not directly related to the percentage of nitrogen (N2) indicated in the machine's parameters report. Even with a low percentage of air entry, there can still be a significant impact on the Total Ion Chromatogram (TIC) data. This problem led to the decision of excluding the first ten minutes of data during result presentation to mitigate the effect of air entry. However, this approach resulted in the loss of valuable information present in that time range. To avoid this loss of information while still addressing the air entry issue, a 3D extraction was performed. This involved removing the air ion values and recalculating the sum of the abundances of each non-deleted ion for every point of the pyrogram. By implementing this method, the influence of air entry on the results was effectively minimized.

Preliminary tests were also conducted on the undifferentiated samples to assess the method's sensitivity and the isolation of the basecoat. These tests followed the procedure outlined in 6.5.1. Results demonstrated that increasing the electron multiplier voltage (EMV) by 200 could improve the detector's amplification and enhance sensitivity. Pyrogram comparisons indicated that increasing the EMV by 200 not only maintained the desired peak abundance but also reduced air entry.

Based on the analysis of the reference polyurethane samples and the tests conducted on the sample set, the optimized parameters summarized in will be utilized for the analysis of the entire sample set.

Pyrolysis parameters		
	Temperature of pyrolysis [°C]	650
	Pyrolysis time [s]	12
	Interface [°C]	300
Gas chromatography parameters		
	Initial temperature	40°C for 3 min
	Ramp	10°C/min
	Final temperature	320°C for 10 min
	Injector temperature	280°C
	Split Ratio	50 :1
	Carrier gas	He
	Flow	1 ml/min
	MSD Transfer Line	300°C
	Column type	35% phenyl- 65% dimethyl polysiloxane capillary column (30 m, 0.25 mm, 0.25 µm)
Mass spectrometry parameters		
	Tune Type	EI (Electron Impact)
	Scanning parameters	Weights: 29 - 550 amu Threshold: 30 Scan speed [u/s]: 1.562 Frequency [scans/s]: 2.8
	Electron multiplier voltage (ΔEMV)	200

6.5.4. Standardization of analytical strategy for the target sample set

Pyrolysis-GC/MS offers the potential to provide additional information and distinction for samples that remain indistinguishable through FTIR and Raman analyses. Consequently, the Py-GC/MS analysis will be applied to the basecoat of undifferentiated samples. However, considering the challenges and labor involved in isolating the basecoat from OEM4 samples, this thesis will not address the undifferentiated OEM4 samples.

Of particular note is that, based on IR analysis, the majority of undifferentiated basecoat samples stem from OEM3 paint samples with a polyurethane binder. The preliminary tests conducted in the master project have developed a specific protocol tailored to the characteristics of the polyurethane basecoat samples in this study. Thus, for the samples that could not be differentiated via FTIR and Raman, they were initially prepared following the protocol outlined in Chapter 6.5.1.2 , and subsequently subjected to Py-GC/MS analysis using the parameters outlined in *Table 25.* The gathered data were then characterized by identifying the compounds generated and their corresponding retention times. Discrimination was pursued through visual comparison and statistical analysis of the 3D extraction data.

7. Microscopic characterization of the sample set

The whole sample set, including 62 samples and 135 sub-samples, was prepared, and examined using the protocol presented in chapter 6.2.5. The results are discussed in the following subchapters.

7.1. Intra-sample variability

To clarify, in this context, the term "intra-sample variability" refers to the observed differences within the subsamples collected from various positions of a vehicle. Due to the practical conditions under which the samples were collected, 19 out of the 62 samples were collected from a single position. This means that analyzing variations within subsamples was not possible for these samples. For the remaining 43 samples, an analysis of layer structure, relative layer thickness, layer color, and layer morphology was conducted to investigate intra-sample variability. Among these 43 samples, 34 (79%) exhibited significant intra-sample variability in terms of layer structure or relative layer thickness. The reasons behind this substantial intra-sample variability in this sample set were investigated. *Figure 49* illustrates the distribution of samples resulting from the examination of intra-sample variability, along with the identified causes for such variability. *Figure 50* exhibits the intra sample variability of some samples.
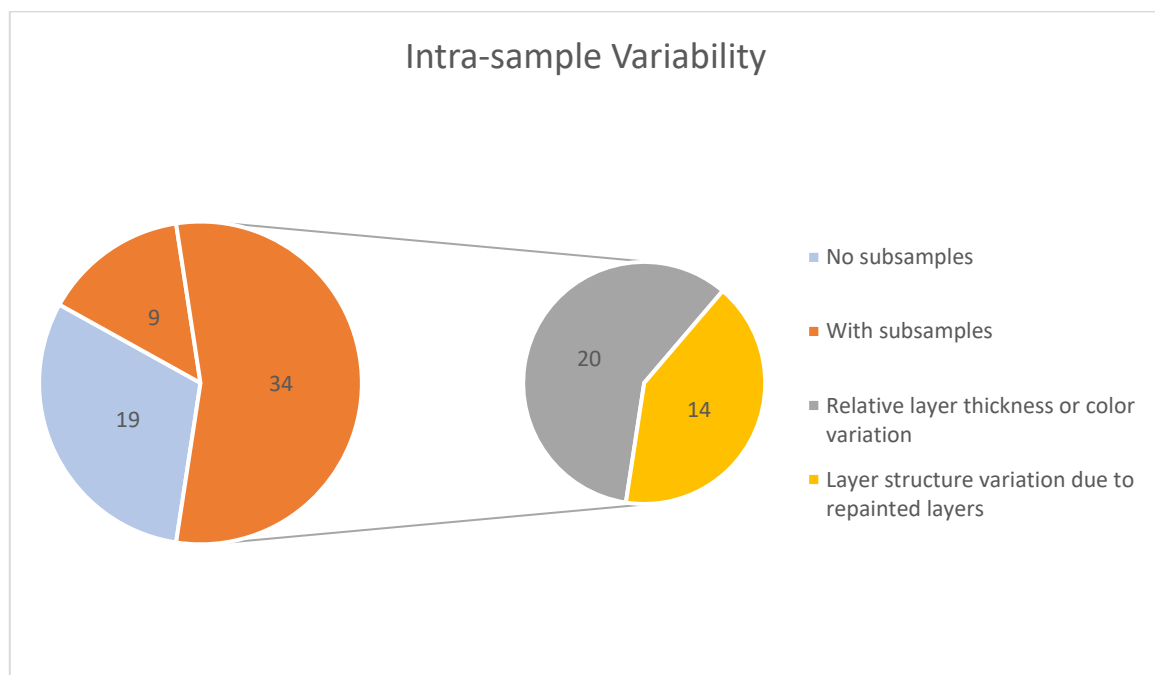
Figure 49. Pie chart showing distribution of samples and identified causes of intra-sample variability.
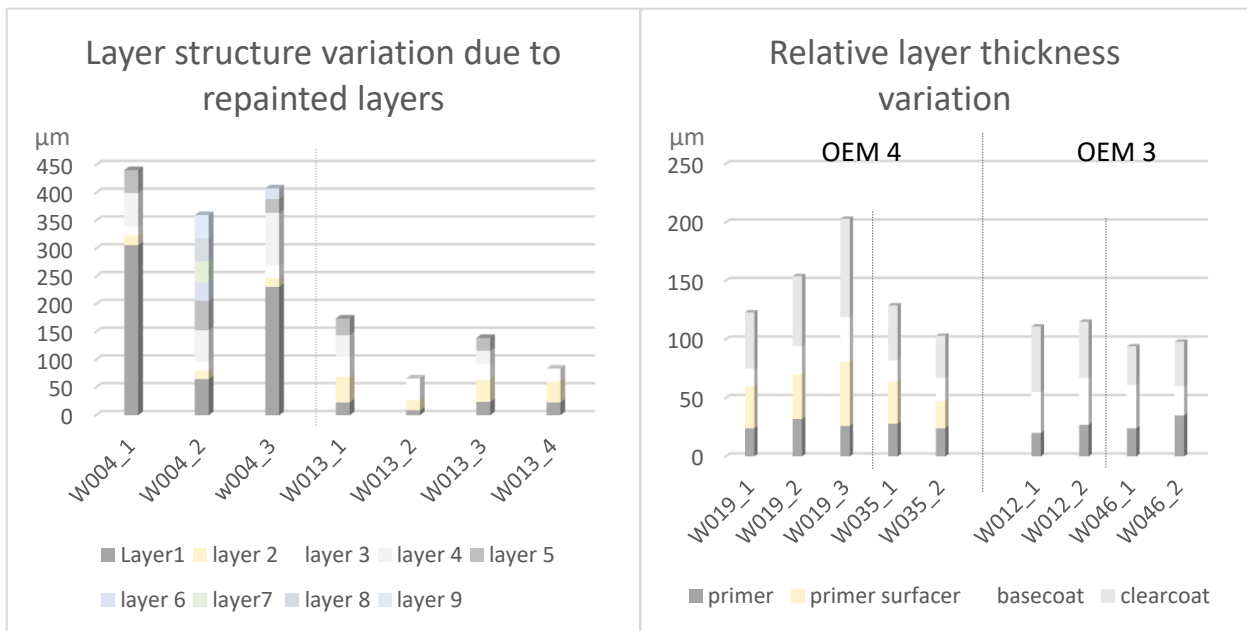
Figure 50. Illustration of intra sample variability revealed from microscopic examination.

First, it is noted that most of the layer structure variability occurred when the involved vehicle had been repainted. 41.2% (14 out of 34) of the intra-sample variability is caused by this repainted fact. In this study, samples were collected from vehicles placed in accident vehicle parking lots or VW service shops. It is highly likely that these vehicles have suffered at least one damage or one scratch. Unlike the OEM coating system, there is no standardized layer sequence for a refinishing paint system. This results in an unusual paint layer structure and makes the repainted layer more distinguishable than the OEM system. When a vehicle has been repainted, samples taken from different locations may have very dissimilar layer structures and colors, as illustrated in *Figure 51*, where the four subsamples from different locations of sample W024 have distinct layer structures, with only sample W024_6 maintaining the original paint system (OEM paint) and the other three locations having only the repainted paint system.

Second, the remaining 58.8% (20 out of 34) of the intra-sample variability is due to relative layer thickness variation or color difference. Sample preparation can inevitably introduce errors to the absolute thickness of each layer; however, the relative layer thickness is not easy to change. Thus, if the relative layer thickness variation is observed, it can be concluded that this variation comes from the sample itself rather than from the sample preparation. *Figure 52* provides an example of the relative layer thickness variation between the subsamples. Both sample W019_1 and sample W019_3 have 4 layers and can be identified as OEM paint, but the relative layer thickness regarding clearcoat, basecoat, and primer surface of the two subsamples are not negligible.

It is surprising that such widespread variation was observed in this sample set, as a standardized paint line should produce paint layers with consistent characteristics regardless of which segment of the vehicle enters the paint shop. Nevertheless, the absolute layer thickness difference of one specific layer is scaled in micron and is often less than 5 µm. This subtle variation is acceptable when comparing to the size of the operation machine.
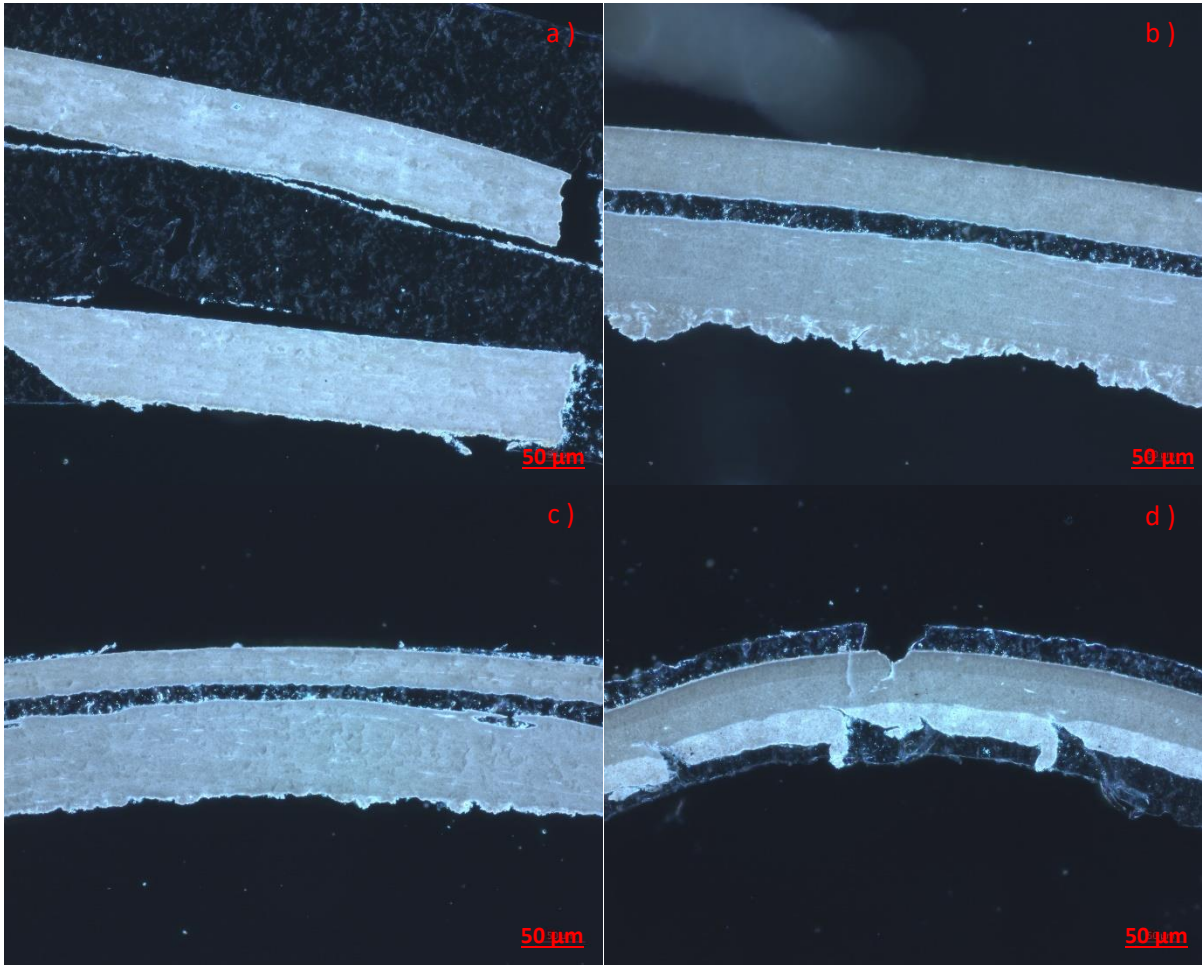
Figure 51. Images of cross-sections of 4 sub-samples from sample W024 under transmitted light dark field, a) sample W024_2, from the right front door; b) sample W024_3, from the front hood; c) sample W024_5, from left front door and d) sample W024_6 from the right rear door.
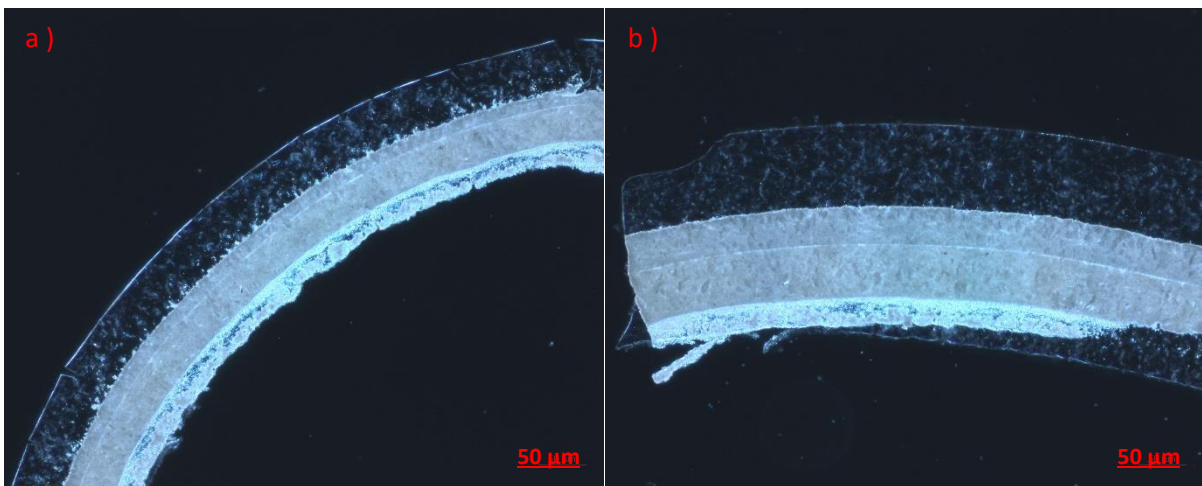
Figure 52. Images of cross-sections of 2 sub-samples from sample W019 under transmitted light dark field, a) sample W019_1, from the front hood; b) sample W019_3, from the left front door.

The presence of intra-sample variability is an important consideration for forensic practitioners when collecting reference samples for comparative analysis in actual casework. In the present study, 79% of the samples exhibited significant intra-sample variability in terms of layer structure, relative layer thickness and layer color. While this variability provides important reminders about the importance of collecting reference samples in close proximity to the area of damage, it poses a significant challenge for inter-sample comparisons. Specifically, differentiation based on relative layer thickness between samples is extremely difficult and can lead to substantial uncertainty in the results.

7.2.   Layer structure and distribution

Based on the layer structure of each sample, the whole sample set can be divided into three main groups:

Group OEM3: a **three-layer structure**, defined as **OEM3**. The paints in this group, from the innermost to the outmost, consist of primer, basecoat, and clearcoat, as shown in *Figure 53a*.

Group OEM4: a **four-layer structure**, named **OEM4**, contains primer, primer surfacer, basecoat and clearcoat (see *Figure 53b*).

Group Repainted: a **repainted structure**, called **repainted**. This group of paints retains **no OEM system** at all, and the layer structure has no specific pattern. The number of layers can vary from only one layer to nine layers, as shown in *Figure 53c* and *Figure 53d*. For those repainted samples, only the innermost and outmost layer can be firmly defined as primer and basecoat, respectively. For the remaining layers in between, It is hard to tell the function of every layer.

To be noticed, some samples had refinishing layers on top of their OEM system. They were either repainted in the refinishing department of original carmaker before delivery to customers, this type of refinish often has an extra basecoat and clearcoat that share the same characteristics as the OEM basecoat and clearcoat (confirmed by IR analysis), as shown in *Figure 54a*. In this study they are defined as original refinishing (OR). Another type of refinishing layers has no such ordered layer structure. They were often repainted in either repair shop or local workshop and have very dissimilar characteristics, as presented in *Figure 54b*. This type of refinish is given a symbol R. These two types of samples were grouped according to their retained OEM systems regardless of the refinishing layers.

When considering each sub-sample as an individual sample, the layer distribution of the whole sample set (n=135) is illustrated in *Figure 55*. Due to the widespread intra-sample variability, some sub-samples from the same vehicle might belong to different groups. Among 135 sub-samples, 106 sub-samples have OEM paint system. These samples have adequate value to meet the research goal of this thesis.

When counting the layer distribution per vehicle, samples were categorized into OEM groups as long as OEM system remained in one of the sub-samples. Samples were classified into repainted group only if there was no OEM system in any of the sub-samples. Therefore, the layer distribution per vehicle is determined and presented in *Figure 56*. In this sample set, 26 samples (41.9%) belong to group OEM3, 28 samples (45.2%) belong to group OEM4, 8 samples (12.9%) have no OEM system and belong to group repainted.
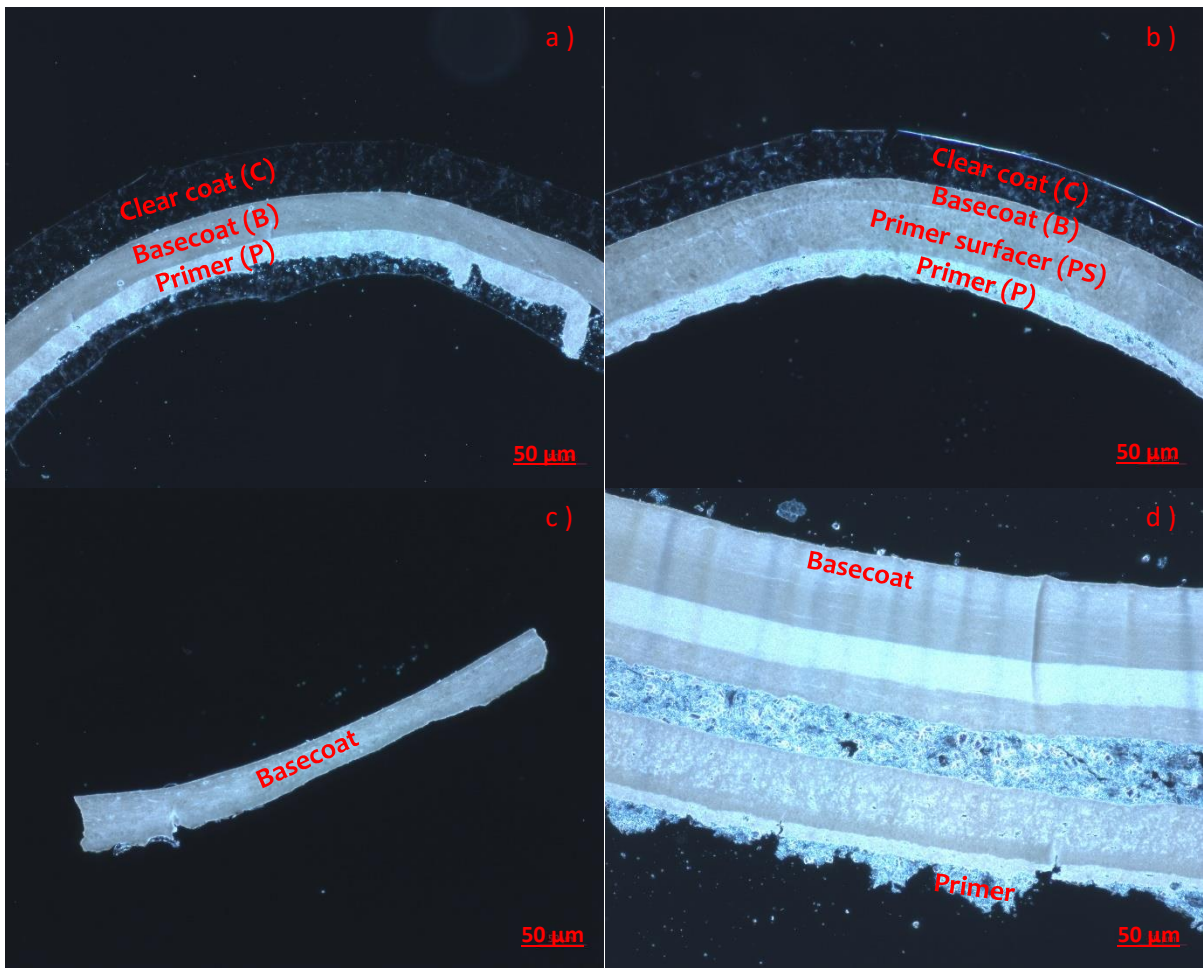
Figure 53. Dark field images of cross-sections of a) Sample W023_1 with three OEM layers; b) Sample W050_2 with four OEM layers; c) Sample W022_1 with one layer; d) Sample W004_2 with nine layers.
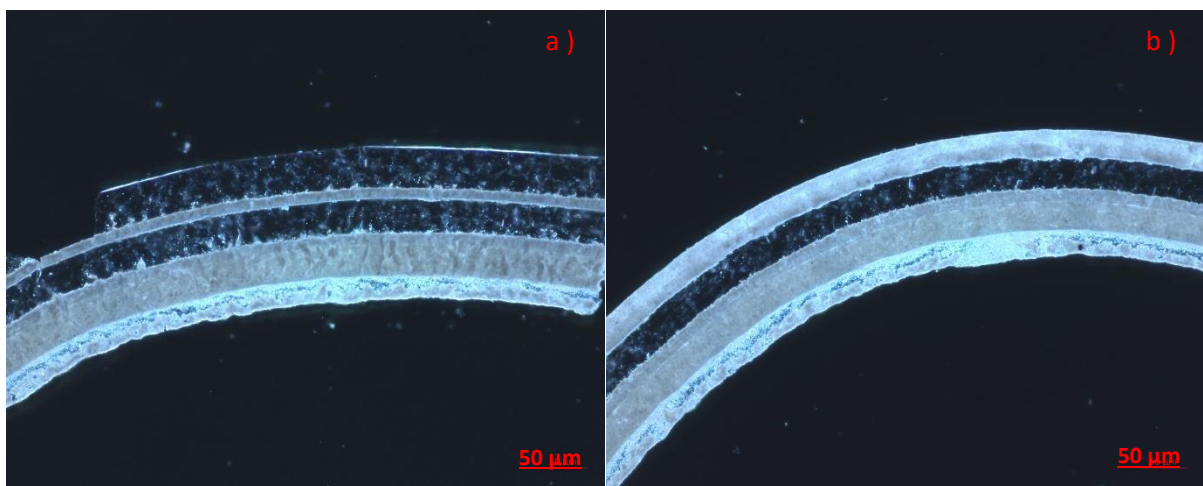
Figure 54. Dark field images of cross-sections of a) Sample W025_3, with original refinishing (OR) layers on top of the OEM four-layer system, and b) Sample W040, with refinishing (R) layers on top of the OEM four-layer system.
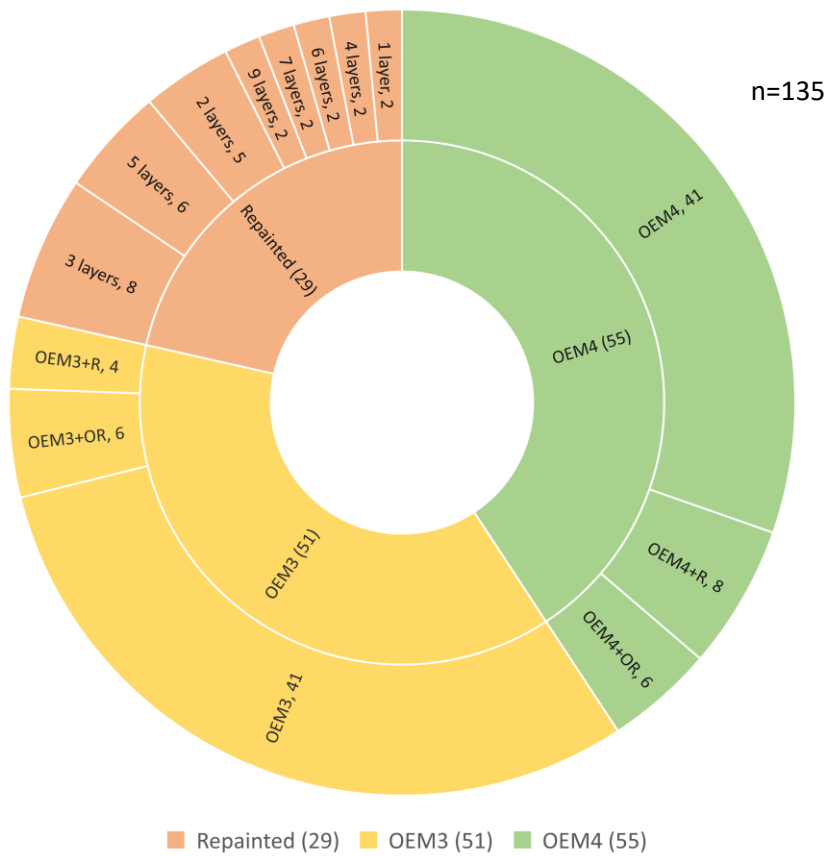
Figure 55. Layer distribution of the whole sample set per sub-sample (n=135): OEM3 and OEM4 refers to the paints having original three-layer structure or four-layer structure, respectively; OEM3/4 + OR refers to the paints having extra original refinishing layers on top of their OEM system; OEM3/4 + R refers to the paints having extra refinishing layers on top of their OEM system.
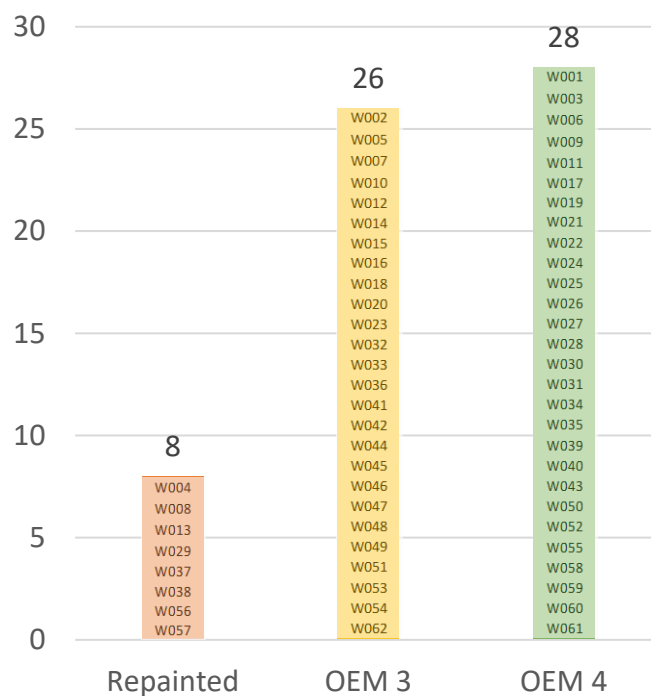
Figure 56. Layer distribution of the whole sample set per vehicle (n=62).

7.3.   Characterization and classification

Group OEM3: The samples within this group consist of three layers. Although slight differences are present among the samples in terms of layer thickness, color, and morphology, since they are produced by the same manufacturer and featured the same color, they definitely share several common characteristics. The innermost layer in this three-layer structure is the primer. It exhibits a granular morphology and is often light grey in color. Typically, the primer's thickness falls within the 15-25 µm range. Notably, since paint chips are scraped from the car body, complete separation from the car body is occasionally unattainable due to paint adhesion. This leads to the fact that the measured primer thickness in this study is thinner than the actual thickness that the primer should have achieved during the coating process. The basecoat within this group is homogeneously white and thicker than primer, typically ranging from 23-40 µm. Microscopic observation reveals little variation in basecoat color. However, layer thickness varies significantly across samples. Additionally, birefringent particles have been identified in the basecoat, but they are not evenly distributed, contributing to some degree of heterogeneity. The outmost layer is the clearcoat, which is transparent and homogeneous. No particles were detected in this layer. Layer thickness of clearcoat can vary from 28 µm up to 74 µm. Samples within this group are readily distinguishable from the other two groups based on their layer structure. Within-group comparison yields differentiation primarily through the color of the primer and the relative layer thickness between the basecoat and clearcoat.

Group OEM4: This particular group comprises 28 samples and features four original layers. As usual, the innermost layer is the granular primer, grey in color. In contrast to Group OEM3, samples in this category possess an additional layer referred to as the primer surfacer, positioned between the primer and basecoat. This layer is relatively thick and appears white, containing birefringent particles. Its color and morphology closely resemble the characteristics of the basecoat. The layer thickness falls within the range of 23-55 µm. Basecoat of this group is a thin, homogeneous white layer without any birefringent particles inside. Layer thickness is in the range of 10-38 µm. Notably, the relative layer thickness between the primer surfacer and basecoat can vary significantly, reaching ratios as high as 3.5:1. The outmost clearcoat is also homogeneous, with the thickness between 28 and 85 µm.

Group repainted: Each sample belonging to this specific group exhibits a very distinct layer structure. It is challenging to pinpoint common features that can be summarized. Only the innermost layer can be identified as primer. Normally, primer in this group has different characteristics not only comparing to group OEM3 and OEM4, but also from sample to sample within the same group. In general, the primer in this category still retains granular morphology. However, there are added birefringent particles of large size in primer and the color vary from grey to light brown, some of them are brighter than others. It is worth noting that repainted structures often lack a clearcoat, thus making the basecoat the outermost layer in these samples. The basecoat's color and morphology exhibit significant variations, with some even displaying a granular texture and looking more silver than white under transmitted dark field illumination. The layers in between have no similar features at all.

These intermediary layers either consist of several overlapping white layers, or suddenly in the middle there is a thick filler layer in between two white layers. The functions of those layers are hard to categorize. These unusual structure and irregular characteristics make samples from this group easy to differentiate from the rest of samples.

After classifying the entire sample set into three distinct groups based on their layer structures, the focus shifted towards classifying samples within each group. As previously noted, the prevalence of intra-sample variability proved to be remarkably high, which in turn posed a substantial challenge during inter-sample comparisons. Even when considering variations in relative layer thickness, achieving definitive discrimination became an intricate task.

Furthermore, in the dark field examination, heterogeneity within the basecoat regarding color was observed. Stripes displaying varying color shades were evident across most of the samples. The underlying reasons for this phenomenon were investigated. It is possible that this observation could be attributed to the unevenness of the sample itself, similar to the lighter stripe noted in *Figure 57a*. Another hypothesis proposes that the microtomic process introduced an inevitable rough surface to the samples, potentially leading to variations in color shade. As illustrated in *Figure 57b*, the section within the red circle appears to encompass numerous small patches, each exhibiting a different white color shade. This form of heterogeneity, although subtle, can make the differentiation of samples somewhat challenging.
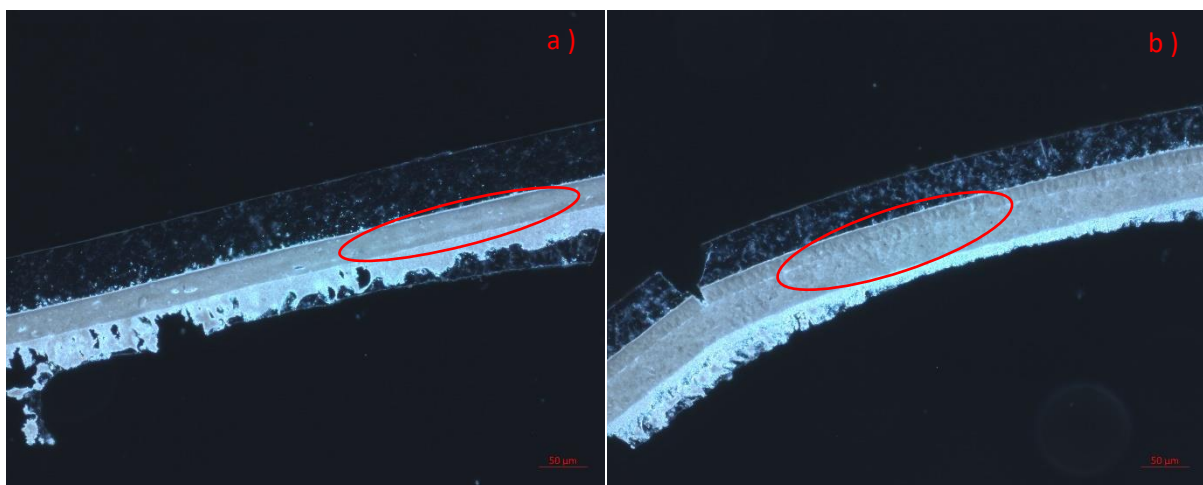
Figure 57. Dark field images of cross-sections of a) Sample W032_2, a lighter stripe presents in the red circle; and b) Sample W021_3, color shade due to rough surface.

Initially, the approach was to designate a solitary sub-sample as the representative for the entire vehicle and employ this sub-sample for comparisons with other samples. However, this strategy encountered a major stumbling block - the rational selection criteria can't be reasonably determined. The inter-sample variability curve and the intra-sample variability curve often exhibited substantial overlap. Consequently, choosing different sub-samples from two samples and conducting comparisons could yield disparate conclusions.

Hence, the author opted for a revised strategy. The new approach for comparisons was shaped as follows:

1) When conducting comparisons within group OEM3 or OEM4, only the OEM system is taken into consideration. While the presence of additional OR or R layers indeed renders the sample distinct from the standard OEM3 samples, It is important to note that this study primarily concentrates on discriminating OEM paints. Any supplementary differentiation brought about by additional repainted layers is not pertinent to the objectives of this study and, consequently, will not be considered.

2) Given the uniform color of each layer in the sub-sample, discrimination should primarily focus on comparing the colors of individual layers, particularly the primer.

3) If differentiation can't be achieved based on color, the comparison should shift to relative layer thickness, but excluding the primer. The ratio between the remaining layers, such as basecoat versus clearcoat for group OEM3, and primer surfacer versus basecoat versus clearcoat for group OEM4, should be computed and summarized. Subsequently, the ranges of these ratios for two samples must be compared. If the ranges do not overlap, the samples should be deemed distinct. Conversely, if the ranges significantly overlap, the samples should be classified as indistinguishable.

With these criteria, classification results based on transmitted light bright field and then dark field is presented in *Figure 58*. The discriminating power for both illuminations has been computed and is presented in *Table 26*. The undifferentiated pairs after these two illuminations are further observed and compared using polarized light and Alexa Fluor 488 fluorescence illumination. The discriminating powers resulting from adding these two illuminations are also presented in *Table 26*.

It should be noted that the final discrimination results differ from the preliminary test. The preliminary test achieved a higher discriminating power for both bright field and dark field than the final discriminating power. In the preliminary test, only one subsample was chosen and compared with other subsamples, excluding consideration of intra-sample variability. However, with the inclusion of more subsamples in the comparison, the range of intra-sample variability has expanded, sometimes fully overlapping with inter-sample variability, rendering discrimination difficult to achieve. Consequently, the final discriminating power is lower than that of the preliminary test. In practical applications, the collection of more reference samples becomes essential to establish a range of intra-sample variability, thereby preventing false negatives.
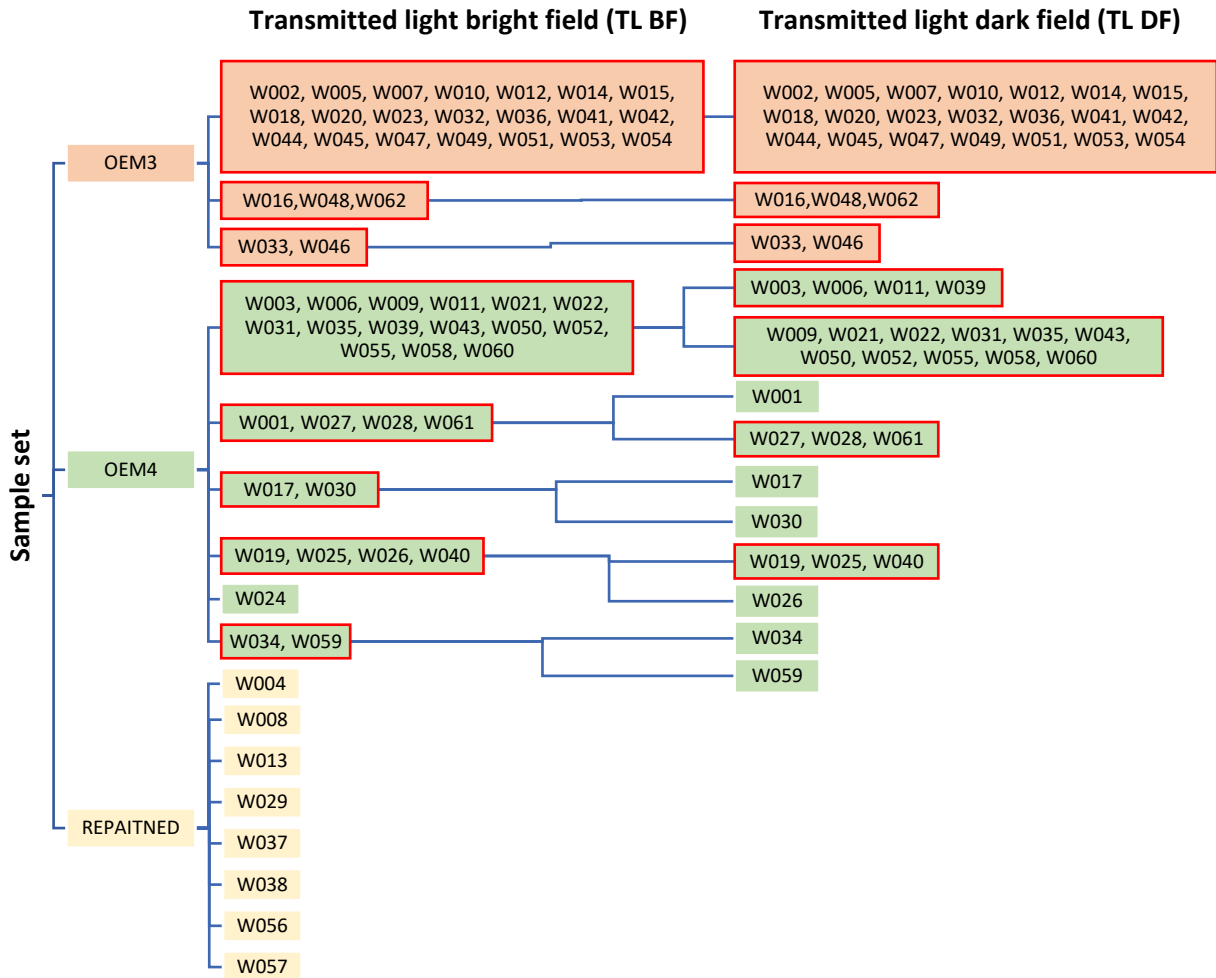
Figure 58. Classification of the whole sample set (considering only OEM layers) using transmitted light bright field and dark field illumination. Red boxes indicate the undifferentiated pairs.

Table 26. Discriminating power of microscopic examination using transmitted light bright field and dark field as well as polarized light and fluorescence AF488 when considering only OEM layers.

Illumination	Undifferentiated pairs	DP (n=62)
TL BF	333	82.4%
TL DF	281	85.1%
TL DF+POL	281	85.1%
TL DF+AF 488	**150**	**92.1%**

It is important to note that this discriminating power is the outcome of solely considering the OEM paint system for the samples belonging to Group OEM3 or OEM4. Differentiation resulting from the addition of extra repainted layers on top of the OEM paint system has not been factored into this analysis. However, It is still valuable to examine the discrimination outcomes when accounting for all existing layers of samples. This would likely lead to a higher discriminating power, providing a representation of the true inter-sample variability within the entire sample set. This is summarized in *Table 27*.

Table 27. Discriminating power of microscopic examination using transmitted light bright field and dark field as well as polarized light and fluorescence AF488 when considering all existing layers.

Illumination	Undifferentiated pairs	DP (n=62)
TL BF	193	89.7%
TL DF	163	91.4%
TL DF+POL	163	91.1%
TL DF+AF 488	**79**	**95.8%**

Consequently, upon the completion of the microscopic examination encompassing transmitted light bright field, dark field, polarized light, and Alexa Fluor 488 fluorescence illumination, a total of 150 pairs of samples within this set were found to be undifferentiated when solely considering OEM layers of a given sample. This number decreases to 79 pairs when taking into account all the existing layers of the samples.

7.4.   Correlation between physical properties and sample origin

Once the characterization and classification were done, the correlation between physical properties and sample origin was explored. When doing this, since repainted samples had no OEM paint system, they are not taken into consideration. Therefore, only 54 samples that belong to either group OEM3 or OEM4 are counted. Results showed that the layer sequence can be correlated to assembly plant. The distribution of samples with regards to six plants and the layer system is presented in *Figure 59*. In most of the cases, one assembly plant produces only one type of layer system regardless of the model and production year. Among the five plants, plant Anting seems to produce more than one layer system. After the investigation, the plant Anting uses the same plant code "2" but actually there are three sub-plants under this code, named Anting I, Anting II, and Anting III. With regards to each sub-plant, only one type of layer system is produced. Surprisingly, exceptions were discovered. Sample W009, W043, and W055 belong to Lavida family, all the other samples from Lavida family have an OEM3 layer structure but these three samples had OEM4 layer structures. The reason behind it was not clear. Perhaps there are more plants behind the plant code, maybe these vehicles are actually produced in other production lines. But in general, **it is the plant that determines the layer structure of a vehicle**.
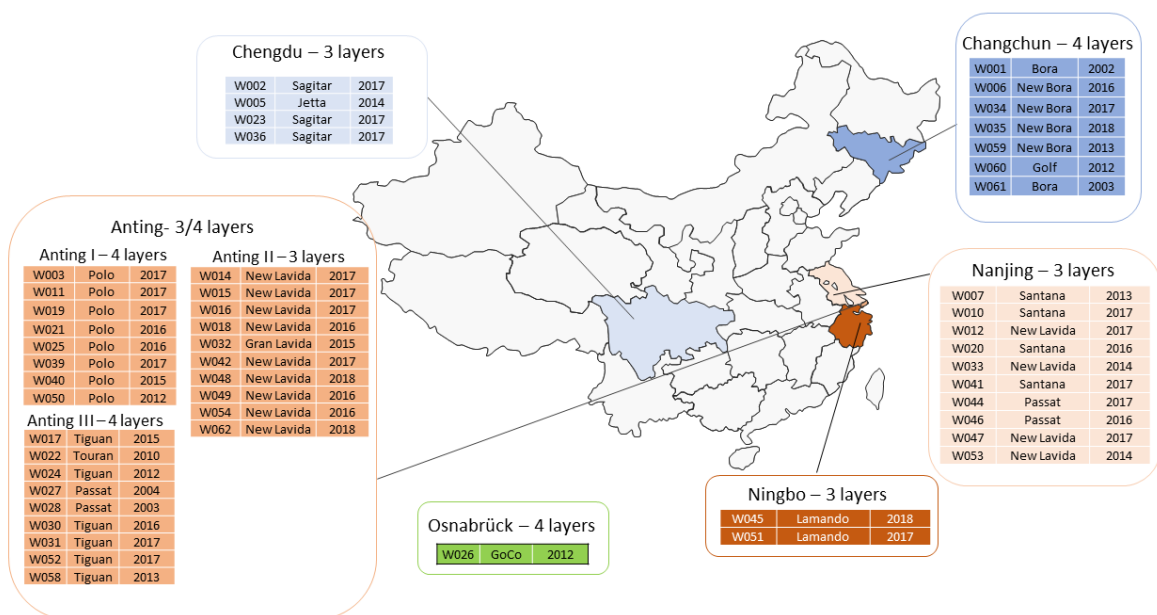
Figure 59. Sample distribution with regards to assembly plants and the layer system.

Regarding the color code of the paint samples, it is noteworthy that it can be linked to the manufacturing company and plants. Specifically, the sample set contains two manufacturing companies (F-VW and S-VW), and three types of color codes, namely LB9A, LC9A, and LY9H. Each plant employs two color codes for their products, with LC9A exclusively used in two F-VW plants and LY9H solely present in two S-VW plants. However, LB9A is utilized by all plants and is the only color code included in the European paint database, implying its worldwide applicability. Intriguingly, the color code demonstrates no association with either the layer structure or color of the samples. Due to the diverse basecoat color, differentiation based on color is not achievable via microscopic observation. Thus, the role of color code in distinguishing between samples is unclear, and further exploration is warranted to investigate any potential correlation between the color code and the chemical composition of the samples.

Despite being produced on the same production line, samples of the same model still exhibit variability, particularly in terms of the color of the primer and relative thickness. This was demonstrated in the preliminary study (Chapter 6.2.4), where samples W034 and W035, although of the same model and produced in the same plant, differed in primer color due to being manufactured in different years. Similarly, samples W014 and W016, which shared identical production information, including production date and plant location, had different clearcoat to basecoat layer thickness ratios. Although the basecoat layer thickness was consistent for both samples, the clearcoat of Sample W016 was significantly thicker than that of Sample W014. This disparity in clearcoat thickness can be attributed to the inability of the coating devices to precisely control the thickness of the paint layer. Thus, it is crucial to consider the potential impact of production variations and equipment limitations when analyzing automotive paint samples.

The high level of intra-sample variability observed during the microscopic examination has raised questions about the potential impact of coating quality on the chemical stability of the samples. To further investigate this possibility, all 135 sub-samples were subjected to FTIR analysis to assess their chemical composition. The results of this analysis will be discussed in the upcoming chapter, providing insight into the extent to which intra-sample variability may exist with regard to the chemical properties of the samples.

8. Characterization and classification with FTIR

The microscopic examination of the sample set provided initial insights and led to the classification of samples into three distinct groups based on their physical features. However, a large number of samples (150 pairs), still remained indistinguishable using this method alone. Therefore, it became necessary to explore the chemical composition of the samples in order to achieve further discrimination. FTIR was chosen as the second method of analysis after microscopy due to its ability to reveal the chemical components of paint layers such as binders, pigments, or additives. Given the observed intra-sample variability of samples with respect to relative layer thickness, it was decided that all samples (n=62) and their subsamples (n=135) should be analyzed with FTIR to determine if the chemical composition of each layer also exhibits such variability. Each layer of every sample was measured using the same calibrated instrument and under identical conditions, as outlined in *Table 18* (Chapter 6.3.4). The measuring window was adapted in accordance with the thickness of each layer in the paint system being considered (10-50 µm x 50 µm).

The characterization of each layer was performed by comparing the characteristic bands of chemical groups with several reference books (Caddy,2001; MacDougall *et al.*,2001; Buzzini and Stoecklein,2005; Ryland and Suzuki,2011), commercial IR databases of coatings, polymers, additives, inorganics that are presented in Thermo Fisher's Omnic software (HR coatings technology, HR Comprehensive Forensic FT-IR collection, HR Polymer and Additives, HR Inorganics, HR Polymer Additives and Plasticizers, HR Polymer Sample Library, Industrial Coatings), and European databases of paints available in EUCAP. The reference spectra employed for comparison with the IR spectra of automotive paint samples within this thesis, discussed in the subsequent subchapters, were sourced from the databases mentioned above.

8.1.   Intra-sample variability

After conducting microscopic analysis, all 135 sub-samples underwent FTIR analysis. Measurements were taken from each layer of every sample, with three replicates obtained from each layer. It is important to note that in this context, the term "intra-sample variability" encompasses not only the variability observed among subsamples collected from different positions of a vehicle but also within the three replicates obtained from the same layer.

Regarding the variability within replicates acquired from different positions of the same layer, it was found to be minimal. The spectra exhibited homogeneity in terms of peak position and relative peak intensity (see *Figure 60*). However, there were instances where the replicates slightly differed in baseline variations, as illustrated in *Figure 61*. This type of variability could be easily eliminated through baseline correction and normalization, posing no challenges for inter-sample comparisons.
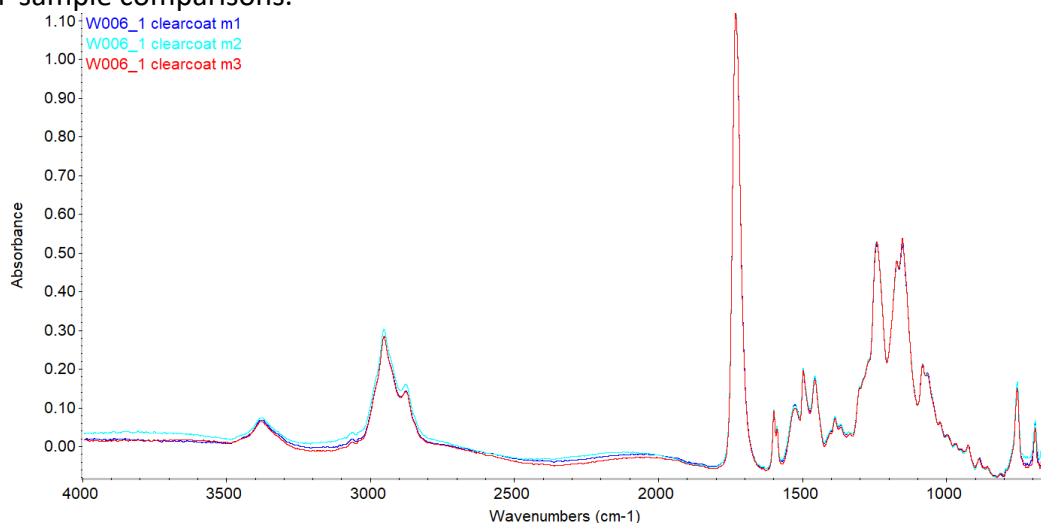
Figure 60. Three IR raw spectra measured from the clearcoat of sample W006_1, showing the homogeneity within the replicates.
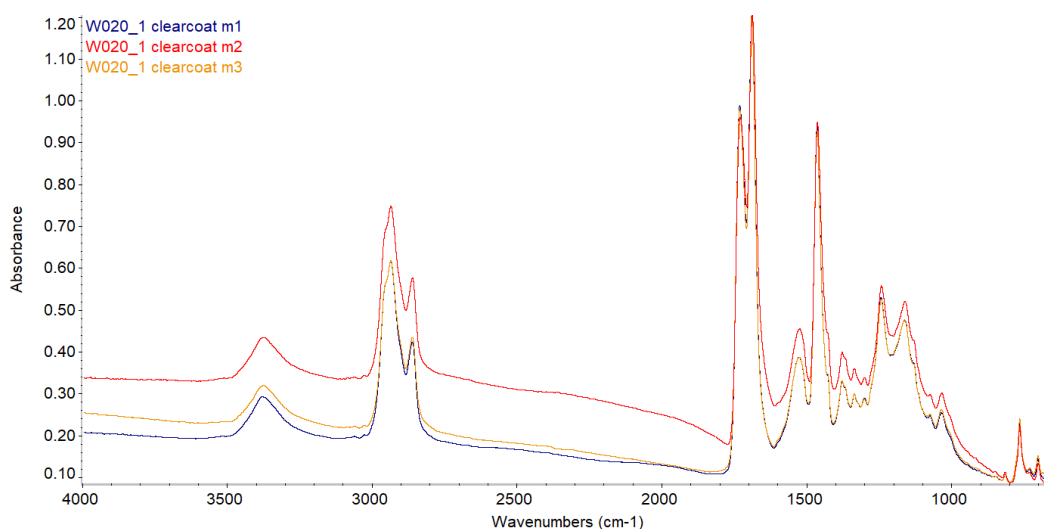
Figure 61. Three IR raw spectra measured from the clearcoat of sample W020_1, showing the variability within the replicates in terms of baseline variation.

Since the IR measuring window was adjusted to match the thickness of each layer in this study, thinner layers were more likely to capture components from adjacent layers, leading to increased intra-sample variability. In some cases, layers were too thin to be effectively measured (e.g., layers thinner than 10 μm). Variability could arise from the situation where the measuring window was too thin and the boundary between two layers was indistinct, causing the IR measurement of a layer to capture components from the adjacent layer. For instance, *Figure 62* presents five IR spectra measured from the basecoat of sample W021_4, with a layer thickness of only 10 μm. Variations in the intensity of the peak at 1510 cm^{-1} were observed among these five replicates. However, this variation was caused by "contamination" from the primer surfacer, which exhibits a strong, sharp peak at 1510 cm^{-1}. This type of variability was specific to the basecoat of samples from Group OEM4 due to their thin layer thickness. To mitigate this issue, after each measurement, the IR spectra of the basecoat were carefully examined and compared with those of the primer surfacer or clearcoat to identify potential "contaminations."
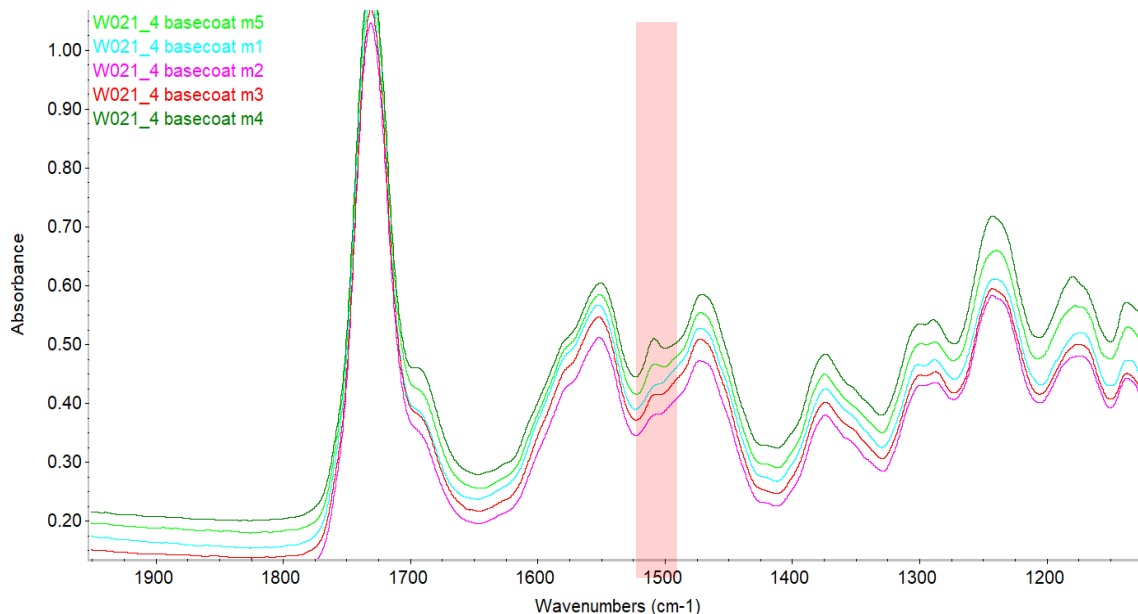
Figure 62. Five IR spectra measured from the basecoat of sample W021_4, showing intra variabilities due to the thin measuring window size. The variation observed from the 5 replicates are highlighted in red.

Figure 50 visually represents the intra-sample variability as observed during the microscopic examination. Within this context, layer structure variations due to repainting effects as well as the variations in relative layer thickness and color were the two main reasons behind intra-sample variability concerning physical characteristics. To assess the intra-sample variability in terms of chemical composition for these two types of samples, a separate evaluation was undertaken.

Specifically, for subsamples with varying layer structures, the chemical composition was compared between layers of the same type. In most cases, only the basecoat composition could be compared. It was observed that although the layer structure may vary due to repainting effects, the original equipment manufacturer (OEM) layers remained relatively homogeneous, while the repainted basecoat differed significantly from the OEM layer. For example, *Figure 63* illustrates the IR spectra obtained from the basecoat of sample W002. Within this sample, subsamples W002_3 and W002_4 exhibited different layer structures, with W002_4 having two additional repainted layers on top of the OEM paint system. However, the original basecoat of W002_3 and W002_4 displayed spectra that were indistinguishable, while the extra repainted basecoat of W002_4 exhibited a distinct chemical composition compared to the original basecoat. As a result, when comparing between samples, only those with an exclusively OEM system are taken into consideration to ensure consistency and accuracy in the analysis.
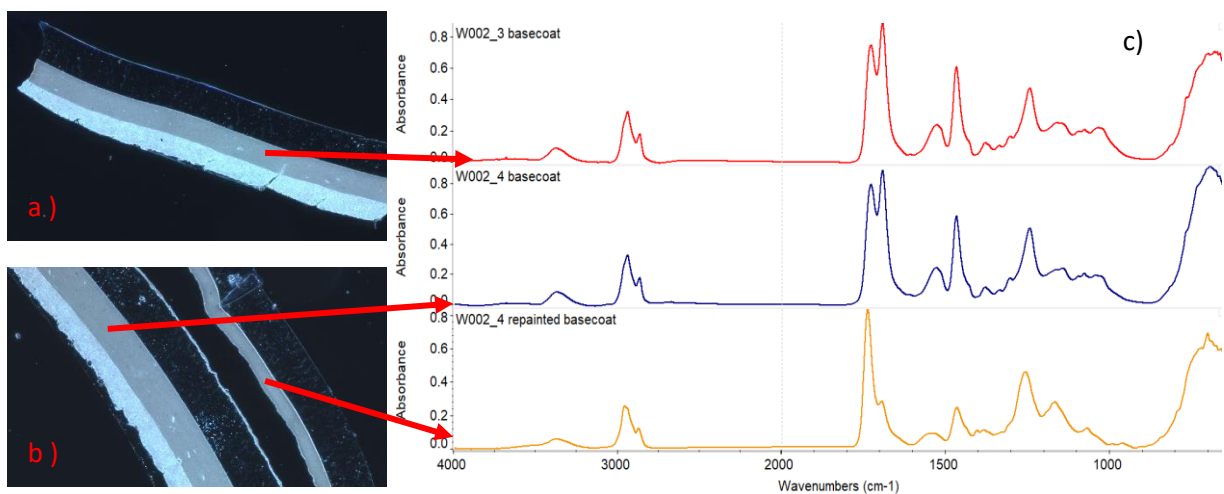
Figure 63. Dark field images of sample W002_3 (a) and sample W002_4 (b) and IR spectra obtained from basecoats of these samples (c).

In the case of subsamples from repainted vehicles where no OEM paint system remained, a comparison between the primer and basecoat revealed that the basecoat exhibited greater intra-sample variability compared to the primer. The primer of these subsamples displayed relatively homogeneous characteristics, while the basecoat showed variations depending on the location. This is exemplified in *Figure 64*, where subsamples W013_3 and W013_4 showcase uniform primer but distinct basecoat characteristics. This variability could potentially introduce complexities in inter-sample comparisons.

However, it should be noted that the coating formula of refinished layers differed significantly from that of OEM paint. Despite the intra-sample variability, the refinished paint could still be easily differentiated from OEM paint due to their distinct formulations. This distinction is evident in *Figure 65*, where the basecoat of repainted sample W013 differs from the basecoat of OEM sample W014. This differentiation remains irrespective of the intra-sample variability seen in sample W013.
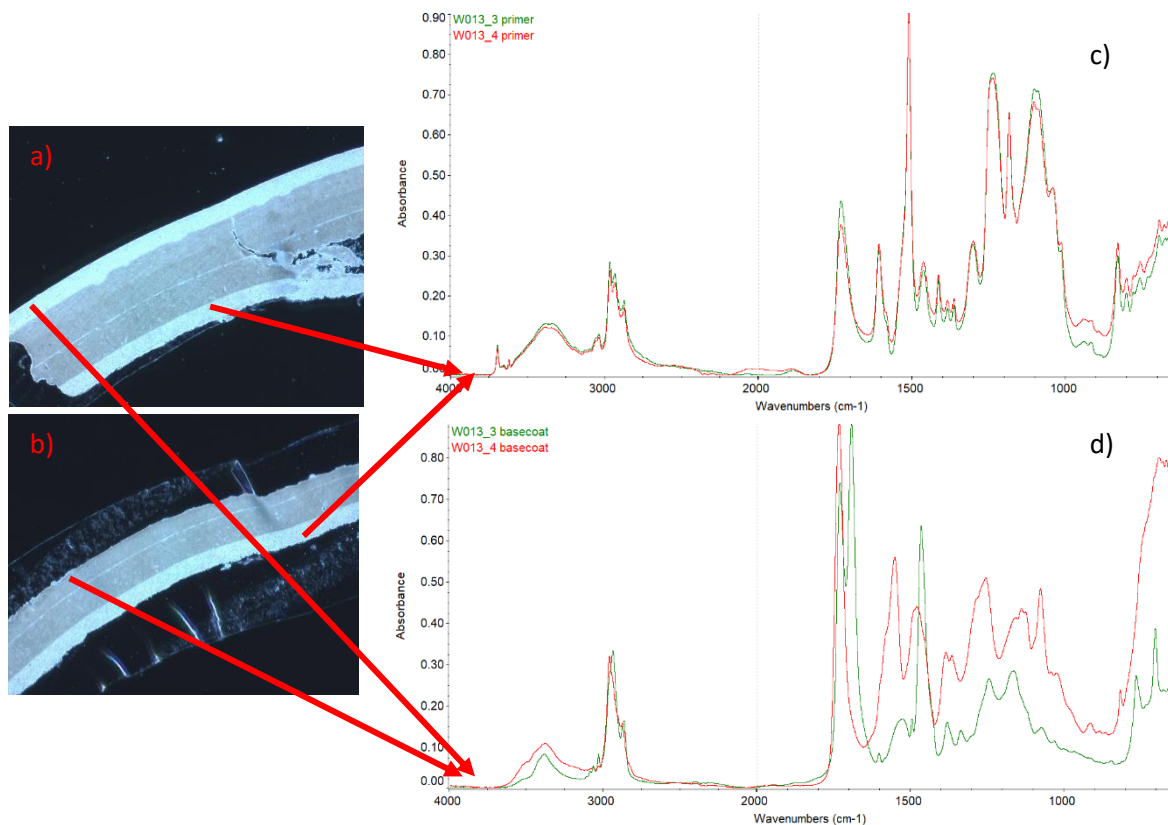
Figure 64. Dark field images of sample W013_3 (a) and sample W013_4 (b) and IR spectra obtained from the primer (c) and the basecoat (d) of these samples.
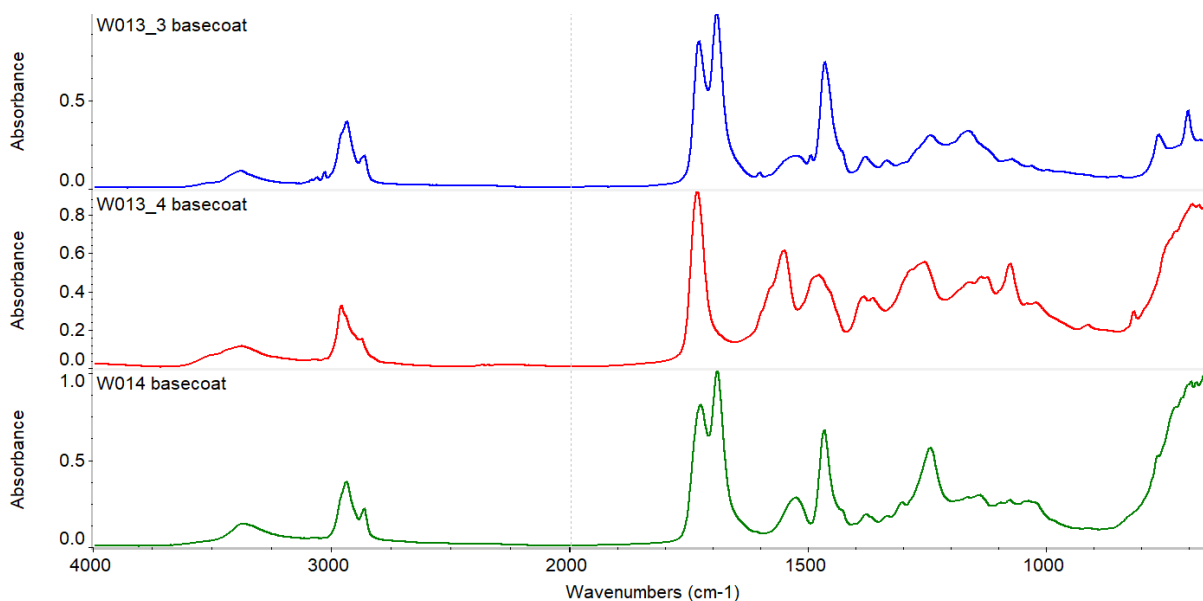
Figure 65. IR spectra obtained from sample W013_3(top), sample W013_4 (middle) and sample W014(bottom).

In samples displaying differences in relative layer thickness or layer color, the OEM paint layers generally exhibited homogeneity. It is worth addressing that intra-variability in the physical characteristics of a sample does not necessarily indicate variability in its chemical characteristics. *Figure 66* illustrates this point, where two non-differentiated IR spectra obtained from the primer of sample W062_2 and W062_3 are shown, despite their color difference in primer.

However, subtle intra-sample variability was still observed in some samples. This variability was observed across all layers, as shown in *Figure 67* with two IR spectra obtained from sample W019_2 and W019_3, highlighting the subtle intra-sample variability (indicated in the red zone) among their clearcoat. Among the layers, the primer exhibited the greatest intra-sample variability, likely due to its lower spectral quality and less homogeneous nature compared to the other layers. This can be observed in the PCA score plots of primer spectra, where spectra from the same sample were projected discreetly and displayed a large distance between each other (see chapter 8.5.6).

The number of samples that contain intra-sample variability related to peak present/absence within each layer were calculated, which from clearcoat to primer, is 3, 6, 1, 6 respectively. When visually comparing samples, all subsamples and respective replicates were taken into consideration. It is important to note that all the observed intra-sample variabilities did not affect the characterization of chemical categories.

In conclusion, the IR analysis conducted on the whole sample set revealed minimal intra-sample variability in terms of chemical characteristics. This finding indicates that the chemical compositions of the samples could be accurately characterized, facilitating reliable comparisons between them. It is important to note that all subsequent characterizations and

classifications discussed in the subsequent chapters will be grounded in the analysis of individual vehicles (n=62).
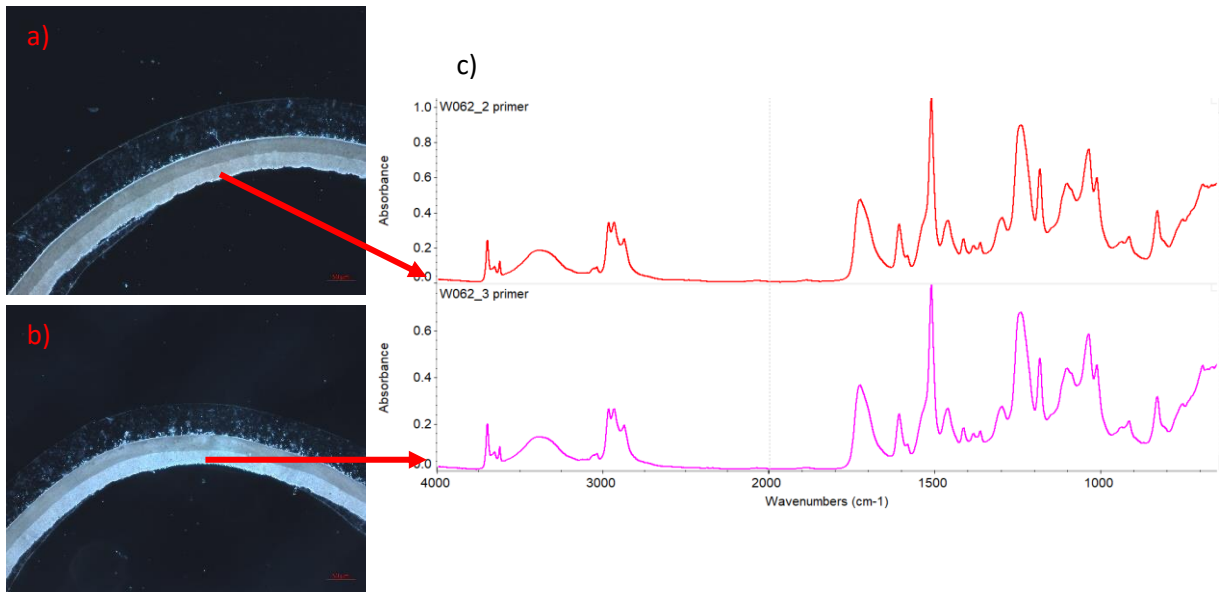
Figure 66. Dark field images of sample W062_2 (a) and sample W062_3 (b) and IR spectra obtained from primer of these samples (c).
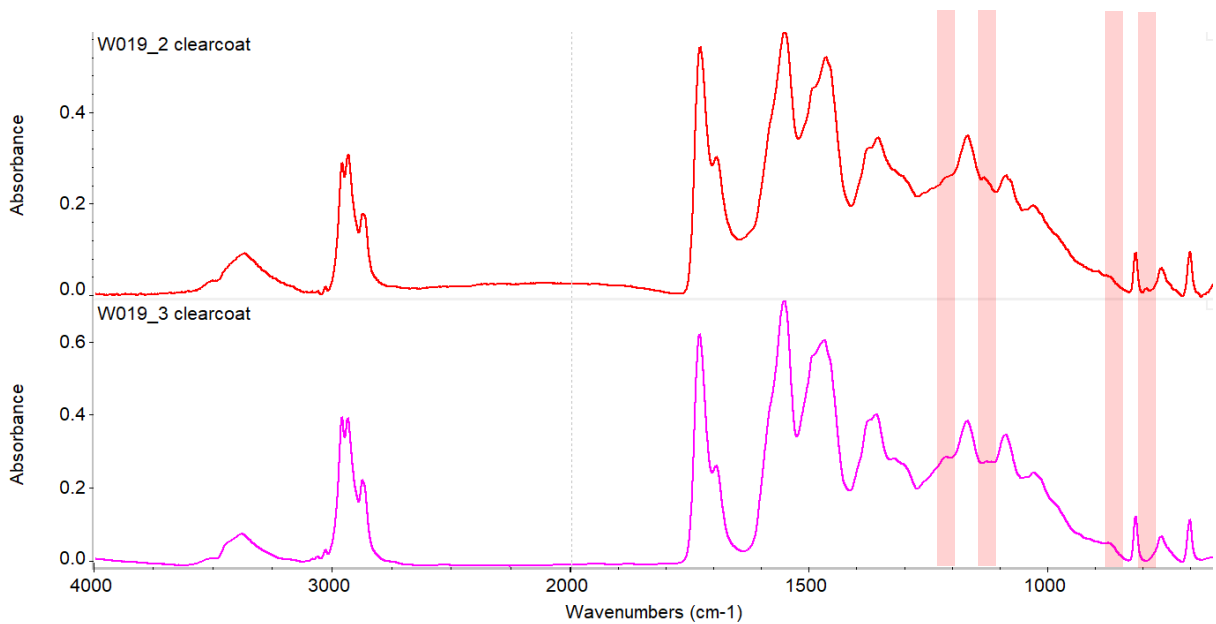
Figure 67. IR spectra obtained from sample W019_2(top) and sample W019_3(bottom). The observed differences are highlighted in red zone.

8.2.   Characterization of clearcoat

Out of the 62 samples in the sample set, eight of them belong to the repainted group and have no clearcoat, while three samples (W017, W022, W030) failed to acquire spectra data due to sample preparation, only 51 samples contain clearcoat. Based on the previous three groups generated by microscopic examination, further discrimination and characterization were made. Notably, only OEM systems were taken into account for samples that featured additional repainted layers. In these 51 samples, 3 were found to have intra-sample variability related to the presence or absence of small peaks.

Table 28 summarizes the results of the visual characterization of FTIR spectra obtained from the clearcoat of all white automotive paints, classifying the samples into two main groups based on the chemical categories of the binders used in the paint. Each group of spectra is then individually analyzed to identify the constituents detected by FTIR in the investigated paints. Further visual comparisons were carried out to identify distinguishable subgroups within each group. These comparisons relied on the presence or absence of certain peaks and the relative intensities of the peaks detected in the IR spectra. To ensure the homogeneity of the analyses, all replicas of each sample were taken into consideration. The subgroups were also summarized in *Table 28*, which highlights the main differences observed between the spectra of samples with similar characterization.

Table 28. Summary of visual characterization and groupings based on the FTIR spectra of the clearcoat of the automotive paint samples in this thesis (n=51).

GROUP/BINDER TYPE	SUB-GROUP	SAMPLES	DIFFERENCE WITHIN THE GROUP
GROUP 1 **PUR+(STY)**	1.1	W002, W007, W020, W023, W036, W053	Peaks presented at 1728 cm^{-1} and 1157 cm^{-1}, additional peak at 846 cm^{-1}
	1.2	W010, W012, W014, W015, W016, W018, W032, W041, W042, W044, W045, W047, W049, W051, W054	Peaks presented at 1733 cm^{-1} and 1162 cm^{-1}
	1.3	W005, W033, W046	Sharper peak at 1130 cm^{-1}, absence of peaks at 3084 cm^{-1}, 3061 cm^{-1}, 3027 cm^{-1}, and 700 cm^{-1}
	1.4	W048, W062	Broad peak at 1546 cm^{-1}
	1.5	W026	Additional peak at 1550 cm^{-1}
GROUP 2 **ACR+PUR+STY+MEL**	2.1	W001, W027, W028, W034, W061	Low intensity of peak at 1690 cm^{-1}, additional peak at 1455 cm^{-1}
	2.2	W003, W011, W019, W021, W031, W039, W050, W052, W055	High intensity of peaks at 1550 cm^{-1}, 1470 cm^{-1}, and 1360 cm^{-1}
	2.3	W006, W009, W024, W035, W043, W058, W059, W060	High intensites of peaks at 1690 cm^{-1}, 1465 cm^{-1}, and 1242 cm^{-1}
	2.4	W025, W040	Highest intensities of peaks at 1690 cm^{-1}, 1465 cm^{-1}, and 1242 cm^{-1}

8.2.1. Group 1 – clearcoat

This group comprises 27 samples (see Group 1 in *Table 28*), which share the same chemical information as determined by FTIR analysis, representing approximately 53% of the total sampling in this study. A typical spectrum of the analyzed group displays significant characteristic absorption peaks at 3380, 2936, 2862, 1732, 1690, 1526, 1465, 1242, 1162, and 765 cm^{-1}. The broad peak at 3380 cm^{-1} is attributed to the stretching vibration of the O-H group, while the bands around 2936 and 2860 cm^{-1} correspond to the C-H asymmetric and symmetric stretching vibrations, respectively. The strong absorption peaks at 1732 and 1690 cm^{-1} can be attributed to the stretching vibration of the carbonyl group (C=O). The peak at 1526 cm^{-1} is due to the stretching vibration of C-N and N-H bond in urethane, while the peak at 1465 cm^{-1} can be attributed to the symmetric bending vibration of the methylene (-CH$_2$-) groups. The peak at 1242 cm^{-1} corresponds to the stretching vibration of the C-O bond, while the peak at 1162 cm^{-1} corresponds to the stretching vibration of the C-O-C bond in ether. Finally, the absorption at 765 cm^{-1} is attributed to the out-of-plane bending vibration of the C-H group. Overall, these characteristic peaks are consistent with those that constitute the FTIR fingerprints of polyurethane. The characteristic peaks of this group as well as a comparison between a reference polyurethane clearcoat produced by Dupont are shown in *Figure 68*.
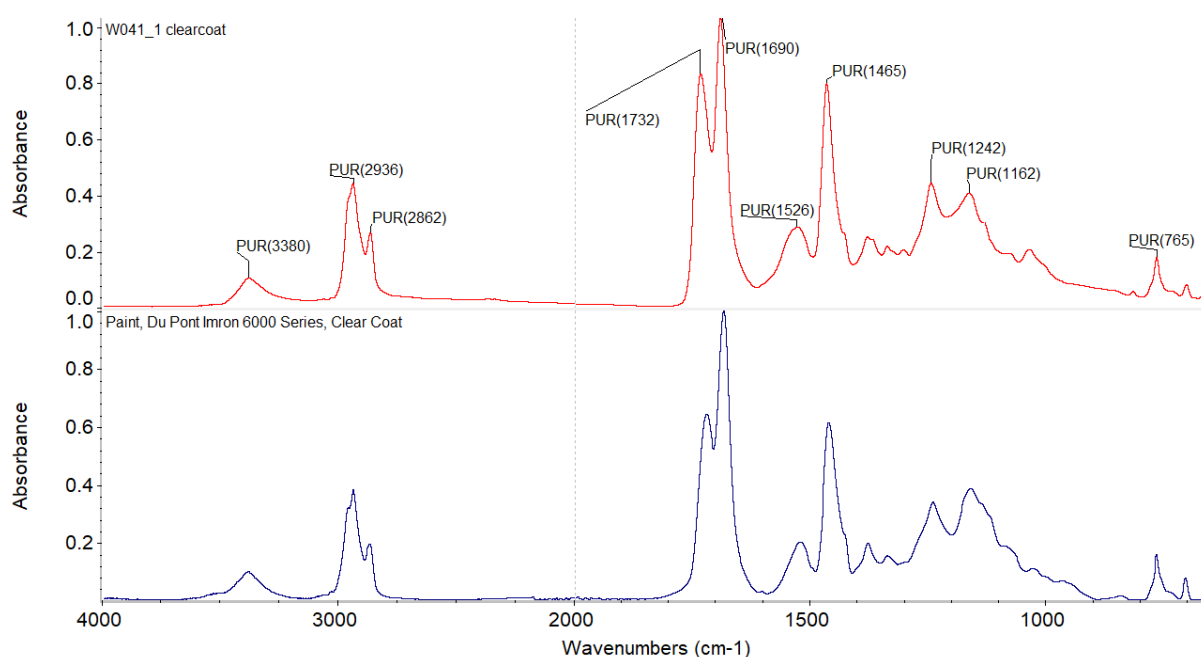
Figure 68. Comparison of a representative IR spectrum of the clearcoat of sample W041_1 (top) with a reference polyurethane clearcoat (bottom) produced by DuPont (DuPont Imron 6000 series, clearcoat). Characteristic peaks of polyurethane are annotated on the spectrum of sample W041_1.

In addition to polyurethane, a significant number of samples in this group also exhibit faint peaks at 3060, 3026, and 700 cm^{-1} in their IR spectra. The two subtle peaks located at 3060 and 3026 cm^{-1} correspond to the stretching vibrations of the aromatic C-H bond, while the peak at 700 cm^{-1} is attributed to the out-of-plane bending vibration of the aromatic ring. These characteristic peaks align with the IR spectrum of styrene, a commonly utilized polymer in industry. A graphical representation of the characteristic styrene peaks observed in the sample, along with a comparison to a standard styrene IR spectrum, is depicted in *Figure 69*.
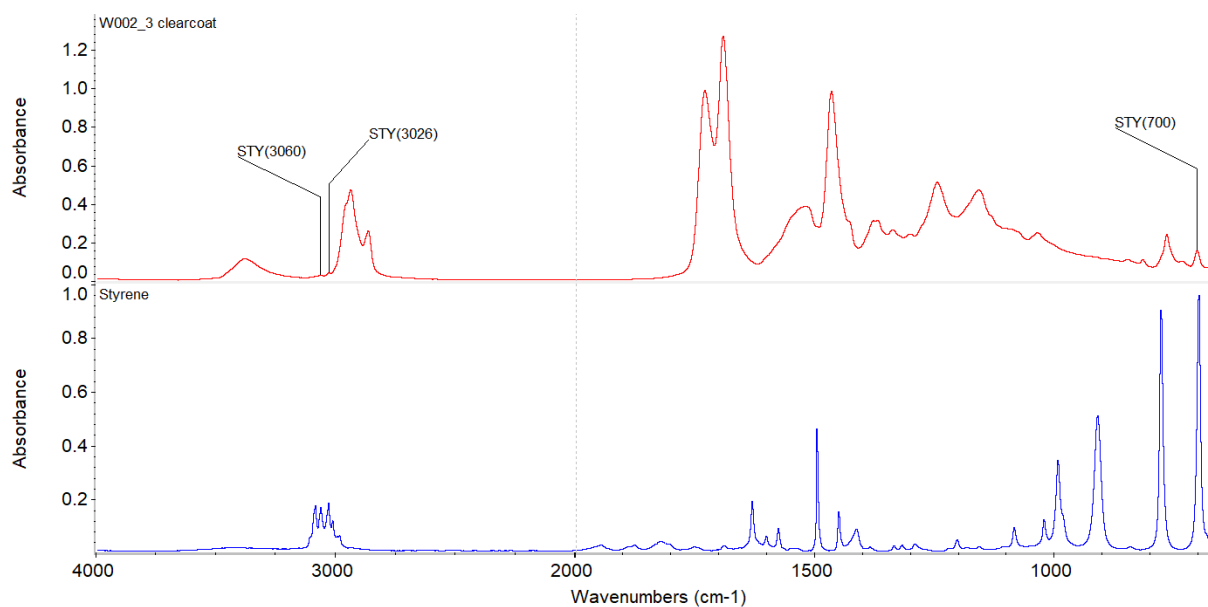
Figure 69. Comparison of a representative IR spectrum of the clearcoat of sample W002_3 (top) with a standard styrene spectrum (bottom). Characteristic peaks of styrene are annotated on the spectrum of sample W002_3.

8.2.2. Group 2 – clearcoat

This group is composed of 24 samples (see Group 2 in *Table 28*), accounting for approximately 47% of the total sample set. The IR spectra of these 24 samples reveal distinct absorption bands, which include a broad band at 3380 cm^{-1}, corresponding to the O-H stretching vibration. The medium bands observed at 2957, 2930, and 2873 cm^{-1} represent the C-H asymmetric and symmetric stretching vibrations. Furthermore, a strong band located at 1730 cm^{-1} is attributed to the stretching vibration of the carbonyl group (C=O). Additionally, the medium band at 1380 cm^{-1} arises from the C-H bending vibration, while the strong band at 1170 cm^{-1} corresponds to the C-O-C stretching vibration. Lastly, the medium band observed at 1088 cm^{-1} can be assigned to the C=O stretching vibration. These characteristic bands are consistent with those typically observed for acrylic resins. Based on the results of the IR spectrum analysis, it can be inferred that acrylic resin is the primary resin present in these 24 samples. *Figure 70* displays the characteristic peaks of acrylic from the sample as well as a comparison between a reference acrylic paint produced by Dupont.
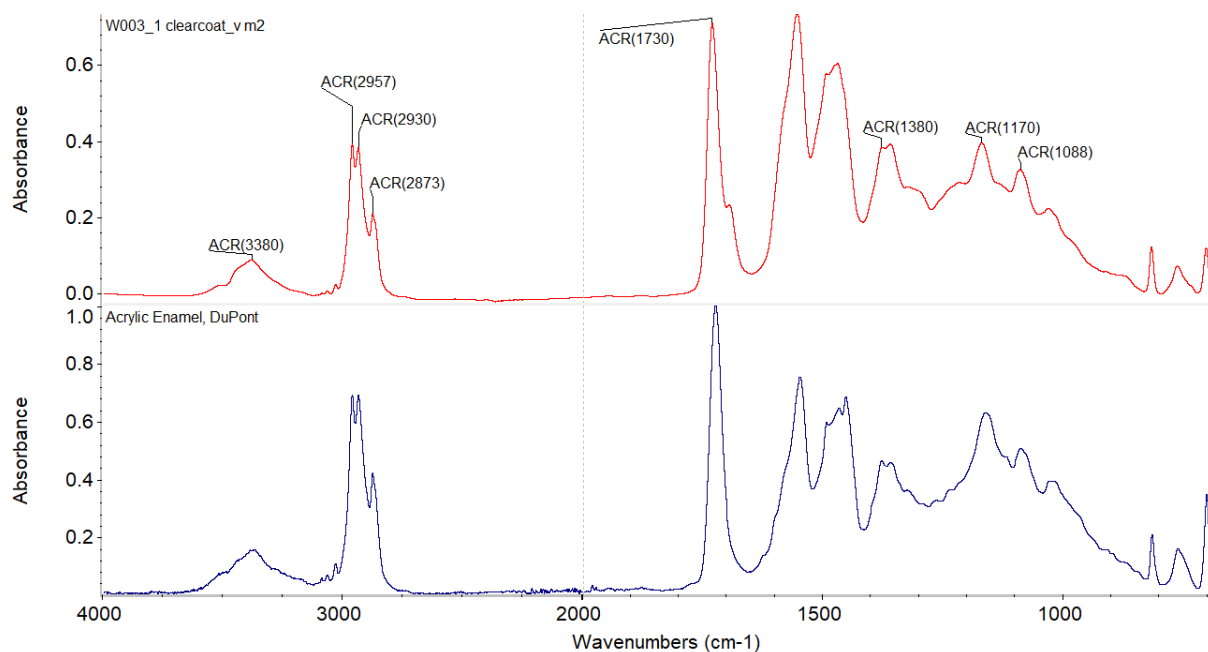
Figure 70. Comparison of a representative IR spectrum of the clearcoat of sample W003_1 (top) with a reference acrylic paint (bottom) produced by DuPont (Acrylic Enamel, DuPont). Characteristic peaks of acrylic are annotated on the spectrum of sample W003_1.

Apart from the primary resin, the IR spectra of the sample set revealed characteristic peaks from additional resins. All the samples in this group exhibit characteristic peaks at 3084, 3061, 3027, 1490, 760, and 700 cm^{-1}. The three weak peaks at 3084, 3061, and 3027 cm^{-1} correspond to the stretching vibrations of the aromatic C-H bond. The peak at 1490 cm^{-1} is attributed to the deformation of the aromatic ring, while the peak at 760 cm^{-1} corresponds to the bending of the C-H bond in the aromatic ring. The peak at 700 cm^{-1} is assigned to the out-of-plane bending vibration of the aromatic ring. These characteristic peaks are consistent with the IR spectrum of styrene. Therefore, based on the analysis of the IR spectra, it can be concluded that the samples in this group contain styrene as one of the additional resins in their clearcoat. Characteristic peaks of styrene presented in the sample as well as a comparison between a standard styrene IR spectrum is illustrated in *Figure 71*.

The IR spectra of the 24 samples also revealed the presence of additional peaks at 1550 and 815 cm^{-1}. These peaks were observed in all the samples of the group and can be assigned to the symmetric and asymmetric triazine ring breathing vibrations of melamine, respectively. Melamine is a nitrogen-rich compound commonly used in the production of formaldehyde-melamine resins, which are widely used in coatings and adhesives due to their excellent properties such as hardness, scratch resistance, and durability (Lambourne and Strivens,1999). The presence of melamine in these samples can be attributed to its use as a crosslinking agent in the formulation of the clearcoat (Caddy,2001). *Figure 71* illustrates the distinctive peaks of melamine found in the sample, along with a comparison to a standard butylated melamine-formaldehyde resin.
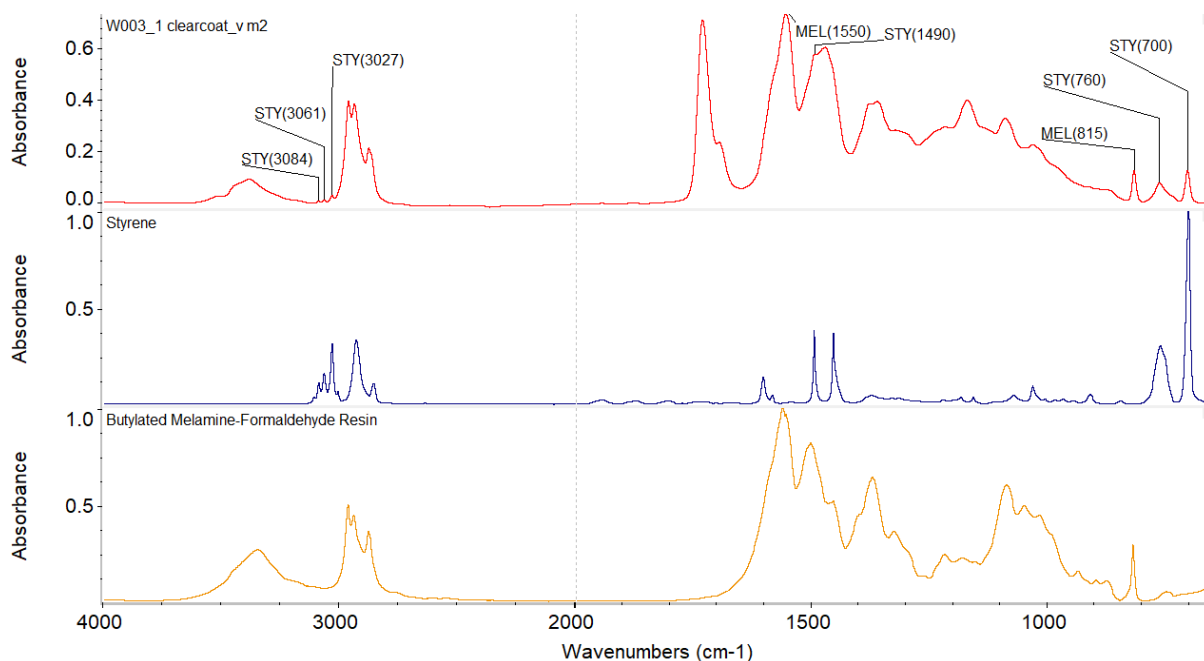
Figure 71. Comparison of the representative IR spectrum of the clearcoat from sample W003_1 (top) containing styrene and melamine with a standard styrene spectrum (middle) and a standard melamine spectrum (bottom). The characteristic peaks of styrene and melamine are annotated on the spectrum of sample W003_1.

Polyurethane peaks were detected in all samples within this group. Depending on the concentration of polyurethane in the clearcoat, the peaks at 1690 and 1465 cm^{-1} may vary in intensity between samples. *Figure 72* shows the clearcoat spectra of two samples in this group, with one sample exhibiting a strong polyurethane peak while the other does not.
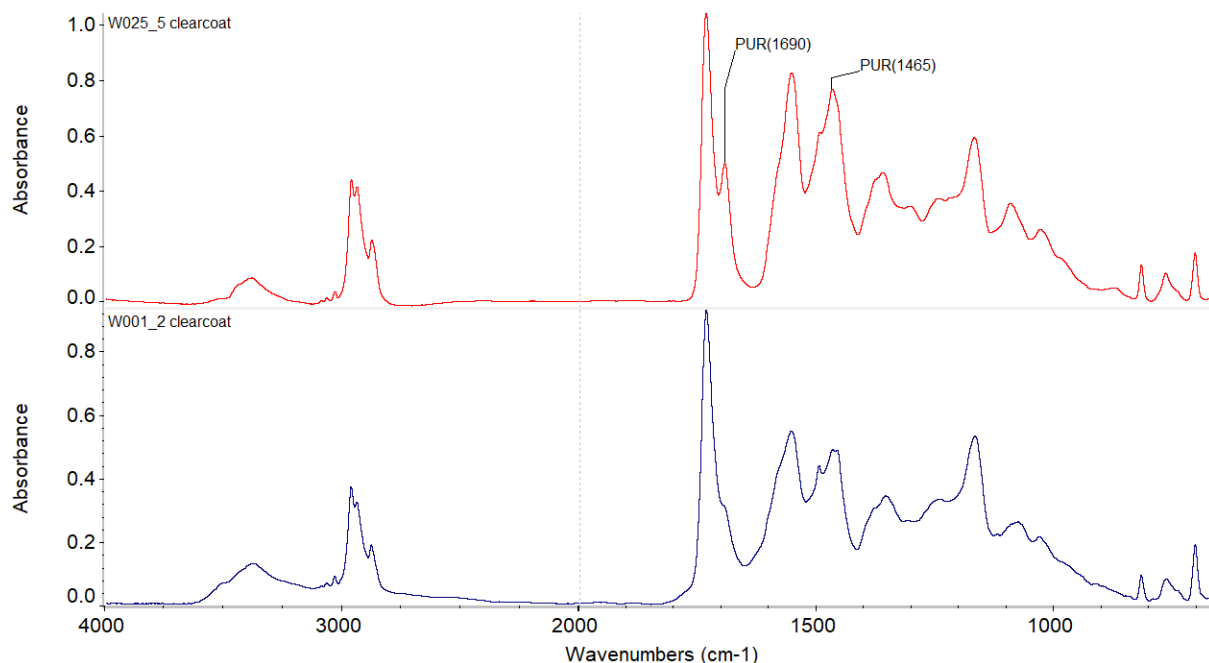
Figure 72. Comparison of the IR spectra of two samples in the group; sample W025_5 (top) showing strong peaks from polyurethane and sample W001 (bottom) with very low concentration of polyurethane. The polyurethane characteristic peaks are annotated on the spectrum of sample W025_5.

8.2.3. Classification and discrimination of clearcoat

Table 29 provides a summary of the characteristic compounds identified from the IR spectra of the clearcoat for each sample examined in this study.

Table 29. Summary of characteristic compound based on the FTIR spectra of the clearcoat of the automotive paint samples in this thesis (n=51)

Sample\ Composition	PUR	ACR	ALK IPH	ALK OPH	MEL	STY
BINDER						
W001		X			X	X
W002	X					X
W003	X	X			X	X
W005	X					
W006	X	X			X	X
W007	X					X
W009	X	X			X	X
W010	X					X
W011	X	X			X	X
W012	X					X
W014	X					X
W015	X					X
W016	X					X
W018	X					X
W019	X	X			X	X
W020	X					X
W021	X	X			X	X
W023	X					X
W024	X	X			X	X
W025	X	X			X	X
W026	X				X	X
W027		X			X	X
W028		X			X	X
W031	X	X			X	X
W032	X					X
W033	X					
W034		X			X	X
W035	X	X			X	X
W036	X					X
W039	X	X			X	X
W040	X	X			X	X
W041	X					X
W042	X					X
W043	X	X			X	X
W044	X					X
W045	X					X
W046	X					
W047	X					X
W048	X					X
W049	X					X
W050	X	X			X	X
W051	X					X
W052	X	X			X	X
W053	X					X
W054	X					X
W055	X	X			X	X
W058	X	X			X	X
W059	X	X			X	X
W060	X	X			X	X
W061	X	X			X	X
W062	X					X
Total	**47**	**24**			**25**	**48**

Based on the chemical composition of the binders in the analyzed paint, two main groups can be distinguished among the considered samples (see *Figure 73)*. The majority of samples (53%) contain polyurethane resin as the binder, alongside additional styrene. The remaining 24 samples (47%) utilize acrylic resin as the primary binder, in conjunction with polyurethane, styrene, and melamine as additional resins. This outcome is consistent with findings from various studies, in which the authors concluded that polyurethane and acrylic-melamine resins are most commonly detected in clear coats (Maric *et al.*,2012; Bender,2013; Lavine *et al.*,2014b; Houck and Siegel,2015).
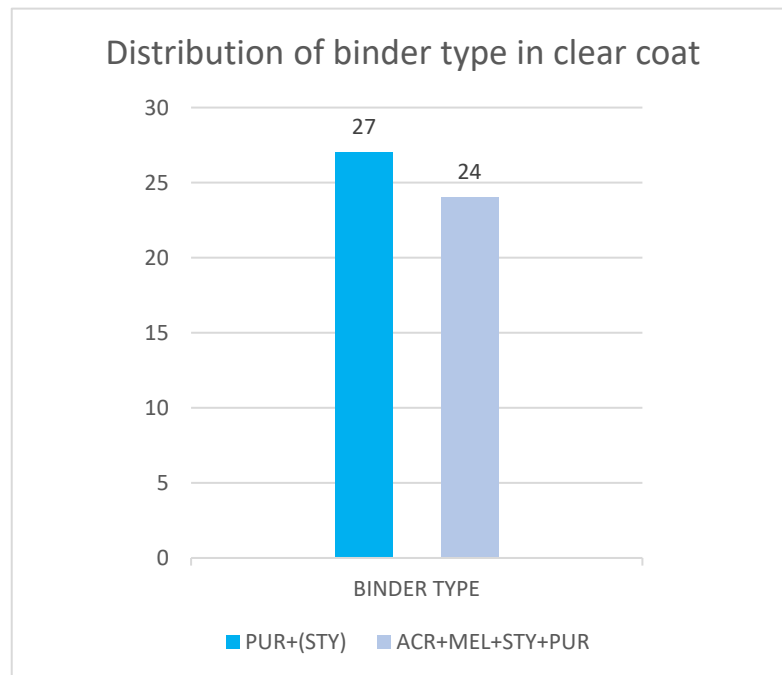
Figure 73. Distribution of binder type characterized in clearcoat.

Based on the subgroups presented in *Table 28*, it is possible to determine the discriminating power of visual comparisons of spectra obtained for clearcoat using FTIR. The discriminating power (DP) can be calculated according to Smalldon and Moffat (Smalldon and Moffat,1973) based on the number of pairs of undifferentiated samples (199 pairs, for a total of 51 samples). The subgroups of spectra after visual comparisons result in a DP of 84.4%.

To gain further insight into the groupings, the original information and physical features were examined. An interesting observation is that the chemical composition of the clearcoat appears to be closely associated with the layer sequence. For instance, all samples in Group 1 except Sample W026, which contain polyurethane binder type, display the OEM3 paint system. Similarly, all the samples in Group 2, which have an acrylic with styrene and melamine modified binder type, exhibit the OEM4 system. Sample W026 was collected from a vehicle produced in Germany. The observed non-conformity of this sample with the pattern observed in the other Chinese-produced samples can be attributed to its distinct origin. However, except for the pattern observed for the binder type of the clearcoat in relation to the layer structure, no correlation was found within the identifying factor for the undifferentiated pairs.

8.2.4. Exploratory analysis

A comprehensive analysis of 318 IR spectra of clearcoat (from 51 samples with 106 subsamples) was conducted using a global PCA to effectively visualize the underlying data structure. All the spectra were pre-treated with baseline offset, SNV normalization and detrended with a polynomial order of 2, following the established procedure. The variables in the range of 3100-2828 and 1800-680 cm^{-1} (2888 points) were selected for.

Figure 74 provides an overview of the PCA model, displaying the projections of IR spectra based on the first two principal components (PC1 and PC2), which account for 95% of the total sampling variance. Remarkably, the PCA analysis yielded the same groupings as those observed through visual comparison of the IR spectra, which were based on the binder types employed in the clearcoat. Two prominent clusters were formed on the PCA score plot, aligning with the distinct binder types (as depicted in *Figure 74a*). Further interpretation of the loadings associated with the first principal component (PC1, as shown in *Figure 74b*) revealed the positive influence of wave numbers corresponding to characteristic peaks of polyurethane, while negative values predominantly stemmed from the signal corresponding to characteristic peaks of acrylic, melamine, and styrene. Moreover, the loading for the second principal component (PC2, illustrated in *Figure 74d*) reflected the signal of polyurethane present in certain samples where acrylic, melamine, and styrene served as the main binder types, effectively separating these samples into two distinct subgroups. The PCA score plot, when examined individually for each sample, provided a detailed depiction of the groupings that aligned consistently with those obtained through visual comparison (*Figure 74c*).

To explore deeper into the differentiation within each binder group, additional PCA analyses were undertaken. However, the outcomes of these analyses fell short of the desired separation results. The majority of samples exhibited close projection, making it challenging to discern distinct clusters. Visual examination revealed that many samples were distinguished by minute peaks or, in some instances, remained undifferentiated. A proven method to enhance this situation involves baseline treatment through Savitzky-Golay type 1st derivative (with polynomial order 2 and 5 smoothing points), which has been demonstrated to maximize inter-sample distances (Lambert,2017). Subsequently, the baseline-offset data underwent this treatment, followed by SNV normalization. The overall PCA results reaffirmed the same separation pattern based on binder type as shown in *Figure 74*. However, when individual PCA analyses were conducted on each binder group, improved separation was attained. *Figure 75* and *Figure 76* present the results of PCA separation and the relative similarity of samples within the two chemical classes, respectively.

Figure 75 shows that when considering the first two principal components (which account for 75% of the total variance), only three distinct clusters were observed. The loading plot of PC1 indicates that the separation was based on the peaks at 1733, 1460, 1162, 1130, and 846 cm^{-1}. The presence, absence, or peak shift at these positions explain why samples within the same chemical class can be differentiated into subgroups. With the addition of PC3 and PC4, two

more clusters can be distinguished based on the peak at 1540 cm^{-1}. Consistent with visual comparison, the polyurethane group exhibits five clusters when considering the first four principal components of this model.

*Figure 76*Figure 75 depicts the PCA separation results within the class of acrylic-melamine-styrene. Four clusters can be distinguished based on the first two principal components, which account for 64% and 14% of the total variance. This separation aligns with the visual groupings. The weights of PC1 and PC2 reveal that peaks at 1690, 1550, 1465, and 1130 cm^{-1} have a significant impact on the separation. The relative intensity of these peaks is the reason behind the visual groupings. The addition of more PCs does not add more distinct groups.

The visual comparison of clearcoat IR spectra revealed nine clusters, and these clusters were successfully visualized using the first four principal components of the PCA model (see *Table 28*). Therefore, based on these groups, a discriminatory power of 84.4% can be obtained by PCA observation of the IR spectra of the clearcoat of the paint systems in this study (199 undifferentiated pairs, for a total of 51 samples).
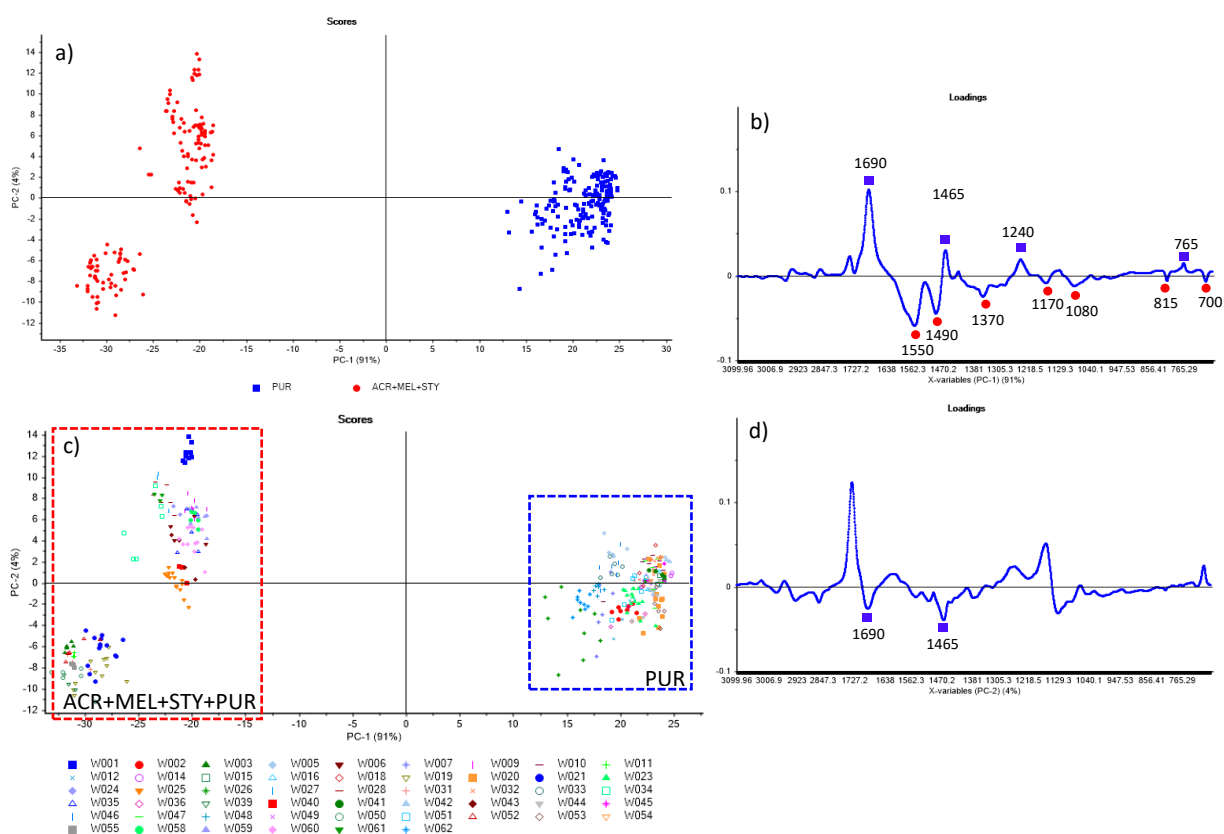
Figure 74. PCA score and loading plots according to the first two principal components for the IR spectra dataset of clearcoat (n=51): (a) PCA score plot where spectra were represented using different colors and shapes according to the binder type characterized on the spectra; (b) loading plot of PC1, with peaks of characterized binder that significantly impact the separation on PC1 highlighting on the plot; (c) sample distribution based on PC1 and PC2, which account for 95% of total variance; (d) loading plot of PC2, with peaks of characterized binder that significantly impact the separation on PC1 highlighting on the plot.

134
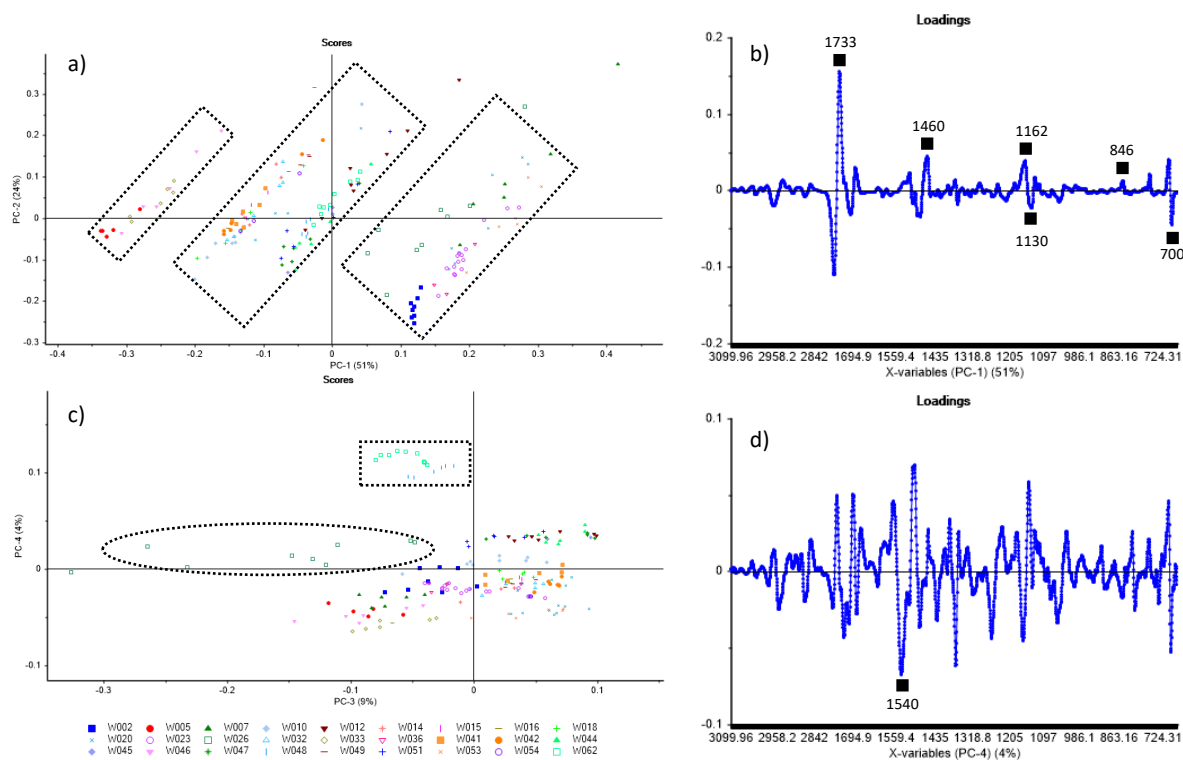
Figure 75. PCA score and loading plots for clearcoat IR spectra of samples from group polyurethane (n=27): (a) PCA score plot based on PC1 and PC2, which account for 51% and 24% of the total variance, respectively. 4 clusters were generated on this score plot; (b) loading plot of PC1, with peaks of characterized binder that significantly impact the separation on PC1 highlighting on the plot; (c) PCA score plot based on PC3 and PC4, accounting for 9% and 4% of the total variance, respectively. Two more clusters can be separated based on PC4; (d) loading plot of PC4, with peaks that significantly impact the separation on PC4 highlighting on the plot.
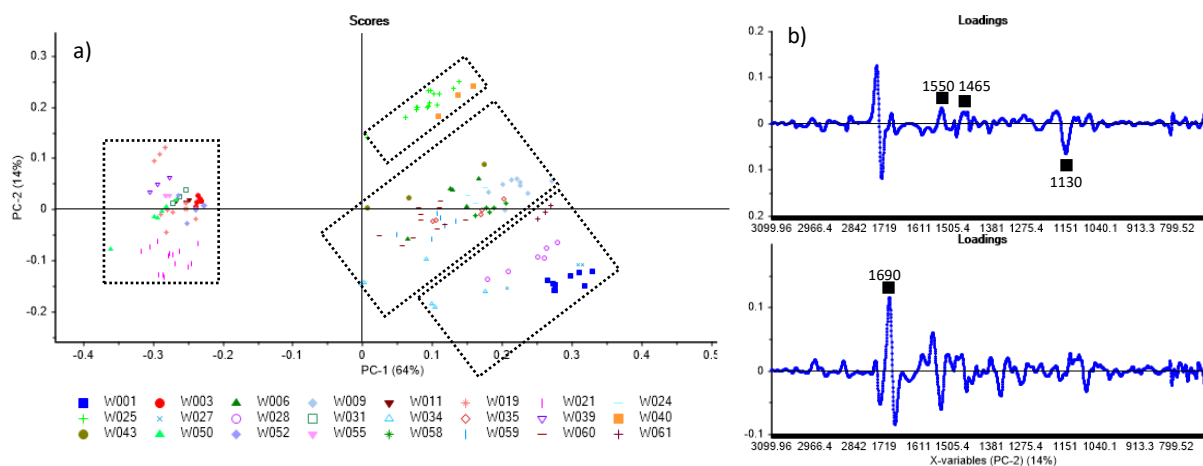
Figure 76. PCA score and loading plots for clearcoat IR spectra of samples from group acrylic modified by melamine and styrene (n=24): (a) PCA score plot based on PC1 and PC2, which account for 64% and 14% of the total variance, respectively. 4 clusters were generated on this score plot; (b) loading plot of PC1 and PC2, with peaks that significantly impact the separation highlighting on the plot.

Apart from the chemical class and individual sample number, the data structure can also be elucidated based on several predetermined identifying factors, as depicted in *Figure 77*. The PCA score plots of clearcoat IR spectra are presented in relation to manufacturing companies (*Figure 77a*), layer structure of paint samples (*Figure 77b*), assembly plants (*Figure 77c*), and vehicle models (*Figure 77d*). Analyzing these PCA score plots reveals that, with the exception of sample W026, all samples displaying the OEM3 layer structure exhibit the polyurethane binder type, whereas samples with the OEM4 paint system consistently contain an acrylic binder type modified with styrene and melamine.

No discernible structure linked to the manufacturing company, assembly plant, or vehicle model emerges from this exploratory analysis (*Figure 77b-d*). It appears that both F-VW and S-VW manufacturing companies in China employ both types of binder in their clearcoat application formula. Most assembly plants (Plant Changchun, Plant Chengdu, Plant Ningbo, and Plant Osnabrück) exclusively utilize a single type of binder in their clearcoat. An exception was observed in Plant Anting and Plant Nanjing, where two different binder types were found in their respective products. Upon further investigation, it was revealed that Plant Anting consists of three sub-plants sharing the same plant code. Each sub-plant operates its independent production line, employing different layer systems and thus utilizing different binder types. However, the exception in Plant Nanjing remains unexplained. Apart from that exception (Sample W009), all other vehicles produced in Plant Nanjing exhibit the same layer system and binder type. Furthermore, Sample W009 corresponds to the New Lavida model, while all other vehicles of the same model display the OEM3 layer system, whereas only Sample W009 has the OEM4 system.
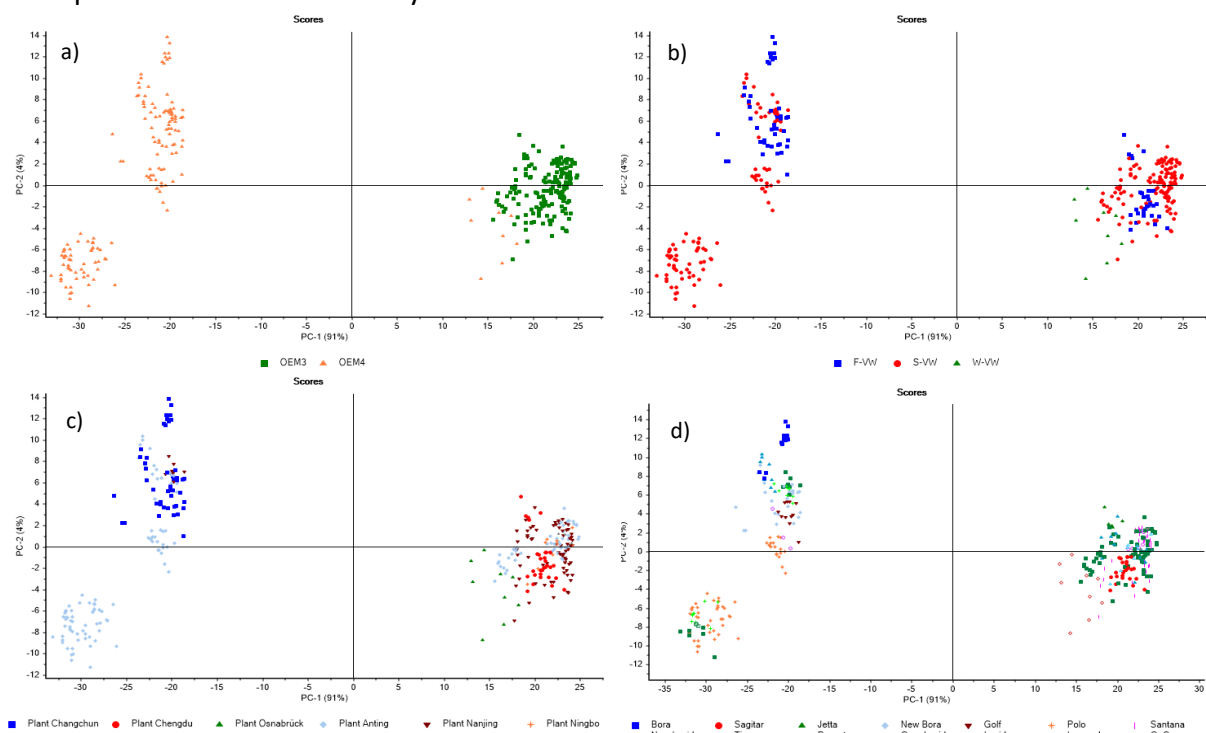
Figure 77. PCA score plots according to the first two principal components of all IR spectra of clearcoats, respectively according to the layer structure (a), their manufacturing companies (b), their assembly plants (c) and the model of vehicles(d).

8.3. Characterization of basecoat

In this section, the characterization of a total of 62 samples is presented. Among these samples, some did not have an original equipment manufacturer (OEM) system, and in these cases, the outmost layers were considered as basecoat. These samples were exclusively found in the repainted group. On the other hand, for samples that retained their OEM system, only the original basecoat was taken into account for analysis, despite their additional repainted layers.

Table 30 summarizes the results of the visual comparison of FTIR spectra obtained from the basecoat of all white automotive paints, classifying the samples into 7 groups based on the chemical categories of the binders, pigments and extenders used in the paint. Each group of spectra is then individually analyzed to identify the constituents detected by FTIR in the investigated paints. Further visual comparisons were carried out to identify distinguishable subgroups within each group, as presented in the table.

Table 30. Summary of visual characterization and groupings based on the FTIR spectra of the basecoat of the automotive paint samples in this thesis (n=62).

GROUP/COMPOSITION	SUB-GROUP	SAMPLES	DIFFERENCE WITHIN THE GROUP
Group 1 **PUR+ALK IPH+TALC+TIO2**	1.1	W002, W005, W010, W012, W014, W015, W016, W018, W020, W023, W032, W033, W036, W041, W042, W044, W045, W046, W047, W049, W051, W053, W054	Sample different from others as follows
	1.2	W007	Relative intensities of peaks at 1730 and 1690 cm^{-1}
Group 2 **PUR+MEL+TIO2**	2.1	W048	Samples different from others as follows
	2.2	W062	Absence of peak at 1515 cm^{-1}, additional peak at 915 cm^{-1}
Group 3 **ACR+ALK IPH+MEL+PUR** **+TIO2**	3.1	W001, W061	Shoulder peak at 1690 cm^{-1}
	3.2	W027, W028, W050	Relative intensities of peaks at 1305 and 1240 cm^{-1}
	3.3	W003, W011, W021, W039	Relative intensities of peaks at 2933, 1690 and 1140 cm^{-1}
	3.4	W017, W043	Higher peak at 1690 cm^{-1}
	3.5	W006, W059	Relative intensities of peaks at 2933 and 1690 cm^{-1}
	3.6	W022, W024, W058, W060	Relative intensities of peaks at 2933,1305 and 1040 cm^{-1}
	3.7	W030, W031, W052	Relative intensities of peaks at 2933 and 1305 cm^{-1}
	3.8	W009	Relative intensities of peaks at 2933, 1690 and 1305 cm^{-1}
	3.9	W034	Relative intensities of peaks at 2933,1305 and 1096 cm^{-1}
	3.10	W035	Relative intensities of peaks at 1690, 1305 and 1096 cm^{-1}
	3.11	W019, W025, W040	Relative intensities of peaks at 1690, 1305, 1240, 1170 and 1130 cm^{-1}
	3.12	W055	Peak broader at around 1240 cm^{-1}
Group 4 **ACR+PUR+MEL+TALC+TIO2**	-	W026	Single sample of the group
Group 5 **PUR+ STY+TIO2**	5.1	W004	Samples different from others as follows
	5.2	W029	Absence of peak at 1165 cm^{-1}
	5.3	W037	Additional peak at 1175 cm^{-1}, absence of peak at 1165 cm^{-1}
	5.4	W038	Broader peak at 1165 cm^{-1}
	5.5	W056	Additional peaks at 1270 and 1126 cm^{-1}
	5.6	W057	Relative intensities of peaks at 1075 and 1030 cm^{-1}
Group 6 **ALK OPH+MEL+TIO2**	-	W008	Single sample of the group
Group 7 **ACR+MEL+STY+TIO2**	-	W013	Single sample of the group

8.3.1. Group 1 – basecoat

Representing approximately 39% of the total samples in this study, this group is composed of 24 samples that share the same binder type as determined by FTIR analysis (see Group 1 in *Table 30)*. A typical spectrum of the analyzed group displays diagnostic absorption peaks at 3370, 2935, 2860, 1725, 1690, 1526, 1465, 1378, 1302, 1242, 1140, 1095, 1075 and 730 cm^{-1}. The broad peak at 3370 cm^{-1} is a characteristic stretching vibration of the hydroxyl (-OH) group. The peaks at 2935 and 2860 cm^{-1} correspond to the symmetric and asymmetric stretching vibrations, respectively, of the methylene (-CH2-) groups. The strong peak at 1725 cm^{-1} is attributed to the stretching vibration of the carbonyl (C=O) group, while the strong peak at 1690 cm^{-1} is attributed to the C=O stretching vibration of the urethane groups. The medium peak at 1526 cm^{-1} is due to the stretching vibration of C-H and N-H bond of the urethane groups, while the strong peak at 1465 cm^{-1} can be attributed to C-H bending vibrations. The weak peaks at 1378 cm^{-1} could be attributed to the deformation vibrations of the C-H group in the aromatic ring, while the peak at 1302 and 1242 cm^{-1} was due to the C-O vibration of isophthalic ester. The peaks at 1140, 1095 and 1075 cm^{-1} can all correspond to the C-O-C stretching. Based on the distinctive absorption peaks identified in the analyzed group, it can be inferred that the primary resin in the basecoat is polyurethane, with isophthalic alkyd serving as an additional resin. *Figure 78* illustrates the diagnostic peaks of polyurethane as well as isophthalic alkyd found in the sample.
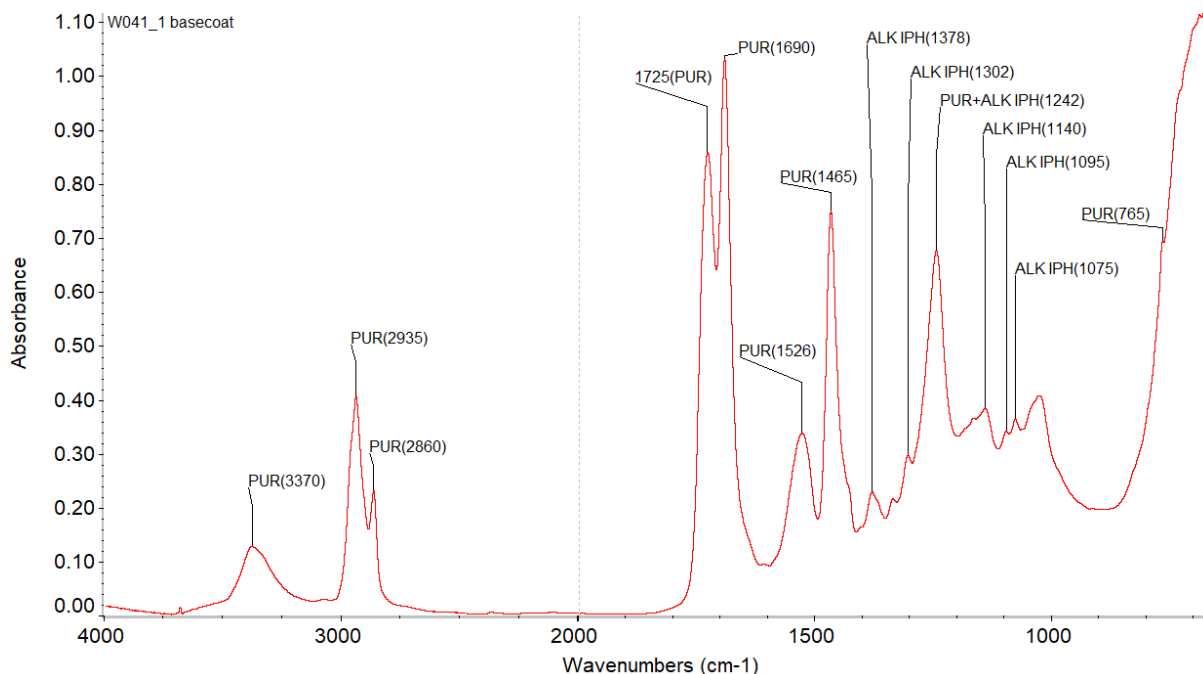
Figure 78. A representative IR spectrum of the basecoat of sample W041_1 with characteristic peaks of polyurethane and isophthalic alkyd annotated on the spectrum.

In addition to the binder types, FTIR analysis also revealed the presence of pigments and extenders in the analyzed samples. The IR spectra showed a rising absorbance towards 700 cm^{-1}, indicating the presence of titanium dioxide (TiO$_2$), which is the most common inorganic pigment used for generating white color in paint. The characteristic peaks at 3678 and 1020 cm^{-1} correspond to the peaks of talc, a commonly used extender in paint formulations. Overall, these results suggest that the analyzed basecoats contain TiO$_2$ as a white pigment and talc as an extender. *Figure 79* illustrates the distinctive peaks of TiO$_2$ and talc found in the sample, along with a comparison to the reference spectra of pure TiO$_2$ and talc.
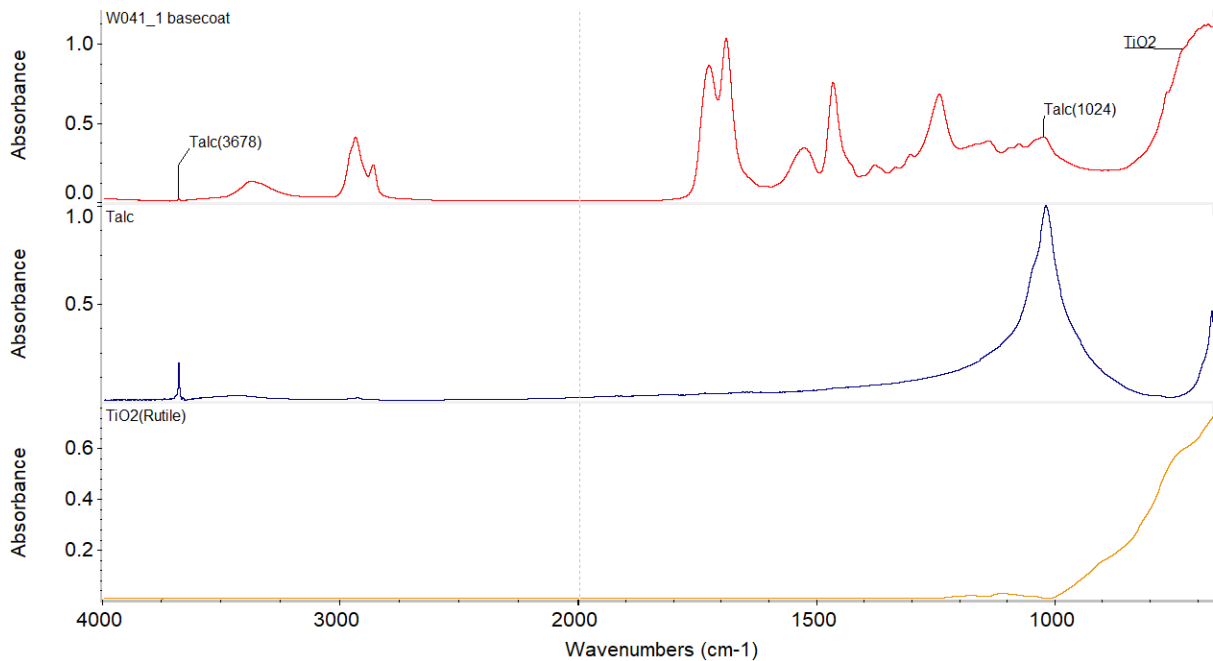
Figure 79. Comparison of the representative IR spectrum of the basecoat from sample W041_1 (top) containing talc and TiO$_2$ with reference spectra of pure talc (middle) and pure TiO$_2$ (bottom). The characteristic peaks of talc and TiO2 are annotated on the spectrum of sample W041_1.

8.3.2. Group 2 – basecoat

Out of the total sample set, this group is comprised of only 2 samples (see Group 2 in *Table 30*), accounting for a mere 3% of the total sample set. The primary resin present in this group has been identified as polyurethane, based on the distinctive absorption peaks observed in the FTIR spectra. In addition, melamine has also been detected in these samples, suggesting its use as an additional resin in the formulation. The characteristic absorption peaks of both polyurethane and melamine are illustrated in detail in *Figure 80*, providing a clear representation of their respective IR spectra.

In this group of basecoats, the presence of TiO_2 was detected as expected. However, interestingly, no talc was detected in any of the samples, which suggests that talc was not added as an extender in the basecoat formulation. The absence of talc in these basecoats may indicate the use of different formulation strategies.
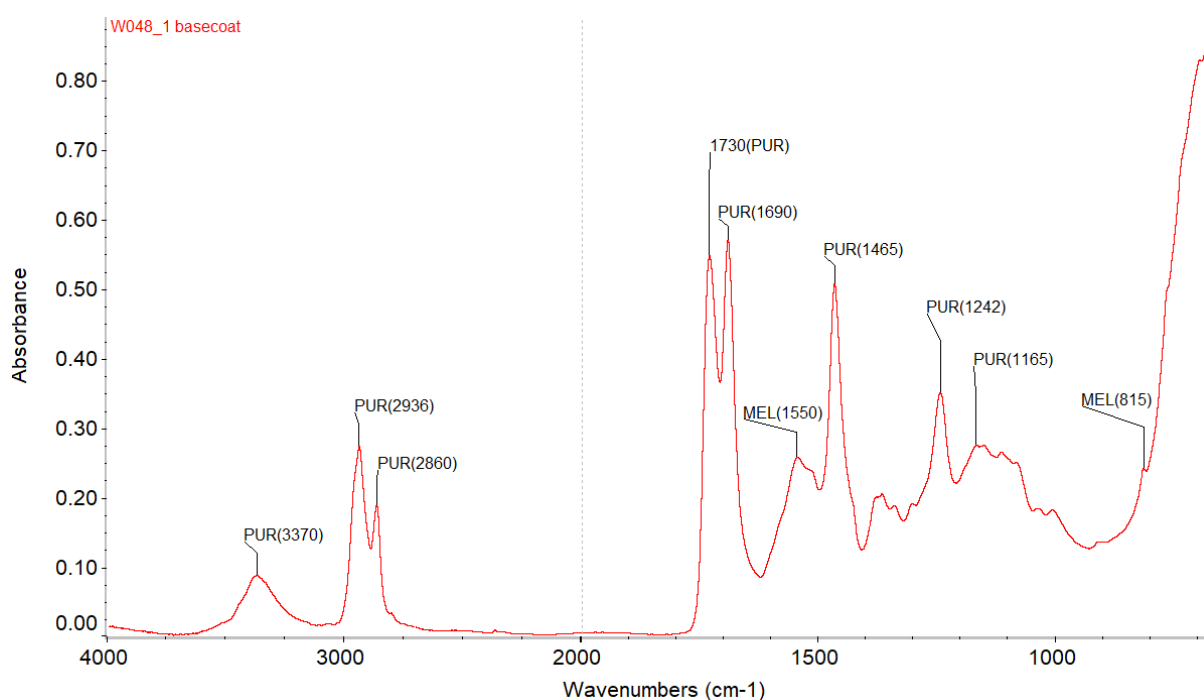
Figure 80. A representative IR spectrum of the basecoat of sample W048_1 with characteristic peaks of polyurethane and melamine annotated on the spectrum.

8.3.3. Group 3 – basecoat

This group is composed of 27 samples, representing 43.5% of the total samples (see Group 3 in *Table 30*). Based on the observed peaks in the IR spectra of this group, several absorption bands can be attributed to specific functional groups present in the basecoat. The peaks at 2960, 2934 and 2874 cm^{-1} can be attributed to aliphatic C-H stretching, while the strong peak at 1730 cm^{-1} corresponds to the stretching vibrations of carbonyl groups (C=O). The peaks at 1472 and 1373cm^{-1} can be attributed to the deformation vibrations of methyl and methylene groups. The peak at 1302 and 1240 cm^{-1} correspond to the C-O stretching vibrations of the isophthalic ester. The peaks at 1170 and 1070 cm^{-1} correspond to C-O stretching vibrations. Finally, the peak at 730 cm^{-1} is due to the out-of-plane bending of four adjacent hydrogens on the aromatic ring. Based on the identified functional groups, the primary resin in this group of basecoats may be a mixture of acrylic and isophthalic alkyd. The distinctive peaks of acrylic and isophthalic alkyd found in the sample, along with a comparison to a reference spectrum of acrylic modified alkyd, are illustrated in *Figure 81*.

In addition to the primary resin peaks, the FTIR spectra of the basecoat revealed two additional diagnostic peaks. The peak at 1550 cm^{-1} is attributed to the in-plane deformation of the triazine ring, while a small sharp peak at 815 cm^{-1} corresponds to the out-of-plane triazine ring vibration (see *Figure 81*). These two peaks suggest the presence of melamine as an additional resin in the formulation. TiO_2 was also detected in the basecoat, as expected.

There is one distinguishing characteristic of this group - the presence of a peak at 1690 cm^{-1}. This peak confirms the presence of polyurethane in the formulation, which allows further discrimination within this group according to the relative intensity of this peak.
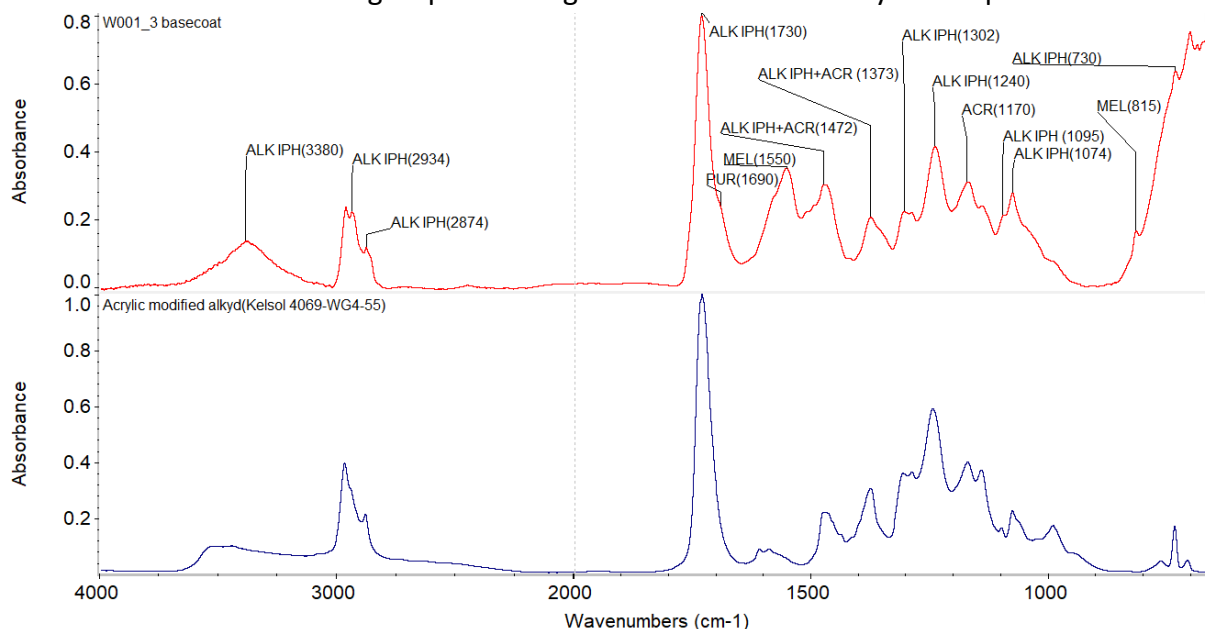
Figure 81. Comparison of the representative IR spectrum of the basecoat from sample W001_3 (top) containing acrylic and isophthalic alkyd with a reference spectrum of acrylic modified alkyd (bottom). The characteristic peaks of isophthalic alkyd, acrylic and melamine are annotated on the spectrum of sample W001_3.

8.3.4. Group 4 – basecoat

The analysis of this group revealed a single sample, which accounted for only 1% of the total samples (see Group 4 in *Table 30*). The observed peaks in the IR spectra of this group suggest the presence of both acrylic and polyurethane resins in the basecoat, with the former being the primary resin. Specifically, the absorption bands at 2960, 2873, 1380, 1170, and 1075 cm^{-1} are characteristic of acrylic resin, while the peaks at 1690, 1465, and 1242 cm^{-1} indicate the presence of polyurethane. Additionally, the peaks at 1550 and 815 cm^{-1} confirm the presence of melamine as an additional resin. Furthermore, the absorption bands at 3678 and 1020 cm^{-1} are indicative of talc usage as an extender in the formulation. TiO$_2$ was also detected in the basecoat, as expected. A representative spectrum from this group is shown in *Figure 82*, with relevant peaks annotated for ease of interpretation.
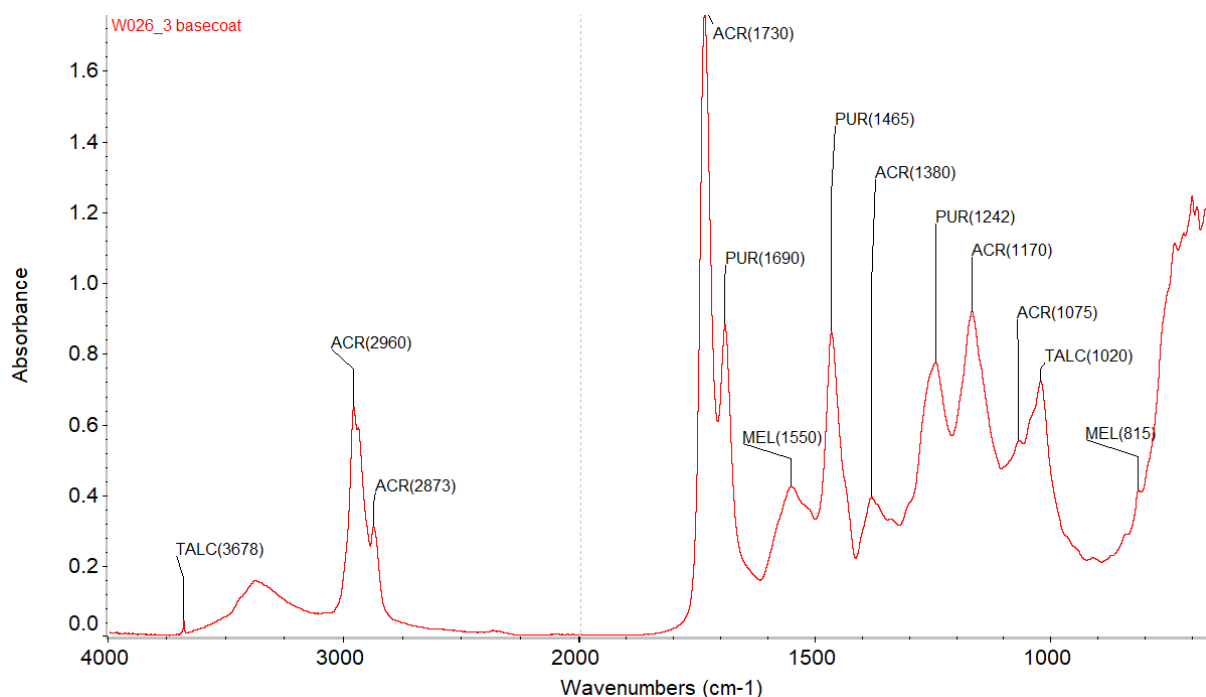
Figure 82. A representative IR spectrum of the basecoat of sample W026_3 with characteristic peaks of acrylic, polyurethane, melamine, and talc annotated on the spectrum.

8.3.5. Group 5 – basecoat

This group consists of 6 samples, accounting for 10% of the total samples and is characterized by distinctive peaks in the FTIR spectra (see Group 5 in *Table 30*). The peaks at 3380, 2933, 2860, 1690, 1526, 1465, 1243, 1162, and 762 cm^{-1} are indicative of the presence of polyurethane, which is identified as the primary resin in this group. In addition, peaks at 3083, 3060, 3027, 1601, 1490, 762, and 700 cm^{-1} can be attributed to styrene, which is used as an additional resin in the formulation. *Figure 83* illustrates a representative spectrum from this group with annotated peaks corresponding to polyurethane and styrene. TiO_2 was found in this group, but the concentration was notably lower compared to the previous groups. This can be inferred from the gradual rise in the spectrum towards 700 cm^{-1}.
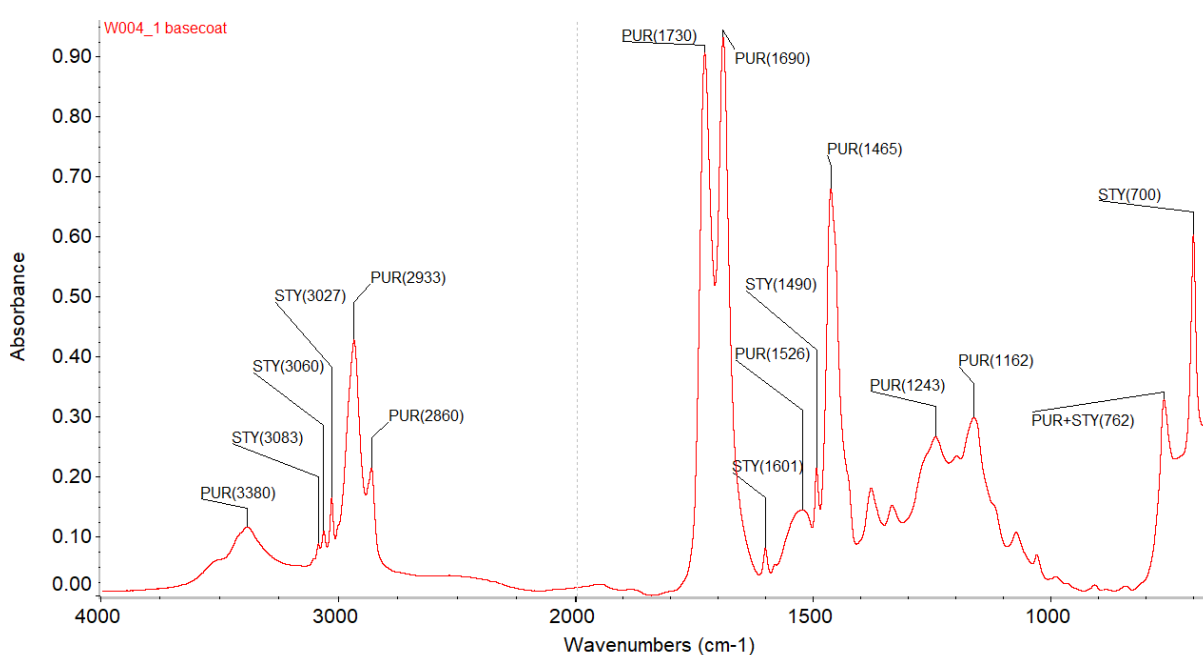
Figure 83. A representative IR spectrum of the basecoat of sample W004_1 with characteristic peaks of polyurethane and styrene annotated on the spectrum.

8.3.6. Group 6 – basecoat

This group comprises only one sample, representing a negligible 1% of the total samples analyzed (see Group 6 in *Table 30*). The sample spectrum exhibits diagnostic absorption peaks at various wavenumbers, including a carbonyl stretch at 1730 cm^{-1}, an aromatic C=C stretch at 1580 cm^{-1}, a C-H bending of an aromatic ring at 1470 cm^{-1}, a C-H stretching vibration of aliphatic groups at 1265 cm^{-1}, and C-O stretching vibrations at 1120 cm^{-1}, 1070 cm^{-1}, and 1040 cm^{-1}. The presence of these peaks collectively suggests the presence of ortho-phthalic alkyd resin in the sample. Furthermore, the detection of peaks at 1550 cm^{-1} and 815 cm^{-1} signifies the presence of melamine as an additional resin. *Figure 84* illustrates the characteristic peaks of this group and a comparison between a reference alkyd melamine binder.
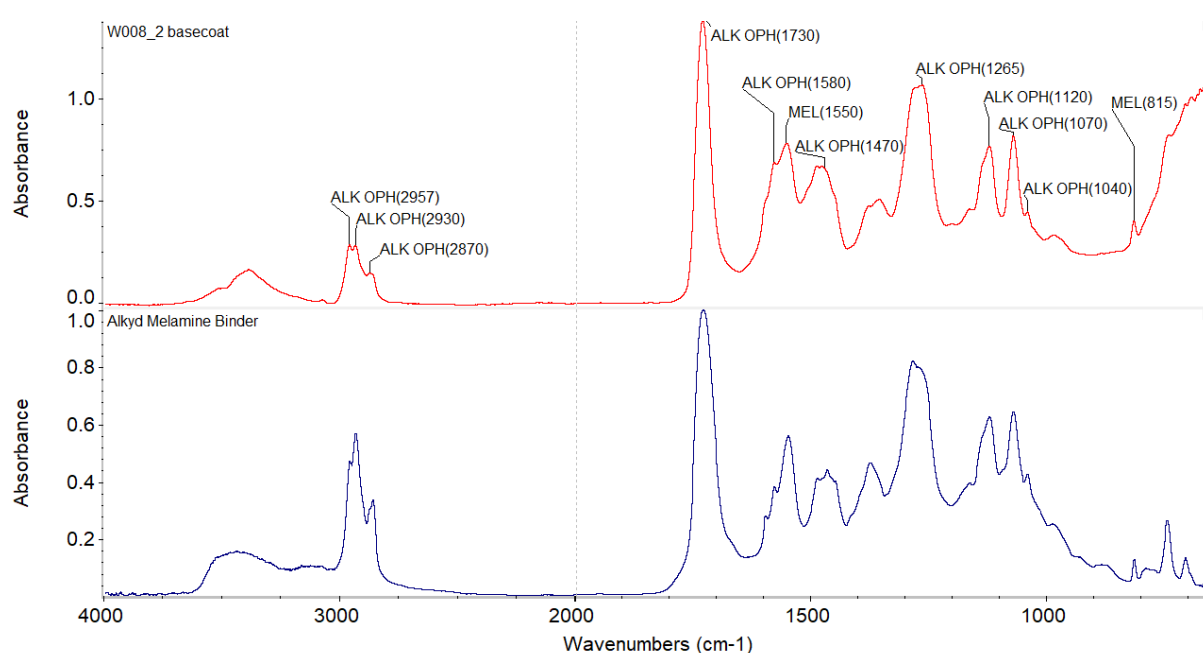
Figure 84. Comparison of a representative IR spectrum of the basecoat of sample W008_2 (top) with a reference alkyd melamine binder (bottom). Characteristic peaks of ortho-phthalic alkyd and melamine are annotated on the spectrum of sample W008_2.

8.3.7. Group 7 – basecoat

Within this particular group, there was a sole sample that constituted a mere 1% of the overall sample set (see Group 7 in *Table 30*). The analysis of this sample's IR spectra unveiled distinct peaks indicating the presence of acrylic resin in the basecoat. Notably, absorption bands at 2960, 2873, 1480, 1380, 1370, 1260, 1160, and 1075 cm^{-1} exhibited characteristic peaks of acrylic resin. Furthermore, the peaks observed at 1550 and 815 cm^{-1} confirm the presence of melamine as additional resin. Despite their subtle nature, the peaks at 3062, 3027, and 1490 cm^{-1} further indicated the existence of styrene. As anticipated, the basecoat also demonstrated the detection of TiO$_2$. A representative spectrum from this specific group has been provided in *Figure 85,* with characteristic peaks labeled accordingly.
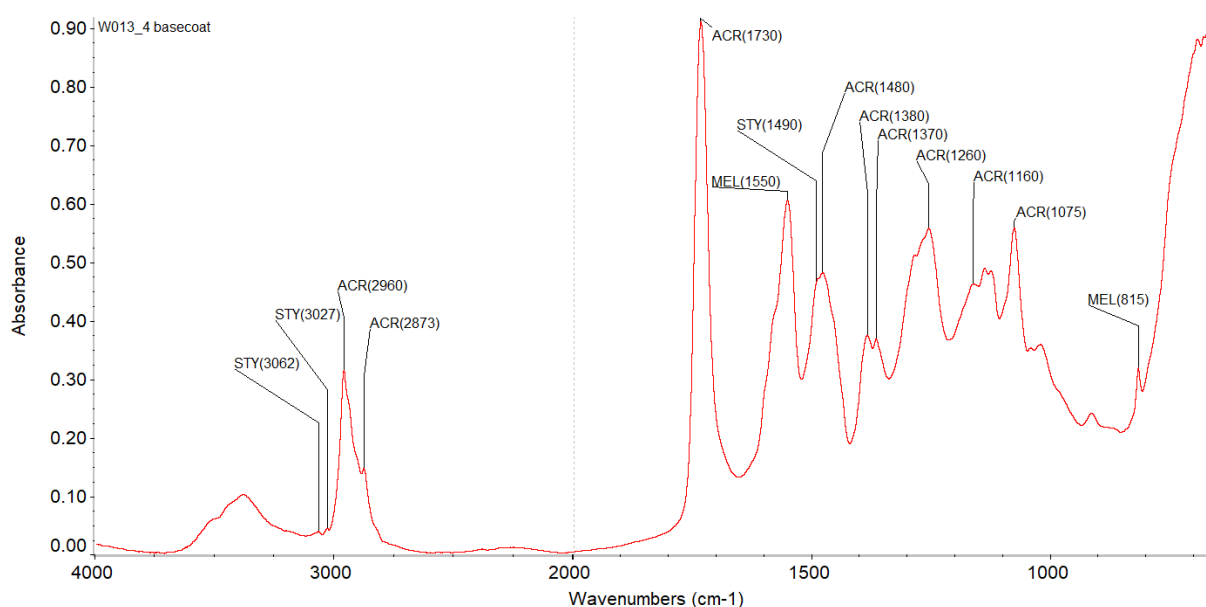
Figure 85. A representative IR spectrum of the basecoat of sample W013_1 with characteristic peaks of acrylic, melamine and styrene annotated on the spectrum.

8.3.8. Classification and discrimination of basecoat

Table 31 provides a summary of the characteristic compounds identified from the IR spectra of the basecoat for each sample examined in this study. Based on the analysis of the chemical composition of binders, pigments, and extenders in the paint samples, the basecoats were classified into seven distinct groups, as depicted in *Figure 86*. Notably, two major groups were observed in the figure. The first group, representing 43.5% of the total sample set, displayed a mixture of acrylic and isophthalic alkyd binders. Furthermore, this group included melamine and polyurethane resins, along with TiO_2 as the pigment. The second major group, comprising 38.7% of the total sample set, exhibited a combination of polyurethane resin, isophthalic alkyd, and melamine resins. Additionally, this group contained TiO_2 and talc as pigments and extenders, respectively. By identifying these distinct groups based on their chemical compositions, a comprehensive understanding of the basecoats was obtained.

The analysis of basecoat spectra in the studied samples has provided valuable insights into the composition of the resins and the presence of additional components, as illustrated in *Figure 87*. Polyurethane resin emerged as the most common binder, accounting for 96.8% of the total samples. The second largest binder type was isophthalic alkyd, found in 82.3 % of the samples. Acrylic resin constituted a smaller proportion of 46.8%, while orthophthalic alkyd resin was detected in only 1.6% of the samples.

Additionally, the analysis revealed the presence of additional resins in the majority of the samples. Melamine was commonly detected as an additional resin, present in 51.6% of the samples. Styrene was detected in 11.3% of the samples as an additional component, mainly among repainted samples with the primary resin being polyurethane.

Regarding pigments and extenders, the presence of TiO_2 was detected in all samples, which aligns with its role in imparting the characteristic white color observed under microscopic analysis. Talc, on the other hand, was the most commonly detected extender, found in 40% of the samples.

Through visual comparison and groupings of the basecoats obtained from IR analysis (summarized in *Table 30*), a total of 278 sample pairs remained undifferentiated, resulting in a discriminating power of 85.3% (278 undifferentiated pairs out of a total of 62 samples).

Table 31. Summary of characteristic compound based on the FTIR spectra of the basecoat of the automotive paint samples in this thesis (n=62)

Sample\Composition	BINDER						PIGMENTS/EXTENDERS	
	PUR	ACR	ALK IPH	ALK OPH	MEL	STY	TiO$_2$	Talc
W001	X	X	X		X		X	
W002	X		X				X	X
W003	X	X	X		X		X	
W004	X					X	X	
W005	X		X				X	X
W006	X	X	X		X		X	
W007	X		X				X	X
W008				X	X		X	
W009	X	X	X		X		X	
W010	X		X				X	X
W011	X	X	X		X		X	
W012	X		X				X	X
W013		X			X	X	X	
W014	X		X				X	X
W015	X		X				X	X
W016	X		X				X	X
W017	X	X	X		X		X	
W018	X		X				X	X
W019	X	X	X		X		X	
W020	X		X				X	X
W021	X	X	X		X		X	
W022	X	X	X		X		X	
W023	X		X				X	X
W024	X	X	X		X		X	
W025	X	X	X		X		X	
W026	X	X			X		X	X
W027	X	X	X		X		X	
W028	X	X	X		X		X	
W029	X					X	X	
W030	X	X	X		X		X	
W031	X	X	X		X		X	
W032	X		X				X	X
W033	X		X				X	X
W034	X	X	X		X		X	
W035	X	X	X		X		X	
W036	X		X				X	X
W037	X					X	X	
W038	X					X	X	
W039	X	X	X		X		X	
W040	X	X	X		X		X	
W041	X		X				X	X
W042	X		X				X	X
W043	X	X	X		X		X	
W044	X		X				X	X
W045	X		X				X	X
W046	X		X				X	X
W047	X		X				X	X
W048	X				X		X	
W049	X		X				X	X
W050	X	X	X		X		X	
W051	X		X				X	X
W052	X	X	X		X		X	
W053	X		X				X	X
W054	X		X				X	X
W055	X	X	X		X		X	
W056	X					X	X	
W057	X					X	X	
W058	X	X	X		X		X	
W059	X	X	X		X		X	
W060	X	X	X		X		X	
W061	X	X	X		X		X	
W062	X				X		X	
Total	**60**	**29**	**51**	**1**	**32**	**7**	**62**	**25**
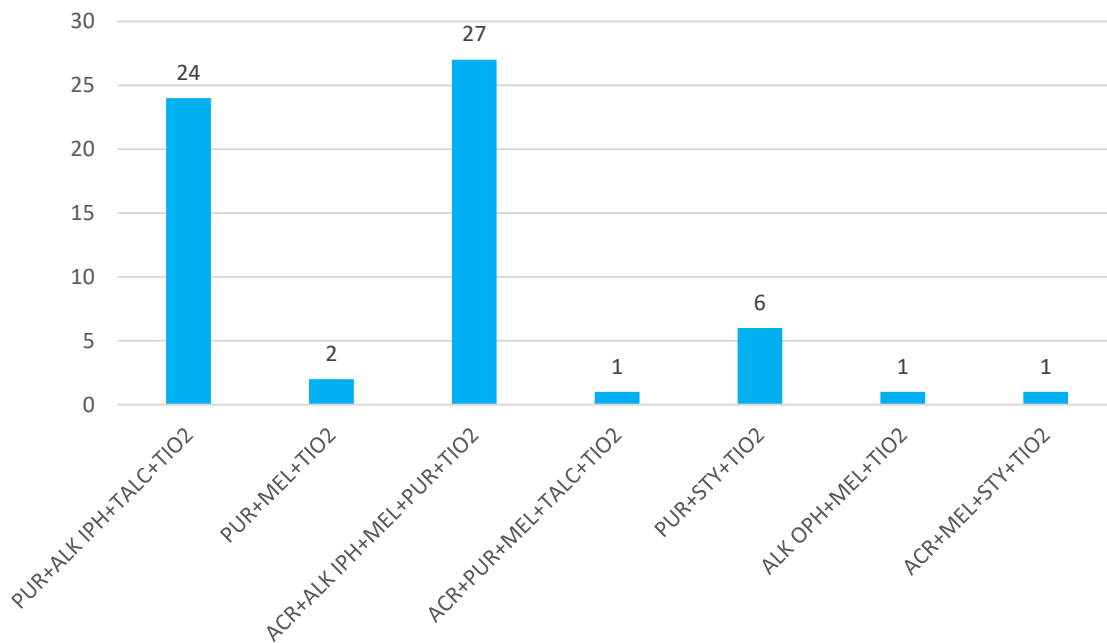
Figure 86. Proportion of samples according to the combination of infrared characterizations. Seven groups (combinations) can be distinguished.
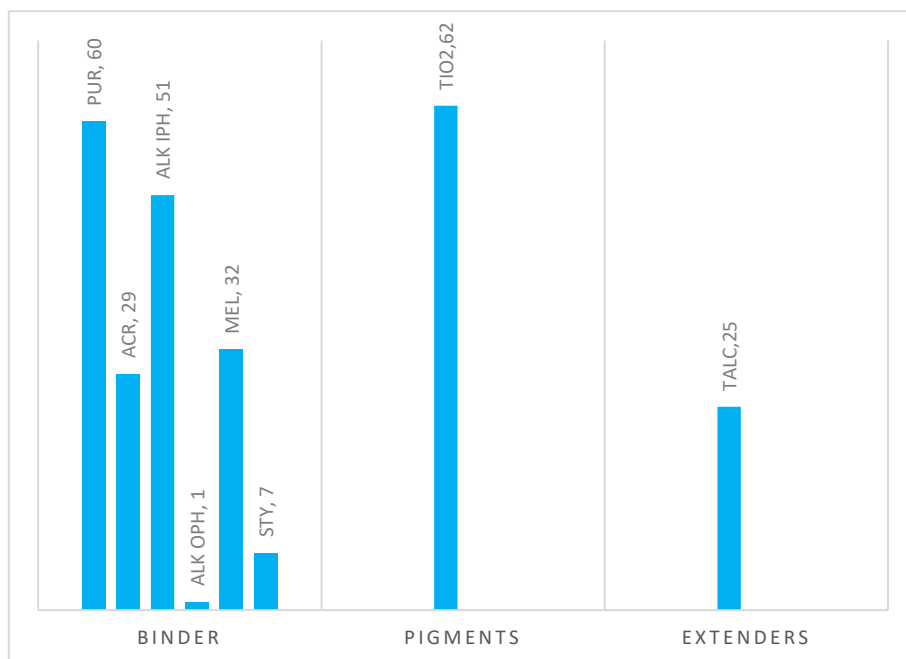
Figure 87. Distribution of infrared characterizations with the basecoat of 62 vehicles.

148

After conducting visual comparisons and groupings, the relationship between chemical composition and the original vehicle information was examined. Similar to the observations made for the clearcoat, the chemical composition of the basecoat also appears to be closely tied to the layer structure. For instance, it was found that all samples belonging to the OEM3 paint system exhibited a polyurethane binder type. Furthermore, all 27 samples in Group 3 (see *Table 30*), characterized by an acrylic mixed with isophthalic alkyd binder type, corresponded to the OEM4 system. As expected, Sample W026 displayed a unique chemical profile that differed from the rest of the Chinese-produced samples, owing to its distinct origin. In addition, the basecoat compositions of repainted samples exhibited distinct chemical features that were easily distinguishable from both the OEM paint and from each other.

8.3.9. Exploratory analysis

A total of 321 IR spectra of basecoats, obtained from 62 samples with 107 subsamples, were subjected to PCA analysis. Prior to analysis, the dataset underwent the same preprocessing steps, including baseline offset, SNV normalization, and detrending with a polynomial order of 2. The analysis specifically focused on variables within the range of 3700-3650 cm^{-1}, 3100-2828 cm^{-1}, and 1800-680 cm^{-1}, resulting in a dataset comprising 3035 variables. These preprocessing steps and the defined spectral range aimed to enhance the quality and relevance of the data for the subsequent PCA analysis.

Figure 88 provides an overview of the PCA model generated from the analyzed dataset, showing the projections of IR spectra based on the first four principal components (PC1 to PC4), which collectively account for 89% of the total variance. The corresponding loading plots are displayed in *Figure 89.*

In the PCA scatter plot (*Figure 88a*), samples are projected based on PC1 and PC2, revealing 13 distinct clusters (marked in dashed circle and rectangular). Examining the loading plot for PC1 (*Figure 89a*), wavenumbers at 1690 and 1465 cm^{-1}, associated with polyurethane, exhibit the highest positive correlation. Conversely, wavenumbers at 1730, 1550, 1480, 1280, 1170, and 1075 cm^{-1} show notable negative correlation, corresponding to spectral features of acrylic and melamine. The loading plot for PC2 (*Figure 89b*) indicates that PC2 is influenced by the signals of polyurethane, acrylic, and isophthalic alkyd. These factors contribute significantly to the observed separation in the score plot. Samples projected on the right side of the scatter plot mainly contain polyurethane, while those on the left side mainly contain acrylic and melamine. Therefore, the observed separation primarily arises from the different chemical categories or compositions of the samples, aligning with visual characterization and comparison results.

However, 7 groups of samples remained undifferentiated, and there were overlaps among groups with identical chemical classes in the scatter plot based on PC1 and PC2 (marked in dashed rectangular *in Figure 88a*). The addition of PC3 successfully separated 3 samples from Group 6 (highlighted in a red dashed rectangular in *Figure 88a*) into individual cluster, as shown in the red dashed circle in *Figure 88b*. Group 3 also became well separated from Group 2 in *Figure 88b*. Furthermore, the addition of PC4 allowed the differentiation of two samples in Group 7 (highlighted with green dashed line in *Figure 88a* and *Figure 88c*), and some samples from Group 2 are well separated from the rest (indicated with a blue dashed line in *Figure 88a* and *Figure 88c*). PC3 primarily relates to polyurethane and melamine, while PC4 is influenced by talc and styrene (*Figure 89c-d*).

This PCA model failed to differentiate samples from Group 1 to Group 5. As a result, additional PCA analyses were performed on samples from each of these groups individually. However, even with these additional analyses, the samples from Group 1 to Group 3 could not be effectively differentiated.

Eventually, a total of 25 groups could be distinguished using the PCA model. The grouping results of the PCA analysis is presented in *Table 32.* This resulted in a total of 361 pairs of samples remaining undifferentiated, leading to a discriminating power of 81% for the PCA observation.
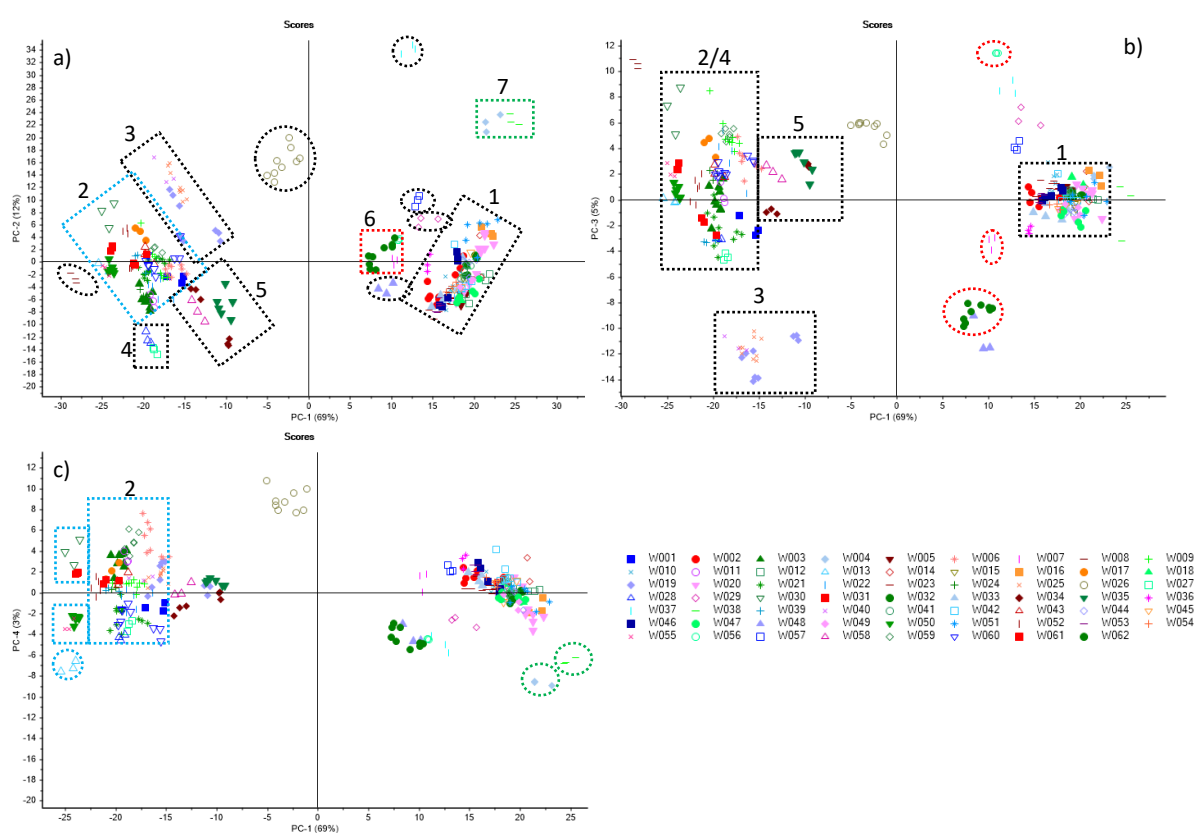
Figure 88. PCA score plots according to the first four principal components of the dataset of IR spectra of basecoat (n=62): a) projections according to PC1 and PC2; b) projections according to PC1 and PC3; c) projections according to PC1 and PC4. 7 groups of undifferentiated spectra according to the set of principal components of the model are highlighted with dashed rectangles (groups observed according to the dispersions of the spectra). Samples that well separated from the rest were highlighted in dashed circle.
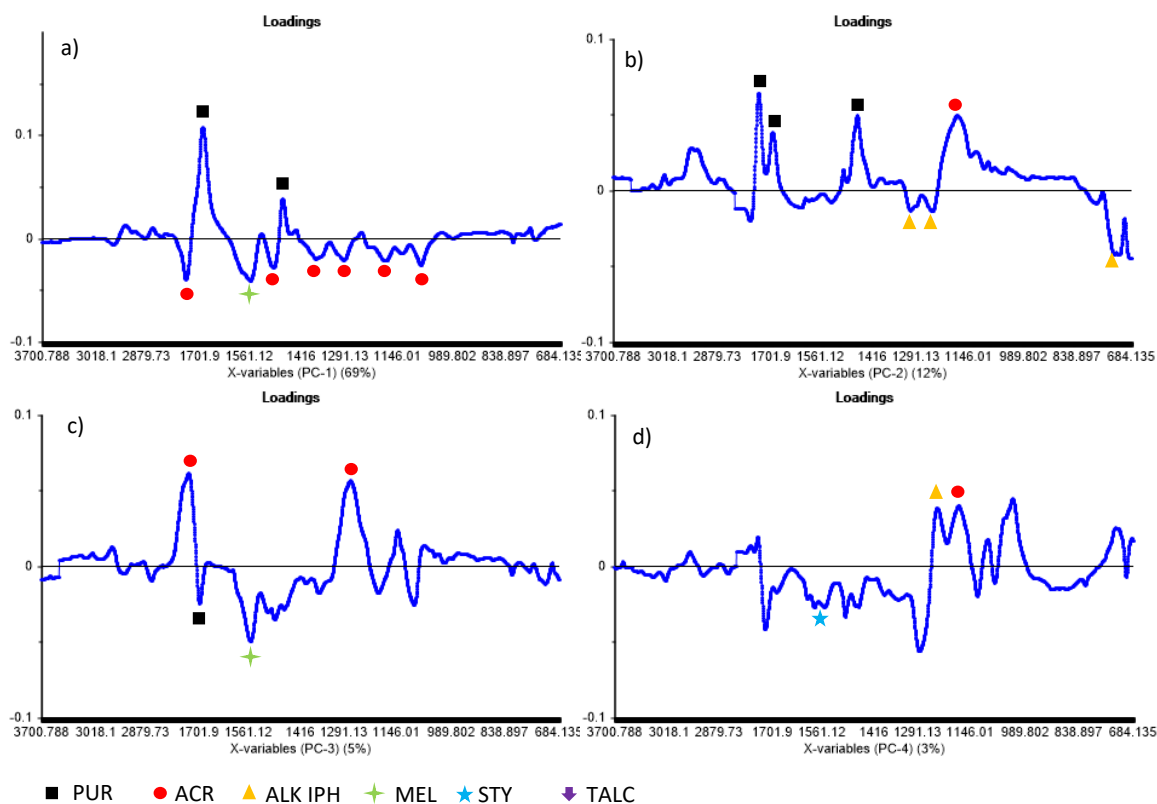
Figure 89. loadings of the first four principal components (a to d, respectively) of the PCA model on the 321 IR spectra of basecoat. The wave numbers corresponding to characteristic peaks of the characterized resin or extenders are highlighted using different shapes and colors.

Table 32. Summary of PCA-based groupings of basecoat (n=62)

GROUP	SAMPLES	CHEMICAL COMPOSITION
1	W002, W005, W010, W012, W014, W015, W016, W018, W020, W023, W032, W033, W036, W041, W042, W044, W045, W046, W047, W049, W051, W053, W054	PUR+ALK IPH+TALC+TIO2
2	W001, W003, W006, W009, W011, W017, W021, W022, W024, W039, W043, W052, W059, W060, W061	ACR+ALK IPH+MEL+PUR+TIO2
3	W019, W025, W040	ACR+ALK IPH+MEL+PUR+TIO2
4	W007	PUR+ALK IPH+TALC+TIO2
5	W048	PUR+MEL+TIO2
6	W062	PUR+MEL+TIO2
7	W026	ACR+PUR+MEL+TALC+TIO2
8	W027	ACR+ALK IPH+MEL+PUR+TIO2
10	W028	ACR+ALK IPH+MEL+PUR+TIO2
11	W030	ACR+ALK IPH+MEL+PUR+TIO2
12	W031	ACR+ALK IPH+MEL+PUR+TIO2
13	W034	ACR+ALK IPH+MEL+PUR+TIO2
14	W035	ACR+ALK IPH+MEL+PUR+TIO2
15	W050	ACR+ALK IPH+MEL+PUR+TIO2
16	W055	ACR+ALK IPH+MEL+PUR+TIO2
17	W058	ACR+ALK IPH+MEL+PUR+TIO2
18	W004	PUR+ STY+TIO2
19	W008	ALK OPH+MEL+TIO2
20	W013	ACR+MEL+STY+TIO2
21	W029	PUR+ STY+TIO2
22	W037	PUR+ STY+TIO2
23	W038	PUR+ STY+TIO2
24	W056	PUR+ STY+TIO2
25	W057	PUR+ STY+TIO2

The data structure of the IR spectra of the basecoats, specifically focusing on 54 OEM paint samples, was investigated and depicted in *Figure 90.* The PCA score plots were generated to analyze the dataset according to the first two principal components, highlighted by chemical categories (*Figure 90a*), layer structure (*Figure 90b*), manufacturing companies (*Figure 90c*), assembly plants (*Figure 90d*), topcoat color codes (*Figure 90e*), and vehicle models (*Figure 90f*).

Figure 90a indicate that the samples were well separated based on the different binder type as samples projected on right side of the scatter plot mainly contain polyurethane as their main binder type, while those on the left side are mainly acrylic based binder.

Analyzing these PCA scatter plots reveals that, for the chemical characteristic of samples with regards to layer structure, manufacturing company, assembly plant, topcoat color codes and vehicle models, similar pattern as what was observed for clearcoat, emerges from this exploratory analysis (*Figure 90b-f*), were describes as follows:

1) All samples displaying the OEM3 layer structure exhibit the polyurethane-based binder type, whereas samples with the OEM4 paint system consistently contain an acrylic based binder type (*Figure 90b*).
2) It appears that both F-VW and S-VW manufacturing companies in China employ both types of binder in their basecoat application formula (*Figure 90c*).
3) Most assembly plants (Plant Changchun, Plant Chengdu, Plant Ningbo, and Plant Osnabrück) exclusively utilize a single type of binder in their basecoat. On the contrary, for Plant Anting and Plant Nanjing, two different binder types were found in their respective products. The reason behind was consistent with what was found for clearcoat as Plant Anting actually consists of three sub-plants operating its independent production line (*Figure 90d*).
4) It was found that samples that share the same topcoat color code do not always have identical chemical composition for their basecoat (*Figure 90e*). The reason behind needs to be further investigated.
5) Variations were found among samples of the same model. *Figure 90f* depicts samples of the model 'New Lavida' represented by a brown horizontal line, and these samples are widely scattered in the scatter plot, indicating batch variations within the same vehicle model. The same observation was obtained among the samples of the model 'Passat' represented by a pink circle in the figure.
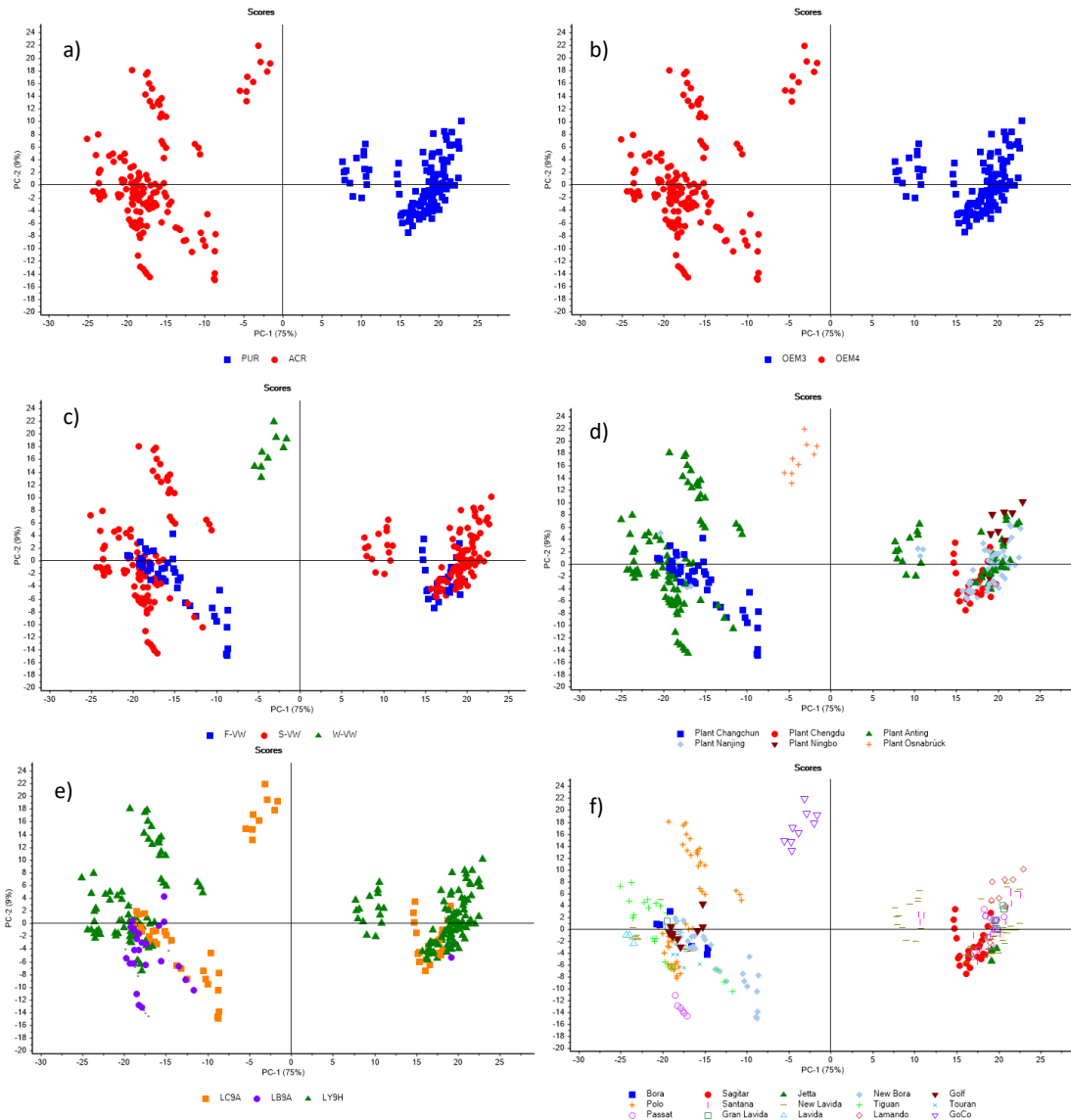
Figure 90. PCA score plots according to the first two principal components of all IR spectra of basecoats, respectively highlighted by the chemical categories (a), layer structure (b), their manufacturing companies (c), their assembly plants (d), their topcoat color codes (e), and the model of vehicles(f).

8.4. Characterization of primer surfacer

Out of the 62 samples in the sample set, only 28 samples were investigated for the characterization of primer surfacer since it only exists in paint that has an OEM4 structure. Of the remaining 34 samples that were not analyzed, 26 belonged to group OEM3, which did not have primer surfacer, and 8 from the repainted group failed to identify the layer of primer surfacer due to their irregular layer structure.

The results of the visual characterization of FTIR spectra obtained from the primer surfacer of the 28 samples are summarized in *Table 33*, which classifies the samples into five groups based on the chemical categories of the binders, pigments, and extenders used in the layer. Each group of spectra is then individually analyzed to identify the constituents detected by FTIR in the investigated paints. Further visual comparisons were carried out to identify distinguishable subgroups within each group, as presented in the table, highlighting the main differences observed between the spectra of samples with similar characterization.

Table 33. Summary of visual characterization and groupings based on the FTIR spectra of the primer surfacer of the automotive paint samples in this thesis (n=28).

GROUP/COMPOSITION	SUB-GROUP	SAMPLES	DIFFERENCE WITHIN THE GROUP
GROUP 1 **EPY+PUR+MEL** **+TALC+BAS+TIO2**	-	W003, W006, W009, W011, W017, W019, W021, W022, W024, W025, W027, W028, W030, W031, W039, W040, W043, W050, W052, W055, W058, W059, W060	Non differentiated within the group
GROUP 2 **ALK IPH+EPY+MEL** **TALC+TIO2**	-	W001	Single sample in the group
GROUP 3 **ALK IPH+PUR+EPY** **+TALC+ALS+TIO2**	3.1	W035	High intensity of peak at 1690 cm^{-1}
	3.2	W061	Low intensity of peaks at 1690 cm^{-1}
GROUP 4 **ALK IPH+MEL+** **TALC+TIO2**	-	W034	Single sample in the group
GROUP 5 **ALK TER+ACR+MEL+** **BAS+TIO2**	-	W026	Single sample in the group

8.4.1. Group 1 – primer surfacer

This group is composed of 23 samples, representing the majority of the total samples at 82% (see Group 1 in *Table 33*), and displays abundant absorption peaks in a typical spectrum. The peaks observed at 1610, 1510, 1240, 1180, and 830 cm^{-1} are indicative of the presence of epoxy resin in the samples of this group. The peak at 1610 cm^{-1} corresponds to the C=C stretching vibrations of the aromatic ring, while the peak at 1510 cm^{-1} corresponds to the C=C stretching vibrations of the aliphatic ring. The peak at 1240 cm^{-1} corresponds to the C-O-C stretching vibration. The peaks at 1180 and 830 cm^{-1} correspond to the C-O and C-H bending vibrations, respectively. Together, these peaks suggest the presence of epoxy resin in the samples of this group. The peaks at 1730 and 1690 cm^{-1}, which corresponds to the stretching vibration of the carbonyl group (C=O) of polyurethane, is a prominent feature in the spectra of this group. The existence of polyurethane is further confirmed by the presence of peaks at 1465 cm^{-1}, which correspond to the symmetric bending vibration of the methylene (-CH2-) groups. Apart from the two resins, the peaks at 1550 (in-plane deformation of the triazine ring) and 815 cm^{-1} (out of plane triazin ring vibration) indicate the presence of melamine, which is commonly used as a crosslinker in coating formulations. The rising trend in the spectrum towards 700 cm^{-1} is attributed to the presence of TiO$_2$, which is consistent with the microscopic observation of a white color in the primer surfacer. The presence of talc as an extender in this group is evidenced by the absorption peaks observed at 3676 and 1020 cm^{-1}. Moreover, the strong peaks detected at 1180, 1120 and 1080 cm^{-1} suggest a high concentration of barium sulfate. It is worth noting that talc and barium sulfate are commonly used as fillers in paint formulations to improve their properties such as hiding power and abrasion resistance. The identification of these fillers in this group can provide valuable insights into the composition of the paint and its potential performance. *Figure 91* illustrates a representative spectrum of this group, with the characteristic peaks of polyurethane, epoxy, melamine, talc, and barium sulfate labeled accordingly, in comparison with the reference spectra of epoxy, melamine, talc and barium sulfate.
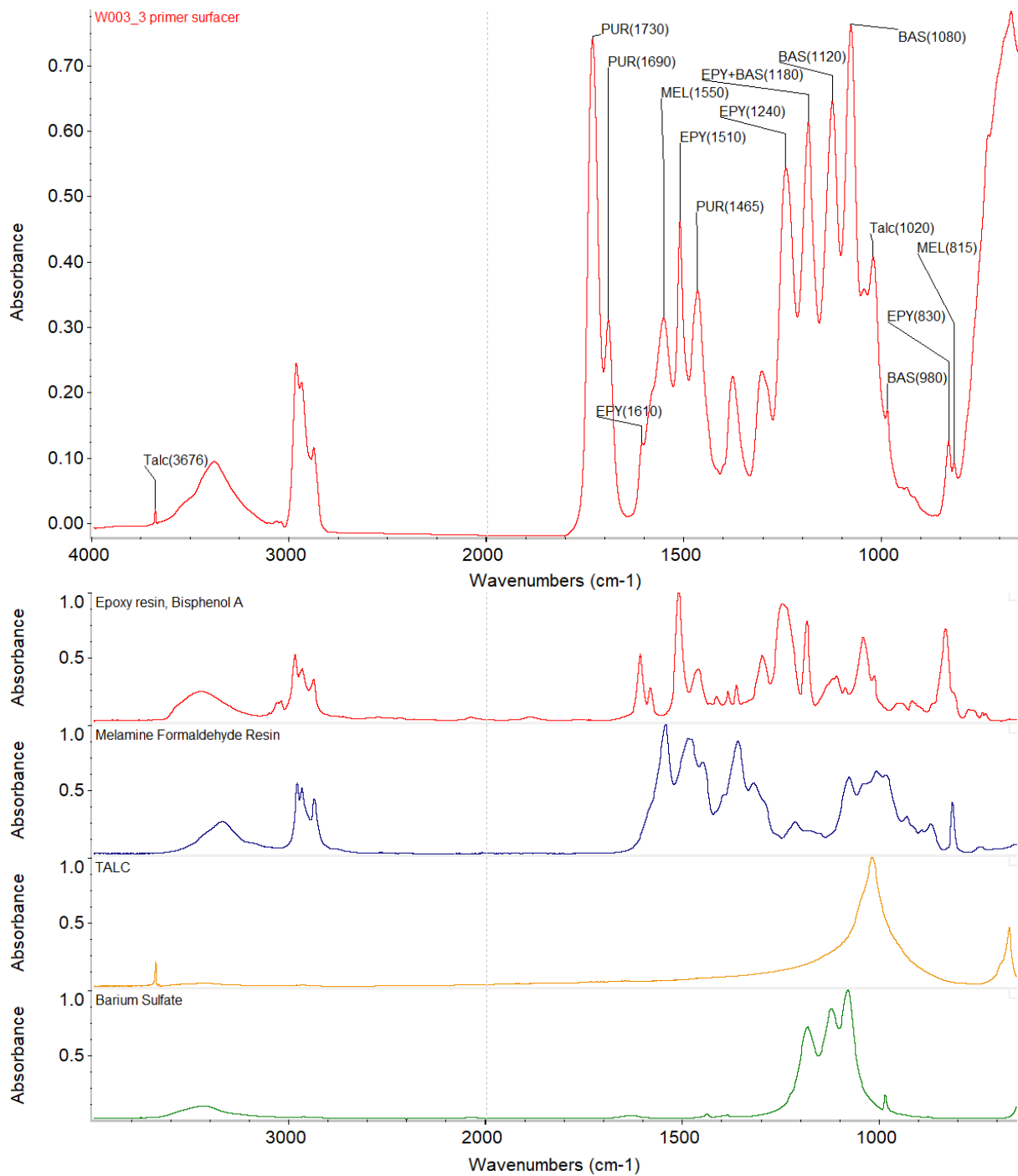
Figure 91. Representative Spectrum of the primer surfacer of sample W003_3 (up) with reference spectra of epoxy, melamine, talc, and barium sulfate (bottom). Characteristic peaks of polyurethane, epoxy, melamine, talc, and barium sulfate are annotated on the spectrum.

8.4.2. Group 2 – primer surfacer

This group comprises a single sample, representing only 3% of the total sample set (see Group 2 in *Table 33*). The spectrum of this group displays prominent absorption peaks, which were analyzed to identify the constituents present in the primer surfacer. The strong peak observed at 1728 cm^{-1} corresponds to the stretching vibration of the carbonyl (C=O) group, while the peaks at 1467, and 1375cm^{-1} are attributed to the deformation vibrations of the C-H group deformation vibrations of methyl and methylene groups. The peaks observed at 1303, 1240, 1140, 1095 and 1075 cm^{-1} can all correspond to the C-O stretching vibrations of the isophthalic ester. The peak at 730 cm^{-1} corresponds to the out-of-plane bending vibration of C-H groups in aromatic rings. Based on the distinctive absorption peaks identified in the analyzed group, it can be inferred that the primary resin present in the primer surfacer of this group is isophthalic alkyd. In addition to that, peaks at 1610, 1510 and 830 cm^{-1} reveal the presence of epoxy, while the peaks at 1550 and 815 cm^{-1} indicate the presence of melamine. TiO$_2$ and talc were also detected in this group. *Figure 92* illustrates a representative spectrum of this group, with the characteristic peaks of isophthalic alkyd, epoxy, melamine, and labeled accordingly.
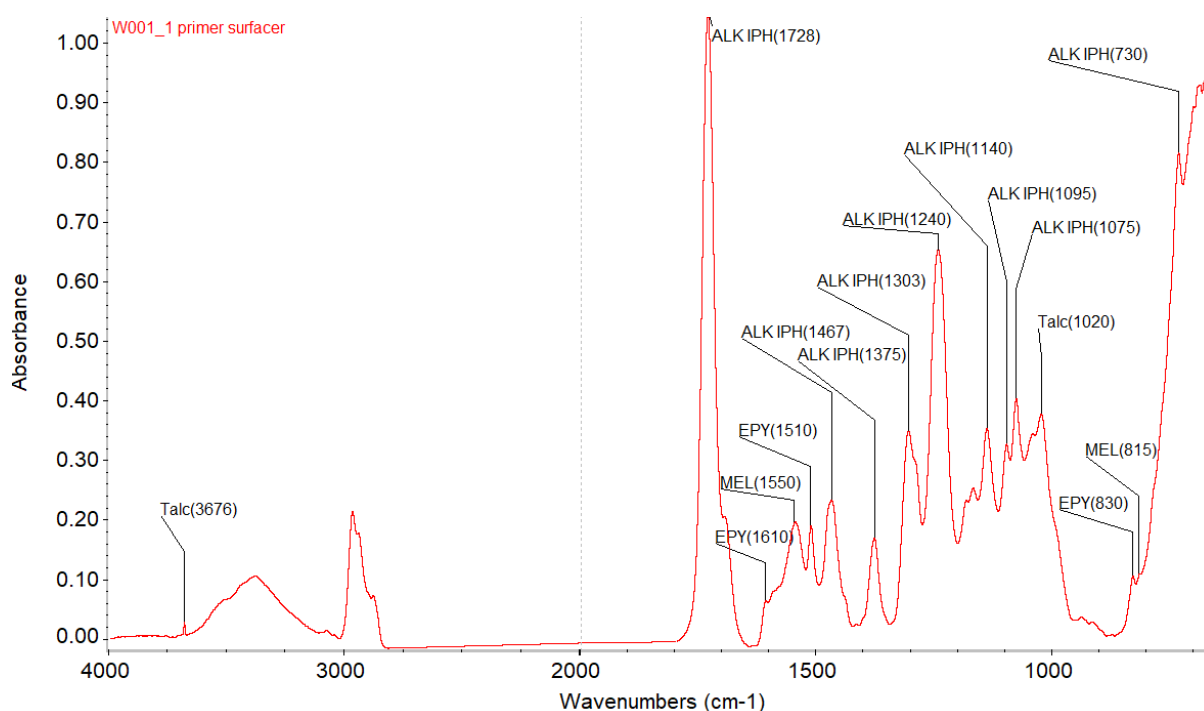
Figure 92. A representative IR spectrum of the primer surfacer of sample W001_1 with characteristic peaks of isophthalic alkyd, epoxy, melamine, and talc annotated on the spectrum.

8.4.3. Group 3 – primer surfacer

This particular group is composed two samples, accounting for 7% of the overall sample set (see Group 3 in *Table 33)*. Despite its small representation, the spectrum of this group displays notable absorption peaks, which were carefully analyzed to identify the constituents present in the primer surfacer. Notably, the strong peak observed at 1728 cm^{-1} corresponds to the stretching vibration of the carbonyl (C=O) group, while the peaks at 1375 cm^{-1} is attributed to the deformation vibrations of the C-H group in the aromatic ring. Additionally, the peaks observed at 1304, 1240, 1095, and 1075 cm^{-1} all correspond to the C-O stretching vibrations of the isophthalic ester. The peak at 730 cm^{-1} corresponds to the out-of-plane bending vibration of C-H groups in aromatic rings. These distinctive absorption peaks point to the primary resin present in the primer surfacer of this group being isophthalic alkyd.

Further analysis of the spectrum revealed the presence of other chemical constituents. Peaks at 1690 and 1465 cm^{-1} confirmed the presence of polyurethane, while peaks at 1610, 1510, and 830 cm^{-1} revealed the presence of epoxy. TiO$_2$ and talc were also detected in this group, and It is worth noting that peaks at 3700 and 3620 cm^{-1} indicate the presence of aluminum silicate, also known as clay or kaolinite. It is a type of clay mineral commonly used as a filler in paint formulations. It can contribute to the hiding power of the paint, allowing it to cover and hide the substrate effectively.

To provide a clear and detailed representation of this group's spectrum, *Figure 93* illustrates a representative spectrum with the characteristic peaks of isophthalic alkyd, epoxy, polyurethane, talc, kaolinite, and their respective labels.
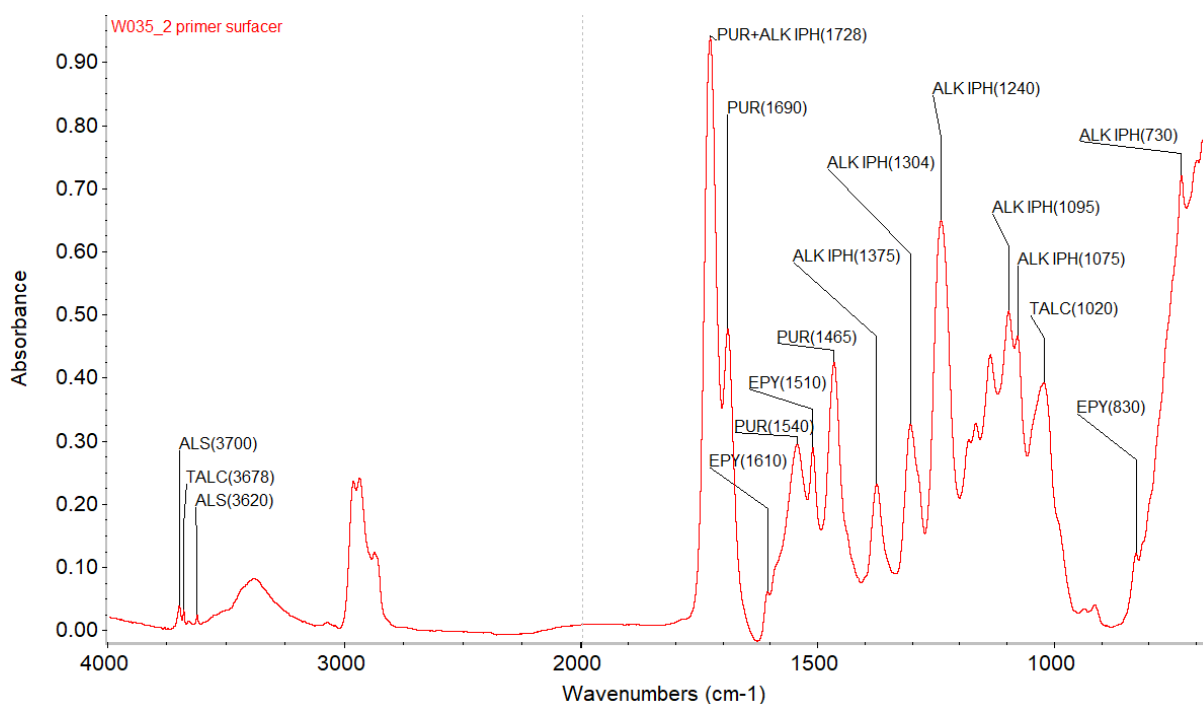
Figure 93. A representative IR spectrum of the primer surfacer of sample W035_1 with characteristic peaks of isophthalic alkyd, epoxy, polyurethane, talc and kaolinite annotated on the spectrum.

8.4.4. Group 4 – primer surfacer

This group is represented by a single sample, which accounts for only 3% of the total sample set (see Group 4 in *Table 33*). The spectrum of this group contains several absorption peaks, including a strong peak at 1728 cm^{-1} as well as peaks at 1475, 1373, 1304,1240, 1095, 1075, and 730 cm^{-1}. Based on these distinctive peaks, it can be inferred that the primary resin in the primer surfacer of this group is isophthalic alkyd. Additionally, peaks at 1550 and 815 cm^{-1} confirmed the presence of melamine, while TiO$_2$ and talc were also detected. A representative spectrum of this group with the characteristic peaks of isophthalic alkyd, melamine, talc, and their respective labels can be seen in *Figure 94*.
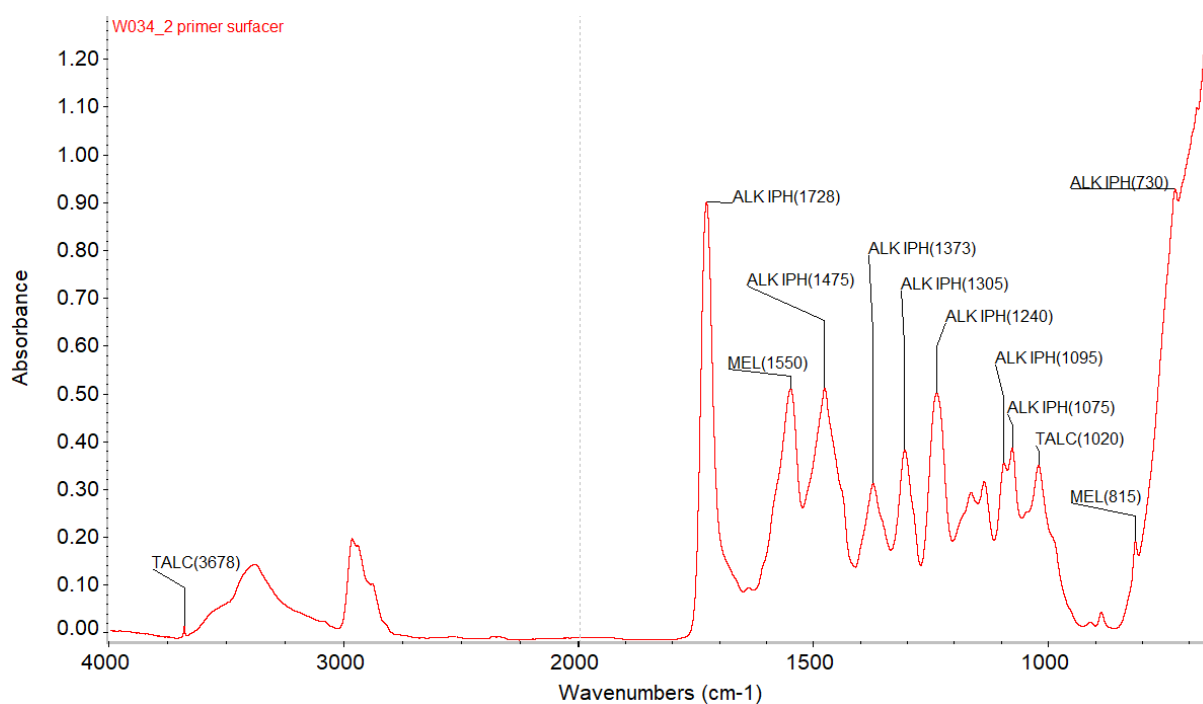
Figure 94. A representative IR spectrum of the primer surfacer of sample W034_2 with characteristic peaks of isophthalic alkyd, melamine, and talc annotated on the spectrum.

8.4.5. Group 5 – primer surfacer

This group comprises a single sample, representing only 3% of the total sample set (see Group 5 in *Table 33*). The spectrum of this group displays several prominent absorption peaks, which were analyzed to identify the constituents present in the primer surfacer. The strong peak observed at 1727 cm^{-1} corresponds to the stretching vibration of the carbonyl (C=O) group. The peak at 1270 cm^{-1} is attributed to the C-H bending vibrations in the aromatic ring. Peaks at 1120 cm^{-1} and 1104 cm^{-1} correspond to the C-O-C stretching. The peak at 1020 cm^{-1} is attributed to the C-H bending vibrations in the aliphatic chain. The peak at 730 cm^{-1} corresponds to the out-of-plane bending vibration of C-H groups in aromatic rings. Based on these distinctive absorption peaks, it can be inferred that the primary resin present in the primer surfacer of this group is terephthalic alkyd. In addition to the presence of terephthalic alkyd, peaks at 1475 cm^{-1}, 1373 cm^{-1}, 1180 cm^{-1}, and 1080 cm^{-1} indicate the presence of acrylic. Furthermore, peaks at 1550 cm^{-1} and 815 cm^{-1} show the presence of melamine. Barium sulfate was also detected, due to the strong absorption peaks at 1120 cm^{-1}, 1080 cm^{-1}, and 983 cm^{-1}. The rising trend towards 700 cm-1 indicates the presence of TiO$_2$. *Figure 95* shows a representative spectrum with the characteristic peaks of terephthalic alkyd, acrylic, melamine, barium sulfate and their respective labels.
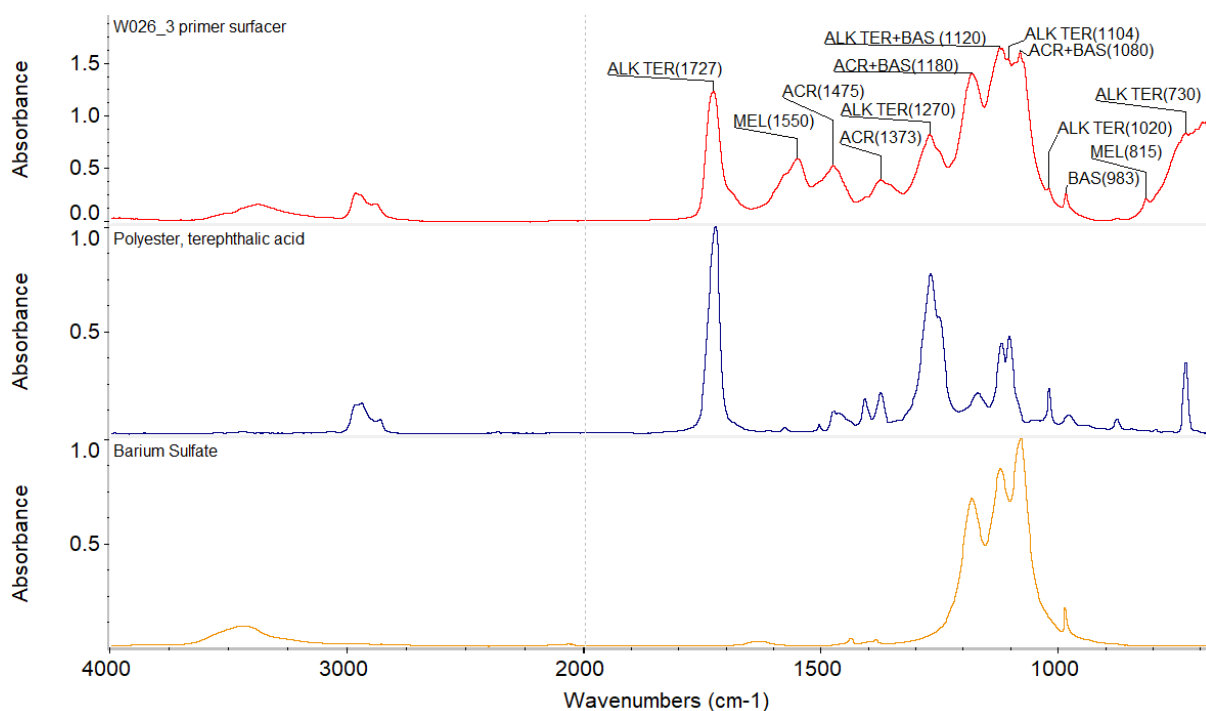
Figure 95. A representative IR spectrum of the primer surfacer of sample W026_3 (top) in comparison with reference spectra of terephthalic alkyd (middle) and barium sulfate (bottom). Characteristic peaks of isophthalic alkyd, acrylic, and barium sulfate are annotated on the spectrum.

8.4.6. Classification and discrimination of primer surfacer

Table 34 provides a summary of the characteristic compounds identified from the IR spectra of the primer surfacer for each sample examined in this study. Upon analyzing the various combinations of binder, pigments and extenders, it was found that the primer surfacer samples could be categorized into five groups (as illustrated in *Figure 96*). The predominant group of samples (accounting for 82% of the total sample set) exhibited an epoxy resin in combination with polyurethane and melamine resins, accompanied by the presence of TiO_2, talc, and barium sulfate as pigments and extenders.

Table 34. Summary of characteristic compound types based on the FTIR spectrum of the primer surfacer of the automotive paint samples in this thesis (28 samples)

Sample\Composition	BINDER						PIGMENTS/EXTENDERS			
	EPY	PUR	ACR	ALK IPH	ALK TER	MEL	TiO$_2$	ALS	BAS	TALC
W001	X			X		X	X			X
W003	X	X				X	X		X	X
W006	X	X				X	X		X	X
W009	X	X				X	X		X	X
W011	X	X				X	X		X	X
W017	X	X				X	X		X	X
W019	X	X				X	X		X	X
W021	X	X				X	X		X	X
W022	X	X				X	X		X	X
W024	X	X				X	X		X	X
W025	X	X				X	X		X	X
W026			X		X	X	X		X	
W027	X	X				X	X		X	X
W028	X	X				X	X		X	X
W030	X	X				X	X		X	X
W031	X	X				X	X		X	X
W034				X		X	X			X
W035	X	X		X			X	X		X
W039	X	X				X	X		X	X
W040	X	X				X	X		X	X
W043	X	X				X	X		X	X
W050	X	X				X	X		X	X
W052	X	X				X	X		X	X
W055	X	X				X	X		X	X
W058	X	X				X	X		X	X
W059	X	X				X	X		X	X
W060	X	X				X	X		X	X
W061		X			X		X	X		X
Total	25	25	1	3	3	26	28	2	24	25

The characterization of primer surfacer spectra in the studied samples has revealed the presence of five binder types (see *Figure 97*). Epoxy resin combined with polyurethane is the predominant type, comprising 82% of the total samples, while isophthalic alkyd, terephthalic alkyd and acrylic are present at lower proportions of 10.7%, 10.7% and 3.5%, respectively. Furthermore, melamine is a commonly detected additional resin in 93% of the samples, often found in association with epoxy and polyurethane, which was identified in 89% of the samples. The presence of TiO_2 was detected in all samples, consistent with its role in providing the characteristic white color observed under microscopic analysis. Talc was the most commonly detected extender, found in a majority of the samples (89%). Barium sulfate, another type of extender, was also detected in 86% of the samples, primarily in conjunction with an epoxy-polyurethane- melamine type of binder. In addition, a small number of samples (7%) contained aluminum silicate.
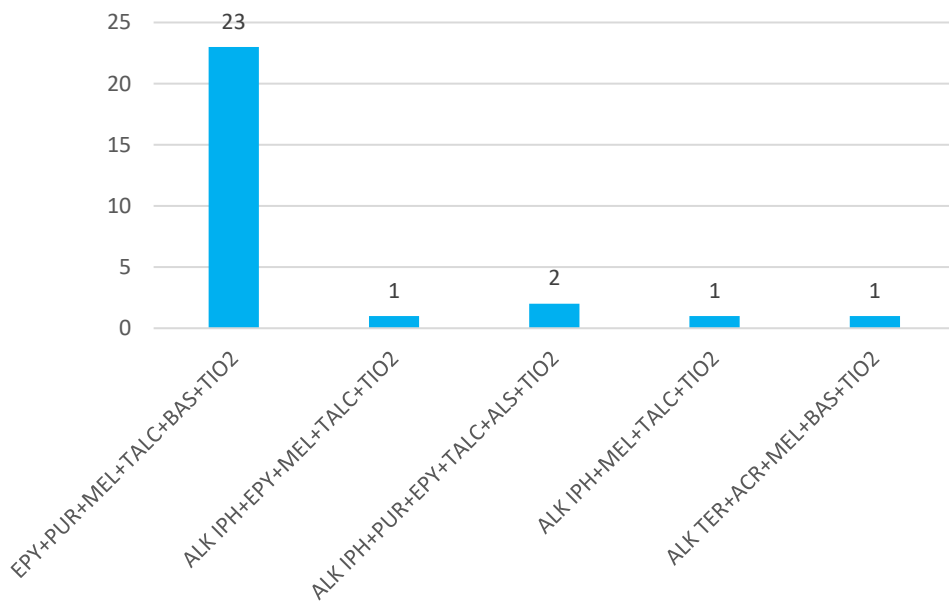
Figure 96. Proportion of samples according to the combination of infrared characterizations. Five groups (combinations) can be distinguished.
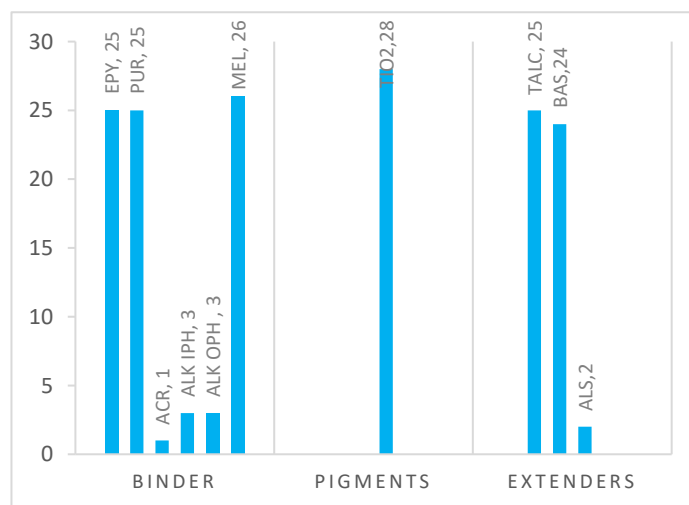
Figure 97. Distribution of infrared characterizations with the primer surfacer of 28 vehicles.

The discriminating power for the visual comparisons of primer surfacer spectra was determined based on the subgroups presented in *Table 33*, taking into account the number of pairs of undifferentiated samples (253 pairs, for a total of 28 samples). This resulted in a discriminating power of 33.1%.

After characterizing and classifying the undifferentiated samples, the correlation between their chemical properties and origin was investigated. The samples with an OEM4 layer structure were found to originate from three different assembly plants: 20 vehicles from Plant Anting of S-VW company, 7 vehicles from Plant Changchun of F-VW company, and 1 vehicle from Plant Osnabrück in Germany. The primer surfacer formulations of the 20 vehicles from Plant Anting were found to be very consistent, with no differentiation observed based on their IR spectra despite variations in model and production year. In contrast, the primer surfacer formulations of the 7 vehicles from Plant Changchun were diverse, with four different types of primer surfacer composition observed. The consistency of primer surfacer formulations at Plant Anting could potentially make it easier to link a paint sample to a specific plant or production batch. However, it could make it more difficult to link the paint sample to a particular model or production year of a vehicle.

8.4.7. Exploratory analysis

An exploratory analysis of all 165 IR spectra of primer surfacer (from 28 samples with 55 subsamples) was conducted using PCA to effectively visualize the underlying data structure. Baseline correction, SNV normalization and detrending with a polynomial order 2 were applied for the pretreatment of the dataset. The variables in the range of 3750-3600, 3100-2828 and 1800-680 cm^{-1}(3200 points) were selected for analysis.

Figure 98 provides an overview of the PCA model generated from this dataset, displaying the projections of IR spectra based on the first two principal components (PC1 and PC2) and relevant loading plots. *Figure 98a* presents a PCA score plot obtained from the analysis of all samples. The plot reveals three prominent clusters. Upon examining the loading plot on PC1 (*Figure 98b*), it is evident that wavenumbers at 1270, 1180, 1120, and 1080 cm^{-1} exhibit the greatest positive correlation, which are associated with terephthalic alkyd and barium sulfate, suggesting that these factors are responsible for the observed separation in the score plot. Conversely, wavenumbers at 1725, 1305, 1240, and 730 display notable negative correlation, which are the spectral features of isophthalic alkyd, indicating their contribution to the separation of samples as well. Therefore, the separation in *Figure 98*a is primarily driven by the different chemical categories or compositions of the samples, which is consistent with that of visual characterization and comparison.

However, the first two PCs explain only 73% of the total variance, the addition of more PCs does not add more distinct groups. Additional PCA analysis was therefore conducted on the overlapping clusters (highlighted in red and green dashed line in *Figure 98a*), in order to achieve further separation and differentiation. *Figure 98c* and *Figure 98d* illustrate the resulting score plots derived from the first two PCs. These plots provide enhanced visualization and improved separation of the samples, enabling a clearer distinction between the previously overlapping clusters. To comprehend the reasons behind this improved separation, *Figure 98e* and *Figure 98f* depicts the loading plots focusing on PC1. These loading plots highlight the spectral features or wavenumbers that contribute significantly to the separation observed in the score plots. As showed in *Figure 98c* and *Figure 98e*, sample W035 and sample W061 can be separated due to the spectral features that correspond to that of polyurethane, indicating the concentration of polyurethan in these two samples are different. As for *Figure 98d*, sample W003, W006 and W011 are separated from the rest of samples due to the wavenumber at 1020 cm^{-1}, which is the characteristic peak of talc. When checking back the spectra, the intensity of talc in these samples are different from the rest.

Additional PCA was performed on the undifferentiated samples, as indicated by the dashed line in *Figure 98d*. In the end, PCA analysis resulted in the generation of 9 distinct groups as presented in *Table 35*. However, there were still 20 samples that could not be differentiated based on the PCA results. Based on these groups, a discriminatory power of 49.7% can be obtained by PCA analysis of the IR spectra of primer surfacer (190 undifferentiated pairs, for a total of 28 samples).
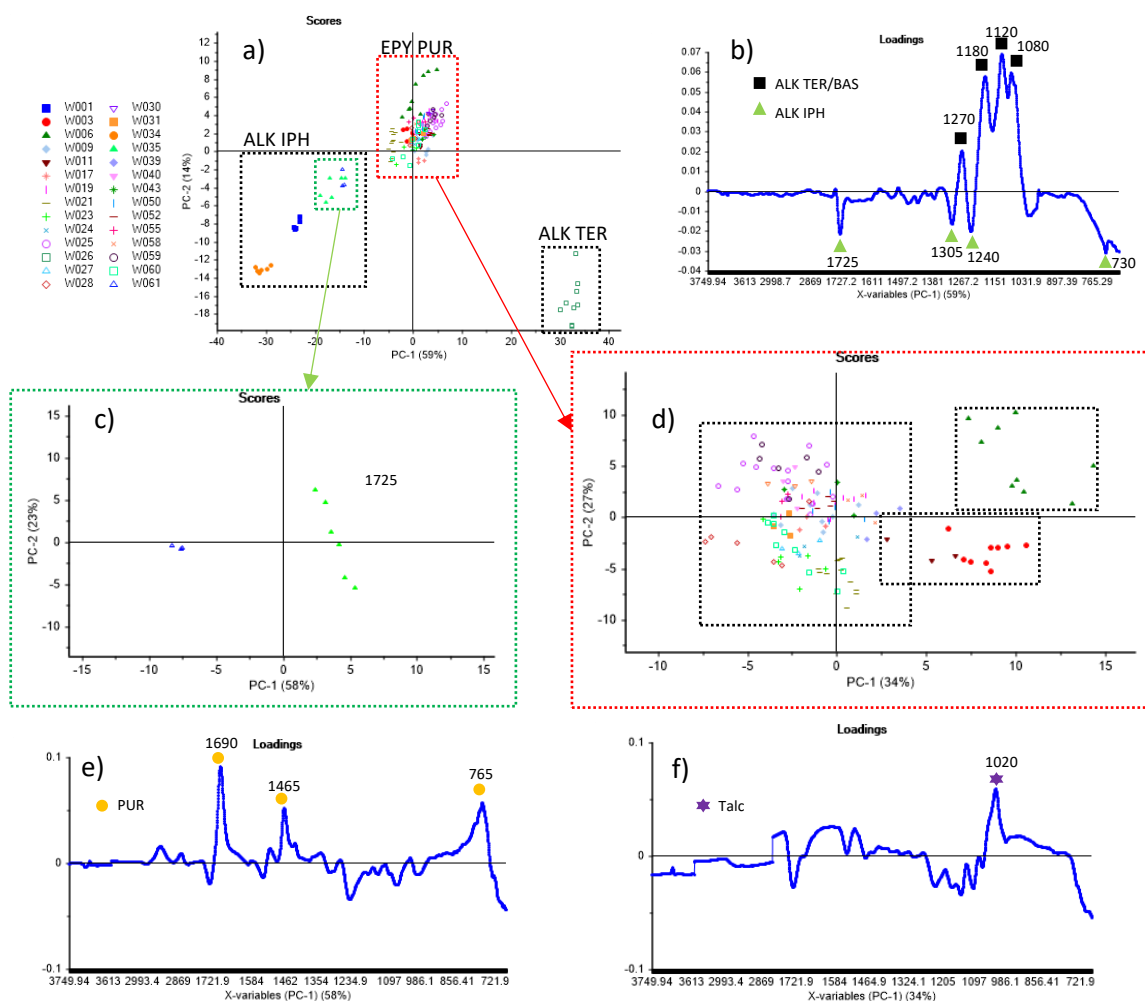
Figure 98. PCA score and loading plots obtained from the dataset: a) PCA score plot obtained from the analysis of all samples (n=28), employing the first two principal components (PCs). The different chemical categories are marked on the figure; b) loading plot specifically focusing on PC1, highlighting the underlying wavenumbers and spectra features responsible for the observed separation in the score plot; c) Additional PCA score plot derived from the first two PCs. This PCA analysis was conducted on the overlapping samples in the green box; d) Additional PCA score plot derived from the first two PCs. This PCA analysis was conducted on overlapping samples in the red box; e) loading plots focusing on PC1. This loading plot highlights the spectral features that contribute significantly to the separation observed in c); f) loading plots focusing on PC1. This loading plot highlights the spectral features that contribute significantly to the separation observed in d).

Table 35. Summary of PCA-based groupings of primer surfacer (n=28)

GROUP	SAMPLES	CHEMICAL COMPOSITION
1	W009, W017, W019, W021, W022, W024, W025, W027, W028, W030, W031, W040, W043, W050, W052, W055, W058, W059, W060	EPY+PUR+MEL+TALC+BAS+TIO2
2	W001	ALK IPH+EPY+MEL TALC+TIO2
3	W003	EPY+PUR+MEL+TALC+BAS+TIO2
4	W006	EPY+PUR+MEL+TALC+BAS+TIO2
5	W011	EPY+PUR+MEL+TALC+BAS+TIO2
6	W034	ALK IPH+MEL+TALC+TIO2
7	W035	ALK IPH+PUR+EPY+TALC+ALS+TIO2
8	W061	ALK IPH+PUR+EPY+TALC+ALS+TIO2
9	W026	ALK TER+ACR+MEL+BAS+TIO2

166

The data structure of the IR spectra of the primer surfacer was explored, taking into account several predetermined identifying factors, as illustrated in *Figure 99.* The PCA score plots of the IR spectra, specifically pertaining to manufacturing companies (*Figure 99a*), assembly plants (*Figure 99b*), and vehicle models (*Figure 99c*), were generated to analyze the dataset. Since all samples in this dataset exhibit an OEM4 layer system, the correlation between chemical composition and layer structure was not investigated.

Consistent with visual comparison, the PCA score plots yielded similar conclusions. Notably, samples from Plant Anting of S-VW company showed a high level of consistency, as indicated by the clustering of data points in the score plot (*Figure 99a and Figure 99b*). Despite variations in vehicle model and production year, there was minimal differentiation observed based on their IR spectra. In contrast, samples from Plant Changchun exhibited greater diversity, with more discrete data points represented in the score plot.

Regarding vehicle models, it was found that the paint formulation within the same model is not always consistent. *Figure 99c* illustrates this phenomenon, where the green triangles represent spectra from a specific model called 'New Bora'. These triangles are distributed across different clusters, which are separated based on chemical categories. This indicates the presence of significant batch variance, where the entire paint formulation can undergo changes after a certain period.

In summary, the PCA analysis of the primer surfacer IR spectra, considering factors such as manufacturing companies, assembly plants, and vehicle models, confirmed the findings obtained from visual comparison. The results highlighted the consistency of samples from Plant Anting, the diversity of samples from Plant Changchun, and the existence of batch variance within the same vehicle model.
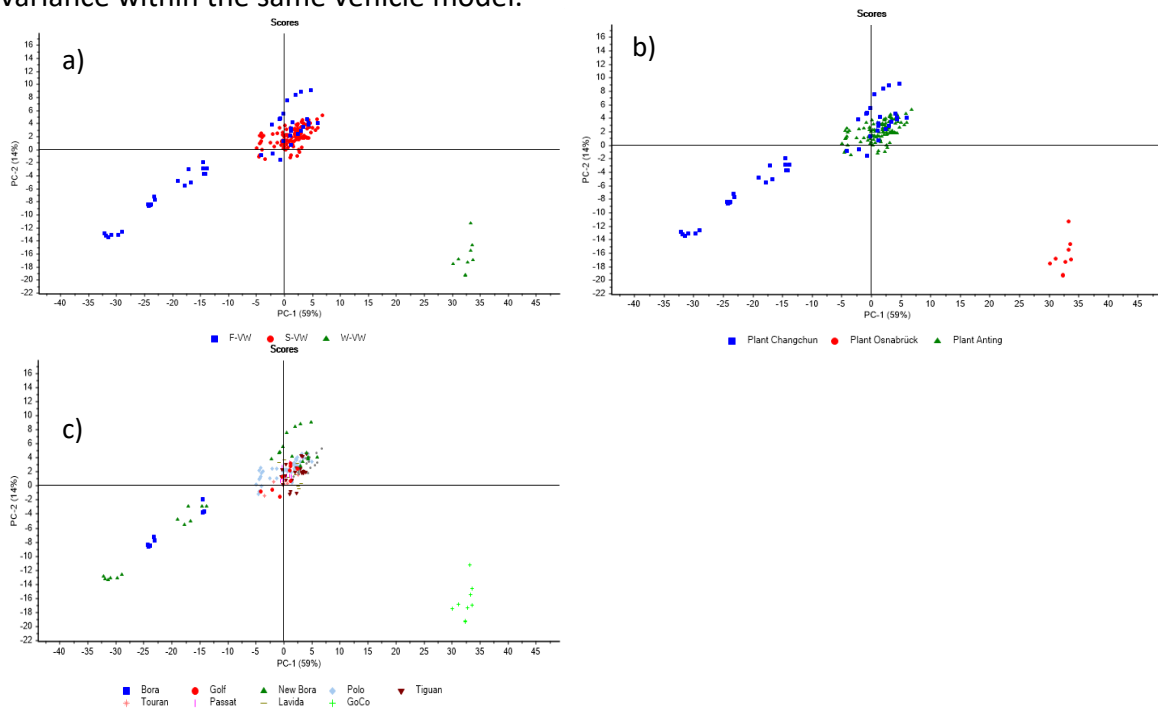
Figure 99. PCA score plots according to the first two principal components of all IR spectra of primer surfacer, respectively according to their manufacturing companies (a), their assembly plants (b) and the model of vehicles(c).

8.5.   Characterization of primer

The characterization of primer was performed on 60 out of the 62 samples in the set, as spectra data could not be obtained for the primer of W029 and W037 due to its thin thickness. The FTIR spectra obtained from the primer of these 60 samples were visually characterized, and the results are presented in *Table 36*. The samples were classified into four groups based on the chemical categories of the binders, pigments, and extenders used in the layer. Further visual comparisons were carried out to identify distinguishable subgroups within each group, as presented in the table, highlighting the main differences observed between the spectra of samples with similar characterization. Each group of spectra was then analyzed individually to identify the constituents detected by FTIR in the investigated paints.

Table 36. Summary of visual characterization and groupings based on the FTIR spectra of the primer of the automotive paint samples in this thesis (n=60).

GROUP/COMPOSITION	SUB-GROUP	SAMPLES	DIFFERENCE WITHIN THE GROUP
GROUP 1 EPY+ALS	1.1	W001	Very high intensities of peaks at 3695, 3620, 1035 and 1012 cm^{-1}, rising towards 700 cm^{-1}
	1.2	W002, W005, W023, W036, W056	Relative intensities of peaks at 3695, 3620, 1035 and 1012 cm^{-1}
	1.3	W007, W033, W046	Relative intensities of peaks at 3695, 3620, 1105, 1083, 1035 and 1012 cm^{-1}
	1.4	W009, W010, W013, W017, W020, W022, W027, W028, W030, W031, W041, W043, W044, W052, W053	Relative intensities of peaks at 1105, 1083, 1035, 1012 and 758 cm^{-1}
	1.5	W012, W014, W015, W016, W018, W032, W042, W047, W048, W049, W054, W062	Relative intensities of peaks at 3695, 3620, 1105, 1083, 1035 and 1012 cm^{-1}
	1.6	W003, W006, W011, W019, W021, W025, W026, W039, W040, W045, W050, W051, W055, W060	Relative intensities of peaks at 3695, 3620, 1105, 1083, 1035 and 1012 cm^{-1}
	1.7	W024	Relative intensities of peaks at 3695, 3620, 1105, 1083, 1035 and 1012 cm^{-1}
	1.8	W034, W058	Relative intensities of peaks at 3695, 3620, 1105, 1083, 1035 and 1012 cm^{-1}
	1.9	W035	Relative intensities of peaks at 3695, 3620, 1105, 1083, 1035, 1012 and 758 cm^{-1}
	1.10	W061	Relative intensities of peaks at 3695, 3620, 1035 1012 cm^{-1} and 700 cm^{-1}
GROUP 2 EPY	2.1	W008	Rising towards 700 cm^{-1}
	2.2	W057	Relative intensities of peaks at 1130 and 1103 cm^{-1}
	2.3	W059	Relative intensities of peaks at 1130 and 1103 cm^{-1}, no rising towards 700 cm^{-1}
GROUP 3 ALK OPH + NCL+BAS+TALC	-	W038	Single sample in the group
GROUP 4 ACR+STY+TALC	-	W004	Single sample in the group

8.5.1. Group 1 – primer

This group comprises the majority of samples, with 55 samples having identical chemical composition, accounting for 92% of the total sample set (see Group 1 *in Table 36*). A typical spectrum of the analyzed group displays diagnostic absorption peaks at 3036, 2955, 2931, 2872, 1610, 1510, 1460, 1413, 1300, 1240, 1180, 1105, 1083, 1040, 1012 and 830 cm^{-1}. The absorption peak between 3000 and 2800 cm^{-1} corresponds to the stretching vibration of C-H bonds in aromatic compounds. The peaks at 1610 and 1510 cm^{-1} are associated with the C= C stretching vibration of the aromatic bisphenol ring. The peaks at 1460 and 1413 cm^{-1} are associated with the bending vibration of the methyl (CH3) group. The peak at 1300 cm^{-1} is associated with the stretching vibration of C-N bonds in amides, which could indicate the presence of an amide binder. The broad peak at 1240 cm^{-1} is due to C6H4-O stretching. The peaks at 1183 and 1103 cm^{-1} are associated with the stretching vibration of C-O bonds. The peak at 1083 and 1040 cm^{-1} correspond to the stretching vibration of C-O bonds in aliphatic compounds. Finally, the peak at 830 cm^{-1} is associated with the out-of-plane bending of two adjacent hydrogens on the aromatic ring. Based on these absorption peaks, it appears that the binder used in the primer is likely to be epoxy resin. In addition to the binder types identified, the spectrum also revealed the presence of pigments and extenders in the analyzed samples. The characteristic peaks at 3695, 3620, 1103, 1035, 1012, and 915 cm^{-1} correspond to the diagnostic peaks of aluminum silicate. *Figure 100* illustrates the distinctive peaks of epoxy resin and clay found in the sample, along with a comparison to the reference spectra of pure epoxy resin and clay.
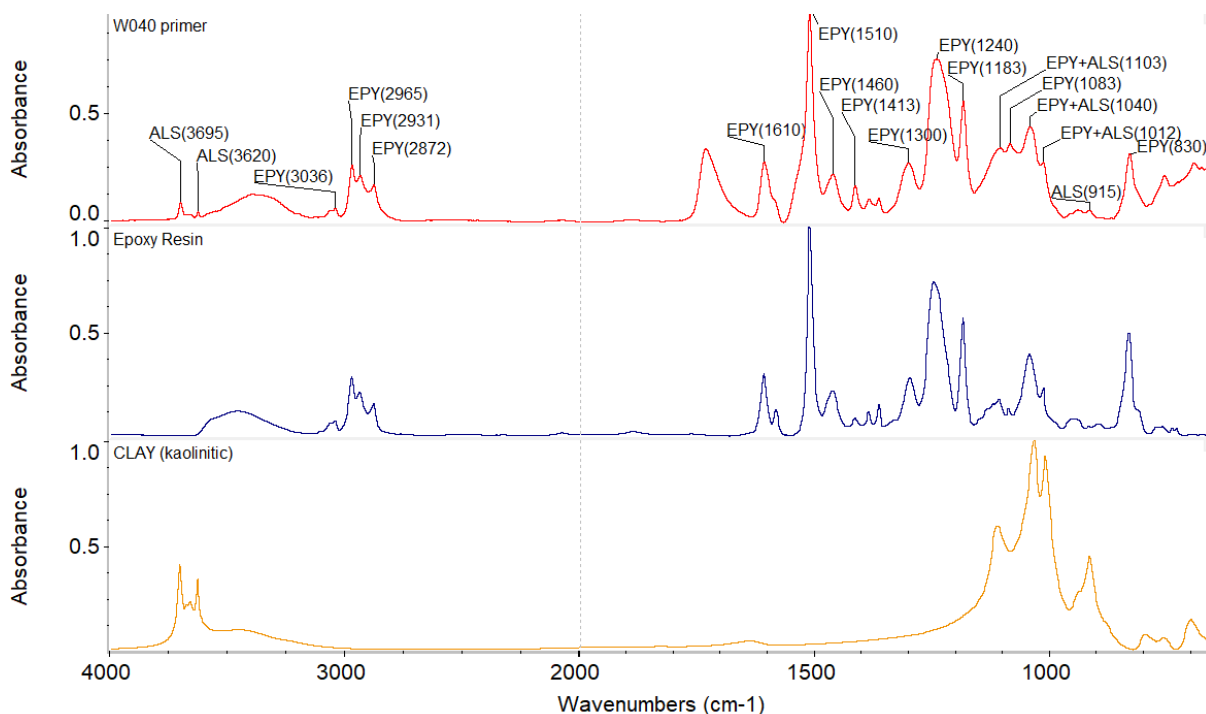
Figure 100. Comparison of the representative IR spectrum of the primer from sample W040 (top) containing epoxy resin and clay with reference spectra of pure epoxy resin (middle) and pure clay (bottom). The characteristic peaks of epoxy and clay are annotated on the spectrum of sample W040.

8.5.2. Group 2 – primer

This group is composed of 3 sample, representing 5% of the total sample set (see Group 2 in *Table 36*). The IR spectrum of this group closely resembles that of group 1, with diagnostic peaks observed at 1610, 1510, 1240, 1180 and 830 cm^{-1}, suggesting the use of epoxy resin as the binder. However, the absence of aluminum silicate in this sample distinguishes it from group 1. *Figure 101* provides a representative spectrum of this group, displaying the characteristic peaks of epoxy resin labeled on the spectrum for reference.
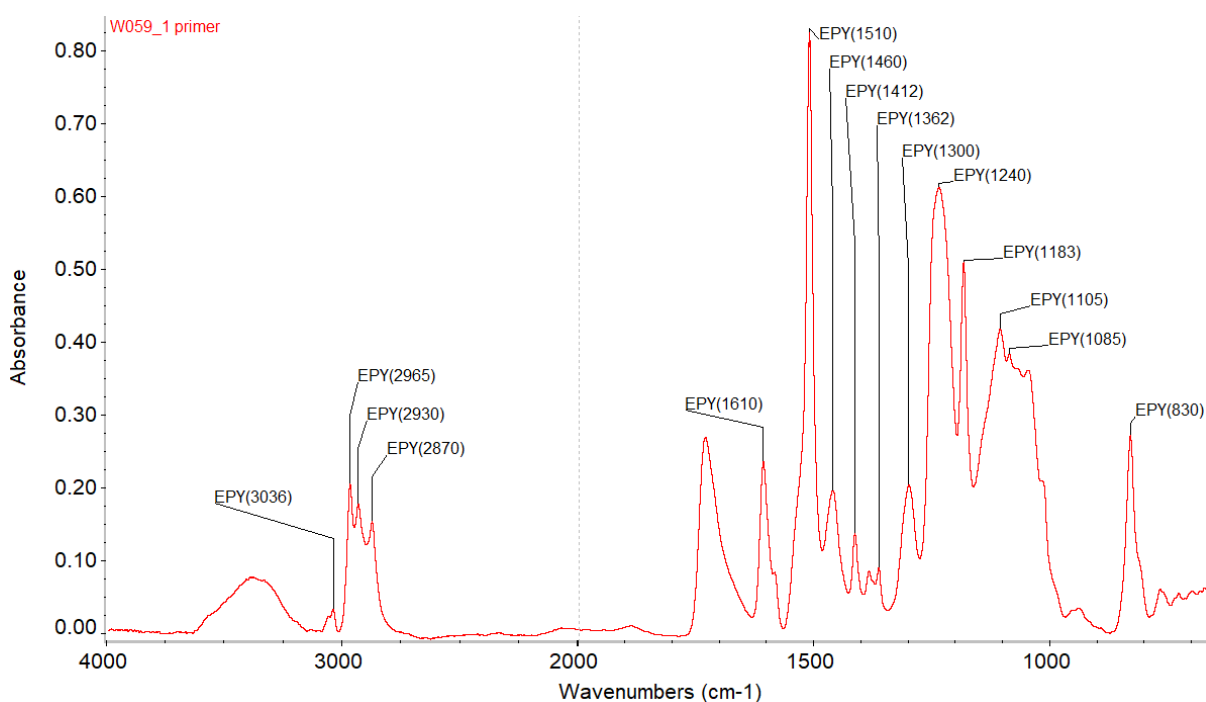
Figure 101. A representative IR spectrum of the primer of sample W059_1 with characteristic peaks of epoxy resin annotated on the spectrum.

8.5.3. Group 3 – primer

This group consists of only one sample, constituting a mere 1.5% of the total sample set (see Group 3 in *Table 36*). In contrast to the previous groups, the spectrum of this particular sample exhibits distinctive absorption peaks, implying the existence of a different type of binder. The peaks at 1650, 1280, 1065, 840 and 750 cm^{-1} correspond to the characteristic vibrations of nitrocellulose. Specifically, the peaks at 1650, 1280 and 840 cm^{-1} are associated with the O-NO_2 stretching vibrations, while the peak at 1065 cm^{-1} is due to the C-O stretching vibration. These findings strongly suggest that the binder type in this sample is nitrocellulose. Additionally, the spectrum also displays peaks at 1727, 1457, 1382, 1123 and 1065 cm^{-1}, which indicate the presence of orthophthalic alkyd. Furthermore, peaks at 3678 and 1020 cm^{-1} are suggestive of the existence of talc, whereas the peaks observed at 1180 and 1123 cm^{-1} may arise from the presence of barium sulfate. A representative spectrum of this group with the characteristic peaks of nitrocellulose, orthophthalic alkyd, talc, barium sulfate, and their respective labels can be seen in *Figure 102*, along with a reference spectrum of nitrocellulose.
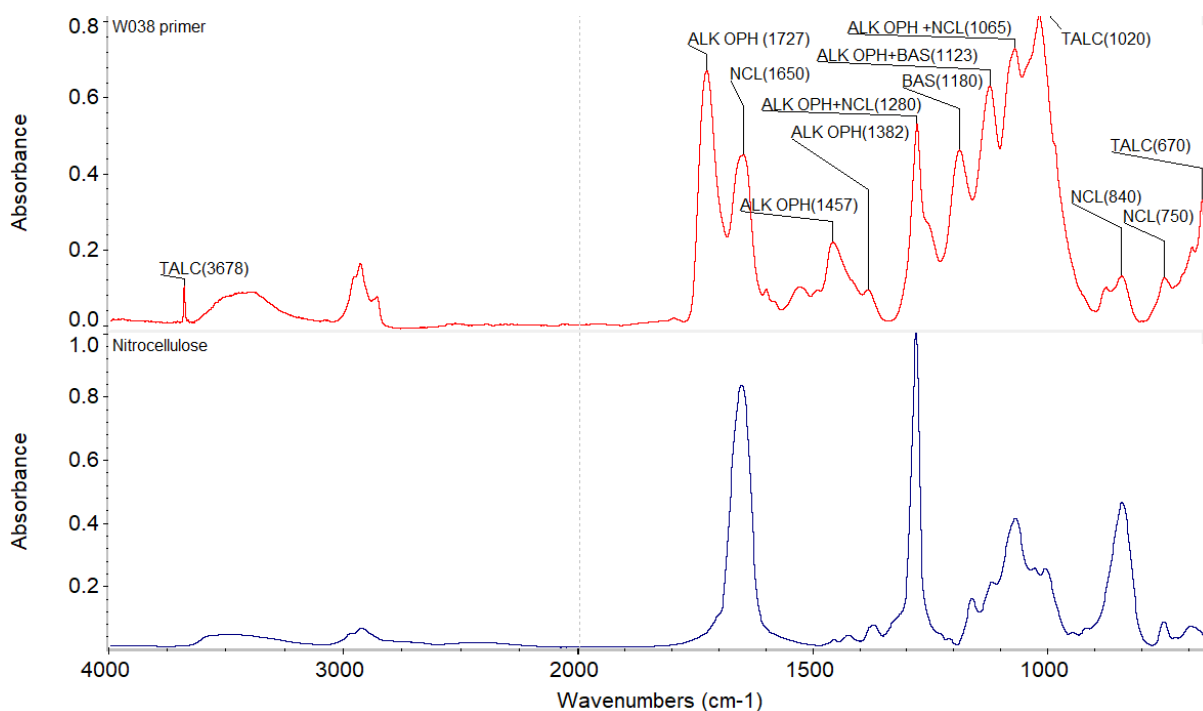
Figure 102. A representative IR spectrum of the primer of sample W038 (top) in comparison with a reference spectrum of nitrocellulose (bottom). Characteristic peaks of nitrocellulose, orthophthalic alkyd, talc and barium sulfate annotated on the spectrum.

8.5.4. Group 4 – primer

This group comprises a solitary sample, representing only 1.5% of the total sample set (see Group 4 in *Table 36*). The corresponding spectrum exhibits a limited number of distinctive peaks. The diagnostic peaks at 1730, 1450, 1380, 1260, 1170, 1150 cm^{-1} strongly suggest the primary resin used in this layer is acrylic. Specifically, these peaks are associated with the characteristic vibrations of the C=O, C-H, and C-O groups of acrylic resin. The peaks at 3060 cm^{-1}, 3026 cm^{-1}, 1601 cm^{-1}, 1490 cm^{-1}, 1450 cm^{-1}, 760 cm^{-1} and 700 cm^{-1} are indicative of styrene, which may be present as a modification. Moreover, the peaks at 3676 cm^{-1}, 1020 cm^{-1} and 670 cm^{-1} suggest the presence of talc. *Figure 103* displays a representative spectrum with the characteristic peaks of acrylic, styrene, talc, and their respective labels.
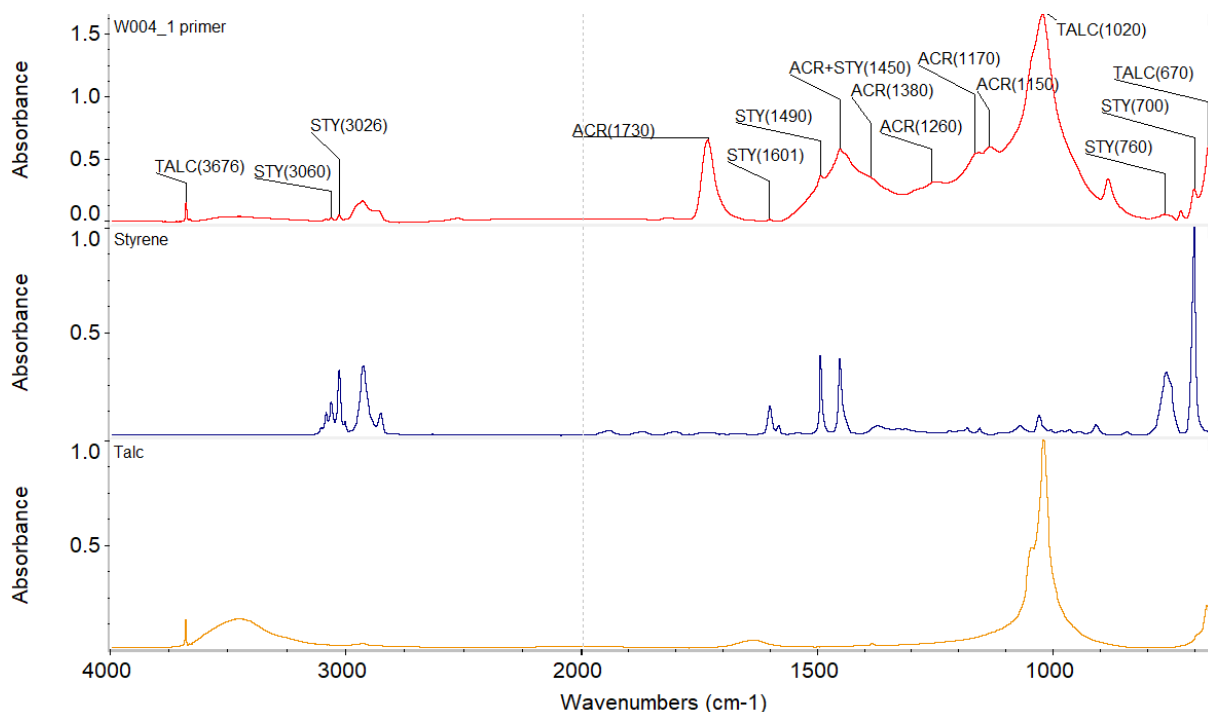
Figure 103. A representative IR spectrum of the primer of sample W004_1 (top) in comparison with reference spectra of styrene (middle) and talc (bottom). Characteristic peaks of acrylic, styrene and talc are annotated on the spectrum.

8.5.5. Classification and discrimination of primer

Table 37 provides a summary of the characteristic compounds identified from the IR spectra of the primer for each sample examined in this study. The primer spectra of the studied samples reveal the presence of three primary resin types, as depicted in *Figure 104*. Epoxy resin is the predominant type, accounting for 97% of the total samples. In contrast, acrylic and orthophthalic alkyd are present at lower proportions of 1.5% each. Furthermore, two types of additional resins were detected in two samples, with one sample containing styrene and one sample containing nitrocellulose, respectively. Aluminum silicate was detected in 92% of the samples, primarily in conjunction with the epoxy resin, while only a small number of samples contained talc.

These findings demonstrate the prevalence of epoxy resin as the primary component of primer, with acrylic and nitrocellulose present in relatively small proportions. Notably, the samples that contain acrylic and nitrocellulose binder types for their primer are those that have been repainted, indicating the great diversity of binders used in refinishing formulations.

After examining the different combinations of primary and additional resins, along with the presence or absence of certain extenders, the primer samples could be classified into four distinct groups (as shown in *Figure 105*). The majority of the samples (92% of the total sample set) were found to contain epoxy resin combined with aluminum silicate as extenders.

The discriminating power for visual comparisons of primer spectra was calculated using the subgroups listed in *Table 36*, taking into account the number of undifferentiated pairs (totaling 276 pairs from 60 samples), resulting in a discriminating power of 84.4 %.

Following the classification of undifferentiated samples, an investigation was conducted to explore any potential correlation between their chemical properties and origin. However, no discernible pattern was found that could be linked to any specific identifying factors, such as company, model, assembly plant, or production year. Unlike clearcoat or basecoat layers, the primer type could not be associated with the layer structure. In other words, paint samples from different company, model, layer structure or assembly plant could have undifferentiated primer compositions.

173

Table 37. Summary of characteristic compound types based on the FTIR spectra of the primer of the automotive paint samples in this thesis (60 samples)

Sample\Composition	BINDER					PIGMENTS/EXTENDERS			
	EPY	ALK OPH	ACR	STY	NCL	BAS	ALS	TiO$_2$	Talc
W001	X						X	X	
W002	X						X		
W003	X						X		
W004			X	X					X
W005	X						X		
W006	X						X		
W007	X						X		
W008	X							X	
W009	X						X		
W010	X						X		
W011	X						X		
W012	X						X		
W013	X						X		
W014	X						X		
W015	X						X		
W016	X						X		
W017	X						X		
W018	X						X		
W019	X						X		
W020	X						X		
W021	X						X		
W022	X						X		
W023	X						X		
W024	X						X		
W025	X						X		
W026	X						X		
W027	X						X		
W028	X						X		
W030	X						X		
W031	X						X		
W032	X						X		
W033	X						X		
W034	X						X		
W035	X						X		
W036	X						X		
W038		X			X	X			X
W039	X						X		
W040	X						X		
W041	X						X		
W042	X						X		
W043	X						X		
W044	X						X		
W045	X						X		
W046	X						X		
W047	X						X		
W048	X						X		
W049	X						X		
W050	X						X		
W051	X						X		
W052	X						X		
W053	X						X		
W054	X						X		
W055	X						X		
W056	X						X		
W057	X							X	
W058	X						X		
W059	X								
W060	X						X		
W061	X						X	X	
W062	X						X		
Total	58	1	1	1	1	1	55	3	2
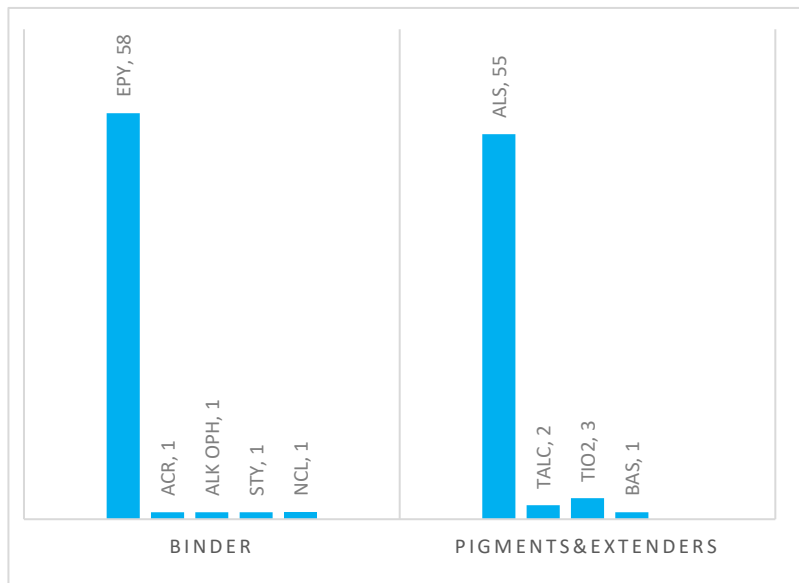
Figure 104. Distribution of infrared characterizations with the primer of 60 vehicles.
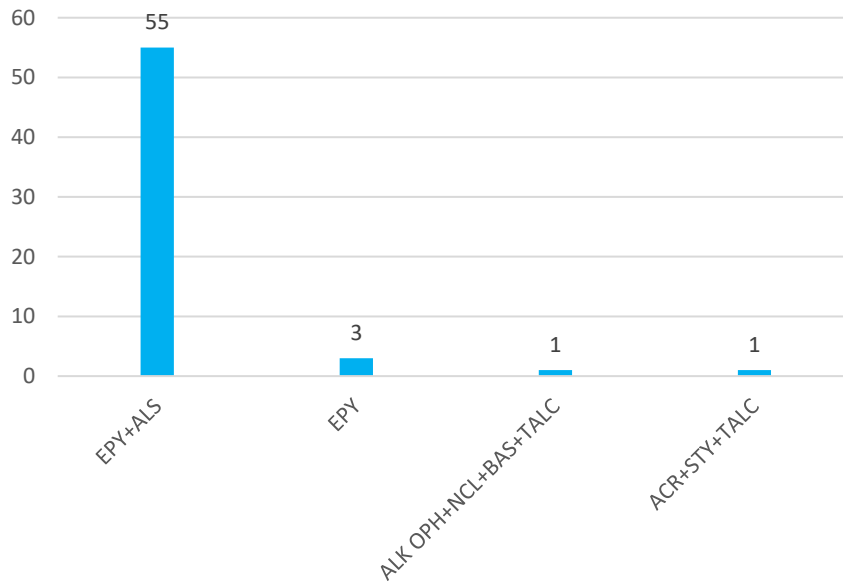
Figure 105. Proportion of samples according to the combination of infrared characterizations. Four groups (combinations) can be distinguished.

8.5.6. Exploratory analysis

A total of 339 IR spectra of primer (from 60 samples with 113 subsamples) was analyzed using PCA to visualize the underlying data structure. The dataset underwent baseline correction, SNV normalization and detrending with a polynomial order of 2 were as preprocessing steps. The analysis focused on variables in the range of 3750-3600, 3100-2828 and 1800-680 cm^{-1} (3200 points).

Figure 106 illustrates the PCA model generated from this dataset, depicting the projections of IR spectra based on the first four principal components, which account for 84% of the total variance. The scatter plot in Figure 106*a* shows a large group of samples discretely spread out in the center. However, two samples stand out as outliers, positioned far away from the main cluster of spectra (indicated by the dashed line in *Figure 106a*).

The loadings of the first principal component (PC1, *Figure 107a*) help identify the factors responsible for the observed distribution in the scatter plot. PC1 is influenced by positive values corresponding to the spectral features of epoxy, as well as by negative values associated with characteristic peaks of aluminum silicate. Analyzing the loadings of the second principal component (PC2, *Figure 107b*), it becomes apparent that wavenumbers at 1510, 1240, and 830 cm^{-1} exhibit significant negative correlation, indicating their association with epoxy resin. Conversely, positive values in PC2 primarily relate to peak at 1105 cm^{-1} which belongs to epoxy. Despite PC1 and PC2 explaining 60% of the total variance, it is challenging to separate samples based on these two components due to the majority of spectra having similar chemical compositions.

By considering the third and fourth principal components, additional separation becomes possible. Five samples, marked by the dashed line in *Figure 107b to d*, can be differentiated from the majority of the spectra. The loadings of the third principal component (PC3, *Figure 107c*) indicate that the separation is based on the concentration of TiO2 in the samples, while the loadings of the fourth principal component (PC4, *Figure 107d*) are predominantly influenced by positive values corresponding to characteristic peaks of epoxy.

Notably, most of the separated samples are identified as outliers since the PCA model primarily captures the components of epoxy resin and aluminum silicate. Samples that deviate from this chemical composition are considered outliers and cannot be effectively represented by this model. Ultimately, seven samples can be distinguished from the majority of the spectral cloud when considering the first four principal components, leaving 53 samples undifferentiated.

Subsequently, an additional PCA was performed on the IR spectra from these 53 samples, excluding the previously identified outliers and those samples that could be differentiated in the previous model. The goal is to determine if there are any internal variations or similarities among these samples that can be captured by the PCA analysis.
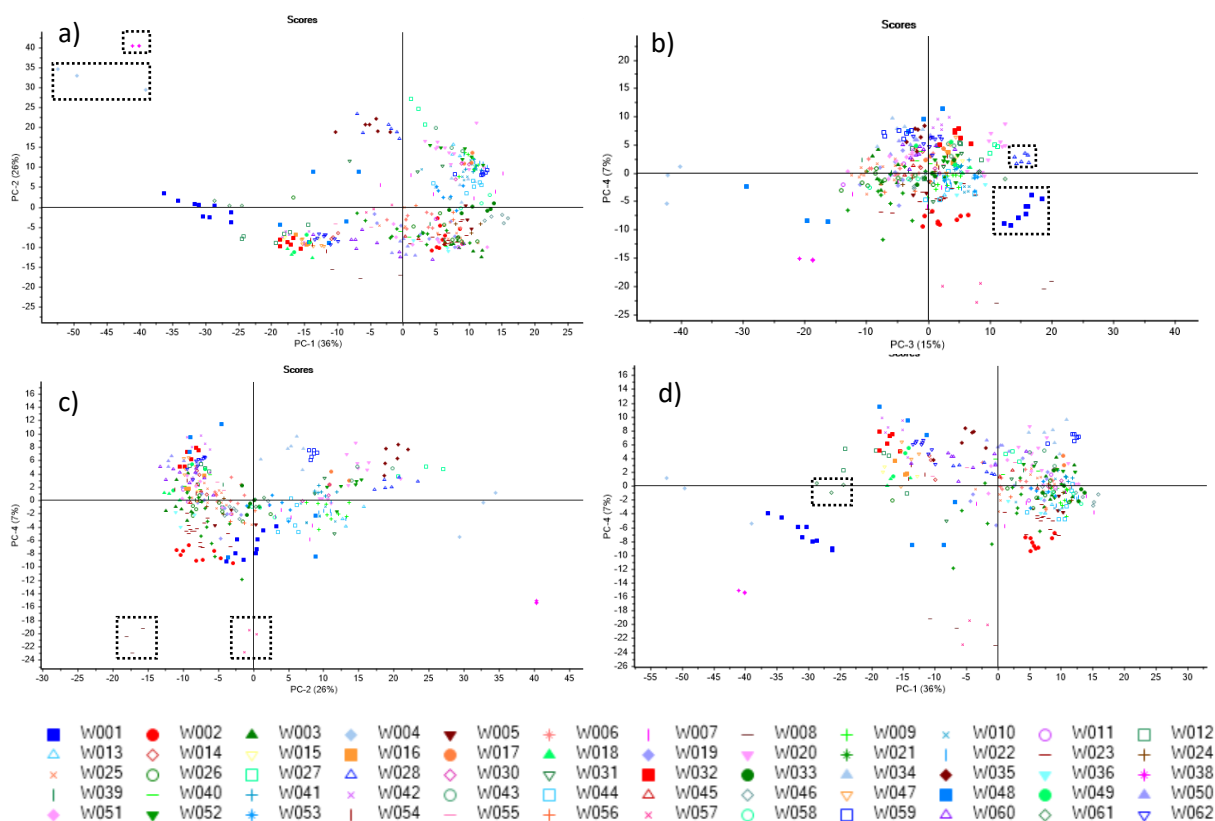
Figure 106. PCA score plots according to the first four principal components of the dataset of IR spectra of primer (n=60): a) projections according to PC1 and PC2; b) projections according to PC3 and PC4; c) projections according to PC2 and PC4; d) projections according to PC1 and PC4. Samples that well separated from the rest were highlighted in dashed rectangular.
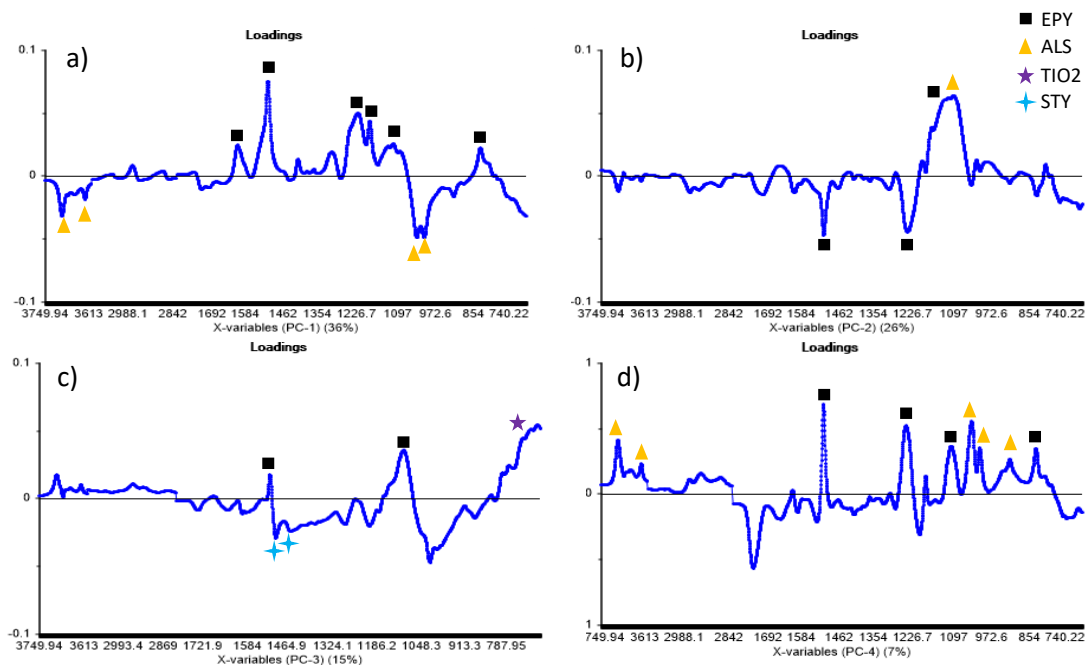
Figure 107. loadings of the first four principal components (a to d, respectively) of the PCA model on the 339 IR spectra of primer. The wave numbers corresponding to characteristic peaks of the characterized resin or extenders are highlighted using different shapes and colors.

Figure 108 displays the scatter plots resulting from PCA analysis on the 53 samples, revealing distinct patterns and enabling further separation within this subset of data. In the scatter plot based on the first two PCs (*Figure 108a*), four clusters can be observed, denoted by dashed lines. However, there is noticeable overlap between these clusters. The loadings of these PCs (*Figure 109*) indicate that the separation is primarily driven by peaks related to epoxy and aluminum silicate. Since all samples in this PCA model contain epoxy and aluminum silicate, the differentiation is mainly based on variations in peak intensity rather than the presence or absence of specific components. The sample in green dashed line was identified as outlier and thus separated from the rest sample set. PC1 accounts for 43% of the total variance and mainly contributes to the separation between clusters. Although PC4 has a lesser impact on the separation, combining PC1 and PC4 leads to improved cluster separation, as depicted in *Figure 108b*. One cluster (highlighted by a red dashed line) is completely distinct from the others, while the remaining two clusters still exhibit some overlap. Consequently, additional PCA was performed on the samples from the two overlapped clusters in an attempt to achieve further separation. However, despite these efforts, satisfactory differentiation between the samples could not be achieved, and it was determined that they would remain undifferentiated.

It is important to note that there is slightly higher intra-sample variability in the IR spectra of the primer due to inconsistent baseline (could not be fully eliminated by pretreatment), contributing to the overlap between clusters. This variability within the same sample limits the effectiveness of PCA separation compared to visual comparison. After conducting PCA analysis on the IR spectra of the primer, a total of 11 groups were generated, as presented in *Table 38*. However, despite these efforts, 846 pairs of samples out of the total of 60 remained undifferentiated. This outcome resulted in an overall discriminating power of 55.2%.
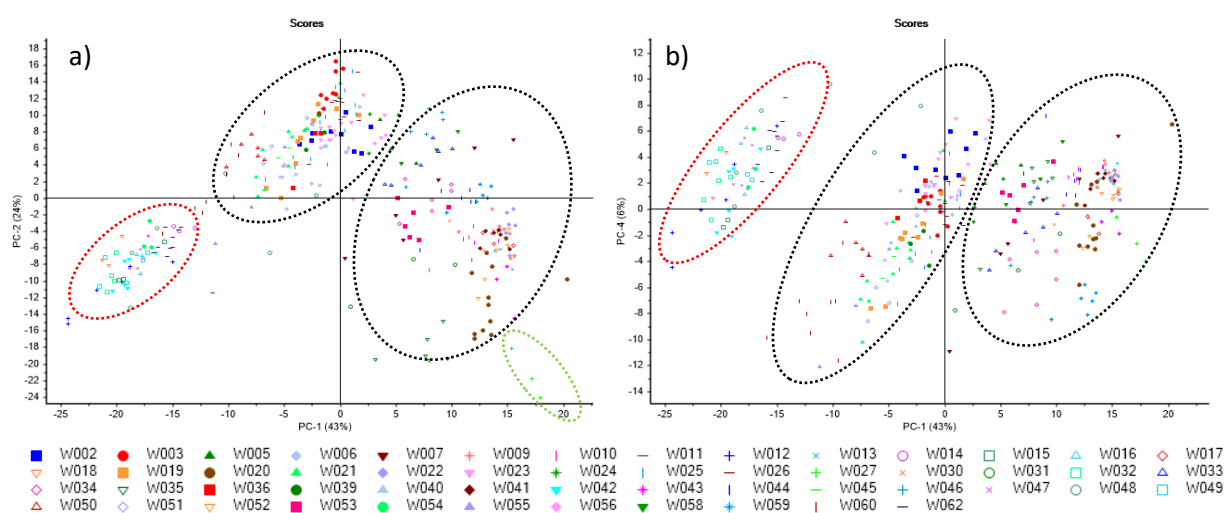
Figure 108. PCA score plots of IR spectra of primer (n=53): a) projections according to PC1 and PC2; b) projections according to PC1 and PC4
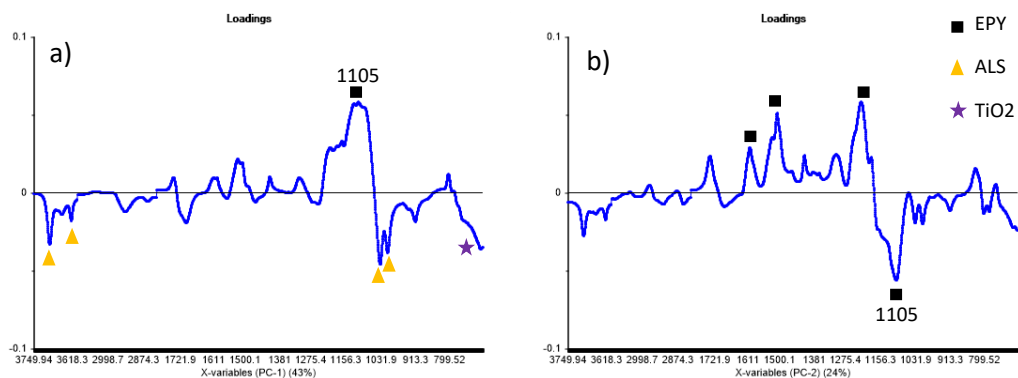
Figure 109. loadings of the first two principal components (a and d, respectively) of the additional PCA model on IR spectra of primer(n=53). The wave numbers corresponding to characteristic peaks of the characterized resin or extenders are highlighted using different shapes and colors.

Table 38. Summary of PCA-based groupings of primer (n=60)

GROUP	SAMPLES	CHEMICAL COMPOSITION
1	W012, W014, W015, W016, W018, W032, W042, W047, W048, W049, W054, W062	EPY+ALS
2	W002, W003, W005, W006, W007, W009, W010, W011, W013, W017, W019, W020, W021, W022, W023, W024, W025, W026, W030, W031, W033, W034, W035, W036, W039, W040, W041, W043, W044, W045, W046, W050, W051, W052, W053, W055, W056, W058, W059, W060	EPY+ALS
3	W001	EPY+ALS
4	W061	EPY+ALS
5	W027	EPY+ALS
6	W028	EPY+ALS
7	W004	ACR+STY+TALC
8	W008	EPY
10	W038	ALK OPH +NCL+BAS+TALC
11	W057	EPY

The data structure of the IR spectra of the primer, specifically focusing on 54 OEM paint samples, was investigated and depicted in *Figure 110*. The PCA score plots were generated to analyze the dataset based on manufacturing companies (*Figure 110a*), layer structure (*Figure 110b*), assembly plants (*Figure 110c*), and vehicle models (*Figure 110d*). However, no noticeable structure linked to these factors could be discerned from the exploratory analysis, as the majority of primer exhibited the same chemical composition.

However, variations were observed among samples from the same assembly plant, as well as among samples of the same vehicle model. For instance, in *Figure 110c*, the scatter plot highlights IR spectra of samples from Plant Nanjing (indicated by orange diamonds), are widely dispersed and projected in different regions, indicating batch variations within the plant. Similarly, *Figure 110d* depicts samples of the model 'New Lavida' represented by a purple horizontal line, and these samples are also widely scattered in the scatter plot, indicating batch variations within the same vehicle model. These observations further emphasize the existence of variability within the primer samples, even when they share the same chemical class.
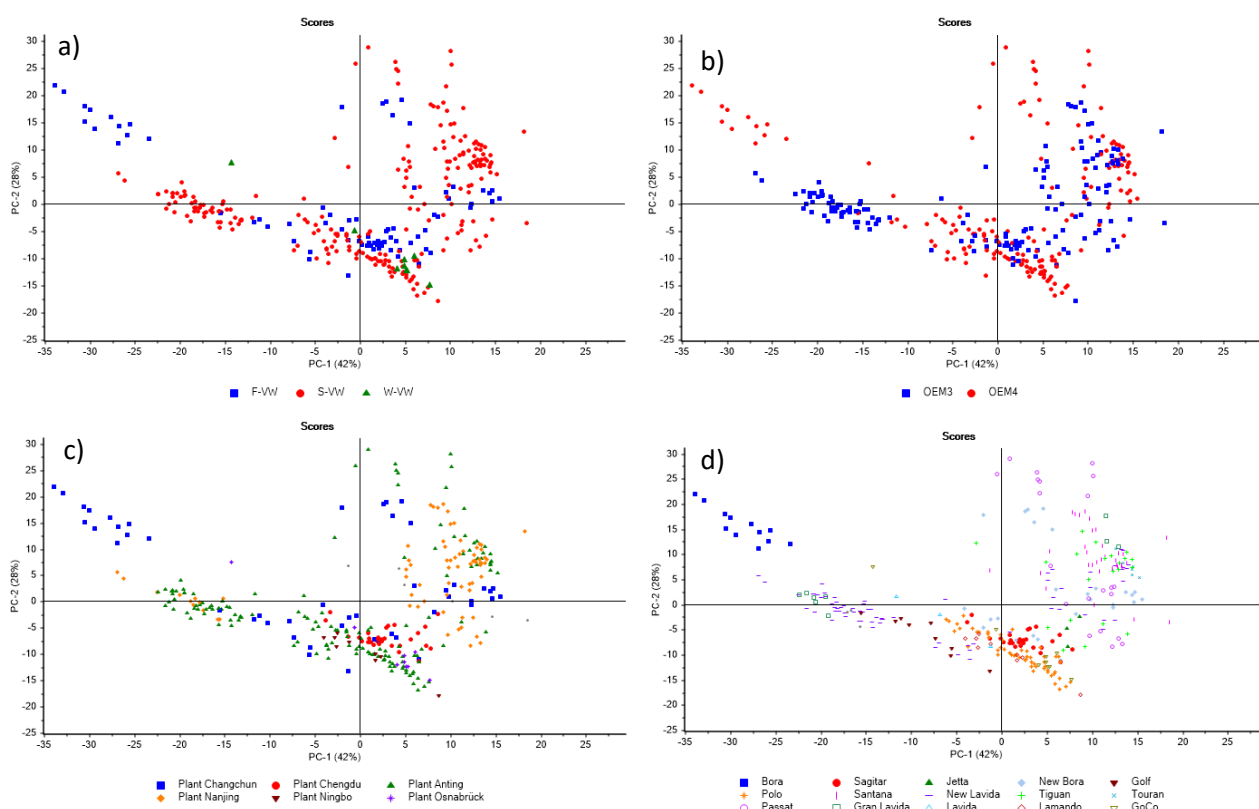
Figure 110. PCA score plots according to the first two principal components of all IR spectra of primer, respectively according to their manufacturing companies (a), their layer structure (b), their assembly plants (c) and the model of vehicles(d).

180

8.6.   Discussion

8.6.1. Blind test

Although this research focuses on the exploratory analysis of paint variation within the same car make and color, it is important to validate that the adopted analytical procedure can be relied upon for the discrimination of these samples. To validate the adopted procedure, blind tests were executed. Five samples (one subsample from each vehicle), designated as A to E, were randomly chosen by a collaborator. Measurement was conducted by another collaborator.

The complete statistical procedure was subsequently applied to these selected samples in a blind manner. For enhanced sample classification accuracy, initial PCA projections were conducted to determine the chemical class of each sample (see *Figure 111)*. Then PCA models were selected for LDA and SIMCA classification. Specifically, the PCA scores were utilized for LDA (3 components used), while individual PCA models were employed for SIMCA classification. The predicted classifications for each replicate of each layer were then integrated to generate the prospective class assignment for each sample. The databases containing all the spectra (including all replicates) from this study were constructed using the OMNIC software and subsequently employed for database searches. The outcomes of the classification are comprehensively detailed in *Table 39*.

Due to the extensive number of undifferentiated samples within each layer, the accuracy of classification using LDA posed challenges, as it can only assign a single class. Despite combining classified results from all replicates, LDA struggled to accurately classify samples. Predicting the class of each layer from a single sample using LDA did not result in a consensus classification, consequently leading to classification failure. Nevertheless, all the false positives identified by LDA were, in fact, attributed to the actual undifferentiated groups the samples originated from, which often contains at least 15 undifferentiated samples.

In contrast, SIMCA and database search exhibited the advantage of providing multiple potential sources, some of which included the actual class of these samples. However, correctly classifying A, C, and E proved to be quite difficult, given their highly similar chemical profiles, resulting in elevated false positive rates. Another complicating factor in the blind tests was the influence of baseline variations. Certain samples exhibited curved baselines due to uneven surfaces during measurement. This occasionally caused projections of these samples to diverge significantly from the original dataset. Consequently, SIMCA classified these samples into no class at the 5% significance level. Successful classification requires the manual correction of the baseline effect and reducing the significance level to 1%.

Conventional database search, based on 'correlation' between search spectra and database spectra, generally yielded good results regardless of baseline effects. Due to the high similarity, the hit list sometimes presented exceedingly high 'match values' over 99% even after 100 hits. All the hits with a 'match value' obtained from the correlation algorithm

surpassing 98% were documented. Furthermore, a visual comparison of spectra was conducted before any potential hits were recorded, ensuring a reliable classification process.

Ultimately, all samples were accurately classified through SIMCA and database search.
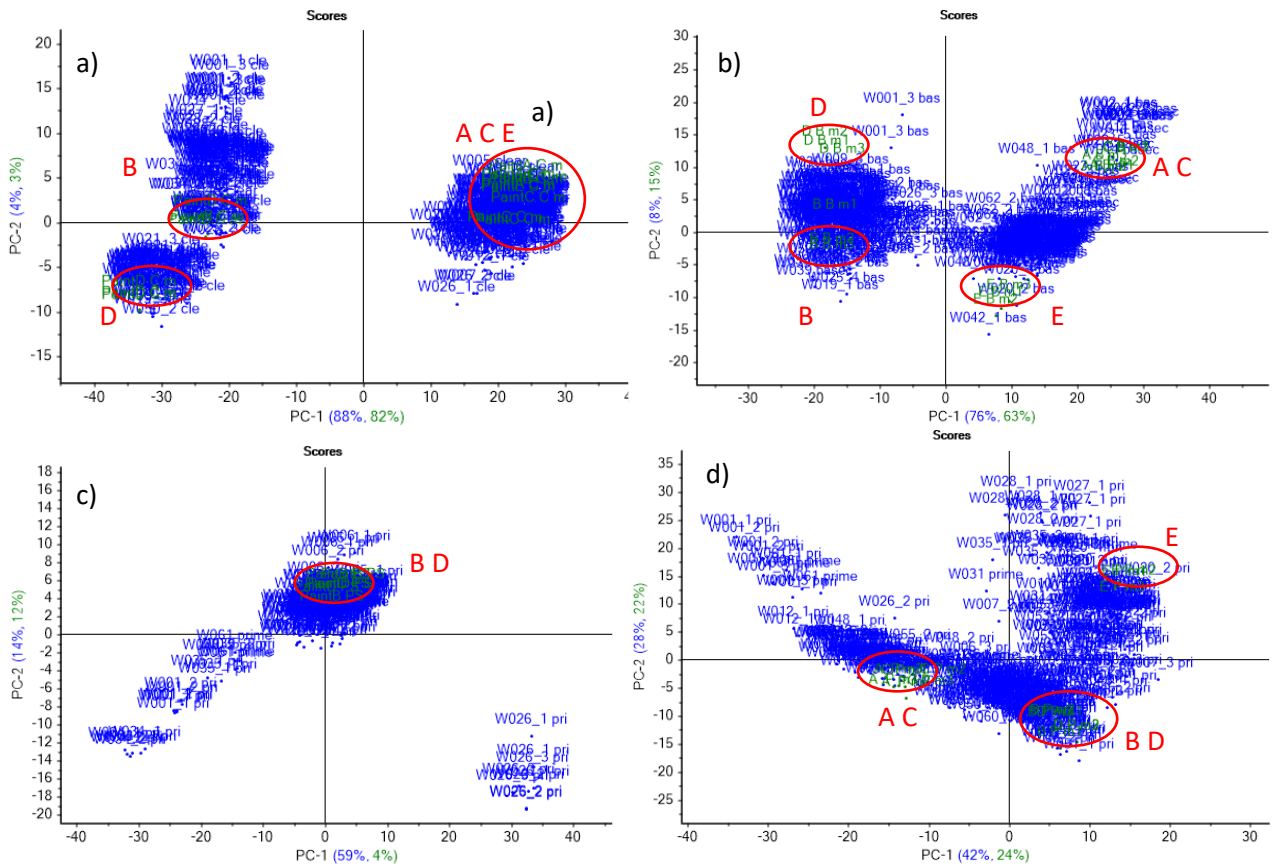
Figure 111. PCA projections for blind test samples (scatter plot in green, highlighted in red circles): a) clearcoat; b) basecoat; c) primer surfacer and d) primer.

Table 39. Blind tests results of LDA, SIMCA classification and database searches for 5 unknown samples.

SAMPLE	LAYER	PCA PROJECTED CHEMICAL CLASS	LDA	SIMCA (1%)	DATABASE SEARCH (>98%)	INTEGRATED PREDICTION	ACTUAL SAMPLE
A	C	PUR	W051, W033, W023	W036, W049, W010, W018, W007, W051, W054	W018, W010, W032, W054, W042, W016, W041, W051, W047, W044, W014, W015, W045	**LDA** Fail **SIMCA** **W049** **Database** W054, **W049**, W047, W032, W018, W014, W015	W049
	B	PUR	W018, W014, W020	W047, W049, W054	W015, W054, W049, W044, W045, W041, W047, W010, W020, W032, W046, W014, W012, W005, W018		
	P	EPY+ALS	W047, W062	W049, W015, W047, W011	W047, W049, W032, W054, W016, W062, W018, W015, W014, W012, W042, W048		
B	C	ACR+MEL+STY+PUR	W034, W061	W040	W025, W040	**LDA** Fail **SIMCA** **W040** **Database** W025, **W040**	W040
	B	ACR	W030, W052	W040, W043, W061	W040, W025, W019		
	PS	EPY+PUR	W025, W028	W040, W043	W025, W040, W055, W059, W050, W060, W043, W021		
	P	EPY+ALS	W053	W040, W039, W011, W005, W058	W003, W011, W040, W051, W050, W039, W019, W055, W025		
C	C	PUR	W002, W048, W053	W036, W049, W007, W051, W018, W041, W044, W047, W054, W010, W014	W047, W051, W044, W045, W032, W020, W010, W012, W016, W018, W041, W042, W054, W015, W049	**LDA** Fail **SIMCA** **W047** **Database** **W047**, W032, W015, W012, W016, W018, W042, W054, W049	W047
	B	PUR	W014, W016	W002, W014, W005, W047, W054, W015	W054, W044, W047, W015, W041, W016, W049, W042, W020, W032, W012, W014, W010, W018, W016		
	P	EPY+ALS	W060, W062	W047, W049, W015, W011	W047, W049, W054, W016, W062, W048, W015, W014, W032, W012, W042, W018		
D	C	ACR+MEL+STY+PUR	W003	W031, W039, W052, W050	W039, W003, W052, W055, W031, W019, W011	**LDA** Fail **SIMCA** **W039** **Database** W003, **W039**, W011	W039
	B	ACR	W055	W040, W039, W043	W003, W039, W011, W021, W052, W031		
	PS	EPY+PUR	W003	W039	W039, W003, W011, W019, W021, W030, W055, W052, W050, W031, W027, W028		
	P	EPY+ALS	W017, W031	W040, W039, W011, W058, W005	W003, W051, W011, W040, W039, W060		
E	C	PUR	W023	W020, W007, W051, W018	W018, W010, W032, W020, W047, W051, W054, W042, W016, W018, W045, W044, W014, W012, W049,	**LDA** Fail **SIMCA** **W020** **Database** **W020**	W020
	B	PUR	W007, W053	W020, W042, W036, W062	W041, W020, W044, W054, W032, W049, W016, W047, W015		
	P	EPY+ALS	W046	W020, W011	W020, W027		

8.6.2. Discriminating power and inter-sample variability

Inter-sample variability refers to the differences or variations observed between different samples within the dataset. It reflects the diversity and heterogeneity among individual samples, providing insights into the range of characteristics present within the group. In this study, inter-sample variability is assessed based on the chemical categories of samples and the discriminating power (DP) obtained from the IR analysis of each layer.

Table 40 presents a summary of the discriminating power with regards to each individual layer, considering visual comparison and PCA-based separation across the entire sample set (n=62). Visual comparison revealed varying levels of discrimination capability among different layers, with the basecoat exhibiting the highest discriminating power and the primer surfacer displaying the lowest. The discriminating power obtained from PCA slightly differed from those of visual comparison. However, it is important to note that the PCA models established might not fully represent the true classification, as PCA is an unsupervised method. To build a more accurate classification model, supervised statistical methods such as linear discriminant analysis should be utilized. Therefore, in this study, PCA was primarily used for data structure visualization, and the further discussion on classification and discrimination relied on visual comparison.

Table 41 provides an overview of the chemical categories identified from each layer through IR analysis, along with the number of samples within each category. *Table 42* summarizes the groups of samples that could not be differentiated based on each layer. It was observed that the chemical classes identified from each layer within this sample set were quite diverse, particularly for the basecoat. However, this diversity primarily stemmed from the variations in chemical compositions among repainted samples. With the exception of the primer layer, where the primer of two repainted samples could not be differentiated from that of OEM samples, all the undifferentiated samples from other layers were OEM paint samples.

Table 40. Discriminating power of each layer based on visual comparison and PCA (n=62)

Layer type	DP of Visual comparison	Undifferentiated pairs of visual comparison	DP of PCA	Undifferentiated pairs of PCA	Total number of samples
Primer	84.4%	276	55.2%	846	60
Primer surfacer	33.1%	253	49.7%	190	28
Basecoat	85.3%	277	81%	361	62
Clearcoat	84.4%	199	84.4%	199	51

Table 41. Chemical categories identified from each layer by IR analysis (n=62).

Layer type	Number of class	Identified chemical class	Number of samples within each class	Total sample number
Primer	1	EPY+ALS	55	
	2	EPY	3	60
	3	ALK OPH + NCL+BAS+TALC	1	
	4	ACR+STY+TALC	1	
Primer surfacer	1	EPY+PUR+MEL+TALC+BAS+TIO2	23	
	2	ALK IPH+EPY+MEL+TALC+TIO2	1	
	3	ALK IPH+PUR+EPY+TALC+ALS+TIO2	2	28
	4	ALK IPH+MEL+TALC+TIO2	1	
	5	ALK TER+ACR+MEL+BAS+TIO2	1	
Basecoat	1	PUR+ALK IPH+TALC+TIO2	24	
	2	PUR+MEL+TIO2	2	
	3	ACR+ALK IPH+MEL+PUR+TIO2	27	
	4	ACR+PUR+MEL+TALC+TIO2	1	62
	5	PUR+STY+TIO2	6	
	6	ALK OPH+MEL+TIO2	1	
	7	ACR+MEL+STY+TIO2	1	
Clearcoat	1	PUR+(STY)	27	51
	2	ACR+MEL+STY+PUR	24	

Table 42. Groups of samples that could not be differentiated from IR analysis based on each layer(n=62).

Layer type	Group No.	Undifferentiated samples
Primer	1	W002, W005, W023, W036, W056
	2	W007, W033, W046
	3	W009, W010, W013, W017, W020, W022, W027, W028, W030, W031, W041, W043, W044, W052, W053
	4	W012, W014, W015, W016, W018, W032, W042, W047, W048, W049, W054, W062
	5	W003, W006, W011, W019, W021, W025, W026, W039, W040, W045, W050, W051, W055, W060
	6	W034, W058
Primer surfacer	1	W003, W006, W009, W011, W017, W019, W021, W022, W024, W025, W027, W028, W030, W031, W039, W040, W043, W050, W052, W055, W058, W059, W060
Basecoat	1	W002, W005, W010, W012, W014, W015, W016, W018, W020, W023, W032, W033, W036, W041, W042, W044, W045, W046, W047, W049, W051, W053, W054
	2	W001, W061
	3	W027, W028, W050
	4	W003, W011, W021, W039
	5	W017, W043
	6	W006, W059
	7	W022, W024, W058, W060
	8	W030, W031, W052
	9	W019, W025, W040
Clearcoat	1	W002, W007, W020, W023, W036, W053
	2	W010, W012, W014, W015, W016, W018, W032, W041, W042, W044, W045, W047, W049, W051, W054
	3	W005, W033, W046
	4	W048, W062
	5	W001, W027, W028, W034, W061
	6	W003, W011, W019, W021, W031, W039, W050, W052, W055
	7	W006, W009, W024, W035, W043, W058, W059, W060
	8	W025, W040

To enhance the practicality of the results and ensure a clearer understanding of the chemical characteristics and differences among OEM paints of the same manufacturer and color, the data were further analyzed by focusing solely on OEM paint. By considering the inter-sample variability and recalculating the discriminating power within the OEM sample subset (n=54), the obtained data becomes more precise for interpretation.

The chemical classes associated with each layer in these OEM samples are summarized in *Table 43*. It was observed that epoxy binder was the only binder type used in the primer of OEM paint samples analyzed in this study. Although the discrimination power of the primer surfacer layer was low, it exhibited a diverse range of chemical classes. In the case of the basecoat layer, despite the presence of four chemical classes, polyurethane and acrylic-based resins were the predominant binder types used. The same trend was observed for the clearcoat layer.

Table 43. Chemical categories identified from each layer in OEM samples by IR analysis (n=54)

Layer type	Class No.	Identified chemical class	Number of samples within each class	Total sample number
Primer	1	EPY+ALS	53	54
	2	EPY	1	
Primer surfacer	1	EPY+PUR+MEL+TALC+BAS+TIO2	23	28
	2	ALK IPH+EPY+MEL+TALC+TIO2	1	
	3	ALK IPH+PUR+EPY+TALC+ALS+TIO2	2	
	4	ALK IPH+MEL+TALC+TIO2	1	
	5	ALK TER+ACR+MEL+BAS+TIO2	1	
Basecoat	1	PUR+ALK IPH+TALC+TIO2	24	54
	2	PUR+MEL+TIO2	2	
	3	ACR+ALK IPH+MEL+PUR+TIO2	27	
	4	ACR+PUR+MEL+TALC+TIO2	1	
Clearcoat	1	PUR+(STY)	27	51
	2	ACR+MEL+STY+PUR	24	

The discriminating power of each paint layer was recalculated using a dataset limited to 54 OEM paint samples. The discrimination capabilities of different layer combinations were also evaluated to understand their effectiveness in distinguishing OEM paint samples. However, it is important to note that when considering the entire OEM sample set, due to the different layer structure of samples in Group OEM3 or Group OEM4, the total number of samples included in each layer combination varies. To homogenize layer structure and the total number of samples within each combination, a segregation was implemented for Group OEM3 and Group OEM4. Subsequently, the discrimination capabilities of each layer and different layer combinations within the two groups were reassessed. All the results are explicated in *Table 44*.

Generally, the discriminative capability varied among different layers, with the clearcoat being the most discriminative and the primer surfacer the least. The inter-sample variability among OEM paint samples of the same manufacturer and color was relatively high, except for the primer surfacer.

Within the context of Group OEM3, the primer yields the highest discriminating power of 73.5%, while the basecoat displays the least discrimination capability, giving a mere 22.1%. The combination of the primer and clearcoat layers amplifies the discrimination potential of IR analysis, providing the highest discrimination power of 83.1%. It is important to underline that due to the low discrimination of the basecoat, additional measurements of the basecoat only reduced undifferentiated pairs by one. Consequently, the final discriminative power derived from IR analysis of all layers in Group OEM3 (n=26) is 83.3%.

In contrast, Group OEM4 exhibited a different trend. The basecoat layer in Group OEM4 showed the highest discriminative potential at 93.7%, while the primer surfacer had the lowest at 33.1%. Combining the primer and basecoat layers provided the highest discrimination capability, resulting in a peak discriminative power of 96.3%. Interestingly, additional clearcoat or primer surfacer measurements minimally enhanced discrimination. Consequently, the ultimate discriminative power extracted from comprehensive IR analysis of all layers within the samples of Group OEM4 (n=28) is 96.8%.

Table 44. Discriminating power of individual layer and different layer combination from IR analysis of OEM paint (n=54).

Layer type	Whole OEM sample set (n=54)		Group OEM3 (n=26)	Group OEM4 (n=28)
	DP (Undifferentiated pairs)	Total number of samples	DP (Undifferentiated pairs)	DP (Undifferentiated pairs)
Primer (P)	**82.0% (258)**	54	**73.5% (86)**	72.8% (103)
Primer surfacer (PS)	**33.1% (253)**	28		33.1% (253)
Basecoat (B)	**80.6% (277)**	54	22.1% (253)	**93.7% (24)**
Clearcoat (C)	**84.4% (199)**	51	61.8% (124)	80.1% (75)
P+PS	75.9% (91)	28		75.9% (91)
P+B	**94.6% (77)**	54	80.6% (63)	**96.3% (14)**
P+C	93.7% (90)	54	**83.1% (55)**	90.7% (35)
PS+B	93.9% (23)	28		93.9% (23)
PS+C	78.0% (83)	28		78.0% (83)
B+C	90.4% (138)	54	63.7% (118)	94.7% (20)
P+PS+B	96.3% (14)	28		96.3% (14)
P+PS+C	90.7% (35)	28		90.7% (35)
P+B+C	**95.4% (66)**	54	**83.4% (54)**	**96.8% (12)**
PS+B+C	95.0% (19)	28		95.0% (19)
P+PS+B+C	**96.8% (12)**	28		**96.8% (12)**
Final DP	**95.4% (66)**	54	**83.4% (54)**	**96.8% (12)**

When combining the final discrimination results of Group OEM3 and Group OEM4, a total of 66 pairs of samples remained undifferentiated, as summarized in *Table 45*, which also includes the corresponding vehicle information. **Notably, the overall discriminating power achieved from the IR analysis of the sample set of 54 OEM white VW automotive paint samples was 95.4%. Considering the entire sample set (n=62), the discriminating power obtained from IR analysis was 96.5%.** These results highlight the effectiveness of FTIR analysis in differentiating automotive paint samples, even within a specific sample set consisting of paint from the same manufacturer and color (white). Despite the limited diversity in pigment among white automotive paints, FTIR analysis proved to be a reliable

method for characterizing and discriminating automotive paint samples. This also underscores the rarity of physical and chemical characteristics within the automotive paint samples, further reinforcing the evidential value of paint analysis in forensic investigations.

Upon examining the vehicle information of the undifferentiated sample pairs, it was observed that most of the undifferentiated samples were produced by the same manufacturing company (S-VW), despite differences in models, production years, and assembly plants (e.g., samples in Group 2, 3, 4, 10). It is worth noting that the assembly plants of this company are geographically close to each other, suggesting the possibility of using the same paint supplier and coating formula for these plants. In contrast, samples from the other company (F-VW) could be mostly differentiated, except for one group of samples that share the same model, production year, and assembly plant (Group 1). Generally, samples from the two different joint ventures can be easily distinguished. The geographic distribution of these undifferentiated samples associated with assembly plants is illustrated in *Figure 112*.

Table 45. Properties of undifferentiated sample groups by visual comparison of IR spectra of all layers

Group No.	Sample No.	Manufacturing company	Model	Production year	Topcoat color code	Assembly plant	Layer structure
1	W002	F-VW	Sagitar	2017	LC9A	Chengdu	OEM3
	W023	F-VW	Sagitar	2017	LC9A	Chengdu	OEM3
	W036	F-VW	Sagitar	2017	LC9A	Chengdu	OEM3
2	W033	S-VW	New Lavida	2014	LY9H	Nanjing	OEM3
	W046	S-VW	Passat	2013	LY9H	Nanjing	OEM3
3	W010	S-VW	Santana	2017	LY9H	Nanjing	OEM3
	W041	S-VW	Santana	2017	LY9H	Nanjing	OEM3
	W044	S-VW	Passat	2017	LY9H	Nanjing	OEM3
4	W020	S-VW	Santana	2016	LY9H	Nanjing	OEM3
	W053	S-VW	New Lavida	2014	LY9H	Nanjing	OEM3
5	W045	S-VW	Lamando	2018	LY9H	Ningbo	OEM3
	W051	S-VW	Lamando	2017	LY9H	Ningbo	OEM3
6	W012	S-VW	New Lavida	2017	LY9H	Nanjing	OEM3
	W014	S-VW	New Lavida	2017	LY9H	Anting	OEM3
	W015	S-VW	New Lavida	2017	LY9H	Anting	OEM3
	W016	S-VW	New Lavida	2017	LY9H	Anting	OEM3
	W018	S-VW	New Lavida	2016	LY9H	Anting	OEM3
	W032	S-VW	Gran Lavida	2015	LY9H	Anting	OEM3
	W042	S-VW	New Lavida	2017	LY9H	Anting	OEM3
	W047	S-VW	New Lavida	2017	LY9H	Nanjing	OEM3
	W049	S-VW	New Lavida	2016	LY9H	Anting	OEM3
	W054	S-VW	New Lavida	2016	LY9H	Anting	OEM3
7	W003	S-VW	Polo	2017	Unknown	Anting	OEM4
	W011	S-VW	Polo	2017	LY9H	Anting	OEM4
	W021	S-VW	Polo	2016	LY9H	Anting	OEM4
	W039	S-VW	Polo	2017	LY9H	Anting	OEM4
8	W027	S-VW	Passat	2004	Unknown	Anting	OEM4
	W028	S-VW	Passat	2003	LB9A	Anting	OEM4
9	W030	S-VW	Tiguan	2016	LY9H	Anting	OEM4
	W031	S-VW	Tiguan	2017	LY9H	Anting	OEM4
	W052	S-VW	Tiguan	2017	LY9H	Anting	OEM4
10	W017	S-VW	Tiguan	2015	LY9H	Anting	OEM4
	W043	S-VW	Gran Lavida	2015	LY9H	Anting	OEM4
11	W025	S-VW	Polo	2016	LY9H	Anting	OEM4
	W040	S-VW	Polo	2015	LY9H	Anting	OEM4
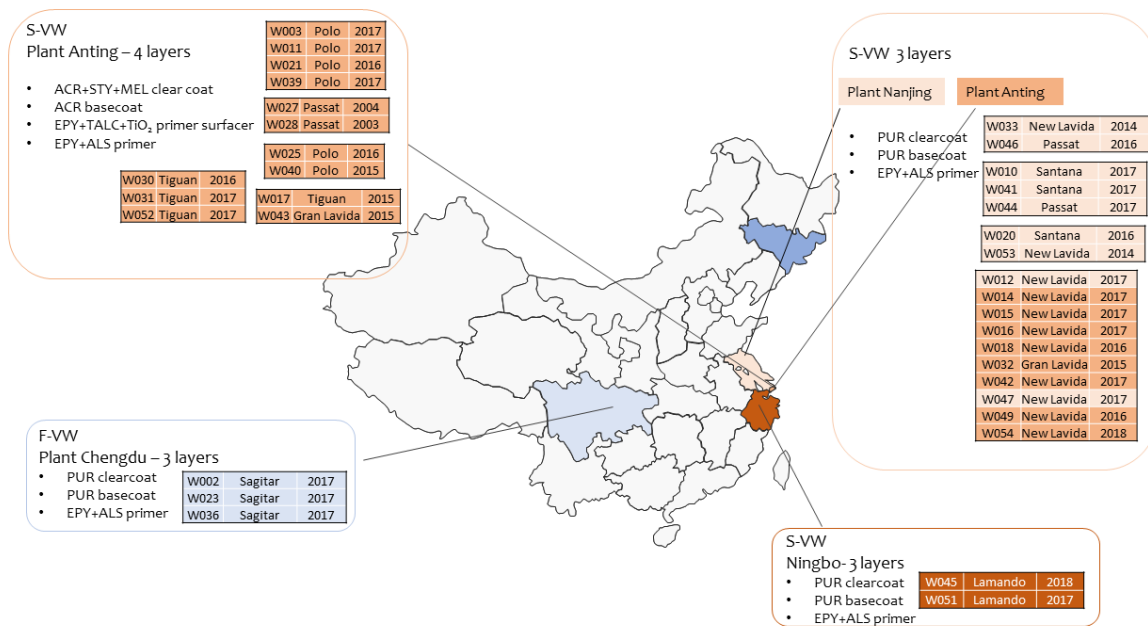
Figure 112. Geographic distribution of undifferentiated samples associated with assembly plants. The chemical profiles (IR) of each undifferentiated samples pairs are listed in the figure.

8.6.3. Correlation between chemical properties and vehicle information

In this section, a specific subset of the dataset consisting of 54 OEM paint samples was investigated. Previous sections have discussed the correlation between chemical properties and sample origin, with a focus on each layer. To gain a deeper understanding of the complete chemical profiles combining all layers, The samples were further analyzed in relation to manufacturing company, assembly plant, and the layer system. *Figure 113* provides an overview of the associations between these factors and the chemical characteristics.

Notably, sample W026 stood out as it exhibited a completely different chemical profile compared to the remaining 53 Chinese-produced vehicles. This finding suggests the presence of geographic variation among samples from the same manufacturer. It was discovered that for the 53 Chinese-produced OEM paint samples, the chemical composition of samples varied significantly depending on the layer system. Samples with an OEM3 paint system displayed distinct chemical profiles compared to those with an OEM4 system, regardless of their manufacturing company or assembly plant.

The assembly plant emerged as a key determinant of the chemical properties, as samples from the same plant tended to exhibit similar chemical profiles. This trend held true regardless of the specific manufacturing company, model, or production year. However, it is important to note that within each assembly plant, there were still variations and undifferentiated groups of samples, as depicted in *Figure 113*.

These findings highlight the intricate relationship between chemical properties, sample origin, and the layer system. The presence of geographic variation and the influence of the assembly plant underscore the complexity of the factors shaping the chemical profiles of the automotive paint samples.

It was observed that even among OEM paint samples that originated from the same manufacturing company, shared the same color and model, and were produced in the same assembly plant in the same year, there were instances where their chemical features differed. For instance, sample W019 exhibited distinct chemical characteristics compared to other samples with the same model "Polo," despite being produced in the same year as samples W003, W011, or W039. Similarly, samples W048 and W062 could be differentiated from each other, despite sharing identical vehicle information, including manufacturing company, model, production year, and assembly plant.
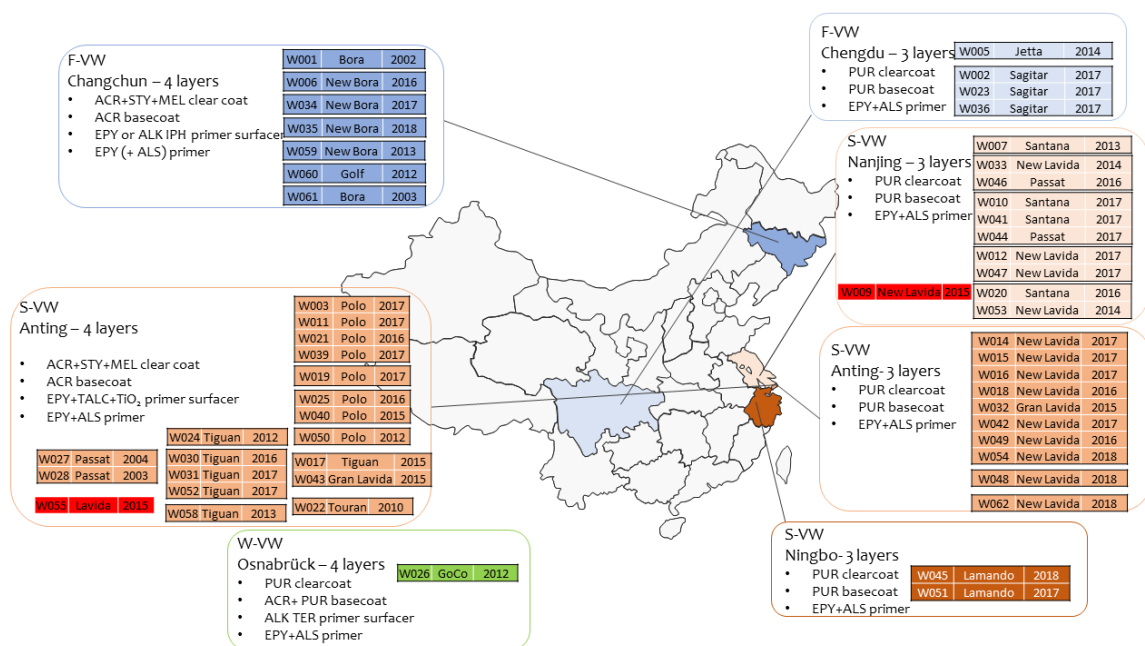
Figure 113. Chemical profiles (IR) of the entire samples in relation to manufacturing company, assembly plant, and the layer system. Groupings obtained from visual comparison within each plant are listed. Samples highlighted in red represent those that have a different layer structure from the rest of the samples. Samples highlighted in green represent those that were not produced in China.

These variations in chemical features within such closely matched samples can be attributed to batch variations. This factor can introduce subtle but significant differences in the chemical composition of the paint samples. Hence, even in cases where the vehicle information is identical, the chemical profiles may vary, indicating the rarity of chemical features of a specific vehicle.

Regarding the topcoat color code, information is available for 50 out of the 54 OEM samples. *Table 46* presents the groupings of samples within each topcoat color code group, determined through visual comparison of the basecoat. As discussed earlier during the exploratory analysis of the basecoat, it was evident that samples sharing the same topcoat color code do not consistently exhibit identical chemical compositions in their basecoat. Instead, these samples with the same color code can be further differentiated into multiple groups, indicating significant variations in their chemical characteristics.

Table 46. groupings of samples within each topcoat color code group based on IR analysis of basecoats (n=50)

Topcoat color code	Group No.	Sample No.	Manufacturing company	Model	Production year	Assembly plant	Layer structure
LC9A	1	W002	F-VW	Sagitar	2017	Chengdu	OEM3
	1	W023	F-VW	Sagitar	2017	Chengdu	OEM3
		W036	F-VW	Sagitar	2017	Chengdu	OEM3
	2	W006	F-VW	New bora	2016	Changchun	OEM4
	2	W059	F-VW	New bora	2013	Changchun	OEM4
	3	W034	F-VW	New bora	2017	Changchun	OEM4
	4	W035	F-VW	New bora	2018	Changchun	OEM4
	5	W026	W-VW	GoCo	2012	Osnabrück	OEM4
LB9A	1	W005	F-VW	Jetta	2014	Chengdu	OEM3
	2	W060	F-VW	Golf	2012	Changchun	OEM4
	3	W022	S-VW	Touran	2010	Anting	OEM4
	3	W024	S-VW	Tiguan	2012	Anting	OEM4
		W058	S-VW	Tiguan	2013	Anting	OEM4
	4	W028	S-VW	Passat	2003	Anting	OEM4
LY9H	1	W010	S-VW	Santana	2017	Nanjing	OEM3
		W012	S-VW	New Lavida	2017	Nanjing	OEM3
		W014	S-VW	New Lavida	2017	Anting	OEM3
		W015	S-VW	New Lavida	2017	Anting	OEM3
		W016	S-VW	New Lavida	2017	Anting	OEM3
		W018	S-VW	New Lavida	2016	Anting	OEM3
		W020	S-VW	Santana	2016	Nanjing	OEM3
		W032	S-VW	Gran Lavida	2015	Anting	OEM3
		W033	S-VW	New Lavida	2014	Nanjing	OEM3
	1	W041	S-VW	Santana	2017	Nanjing	OEM3
		W042	S-VW	New Lavida	2017	Anting	OEM3
		W044	S-VW	Passat	2017	Nanjing	OEM3
		W045	S-VW	Lamando	2018	Ningbo	OEM3
		W046	S-VW	Passat	2016	Nanjing	OEM3
		W047	S-VW	New Lavida	2017	Nanjing	OEM3
		W049	S-VW	New Lavida	2016	Anting	OEM3
		W051	S-VW	Lamando	2017	Ningbo	OEM3
		W053	S-VW	New Lavida	2014	Nanjing	OEM3
		W054	S-VW	New Lavida	2016	Anting	OEM3
	2	W007	S-VW	Santana	2013	Nanjing	OEM3
	3	W048	S-VW	New Lavida	2018	Anting	OEM3
	4	W062	S-VW	New Lavida	2018	Anting	OEM3
	5	W011	S-VW	Polo	2017	Anting	OEM4
	5	W021	S-VW	Polo	2016	Anting	OEM4
		W039	S-VW	Polo	2017	Anting	OEM4
	6	W017	S-VW	Tiguan	2015	Anting	OEM4
	6	W043	S-VW	Gran LAVIDA	2015	Anting	OEM4
	7	W019	S-VW	Polo	2017	Anting	OEM4
	7	W025	S-VW	Polo	2016	Anting	OEM4
		W040	S-VW	Polo	2015	Anting	OEM4
	8	W030	S-VW	Tiguan	2016	Anting	OEM4
	8	W031	S-VW	Tiguan	2017	Anting	OEM4
		W052	S-VW	Tiguan	2017	Anting	OEM4
	9	W009	S-VW	New Lavida	2015	Nanjing	OEM4
	10	W050	S-VW	Polo	2012	Anting	OEM4
	11	W055	S-VW	Lavida	2014	Anting	OEM4

9. Characterization and classification with Raman

The FTIR analysis of the entire sample set has provided valuable insights into the chemical composition of each layer of the paint samples. However, there are still 66 pairs of samples that remain undifferentiated. To further discriminate these pairs, it becomes necessary to perform Raman analysis. While Raman spectroscopy is often used in conjunction with IR spectroscopy as a complementary technology, its potential for differentiating all layers of automotive paint samples with the same car make and color has not been extensively explored. Conducting a comprehensive Raman analysis on the entire sample set can provide a deeper understanding of the diversity in chemical composition within this closely related set of samples.

To streamline the Raman analysis, it was decided to include only 54 OEM paint samples. This decision was based on several factors. Firstly, all repainted samples have already been differentiated from the rest of the OEM samples using FTIR analysis, making further discrimination using Raman unnecessary. Secondly, since the valuable and useful data for interpretation would be obtained only from OEM paint samples, there is no need to consider the repainted samples. Lastly, all the undifferentiated samples are OEM samples, indicating the need to continue the analytical sequence to achieve further discrimination. One representative subsample from each vehicle was chosen for Raman analysis, resulting in the analysis of each layer from a total of 54 samples using Raman spectroscopy.

As discussed in Chapter 6.4, the Raman analysis in this study utilized a Raman Renishaw InVia system equipped with a Leica DM2600M microscope with a 50x objective. A near-infrared 785nm diode laser was found to be the most suitable laser for analysis. The laser had a maximum power of 233mW at the sample and 332mW at the source. Laser power modulation was employed to prevent detector saturation for the samples under study. A 1200 l/mm grating was used for all experiments, and the wavenumber range considered was between 200 and 2000 cm^{-1}. The exposure time for each measurement was set at 10s, and the number of accumulations was 8. Data acquisition was performed using Renishaw's software 'Wire 5.5'. To minimize temperature-related variability, all measurements were conducted at a constant room temperature of 22°C. Intra-sample variability was evaluated by performing three replicates for each layer of every paint sample. The obtained spectra were visually compared using Thermo Fisher Scientific Inc.'s software 'Omnic 9.12.928'.

For the characterization of each layer, the characteristic bands of chemical groups were compared with Raman spectra from various commercial Raman databases of coatings, polymers, additives, and inorganics available in Thermo Fisher's Omnic software. These databases include Ahura Raman, Aldrich Raman, FDM Raman Inorganics, FDM Raman Organics 780, HR Raman Inorganics, Law Enforcement and Security Raman Library, Mineral Raman Database, Raman Dyes and Pigments, and Raman Spectroscopic Library of Natural and Synthetic Pigments.

9.1. Intra-sample variability

It is known that the IR analysis conducted on the sample set revealed minimal intra-sample variability in terms of chemical characteristics. In the Raman analysis, one representative subsample from each vehicle was chosen for Raman spectroscopy, resulting in the analysis of a total of 54 samples. Measurements were taken from each layer of every sample, with three replicates obtained from each layer. In this context, "intra-sample variability" refers to the variability observed within the three replicates obtained from different positions within the same layer.

After acquisition, the raw spectra were processed using baseline subtraction and cosmic ray removal in Renishaw's software 'Wire 5.5'. The three replicates for each layer were then compared to assess the intra-sample variability. It was found that the spectra generally exhibited homogeneity in terms of peak position and relative peak intensity. This homogeneity is also reflected in the PCA scatter plots, where the three replicates from one sample are projected close to each other. However, there were instances where the replicates showed slight differences in baseline variations, particularly in clearcoats, as illustrated in *Figure 114a*. These baseline variations can cause the projections of the replicates on the PCA scatter plot to be far apart from each other, even after the spectra underwent preprocessing treatments, as shown in *Figure 114b* (the projections of the three spectra presented in *Figure 114*a are marked in a dashed circle). This introduces uncertainty in PCA-based separation. However, it does not pose a problem for visual comparison. Therefore, when such situations occur in PCA analysis, the spectra are visually verified.

In conclusion, the Raman analysis conducted on the sample set revealed minimal intra-sample variability. This finding indicates that the chemical compositions of the samples can be accurately characterized, enabling reliable comparisons between them.
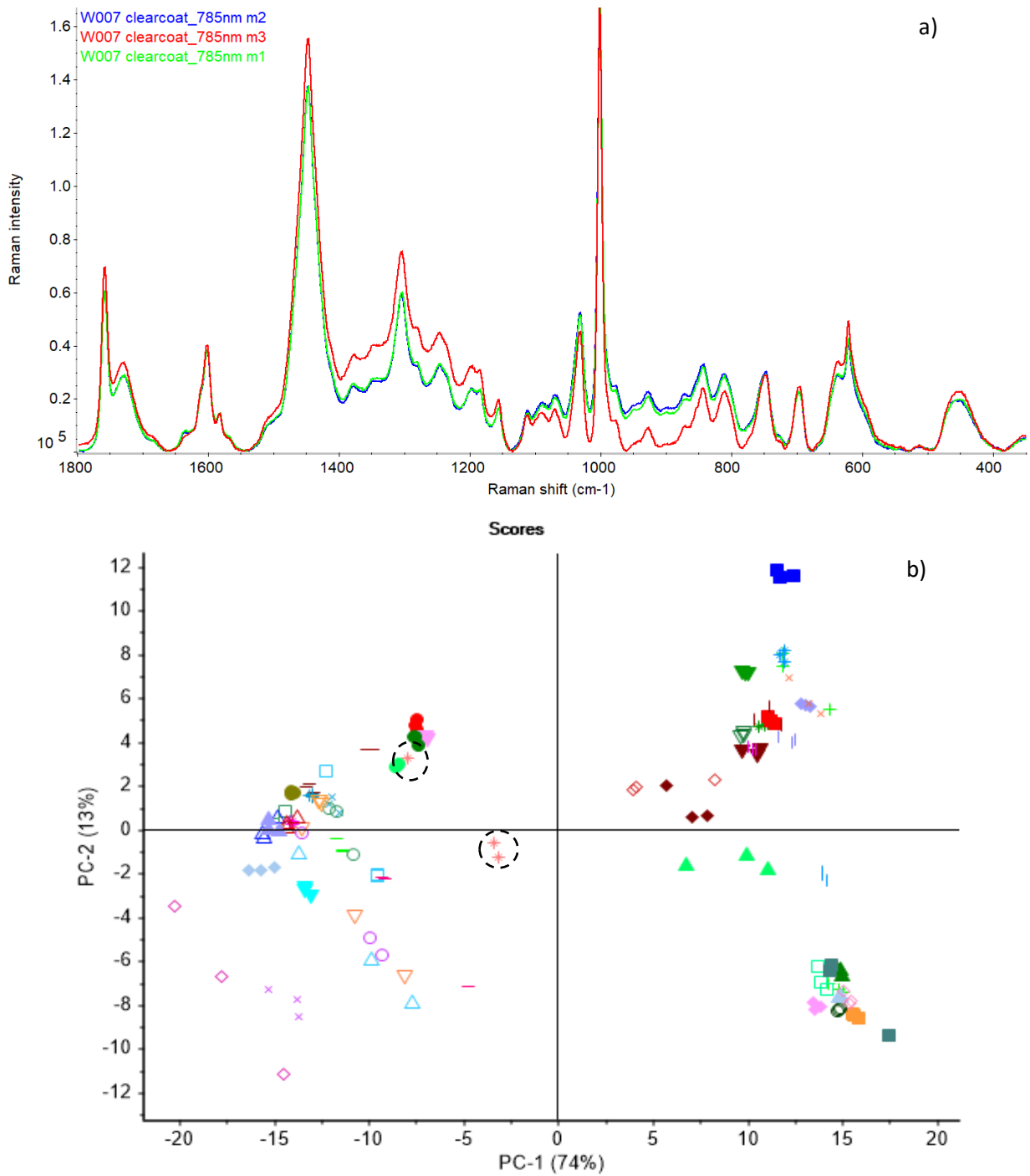
Figure 114. Three Raman spectra measured from the clearcoat of sample W007 (a) and their projections on PCA scatter plot (b), showing the variability within the replicates in terms of baseline variation.

9.2. Characterization of clearcoat

The clearcoat analysis and characterization encompassed all 54 samples in the set, yielding high-quality spectra from 8 accumulations. The samples were then categorized into three distinct groups based on identified chemical categories within the spectra, as presented in *Table 47 (page 199)*. Individual analysis of each group's spectra enabled the identification of Raman-detected constituents in the paints. Detailed discussions of these findings will be presented in the subsequent subchapters.

9.2.1. Group C1

Group C1 consists of a single sample, accounting for 2% of the total samples. As depicted in *Figure 115*, the Raman spectrum of this sample exhibits a fluorescence curve, rendering it incapable of determining the chemical composition through Raman analysis. Consequently, the spectra from this sample remain uncharacterized.
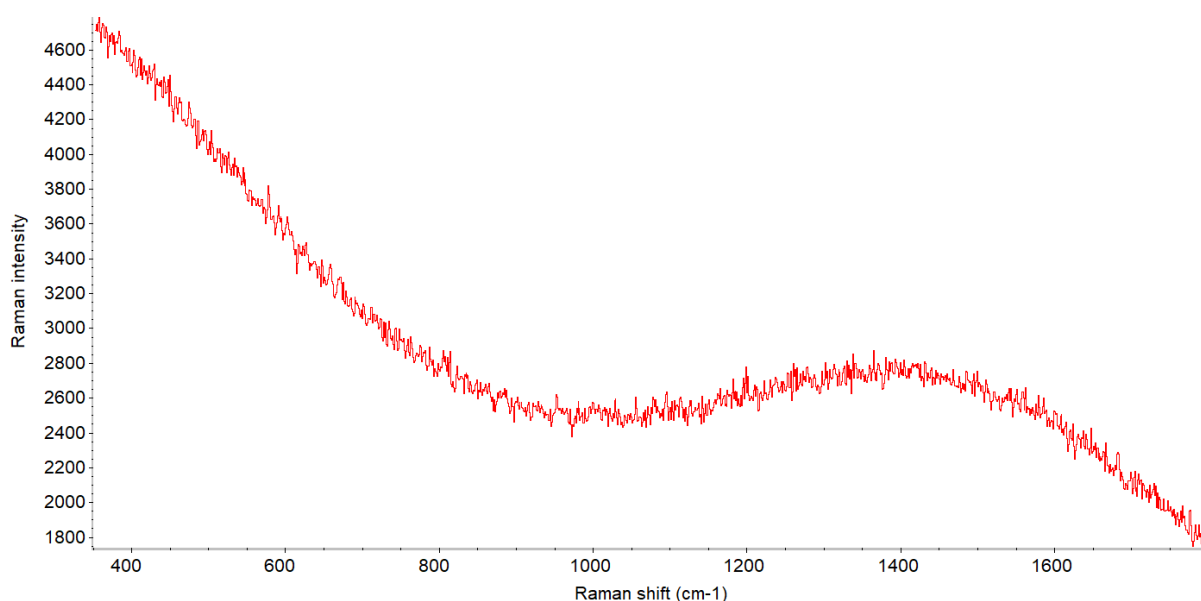
Figure 115. Representative spectrum of the clearcoat of sample W061 from Group C1. Raman spectra (raw) acquired with a laser at 785nm.

9.2.2. Group C2

Group C2 comprises 27 samples, representing 50% of the total sample set. *Figure 116a* displays a representative spectrum from this group, highlighting the characteristic peaks identified in the spectrum. In contrast to other layers, clearcoats do not contain any detected pigment or extender, resulting in an abundance of peaks originating from the binder. One distinctive feature observed in this group is the presence of double peaks at 1756 and 1730 cm^{-1}, attributed to C-O stretches from the polyurethane binders. Furthermore, the spectrum exhibits identifiable peaks at 1602, 1583, 1156, 1031, 1001, and 620 cm^{-1}, which closely align with the reference Raman spectrum of styrene presented in *Figure 116b*. It is worth highlighting that while the IR analysis did not show high concentrations of styrene, it constitutes the major component of the peaks observed in the Raman spectra. Unfortunately, the remaining peaks couldn't be identified using the available databases.
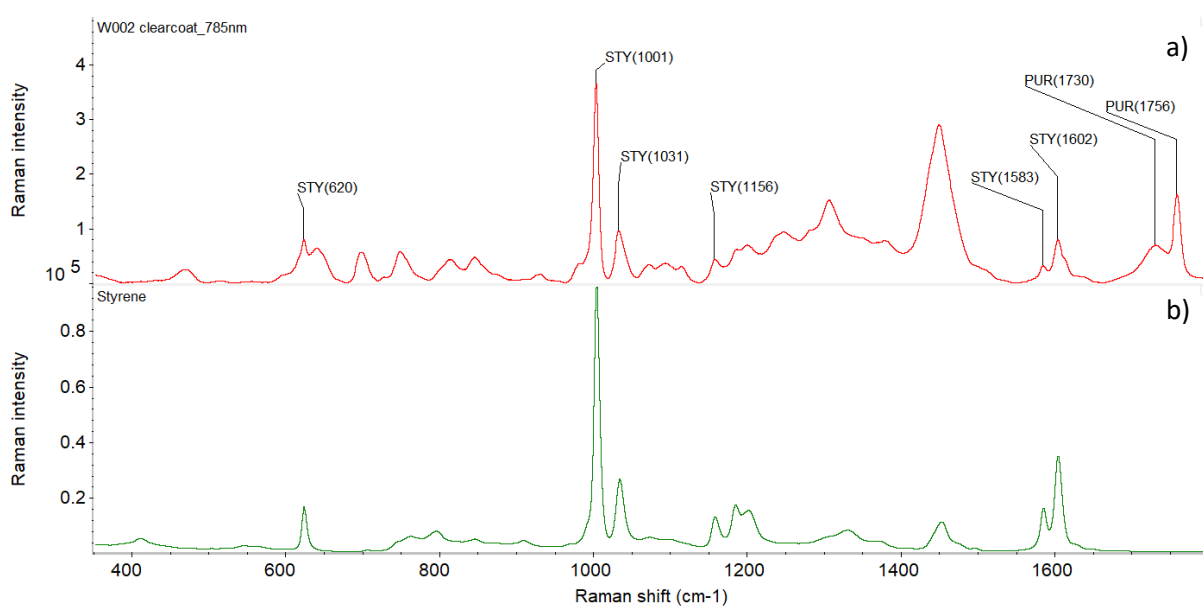
Figure 116. Representative Raman spectrum of the basecoat of sample W002 (up) with reference Raman spectrum of styrene (bottom). Characteristic peaks of polyurethane and styrene are annotated on the spectrum.

9.2.3. Group C3

Group C3 consists of 26 samples, accounting for 48% of the total sample set. *Figure 117* showcases a representative spectrum from this group, emphasizing the characteristic peaks identified within the spectrum. Similar to Group C2, the spectrum exhibits discernible peaks at 1602, 1583, 1156, 1031, 1001, and 620 cm^{-1}, which are associated with styrene. One distinct feature that differentiates this group from Group C2 is the higher intensity of the peak at 1730 cm^{-1}, which can be attributed to C-O stretches of acrylic resin. Although the peak at 1756 cm^{-1} is still present in the spectra, its intensity is relatively low. The variation in peak intensity indicates that the primary binder used in the clearcoat of samples from this group is acrylic resin, a finding that is supported by the results of IR analysis. Another notable discriminative feature is the high intensity of peak at 976 cm^{-1} in all spectra of this group. Unfortunately, the specific composition associated with this peak could not be identified. One hypothesis suggests that it might originate from melamine. However, the reference Raman spectrum of melamine indicates that the key peak of melamine typically appears at 678 cm^{-1}, which is not present in the spectra of this group.
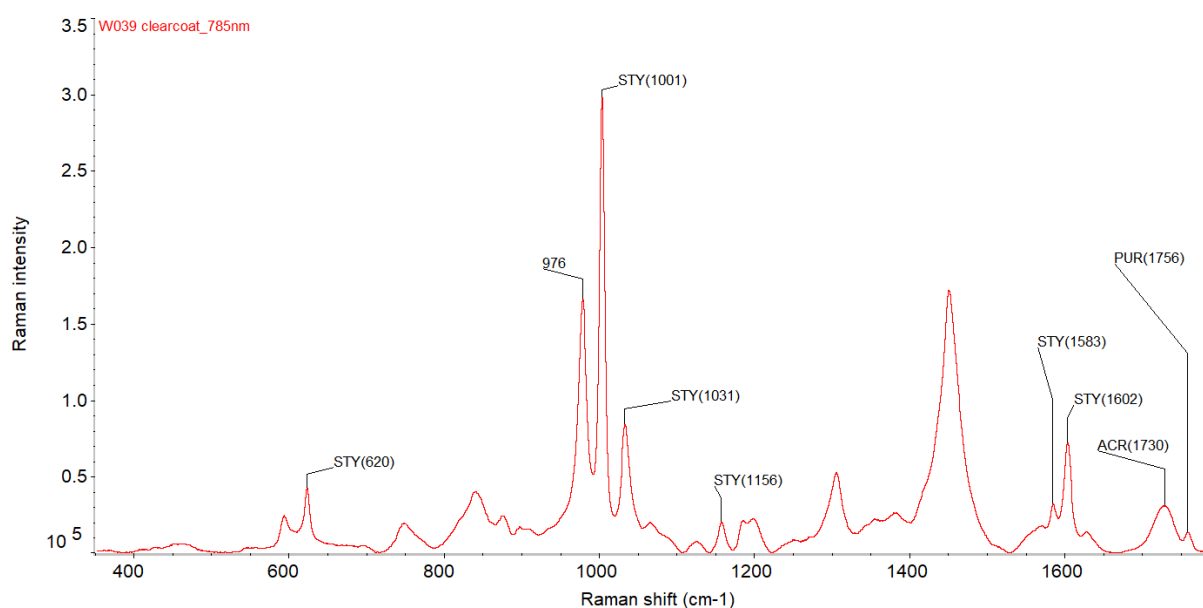
Figure 117. Representative Raman spectrum of clearcoat of sample W039 from Group C3, with annotated characteristic peaks of acrylic, polyurethane, and styrene.

9.2.4. Classification and discrimination of clearcoat

The Raman spectra obtained from clearcoats exhibited overall excellent quality. Only one sample showed uninformative spectra due to fluorescence effects. Although not all peaks in the clearcoat spectra could be identified, it was still possible to classify the chemical class of each group based on differences in peak intensities at 1756 and 1730 cm^{-1}, and further discrimination could be achieved by considering the presence or absence of specific peaks within each group. The results of visual comparison and the corresponding chemical class for each group are summarized in *Table 47*. Additionally, the key differences observed among spectra with similar characterizations are highlighted in the table.

Through visual comparison of the clearcoat spectra obtained using a 785 nm Raman laser, 172 pairs of samples could not be differentiated, resulting in a discriminating power of 88% (172 undifferentiated pairs out of a total of 54 samples).

Table 47. Summary of visual groupings of clearcoat (n=54)

GROUP/COMPOSITION	SUBGROUP	SAMPLES	DIFFERENCE WITHIN THE GROUP
Group C1 **FLUORESCENCE**	-	W061	Fluorescence curve
Group C2 **PUR+STY**	2.1	W002, W007, W023, W036, W053	Identical peaks at 1756, 1730, 1602, 1583, 1156, 1031, 1001 and 620 cm^{-1}.
	2.2	W010, W014, W015, W016, W018	Extra peak at 1640, 1567, 976 cm^{-1}
	2.3	W012, W020, W032 W041, W042, W044, W045, W047, W049, W051, W054	Extra peak at 1567, 976 cm^{-1}
	2.4	W005, W033, W046	Extra peak at 1567, 976 and 857 cm^{-1}, no peak at 845 cm^{-1}
	2.5	W048, W062	Higher peak intensity at 976 cm^{-1}
	2.6	W026	Extra peak at 1280, 976 cm^{-1}
Group C3 **ACR+PUR+STY**	3.1	W003, W011, W019, W021, W030, W031, W039, W050, W052, W055	Identical peaks at 1756, 1730, 1602, 1583, 1156, 1031, 1001, 976 and 620 cm^{-1}
	3.2	W009, W017, W022, W024, W025, W035, W040, W043, W059, W060	Extra peak at 806 cm^{-1}, no peak at 872 cm^{-1}
	3.3	W001	Peak lower at 1756, 976 and 592 cm^{-1}, no peak at 872 cm^{-1}
	3.4	W027, W028, W034	Peak lower at 1756 and 592 cm^{-1}, no peak at 872 cm^{-1}
	3.5	W006	No peak at 1625 cm^{-1}
	3.6	W058	Extra peak at 925 and 792 cm^{-1}

9.2.5. Exploratory analysis

Sample W061 was excluded from the dataset of Raman spectra due to its non-informative fluorescence curve. This resulted in a dataset of 159 Raman spectra obtained from the clearcoat of 53 samples, which were subjected to PCA analysis for visualizing the underlying data structure. Prior to analysis, all spectra underwent pre-treatment steps including baseline offset, and SNV normalization. The analysis focused on variables within the range of 1800-670 cm^{-1}, resulting in a dataset of 1031 variables for PCA analysis.

Figure 118 provides an overview of the PCA model generated from the dataset, displaying the projections of Raman spectra based on the first three principal components, which account for 93% of the total variance. On the scatter plot based on the first two principal components (*Figure 118a*), two distinct clusters were clearly observed and marked within a dashed rectangular. The loadings for PC1 (*Figure 119a*) revealed the positive values were primarily influenced by wave numbers corresponding to characteristic peaks of styrene, while negative values predominantly stemmed from the signal corresponding to characteristic peaks of polyurethane. This separation aligns with the visual comparison results, as samples from Group C2 were projected on the left side of the scatter plot, while samples from Group C3 were projected on the right side. Additionally, the loadings for PC2 and PC3 (*Figure 119b-c*) indicate that the separation was also influenced by uncharacterized peaks at 1450 and 976 cm^{-1}.

Through the PCA analysis, a total of 13 groups were distinguished, as presented in *Table 48*. However, there are still 278 pairs of samples that remain undifferentiated, resulting in a discriminating power of 80.5% (with 278 undifferentiated pairs out of a total of 54 samples).

Table 48. Summary of PCA-based groupings of clearcoat (n=54)

GROUP	SAMPLES	VISUAL GROUPS
1	W061	Group C1
2	W002, W007, W023, W036, W053	Group C2
3	W010, W012, W014, W015, W016, W018, W020, W032, W041, W042, W044, W045, W047, W048, W049, W051, W054, W062	Group C2
4	W005	Group C2
5	W033	Group C2
6	W046	Group C2
7	W026	Group C2
8	W003, W011, W019, W030, W031, W039, W050, W052, W55	Group C3
9	W006, W009, W022, W024, W027, W028, W034, W035, W043, W035, W058, W059, W60	Group C3
10	W021, W040	Group C3
11	W001	Group C3
12	W017	Group C3
13	W025	Group C3
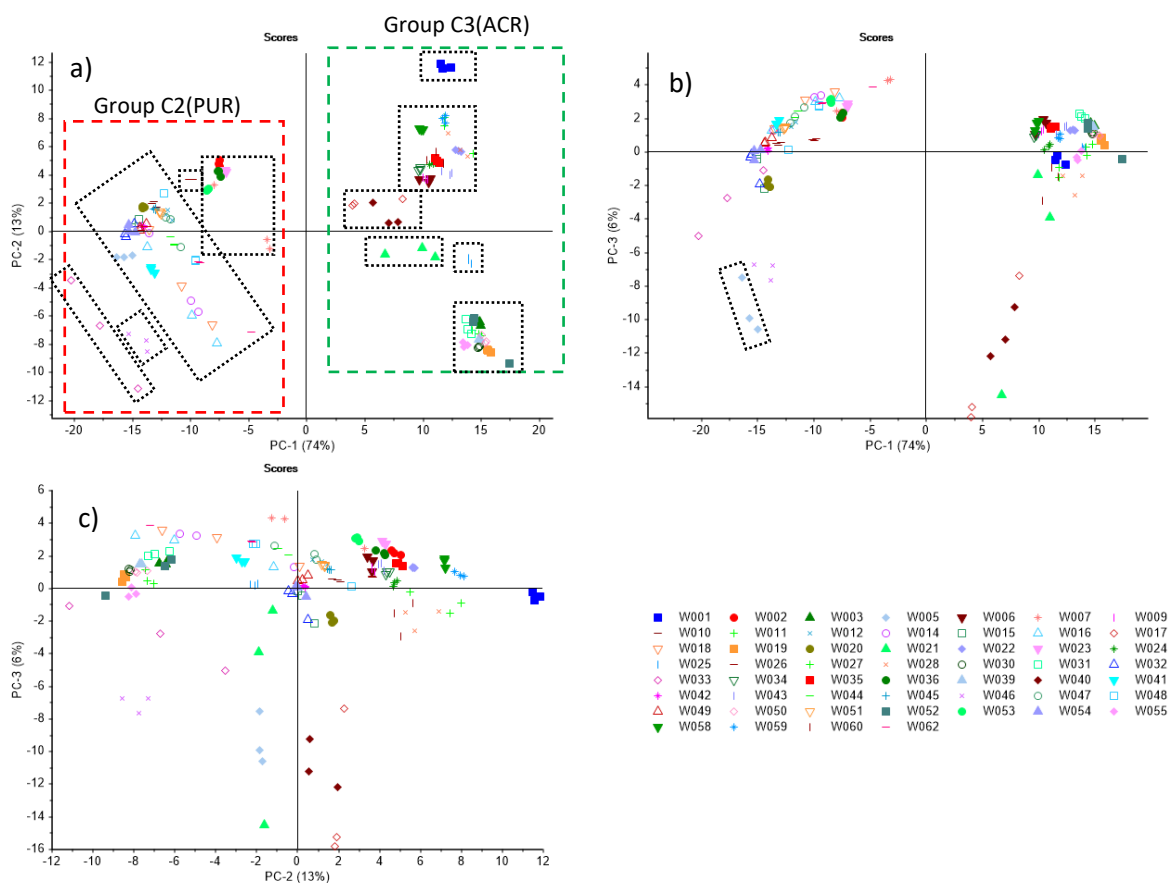
Figure 118. PCA score plots performed on the clearcoats (n=53). The first 3 PCs explained 93% of the total variance and were all considered for discrimination. Two main clusters with 12 finer clusters were generated and marked in dashed line.
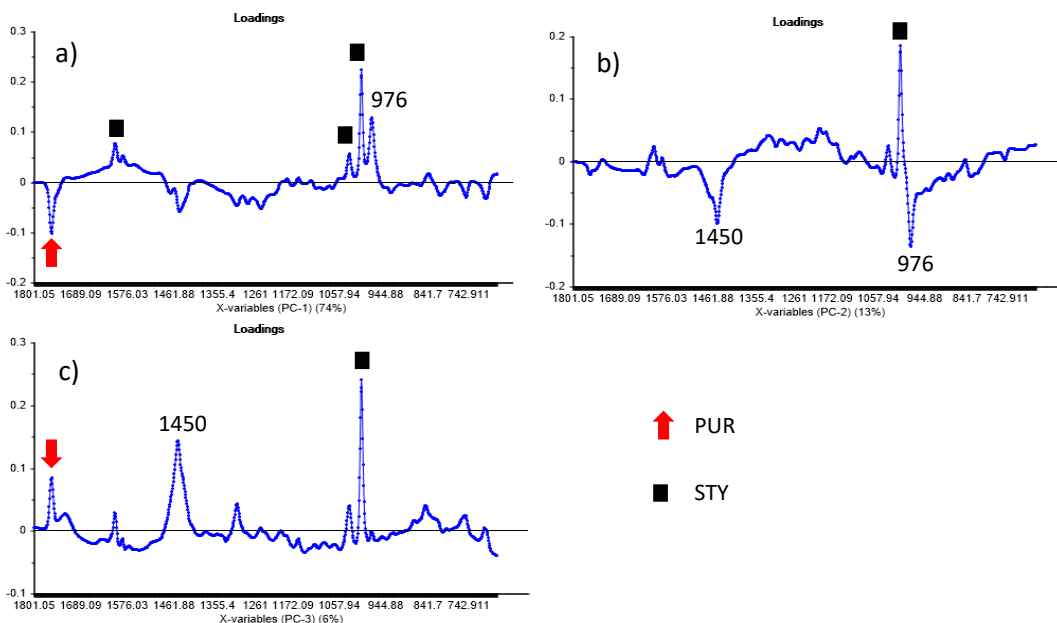
Figure 119. loadings of the first three PCs (a to c, respectively) of the PCA model generated from the clearcoat Raman spectra (n=53). The wave numbers corresponding to characteristic peaks of the characterized component are highlighted using different shapes and colors.

As always, the data structure was investigated based on several predetermined identifying factors, as depicted in *Figure 120*. The PCA score plots of clearcoat Raman spectra are presented in relation to manufacturing companies (*Figure 120a*), layer structure of paint samples (*Figure 120b*), assembly plants (*Figure 120c*), and vehicle models (*Figure 120d*). The observed patterns were largely consistent with the findings from the IR spectra analysis.
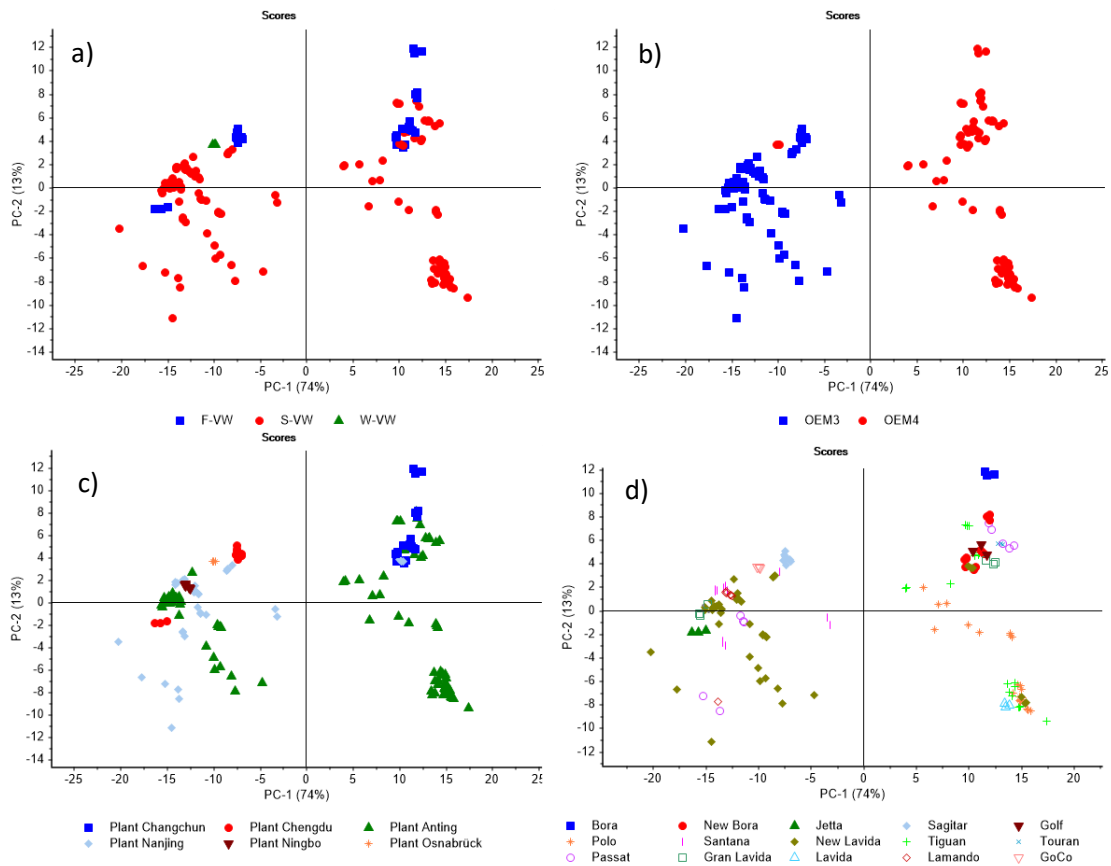
Figure 120. PCA score plots according to the first two principal components of Raman spectra of clearcoat (n=53), respectively highlighted by their manufacturing companies (a), their layer structure (b), their assembly plants (c), and the model of vehicles (d).

9.3. Characterization of basecoat

The analysis and characterization of the basecoat were conducted on the entire set of 54 samples. Subsequently, the samples were classified into three distinct groups based on the identified chemical categories in the spectra, as summarized in *Table 49 (page 206)*. Each group of spectra underwent individual analysis to identify the constituents detected by Raman in the investigated paints. The findings of these analyses will be discussed in the subsequent subchapters.

9.3.1. Group B1

Group B1 comprises a single sample, representing 2% of the total samples. As presented in *Figure 121*, the Raman spectrum of this sample display a fluorescence curve, making it unable to determine the chemical composition through Raman analysis. Consequently, the spectra from this sample remain uncharacterized.
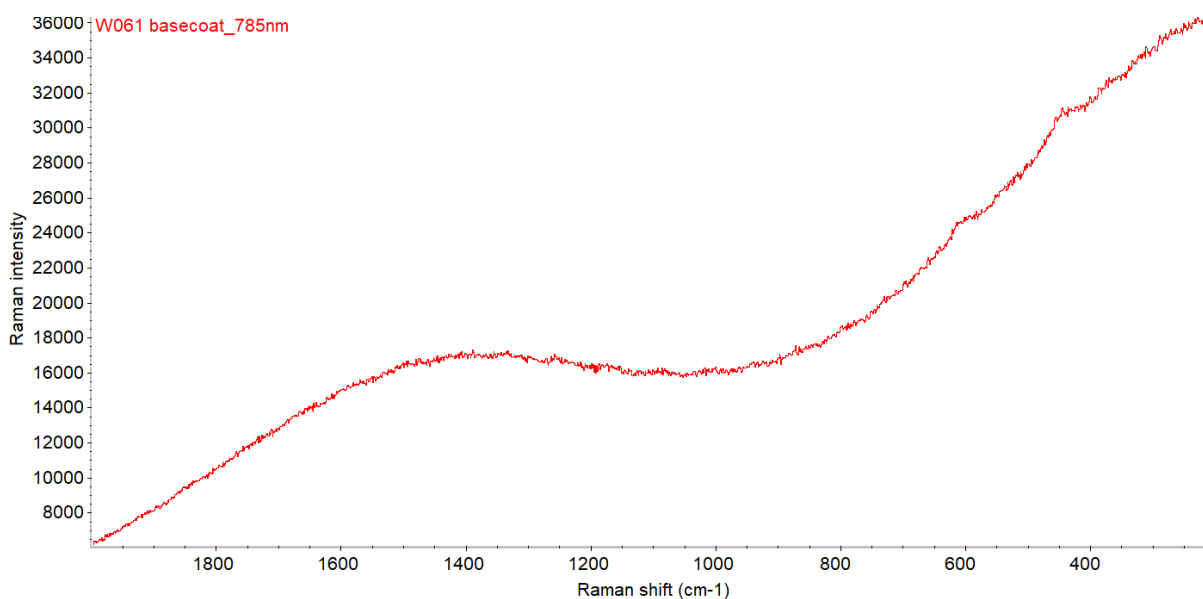
Figure 121. Representative spectrum of the basecoat of sample W061 from Group B1. Raman spectra (raw) acquired with a laser at 785nm.

9.3.2. Group B2

Group B2 consists of 27 samples, accounting for 50% of the total sample set. The Raman spectra in *Figure 122* reveal prominent peaks at 448 and 610 cm^{-1}, indicating the presence of titanium dioxide in the form of rutile, the primary inorganic pigment used in the basecoat. Another distinctive feature observed in this group is the double weak but broad peaks at 1756 and 1730 cm^{-1}, with slightly higher intensity at 1756cm^{-1}. Despite efforts using a commercial database, these peaks could not be identified. However, considering the binder types obtained from IR analysis, all samples in this group contain polyurethane resin. Therefore, it can be inferred that these characteristic peaks originate from the polyurethane resin. Within the group, further differentiation can be made based on variations in the 1700-700 cm^{-1} regions, although confidently identifying each specific peak in these regions remains challenging.
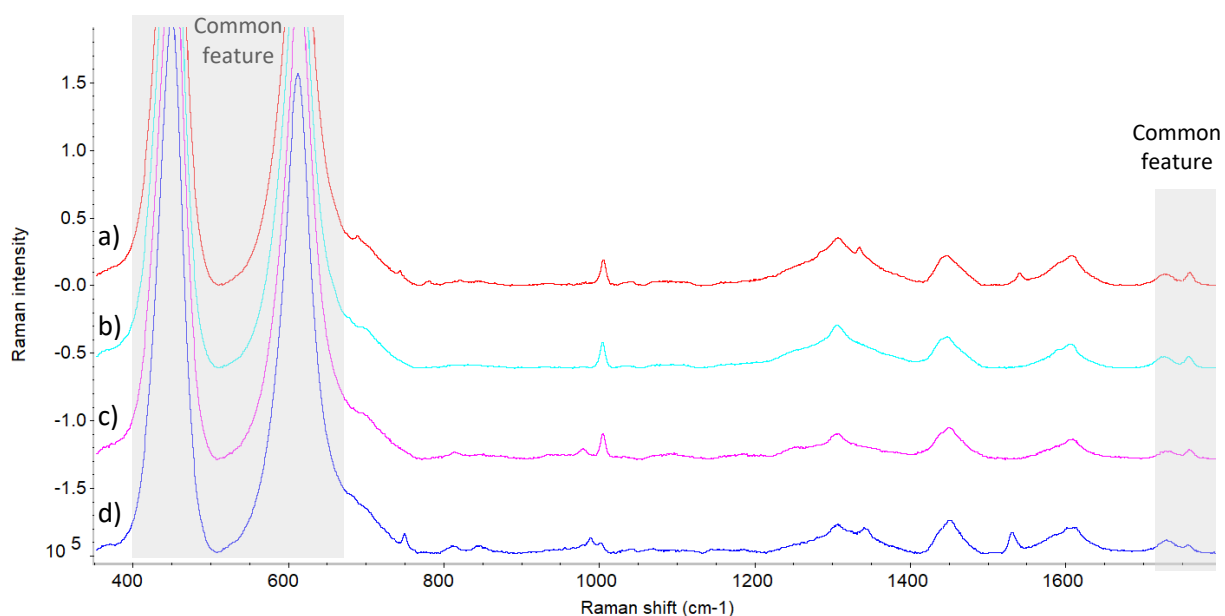
Figure 122. Representative Raman spectra of Group B2 obtained from the basecoat of: a) Sample W023; b) Sample W010; c) Sample W048; d) Sample W026. Common Spectral Features of Group B2 Highlighted in the Figure.

9.3.3. Group B3

Group B3 consists of 26 samples, representing 48% of the total sample set. *Figure 123* displays several spectra of this group, highlighting the key features observed. The dominant characteristics in all the spectra are the two prominent peaks at 448 and 610 cm^{-1} from rutile pigment. Notably, the absence of a peak at 1756 cm^{-1} and the higher intensity of the peak at 1730 cm^{-1} differentiate this group from Group B2. The peaks at 1002 and 1305 cm^{-1} suggest the presence of isophthalic acid. Despite attempts using database search, the specific composition of each peak could not be all determined. However, upon comparing with the results from IR analysis, it is evident that all samples in this group contain acrylic combined with isophthalic alkyd as the primary binder type. Consequently, these samples have been categorized accordingly. Furthermore, subgroups within Group B3 can be formed based on variations observed in the range of 1700-700 cm^{-1}.
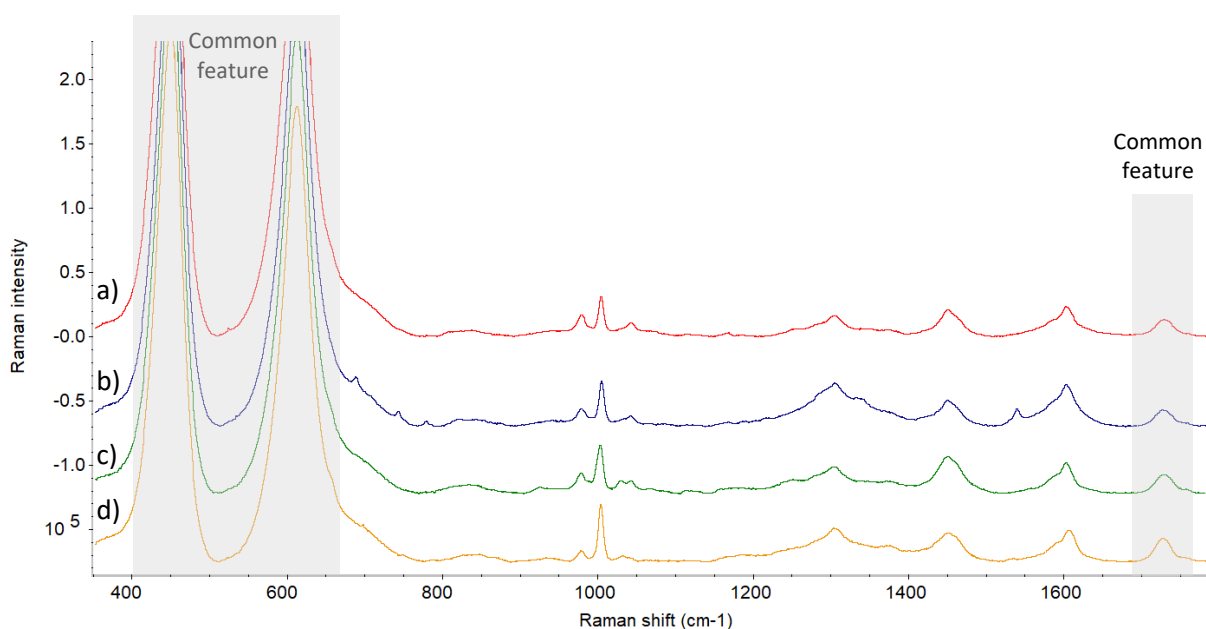
Figure 123. Representative Raman spectra of Group B3 obtained from the basecoat of: a) Sample W003; b) Sample W006; c) Sample W017; d) Sample W035. Common Spectral Features of Group B3 Highlighted in the Figure.

9.3.4. Classification and discrimination of basecoat

Samples with the detected pigment could not be differentiated, similar to the primer surfacer. While identifying the composition of each peak proved challenging, certain trends became evident. The presence or absence of a peak at 1756 cm^{-1} and variations in the peak intensity at 1730 cm^{-1}, which attributed to different binder types, served as key factors in dividing the samples into two primary groups. Notably, significant variations were observed in the 700-1700 cm^{-1} range, enabling visual comparison of spectra for sample discrimination. The findings from visual grouping, along with the identified chemical class for each group, are summarized in *Table 49*. Furthermore, the main differences observed among spectra with similar characterizations are emphasized in the table.

By visually comparing the basecoat spectra acquired through Raman analysis with a 785 nm laser, it was found that 339 pairs of samples could not be differentiated, indicating a discriminating power of 76.3% (339 undifferentiated pairs out of a total of 54 samples).

Table 49. Summary of visual groupings of basecoat (n=54)

GROUP/COMPOSITION	SUBGROUP	SAMPLES	DIFFERENCE WITHIN THE GROUP
Group B1 FLUORESCENCE	-	W061	Fluorescence curve
Group B2 PUR+TIO2	2.1	W005, W007, W010, W012, W014, W015, W016, W018, W020, W032, W033, W041, W042, W044, W045, W046, W047, W049, W051, W053, W054	Identical peaks at 1756, 1730, 1605, 1304, 1002, 610, and 444 cm^{-1}.
	2.2	W002, W023, W036	Extra peak at 1537 cm^{-1}
	2.3	W048, W062	Extra peak at 976 cm^{-1}
	2.4	W026	Extra peaks at 1530, 987 and 750 cm^{-1}
Group B3 ACR+ALK IPH+TIO2	3.1	W003, W009, W011, W021, W022, W024, W027, W028, W030, W031, W039, W043, W050, W052, W055, W058	Identical peaks at 1730, 1605, 1304, 1040, 1002, 976, 610, and 444 cm^{-1}.
	3.2	W006, W059	Extra peaks at 1537, 777,740and 685 cm^{-1}
	3.3	W034, W035	No peak at 1040 cm^{-1}
	3.4	W001	No peak at 976 cm^{-1}
	3.5	W017	Extra peak at 1030 cm^{-1}
	3.6	W060	Extra peak at 990 cm^{-1}
	3.7	W019, W025, W040	Extra peaks at 1756 and 990 cm^{-1}

9.3.5. Exploratory analysis

Due to the presence of fluorescence and its significant impact on the statistical model generation, Sample W061 was excluded from the dataset prior to conducting exploratory analysis. Consequently, the dataset consisted of 159 Raman spectra obtained from the basecoat of 53 samples, which were subjected to PCA analysis to visualize the underlying data structure. Due to extensive similar profile of samples, Raman spectra underwent pre-treatment steps including baseline offset, Savitzky-Golay type 1st derivative baseline treatment and SNV normalization to maximize the inter-sample variability. The analysis specifically focused on variables within the range of 1800-800 cm^{-1}, resulting in a dataset comprising 912 variables for PCA analysis.

Figure 124 illustrates the PCA model generated from the dataset, displaying the projections of Raman spectra based on the first four principal components. These components account for 70% of the total variance. On PC1, which explains 38% of the total variance, the sample set was separated into two primary groups: Group B1 and Group B2 (*Figure 124a*). The loadings for PC1 (*Figure 125a*) revealed that this separation was primarily influenced by the spectral characteristics of polyurethane, acrylic, and isophthalic alkyd. By incorporating PC4, additional discrimination was achieved (*Figure 124b*), particularly within Group B1, where a distinct separation is observed based on a peak at approximately 1540 cm^{-1} (*Figure 125b*). In contrast, the projections of spectra from samples in Group B2 exhibited a more dispersed distribution without clear clusters. To achieve a confident separation, an additional PCA analysis focusing on Group B2 samples was conducted. The resulting PCA scatter plot (*Figure 126a*) displays 11 distinct clusters. The loadings (*Figure 126b*) indicated that the model was primarily influenced by peaks at 1606, 1040, 1002, and 976 cm^{-1}. While the exact compositions corresponding to these peaks could not be determined with certainty, their presence, absence, or relative intensity contribute to the observed separation.

Ultimately, the PCA analysis enabled the distinction of a total of 15 groups. The grouping results are presented in *Table 50*. There are still 306 pairs of samples that remain undifferentiated, resulting in a discriminating power of 78.6% (with 306 undifferentiated pairs out of a total of 54 samples).
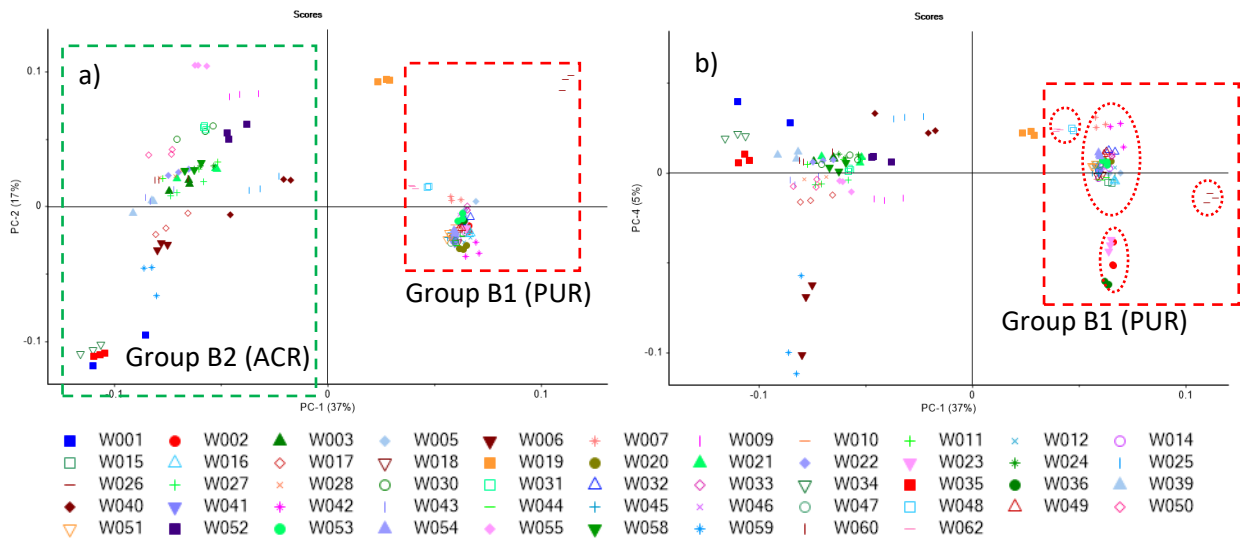
Figure 124. PCA score plots performed on the Raman spectra of basecoats (n=53): a) projections based on PC1 and PC2, two main clusters (Group B1/B2) are marked in dashed rectangular; b) projections based on PC1 and PC4, with more discrimination achieved in Group B1 in red dashed rectangular.
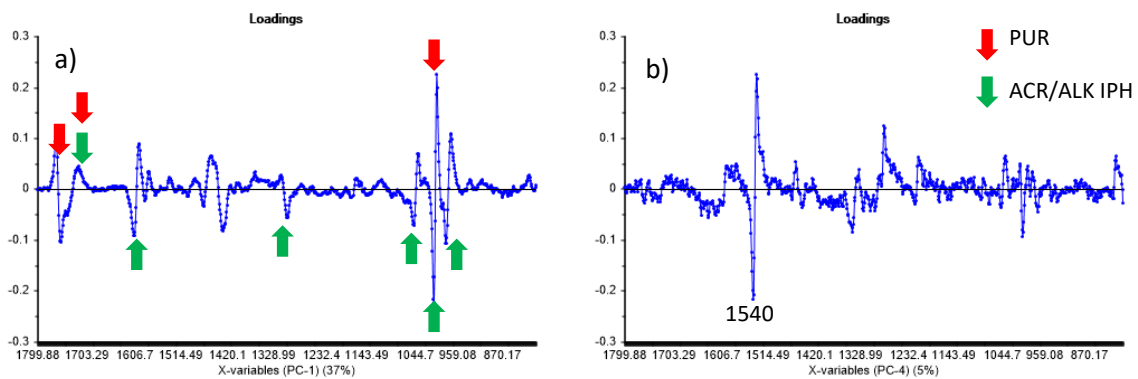
Figure 125. loadings of PC1 (a) and PC4 (b) of the PCA model generated from the basecoat Raman spectra (n=54). The wave numbers corresponding to characteristic peaks of the characterized component are highlighted using different shapes and colors.
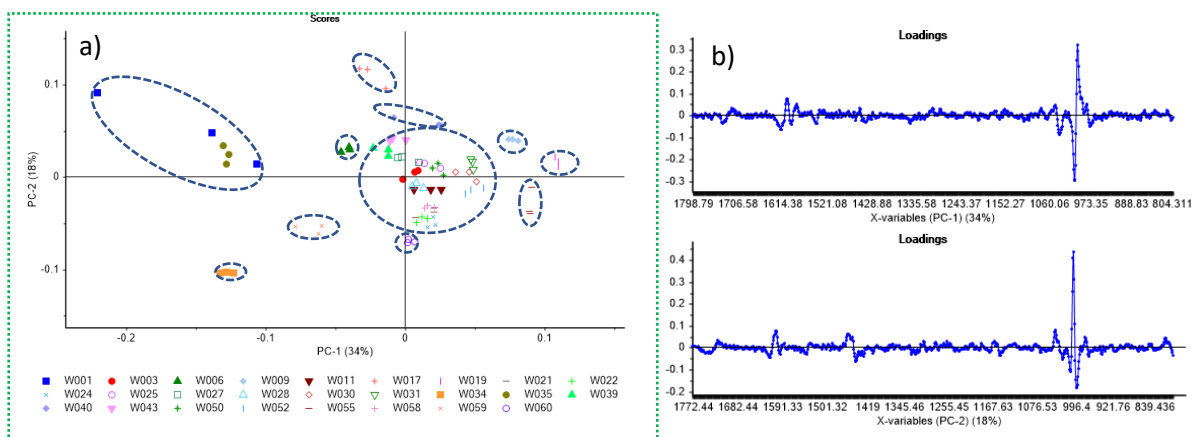
Figure 126. PCA score and loading plot for the basecoat of samples from Group B2 (n=26): a) projections based on the first two PCs. 11 clusters were generated using the first two PCs; b) loading plot for the first two PCs.

Table 50. Summary of PCA-based groupings of basecoat (n=54)

GROUP	SAMPLES	VISUAL GROUPS
1	W061	Group B1
2	W005, W007, W010, W012, W014, W015, W016, W018, W020, W032, W033, W041, W042, W044, W045, W046, W047, W049, W051, W053, W054	Group B2
3	W002, W023, W036	
4	W048, W062	
5	W026	
6	W003, W011, W021, W022, W024, W025, W027, W028, W030, W031, W039, W043, W052, W058	Group B3
7	W001, W035	
8	W040	
9	W034	
10	W009	
11	W006	
12	W019	
13	W017	
14	W055	
15	W059	
16	W060	

Similar to the IR analysis, the data structure of the basecoat Raman spectra was also investigated and visualized in *Figure 127.* PCA score plots were generated to analyze the dataset with regards to various factors, including chemical categories (*Figure 127a*), layer structure (*Figure 127b*), manufacturing companies (*Figure 127c*), assembly plants *(Figure 127d)*, topcoat color codes (*Figure 127e*), and vehicle models (*Figure 127f*). The observed patterns were largely consistent with the findings from the IR spectra analysis, with a few exceptions noted.

1) In *Figure 127a*, the distribution of samples according to the identified chemical classes revealed an interesting observation. One sample categorized as acrylic was projected on the right side of the scatter plot, where all the samples containing polyurethane binder were located. Upon further examination of the Raman spectra for this sample, it was discovered that although it was classified as acrylic, it also contained a high proportion of polyurethane as an additional resin. This finding was subsequently confirmed by cross-checking the IR spectra of the sample.

2) Additionally, in *Figure 127b*, two samples with an OEM4 layer structure were not projected on the same side as the other samples with an OEM4 layer structure. Upon analyzing their IR and Raman spectra, it was revealed that these two samples actually contained both acrylic and polyurethane resins. While the polyurethane served as an additional resin, the proportion of polyurethane in these two samples was significantly higher. This explains why these samples were projected on the right side of the scatter plot.
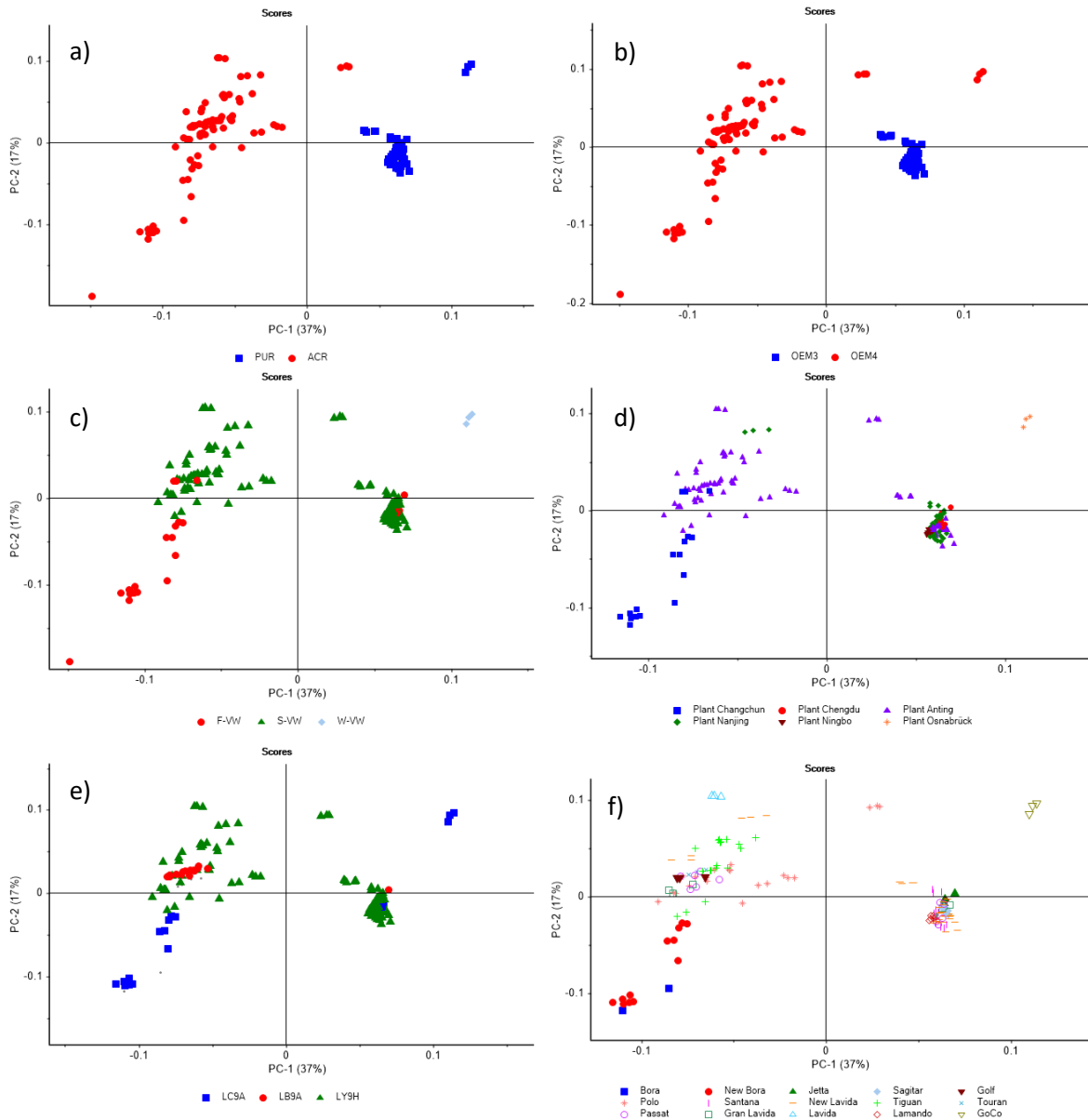
Figure 127. PCA score plots according to the first two principal components of Raman spectra of basecoats (n=53), respectively highlighted by the chemical categories (a), layer structure (b), their manufacturing companies (c), their assembly plants (d), their topcoat color codes (e), and the model of vehicles(f).

9.4. Characterization of primer surfacer

The characterization of primer surfacer was limited to samples with a OEM4 system, resulting in only 28 samples being involved in the analysis. The primer surfacer spectra obtained in this study also exhibited good quality. The samples were subsequently classified into four groups based on the chemical categories identified from the spectra, as summarized in *Table 51* (page 215). Each group of spectra was individually analyzed to identify the constituents detected by Raman in the investigated paints. These findings will be discussed in the subsequent subchapters.

9.4.1. Group PS1

This group consists of only 1 sample, accounting for 3.5% of the total sample set. In *Figure 128*, the Raman spectra of this sample exhibit a distinct characteristic—a fluorescence curve. Unfortunately, this fluorescence curve does not provide sufficient information for the characterization of specific chemical groups. As a result, the spectra from this sample remain uncharacterized, and it is not possible to determine the chemical composition based on the Raman analysis.
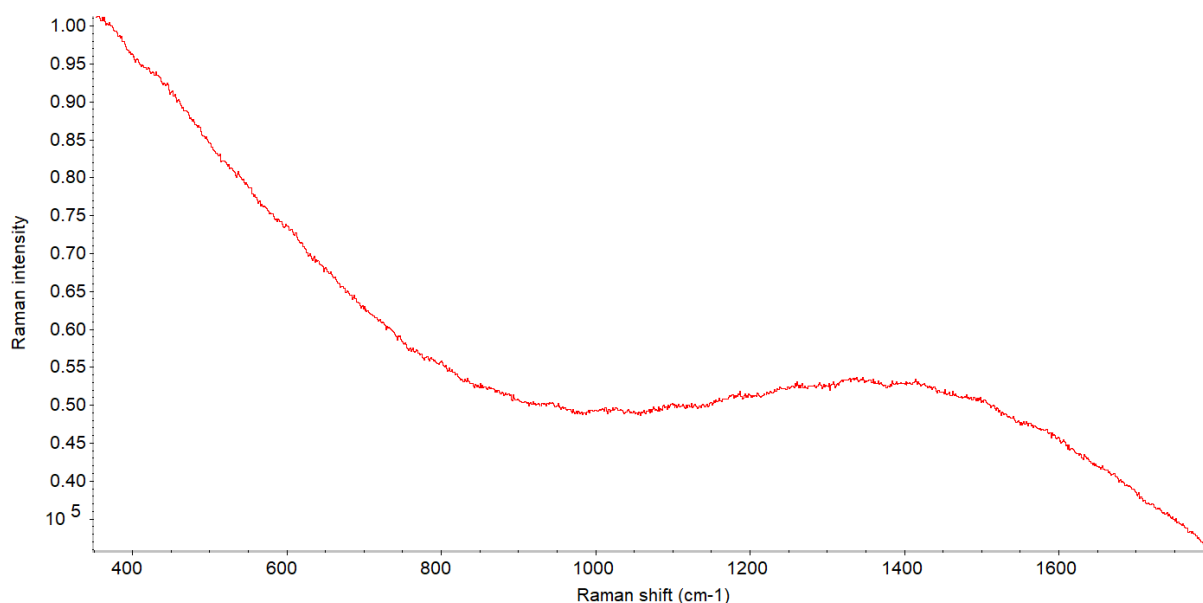
Figure 128. Representative spectrum of the primer surfacer of sample W061 from Group PS1. Raman spectra (raw) acquired with a laser at 785nm.

9.4.2. Group PS2

This group, known as Group PS2, consists of 23 samples, accounting for 82% of the total sample set. The Raman spectra of these samples, depicted in *Figure 129*, exhibited identical peaks at 1730, 1606, 1304, 1188, 1112, 1002, 987, 610, and 444 cm^{-1}. The bands around 444 and 610 cm^{-1} indicated the presence of rutile pigment. The peak at 987 cm^{-1} was attributed to the symmetric stretching vibration of barium sulfate (SO4^{2-}). Additionally, the peaks at approximately 1111 and 1185 cm^{-1} were assigned to C–C backbone and C–C out-of-plane vibrations, respectively, which could be characterized as the epoxy binder(De Gelder *et al.*,2005). The bands at 1606 cm^{-1} also indicated the presence of epoxy resin, while the peak at 1730 cm^{-1} was attributed to C-O stretches from the polyurethane binders. These identifications were further supported by IR analysis, which revealed the presence of epoxy resin combined with polyurethane resins in this group of primer surfacers, along with TiO$_2$ and barium sulfate as pigments and extenders. Notably, isophthalic acid was not identified in the FTIR spectra but was detected in the Raman spectra. Upon revisiting the FTIR spectra of this sample group, it was found that all the spectra exhibited peaks at 1305, 1240, and 730 cm^{-1}, which were not annotated in *Figure 91*. These peaks are actually characteristic peaks of isophthalic alkyd. This finding underscores the importance of combining both IR and Raman analysis for the comprehensive identification and characterization of automotive paint.
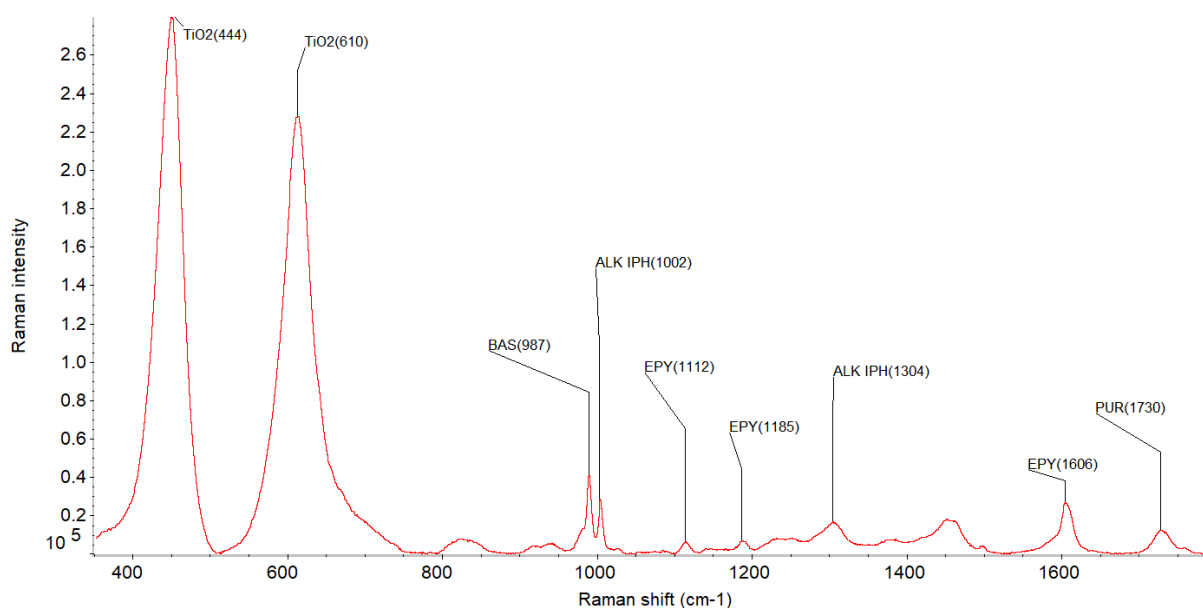
Figure 129. Representative Raman spectrum obtained from the primer surfacer of Sample W009 from Group PS2, with characteristic peaks annotated on the spectrum.

212

9.4.3. Group PS3

Group PS3 consists of 3 samples, representing 11% of the total samples. As depicted in *Figure 130*, a significant distinction between this group and Group PS2 is the absence of a peak at 987 cm^{-1}, indicating that the samples in this group do not contain barium sulfate. A common feature among the samples in Group PS2 is the presence of peaks at 1002 and 1304 cm^{-1}, suggesting the presence of isophthalic acid. This finding was corroborated by FTIR analysis, which confirmed that the IR spectra of samples in this group indeed contained isophthalic alkyd as the primary binder.
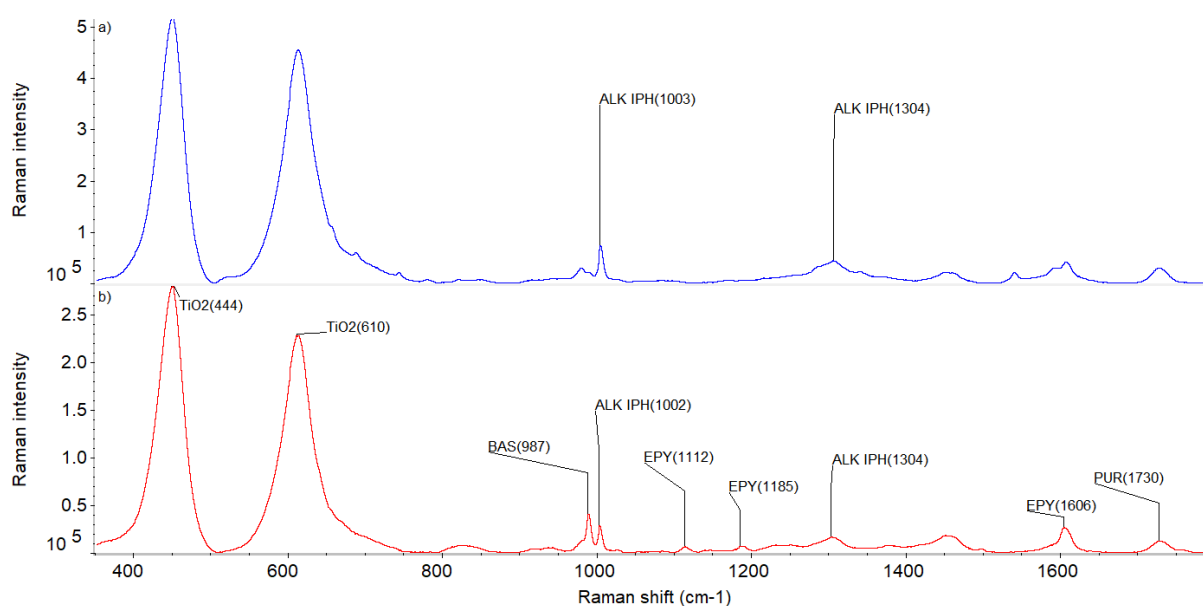
Figure 130. Representative Raman spectra obtained from the primer surfacer of: a) Sample W034 from Group PS3; and b) sample W009 from Group PS2. Characteristic peaks of each group are annotated on the spectra.

9.4.4. Group PS4

Group PS4 consists of only 1 sample, representing 3.5% of the total samples. A notable characteristic that sets this sample apart from the other groups is the absence of a peak at 1002 cm^{-1} and the presence of a relatively strong peak at 987 cm^{-1}. The absence of the peak at 1002 cm^{-1} suggests the presence of a different binder type in this sample, as shown in *Figure 131*. The identification of the IR spectra of this sample confirms this conclusion, as it indicates the presence of terephthalic alkyd combined with acrylic as the binder. However, in the Raman spectra, there are fewer discernible peaks from the binder, making the characterization of the binder in this sample more challenging.
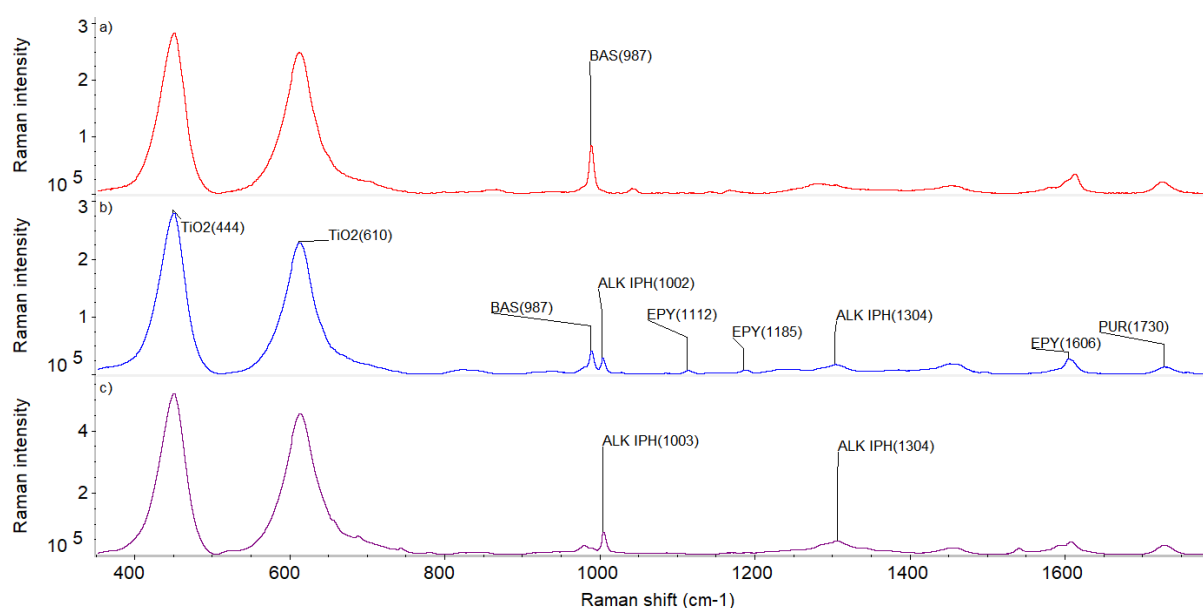
Figure 131. Representative Raman spectra obtained from the primer surfacer of: a) Sample W026 from Group PS4; b) sample W009 from Group PS2; and c) Sample W034 from Group PS3. Characteristic peaks of each group are annotated on the spectra.

9.4.5. Classification and discrimination of primer surfacer

The key features observed in all the obtained spectra were the two large peaks at 448 and 610 cm^{-1}, which were attributed to titanium dioxide in the form of rutile. However, it was not possible to differentiate samples based on the detected pigment alone. The region of 800-1800 cm^{-1} exhibited weak but abundant peaks, allowing for differentiation between samples. However, not all peaks in this region could be identified, even with the assistance of known chemical composition information obtained from IR analysis and database searches. In other words, not all compositions detected from the IR analysis could be identified from the Raman spectra. Consequently, only the compositions that could be confidently identified from the Raman spectra of the primer surfacer were marked. The results of visual grouping and the identified chemical compositions for each group are summarized in *Table 51*. The main differences observed between the spectra of samples with similar characterizations were also emphasized in the table.

Through visual comparison of the primer surfacer spectra obtained from Raman analysis using a 785 nm laser, a total of 191 sample pairs remained undifferentiated, resulting in a discriminating power of 49.5% (191 undifferentiated pairs out of a total of 28 samples).

Table 51. Summary of visual groupings of primer surfacer (n=28)

GROUP/COMPOSITION	SUB-GROUP	SAMPLES	DIFFERENCE WITHIN THE GROUP
Group PS1 FLUORESCENCE	-	W061	Fluorescence curve
Group PS2 EPY+ALK IPH+PUR +BAS+TIO2	2.1	W009, W011, W017, W019, W021, W022, W024, W025, W027, W028, W030, W031, W040, W043, W050, W052, W055, W058, W059, W060	Identical peaks at 1730, 1606, 1304, 1188, 1112, 1002, 984, 610, and 444 cm^{-1}.
	2.2	W003, W039	Extra peak at 1530 cm^{-1}
	2.3	W006	Sharper peak at 1450 cm^{-1}
Group PS3 ALK IPH+TIO2	3.1	W001	Poor quality, only peaks at 1002, 610 and 444 cm^{-1} can be identified
	3.2	W034	Extra peaks at 1538, 990, 745 and 687 cm^{-1}
	3.3	W035	No peaks at 1538, 990, 745 and 687 cm^{-1}
GROUP 4 Uncharacterized binder+BAS+TIO2	-	W026	Single sample in the group

9.4.6. Exploratory analysis

A total of 80 Raman spectra from the primer surfacer of 28 samples were subjected to PCA analysis to visualize the underlying data structure. Considering the large number of undifferentiated samples, all spectra underwent pre-treatment including baseline offset, Savitzky-Golay type 1st derivative baseline treatment and SNV normalization. The analysis focused on variables within the range of 1800-800 cm^{-1}, resulting in a dataset comprising 912 variables for PCA analysis.

Figure 132 illustrates the PCA model generated from this dataset, displaying the projections of Raman spectra based on the first two principal components, which account for 95% of the total variance. However, the presence of significant fluorescence signal in sample W061 and background noise in sample W001 resulted in most of the samples being accumulated in the center without any discernible pattern. To address this issue, the two outliers (W061 and W001) were identified and subsequently removed from the dataset.

Subsequently, an additional PCA analysis was conducted on the remaining 78 Raman spectra from the primer surfacer of the remaining 26 samples. *Figure 133* summarizes the PCA model generated from this new subset, showcasing the projections of Raman spectra based on the first four principal components, which account for 92% of the total variance within this subset. The two-dimensional score plots obtained using PC1 and PC2 confirmed the presence of three larger clusters (with four finer groupings), based on the binder and extender used in the primer surfacer, as depicted in *Figure 133a* (each cluster marked within dashed rectangles). By comparing derivative spectra with the original spectra, the corresponding loading plots for PC1 and PC2 (*Figure 134a* and *Figure 134b*) revealed that peaks at approximately 987, 1002, and 1606 cm^{-1}, corresponding to spectral features of barium sulfate, isophthalic acid, and epoxy, respectively, significantly contributed to the separation of the clusters. The inclusion of PC3 and PC4 allowed for further separation within Group PS2 (highlighted by a red dashed line in *Figure 133b* and *Figure 133c).* PC3 is associated with epoxy, while PC4 is influenced by the extra tiny peak at 1530 cm^{-1}(*Figure 134c* and *Figure 134d*).

Eventually, considering the previously identified outliers, a total of eight groups could be distinguished using the PCA model. The grouping results of the PCA analysis are presented in *Table 52*. However, there is a group of 21 samples that remained undifferentiated, resulting in a discriminating power of 44.4% (with 210 undifferentiated pairs out of a total of 28 samples).

The data structure of the Raman spectra of the primer surfacer, with respect to the information on vehicle origin, was not investigated further. This decision was based on the observation that the grouping results obtained from the Raman spectra analysis mirrored the patterns observed in the IR analysis. Consequently, conducting additional analysis on the Raman spectra did not yield any additional information or insights.
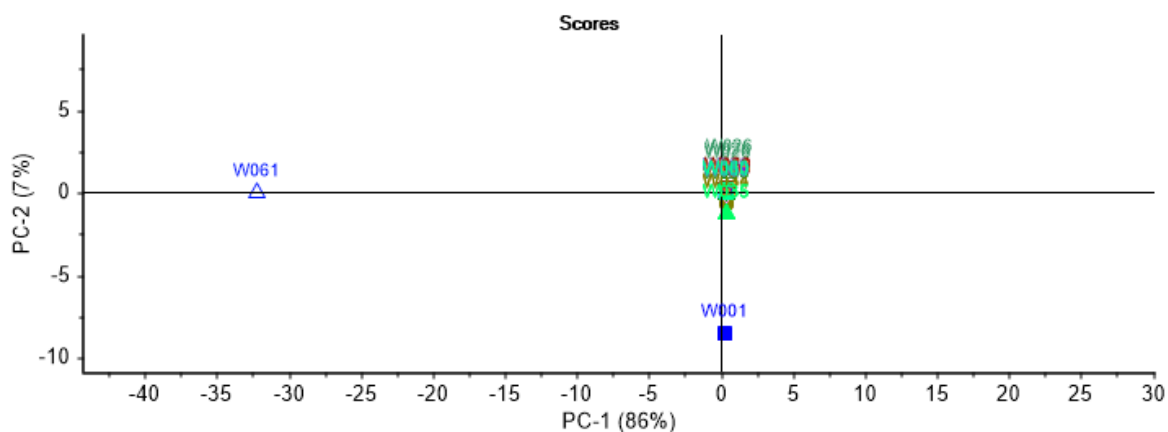
Figure 132. PCA scatter plot of all Raman spectra of primer surfacer (n=28) according to the first two principal components.
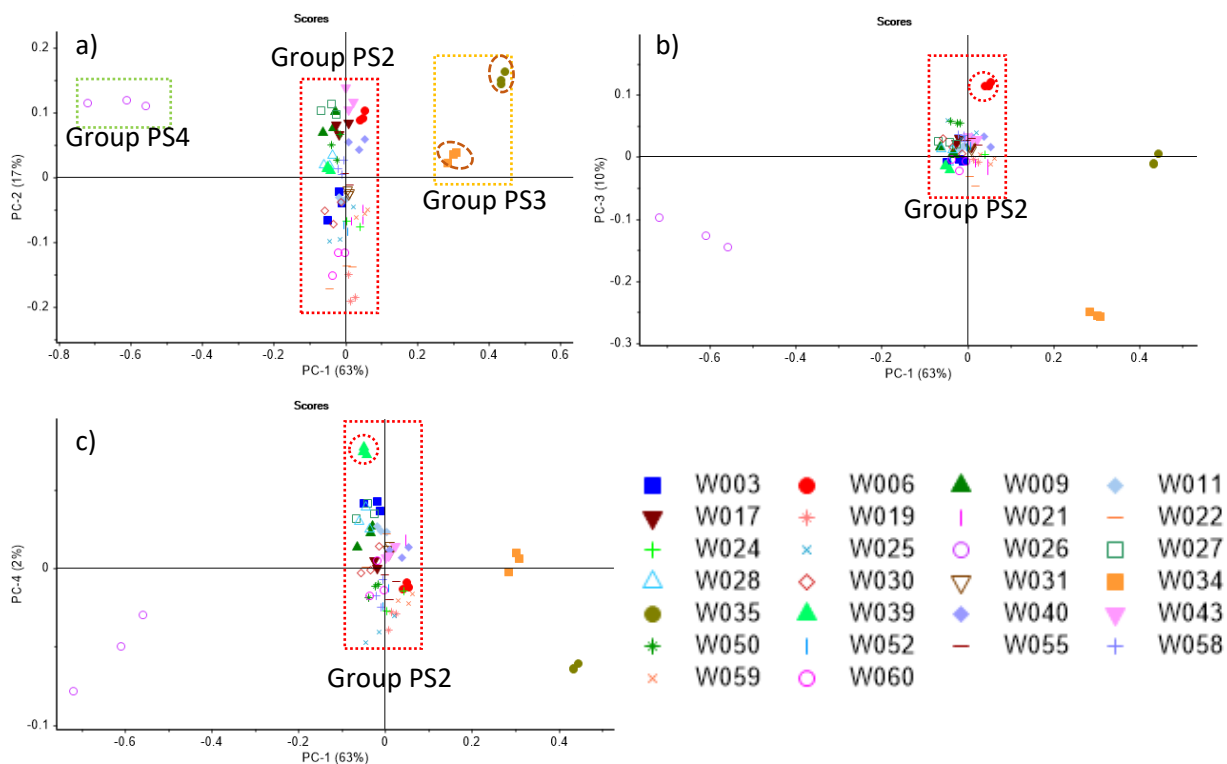
Figure 133. PCA score plots for the primer surfacer Raman spectra of new subset(n=26): (a) Separation for 3 larger groups based on PC1 and PC2, which account for 63% and 17% of the total variance, respectively; (b) projections based on PC1 and PC3, accounting for 63% and 10% of the total variance, respectively, with sample W006 separated from the rest of Group PS2; (c) projections based on PC1 and PC4, accounting for 63% and 2% of the total variance, respectively, with sample W039 separated from the rest of Group PS2.

217
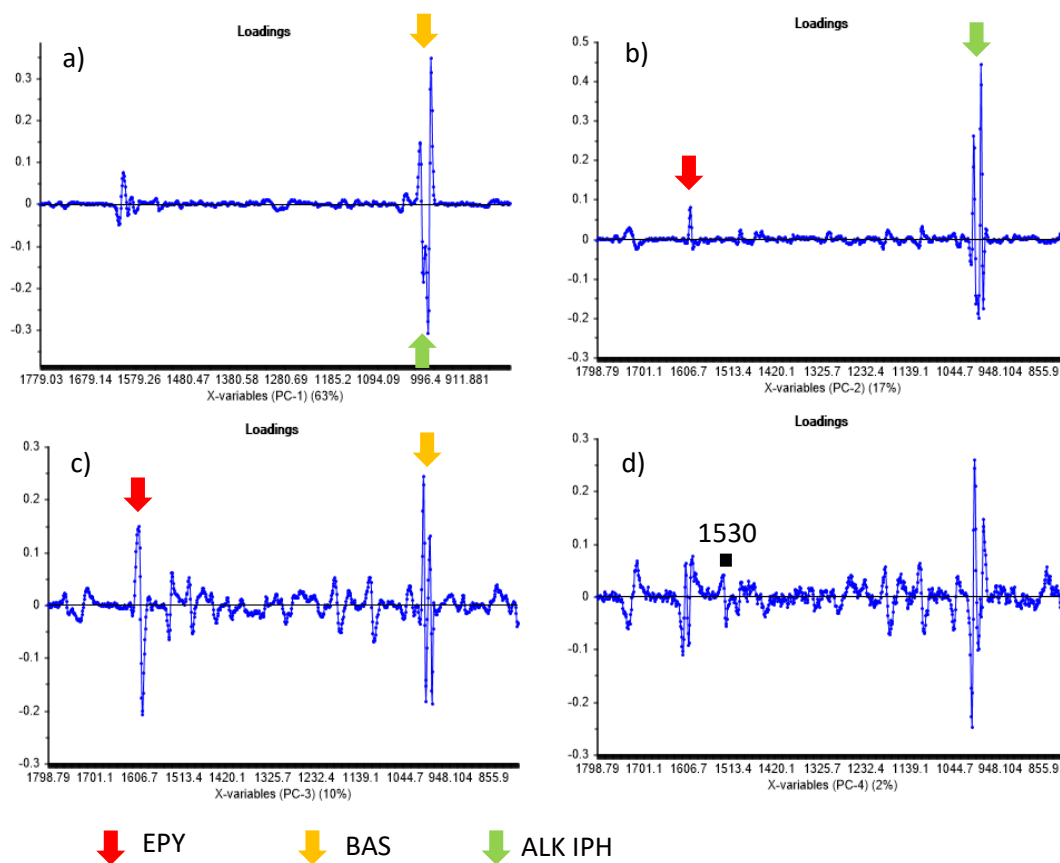
Figure 134. loadings of the first four principal components (a to d, respectively) of the PCA model generated from the primer surfacer Raman spectra of new subset (n=26). The wave numbers corresponding to characteristic peaks of the characterized component are highlighted using different shapes and colors.

Table 52. Summary of PCA-based groupings of primer surfacer (n=28)

GROUP	SAMPLES	VISUAL GROUPS
1	W061	Group PS1
2	W003, W009, W011, W017, W019, W021, W022, W024, W025, W027, W028, W030, W031, W040, W043, W050, W052, W055, W058, W059, W060	Group PS2
3	W039	
4	W006	
5	W001	
6	W034	Group PS3
7	W035	
8	W026	Group PS4

218

9.5.   Characterization of primer

The analysis and characterization of primer was performed on all 54 samples in the set. The primer spectra obtained in this study exhibited mostly poor quality, posing challenges in sample identification and differentiation based on spectral analysis. The response of the primer to the laser varied greatly among samples, requiring different laser powers for accurate measurements. Increasing the laser power often resulted in primer burning, further complicating the acquisition of high-quality spectra. 16 accumulations were added onto the original spectra in order to increase signal to noise ratio, thus obtaining better quality of spectra. Due to the poor quality, only one measurement was taken from each primer. The samples were classified into two groups based on the chemical categories identified from the spectra. Each group of spectra was analyzed individually to identify the constituents detected by Raman in the investigated paints and were discussed in the following subchapters.

9.5.1. Group P1

This particular group, identified as Group P1, consists of 1 sample, representing 1.8% of the total samples. The spectra within this group exhibit a distinct characteristic—they lack discernible peaks or features that would enable the characterization of specific chemical groups. Instead, the spectra in Group P1 only display a fluorescence curve, as depicted in *Figure 135*. As a result, at this stage of the analyses, the spectrum from Group P1 remains uncharacterized, as it does not provide sufficient information for identification or classification.
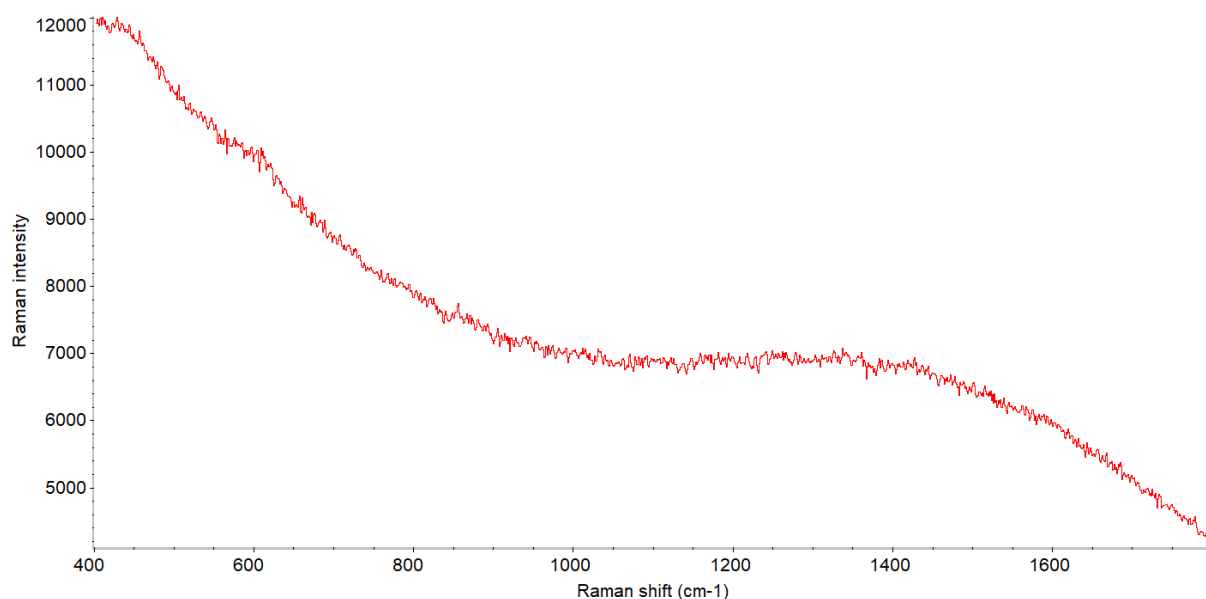
Figure 135. Representative spectra of the primer of samples forming "Group P1". Raman spectra (raw) acquired with a laser at 785nm.

9.5.2. Group P2

Group P2 comprises 53 samples, representing 98.2% of the total sample set. Within this group, a subset of 7 samples exhibited spectra of good quality, enabling the characterization of their chemical composition. However, the remaining 46 samples displayed the same characteristic peaks, albeit with lower intensity, resulting in lower-quality spectra compared to the aforementioned seven samples.

Figure 136 illustrates a spectrum of good quality, exhibiting distinct Raman bands at 1610, 1185, 1111, 638, 610, and 444 cm^{-1}. The IR analysis revealed that all primers in the sample set contained epoxy resin, in combination with titanium dioxide and aluminum silicate as pigments and extenders. In the Raman spectra, the presence of peaks at approximately 610 and 444 cm^{-1} indicated the presence of rutile form of TiO$_2$, while the shoulder peak at approximately 638 cm^{-1} was attributed to the presence of aluminum silicate. The peaks at approximately 1111 and 1185 cm^{-1} were assigned to C–C backbone and C–C out-of-plane vibrations, respectively, originating from the epoxy resin.

Although there are variations in the relative intensity and response to the laser within this group, all the Raman bands show up at the same positions. Consequently, two subgroups were formed within the same chemical class based on spectral quality. One subgroup includes 7 samples with distinct peaks, while the other subgroup contains 46 samples with less intense characteristic peaks. However, this grouping outcome won't serve as a basis for discrimination, all 53 samples in Group P2 remain undifferentiated.
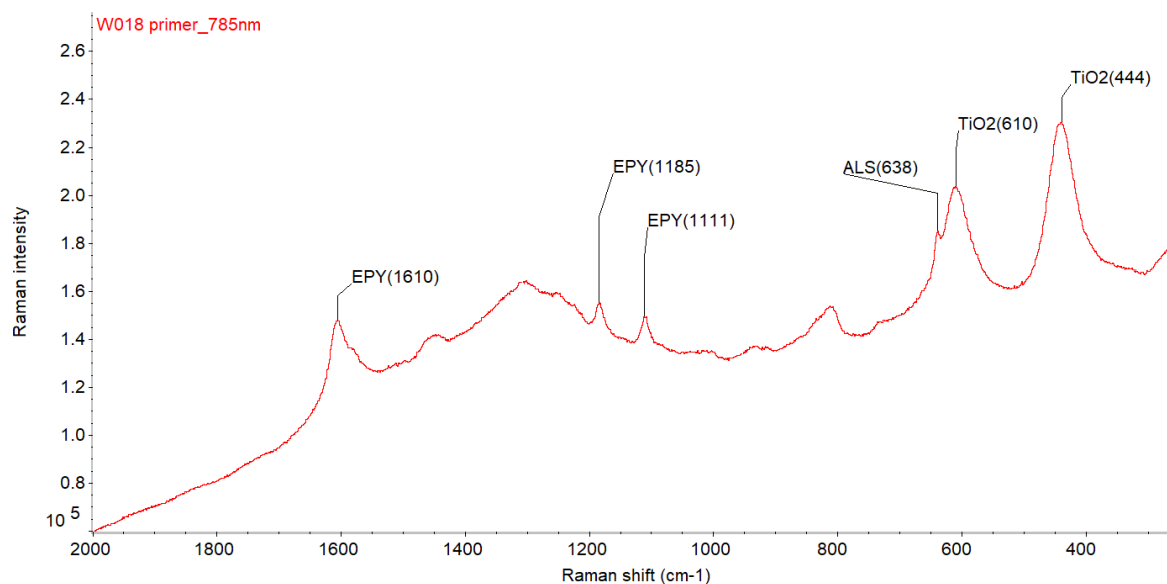
Figure 136. Representative Raman spectrum obtained from the primer of Sample W018 from Group P2, with characteristic peaks annotated on the spectrum.

9.5.3. Classification and discrimination of primer

The analysis of primer spectra posed challenges due to the poor quality of the majority of the spectra. As a result, drawing definitive conclusions based on visual comparison alone proved difficult, and no additional compositional information beyond what was obtained from the IR analysis could be identified from the Raman spectra. Within Group P1, the single sample provided no information.

Furthermore, within Group P2, the primer spectra could not be differentiated from each other based solely on the position of characteristic Raman bands. The results of the grouping, obtained through visual comparison, are summarized in *Table 53*.

A significant number of samples remained undifferentiated following the Raman analysis of the primer, with an exceptionally high number of undifferentiated pairs (1378 pairs). The calculated discriminating power was merely 3.7% (1378 undifferentiated pairs out of a total of 54 samples). Even when accounting for the variations in the relative intensity of peaks observed in Group P2, a substantial 1056 pairs of samples still remained undifferentiated, resulting in a discriminating power of 26.2%. This underscores that the Raman analysis of the primer did not yield the same level of discrimination as offered by the IR analysis. As such, Raman analysis of the primer proves to be less optimal for automotive paint analysis.

Table 53. Summary of visual comparisons within the previously defined groups (primer).

GROUP/COMPOSITION	SUB-GROUP	SAMPLES	DIFFERENCE WITHIN THE GROUP
GROUP P1 FLUORESCENCE	-	W061	All fluorescence, no difference
GROUP 2 EPY+ALS+TIO2	-	W002, W003, W005, W006, W018, W052, W062	Raman bands at 1610, 1185, 1111, 638, 610, and 444 cm^{-1}
	-	W001, W007, W009, W010, W011, W012, W014, W015, W016, W017, W019, W020, W021, W022, W023, W024, W025, W026, W027, W028, W030, W031, W032, W033, W034, W035, W036, W039, W040, W041, W042, W043, W044, W045, W046, W047, W048, W049, W050, W051, W053, W054, W055, W058, W059, W060	Lower intensities at aforementioned position, mainly present only TiO$_2$ peaks

9.5.4. Exploratory analysis

A total of 54 Raman spectra from the primer of the analyzed samples in this study were investigated using PCA to visualize the data structure. Prior to applying the exploratory algorithms, the raw spectra data underwent baseline correction, normalization, and detrending with a polynomial order of 2. Variables in the range of 1640-380 cm^{-1} (1321 points) were selected.

In *Figure 137*a, the PCA model is summarized by displaying the projections of the Raman spectra based on the first two principal components, which account for 95% of the total sampling variance. The majority of samples were projected closely together and close to the center, with only a few samples distributed far away from the center. By examining the weights (loadings) of the first principal component (PC1, *Figure 137*b), the influence of positive values corresponding to titanium dioxide can be highlighted. However, this separation was primarily based on the spectra quality, as the samples distributed far away from the center exhibited discernible peaks with generally higher intensities. Despite these observations, confident discrimination could not be achieved based on this PCA model.
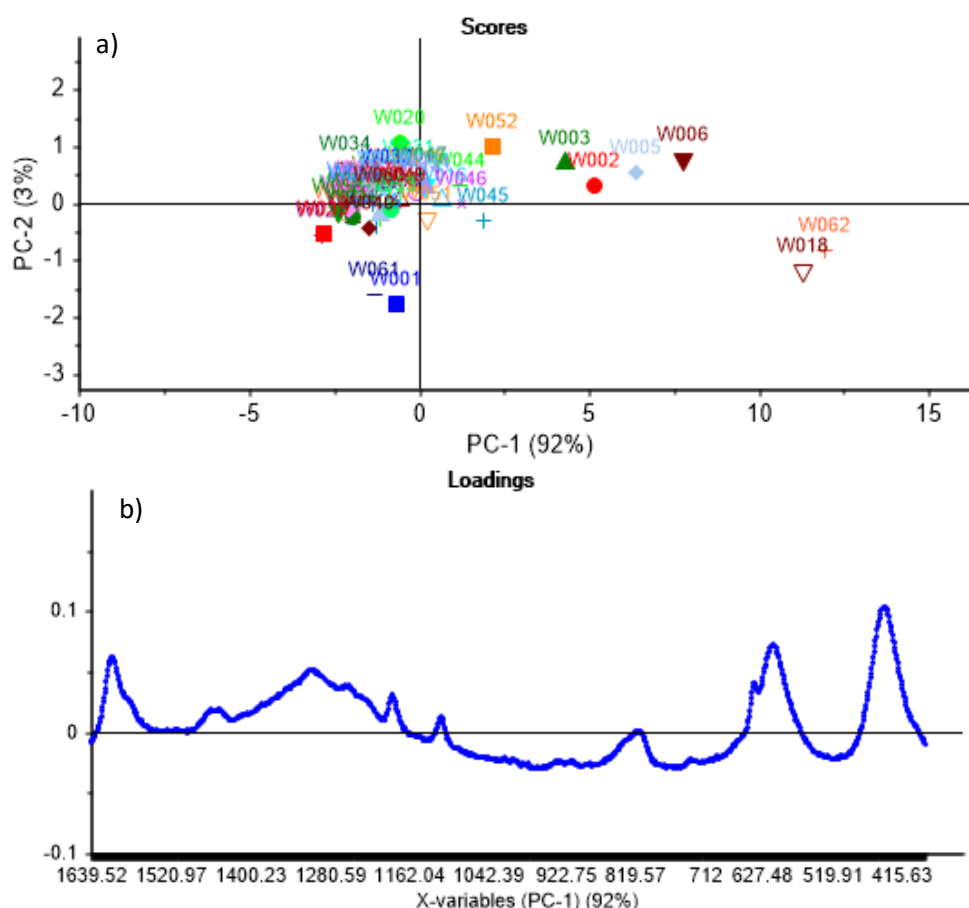
Figure 137. PCA scatter plot according to the first two principal components (a) of the set of Raman spectra of primer (785nm) and the loadings for PC1(b).

222

9.6.   Discussion

9.6.1. Blind test

Blind tests were carried out to validate the Raman protocol. A total of five samples, denoted as A to E, were randomly selected. These samples were measured by a different collaborator. The same procedure as the FTIR blind test was employed in these tests. However, LDA was excluded due to its constrained classification capability for less discriminant sample groups. For enhanced sample classification accuracy, initial PCA projections were conducted to determine the chemical class of each sample (see *Figure 138*). Then PCA models were then selected for SIMCA classification. The classification outcomes achieved using SIMCA and database search are detailed in *Table 54.*

The databases were established using OMNIC software by uploading all spectra, including replicates, acquired from Raman analyses of each layer. The search results were generated using the 'correlation' algorithm. All the hits with a 'match value' obtained from the correlation algorithm surpassing 95% were documented. In this context, the conventional database search stands out for its simplicity and speed—offering distinct advantages. Unlike SIMCA, which requires the determination and creation of individual PCA models one by one—an often-time-consuming process—database search offers a more streamlined approach. Additionally, database search facilitates direct spectra comparison, a feature that proves valuable in the identification and elimination of certain false positives. Given the remarkably identical chemical profiles in the basecoat and primer surfacer—resulting in a group of 21 undifferentiated samples, respectively—numerous potential sources become plausible. However, due to space limitations, only the initial ten samples from this group have been included in the table. This underscores the complexity and challenges associated with distinguishing between such closely related layers in automotive paint analysis.

It is worth noting that the clearcoat of Sample D lacks spectra data due to an incorrect layer identification. However, this does not significantly impact the final classification, as Sample D could be accurately identified using its unique basecoat.

Furthermore, It is important to note that primer classification was initially excluded due to its limited discriminatory capability. However, the quality of primer spectra does offer some level of support to the classification process. While not as robust as other layers, the primer spectra still provide valuable information that contributes to the overall classification efforts.

Ultimately, all samples were accurately classified through these approaches.
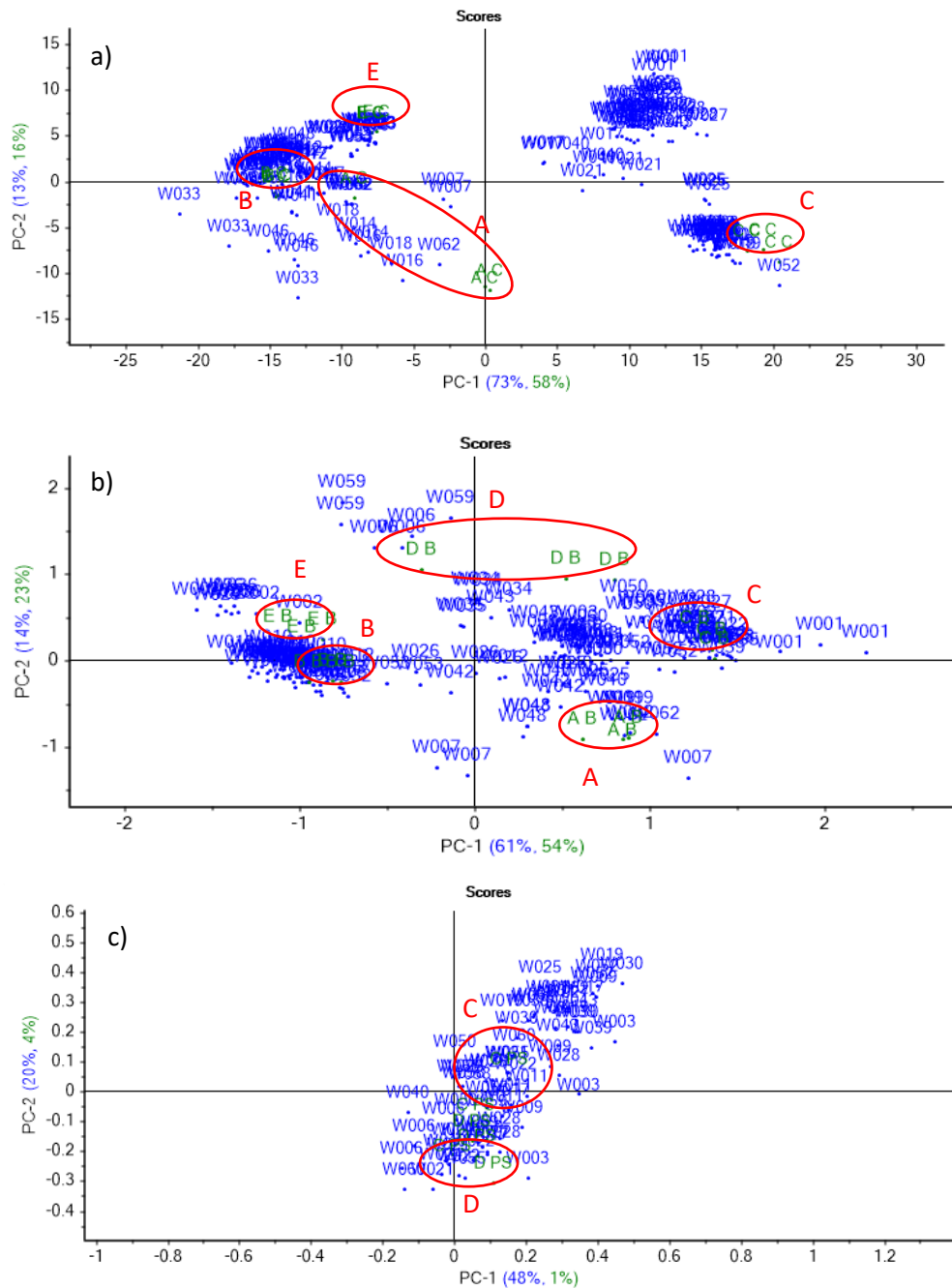
Figure 138. PCA projections for blind test samples (scatter plot in green, highlighted in red circles): a) clearcoat; b) basecoat; c) primer surfacer.

Table 54. Raman blind tests results of SIMCA and database searches for 5 unknown samples.

SAMPLE	LAYER	PCA PROJECTED CHEMICAL CLASS	SIMCA (1% or 5%)	DATABASE SERATCH (>95%)	INTERGREATED PREDICTION	ACTUAL SAMPLE
A	C	Group C2	W048, W062	W062, W048	**SIMCA** **W062** **Database** **W062**	W062
	B	Group B2	W026, W007, W062, W042,	W048, W062		
	P	Group P2	-	W062		
B	C	Group C2	W014, W041, W048, W047	W054, W041, W051, W012, W047, W049, W045, W044	**SIMCA** W014, **W041**, W047 **Database** W054, **W041**, W051, W047, W044	W041
	B	Group B2	W002, W010, W018, W016, W015, W014, W049, W041, W046, W020, W047, W045, W033, W032, W005, W053, W012, W026, W007	W051, W047, W045, W018, W041, W020, W005, W010, W046, W014, W044		
	P	Group P2				
C	C	Group C3	W021, W050	W030, W011, W019, W052, W021, W031, W039, W055, W050, W003	**SIMCA** W021, **W050** **Database** W011, W030, **W050**, W052, W021	W050
	B	Group B3	W035, W052, W043, W060, W050, W030, W039, W021, W024, W031, W028, W027, W003, W022, W058, W055	W024, W022, W011, W058, W021, W052, W030, W003, W028, W050		
	PS	Group PS2	W022, W028, W060, W040, W027, W050, W025, W003, W021, W058, W055, W017, W043, W019, W030, W039, W009	W052, W022, W019, W059, W060, W021, W025, W030, W011, W050, W040, W028		
	P	Group P2				
D	C				**SIMCA** **W006**, W043, W060, W039, W021, W028, W058, W055, **Database** **W006**	W006
	B	Group B3	W006, W059, W043, W060, W050, W039, W021, W024, W031, W028, W003, W022, W058, W055	W006		
	PS	Group PS2	W006, W028, W060, W040, W027, W025, W003, W021, W058, W055, W017, W043, W019, W030, W039, W009	W043, W006, W027, W009		
	P	Group P2	-	W006		
E	C	Group C2	W036, W023, W002, W062	W036, W002, W023	**SIMCA** W002, W036, **W023** **Database** W002, **W023**, W036	W023
	B	Group B2	W002, W023, W036, W012, W007, W014	W002, W036, W023		
	P	Group P2				

225

9.6.2. Discriminating power and Inter-sample variability

Similar to the IR analysis, the inter-sample variability revealed from Raman analysis is assessed by examining the chemical categories of the samples and the discriminating power (DP) obtained from analyzing each layer.

Table 55 presents a summary of the discriminating power for each layer, considering both visual comparison and PCA-based separation across the entire sample set of 54 OEM paint samples. The results show that different layers exhibit varying levels of discrimination capability, with the clearcoat showing the highest discriminating power and the primer displaying the lowest. It should be noted that the discriminating power obtained from PCA may differ slightly from that of visual comparison due to the potential uncertainty introduced by baseline variations, as discussed in the previous section. Therefore, visual comparison is primarily relied upon for classification and discrimination analysis.

Table 56 presents an overview of the chemical categories identified from each layer through Raman analysis, including the number of samples assigned to each category. These categories were determined by cross-referencing the identification from the IR analysis to assist in the classification of the Raman spectra, with only the identifiable features listed. Due to the limited diversity in pigment among white automotive paints, the characterization of Raman spectra revealed mainly the resins used in paint samples as well. No additional pigment or extender composition was detected from Raman analysis.

Table 55. Discriminating power of each layer based on visual comparison and PCA (n=54).

Layer type	DP of Visual comparison	Undifferentiated pairs of visual comparison	DP of PCA	Undifferentiated pairs of PCA	Total number of samples
Primer (P)	**10.7%**	1278	-	-	54
Primer surfacer (PS)	**49.5%**	191	**44.4%**	210	28
Basecoat (B)	**76.3%**	339	**78.6%**	306	54
Clearcoat (C)	**88.0%**	172	**80.5%**	278	54

Table 56. Chemical categories identified from each layer by Raman analysis (n=54).

Layer type	Number of classes	Identified chemical class	Number of samples within each class	Total sample number
Primer	1	Fluorescence	1	54
	2	EPY+ALS+TIO2	53	
Primer surfacer	1	Fluorescence	1	28
	2	EPY+ALK IPH+PUR+BAS+TIO2	23	
	3	ALK IPH+TIO2	3	
	4	Uncharacterized binder+BAS+TIO2	1	
Basecoat	1	Fluorescence	1	54
	2	PUR +TIO2	27	
	3	ACR+ALK IPH+TIO2	26	
Clearcoat	1	Fluorescence	1	54
	2	PUR+STY	27	
	3	ACR+PUR+STY	26	

226

Table 57 summarizes the groups of samples that could not be differentiated based on each layer.

Table 57. Groups of samples that could not be differentiated from Raman analysis of each layer.

Layer type	Group No.	Undifferentiated samples
Primer	1	W001, W002, W003, W005, W006, W007, W009, W010, W011, W012, W014, W015, W016, W017, W018,W019, W020, W021, W022, W023, W024, W025, W026, W027, W028, W030, W031, W032, W033, W034, W035, W036, W039, W040, W041, W042, W043, W044, W045, W046, W047, W048, W049, W050, W051, W052, W053, W054, W055, W058, W059, W060, W062
Primer surfacer	1	W009, W011, W017, W019, W021, W022, W024, W025, W027, W028, W030, W031, W040, W043, W050, W052, W055, W058, W059, W060
	2	W003, W039
Basecoat	1	W005, W007, W010, W012, W014, W015, W016, W018, W020, W032, W033, W041, W042, W044, W045, W046, W047, W049, W051, W053, W054
	2	W002, W023, W036
	3	W048, W062
	4	W003, W009, W011, W021, W022, W024, W027, W028, W030, W031, W039, W043, W050, W052, W055, W058
	5	W034, W035
	6	W006, W059
	7	W019, W025, W040
Clearcoat	1	W002, W007, W023, W036, W053
	2	W010, W014, W015, W016, W018
	3	W012, W020, W032 W041, W042, W044, W045, W047, W049, W051, W054
	4	W005, W033, W046
	5	W048, W062
	6	W003, W011, W019, W021, W030, W031, W039, W050, W052, W055
	7	W009, W017, W022, W024, W025, W035, W040, W043, W059, W060
	8	W027, W028, W034

Similar to the FTIR analysis, the discriminating capabilities of different layer combinations were also assessed, and separate evaluations were conducted for Group OEM3 and Group OEM4. The results are summarized in *Table 58*. It is important to note that while the primer analysis did separate the samples into two groups, the resulting discriminating power remains relatively low. Additionally, the separation is primarily driven by differences in the responses to the laser, and therefore, may not comprehensively reflect the samples' chemical characteristics. The primer analysis does not contribute any supplementary discrimination.

Mirroring the trends observed in the overall sample set's discrimination power, both within Group OEM3 and Group OEM4, the combination of basecoat and clearcoat demonstrated the highest discrimination capability in the case of considering only two layers. Remarkably, within Group OEM3, this specific combination proved to be the sole effective choice, given that primer did not yield any additional discrimination potential. This layer combination ultimately resulted in a discriminating power of 77.5% for Group OEM3. The same principle applies to the three-layer combination within Group OEM4. Here, the integration of primer

227

surfacer, basecoat, and clearcoat forms the genuine three-layer combination, yielding the highest discrimination power of 92.1%. This value also represents the ultimate discriminating power derived from the Raman analysis of samples within Group OEM4.

Table 58. Discrimination power of single layer and different layer combination from Raman analysis (n=54)

Layer type	Whole OEM sample set (n=54)		Group OEM3 (n=26)	Group OEM4 (n=28)
	DP (Undifferentiated pairs)	Total number of samples	DP (Undifferentiated pairs)	DP (Undifferentiated pairs)
Primer (P)	**10.7% (1278)**	54	**0% (325)**	7.1% (351)
Primer surfacer (PS)	**49.5% (191)**	28		49.5% (191)
Basecoat (B)	**76.3% (339)**	54	34.2% (214)	66.9% (125)
Clearcoat (C)	**88.0% (172)**	54	**75.7% (79)**	**75.4% (93)**
P+PS	49.5% (191)	28		49.5% (191)
P+B	76.3% (339)	54	34.2% (214)	66.9% (125)
P+C	88.0% (172)	54	75.7% (79)	75.4% (93)
PS+B	74.9% (95)	28		74.9% (95)
PS+C	82.5% (66)	28		82.5% (66)
B+C	**91.8% (117)**	54	**77.5% (73)**	**88.4% (44)**
P+PS+B	74.9% (95)	28		74.9% (95)
P+PS+C	82.5% (66)	28		82.5% (66)
P+B+C	91.8% (117)	54	**77.5% (73)**	88.4% (44)
PS+B+C	**92.1% (30)**	28		**92.1% (30)**
P+PS+B+C	92.1% (30)	28		92.1% (30)
Final DP	**92.8% (103)**	54	**77.5% (73)**	**92.1% (30)**

When considering the discrimination results of all layers, there were a total of 103 pairs of samples that remained undifferentiated. The undifferentiated groups of samples and the corresponding vehicle information are listed in *Table 59*. This indicates that the overall discriminating power achieved from the Raman analysis of the sample set of 54 OEM white VW automotive paint samples was **92.8%** (103 undifferentiated pairs out of 54 samples). **These findings underscore the potential of Raman analysis as an alternative to FTIR for distinguishing automotive paint samples effectively, although it may not be as robust as FTIR**.

After closely examining the vehicle details of the undifferentiated sample pairs, a consistent pattern became evident, aligning with the observations made during the IR analysis. The majority of undifferentiated samples could be traced back to the same manufacturing company (S-VW), even when considering variations in models, production years, and assembly plants (for example, samples in Groups 2, 4, 7, 10).

However, It is important to highlight that Group 3 displayed a different pattern. Here, undifferentiated samples originated from different manufacturing companies, featuring diverse models and color codes, yet sharing non-differentiable basecoat and clearcoat layers. A cross-reference with the IR analysis outcomes further revealed the inability of IR analysis to differentiate the basecoat and clearcoat of these three samples. Sample W005, produced by a different manufacturing company than W033 and W046, could be distinctly differentiated solely through IR analysis of the primer layer.

In conclusion, the Raman analysis conducted in this study confirmed the identified chemical characteristics of the samples, which were consistent with the findings from the IR analysis. Despite the samples belonging to the same manufacturer and color (white), there was significant diversity and inter-sample variability observed within this specific sample set.

Table 59. Properties of undifferentiated sample groups by visual comparison of Raman spectra of all layers

Group No.	Sample No.	Manufacturing company	Model	Production year	Topcoat color code	Assembly plant	Layer structure
1	W002	F-VW	Sagitar	2017	LC9A	Chengdu	OEM3
	W023	F-VW	Sagitar	2017	LC9A	Chengdu	OEM3
	W036	F-VW	Sagitar	2017	LC9A	Chengdu	OEM3
2	W007	S-VW	Santana	2013	LY9H	Nanjing	OEM3
	W053	S-VW	New Lavida	2014	LY9H	Nanjing	OEM3
3	W005	F-VW	Jetta	2014	LB9A	Chengdu	OEM3
	W033	S-VW	New Lavida	2014	LY9H	Nanjing	OEM3
	W046	S-VW	Passat	2013	LY9H	Nanjing	OEM3
4	W010	S-VW	Santana	2017	LY9H	Nanjing	OEM3
	W014	S-VW	New Lavida	2017	LY9H	Anting	OEM3
	W015	S-VW	New Lavida	2017	LY9H	Anting	OEM3
	W016	S-VW	New Lavida	2017	LY9H	Anting	OEM3
	W018	S-VW	New Lavida	2016	LY9H	Anting	OEM3
5	W012	S-VW	New Lavida	2017	LY9H	Nanjing	OEM3
	W020	S-VW	Santana	2016	LY9H	Nanjing	OEM3
	W032	S-VW	Gran Lavida	2015	LY9H	Anting	OEM3
	W041	S-VW	Santana	2017	LY9H	Nanjing	OEM3
	W042	S-VW	New Lavida	2017	LY9H	Anting	OEM3
	W044	S-VW	Passat	2017	LY9H	Nanjing	OEM3
	W045	S-VW	Lamando	2018	LY9H	Ningbo	OEM3
	W047	S-VW	New Lavida	2017	LY9H	Nanjing	OEM3
	W049	S-VW	New Lavida	2016	LY9H	Anting	OEM3
	W051	S-VW	Lamando	2017	LY9H	Ningbo	OEM3
	W054	S-VW	New Lavida	2016	LY9H	Anting	OEM3
6	W048	S-VW	New Lavida	2018	LY9H	Anting	OEM3
	W062	S-VW	New Lavida	2018	LY9H	Anting	OEM3
7	W011	S-VW	Polo	2017	LY9H	Anting	OEM4
	W021	S-VW	Polo	2016	LY9H	Anting	OEM4
	W030	S-VW	Tiguan	2016	LY9H	Anting	OEM4
	W031	S-VW	Tiguan	2017	LY9H	Anting	OEM4
	W050	S-VW	Polo	2012	LY9H	Anting	OEM4
	W052	S-VW	Tiguan	2017	LY9H	Anting	OEM4
	W055	S-VW	Lavida	2014	LY9H	Anting	OEM4
8	W027	S-VW	Passat	2004	Unknown	Anting	OEM4
	W028	S-VW	Passat	2003	LB9A	Anting	OEM4
9	W003	S-VW	Polo	2017	LY9H	Anting	OEM4
	W039	S-VW	Polo	2017	LY9H	Anting	OEM4
10	W009	S-VW	New Lavida	2015	LY9H	Nanjing	OEM4
	W022	S-VW	Touran	2010	LB9A	Anting	OEM4
	W024	S-VW	Tiguan	2012	LB9A	Anting	OEM4
	W043	S-VW	Gran Lavida	2015	LY9H	Anting	OEM4
11	W025	S-VW	Polo	2016	LY9H	Anting	OEM4
	W040	S-VW	Polo	2015	LY9H	Anting	OEM4

9.6.3. Correlation between chemical properties and vehicle information

Figure 139 provides a summary of the correlation between the chemical properties identified from the Raman analysis and the sample groupings based on vehicle information, including manufacturing company, assembly plant, and the layer system. The observed correlations were consistent with those obtained from the IR analysis. However, no additional patterns or correlations were identified specifically from the Raman analysis. Notably, it was observed that a greater number of distinct groups could be distinguished within each assembly plant compared to the findings from the IR analysis. This suggests that the Raman analysis provided additional resolution and discrimination capabilities for identifying variations in the chemical properties within the same assembly plant.
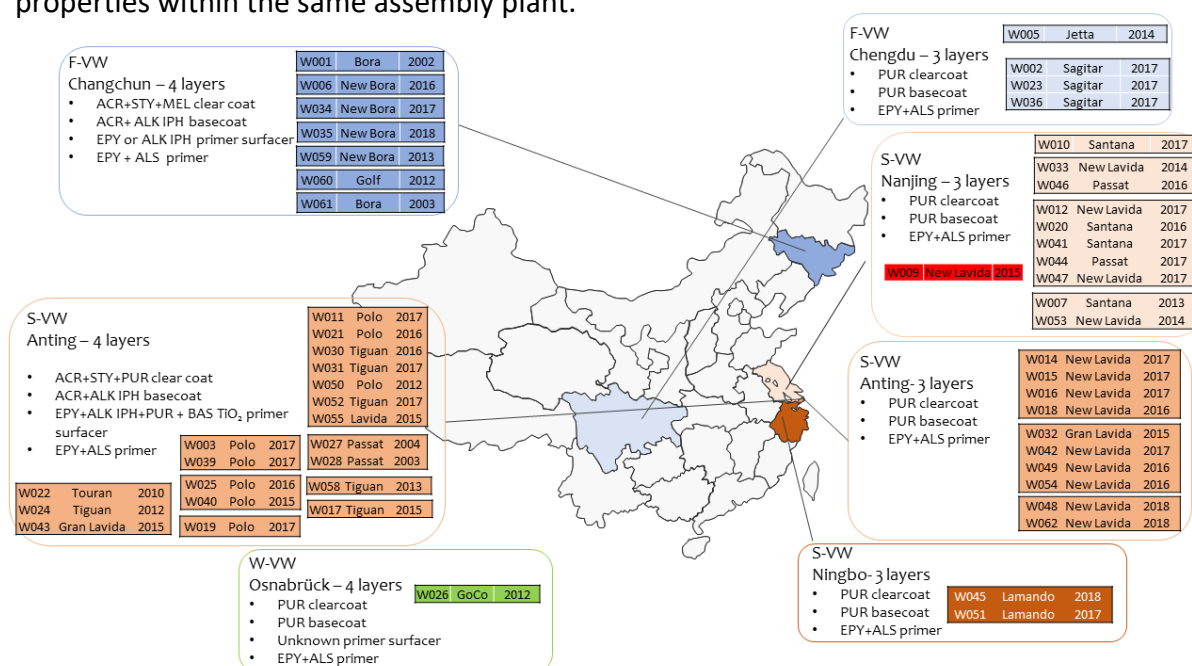
Figure 139. Chemical profiles (Raman) of the entire samples in relation to manufacturing company, assembly plant, and the layer system. Groupings obtained from visual comparison within each plant are listed.

Regarding the topcoat color code, *Table 60* displays the groupings of samples within each topcoat color code group, determined through visual comparison of the basecoat Raman spectra. This analysis was conducted on a subset of 50 OEM paint samples for which the topcoat color code information was available. The results revealed a similar trend to that observed in the IR analysis. While the discriminant power of Raman analysis was slightly lower, it was still able to differentiate samples with the same color code into multiple groups. This indicates substantial variations in the chemical characteristics of the paint samples, even within the context of shared topcoat color codes.

This section mainly discusses the findings from solely Raman analysis. As for the comparison between the results obtained from IR and Raman analysis, as well as the observations derived from combining the findings of both techniques, a detailed discussion will be provided in Chapter 11 of the thesis. Chapter 11 will delve into the similarities, differences, and

complementary aspects of IR and Raman analysis, highlighting their respective strengths and limitations in characterizing the chemical properties of the automotive paint samples.

Table 60. groupings of samples within each topcoat color code group based on Raman analysis of basecoat (n=50)

Topcoat color code	Group No.	Sample No.	Manufacturing company	Model	Production year	Assembly plant	Layer structure
LC9A	1	W002	F-VW	Sagitar	2017	Chengdu	OEM3
	1	W023	F-VW	Sagitar	2017	Chengdu	OEM3
	1	W036	F-VW	Sagitar	2017	Chengdu	OEM3
	2	W006	F-VW	New bora	2016	Changchun	OEM4
	2	W059	F-VW	New bora	2013	Changchun	OEM4
	3	W034	F-VW	New bora	2017	Changchun	OEM4
	3	W035	F-VW	New bora	2018	Changchun	OEM4
	4	W026	W-VW	GoCo	2012	Osnabrück	OEM4
LB9A	1	W005	F-VW	Jetta	2014	Chengdu	OEM3
	2	W060	F-VW	Golf	2012	Changchun	OEM4
	3	W022	S-VW	Touran	2010	Anting	OEM4
	3	W024	S-VW	Tiguan	2012	Anting	OEM4
	3	W058	S-VW	Tiguan	2013	Anting	OEM4
	4	W028	S-VW	Passat	2003	Anting	OEM4
LY9H	1	W007	S-VW	Santana	2013	Nanjing	OEM3
	1	W010	S-VW	Santana	2017	Nanjing	OEM3
	1	W012	S-VW	New Lavida	2017	Nanjing	OEM3
	1	W014	S-VW	New Lavida	2017	Anting	OEM3
	1	W015	S-VW	New Lavida	2017	Anting	OEM3
	1	W016	S-VW	New Lavida	2017	Anting	OEM3
	1	W018	S-VW	New Lavida	2016	Anting	OEM3
	1	W020	S-VW	Santana	2016	Nanjing	OEM3
	1	W032	S-VW	Gran Lavida	2015	Anting	OEM3
	1	W033	S-VW	New Lavida	2014	Nanjing	OEM3
	1	W041	S-VW	Santana	2017	Nanjing	OEM3
	1	W042	S-VW	New Lavida	2017	Anting	OEM3
	1	W044	S-VW	Passat	2017	Nanjing	OEM3
	1	W045	S-VW	Lamando	2018	Ningbo	OEM3
	1	W046	S-VW	Passat	2016	Nanjing	OEM3
	1	W047	S-VW	New Lavida	2017	Nanjing	OEM3
	1	W049	S-VW	New Lavida	2016	Anting	OEM3
	1	W051	S-VW	Lamando	2017	Ningbo	OEM3
	1	W053	S-VW	New Lavida	2014	Nanjing	OEM3
	1	W054	S-VW	New Lavida	2016	Anting	OEM3
	2	W048	S-VW	New Lavida	2018	Anting	OEM3
	2	W062	S-VW	New Lavida	2018	Anting	OEM3
	3	W009	S-VW	New Lavida	2015	Nanjing	OEM4
	3	W011	S-VW	Polo	2017	Anting	OEM4
	3	W021	S-VW	Polo	2016	Anting	OEM4
	3	W030	S-VW	Tiguan	2016	Anting	OEM4
	3	W031	S-VW	Tiguan	2017	Anting	OEM4
	3	W039	S-VW	Polo	2017	Anting	OEM4
	3	W043	S-VW	Gran LAVIDA	2015	Anting	OEM4
	3	W050	S-VW	Polo	2012	Anting	OEM4
	3	W052	S-VW	Tiguan	2017	Anting	OEM4
	3	W055	S-VW	Lavida	2014	Anting	OEM4
	4	W019	S-VW	Polo	2017	Anting	OEM4
	4	W025	S-VW	Polo	2016	Anting	OEM4
	4	W040	S-VW	Polo	2015	Anting	OEM4
	5	W017	S-VW	Tiguan	2015	Anting	OEM4

10. Characterization and classification with Py-GC/MS

As mentioned previously, this chapter was summarized from a master project.

During the IR analysis of the basecoat samples, it was observed that among the 26 samples with an OEM3 layer system, all of them contained polyurethane basecoat. However, 23 of these samples could not be differentiated using FTIR analysis, indicating limited discrimination power. Raman analysis also did not provide significant additional discrimination, as 21 of the samples remained undifferentiated. To further enhance the discrimination capabilities, Pyrolysis-GC/MS analysis was performed on these samples following the strategy outlined in Chapter 6.5.

This chapter will present the analysis results obtained from Pyrolysis-GC/MS, showcasing the chemical information and discrimination capabilities provided by this technique. The obtained chromatograms and mass spectra will be analyzed and interpreted to identify key compounds and chemical markers that can differentiate between the samples. The discussion will also address the challenges and limitations encountered during the Pyrolysis-GC/MS analysis of the paint samples.

10.1. Sample set

Basecoat samples from 23 vehicles with an OEM3 layer system, which were undifferentiated in the IR analysis, were selected for pyrolysis GC/MS analysis. The sample information for this group is provided in *Table 61*. This represents the largest undifferentiated group of samples even after Raman analysis.

By focusing on the basecoat layer, further exploration of the correlation between topcoat color code and chemical characteristics can be conducted. In this group, all the samples were found to contain polyurethane as the primary binder, with isophthalic resin serving as an additional resin in the basecoat formulation.

The pyrolysis GC/MS analysis of these samples aims to identify and analyze the pyrolysis products, providing detailed information about the chemical compounds present in the basecoat layer.

Table 61. Sample set involved in pyrolysis GC/MS analysis and vehicle information.

Sample No.	Company	Model	Production year	Topcoat color code	Assembly plant
W002	F-VW	Sagitar	2017	LC9A	Chengdu
W005	F-VW	Jetta	2014	LB9A	Chengdu
W010	S-VW	Santana	2017	LY9H	Nanjing
W012	S-VW	New Lavida	2017	LY9H	Nanjing
W014	S-VW	New Lavida	2017	LY9H	Anting
W015	S-VW	New Lavida	2017	LY9H	Anting
W016	S-VW	New Lavida	2017	LY9H	Anting
W018	S-VW	New Lavida	2016	LY9H	Anting
W020	S-VW	Santana	2016	LY9H	Nanjing
W023	F-VW	Sagitar	2017	LC9A	Chengdu
W032	S-VW	Gran Lavida	2015	LY9H	Anting
W033	S-VW	New Lavida	2014	LY9H	Nanjing
W036	F-VW	Sagitar	2017	LC9A	Chengdu
W041	S-VW	Santana	2017	LY9H	Nanjing
W042	S-VW	New Lavida	2017	LY9H	Anting
W044	S-VW	Passat	2017	LY9H	Nanjing
W045	S-VW	Lamando	2018	LY9H	Ningbo
W046	S-VW	Passat	2013	LY9H	Nanjing
W047	S-VW	New Lavida	2017	LY9H	Nanjing
W049	S-VW	New Lavida	2016	LY9H	Anting
W051	S-VW	Lamando	2017	LY9H	Ningbo
W053	S-VW	New Lavida	2014	LY9H	Nanjing
W054	S-VW	New Lavida	2016	LY9H	Anting

10.2.   Results and discussion

The 23 samples that initially showed indistinguishable basecoat by FTIR analysis were prepared and measured using Py-GC/MS with the optimized experimental parameters. Three replicates were performed for each sample to assess the intra-sample variability and ensure reliable results. During the analysis, the sample cups were placed in the autosampler of the pyrolyzer, with an empty cup inserted between each sample as a blank run to account for any potential background signals or contamination.

10.2.1.   Intra-sample variability

To evaluate the intra-sample variability, the pyrograms of each sample were visually compared within the replicates. It should be noted that intra-variability between the three replicates of the same sample were rarely observed. When such variabilities did emerge, they usually pertained to variations in relative intensities, or the presence/absence of a peak situated closely to the background. Six samples demonstrated this type of intra-sample variability. *Figure 140* provides an illustration of intra-sample variability attributed to the presence or absence of a peak in close proximity to the background, as observed in Sample W044.
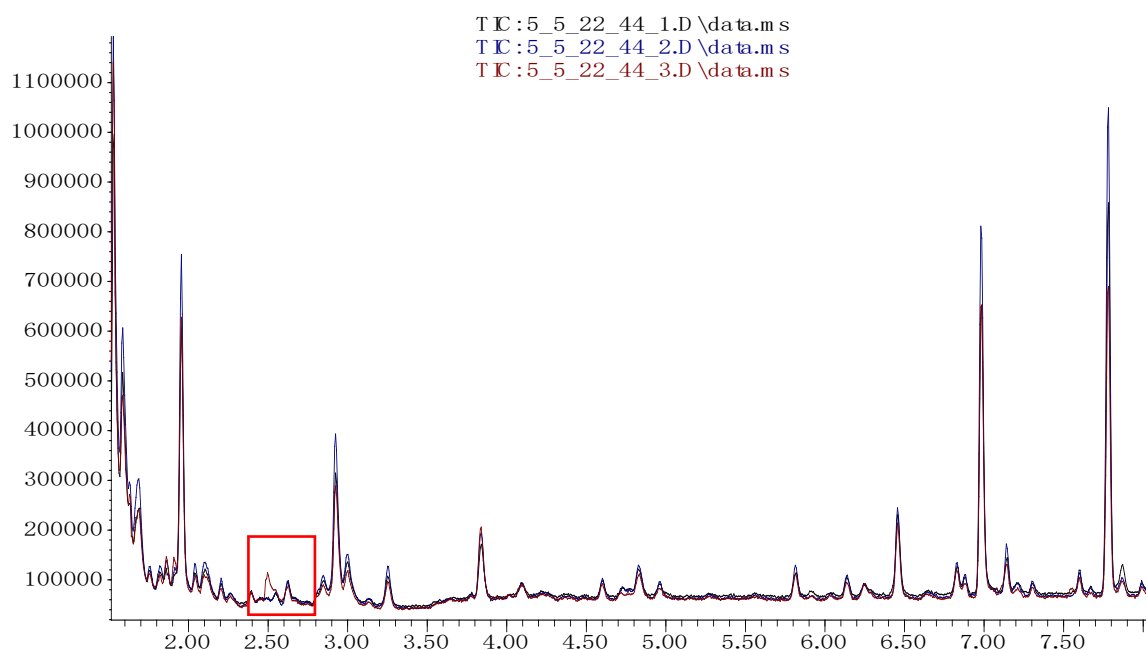
Figure 140. Three pyrograms of sample W044, showing the intra-sample variability which is marked in rectangular.

A single sample (W046) exhibited significant intra-sample variability in one of its three replicates. As depicted in *Figure 141*, in one of the replicates of Sample W046, a prominent peak emerged around 5.00 minutes, whereas this peak was absent in the pyrograms of the other replicates. Notably, the peaks differing among the replicates did not align with the peaks observed in the pyrogram of the mounting resin used to embed the analyzed paint.
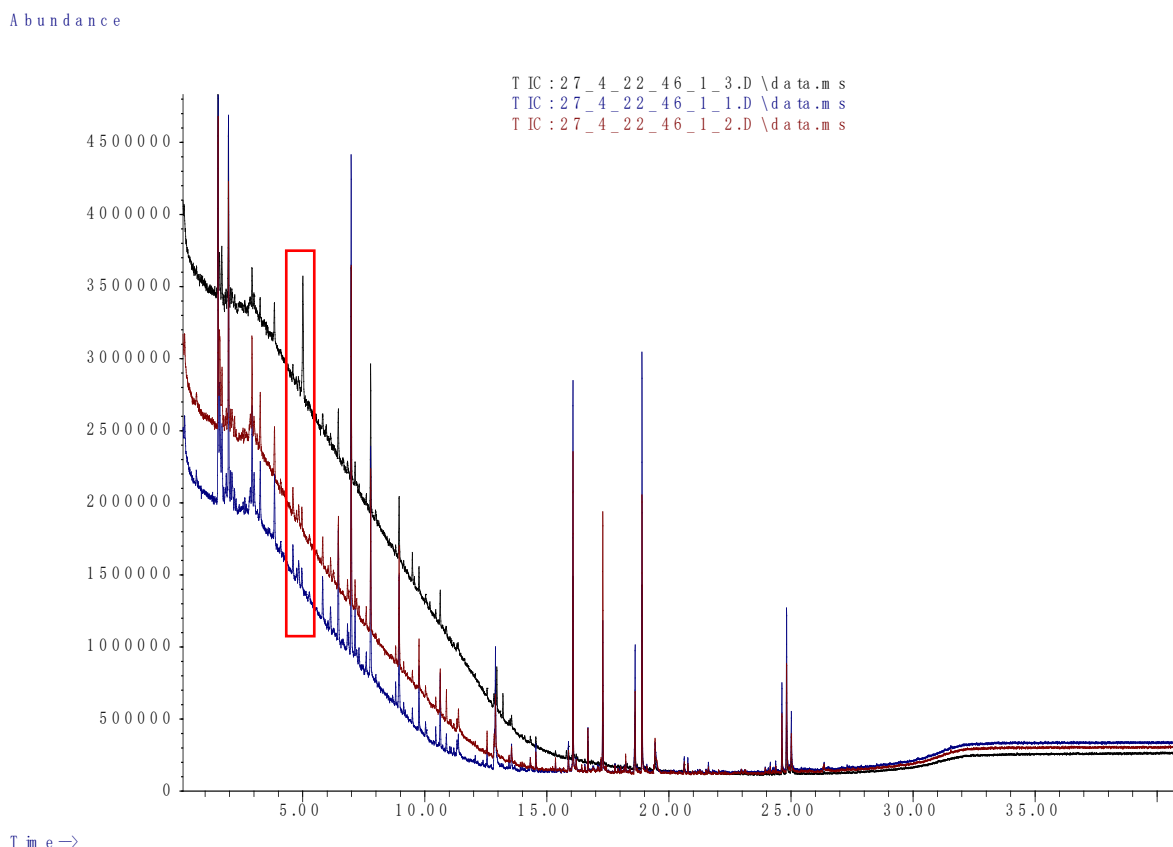
Figure 141. Three pyrograms of sample W046, showing the intra-sample variability which is marked in rectangular.

In the context of the existing intra-sample variability, when comparing samples, if the three replicates exhibited no notable variability, a single representative pyrogram was chosen for further comparison with other samples. Conversely, if the replicates displayed noticeable variation, all three were retained for inter-sample comparison. Any variations observed in the inter-sample comparison were deemed significant only when all three replicates distinctly deviated from the pyrograms of other samples.

In addition to this, statistical techniques, specifically PCA, were employed to visualize the structure of the data and identify patterns within the dataset. The pyrogram data were extracted in 3D (similar to the approach used for reference samples), and values attributed to light ions, particularly those originating from the air, were eliminated to enhance data quality. The outcomes of these analyses will be elaborated upon in the subsequent chapter.

10.2.2. Identification of compound and visual comparison

In *Figure 142*, a typical pyrogram obtained from the analysis is displayed, showcasing the main peaks observed. The mass spectra of these peaks were identified using the NIST17 Mass Spectral Library, which is a valuable resource for compound identification. Visual comparisons were conducted by overlaying the pyrograms and examining the presence or absence of specific peaks.

Table 62 provides a comprehensive list of the peaks observed in the 23 samples, along with the identification of compounds based on the NIST17 database. Up to 95 compounds were found in the chromatographic pattern obtained from the samples. It is worth noting that several compounds could not be conclusively identified using the database and are labeled as "unknown." However, some of these unknown compounds play a significant role in distinguishing one sample from another, highlighting their importance in the analysis. These differences serve as distinguishing factors that contribute to the unique characteristics of each sample. *Table 63* presents the summary of the visual groupings conducted between samples, based on the differences observed and outlined in *Table 62.*
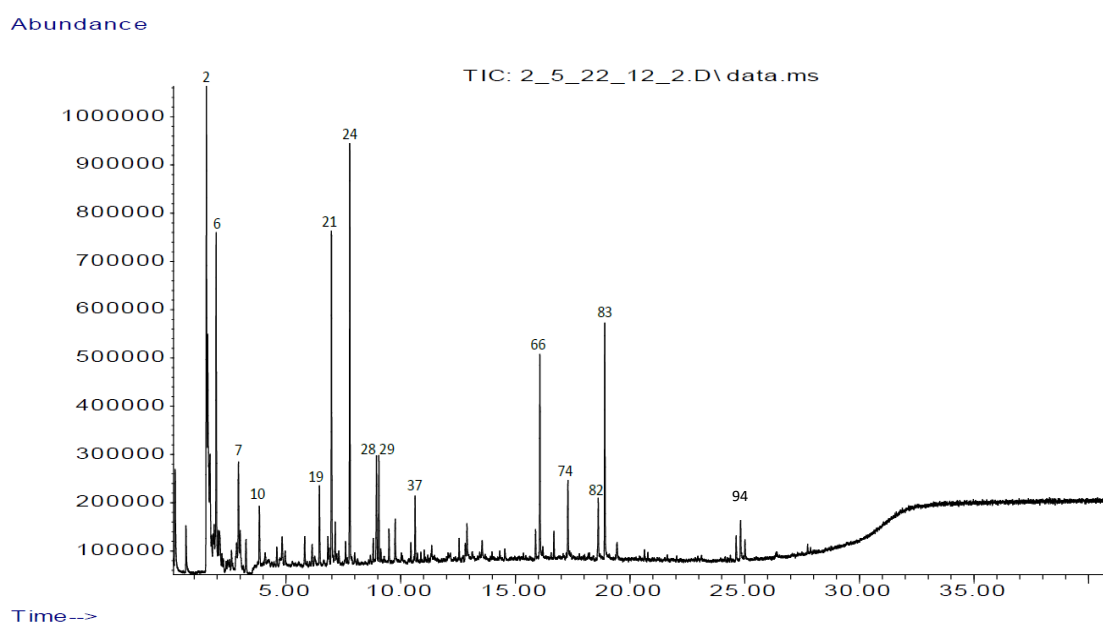
Figure 142. representative pyrogram of sample W012, with main peaks marked on the pyrogram. The identification of these peaks is presented in Table 62.

Table 62. List of Compounds Identified in the Samples.

n°	Rt	Compound (Qual NIST 17)	W002	W005	W010	W012	W014	W015	W016	W018	W020	W023	W032	W033	W036	W041	W042	W044	W045	W046	W047	W049	W051	W053	W054
1	0.16	unknown																							
2	1.53	unknown																							
3	1.59	1-propene, 2-methyl- (87)																							
4	1.69	unknown																							
5	1.87	unknown																							
6	1.96	unknown																							
7	2.92	1-butanol (90)																							
8	3.00	benzene (91)																							
9	3.26	unknown																							
10	3.84	2-propenoic acid, 2-methyl- , methyl ester (94)																							
11	4.10	unknown																							
12	4.60	unknown																							
13	4.73	2-propenoic acid, 2-methyl- (81)																							
14	4.84	unknown																							
15	4.96	unknown																							
16	5.81	unknown																							
17	6.14	oxepane (83)																							
18	6.25	unknown	x	x							x	x		x	x				x	x	x	x	x	x	
19	6.46	cyclopentanone (91)																							
20	6.83	unknown																							
21	6.99	ethylidenecyclobutane (80)																							
22	7.15	unknown																							
23	7.60	2-propenoic acid, butyl ester (83)																							
24	7.78	styrene (94) or 1,3,5,7-cyclooctatetraene (94)																							
25	8.63	hexanal, 2-ethyl- (80)		x	x	x	x	x	x	x		x	x	x	x	x	x	x	x	x	x	x	x		x
26	8.69	benzene (90)		x										x						x			x		
27	8.81	unknown																							
28	8.94	unknown																							
29	9.06	2-propenoic acid, 2-methyl-, butyl ester (83)		x										x						x					
30	9.13	unknown																							
31	9.50	alpha-methylstyrene (81)																							
32	9.76	unknown																							
33	10.03	benzaldehyde (87)																							
34	10.18	unknown		x	x	x	x	x	x	x		x	x		x	x	x	x	x	x	x	x	x		x
35	10.36	unknown		x	x	x	x	x	x	x		x	x		x	x	x	x	x	x	x	x	x		x
36	10.45	benzene, 3-butenyl- (86)																							
37	10.63	benzonitrile (91) or tricyclo-hex-3-ene-3-carbonitrile (91)																							
38	10.74	benzene (90)																							
39	10.80	unknown		x	x	x	x	x	x			x			x	x	x	x		x	x	x			x
40	10.88	unknown																							
41	11.02	benzene, 1-ethynyl-4-methyl- (86)																							
42	11.19	unknown																							
43	11.32	unknown																							
44	11.36	unknown																							
45	11.47	unknown		x	x	x	x	x	x	x		x	x		x	x	x	x	x				x		x
46	11.54	unknown		x	x	x		x	x	x		x			x	x	x	x			x	x	x	x	x
47	12.07	unknown							x	x															
48	12.55	benzylisocyanate (95)																							
49	12.73	unknown																							
50	12.83	benzoic acid (90)							x	x															
51	12.90	unknown																							
52	13.12	ethanol, 2-(2-butoxyethoxy)- (90)	x	x		x	x	x	x	x	x	x	x	x	x	x	x				x		x	x	x
53	13.45	unknown																							
54	13.56	unknown																							
55	13.69	unknown							x	x															
56	13.85	dimethylbenzonitrile (94)			x	x	x	x	x	x		x			x	x	x	x	x	x	x	x	x		x
57	13.92	unknown							x	x															
58	13.98	unknown							x	x															
59	14.33	benzene, 1-methylethenyl- (91)							x	x					x					x					
60	14.35	unknown	x	x		x					x	x	x	x		x	x			x	x	x	x		x
61	14.54	unknown																							
62	15.24	benzene, 1,2,3,5-tetramethyl- (80)		x	x	x	x	x	x	x		x	x		x	x	x	x	x	x	x				x
63	15.36	unknown							x	x															
64	15.40	unknown		x	x	x	x	x	x	x		x	x	x	x	x	x	x	x	x	x	x	x		x
65	15.86	unknown																							
66	16.07	hexane, 1,6-diisocyanato- (90)																							
67	16.20	1,3-benzenedicarbonitrile (81)																							
68	16.43	unknown	x		x	x	x	x	x	x	x	x	x		x	x	x	x	x		x	x	x	x	x
69	16.56	naphthalene, 2-ethenyl- (81)																							

237

No	Rt	Compound	1	2	3	4	5	6	7	8	9	10	11	12	13	14	15	16	17	18	19	20	21	22	23
70	16.68	phthalic anhydride (94)																							
71	17.08	unknown																							
72	17.12	unknown																							
73	17.21	unknown																							
74	17.29	cyclohexene (87)																							
75	17.79	unknown	x			x	x	x	x	x	x		x			x			x			x	x		
76	17.91	unknown		x	x	x	x	x	x	x		x		x	x	x	x	x				x			x
77	17.96	unknown																							
78	18.03	unknown						x	x																
79	18.18	unknown						x	x																
80	18.23	unknown						x	x																
81	18.40	unknown						x	x																
82	18.61	cyclohexane, 5-isocyanato-1-(isocyanatomethyl)-1,3,3-trimethyl- (90)						x	x																
83	18.90	cyclohexane, 5-isocyanato-1-(isocyanatomethyl)-1,3,3-trimethyl- (83)																							
84	19.43	unknown																							
85	20.63	unknown																							
86	20.77	unknown											x												
87	20.98	1-hexadecene (89)		x	x	x	x	x	x	x		x	x		x	x	x					x	x	x	x
88	21.62	unknown						x	x																
89	21.83	unknown	x	x	x	x	x	x	x			x	x		x	x	x	x	x	x	x	x			x
90	22.04	1,2-benzenedicarboxylic acid (83)																							
91	22.97	pentafluoropropionic acid, 4-hexadecyl ester (91)		x					x															x	
92	23.12	unknown		x																					
93	24.63	unknown											x												
94	24.82	unknown											x												
95	25.01	unknown											x												

Note: "Rt" refers to the retention time of each compound. The compound names provided are the result of a search in the NIST17 database. The "Qual" column indicates the comparison value assigned by NIST17. Columns 3-25 indicate the presence or absence of the corresponding peak or compound in each sample. Absence of the peak is marked with 'x' in the table.

Table 63. Summary of visual groupings based on the pyrograms of the basecoat of the samples in this sample set (n=23).

Group	Sample No.	Company	Model	Production year	Topcoat color code	Assembly plant
1	W002	F-VW	Sagitar	2017	LC9A	Chengdu
	W023	F-VW	Sagitar	2017	LC9A	Chengdu
2	W005	F-VW	Jetta	2014	LB9A	Chengdu
	W033	S-VW	New Lavida	2014	LY9H	Nanjing
	W046	S-VW	Passat	2013	LY9H	Nanjing
3	W014	S-VW	New Lavida	2017	LY9H	Anting
	W015	S-VW	New Lavida	2017	LY9H	Anting
4	W016	S-VW	New Lavida	2017	LY9H	Anting
	W018	S-VW	New Lavida	2016	LY9H	Anting
5	W047	S-VW	New Lavida	2017	LY9H	Nanjing
	W049	S-VW	New Lavida	2016	LY9H	Anting
6	W012	S-VW	New Lavida	2017	LY9H	Nanjing
	W032	S-VW	Gran Lavida	2015	LY9H	Anting
	W041	S-VW	Santana	2017	LY9H	Nanjing
	W042	S-VW	New Lavida	2017	LY9H	Anting
	W054	S-VW	New Lavida	2016	LY9H	Anting
7	W036	F-VW	Sagitar	2017	LC9A	Chengdu
8	W020	S-VW	Santana	2016	LY9H	Nanjing
9	W045	S-VW	Lamando	2018	LY9H	Ningbo
10	W010	S-VW	Santana	2017	LY9H	Nanjing
11	W044	S-VW	Passat	2017	LY9H	Nanjing
12	W051	S-VW	Lamando	2017	LY9H	Ningbo
13	W053	S-VW	New Lavida	2014	LY9H	Nanjing

By analyzing the grouping results in *Table 63*, it is observed that there are 17 pairs of samples that could not be differentiated from each other, resulting in a discriminating power of 93.3% (17 undifferentiated pairs out of 23 samples).

Upon examining the vehicle information of the undifferentiated sample pairs, a noticeable pattern emerged across six undifferentiated sample groups. Among these groups, the majority of undifferentiated sample pairs (for instance, those in Groups 1, 3, 4) were manufactured within the same assembly plant, during the same or similar production years, and had identical topcoat color codes. Likewise, samples in Group 5 and 6 shared the same manufacturing company (S-VW), despite variations in models, production years, or assembly plants. However, an interesting observation arises in Group 2. Despite their undifferentiated nature, these three samples have remarkably distinct origins, originating from different manufacturing companies, featuring diverse models, assembly plants, and topcoat color codes.

Conversely, upon reviewing the vehicle information of distinguishable samples, it was found that samples which initially shared indistinguishable vehicle information could indeed be differentiated through Py-GC/MS analysis. This phenomenon is illustrated in *Figure 143*, wherein the pyrograms of the basecoat for both Sample W002 and Sample W036 are displayed. Notably, these two samples, which remained undifferentiated through IR or Raman analysis, share identical origins, including the manufacturer, assembly plant, production year, and topcoat color code. However, their pyrograms showcase a pronounced dissimilarity.
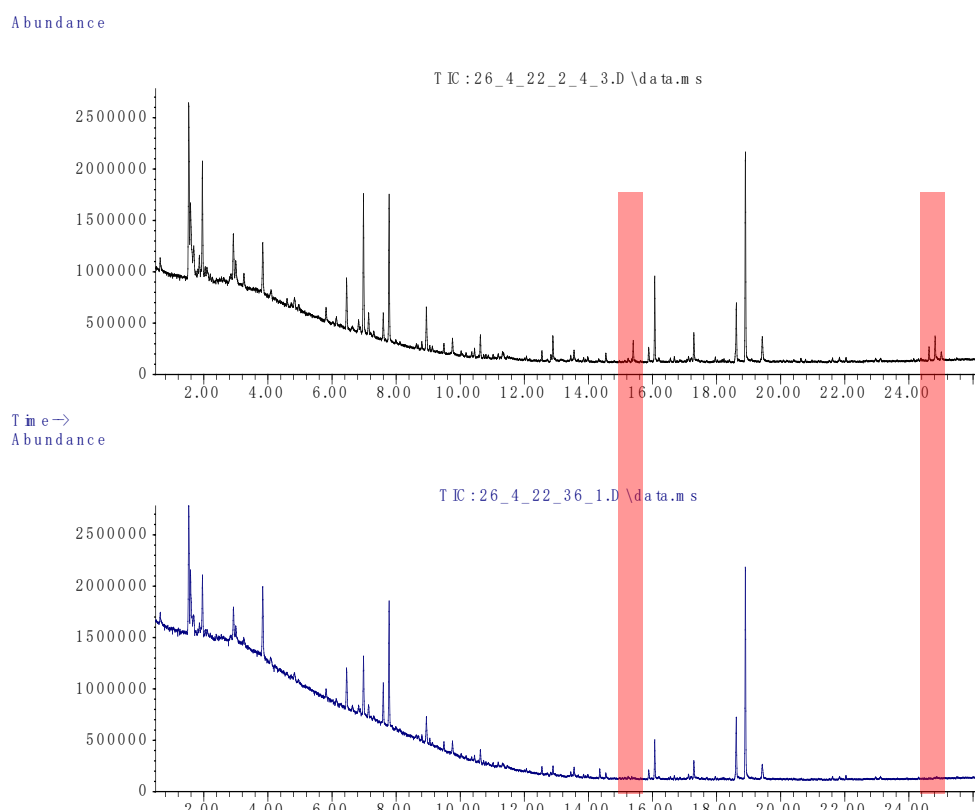
Figure 143. Pyrograms of basecoat of Sample W002 (top) and Sample 036 (bottom). The observed differences are highlighted in red.

239

10.2.3.   Exploratory analysis

The pyrogram data underwent a 3D extraction process to eliminate the influence of light ion values, particularly those originating from air entry. This extraction involved removing the light ion values and recalculating the sum of the abundances for each non-deleted ion at every data point. The dataset was then normalized using the area sum and subjected to a double square root transformation as a preprocessing step for statistical analysis. PCA was subsequently conducted on the normalized data. Groupings related to the identifying factors such as plant, model, and topcoat color code were examined to investigate whether any discernible patterns could be identified based on these factors.

Figure 144 provides an overview of the PCA model generated from the dataset, displaying the projections of pyrograms based on the first two principal components, which account for 95% of the total variance, highlighted by individual sample number (*Figure 144a*), assembly plants (Figure 144*b*), topcoat color codes *(*Figure 144*c*), and vehicle models (*Figure 144d*).
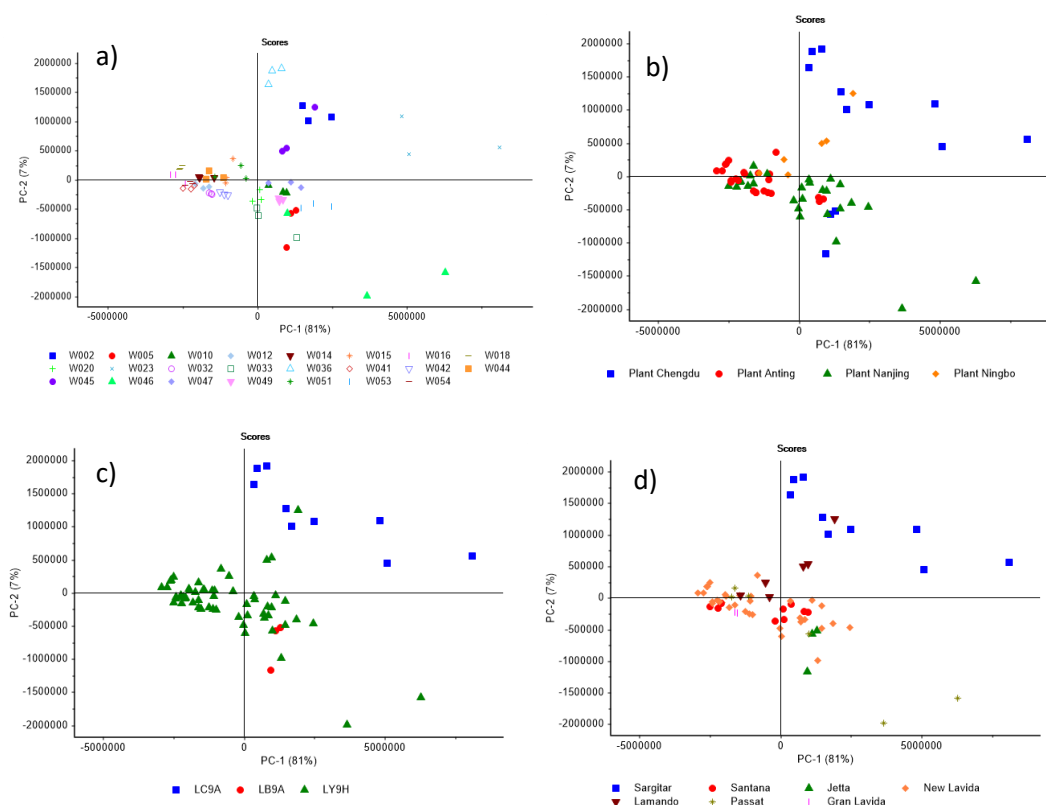
Figure 144. PCA score plots according to the first two principal components of pyrograms of basecoat (n=23), respectively highlighted by their individual sample number (a), their assembly plant (b), their topcoat color codes (c), and the model of vehicles (d).

240

The repeatability of the pyrograms between replicates is an important observation and indicates the consistency of the analytical method. In this study, the pyrograms of the three replicates of the same sample show no major visual differences, it suggests that the analysis is producing consistent and reproducible results for that particular sample. This is further supported by the close projections of the three replicates in the PCA scatter plot. However, it is worth noting that some samples exhibit significant intra-sample variability, where the projections of the three replicates are far away from each other in the PCA plot. This variability could be attributed to the differences in the relative intensities or in the presence/absence of a peak very close to the background.

The observation that three samples with a different color code (LC9A) are clearly separated from the rest of the cluster in the PCA model suggests that there is a distinct chemical composition associated with these specific color codes (*Figure 144c*). On the other hand, the lack of a discernible pattern related to assembly plants or vehicle models suggests that these factors may have a minimal influence on the chemical composition of the paint samples in this study.

It is important to note that the PCA analysis conducted on the whole dataset without pre-selecting the variables may not fully capture the observed differences obtained from visual comparison. In order to optimize the analysis and consider the relevance of each compound, a selection of variables should be performed by examining the correlation of the variables using loading plots and considering the coefficient of variations for each compound. However, due to time limitations, this step was not completed in the scope of this study.

Indeed, even though the PCA model may not be optimized for further discrimination, it can still provide valuable insights into the chemical properties of the sample set. The patterns observed in the PCA plot can help in gaining a deeper understanding of the relationships and similarities among the samples based on their chemical profiles.

While additional analyses and variable selection techniques could enhance the discrimination capabilities, the initial patterns observed in the PCA model can serve as a starting point for further investigations and discussions.

Analyzing and identifying automotive paint using Py-GC/MS is indeed a challenging task, and further research can be conducted to delve deeper into this topic. While this thesis did not explore the full extent of this direction, it provides a foundation for future projects to expand upon.

10.2.4. Blind test

In this study, two samples were chosen at random, and blind test was performed on both samples using the same protocol for validation. To gain a better understanding of the data and its potential distribution, PCA projection was initially employed, and the results are visually represented in *Figure 145*. This visualization allowed for an initial exploration of the data's underlying patterns and variations.

Subsequently, LDA was employed as a classification technique to further investigate the samples. The results of this analysis are presented in *Table 64*. It is noteworthy that while the predictive potential of the model was relatively lower, it is still significant that all the samples were correctly classified.

These results demonstrate the potential utility of Py-GC/MS in characterizing and further discriminating automotive paint samples. Further refinement and optimization of the variable selection could potentially enhance its predictive capabilities in future studies.
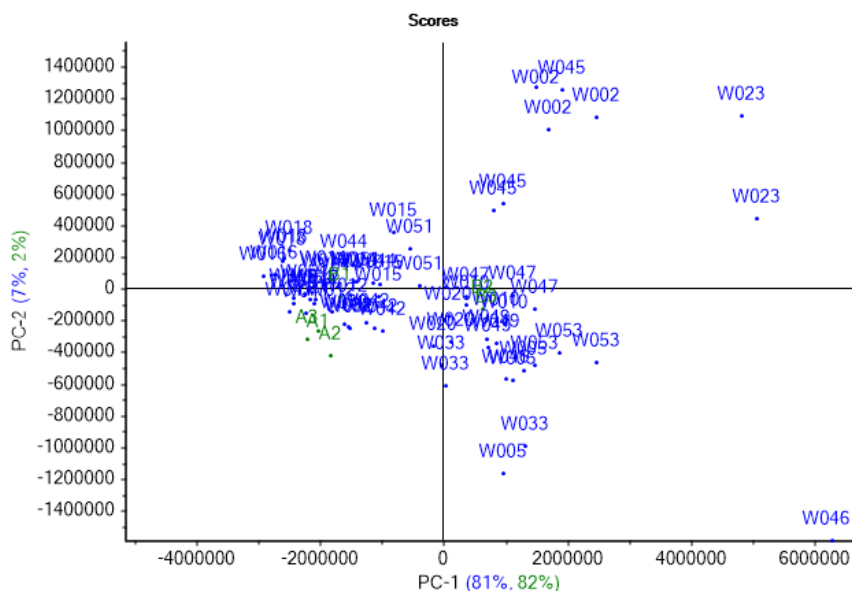
Figure 145. PCA projections for blind test samples (in green).

Table 64. Blind test results from LDA for 2 unknown samples.

SAMPLE	LDA CLASSIFICATION (PREDICTIVE POTENTIAL)	ACTUAL SAMPLE
A	W005(56%), W033(21.5%), W014(20.5%)	W033
B	W047(50.6%), W010(32%), W049 (17%)	W047

10.2.5.   Discussion

The Py-GC/MS analysis conducted within the scope of this study has demonstrated its utility as a powerful tool for characterizing and discriminating white basecoats. This capability is particularly pronounced in cases where FTIR and Raman spectroscopy exhibit limited discriminating power. Nevertheless, the achievement of reproducible and reliable results through Py-GC/MS analysis demanded a substantial investment of effort. The determination of optimal sample preparation methods and experimental parameters specific to each paint type required extensive experimentation and diligence.

As discussed in chapter 6.5.1.2, the isolation of the basecoat from a multi-layer system, particularly when the layer was exceedingly thin and closely resembled adjacent layers in color, posed an exceeded challenge. In practical terms, this practical challenge must be factored into the analytical process, given that the enhanced discriminatory capabilities of Py-GC/MS may be difficult to achieve if the quantity and quality of the sample, as well as the timeframe, do not permit for a robust analysis.

Another issue that emerged during the analysis pertains to the air entry into some of the samples. This phenomenon not only affects visual comparisons but also presents a notable impact on statistical analyses. Consequently, it becomes imperative to devise a strategy to mitigate the influence. The adoption of a 3D data extraction approach, on the one hand, facilitates the removal of ions originating from the air, thereby enabling a more precise comparison of the information derived solely from the samples themselves. However, it should be noted that this approach leads to larger data files and a long data processing duration.

Upon examination of the discrimination outcomes, it was observed that samples sharing a common origin could be effectively distinguished through the application of Py-GC/MS analysis. This subtle differentiation, which is uniquely unveiled through Py-GC/MS analysis, primarily arises from batch variation. Nevertheless, it is noteworthy that despite the comprehensive differentiation capacity of Py-GC/MS, there were instances where three samples, each originating from distinct manufacturing companies, featuring diverse models, assembly plants, and topcoat color codes, remained indistinguishable following Py-GC/MS analysis.

11. General discussion

In this chapter, the discussion will address any unique insights or additional information that emerged from combining all the analytical results, providing a comprehensive understanding of the paint samples' physical and chemical characteristics. Only OEM paint samples were considered in this chapter.

11.1. Comparison of IR and Raman analysis results

Traditionally, IR and Raman analysis have been utilized to investigate the composition of samples from different perspectives. IR analysis is primarily employed for the characterization and identification of binders and additives used in paint, while Raman analysis focuses more on the pigments and extenders present in the paint. However, in the context of this study, which specifically focuses on white-colored samples, there may be limited information about the pigments available for Raman detection and identification. As such, it is crucial to conduct a comparison between IR and Raman analysis individually to ascertain the type of information that can be obtained from each technique. This comparative analysis will aid in understanding the strengths and limitations of each method.

Table 65 offers a comprehensive overview of the chemical composition attributed to each layer, as determined through the application of FTIR and Raman technique. Both IR and Raman analysis can provide valuable insights into the composition of the samples from similar aspects, including the binders, pigments, and extenders, with FTIR offering a more detailed identification. It is worth noting that while Raman analysis is based on the results of FTIR identification, it can still reveal additional compositional information that may have been missed initially. For instance, the Raman spectra of the primer surfacer layer consistently indicated the presence of isophthalic alkyd, which was not initially identified in all FTIR spectra. Upon revisiting the FTIR spectra, it was discovered that isophthalic alkyd resin was indeed present in the majority of primer surfacer, but its identification may have been overlooked due to other abundant peaks information from other components. Therefore, Raman analysis could complement the chemical profile obtained from FTIR analysis, serving as a confirmation tool. However, no additional binders, pigments, or extenders were detected through Raman analysis that were not already identified in the FTIR spectra.

Table 65. Comparison of chemical composition of each layer identified from FTIR and Raman

Layer type	Class No.	Identified chemical class from FTIR	Identified chemical class from Raman
Primer	1	EPY+ALS	EPY+ALS+TIO2
	2	EPY	
Primer surfacer	1	EPY+PUR+MEL+TALC+BAS+TIO2	EPY+ALK IPH+PUR+BAS+TIO2
	2	ALK IPH+EPY+MEL+TALC+TIO2	ALK IPH+TIO2
	3	ALK IPH+PUR+EPY+TALC+ALS+TIO2	Uncharacterized binder+BAS+TIO2
	4	ALK IPH+MEL+TALC+TIO2	
	5	ALK TER+ACR+MEL+BAS+TIO2	
Basecoat	1	PUR+ALK IPH+TALC+TIO2	PUR +TIO2
	2	PUR+MEL+TIO2	ACR+ALK IPH+TIO2
	3	ACR+ALK IPH+MEL+PUR+TIO2	
	4	ACR+PUR+MEL+TALC+TIO2	
Clearcoat	1	PUR+(STY)	PUR+STY
	2	ACR+MEL+STY+ PUR	ACR+PUR+STY

Table 66 provides a comparison of the discriminating power (DP) of FTIR and Raman analysis for different layers and layer combinations in 54 OEM automotive paint samples as well as a separated evaluation for Group OEM3 and Group OEM4. The DP values represent the ability of each technique to differentiate between samples based on their composition. The results were obtained from visual comparison.

When considering individual layers, both FTIR and Raman techniques demonstrate comparable performance in distinguishing clearcoat, basecoat and primer surfacer. Clearcoat stands out as the layer with the highest discrimination capability when analyzed using Raman analysis, even higher than that of using IR analysis. This finding was consistent with the study by Maric *et al.*, where they demonstrated that Raman spectroscopy is more discriminating than IR spectroscopy for analyzing automotive clearcoats (Maric *et al.*,2016). However, the discrimination power of primer surfacer is relatively low for both FTIR and Raman techniques. This limitation can be attributed to the limited sample size and the lack of diversity in the sample origin, as the majority of the samples were produced in the same plant. IR and Raman techniques exhibit notably differing discrimination capabilities when applied to primer analysis. IR analysis yields a high discriminating power (DP) of 82.0%, while Raman analysis provides only a marginal 10%. Raman's low discrimination capability for primer primarily stems from the poor quality of spectra and the limited information they convey. Consequently, for effective primer discrimination, IR analysis is the preferred choice. Conversely, Raman proves to be more potent in differentiating the clearcoat layer.

Moving on to layer combinations, it can be seen that the discrimination power varies depending on the specific combination. However, It is generally observed that IR analysis offers superior discriminatory capability compared to Raman analysis.

Table 66. *Comparison of discriminating power of IR and Raman analysis of each layer and layer combination for OEM sample set (n=54)*

Single layer/ Layer combination	Whole sample set (n=54)			Group OEM3 (n=26)		Group OEM4 (n=28)	
	DP of FTIR	DP of Raman	Total number of samples	DP of FTIR	DP of Raman	DP of FTIR	DP of Raman
P	**82.0%**	10.7%	54	73.5%	0	**72.8%**	7.1%
PS	33.1%	**49.5%**	28			33.1%	**49.5%**
B	**80.6%**	76.3%	54	22.1%	**34.2%**	**93.7%**	66.9%
C	84.4%	**88.0%**	54	61.8%	**75.7%**	75%	**75.4%**
P+PS	75.9%	49.5%	28			75.9%	49.5%
P+B	**94.6%**	76.3%	54	80.6%	34.2%	**96.3%**	66.9%
P+C	93.7%	88.0%	54	**83.1%**	75.7%	90.7%	75.4%
PS+B	93.9%	74.9%	28			93.9%	74.9%
PS+C	78.0%	82.5%	28			78.0%	82.5%
B+C	90.4%	**91.8%**	54	63.7%	77.5%	94.7%	**88.4%**
P+PS+B	96.3%	74.9%	28			96.3%	74.9%
P+PS+C	90.7%	82.5%	28			90.7%	82.5%
PS+B+C	95.0%	**92.1%**	28			95.0%	**92.1%**
P+B+C	**95.4%**	91.8%	54	83.4%	**77.5%**	**96.8%**	88.4%
P+PS+B+C	**96.8%**	92.1%	28			**96.8%**	92.1%
Final DP (pairs)	**95.4% (66)**	**92.8% (103)**	**54**	**83.4% (54)**	**77.5% (73)**	**96.8% (12)**	**92.1% (30)**

Overall, both IR and Raman analysis demonstrate comparable capabilities in characterizing and distinguishing OEM automotive white paint samples. Each technique can effectively differentiate the individual layers of automotive paint, with IR offering a slightly better discriminating result. This study demonstrated Raman spectroscopy can serve as an alternative to FT-IR for discrimination of white automotive paint. However, the combination of both techniques might provide a more comprehensive chemical profile of the automotive paints and enhance the certainty of identification. By utilizing both IR and Raman analysis, a more robust and reliable characterization of the paint samples can be achieved.

11.2. Combination of IR and Raman analysis results

As previously mentioned, the combination of FTIR and Raman analysis provides a more comprehensive chemical profile of automotive paints. In this section, the chemical profiles of 54 OEM automotive white paints obtained from the integrated analysis of both techniques will be summarized. Additionally, the undifferentiated samples, inter-sample variability, and potential correlations between the chemical profiles and vehicle information will be explored based on the integrated information.

Initially, there was a plan to adapt multiblock statistical methods to combine the IR and Raman analysis results. However, upon closer examination, it was found that the IR and Raman analysis provided similar information from a similar perspective. Consequently, the statistical combination of the two data sets did not yield additional information but rather resulted in overlapping information. Therefore, it was decided not to include this method in the thesis. Instead, the combined information was obtained by simply merging the grouping results from visual comparison to determine the undifferentiated groups.

11.2.1. General combination results

Table 67 displays the chemical profiles revealed within each OEM paint layer through the integration of FTIR and Raman analyses. Moreover, the table indicates the outcomes of grouping within each class, where samples from Group OEM3 are denoted in blue and those from Group OEM4 are highlighted in orange. The undifferentiated groups of samples are indicated by underlined entries.

Concerning the chemical profile, in the primer layer, it was observed that epoxy binder was the only type used in the OEM paint samples. Aluminum silicate was commonly combined with the epoxy binder as an extender, and titanium was also detected in most of the samples. Moving on to the primer surfacer layer, although a diverse range of chemical classes was identified, the majority of samples contained isophthalic alkyd combined with epoxy binder. The variation in chemical classes was attributed to the presence of additional resins such as polyurethane or melamine, as well as the use of different extenders like barium sulfate or talc. In the basecoat layer, it was found that both polyurethane-based and acrylic-based resins were predominantly used as binders. The chemical profile of the basecoat layer was strongly influenced by the layer structure. Similar trends were observed in the clearcoat layer, with the presence of polyurethane-based and acrylic-based resins. Within each chemical class, the samples exhibited further differentiation into several groups, indicating a high level of inter-sample variability. The high discriminating power achieved through the combined FTIR and Raman analysis of white automotive paint samples not only highlights the discrimination capabilities of both techniques but also underscores the significant inter-sample variability within this specific sample set.

Table 67. Chemical composition of each layer identified from integrated FTIR and Raman analysis and the groupings (OEM3 in blue and OEM4 in orange).

Layer type	Class No.	Identified chemical class		Sample groupings
Primer (54)	1	EPY+ALS+TIO2	1)	W002, W005, W023, W036
			2)	W007, W033, W046
			3)	W009, W010, W017, W020, W022, W027, W028, W030, W031, W041, W043, W044, W052, W053
			4)	W012, W014, W015, W016, W018, W032, W042, W047, W048, W049, W054, W062
			5)	W003, W006, W011, W019, W021, W025, W026, W039, W040, W045, W050, W051, W055, W060
			6)	W034, W058
			7)	W001
			8)	W024
			9)	W035
			10)	W061
	2	EPY	11)	W059
Primer surfacer (28)	1	EPY+ALK IPH+PUR+MEL +TALC+BAS+TIO2	1)	W009, W011, W017, W019, W021, W022, W024, W025, W027, W028, W030, W031, W040, W043, W050, W052, W055, W058, W059, W060
			2)	W003, W039
			3)	W006
	2	ALK IPH+EPY+MEL+TALC+TIO2	4)	W001
	3	ALK IPH+PUR+EPY +TALC+ALS+TIO2	5)	W035
			6)	W061
	4	ALK IPH+MEL+TALC+TIO2	7)	W034
	5	ALK TER+ACR+MEL+BAS+TIO2	8)	W026
Basecoat (54)	1	PUR+ALK IPH+TALC+TIO2	1)	W005, W010, W012, W014, W015, W016, W018, W020, W032, W033, W041, W042, W044, W045, W046, W047, W049, W051, W053, W054
			2)	W002, W023, W036
			3)	W007
	2	PUR+MEL+TIO2	4)	W048
			5)	W062
	3	ACR+ALK IPH+MEL+PUR+ TIO2	6)	W003, W011, W021, W039
			7)	W006, W059
			8)	W019, W025, W040
			9)	W022, W024, W058, W060
			10)	W027, W028, W050
			11)	W030, W031, W052
			12)	W001
			13)	W009
			14)	W017
			15)	W034
			16)	W035
			17)	W043
			18)	W055
			19)	W061
	4	ACR+PUR+MEL+TALC+TIO2	20)	W026
Clearcoat (54)	1	PUR+STY	1)	W002, W007, W023, W036, W053
			2)	W020
			3)	W010, W014, W015, W016, W018
			4)	W012, W032, W041, W042, W044, W045, W047, W049, W051, W054
			5)	W048, W062
			6)	W005, W033, W046
			7)	W026
	2	ACR+MEL+STY+(PUR)	8)	W003, W011, W019, W021, W030, W031, W039, W050, W052, W055
			9)	W009, W017, W022, W024, W035, W043, W059, W060
			10)	W025, W040
			11)	W027, W028, W034
			12)	W001
			13)	W006
			14)	W058
			15)	W061

The discriminating power of combining both FTIR and Raman techniques for the analysis of each layer, as well as different layer combinations, was calculated. A division was also applied to Group OEM3 and Group OEM4. All the results are presented in *Table 68*.

The combined technique demonstrates higher discriminative capability for samples within Group OEM4 compared to those within Group OEM3, resulting in only 7 pairs of samples remaining undifferentiated and yielding a robust discriminating power of 98.1%. The relatively lower discrimination within Group OEM3 can be attributed to the high similarity of basecoat compositions among OEM3 samples.

Table 68. Discriminating power of combined FTIR and Raman analysis for each layer and layer combinations within OEM sample set (n=54).

Single layer/ Layer combination	Whole OEM sample set (n=54)		Group OEM3 (n=26)	Group OEM4 (n=28)
	DP (Undifferentiated pairs)	Total number of samples	DP (Undifferentiated pairs)	DP (Undifferentiated pairs)
P	82.0% (258)	54	73.5% (86)	72.8% (103)
PS	49.5% (191)	28		49.5% (191)
B	85.0% (215)	54	40.6% (193)	94.2% (22)
C	90.5% (136)	54	78.8% (69)	82.3% (67)
P+PS	82.8% (65)	28		82.8% (65)
P+B	94.9% (73)	54	81.5% (60)	96.6% (13)
P+C	95.8% (60)	54	91.4% (28)	91.5% (32)
PS+B	95.5% (17)	28		95.5% (17)
PS+C	86.2% (52)	28		86.2% (52)
B+C	94.8% (75)	54	81.2% (61)	96.3% (14)
P+PS+B	97.6% (9)	28		97.6% (9)
P+PS+C	94.4% (21)	28		94.4% (21)
PS+B+C	97.4% (10)	28		97.4% (10)
P+B+C	97.3% (38)	54	91.7% (27)	97.1% (11)
P+PS+B+C	98.1% (7)	28		98.1% (7)
Final	**97.6% (34)**	**54**	**91.7% (27)**	**98.1% (7)**

After combining the FTIR and Raman analysis results of all layers in the 54 OEM automotive white paint samples, a total of 34 sample pairs remained undifferentiated, resulting in a discriminating power of 97.6%. The undifferentiated sample groups and their corresponding vehicle information are listed in *Table 69*. The geographic distribution of these undifferentiated samples associated with assembly plants is illustrated in *Figure 146*.

Upon conducting the integrated analysis, it was found that there are a total of 11 distinct groups of samples, while 34 sample pairs remain undifferentiated. Those samples in Group 1, 2, 5, 9, 10, 11 that were undistinguished by IR analysis, retained their undifferentiated status following subsequent Raman analysis. Conversely, Raman analysis contributed to the further discrimination of the rest samples. For instance, samples from Group 4 and Group 6 or samples from Group 7 and Group 8, originally assigned to the same undifferentiated sample group in IR analysis, could indeed be differentiated through Raman analysis.

Further examination of the vehicle information associated with these undifferentiated sample pairs revealed interesting insights. Most of the undifferentiated samples shared the same model, were produced in the same assembly plants, and had the same or similar production year and topcoat color code. Assembly plants are found to be a significant factor contributing to the lack of discrimination. Despite variations in model or production year, samples from the same assembly plant may be undifferentiated, as shown in Group 2, 3, and 6. This suggests that the assembly plant plays a crucial role in determining the chemical composition of the automotive paint used.

It was also found that the majority of these undifferentiated sample groups originated from the same company (S-VW), indicating a high level of consistency in the paint formula used by S-VW. In contrast, samples from the other company, F-VW, displayed a higher level of differentiation, with only one undifferentiated sample group (Group 1) identified. This suggests that F-VW utilizes different paint formulations or suppliers, resulting in more distinguishable chemical profiles.

Interestingly, it was observed that even when samples shared the same model, were produced in the same assembly plant, and had the same production year, they could still exhibit subtle differences. For example, sample W011 (Polo 2017) and sample W039 (Polo 2017) displayed slight variations despite their identical vehicle information. These differences were only revealed by Raman analysis and could be attributed to batch variations. Further discussion on these subtle differences will be explored in the next sections.

Table 69. Undifferentiated sample groups by combined IR and Raman analysis of all layers.

| Group No.	Sample No.	Manufacturing company	Model	Production year	Topcoat color code	Assembly plant	Layer structure
1	W002	F-VW	Sagitar	2017	LC9A	Chengdu	OEM3
	W023	F-VW	Sagitar	2017	LC9A	Chengdu	OEM3
	W036	F-VW	Sagitar	2017	LC9A	Chengdu	OEM3
2	W033	S-VW	New Lavida	2014	LY9H	Nanjing	OEM3
	W046	S-VW	Passat	2013	LY9H	Nanjing	OEM3
3	W041	S-VW	Santana	2017	LY9H	Nanjing	OEM3
	W044	S-VW	Passat	2017	LY9H	Nanjing	OEM3
4	W014	S-VW	New Lavida	2017	LY9H	Anting	OEM3
	W015	S-VW	New Lavida	2017	LY9H	Anting	OEM3
	W016	S-VW	New Lavida	2017	LY9H	Anting	OEM3
	W018	S-VW	New Lavida	2016	LY9H	Anting	OEM3
5	W045	S-VW	Lamando	2018	LY9H	Ningbo	OEM3
	W051	S-VW	Lamando	2017	LY9H	Ningbo	OEM3
6	W012	S-VW	New Lavida	2017	LY9H	Nanjing	OEM3
	W032	S-VW	Gran Lavida	2015	LY9H	Anting	OEM3
	W042	S-VW	New Lavida	2017	LY9H	Anting	OEM3
	W047	S-VW	New Lavida	2017	LY9H	Nanjing	OEM3
	W049	S-VW	New Lavida	2016	LY9H	Anting	OEM3
	W054	S-VW	New Lavida	2016	LY9H	Anting	OEM3
7	W003	S-VW	Polo	2017	Unknown	Anting	OEM4
	W039	S-VW	Polo	2017	LY9H	Anting	OEM4
8	W011	S-VW	Polo	2017	LY9H	Anting	OEM4
	W021	S-VW	Polo	2016	LY9H	Anting	OEM4
9	W025	S-VW	Polo	2016	LY9H	Anting	OEM4
	W040	S-VW	Polo	2015	LY9H	Anting	OEM4
10	W027	S-VW	Passat	2004	Unknown	Anting	OEM4
	W028	S-VW	Passat	2003	LB9A	Anting	OEM4
11	W030	S-VW	Tiguan	2016	LY9H	Anting	OEM4
	W031	S-VW	Tiguan	2017	LY9H	Anting	OEM4
	W052	S-VW	Tiguan	2017	LY9H	Anting	OEM4
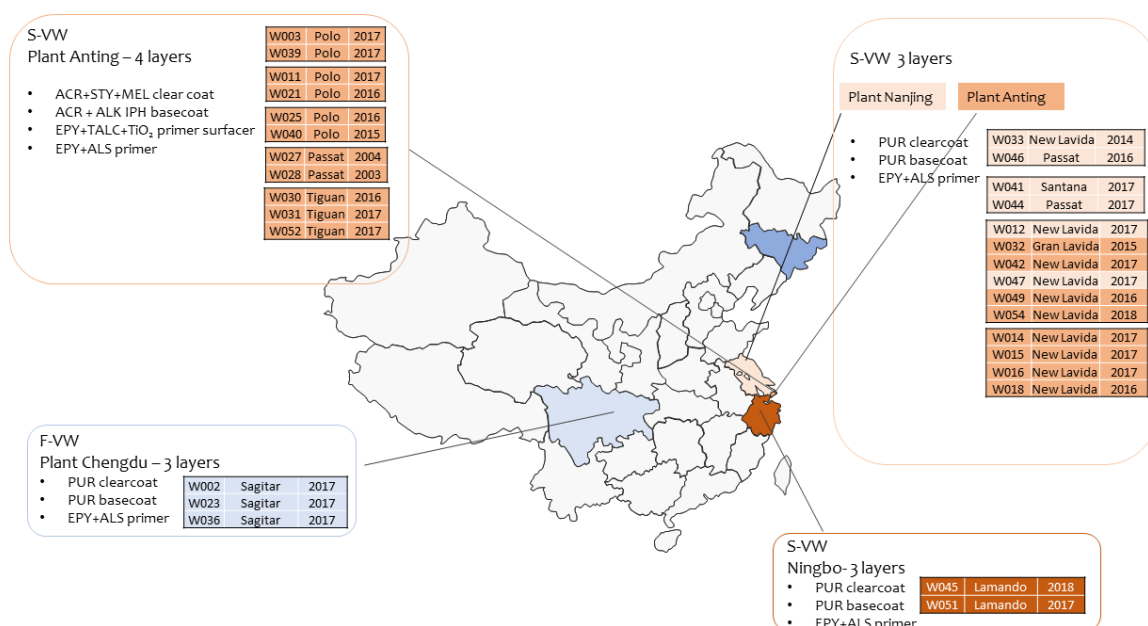
Figure 146. Geographic distribution of undifferentiated samples associated with assembly plants. The chemical profiles of each undifferentiated sample pair are listed in the figure.

251

11.2.2.　　Choice of technique / layer

Automotive paint constitutes a complex multilayer coating system. In forensic analyses of such paints, the procedure often entails a layer-by-layer examination and identification utilizing various instruments. This approach can be time-intensive and cost-inefficient if applied to all layers. This study has evaluated and summarized the discriminative capabilities of IR and Raman techniques for each layer as well as their combinations, as outlined in *Table 66* and *Table 68*. Through the combination of these two tables, the optimal technique for each layer analysis and the most suitable layers for achieving best discrimination can be discerned. The decision on layer/technique selection, along with the comparison of results to existing literature that addresses this matter, is presented in *Table 70*. This decision-making process was guided by the highest achieved discriminating power.

By comparing the discriminating power of IR and Raman analyses for individual layers, the superior technique for discriminating samples using a singular layer was determined. For instance, in the case of analyzing clearcoat, Raman has exhibited a more effective discrimination capacity than IR. This observation aligns with research findings of Maric and Affadu-Danful *et al*. (Maric,2014; Affadu-Danful *et al*.,2023).

In scenarios where only IR is available, the examination of a sole layer points to clearcoat as the most discriminatory in this sample set. This outcome is also in harmony with the findings of Eyring *et al*., who have demonstrated that samples with identical color codes can largely be differentiated by solely examining the clear coat (Eyring *et al*.,2007). They further indicated that, through supplementary primer analysis, robust discrimination can be achieved without the necessity of analyzing the basecoat. Notably, the outcome contrasts with the conclusions drawn by Massonnet, whose study indicated that, within her sample set, clearcoat offered the least discriminating power, while primer surfacer yielded the highest (Massonnet,1996).

In this study, the discriminative power obtained from clearcoat and primer analyses almost paralleled that of Eyring's study, albeit not representing the optimal discrimination result within this sample set. Remarkably, the combination of primer and basecoat yielded a higher discriminating power of 94.9%. The addition of the clearcoat further elevated the overall discriminating power to 97.3%, emerging as the most fitting choice for a three-layer combination. In this context, delving into primer surfacer analysis didn't yield additional discrimination, rendering it unnecessary.

In the context of Raman analysis, the choice of layers is notably constrained due to the virtually non-existent discriminative capability of Raman analysis of primer and the limited discrimination yielded from primer surfacer analysis. This limitation narrows down the preferable layers to basecoat and clearcoat. When it comes to a three-layer combination, the inclusion of primer surfacer marginally enhances the overall discrimination outcome by resolving four pairs of previously undifferentiated samples. This modification results in an improved discriminating power of 91.8%.

If both techniques are accessible and employed for the analysis of individual layers, the integrated discriminating outcomes have been summarized in *Table 68*. Given that the most

effective technique for discriminating individual layers alternates between the two methods, it becomes interesting to combine the most effective discriminative outcomes of single layers. This assessment aims to evaluate whether the optimal combination can yield effective discriminative power while also reducing the measurement efforts by half. This combined result is summarized in *Table 71*. Upon comparison with the results in *Table 68***Error! Reference source not found.**, it becomes evident that **this optimized combination yielded nearly identical discriminative capabilities as when both techniques were employed**. Employing both techniques for analyzing each layer results in a reduction of a maximum of 14 undifferentiated sample pairs and an increase of only 1% in discriminating power. By integrating the best technique for each layer, the optimal combination results in 37 pairs of undifferentiated samples (3 more pairs compared to when both techniques were employed), thus achieving a highly notable discriminating power of 97.4% (97.6% when both techniques were employed and combined).

This highlights that utilizing both techniques for individual layer analysis is not indispensable for this sample set. If both techniques are at hand, analyzing primer with FTIR and clearcoat with Raman can yield exceptionally effective discriminative results, culminating in a discriminating power of 95.7%. These layers often constitute the surface layer and require minimal sample preparation.

Table 70. Summary of choice of technique / layer of this study and the existing literature

Choice of technique for single layer analysis			
Existing literature	**Involved layer**	**Best technique**	**Achieved DP**
This study	Clearcoat (C)	Raman	88.0%
	Basecoat (B)	IR	80.6%
	Primer surfacer (PS)	Raman	49.5%
	Primer (P)	IR	82.0%
Maric, 2014	Clearcoat	Raman	97.6%
Affadu-Danful *et al.* 2023	clearcoat	Raman	Not provided
Choice of layer for best discrimination if only FTIR available			
Existing literature	**Involved layer No.**	**Layer combination**	**Achieved DP**
This study	1	C	84.4%
	2	P+B/P+C	94.9%/93.2%
	3	P+B+C	97.3%
Eyring *et al.*, 2007	1	C	Not provided
	2	P+C	93%
Massonnet, 1999	1	PS	98%
	2	P+PS	99%
	3	P+PS+B	99%
Choice of layer for the best discrimination if only Raman available			
Existing literature	No. Of choice	Choice of layer	Achieved DP
This study	1	C	88%
	2	B+C	91.8%
	3 (only for Group OEM4)	PS+B+C	92.1%
De Gelder *et al.*, 2005	1	B	Not provided
Choice of layer for the best discrimination if both technique available			
Existing literature	**No. of choice**	**Choice of layer (employed technique)**	**Achieved DP**
This study	1	C (Raman)	88%
	2	P(IR)+C(Raman)	95.7%

253

	3	P(IR)+B(IR)+C(Raman)	97.1%

Table 71. Discriminating power of combined FTIR and Raman analysis when only one technique is employed for analysis individual layers.

Layer combination (best technique)	Whole OEM sample set (n=54)		Group OEM3 (n=26)	Group OEM4 (n=28)
	DP (Undifferentiated pairs)	Total number of samples	DP (Undifferentiated pairs)	DP (Undifferentiated pairs)
P(IR)+PS (Raman)	82.8% (65)	28		82.8% (65)
P(IR)+B(IR)	94.6% (77)	54	80.6% (63)	96.3% (14)
P(IR)+C (Raman)	**95.7% (62)**	54	90.8% (30)	91.5% (32)
PS(Raman)+B(IR)	95.5% (17)	28		95.5% (17)
PS(Raman)+C(IR)	82.5% (66)	28		82.5% (66)
B(IR)+C(Raman)	93.8% (89)	54	77.2% (74)	96.0% (15)
P(IR)+PS (Raman)+ B(IR)	97.4% (10)	28		97.4% (10)
P(IR)+PS (Raman)+C(Raman)	94.2% (22)	28		94.2% (22)
P(IR)+B(IR)+C(Raman)	**97.1% (41)**	54	91.1% (29)	96.8% (12)
PS (Raman)+ B(IR)+C(Raman)	97.1% (11)	28		97.1% (11)
P(IR)+PS (Raman)+ B(IR)+ C(Raman)	97.9% (8)	28		97.9% (8)
Final DP	**97.4% (37)**	**54**	**91.1% (29)**	**97.9% (8)**

11.2.3. Correlations between chemical compound and vehicle information

Figure 147 presents an overview of the correlation between the chemical characteristics of 54 OEM automotive white paints, as identified from IR and Raman analysis, and various vehicle information including manufacturing company, layer structure, assembly plant, vehicle model, and production year. A significant observation is that a considerable number of distinct groups can be distinguished within each assembly plant.

As observed from individual IR and Raman analyses, a distinct chemical profile was identified in an OEM paint sample (W026) from Germany, which sets it apart from the white OEM paint samples produced in China. The chemical characteristics of white OEM paint samples produced in China were found to be highly related to their layer structure, with all paints having an OEM3 layer structure exhibiting identical chemical classes regardless of manufacturing company, assembly plant, or model. The groupings observed within each assembly plant were primarily based on the addition or combination of different additional resins or extenders, although these differences were subtle.

Furthermore, it is important to note that even samples with identical vehicle information may exhibit differentiation due to factors such as batch variation or weathering effects. These factors contribute to the nuanced variations observed within the sample set.

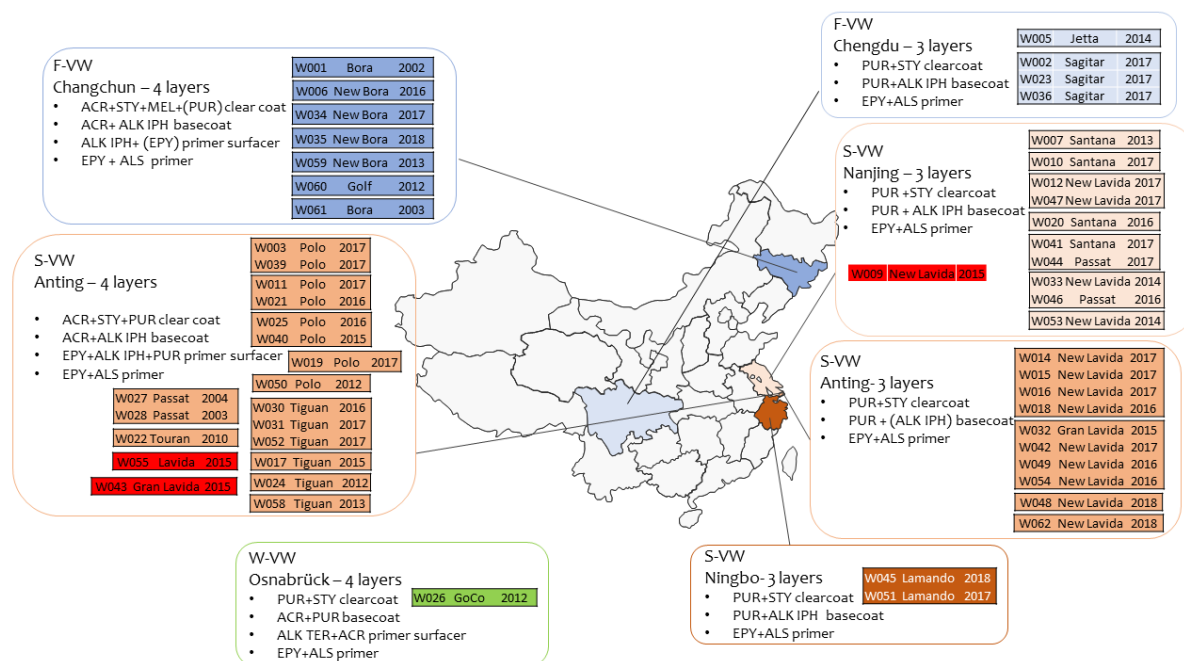In the following sections, the inter-sample variability within each identify factor will be discussed.

Figure 147. Chemical profiles identified from both IR and Raman analysis of OEM paint samples in relation to manufacturing company, assembly plant, and the layer system. Groupings within each plant based on the integrated analysis result are listed.

11.2.4.   Sample variation related to topcoat color code

Table 72 presents the color codes of samples within two groups of undifferentiated basecoat, as determined from the integrated IR and Raman analysis. It is evident from the table that different color codes do not necessarily indicate different chemical compositions, as undifferentiated basecoat samples may have different color codes. On the other hand, *Table 73* displays the groupings of samples within each topcoat color code group. The results obtained are consistent with the findings from the individual IR and Raman analyses, demonstrating that samples sharing the same topcoat color code do not consistently exhibit identical chemical compositions in their basecoat. Instead, samples with the same color code can be further differentiated into multiple groups, highlighting significant variations in their chemical characteristics. Moreover, it is important to note that different manufacturers, such as Volkswagen (VW), Audi, and Subaru, can use the same topcoat color code while utilizing entirely different binders in their paint formulations. This underscores that the observed lack of correlation between topcoat color codes and the chemical composition of the basecoat is an expected outcome

In conclusion, the discrimination of samples does not show any correlation with the topcoat color code.

Table 72. Topcoat color code of samples within two groups of undifferentiated basecoat samples. The undifferentiated basecoat samples that have different color codes are highlighted in bold.

Group No.	Sample No.	Manufacturing company	Model	Production year	Topcoat color code	Assembly plant	Layer structure
1	**W005**	**F-VW**	**Jetta**	**2014**	**LB9A**	**Chengdu**	**OEM3**
	W010	S-VW	Santana	2017	LY9H	Nanjing	OEM3
	W012	S-VW	New Lavida	2017	LY9H	Nanjing	OEM3
	W014	S-VW	New Lavida	2017	LY9H	Anting	OEM3
	W015	S-VW	New Lavida	2017	LY9H	Anting	OEM3
	W016	S-VW	New Lavida	2017	LY9H	Anting	OEM3
	W018	S-VW	New Lavida	2016	LY9H	Anting	OEM3
	W020	S-VW	Santana	2016	LY9H	Nanjing	OEM3
	W032	S-VW	Gran Lavida	2015	LY9H	Anting	OEM3
	W033	S-VW	New Lavida	2014	LY9H	Nanjing	OEM3
	W041	S-VW	Santana	2017	LY9H	Nanjing	OEM3
	W042	S-VW	New Lavida	2017	LY9H	Anting	OEM3
	W044	S-VW	Passat	2017	LY9H	Nanjing	OEM3
	W045	S-VW	Lamando	2018	LY9H	Ningbo	OEM3
	W046	S-VW	Passat	2016	LY9H	Nanjing	OEM3
	W047	S-VW	New Lavida	2017	LY9H	Nanjing	OEM3
	W049	S-VW	New Lavida	2016	LY9H	Anting	OEM3
	W051	S-VW	Lamando	2017	LY9H	Ningbo	OEM3
	W053	S-VW	New Lavida	2014	LY9H	Nanjing	OEM3
	W054	S-VW	New Lavida	2016	LY9H	Anting	OEM3
2	W027	S-VW	Passat	2004	Unknown	Anting	OEM4
	W028	S-VW	Passat	2003	LB9A	Anting	OEM4
	W050	**S-VW**	**Polo**	**2012**	**LY9H**	**Anting**	**OEM4**

Table 73. groupings of samples within each topcoat color code group based on IR and Raman analysis of basecoats (n=50)

Topcoat color code	Group No.	Sample No.	Manufacturing company	Model	Production year	Assembly plant	Layer structure
LC9A	1	W002	F-VW	Sagitar	2017	Chengdu	OEM3
		W023	F-VW	Sagitar	2017	Chengdu	OEM3
		W036	F-VW	Sagitar	2017	Chengdu	OEM3
	2	W006	F-VW	New bora	2016	Changchun	OEM4
		W059	F-VW	New bora	2013	Changchun	OEM4
	3	W034	F-VW	New bora	2017	Changchun	OEM4
	4	W035	F-VW	New bora	2018	Changchun	OEM4
	5	W026	W-VW	GoCo	2012	Osnabrück	OEM4
LB9A	1	W005	F-VW	Jetta	2014	Chengdu	OEM3
	2	W060	F-VW	Golf	2012	Changchun	OEM4
	3	W022	S-VW	Touran	2010	Anting	OEM4
		W024	S-VW	Tiguan	2012	Anting	OEM4
		W058	S-VW	Tiguan	2013	Anting	OEM4
	4	W028	S-VW	Passat	2003	Anting	OEM4
LY9H	1	W010	S-VW	Santana	2017	Nanjing	OEM3
		W012	S-VW	New Lavida	2017	Nanjing	OEM3
		W014	S-VW	New Lavida	2017	Anting	OEM3
		W015	S-VW	New Lavida	2017	Anting	OEM3
		W016	S-VW	New Lavida	2017	Anting	OEM3
		W018	S-VW	New Lavida	2016	Anting	OEM3
		W020	S-VW	Santana	2016	Nanjing	OEM3
		W032	S-VW	Gran Lavida	2015	Anting	OEM3
		W033	S-VW	New Lavida	2014	Nanjing	OEM3
		W041	S-VW	Santana	2017	Nanjing	OEM3
		W042	S-VW	New Lavida	2017	Anting	OEM3
		W044	S-VW	Passat	2017	Nanjing	OEM3
		W045	S-VW	Lamando	2018	Ningbo	OEM3
		W046	S-VW	Passat	2016	Nanjing	OEM3
		W047	S-VW	New Lavida	2017	Nanjing	OEM3
		W049	S-VW	New Lavida	2016	Anting	OEM3
		W051	S-VW	Lamando	2017	Ningbo	OEM3
		W053	S-VW	New Lavida	2014	Nanjing	OEM3
		W054	S-VW	New Lavida	2016	Anting	OEM3
	2	W007	S-VW	Santana	2013	Nanjing	OEM3
	3	W048	S-VW	New Lavida	2018	Anting	OEM3
	4	W062	S-VW	New Lavida	2018	Anting	OEM3
	5	W011	S-VW	Polo	2017	Anting	OEM4
		W021	S-VW	Polo	2016	Anting	OEM4
		W039	S-VW	Polo	2017	Anting	OEM4
	6	W017	S-VW	Tiguan	2015	Anting	OEM4
	7	W043	S-VW	Gran LAVIDA	2015	Anting	OEM4
	8	W019	S-VW	Polo	2017	Anting	OEM4
		W025	S-VW	Polo	2016	Anting	OEM4
		W040	S-VW	Polo	2015	Anting	OEM4
	9	W030	S-VW	Tiguan	2016	Anting	OEM4
		W031	S-VW	Tiguan	2017	Anting	OEM4
		W052	S-VW	Tiguan	2017	Anting	OEM4
	10	W009	S-VW	New Lavida	2015	Nanjing	OEM4
	11	W050	S-VW	Polo	2012	Anting	OEM4
	12	W055	S-VW	Lavida	2014	Anting	OEM4

11.2.5. Sample variation related to production year

The production year of paint can have a significant influence on sample variation, as manufacturers often engage in renovation efforts that may involve changing production lines or altering paint formulations for specific car models over time. To illustrate, consider the case of the 'Passat' vehicle model. Initially, it was manufactured at Plant Anting during its early years. For instance, Sample W028, produced in 2003, and Sample W027, produced in 2004, both exhibited an OEM4 layer system, with clearcoat and basecoat formulas based on acrylic binders. Subsequently, a new production line was established at Plant Nanjing for this model. All vehicles manufactured in this new line at the new plant, such as W046 in 2016 and W044 in 2017, featured an OEM3 layer system and utilized polyurethane-based binders for their clearcoat and basecoat. This exemplifies how the production year and manufacturing changes can impact the paint characteristics of specific car models.

The variation in samples related to the production year was also systematically investigated by maintaining consistency in identifying factors, such as manufacturing company, assembly plant, and model, while varying only the sample production year. Two specific models, one with an OEM3 layer structure (New Lavida) and another with an OEM4 system (Polo), were selected for this analysis, resulting in the creation of two distinct sample sets. The specific details of these sample sets are summarized in *Table 74*. Each layer of the samples was analyzed separately to gain insights into how the production year influences the variation within each layer. The resulting groupings of each layer are presented *Table 75*. Samples within each group were undifferentiated and the production year contained in the undifferentiated sample group are listed in the table.

From *Table 75*, it is evident that different production years do not necessarily result in sample variation, as samples produced in different years were found to have undifferentiated layers. For example, in both sample sets, the primer layer remains undifferentiated regardless of the production year. Conversely, samples produced in the same year may exhibit distinguished layers, as observed in set 2 where four samples of Model Polo produced in 2017 show differentiation in the primer surfacer layer. This difference is likely attributed to batch variation rather than weathering effects, as primer surfacer is not an outer layer and the clearcoat, which is more susceptible to weathering, remains undifferentiated among these four samples. These findings indicate that production year alone is not a significant factor contributing to sample differentiation or non-differentiation. Any sample variation related to the production year is most probably due to batch variation, which will be discussed in the next section.

Table 74. Information of two sample sets used for the investigation of sample variation related to the production year.

Sample set	Manufacturing company	Model	Assembly plant	Layer structure	Sample no.	Production year
Set 1 (9)	S-VW	New Lavida	Anting	OEM3	W014	2017
					W015	2017
					W016	2017
					W018	2016
					W042	2017
					W048	2018
					W049	2016
					W054	2016
					W062	2018
Set 2 (8)	S-VW	Polo	Anting	OEM4	W003	2017
					W011	2017
					W019	2017
					W021	2016
					W025	2016
					W039	2017
					W040	2015
					W050	2012

Table 75. Groupings within each layer related to production year.

Sample set	Layer type	Group no.	Production year contained in the undifferentiated sample groups
Set 1 **S-VW** **Anting** **OEM3** **New Lavida**	Primer	-	2016 (W018, W049, W054) 2017 (W014, W015, W016, W042) 2018 (W048, W062)
	basecoat	1	2016 (W018, W049, W054) 2017 (W014, W015, W016, W042)
		2	2018 (W048)
		3	2018 (W062)
	clearcoat	1	2016 (W018) 2017 (W014, W015, W016)
		2	2016 (W049, W054) 2017 (W042)
		3	2018 (W048, W062)
Set 2 **S-VW** **Anting** **OEM4** **Polo**	Primer	-	2012 (W050) 2015 (W040) 2016 (W021, W025) 2017 (W003, W011, W019, W039)
	Primer surfacer	1	2012 (W050) 2015 (W040) 2016 (W021, W025) 2017 (W011, W019)
		2	2017 (W003, W039)
	basecoat	1	2016 (W021) 2017 (W003, W011, W039)
		2	2015 (W040) 2016 (W025) 2017 (W019)
		3	2012 (W050)
	clearcoat	1	2012 (W050) 2016 (W021) 2017 (W003, W011, W019, W039)
		2	2015 (W040) 2016 (W025)

11.2.6. Batch variation

Automotive paint batch refers to a specific quantity of vehicles that undergoes painting under uniform conditions and is assigned a unique identification or batch number for the paint. It typically represents a distinct manufacturing run or production cycle. Based on the existing literature, it is apparent that differentiation at the level of paint production batches is often arbitrary and influenced by various unknown factors, such as adjustments made during the manufacturing process, the diverse sources of raw materials, and the manufacturer's decisions regarding changes in paint formulations (Quevillon *et al.*,2019). It is important to note that paint batch differentiation is not strictly tied to the vehicle production year but rather associated with the size of the batch, which is often undisclosed to customers.

Consequently, batch-to-batch variation cannot be reliably predicted or consistently observed. However, such variation can lead to significantly distinct chemical profiles, potentially enabling the differentiation of one production batch from others. In this study, no significant paint formula variations were detected.

Alternatively, the batch variation may be so subtle that it may be ignored or may not be detectable. As previously discussed, the observed sample variation related to different production years is likely attributed to batch variation. In this study, subtle batch variations were observed when comparing samples with identical manufacturing company, model, and assembly plant but different production years, as indicated in *Table 75*.

As shown in *Table 75*, within Set 1 for the vehicle model 'New Lavida', the basecoat of two samples (W048 and W062) produced in 2018 can be distinguished from those produced in 2016 and 2017. *Figure 148* displays the IR spectra of the basecoat from two samples produced in 2018 (W048 and W062) and one sample produced in 2017 (W042), highlighting batch variation resulting from different production years and within the same production year. The differentiation between the samples from 2018 and the sample from 2017 can be attributed to small changes in the paint formula, where the basecoat from 2018 includes melamine but excludes talc. Additionally, the samples from 2018 exhibit differentiation from each other due to variations in the concentration of melamine.

Another example of batch variation can be observed within Set 2 for the vehicle model 'Polo'. Samples W021 and W025, both produced in 2016, exhibit undifferentiated primer and primer surfacer layers. However, differentiation between these samples can be observed in their basecoat and clearcoat layers. *Figure 149* illustrates the variation detected in the IR spectra of the basecoat and clearcoat, indicating that the variation is attributed to differences in the concentration of polyurethane used in the basecoat and clearcoat layers.

Subtle batch variation was also identified within Set 2. Sample W011 and W039, both produced in 2017, exhibit undifferentiated primer, basecoat, and clearcoat. However, these samples can be differentiated from each other based on subtle variations observed in the primer surfacer layer, as revealed by Raman analysis in *Figure 150*.

Py-GC/MS can also reveal subtle batch variation that could not detected by IR and Raman analysis, as shown in *Figure 143*.

Since automotive paint consists of multiple layers, each layer is produced in separate batches. This means that while working with a specific batch of basecoat, changes in the batches of primer surfacer or clearcoat may occur. These variations in batch can contribute significantly to the inter-sample variability.

In conclusion, these observations highlight the significant contribution of batch variation to the discrimination of samples with identical vehicle information. Variations in batch compositions can be effectively detected using IR, Raman and Py-GC/MS analysis.
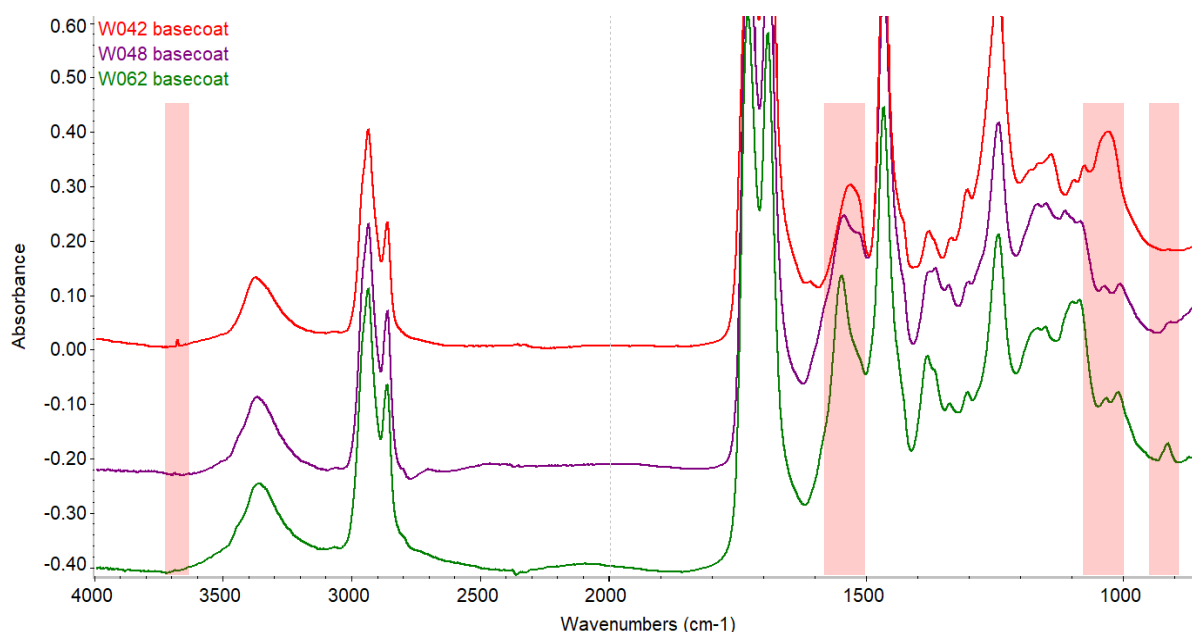
Figure 148. IR spectra of basecoat of sample W042(red), sample W048 (purple) and sample W062 (green), showcasing the batch variation among these samples. The observed variations are highlighted in red.
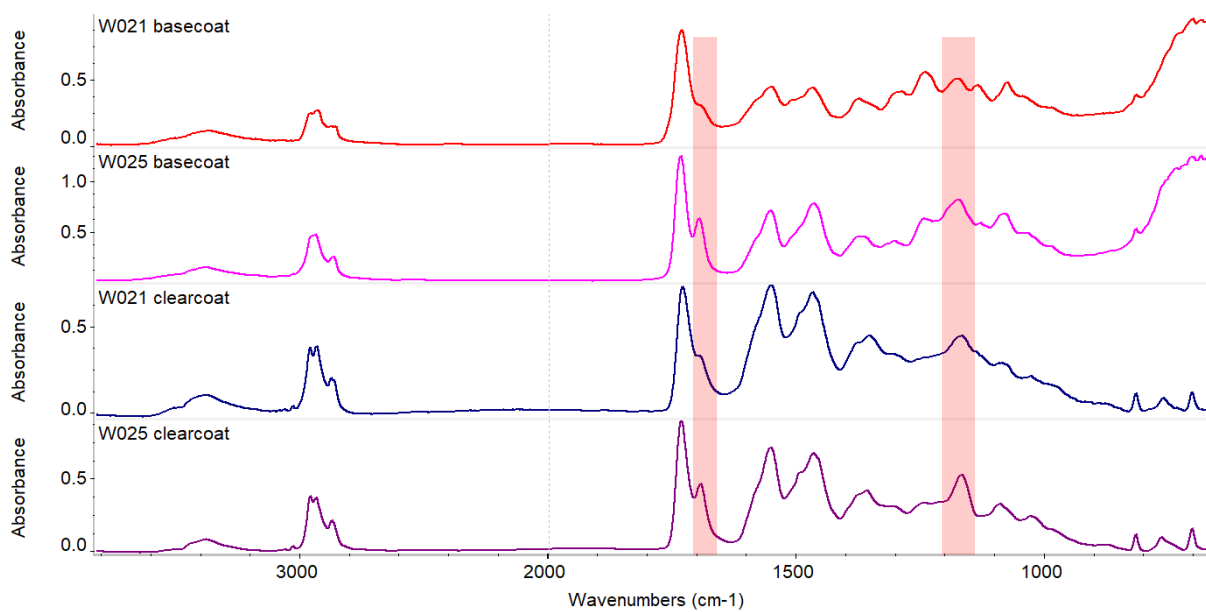
Figure 149. IR spectra of basecoat and clear coat of sample W021 and W025, showcasing the batch variation among these samples. The observed variations are highlighted in red.
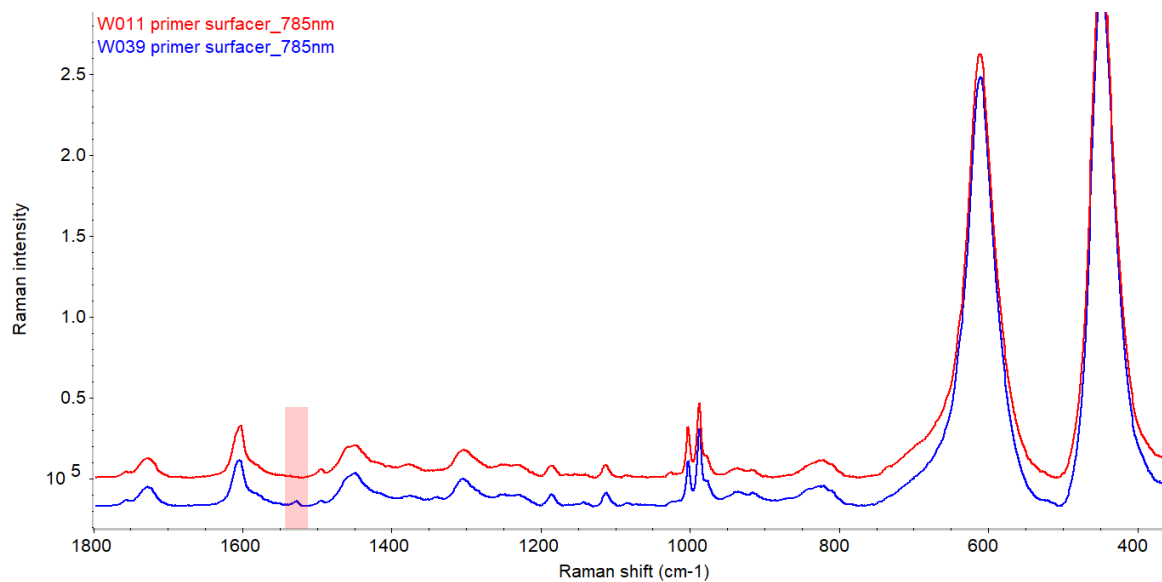

Figure 150. Raman spectra of primer surfacer of sample W011(red) and W039 (blue), showcasing the batch variation among these samples. The observed variations are highlighted in red.

11.3. Combination of IR and Raman results with other techniques

11.3.1. IR + Raman + Microscopy

Upon merging microscopic observations with FTIR and Raman results for 54 OEM automotive white paint samples (considering only OEM paint layers), 22 pairs of samples were indistinguishable, resulting in a discriminating power of 98.5%. The geographic distribution of these undifferentiated samples associated with assembly plants is illustrated in *Figure 151* and their corresponding vehicle details are outlined in *Table 76*.

However, some OEM paint samples might have additional repainted layers on top of their OEM layers, the layer structures of these samples were actually different from those have no repainted layers. When taking this factor into consideration, an additional 4 pairs could be differentiated due to variations in layer structure (samples highlighted in grey within the table), reducing undistinguished pairs to 18, elevating discriminating power to 98.7%. When evaluated independently for Group OEM3 and Group OEM4 for OEM layers, the overall discrimination is 94.2%, leaving 19 pairs indistinguishable among 26 samples in Group OEM3, while only 3 pairs out of 28 remain indistinguishable in Group OEM4, resulting in a discriminating power of 98.9%. These values increase to 94.8% (17 indistinguishable pairs) and 99.7% (1 indistinguishable pairs) when considering all layers.

If we consider the collective discriminating capacity derived from microscopy, IR, and Raman analyses across the entire sample set (n=62), the overall discriminating power rises to **99%**.
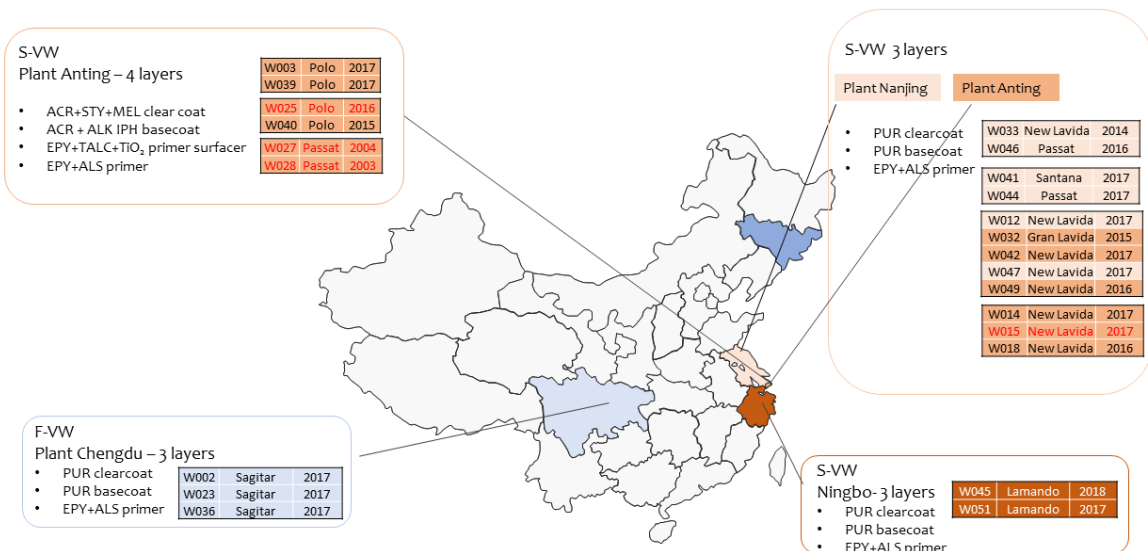
Figure 151. Geographic distribution of undifferentiated samples associated with assembly plants after microscopy, IR and Raman analysis.

Table 76. Undifferentiated sample groups by combined microscopy, IR and Raman analysis. (Samples that actually have different layer structure were marked in grey).

Group No.	Sample No.	Manufacturing company	Model	Production year	Topcoat color code	Assembly plant	Layer structure
1	W002	F-VW	Sagitar	2017	LC9A	Chengdu	OEM3
	W023	F-VW	Sagitar	2017	LC9A	Chengdu	OEM3
	W036	F-VW	Sagitar	2017	LC9A	Chengdu	OEM3
2	W033	S-VW	New Lavida	2014	LY9H	Nanjing	OEM3
	W046	S-VW	Passat	2013	LY9H	Nanjing	OEM3
3	W041	S-VW	Santana	2017	LY9H	Nanjing	OEM3
	W044	S-VW	Passat	2017	LY9H	Nanjing	OEM3
4	W014	S-VW	New Lavida	2017	LY9H	Anting	OEM3
	W015	S-VW	New Lavida	2017	LY9H	Anting	OEM3
	W018	S-VW	New Lavida	2016	LY9H	Anting	OEM3
5	W045	S-VW	Lamando	2018	LY9H	Ningbo	OEM3
	W051	S-VW	Lamando	2017	LY9H	Ningbo	OEM3
6	W012	S-VW	New Lavida	2017	LY9H	Nanjing	OEM3
	W032	S-VW	Gran Lavida	2015	LY9H	Anting	OEM3
	W042	S-VW	New Lavida	2017	LY9H	Anting	OEM3
	W047	S-VW	New Lavida	2017	LY9H	Nanjing	OEM3
	W049	S-VW	New Lavida	2016	LY9H	Anting	OEM3
7	W003	S-VW	Polo	2017	Unknown	Anting	OEM4
	W039	S-VW	Polo	2017	LY9H	Anting	OEM4
8	W025	S-VW	Polo	2016	LY9H	Anting	OEM4
	W040	S-VW	Polo	2015	LY9H	Anting	OEM4
9	W027	S-VW	Passat	2004	Unknown	Anting	OEM4
	W028	S-VW	Passat	2003	LB9A	Anting	OEM4

11.3.2.   IR + Raman + Py-GC/MS for samples within Group OEM3

As presented in *Table 68*, the overall capacity to differentiate samples within Group OEM3 wasn't as robust as achieved for Group OEM4. The combined IR and Raman analysis across all three layers resulted in a discriminating power of 91.7%, leaving 27 pairs of samples undistinguished. Conversely, for Group OEM4, the discrimination power reached an impressive 98.1% with only 7 pairs remaining undistinguished. Py-GC/MS was employed on a limited subset comprising 23 samples belonging to Group OEM3, specifically those whose basecoat could not be differentiated through IR and Raman analysis.

Upon integrating the discriminatory outcomes from Py-GC/MS with the results of FTIR and Raman analyses for the 26 automotive white paint samples within Group OEM3, a total 10 pairs of samples were deemed indistinguishable, resulting in a discriminating power of 97%. The specific pairs of undistinguished samples and their corresponding vehicle information are detailed in *Table 77*. The geographic distribution of these undifferentiated samples associated with assembly plants is illustrated in *Figure 152*.

It was noticed that combining Py-GC/MS did not significantly enhance the overall discriminatory power of Group OEM3 to match the discriminative ability observed in Group

OEM4. This observation suggests that samples with three layers share a remarkably similar profile within the same manufacturing company, regardless of varying models, production years, or assembly plants.

Table 77. Undifferentiated sample groups by combined IR, Raman and Py-GC/MS analysis of samples within Group OEM3

| Group No.	Sample No.	Manufacturing company	Model	Production year	Topcoat color code	Assembly plant
1	W002	F-VW	Sagitar	2017	LC9A	Chengdu
	W023	F-VW	Sagitar	2017	LC9A	Chengdu
2	W033	S-VW	New Lavida	2014	LY9H	Nanjing
	W046	S-VW	Passat	2013	LY9H	Nanjing
3	W014	S-VW	New Lavida	2017	LY9H	Anting
	W015	S-VW	New Lavida	2017	LY9H	Anting
4	W016	S-VW	New Lavida	2017	LY9H	Anting
	W018	S-VW	New Lavida	2016	LY9H	Anting
5	W012	S-VW	New Lavida	2017	LY9H	Nanjing
	W032	S-VW	Gran Lavida	2015	LY9H	Anting
	W042	S-VW	New Lavida	2017	LY9H	Anting
	W054	S-VW	New Lavida	2016	LY9H	Anting
6	W047	S-VW	New Lavida	2017	LY9H	Nanjing
	W049	S-VW	New Lavida	2016	LY9H	Anting
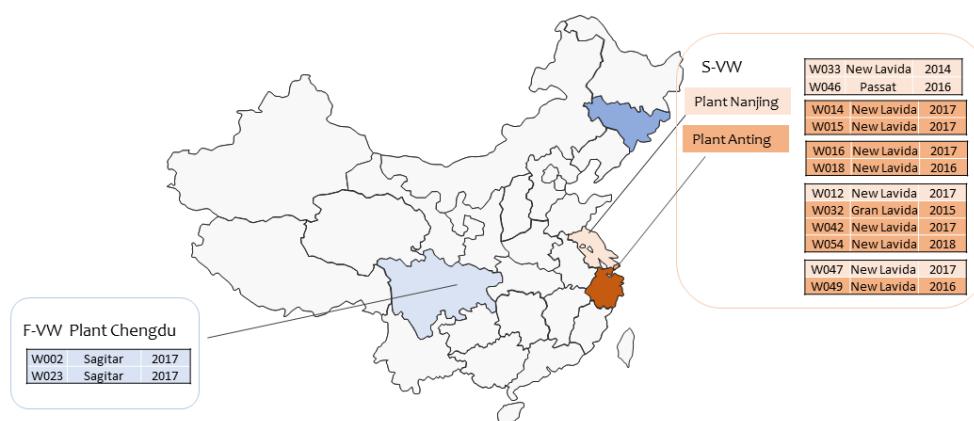
Figure 152. Geographic distribution of undifferentiated samples associated with assembly plants after IR, Raman and Py-GC/MS analysis.

11.4.   Global discriminating power

The global discriminating power of each technique and that in each step of analytical sequence for the differentiation of 54 OEM paint (only consider the OEM layer) is summarized in *Table 78*. Samples originating from Group OEM4 generally exhibited a higher level of discriminative characteristics compared to samples from Group OEM3. The cumulative discriminatory power achieved through the utilization of all techniques to differentiate the set of 54 white OEM automotive paint samples reached 99.3%, resulting in only 10 pairs of samples remaining undifferentiated.

Table 78. Discriminating power of each technique distinguishing among the 54 OEM automotive paint samples as well as the two layer groups (OEM3 and OEM4)

STEPS	TECHNIQUE	OEM3 (N=26)	OEM4 (N=28)	TOTAL OEM (N=54)
1	Microscopy	62.5% (122)	92.6% (28)	92.1% (150)
2	FTIR	83.4% (54)	96.8% (12)	95.4% (66)
3	Raman	77.5% (73)	92.1% (30)	92.8% (103)
5	Microscopy + IR	93.8% (20)	98.7% (5)	98.3% (25)
6	Microscopy + IR + Raman	94.2% (19)	98.9% (3)	98.5% (22)
7	Microscopy + IR + Raman + Py-GC/MS	97.8%(7)	-	99.3% (10)

Table 79 provides a comprehensive overview of the collective discriminatory power of all techniques employed for distinguishing the entire sample set considering all the layers (taking into account actual different layer structure due to additional repainted layer on top of OEM system). Through the completion of the analytical sequence defined in this study, an impressive discriminative power of 99.6% was attained for this particular sample set, resulting in only 7 pairs of samples remaining undifferentiated. Further details concerning the vehicle information of these undifferentiated samples are presented in *Table 80*. The geographic distribution of these undifferentiated samples associated with assembly plants is illustrated in *Figure 153.*

The findings indicate that while Raman analysis proved effective in distinguishing white automotive paint samples, it did not substantially enhance discrimination beyond the results of microscopy and IR analysis. Furthermore, the information revealed by Raman analysis demonstrated remarkable consistency with the outcomes of IR analysis. Consequently, in practical applications, conducting both IR and Raman analyses appears redundant for white automotive paint.

However, considering the higher discriminating power demonstrated by Raman analysis in differentiating clearcoat layers, it could be advantageous to apply only one technique to each specific layer. This strategic approach has the potential to yield a higher discriminating power than a single technique could achieve on its own. Ultimately, this would lead to an equivalent discriminatory capability as employing both techniques, while streamlining the analytical process, as discussed in chapter 11.2.2.

Table 79. Discriminating power obtained from each stage of analytical sequence for differentiating 62 automotive paint samples in this sample set.

TECHNIQUE	ENTIRE SAMPLE SET ALL THE LAYERS (N=62)
MICROSCOPY	95.8% (79)
MICROSCOPY + IR	98.9% (20)
MICROSCOPY + IR + RAMAN	99% (18)
MICROSCOPY + IR + RAMAN + PY-GC/MS	99.6% (7)

Table 80. Vehicle information of undifferentiated samples by combined microscopy, FTIR, Raman and Py-GC/MS analysis

Group No.	Sample No.	Manufacturing company	Model	Production year	Topcoat color code	Assembly plant	Layer structure
1	W002	F-VW	Sagitar	2017	LC9A	Chengdu	OEM3
	W023	F-VW	Sagitar	2017	LC9A	Chengdu	OEM3
2	W033	S-VW	New Lavida	2014	LY9H	Nanjing	OEM3
	W046	S-VW	Passat	2013	LY9H	Nanjing	OEM3
3	W012	S-VW	New Lavida	2017	LY9H	Nanjing	OEM3
	W032	S-VW	Gran Lavida	2015	LY9H	Anting	OEM3
	W042	S-VW	New Lavida	2017	LY9H	Anting	OEM3
4	W047	S-VW	New Lavida	2017	LY9H	Nanjing	OEM3
	W049	S-VW	New Lavida	2016	LY9H	Anting	OEM3
5	W003	S-VW	Polo	2017	Unknown	Anting	OEM4
	W039	S-VW	Polo	2017	LY9H	Anting	OEM4

Figure 153. Geographic distribution of undifferentiated samples associated with assembly plants after conducting the complete analytical sequence.

In inclusion, the implemented analytical sequence in this study has demonstrated its efficacy in distinguishing samples with exceedingly similar origins. This finding underscores that despite the mass production of automotive paint, the analysis can still yield a notable level of discrimination. This observation underscores the significant evidential value inherent in paint analysis.

## 11.5. Geographic variation in Chinese Produced OEM Paint Samples and Samples from EUCAP Databases

In this section, the geographic variation among Chinese produced OEM paint samples and samples from the EUCAP databases were investigated. The aim is to explore whether there are any discernible differences in the chemical composition of automotive paint samples based on their geographic origin.

Initially, a search was conducted in the EUCAP databases using the keywords 'VW' and 'white' to retrieve IR spectra of basecoat. A total of 166 basecoat spectra were found in five solid basecoat databases from Germany, France, Belgium and Spain. When available (which was not always the case), the basecoat spectra were linked to specific identifiers known as 'FRCAP numbers'. These identifiers facilitated the connection of spectra from other layers originating from the same vehicle within other databases. It is important to note that the registered information for these spectra was frequently incomplete. This included missing production location information, or even instances where details such as model or production year were absent. Certain IR spectra were sourced directly from raw paint materials provided by paint suppliers like BASF and PPG. Often, these samples were not associated with specific vehicle models or production years, further complicating the geographic investigation.

Among the registered spectra, only one topcoat color code (LB9A) and six models (Golf, Polo, Passat, Tiguan, Touran, Jetta) were discovered, which are consistent with either the color code or models produced in China. The six identified models in the EUCAP databases all exhibit a color code LB9A, which is different from the color code LY9H found in the Chinese-produced vehicles. Furthermore, the chemical composition of basecoat and clearcoat within the same model also differs, as depicted in *Figure 154*. This reveals the geographic variation among Chinese and European produced OEM paint in terms of model and color code.

However, It is noteworthy that while the European-produced sample (W026) in this dataset exhibited a distinct chemical profile in comparison to the Chinese-produced vehicles, It is crucial to acknowledge that the chemical classes identified in the Chinese-produced vehicles are not exclusive. Analogous profiles for each layer can also be found within the EUCAP database. For instance, *Figure 155* presents a comparison between a Chinese-produced sample, W014, with a vehicle model 'New Lavida' and a topcoat color code 'LY9H', and a European-produced sample, 15162, with a vehicle model 'Polo' and a topcoat color code 'LB9A'. The primer, basecoat, and clearcoat of these paints were examined and compared. The results depicted in the figure suggest that while not entirely indistinguishable, there are common identifiable chemical compounds used in both European and Chinese vehicles. This observation implies a lack of geographical variation in paint composition, irrespective of differences in model or color codes.

Therefore, the data acquired from this study might not serve as a comprehensive investigative tool for providing specific vehicle information for inquiries in Europe. However, it can still be employed as a valuable data source for the purpose of interpretation.
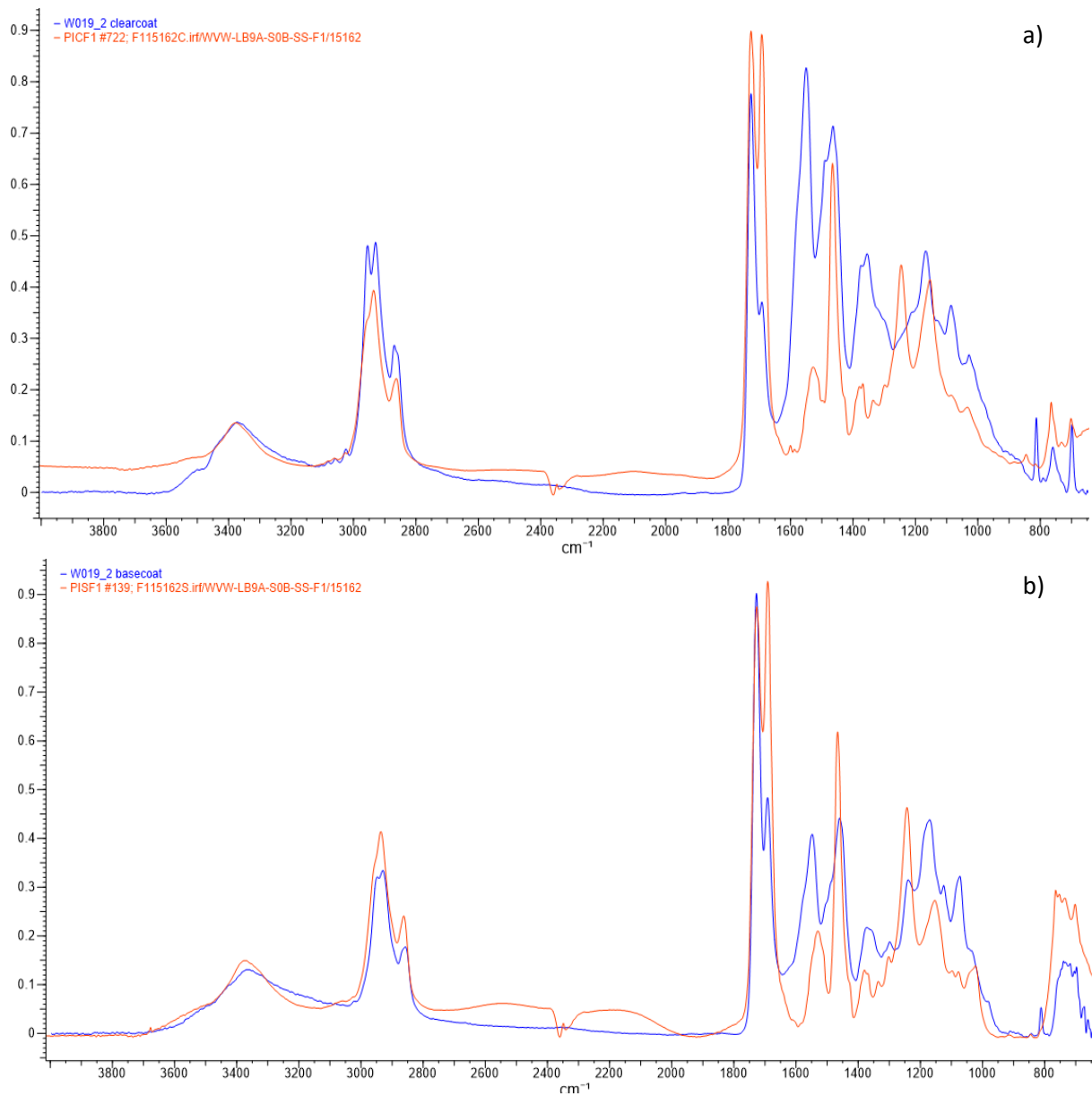
Figure 154. IR spectra of vehicle model 'Polo', one produced in China (Sample W019, spectra in blue) and the other in Europe (Sample 15162, spectra in red), exhibit distinct chemical compositions in the clearcoat (a) and basecoat (b).
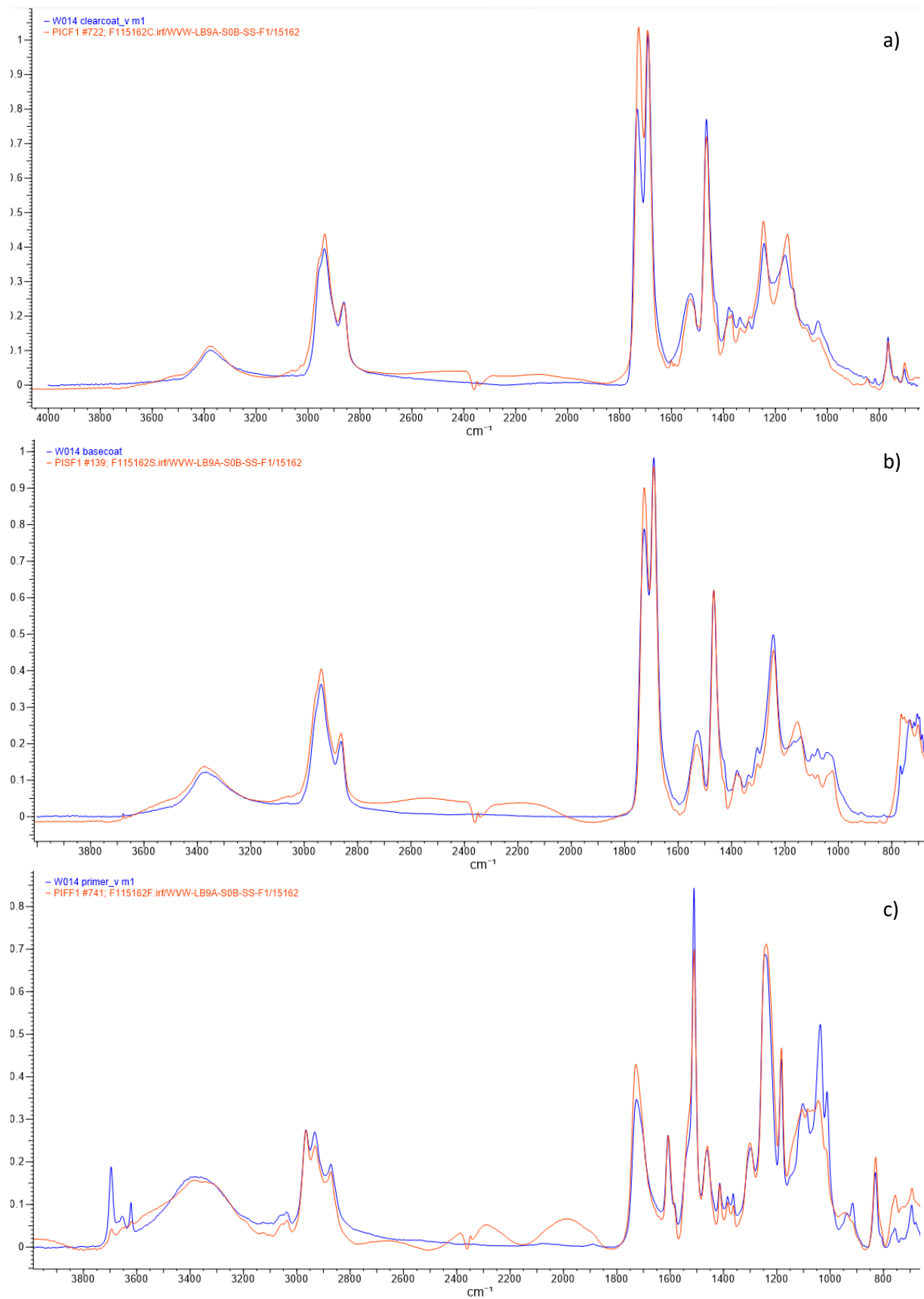
Figure 155. IR spectra of vehicles produced in China (Sample W014, spectra in blue) and Europe (Sample 15162, spectra in red), demonstrating similar chemical profiles in primer (a), basecoat (b) and clearcoat (c) regardless model or color code variation.

11.6. Global vision

This study can be regarded as a specialized color block study, as it not only confines itself to a specific color but also narrows its focus to a particular car manufacturer. The samples selected originate exclusively from Volkswagen (VW) vehicles, all of which share the same color (white) and belong to a limited production timeframe, primarily ranging from 2010 to 2018. It is worth underscoring that this study represents not only the initial but also the sole research in which such a comprehensive and thorough investigation has been conducted on this specific category of closely related samples. The author believes that the investigation of this distinctive sample collection using conventional analytical techniques such as microscopy, FTIR, Raman spectroscopy, and Py-GC/MS can yield novel insights that may prove valuable to forensic practitioners.

1) This study validates the discriminating capabilities of common techniques for closely similar samples. Each technique demonstrates a relatively high discriminating power. **FTIR stands out as the most effective method for discriminating white automotive paint**, with only 66 pairs of samples remaining undifferentiated (DP=95.4%). Additionally, this study **highlights Raman spectroscopy as a viable alternative to FTIR**, as it leaves only 103 pairs of samples undistinguished (DP=92.8%).

2) It becomes evident in this study that, **for white automotive paint, conducting both IR and Raman analyses for all layers may not be necessary**, given the similar insights offered by both techniques. This similarity primarily arises from the limited information available for Raman detection and identification of white paint pigments. The complementary aspect of Raman analysis would become more pronounced when dealing with colored paint, where Raman analysis unveils abundant pigment information. Conversely, **for neutral colors like white, grey, or black, the added discrimination offered by Raman analysis may be limited**.

3) Given the multiple layers in automotive paint, this study identifies the most effective techniques for analyzing individual layers and unveils optimal layer-technique combinations for distinguishing white automotive paint. Raman spectroscopy exhibits superior discriminatory power over IR when analyzing clearcoat, making it the preferred technique for this layer. This finding aligns with other studies conducted on Australian and North American paint samples (Maric *et al.*,2016; Affadu-Danful *et al.*,2023), further suggesting that **Raman spectroscopy offers higher potential over FT-IR in identifying and discriminating automotive clearcoats, regardless of car make or production location**. In this study, combining IR analysis for primer with Raman analysis for clearcoat achieves exceptionally effective discrimination, resulting in a discrimination power of 95.7% (only 62 undifferentiated pairs). This approach is consistent with the findings of Eyring *et al.*, who, using a different sample set, demonstrated that robust discrimination can be attained by analyzing primer and

clearcoat through IR without the need to analyze the basecoat (Eyring *et al.*, 2007). Thus, it is reasonable to infer **that the combination of IR analysis for primer and Raman analysis for clearcoat represents the most effective approach for discriminating automotive paint, irrespective of car make or color**.

4) This study collected samples from various locations within the same vehicle and assessed the intra-sample variability among these subsamples. The examination of white OEM automotive paint samples revealed significant intra-sample variability in terms of physical attributes, as evidenced by microscopic analysis. Out of 43 samples that had subsamples, a notable 79% of them exhibited variations in layer structure, relative layer thickness, and layer color, underscoring the diversity within individual samples in terms of their physical characteristics. Conversely, the intra-sample variability from a chemical standpoint was found to be minimal. Consequently, in practical forensic cases, **it is imperative to gather reference samples from various locations within the vehicle and be cautious when making exclusion decisions solely based on observed microscopic variations**.

5) The analysis of white OEM automotive paint samples delved into the factors contributing to sample differentiation, including the vehicle model, production years, and assembly plant. **This investigation unveiled a significant role played by the assembly plant in determining both the physical attributes and chemical profiles of the paints**. Notably, samples originating from the same assembly plant exhibited identical layer structures and similar chemical compositions, irrespective of variations in the manufacturing company, model, or production year. This underscores the potent influence of the assembly plant in maintaining consistency in the physical and chemical characteristics within a specific group of samples. **By identifying and combining the chemical information obtained from each layer, it is possible to determine the potential assembly plant of paint samples, thus further determine the make and model of a vehicle. Variations related to the production year, on one hand, were attributed to manufacturer decisions regarding changes in production lines or paint formulas for specific models over time, while on the other hand, they were primarily attributed to batch-to-batch variations**. By obtaining these findings, this study offers a more comprehensive perspective on the paint market and manufacturing plants.

6) This study delves deeply into the correlation between the chemical composition of the basecoat and the topcoat color code. Typically, automotive paint's topcoat color code enables the designation of the specific formula for an original color associated with a car brand, implying that identical topcoat color codes should yield identical appearances. However, the findings in this study reveal that **sample discrimination does not align with the topcoat color code**. In other words, **undifferentiated basecoats may possess varying color codes, and samples sharing identical color codes do not consistently display identical chemical compositions in their basecoats**.

This observation challenges the conventional assumption regarding the relationship between color codes and basecoat compositions.

7) Geographic variations were identified between Chinese and European-produced OEM paints concerning both the model and color code. Notably, samples sharing the same model did not consistently belong to the same chemical class and have identical color codes. Consequently, the data generated from this study may not offer a comprehensive investigative tool for providing specific vehicle information within Europe. However, it is worth highlighting that, while not entirely indistinguishable, there are common and identifiable chemical compounds found in both European and Chinese vehicles. This observation suggests a lack of geographical variation in paint composition, regardless of different model or color codes. As such, **the acquired data remains a valuable resource for interpretation purposes**.

8) This study ventured beyond the expectations of a typical population study, delving deeper into the occurrence of paint within a constrained range. In automotive paint interpretation, it is crucial to assess the occurrence of a particular paint being encountered in a relevant population. Typically, this involves multiplying the prevalence of a specific color by the occurrence of its chemical properties, often discerned through IR analysis. To achieve this, database searches are employed to locate matching spectra within the pertinent population. For instance, if the relevant population is limited to white Volkswagen (VW) vehicles, one must consider evaluating the proposition that the suspect's white VW was used in the commission of a crime (Hp) versus another white VW vehicle being involved (Hd).

As previously noted, the available basecoat spectra for white VW vehicles in five EUCAP solid basecoat databases total only 166, a relatively small number compared to the overall 60,000 IR spectra in the EUCAP database. Furthermore, only a fraction of these spectra encompasses complete data from all layers originating from the same vehicle. **By incorporating the IR spectra data obtained from this study into the existing databases, the occurrence of encountering the chemical properties of the given paint can be substantially reduced, particularly when considering all layers**. Moreover, the inclusion of other techniques such as microscopy, Raman, and Py-GC/MS was expected to further diminish the global occurrence of such paint. This study lays the groundwork for introducing a estimate factor aimed at reducing global occurrence. Notably, it became evident in this study that the supplementary use of either microscopy or Raman analysis reduced the number of undifferentiated paint samples by a factor of 2. The additional application of Py-GC/MS led to an even greater reduction, lowering the number of undifferentiated samples by a factor of 2. By incorporating these additional techniques into the assessment, **it was estimated that the overall occurrence, as determined solely by IR analysis, could be reduced to at least ¼, thereby enhancing the final likelihood ratio**.

12. Conclusion & Perspective

In this study, a total of 62 white Volkswagen automotive paint samples with 135 subsamples were collected in China, and they underwent a comprehensive analytical sequence for characterization. The analysis included microscopic examination, FTIR analysis, Raman analysis, and Py-GC/MS analysis.

All these 135 subsamples were undertaken microscopic examination using transmitted light bright field and dark filed, polarized light, and Alexa Fluor 488 fluorescence illumination. Microscopic examination of the samples revealed three types of layer systems (OEM3, OEM4, and repainted) and significant intra-sample variability in terms of layer structure, relative layer thickness, and layer color. The examination identified 150 pairs of samples that remained undifferentiated, resulting in a discriminating power of 92.1%. Extending the consideration to all existing layers, the examination left 79 pairs of samples that were undifferentiated, yielding a discriminative power of 95.8%.

FTIR analysis was then conducted on the entire set of samples, as well as a subset of 54 OEM automotive paint samples, to evaluate inter-sample variability and the correlation between chemical characteristics and sample origin. The analysis revealed minimal intra-sample variability. Repainted samples easily differentiated from OEM paint samples and from each other. The chemical composition of OEM paint samples showed a high correlation with the layer structure, with distinct chemical classes identified in the basecoat and clearcoat of OEM3 and OEM4 groups. However, it is worth noting that the primer layer exhibited a high level of similarity between the OEM3 and OEM4 groups. The chemical composition and characteristics of the primer were found to be quite identical in both groups, indicating a consistent formulation or composition of the primer layer regardless of the overall layer structure. This suggests that the primer layer may play a less significant role in differentiating between the OEM3 and OEM4 groups compared to the other layers in the paint system. The discriminating powers of FTIR analysis for each layer and layer combination were calculated. By combining the discrimination results from all layers, a total of 66 sample pairs remained undifferentiated, resulting in a discriminating power of 96.5% when considering all 62 samples, and 95.4% when considering only the 54 OEM samples.

Raman analysis was conducted on representative samples from the 54 OEM paints, examining each layer individually. It was found that Raman analysis provided similar information to FTIR analysis regarding binders and extenders but had limited contribution in pigment identification due to pigment formulation limitations in white paint. The discriminating powers of Raman analysis for each layer and layer combination were also calculated, with a higher discriminating power observed for the clearcoat compared to FTIR analysis. After combining the results from all layers, 103 sample pairs remained undifferentiated, resulting in a discriminating power of 92.8%.

A separate project focusing on analyzing white automotive paint basecoat using Py-GC/MS was performed. The basecoat of 23 samples that could not be differentiated by FTIR analysis was selected for analysis. The project explored the sample preparation method and optimized instrument settings for the analysis of polyurethane basecoat. Py-GC/MS analysis showed further discrimination for undifferentiated basecoat samples, with only 17 pairs of samples remaining undifferentiated and a discriminating power of 93.3%.

By combining the results of FTIR and Raman analysis, the full chemical characteristics of OEM white automotive paint and the inter-sample variability were investigated. Raman analysis confirmed the chemical composition identified by FTIR analysis and provided additional characterization of certain compounds. The integration of FTIR and Raman analysis resulted in only 34 undifferentiated sample pairs, with a discriminating power of 97.6%. This highlighted the high discrimination capability of both techniques and revealed the unique physical and chemical properties of individual paint samples, providing strong evidential value for automotive paint analysis.

While Raman analysis exhibited effectiveness in differentiating white automotive paint samples, it did not contribute significantly to discrimination beyond the outcomes of microscopy and IR analysis. Consequently, in practical scenarios, the utilization of both IR and Raman analyses appears to be redundant. An insightful approach uncovered in this study involves strategically applying the most discriminatory technique to a specific individual layer. In this context, **employing Raman analysis for clearcoat and primer measurement and utilizing IR for basecoat and primer measurement yields a superior discriminating power (97.4%) than what a single technique could achieve on its own**. Ultimately, this approach could achieve a similar level of discriminatory capability as employing both techniques (97.6%), while simultaneously simplifying the analytical process.

The necessity of analyzing all layers was thoroughly examined, revealing that a highly effective discriminatory outcome can be achieved by analyzing the primer with IR and the clearcoat with Raman spectroscopy. This strategic combination resulted in an impressive discriminating power of 95.7%. Additionally, as these layers frequently constitute the surface layer and demand minimal sample preparation, this pairing emerges as the most efficient and cost-effective choice. By comparing with the existing studies, it is reasonable to infer that **the combination of IR analysis for primer and Raman analysis for clearcoat represents the most effective approach for discriminating automotive paint, irrespective of car make or color**.

Through the completion of the analytical sequence defined in this study, an impressive discriminative power of 99.6% was attained for this particular sample set, resulting in only 7 pairs of samples remaining undifferentiated.

The study thoroughly investigated the undifferentiated sample pairs, the correlation between paint characteristics and sample origin (manufacturing company, model, assembly plant), and the sample variability related to topcoat color, production year, batch variation, and geographic variation using the integrated data. The findings successfully addressed the research questions posed in this study as follows:

1) **To what extent OEM-paint from mass-produced vehicles of same color manufactured by same make, can be differentiated and under what conditions can this be done?**

The investigation of white OEM automotive paint through microscopy, FTIR, Raman spectroscopy and Py-GC/MS revealed that paints originating from the same manufacturer, with the same color and model, and produced in the same assembly plant in the same year can potentially be differentiated based on their physical and chemical characteristics. Both individual FTIR and Raman analysis demonstrated the capability to achieve this level of discrimination. Furthermore, when the two techniques were combined, an even greater level of discrimination was achieved, allowing for further differentiation among the samples. This suggests that the combination of FTIR and Raman spectroscopy can enhance the ability to distinguish between mass-produced vehicles of the same color, manufactured by the same make, under specific conditions. Additionally, Py-GC/MS analysis extends the discriminatory capabilities by distinguishing white basecoats with identical origins that could not be differentiated through FTIR and Raman analyses alone. This study goes beyond the typical scope of population studies, delving deeper into the occurrence of paint within a constrained range and demonstrated the significant rarity of one specific paint encountered in casework.

2) **Which identifying factor (model, topcoat color code, production years, assembly paint) contributes the greatest towards non differentiation of samples?**

The analysis of the white OEM automotive paint samples revealed that the assembly plant played a significant role in determining the chemical properties of the paints. Samples originating from the same assembly plant exhibited similar chemical profiles, regardless of the specific manufacturing company, model, or production year. This indicates that **the assembly plant has a strong influence on the consistency of the chemical composition within a specific group of samples**. However, it is worth noting that even within the same assembly plant, variations in the chemical properties were still observed among the samples. This suggests that while the assembly plant contributes significantly to the non-differentiation of samples, there are other factors at play that contribute to the overall variation in the chemical profiles. **By identifying and combining the chemical information obtained from each layer, it is possible to determine the potential assembly plant of paint samples, thus further determine the make and model of a vehicle.**

3) What is the degree of inter-sample and intra-sample variability as well as batch variation of automotive paint?

The analysis of the white OEM automotive paint samples revealed significant intra-sample variability in terms of physical features, as observed through microscopic examination. Among the 62 samples, 43 had subsamples, and 79% of them showed noticeable variations in layer structure, relative layer thickness, and layer color. This indicates that there is a considerable level of diversity within individual samples. In contrast, the intra-sample variability from a chemical feature perspective was found to be minimal. Both the IR and Raman analyses demonstrated consistent chemical compositions within each sample, indicating a high level of similarity in terms of chemical properties. Consequently, in practical forensic cases, **it is imperative to gather reference samples from various locations within the vehicle and be cautious when making exclusion decisions solely based on observed microscopic variations.**

On the other hand, the inter-sample variability was found to be relatively high. The discrimination power of the microscopic examination (95.8%), IR analysis (96.5%), Raman analysis (92. 8 %), PY-GC/MS analysis (93.3%) all indicated significant variations among the samples within this sample set. This suggests that there are notable differences in the chemical and physical characteristics among the different samples.

Batch variation was detected in this sample set. It was found that batch variation was the primary factor contributing to the differentiation of samples with identical manufacturing company, model, color, assembly plant, and production year. The presence of batch variation further supports the high level of variability observed in the samples.

Overall, the high levels of intra-sample, inter-sample, and batch variation highlight the rarity of the physical and chemical properties exhibited by individual samples. These findings emphasize the importance of comprehensive analysis techniques in differentiating and characterizing automotive paint samples.

4) Which single layer can contribute the greatest distinction and what layer combination examination can provide sufficient evidential value?

The analysis of individual layers using FTIR and Raman spectroscopy demonstrated a relatively high discriminating power, with clearcoat analysis contributing the greatest discrimination among all the layers. In both FTIR and Raman analysis, the clearcoat exhibited the highest discriminating power, with Raman analysis of clearcoat achieving the highest discrimination capability (88.0%) among all the single layer analyses.

When considering the combination of multiple layers, an insightful strategy has been identified: **analyzing the primer with IR and the clearcoat with Raman spectroscopy.** This approach not only demands minimal sample preparation but also yields remarkable discriminatory results, achieving a discriminating power of 95.8%, with a mere 60 pairs of samples remaining undifferentiated. This particular pairing stands out as the most efficient and cost-effective option, regardless of car make or color.

Through the systematic analysis of a meticulously chosen sample set comprising Chinese produced White Volkswagen automotive paint, this research has contributed to a better comprehension of the contemporary variations in manufactured automotive paint. By employing a comprehensive analytical sequence encompassing microscopy, FTIR spectroscopy, Raman spectroscopy, and Pyrolysis GC/MS, a thorough investigation of the chemical properties of the paint was conducted.

Comparing the obtained results with samples from the European Coatings Automotive Paints (EUCAP) databases, it was observed that the chemical characteristics of Chinese produced paint exhibit similarities with those of European produced paints. This finding suggests a reduced level of geographic variation in automotive paint properties.

The insights and data derived from this research hold significant value for the interpretation of automotive paint analysis in forensic casework as it broadens the existing population in current databases and lays the foundation for introducing an estimate factor to diminish global occurrence when employing supplementary techniques for automotive paint analysis. By expanding our understanding of the variations in contemporary automotive paint, forensic scientists and analysts can draw more accurate and informed conclusions when examining paint evidence in investigations.

Although this study has paved the way for a deeper understanding of automotive paint analysis, certain areas remain unexplored. One notable aspect that warrants future investigation is the potential impact of weathering on paint samples. While this study did not delve into weathering effects, a promising avenue for further research lies in employing Attenuated Total Reflectance (ATR) spectroscopy to assess this aspect comprehensively. By including this dimension, a more comprehensive understanding of how paint samples may evolve over time can be gained.

This study has unveiled a certain level of intra-sample variability stemming from distinct locations within the vehicle. To deepen the understanding, further research can focus on the frequency and prevalence of this intra-sample variability. This can be achieved through the collection of multiple samples from various parts of different vehicles. By conducting a systematic investigation on a broader scale, we can gain insights into the consistency of this variability across different contexts and vehicle types. This would not only enhance our comprehension of paint characteristics but also contribute to the refinement of analysis strategy in the context of forensic paint examination.

The rich and informative data produced in this study opens avenues for further exploration into how this knowledge can be optimally utilized in aiding paint evidence interpretation and evaluation. To this end, conducting detailed case studies that apply the insights from this study to real-world scenarios could provide valuable insights. Such case studies would demonstrate their practical application within forensic analysis.

While the statistical model developed in this study has proven valuable in discriminating between various paint samples, it may fall short in capturing subtle variations. As the field of data analysis continues to evolve, there is an opportunity to develop more advanced tools, such as machine learning algorithms, to build more powerful and robust models.

In conclusion, the comprehensive analysis and comparisons conducted in this research provide a solid foundation for future forensic investigations involving automotive paint. The findings contribute to the body of knowledge in this field and enhance the capabilities of forensic experts in determining the origin and characteristics of automotive paint samples.

13. References

Adams, M. J. (2004). Chemometrics in Analytical Spectroscopy. 2nd Edition. The Royal Society of Chemistry.

AdobePhotoshop. "Introduction to Camera Raw." Retrieved Jun 6, 2021, from https://helpx.adobe.com/camera-raw/using/introduction-camera-raw.html.

Affadu-Danful, G. P., Zhong, H., Dahal, K. S., Kalkan, K., Zhang, L. ,Lavine, B. K. (2023). Raman Spectroscopy to Enhance Investigative Lead Information in Automotive Clearcoats. Appl Spectrosc **77**(9): 1064-1072. Doi: http://doi.org/10.1177/00037028231186838

Akafuah, N. K., Poozesh, S., Salaimeh, A., Patrick, G., Lawler, K. ,Saito, K. (2016). Evolution of the Automotive Body Coating Process—A Review. Coatings **6**(2): 24. Doi: https://doi.org/10.3390/coatings6020024

Allen, T. J. (1992a). The examination of thin sections of coloured paints by light microscopy. Forensic Science International **57**(1): 5-16. Doi: https://doi.org/10.1016/0379-0738(92)90040-4

Allen, T. J. (1992b). Paint sample presentation for Fourier transform infrared microscopy. Vibrational Spectroscopy **3**(3): 217-237. Doi: https://doi.org/10.1016/0924-2031(92)87004-Y

Ansdell, D. A. (1999). Automotive paints. In Paint and Surface Coatings(eds Lambourne, R. and Strivens, T. A.). Woodhead Publishing**:** 411-491.

ASTM-D16-19 Standard Terminology for Paint, Related Coatings, Materials, and Applications. West Conshohocken, PA. ASTM International. Doi: https://doi.org/10.1520/D0016-19

ASTM-E1421-99[2015]e1 Standard Practice for Describing and Measuring Performance of Fourier Transform Mid-Infrared (FT-MIR) Spectrometers: Level Zero and Level One Tests. West Conshohocken, PA. ASTM International. Doi: https://doi.org/10.1520/E1421-99R15E01

ASTM-E1610-18 Standard Guide for Forensic Paint Analysis and Comparison. West Conshohocken, PA. ASTM International. Doi: https://doi.org/10.1520/E1610-18

ASTM-E1840-96[2014] Standard Guide for Raman Shift Standards for Spectrometer Calibration. West Conshohocken, PA. ASTM International. Doi: https://doi.org/10.1520/E1840-96R14

ASTM-E1866-97[2013] Standard Guide for Establishing Spectrophotometer Performance Tests. West Conshohocken, PA. ASTM International. Doi: https://doi.org/10.1520/E1866-97R13

ASTM-E2911-13 Standard Guide for Relative Intensity Correction of Raman Spectrometers. West Conshohocken, PA. ASTM International. Doi: https://doi.org/10.1520/E2911-13

ASTM-E2937-18 Standard Guide for Using Infrared Spectroscopy in Forensic Paint Examinations. West Conshohocken, PA. ASTM International. Doi: https://doi.org/10.1520/E2937-18

Audette, R. J. ,Percey, R. F. E. (1982). A rapid systematic, and comprehensive classification system for the identification and comparison of motor vehicle paint samples. ll: Paint data collected from Chrysler-manufactured cars. Journal of Forensic Sciences **27**(3): 622-670. Doi: https://doi.org/10.1520/jfs12173j

Audette, R. J. ,Percy, R. F. E. (1979). A rapid, systematic, and comprehensive classification system for the identification and comparison of motor vehicle paint samples. I: The nature and scope of the classification system. Journal of Forensic Sciences **24**(4): 790-807. Doi: https://doi.org/10.1520/jfs10908j

Bauer, D. R. (1997). Predicting in-service weatherability of automotive coatings: A new approach. Journal of Coatings Technology **69**(864): 85-96. Doi: https://doi.org/10.1007/BF02696095

Bauer, D. R. (2000). Interpreting weathering acceleration factors for automotive coatings using exposure models. Polymer Degradation and Stability **69**(3): 307-316. Doi: https://doi.org/10.1016/S0141-3910(00)00074-4

Beauchaine, J. P., Peterman, J. W. ,Rosenthal, R. J. (1988). Applications of FT-IR/microscopy in forensic analysis. Mikrochimica Acta **94**(1-6): 133-138. Doi: https://doi.org/10.1007/BF01205855

Bell, S. E. J., Fido, L. A., Speers, S. J. ,Armstrong, W. J. (2005c). Rapid forensic analysis and identification of "lilac" architectural finishes using Raman spectroscopy. Applied Spectroscopy **59**(1): 100-108. Doi: https://doi.org/10.1366/0003702052940404

Bell, S. E. J., Fido, L. A., Speers, S. J., Armstrong, W. J. ,Spratt, S. (2005a). Forensic analysis of architectural finishes using fourier transform infrared and raman spectroscopy, part I: The resin bases. Applied Spectroscopy **59**(11): 1333-1339. Doi: https://doi.org/10.1366/000370205774783296

Bell, S. E. J., Fido, L. A., Speers, S. J., Armstrong, W. J. ,Spratt, S. (2005b). Forensic analysis of architectural finishes using fourier transform infrared and raman spectroscopy, part II: White paint. Applied Spectroscopy **59**(11): 1340-1346. Doi: https://doi.org/10.1366/000370205774783232

Bell, S. E. J., Stewart, S. P. ,Armstrong, W. J. (2012). Raman Spectroscopy for Forensic Analysis of Household and Automotive Paints. In Infrared and Raman Spectroscopy in Forensic Science(eds Chalmers, J. M., Edwards, H. G. M. et al.). John Wiley & Sons, Ltd**:** 121-135.

Bender, L. (2013). Automotive Paint. Encyclopedia of Forensic Sciences. Siegel, J. A., Saukko, P. J. et al. Waltham, Academic Press**:** 257-264.

Bonaduce, I. ,Andreotti, A. (2009). Py-GC/MS of Organic Paint Binders. In Organic Mass Spectrometry in Art and Archaeology(eds Colombini, M. P. and Modugno, F.). John Wiley & Sons, Ltd**:** 303-326.

Bradley, M. J., Hobbs, A. L., Wright, D. M. ,Koons, R. D. (2007). Paint and Glass. In International Forensic Science Symposium Interpol Reports 2007(eds Daéid, N. and Houck, M. M.). CRC Press**:** 89-151.

Brereton, R. G. (2007). Applied Chemometrics for Scientists. John Wiley & Sons, Inc.

Brereton, R. G. (2007). Pattern Recognition. In Applied Chemometrics for Scientists. John Wiley & Sons, Inc.**:** 145-191.

Brereton, R. G. (2009). Chemometrics for Pattern Recognition. John Wiley & Sons, Ltd.

Brown, K. L. ,Clark, R. J. H. (2004). Analysis of key Anglo-Saxon manuscripts (8–11th centuries) in the British Library: pigment identification by Raman microscopy. Journal of Raman Spectroscopy **35**(3): 181-189. Doi: https://doi.org/10.1002/jrs.1127

Buckle, J., Fung, T. ,Ohashi, K. (1987). Automotive Topcoat Colours: Occurrence Frequencies in Canada. Canadian Society of Forensic Science Journal **20**(2-3): 45-56. Doi: https://doi.org/10.1080/00085030.1987.10756940

Buckle, J. L., Macdougall, D. A. ,Grant, R. R. (1997). PDQ—paint data queries: The history and technology behind the development of the royal canadian mounted police forensic laboratory services automotive paint database. Journal of the Canadian Society of Forensic Science **30**(4): 199-212. Doi: https://doi.org/10.1080/00085030.1997.10757099

Burns, D. T. ,Doolan, K. P. (2005a). A comparison of pyrolysis-gas chromatography-mass spectrometry and fourier transform infrared spectroscopy for the characterisation of automative paint samples. Analytica Chimica Acta **539**(1-2): 145-155. Doi: https://doi.org/10.1016/j.aca.2005.02.048

Burns, D. T. ,Doolan, K. P. (2005b). The discrimination of automotive clear coat paints indistinguishable by Fourier transform infrared spectroscopy via pyrolysis-gas chromatography-mass spectrometry. Analytica Chimica Acta **539**(1-2): 157-164. Doi: https://doi.org/10.1016/j.aca.2005.02.047

Buzzini, P., Massonnet, G. ,Sermier, F. M. (2006). The micro Raman analysis of paint evidence in criminalistics: Case studies. Journal of Raman Spectroscopy **37**(9): 922-931. Doi: https://doi.org/10.1002/jrs.1522

Buzzini, P. ,Stoecklein, W. (2005). FORENSIC SCIENCES | Paints, Varnishes, and Lacquers. In Encyclopedia of Analytical Science(eds Worsfold, P., Townshend, A. et al.). Elsevier**:** 453-464.

CAAM. (2018). "Sales ranking of the top ten manufacturers of automotive in China 2017(2017 年中国品牌汽车分车型前十家生产企业销量排名)." from http://www.caam.org.cn/chn/4/cate_39/con_5214780.html.

Caddy, B. (2001). Forensic Examination of Glass and Paint : Analysis and Interpretation. 1st edition. CRC Press.

Campanella, B., Palleschi, V. ,Legnaioli, S. (2021). Introduction to vibrational spectroscopies. ChemTexts **7**. Doi: https://doi.org/10.1007/s40828-020-00129-4

Carlesi, S., Ricci, M., Cucci, C., Lofrumento, C., Picollo, M. ,Becucci, M. (2016). Multivariate analysis of combined reflectance FT-NIR and micro-Raman spectra on oil-paint models. Microchemical Journal **124**: 703-711. Doi: https://doi.org/10.1016/j.microc.2015.10.023

Cassista, A. R. ,Sandercock, P. M. L. (1994). Comparison and Identification of Automotive Topcoats: Microchemical Spot Tests, Microspectrophotometry, Pyrolysis-Gas Chromatography, and Diamond Anvil Cell Ftir. Canadian Society of Forensic Science Journal **27**(3): 209-223. Doi: https://doi.org/10.1080/00085030.1994.10757036

Castanys, M., Perez-Pueyo, R., Soneira, M. J., Golobardes, E. ,Fornells, A. (2011). Identification of Raman spectra through a case-based reasoning system: Application to artistic pigments. Journal of Raman Spectroscopy **42**(7): 1553-1561. Doi: https://doi.org/10.1002/jrs.2888

Challinor, J. M. (2001). Pyrolysis techniques for the characterisation and discrimination of paint. In Forensic Examination of Glass and Paint: Analysis(eds Caddy, B.). CRC Press**:** 165-182.

Chalmers, J. M., Edwards, H. G. M. ,Hargreaves, M. D. (2012a). Vibrational Spectroscopy Techniques: Basics and Instrumentation. In Infrared and Raman Spectroscopy in Forensic Science(eds Chalmers, J. M., Edwards, H. G. M. et al.). John Wiley & Sons, Ltd**:** 9-44.

Chalmers, J. M., Edwards, H. G. M. ,Hargreaves, M. D. (2012b). Vibrational Spectroscopy Sampling Techniques. In Infrared and Raman Spectroscopy in Forensic Science(eds Chalmers, J. M., Edwards, H. G. M. et al.). John Wiley & Sons, Ltd**:** 45-86.

Chalmers, J. M., Edwards, H. G. M. ,Hargreaves, M. D. (2012c). Introduction and Scope. In Infrared and Raman Spectroscopy in Forensic Science(eds Chalmers, J. M., Edwards, H. G. M. et al.). John Wiley & Sons, Ltd**:** 1-7.

Chalmers, J. M. ,Griffiths, P. R. (2002). Handbook of vibrational spectroscopy. J. Wiley.

Chaplin, T. D., Clark, R. J. H. ,Beech, D. R. (2002). Comparison of genuine (1851-1852 AD) and forged or reproduction Hawaiian Missionary stamps using Raman microscopy. Journal of Raman Spectroscopy **33**(6): 424-428. Doi: https://doi.org/10.1002/jrs.874

Chen, R., Lv, J. ,Feng, J. (2015). Characterization of Paint by Fourier-Transform Infrared Spectroscopy, Raman Microscopy, and Scanning Electron Microscopy-Energy Dispersive X-ray Spectroscopy. Analytical Letters **48**(9): 1502-1510. Doi: https://doi.org/10.1080/00032719.2014.984190

Clymer, M. ,Wei, H. (2014). Color Calibration of Digital Brightfield Microscope Images Using Colorimetry with a Color Standard Slide. Microscopy & Microanalysis 2014 Meeting, Hartford, CT.https://www.microscopy.org/MandM/2014/abstracts/LB-3.pdf

Darlene, R. ,Brezinski (1991). An Infrared Spectroscopy Atlas for the Coating Industry. Federation of Societies for Coatings Technology.

De Gelder, J., Vandenabeele, P., Govaert, F. ,Moens, L. (2005). Forensic analysis of automotive paints by Raman spectroscopy. Journal of Raman Spectroscopy **36**(11): 1059-1067. Doi: https://doi.org/10.1002/jrs.1408

Doménech, A., Doménech-Carbó, M. T. ,Edwards, H. G. M. (2011). On the interpretation of the Raman spectra of Maya Blue: A review on the literature data. Journal of Raman Spectroscopy **42**(1): 86-96. Doi: https://doi.org/10.1002/jrs.2642

Dössel, K.-F. (2008). In-Plant Repairs. In Automotive Paints and Coatings(eds Streitberger, H. J. and Dössel, K. F.)**:** 377-380.

Duarte, J. M., Sales, N. G. S., Sousa, M. H., Bridge, C., Maric, M. ,Gomes, J. D. A. (2020). Automotive paint analysis: How far has science advanced in the last ten years? TrAC **132**. Doi: https://doi.org/10.1016/j.trac.2020.116061

Edmondstone, G., Hellman, J., Legate, K., Vardy, G. L. ,Lindsay, E. (2004). An assessment of the evidential value of automotive paint comparisons. Journal of the Canadian Society of Forensic Science **37**(3): 147-153. Doi: https://doi.org/10.1080/00085030.2004.10757572

Edwards, H. G. M., Villar, S. E. J., David, A. R. ,De Faria, D. L. A. (2004). Nondestructive analysis of ancient Egyptian funerary relics by Raman spectroscopic techniques. Analytica Chimica Acta **503**(2): 223-233. Doi: https://doi.org/10.1016/j.aca.2003.10.057

EPGT (2022). Best Practice Manual for the Forensic Examination of Paint.

EPGT (2022). Guideline for the forensic examination of paint by SEM/EDX.

EPGT(EPG-GDL-002) (2022). Guideline for the forensic examination of paint by Fourier-transform infrared spectroscopy.

Eyring, M., Lovelace, M. ,Sy, D. (2007). A Study of the Discrimination of Some Automotive Paint Films having Identical Color Codes. Proceedings of the Trace Evidence Symposium, Clearwater Beach, FL.https://projects.nfstc.org/trace/docs/Trace%20Presentations%20CD-2/eyring.pdf

Fasasi, A., Mirjankar, N., Stoian, R. I., White, C., Allen, M., Sandercock, M. P. ,Lavine, B. K. (2015). Pattern recognition-assisted infrared library searching of automotive clear coats. Applied Spectroscopy **69**(1): 84-94. Doi: https://doi.org/10.1366/14-07578

FAW-Volkswagen. "Enterprise Overview." from https://www.faw-vw.com/summary.html.

Ferreira, K. B., Oliveira, A. G. G. ,Gomes, J. A. (2017). Raman spectroscopy of automotive paints: Forensic analysis of variability and spectral quality. Spectroscopy Letters **50**(2): 102-110. Doi: https://doi.org/10.1080/00387010.2017.1288635

Ferreira, K. B., Oliveira, A. G. G., Gonçalves, A. S. ,Gomes, J. A. (2017). Evaluation of Hyperspectral Imaging Visible/Near Infrared Spectroscopy as a forensic tool for automotive paint distinction. Forensic Chemistry **5**: 46-52. Doi: https://doi.org/10.1016/j.forc.2017.06.001

Fremout, W. ,Saverwyns, S. (2012). Identification of synthetic organic pigments: The role of a comprehensive digital Raman spectral library. Journal of Raman Spectroscopy **43**(11): 1536-1544. Doi: https://doi.org/10.1002/jrs.4054

Fukuda, K. (1985). The pyrolysis gas chromatographic examination of Japanese car paint flakes. Forensic Science International **29**(3-4): 227-236. Doi: https://doi.org/10.1016/0379-0738(85)90116-1

Gemperline, P. (2006). Practical Guide To Chemometrics. 2nd Edition. CRC Press.

Ghelardi, E., Degano, I., Colombini, M. P., Mazurek, J., Schilling, M. ,Learner, T. (2015). Py-GC/MS applied to the analysis of synthetic organic pigments: Characterization and identification in paint samples. Analytical and Bioanalytical Chemistry **407**(5): 1415-1431. Doi: https://doi.org/10.1007/s00216-014-8370-y

Gothard, J. A. (1976). Evaluation of automobile paint flakes as evidence. Journal of Forensic Sciences **21**(3): 636-641. Doi: https://doi.org/10.1520/jfs10537j

Griffiths, P. R. ,De Haseth, J. A. D. H. (2007). Fourier Transform Infrared Spectrometry. 2nd edition. John Wiley & Sons, Inc.

Hamer, P. S. (1982). Pigment Analysis in the Forensic Examination of Paints. III. A Guide to Motor Vehicle Paint Examination by Transmitted Light Microscopy. Journal of the Forensic Science Society **22**(2): 187-192. Doi: https://doi.org/10.1016/S0015-7368(82)71469-0

Harkins, T. R., Harris, J. T. ,Shreve, O. D. (1959). Identification of Pigments in Paint Products by Infrared Spectroscopy. Analytical Chemistry **31**(4): 541-545. Doi: https://doi.org/10.1021/ac50164a025

Henson, M. L. ,Jergovich, T. A. (2001). Scanning electron microscopy and energy dispersive X-ray spectrometry (SEM/EDS) for the forensic examination of paints and coatings. In Forensic Examination of Glass and Paint: Analysis(eds Caddy, B.). CRC Press**:** 243-272.

Hodgins, T. (2016). Paint Data Query (PDQ). Trace Evidence Data Workshop: Improving Technology And Measurement In Forensic Science, Gaithersburg,MD

Hodson, J. ,Lander, J. A. (1987). The analysis of cured paint media and a study of the weathering of alkyd paints by FTi.r./PAS. Polymer **28**(2): 251-256. Doi: https://doi.org/10.1016/0032-3861(87)90413-7

Hopen, T. J. ,Davis, M. (2009). Microscopy: Light Microscopes. Wiley Encyclopedia of Forensic Science.

Houck, M. M. ,Siegel, J. A. (2015). Chapter 16 - Paint Analysis. In Fundamentals of Forensic Science (Third Edition)(eds Houck, M. M. and Siegel, J. A.). Academic Press**:** 405-426.

Humecki, H. J. (1995). Practical guide to infrared microspectroscopy. Marcel Dekker, Inc.

HutchColor (2019). HCT^CM Precision Scanner Target user guide.Version 43.

Jackson, F., Bunford, J., Maynard, P. ,Roux, C. (2015). Surveys of vehicle colour frequency and the transfer of vehicle paints to stationary objects in Sydney, Australia. Forensic Science International **248**: 124-128. Doi: https://doi.org/10.1016/j.forsciint.2014.12.010

Kendix, E., Moscardi, G., Mazzeo, R., Baraldi, P., Prati, S., Joseph, E. ,Capelli, S. (2008). Far infrared and Raman spectroscopy analysis of inorganic pigments. Journal of Raman Spectroscopy **39**(8 SPEC. ISS.): 1104-1112. Doi: https://doi.org/10.1002/jrs.1956

Kirkbride, P. (2015). Paint and coatings examination. In Forensic Chemistry- Fundamentals and Applications(eds Siegel, J. A.). Wiley Blackwell**:** 75-134.

Koçak, A. (2011). The Role of Vibrational Spectroscopy in Forensic Chemistry. In Forensic Chemistry Handbook(eds Kobilinsky, L.). John Wiley & Sons, Inc.**:** 251-267.

Kochanowski, B. ,Morgan, S. (2000). Forensic Discrimination of Automotive Paint Samples Using Pyrolysis-Gas Chromatography-Mass Spectrometry with Multivariate Statistics. Journal of chromatographic science **38**: 100-108. Doi: https://doi.org/10.1093/chromsci/38.3.100

Kruglak, K. J., Dubnicka, M., Kammrath, B., Maxwell, V. ,Reffner, J. A. (2019). The Evidentiary Significance of Automotive Paint from the Northeast: A Study of Red Paint. Journal of Forensic Sciences **64**(5): 1345-1358. Doi: https://doi.org/10.1111/1556-4029.14007

Kumano, N., Mori, K., Kato, M. ,Ishii, M. (2019). Degradation of scratch resistance of clear coatings by outdoor weathering. Progress in Organic Coatings **135**: 574-581. Doi: https://doi.org/10.1016/j.porgcoat.2019.06.034

Kuptsov, A. H. (1994). Applications of Fourier transform raman spectroscopy in forensic science. Journal of Forensic Sciences **39**(2): 305-318. Doi: https://doi.org/10.1520/jfs13604j

Lambert, D. (2017) Apport de la spectroscopie Raman dans l'analyse de peintures automobiles, étude de comparabilité inter-laboratoires et combinaison de données spectroscopiques, Université de Lausanne.

Lambert, D. (2018). Data structure analysis through exploratory chemometrics based on EUCAP IR spectra. European Paint & Glass Group 24th Annual Meeting, Paris, France

Lambert, D., Muehlethaler, C., Esseiva, P. ,Massonnet, G. (2016). Combining spectroscopic data in the forensic analysis of paint: Application of a multiblock technique as chemometric tool. Forensic Science International **263**: 39-47. Doi: https://doi.org/10.1016/j.forsciint.2016.03.049

Lambert, D., Muehlethaler, C., Gueissaz, L. ,Massonnet, G. (2014). Raman analysis of multilayer automotive paints in forensic science: Measurement variability and depth profile. Journal of Raman Spectroscopy **45**(11-12): 1285-1292. Doi: https://doi.org/10.1002/jrs.4490

Lambourne, R. ,Strivens, T. A. (1999). Paint and Surface Coatings. 2nd Edition. Woodhead Publishing.

Larkin, P. (2011). Infrared and Raman Spectroscopy. Elsevier.

Lavine, B. K. ,Davidson, C. E. (2006). Classification and pattern recognition. In Practical Guide To Chemometrics(eds Gemperline, P.). CRC Press**:** 339–377.

Lavine, B. K., Fasasi, A., Mirjankar, N. ,Sandercock, M. (2014a). Development of search prefilters for infrared library searching of clear coat paint smears. Talanta **119**: 331-340. Doi: https://doi.org/10.1016/j.talanta.2013.10.066

Lavine, B. K., Fasasi, A., Mirjankar, N., White, C. ,Mehta, J. (2014b). Search prefilters for library matching of infrared spectra in the PDQ database using the autocorrelation transformation. Microchemical Journal **113**: 30-35. Doi: https://doi.org/10.1016/j.microc.2013.11.001

Lavine, B. K., Fasasi, A., Mirjankar, N., White, C. ,Sandercock, M. (2015). Search prefilters to assist in library searching of infrared spectra of automotive clear coats. Talanta **132**: 182-190. Doi: https://doi.org/10.1016/j.talanta.2014.08.061

Lavine, B. K., Fasasi, A. ,Sandercock, M. (2014). Improving PDQ database search strategies to enhance investigative lead information for automotive paints. Microchemical Journal **117**: 133-137. Doi: https://doi.org/10.1016/j.microc.2014.06.007

Lavine, B. K., Mirjankar, N., Ryland, S. ,Sandercock, M. (2011). Wavelets and genetic algorithms applied to search prefilters for spectral library matching in forensics. Talanta **87**(1): 46-52. Doi: https://doi.org/10.1016/j.talanta.2011.09.039

Lavine, B. K., White, C. ,Allen, M. (2016a). Forensic analysis of automotive paints using a pattern recognition assisted infrared library searching system: Ford (2000–2006). Microchemical Journal **129**: 173-183. Doi: https://doi.org/10.1016/j.microc.2016.06.024

Lavine, B. K., White, C., Perera, U., Nishikda, K. ,Allen, M. (2016b). Improving the PDQ Database to Enhance Investigative Lead Information from Automotive Paints. Rockville, MD, National Institute of Justice.https://www.ojp.gov/pdffiles1/nij/grants/249893.pdf

Lavine, B. K., White, C. G., Allen, M. D., Fasasi, A. ,Weakley, A. (2016c). Evidential significance of automotive paint trace evidence using a pattern recognition based infrared library search engine for the Paint Data Query Forensic Database. Talanta **159**: 317-329. Doi: https://doi.org/10.1016/j.talanta.2016.06.035

Lavine, B. K., White, C. G., Allen, M. D. ,Weakley, A. (2017). Pattern recognition-assisted infrared library searching of the paint data query database to enhance lead information from automotive paint trace evidence. Applied Spectroscopy **71**(3): 480-495. Doi: https://doi.org/10.1177/0003702816666287

Lewis, I. ,Edwards, H. (2001). Handbook of Raman Spectroscopy. 1st edition. Marcel Dekker, Inc.

Lv, J., Zhang, W., Liu, S., Chen, R., Feng, J., Zhou, S. ,Liu, Y. (2016). Analysis of 52 automotive coating samples for forensic purposes with Fourier transform infrared spectroscopy (FTIR) and Raman microscopy. Environmental Forensics **17**(1): 59-67. Doi: https://doi.org/10.1080/15275922.2015.1091403

MacDougall, D., Fung, T. ,Beveridge, A. (2001). Use of infrared spectroscopy for the characterisation of paint fragments. In Forensic Examination of Glass and Paint: Analysis and Interpretation(eds Caddy, B.). CRC Press**:** 183-241.

Makki, H., Adema, K. N. S., Peters, E. A. J. F., Laven, J., van der Ven, L. G. J., van Benthem, R. A. T. M. ,de With, G. (2015). Quantitative spectroscopic analysis of weathering of polyester-urethane coatings. Polymer Degradation and Stability **121**: 280-291. Doi: https://doi.org/10.1016/j.polymdegradstab.2015.09.019

Mann, C. K. ,Vickers, T. J. (2001). The Quest for Accuracy in Raman Spectra. In Handbook of Raman Spectroscopy(eds Lewis, I. and Edwards, H.). Marcel Dekker, Inc**:** 251-274.

Maric, M. (2014) Chemical Characterisation and Classification of Forensic Trace Evidence, Curtin University.

Maric, M., Van Bronswijk, W., Lewis, S. W. ,Pitts, K. (2012). Rapid characterisation and classification of automotive clear coats by attenuated total reflectance infrared spectroscopy. Analytical Methods **4**(9): 2687-2693. Doi: https://doi.org/10.1039/c2ay25419k

Maric, M., van Bronswijk, W., Pitts, K. ,Lewis, S. W. (2016). Characterisation and classification of automotive clear coats with Raman spectroscopy and chemometrics for forensic purposes. Journal of Raman Spectroscopy **47**(8): 948-955. Doi: https://doi.org/10.1002/jrs.4925

Mark, H. ,Workman, J. (2007). Chemometrics in Spectroscopy. Academic Press.

Massonnet, G. (1996) Les peintures automobiles en criminalistique, University of Lausanne, IPSC.

Massonnet, G. ,Stoecklein, W. (1999). Identification of organic pigments in coatings: Applications to red automotive topcoats. Part III: Raman spectroscopy (NIR FT-Raman). Science and Justice **39**(3): 181-187. Doi: https://doi.org/10.1016/S1355-0306(99)72045-9

Massonnet, G. ,Stoecklein, W. (1999b). Identification of organic pigments in coatings: Applications to red automotive topcoats. Part II: Infrared spectroscopy. Science and Justice **39**(2): 135-140. Doi: https://doi.org/10.1016/S1355-0306(99)72032-0

Mazerolles, G., Hanafi, M., Dufour, E., Bertrand, D. ,Qannari, E. M. (2006). Common components and specific weights analysis: A chemometric method for dealing with complexity of food products. Chemometrics and Intelligent Laboratory Systems **81**(1): 41-49. Doi: https://doi.org/10.1016/j.chemolab.2005.09.004

McCreery, R. L. (2000). Raman Spectroscopy for Chemical Analysis. John Wiley & Sons, Inc.

McDermott, S. D., Willis, S. M. ,McCullough, J. P. (1999). The evidential value of paint. Part II: A Bayesian approach. Journal of Forensic Sciences **44**(2): 263-269. Doi: https://doi.org/10.1520/jfs14450j

McMinn, D. G., Carlson, T. L. ,Munson, T. O. (1985). Pyrolysis capillary gas chromatography/mass spectrometry for analysis of automotive paints. Journal of Forensic Sciences **30**(4): 1064-1073. Doi: https://doi.org/10.1520/jfs11047j

Milczarek, J. M., Dziadosz, M. ,Zięba-Palus, J. (2009). Way to distinguish car paint traces based on epoxy primer layers analysis by pyrolysis-gas chromatography-mass spectrometry. Chemia Analityczna **54**(2): 173-185. https://milczarek.eu/wp-content/uploads/2012/10/ChemAnal.54.173.2009.173-185.pdf

Moore, J. R. (2017). Automotive Paint Application. In Protective Coatings: Film Formation and Properties(eds Wen, M. and Dušek, K.). Springer International Publishing**:** 465-496.

Muehlethaler, C. (2015) L'exploitation des peintures en spray en criminalistique : mise en place d'une procédure de gestion et de comparaison des spectres infrarouges à l'aide des statistiques multivariées, University of Lausanne.

Muehlethaler, C., Gueissaz, L. ,Massonnet, G. (2013). Forensic Paint Analysis. In Encyclopedia of Forensic Sciences(eds Siegel, J. A., Saukko, P. J. et al.). Academic Press**:** 265-272.

Muehlethaler, C., Massonnet, G., Deviterne, M., Bradley, M., Herrero, A., de Lezana, I. D., . . . Turunen, R. (2013b). Survey on batch-to-batch variation in spray paints: A collaborative study. Forensic Science International **229**(1-3): 80-91. Doi: https://doi.org/10.1016/j.forsciint.2013.02.041

Muehlethaler, C., Massonnet, G. ,Esseiva, P. (2011). The application of chemometrics on Infrared and Raman spectra as a tool for the forensic analysis of paints. Forensic Science International **209**(1): 173-182. Doi: https://doi.org/10.1016/j.forsciint.2011.01.025

Muehlethaler, C., Massonnet, G. ,Esseiva, P. (2014). Discrimination and classification of FTIR spectra of red, blue and green spray paints using a multivariate statistical approach. Forensic Science International **244**: 170-178. Doi: https://doi.org/10.1016/j.forsciint.2014.08.038

Nichols, M., Boisseau, J., Pattison, L., Campbell, D., Quill, J., Zhang, J., . . . Peters, C. (2013). An improved accelerated weathering protocol to anticipate Florida exposure behavior of coatings. Journal of Coatings Technology and Research **10**(2): 153-173. Doi: https://doi.org/10.1007/s11998-012-9467-x

Nichols, M. E., Gerlock, J. L., Smith, C. A. ,Darr, C. A. (1999). Effects of weathering on the mechanical performance of automotive paint systems. Progress in Organic Coatings **35**(1-4): 153-159. Doi: https://doi.org/10.1016/S0300-9440(98)00060-5

Otero, V., Sanches, D., Montagner, C., Vilarigues, M., Carlyle, L., Lopes, J. A. ,Melo, M. J. (2014). Characterisation of metal carboxylates by Raman and infrared spectroscopy in works of art. Journal of Raman Spectroscopy **45**(11-12): 1197-1206. Doi: https://doi.org/10.1002/jrs.4520

Perera, U. D. N., Nishikida, K. ,Lavine, B. K. (2018). Development of Infrared Library Search Prefilters for Automotive Clear Coats from Simulated Attenuated Total Reflection (ATR) Spectra. Applied Spectroscopy **72**(6): 886-895. Doi: https://doi.org/10.1177/0003702818759664

Perrin, F. X., Irigoyen, M., Aragon, E. ,Vernet, J. L. (2001). Evaluation of accelerated weathering tests for three paint systems: A comparative study of their aging behaviour. Polymer Degradation and Stability **72**(1): 115-124. Doi: https://doi.org/10.1016/S0141-3910(01)00005-2

Plage, B., Berg, A. D. ,Luhn, S. (2008). The discrimination of automotive clear coats by pyrolysis-gas chromatography/mass spectrometry and comparison of samples by a chromatogram library software. Forensic Science International **177**(2-3): 146-152. Doi: https://doi.org/10.1016/j.forsciint.2007.11.011

PPG. "Compact Paint Systems." from http://corporate.ppg.com/China/PPG-China-Automotive-OEM-Coatings/Products-and-Service/Compact-Paint-Systems.aspx.

Puomi, P., Ooij, W. J., Yin, Z. ,Seth, A. (2008). Replacement of zinc phosphating and E-coating by a one-step primer? Plating and Surface Finishing **95**: 42-48. https://www.nmfrc.org/pdf/psf2008/010842.pdf

Quevillon, S., Toupin, N., Tremblay, A., Fournier, R. ,Muehlethaler, C. (2019). Batch-to-batch variation in domestic paints: Insights into the newly commercialized recycled paints. Forensic Science International **303**. Doi: 10.1016/j.forsciint.2019.109946

Razin, A. A., Yari, H. ,Ramezanzadeh, B. (2015). Stone-chipping and adhesion deterioration of automotive coating systems caused by outdoor weathering of underneath layers. Journal of Industrial and Engineering Chemistry **31**: 291-300. Doi: https://doi.org/10.1016/j.jiec.2015.07.001

Rencher, A. C. ,Christensen, W. F. (2012). Methods of Multivariate Analysis. 3rd Edition. John Wiley & Sons, Inc.

Reynolds, A., Roberts, K., Thompson, A. ,Runt, E. (2018). Discrimination Power of Automotive Paint Comparisons using a Paint Analytical Scheme. JASTEE **8**(1): 4-15. https://astee.s3.amazonaws.com/320166_JASTEE_2018_8-1_Reynolds.pdf

Rodgers, P. G., Cameron, R., Cartwright, N. S., Clark, W. H., Deak, J. S. ,Norman, E. W. (1976a). The classification of automobile paint by diamond window infrared spectrophotometry part l: Binders and pigments. Journal of the Canadian Society of Forensic Science **9**(1): 1-14. Doi: https://doi.org/10.1080/00085030.1976.10757242

Rodgers, P. G., Cameron, R., Clark, W. H., Cartwright, N. S., Deak, J. S. ,Norman, E. W. W. (1976b). The classification of automotive paint by diamond window infrared spectrophotometry part ll automotive topcoats and undercoats. Journal of the Canadian Society of Forensic Science **9**(2): 49-68. Doi: https://doi.org/10.1080/00085030.1976.10757246

Rodgers, P. G., Cameron, R., Deak, J. S., Cartwright, N. S., Clark, W. H. ,Norman, E. W. W. (1976c). The classification of automotive paint by diamond window infrared spectrophotometry part lll case histories. Journal of the Canadian Society of Forensic Science **9**(3): 103-111. Doi: https://doi.org/10.1080/00085030.1976.10757253

Russell, J., Singer, B. W., Perry, J. J. ,Bacon, A. (2011). The identification of synthetic organic pigments in modern paints and modern paintings using pyrolysis-gas chromatography-mass spectrometry. Analytical and Bioanalytical Chemistry **400**(5): 1473-1491. Doi: https://doi.org/10.1007/s00216-011-4822-9

Ryland, S., Bishea, G., Brun-Conti, L., Eyring, M., Flanagan, B., Jergovich, T., . . . Suzuki, E. (2001). Discrimination of 1990s original automotive paint systems: A collaborative study of black nonmetallic base coat/clear coat finishes using infrared spectroscopy. Journal of Forensic Sciences **46**(1): 31-45. Doi: https://doi.org/10.1520/jfs14908j

Ryland, S. G. (1995). Infrared Microspectroscopy of Forensic Paint Evidence. In Practical guide to infrared microspectroscopy(eds Humecki, H. J.). Marcel Dekker, Inc**:** 163-243.

Ryland, S. G., Jergovich, T. A. ,Kirkbride, K. P. (2006). Current Trends in Forensic Paint Examination. Forensic Science Review **18**(2): 97-117.

Ryland, S. G. ,Kopec, R. J. (1979). The evidential value of automobile paint chips. Journal of Forensic Sciences **24**(1): 140-147. Doi: https://doi.org/10.1520/jfs10800j

Ryland, S. G., Kopec, R. J. ,Somerville, P. N. (1981). The Evidential Value of Automobile Paint. Part II: Frequency of Occurrence of Topcoat Colors. Journal of Forensic Sciences **26**(1): 64-74. Doi: https://doi.org/10.1520/jfs11330J

Ryland, S. G. ,Suzuki, E. M. (2011). Analysis of Paint Evidence. In Forensic Chemistry Handbook(eds Lawrence, K.). John Wiley & Sons, Inc.**:** 131-224.

Saferstein, R. (2018). Criminalistics : an introduction to forensic science. 12th edition. Pearson Education.

SAIC-Volkswagen. "Factory layout(上汽大众工厂布局)." from https://www.csvw.com/csvw-website/about/map.html.

Scalarone, D. ,Chiantore, O. (2009). Py-GC/MS of Natural and Synthetic Resins. In Organic Mass Spectrometry in Art and Archaeology(eds Colombini, M. P. and Modugno, F.). John Wiley & Sons, Ltd**:** 327-361.

Scherrer, N. C., Stefan, Z., Francoise, D., Annette, F. ,Renate, K. (2009). Synthetic organic pigments of the 20th and 21st century relevant to artist's paints: Raman spectra reference collection. Spectrochimica Acta - Part A: Molecular and Biomolecular Spectroscopy **73**(3): 505-524. Doi: https://doi.org/10.1016/j.saa.2008.11.029

Schiering, D. W. (1988). A Beam Condenser/Miniature Diamond Anvil Cell Accessory for the Infrared Microspectrometry of Paint Chips. Applied Spectroscopy **42**(5): 903-906. Doi: https://doi.org/10.1366/0003702884428879

Shaver, J. M. (2001). Chemometrics for Raman Spectroscopy. In Handbook of Raman Spectroscopy(eds Lewis, I. and Edwards, H.). Marcel Dekker, Inc.

Shi, X. ,Croll, S. G. (2010). Recovery of surface defects on epoxy coatings and implications for the use of accelerated weathering. Progress in Organic Coatings **67**(2): 120-128. Doi: https://doi.org/10.1016/j.porgcoat.2009.10.012

Shin, T., Hajime, O. ,Chuichi, W. (2011). Pyrolysis–GC/MS Data Book of Synthetic Polymers. Elsevier.

Smalldon, K. W. ,Moffat, A. C. (1973). The Calculation of Discriminating Power for a Series of Correlated Attributes. Journal of the Forensic Science Society **13**(4): 291-295. Doi: https://doi.org/10.1016/S0015-7368(73)70828-8

Soong, W. Y., Goh, K. Y., Xie, H. ,Lim, T. B. (2020). Assessing the automotive paint evidence in Singapore via population and discrimination studies. Forensic Chemistry **21**. Doi: https://doi.org/10.1016/j.forc.2020.100289

Spathis, P., Karagiannidou, E. ,Magoula, A. E. (2003). Influence of titanium dioxide pigments on the photodegradation of Paraloid acrylic resin. Studies in Conservation **48**(1): 57-64. Doi: https://doi.org/10.1179/sic.2003.48.1.57

Stewart, S. P., Bell, S. E. J., Armstrong, W. J., Kee, G. ,Speers, S. J. (2012). Forensic examination of multilayer white paint by lateral scanning Raman spectroscopy. Journal of Raman Spectroscopy **43**(1): 131-137. Doi: https://doi.org/10.1002/jrs.2982

Stewart, W. D. (1974). Pyrolysis gas chromatographic analysis of automobile paints. Journal of Forensic Sciences **19**(1): 121-129. Doi: https://doi.org/10.1520/jfs10079j

Stoecklein, W. ,Palenik, C. S. (1998). Forensic analysis of automotive paints: Evidential value and the batch problem. the 4th European Paint Group Meeting, Paris

Stone, H. S., Murphy, K. J., Rioux, J. M. ,Stuart, A. W. (1991). Vehicle topcoat colour and manufacturer: Frequency distribution and evidential significance. Part II. Journal of the Canadian Society of Forensic Science **24**(3): 175-185. Doi: https://doi.org/10.1080/00085030.1991.10756994

Streitberger, H. J. ,Dössel, K. F. (2008). Automotive Paints and Coatings. 2nd edition. Wiley‑VCH Verlag GmbH & Co. KGaA.

Suzuki, E. M. (1996a). Infrared spectra of U.S. automobile original topcoats (1974-1989): I. Differentiation and identification based on acrylonitrile and ferrocyanide C$\equiv$N stretching absorptions. Journal of Forensic Sciences **41**(3): 376-392. Doi: https://doi.org/10.1520/JFS13924J

Suzuki, E. M. (1996b). Infrared spectra of U.S. automobile original topcoats (1974-1989): II. Identification of some topcoat inorganic pigments using an extended range (4000-220 cm-1) fourier transform spectrometer. Journal of Forensic Sciences **41**(3): 393-406. Doi: https://doi.org/10.1520/jfs13925j

Suzuki, E. M. (1999a). Infrared spectra of U.S. automobile original topcoats (1974-1989): V. Identification of organic pigments used in red nonmetallic and brown nonmetallic and metallic monocoats - DPP Red BO and thioindigo bordeaux. Journal of Forensic Sciences **44**(2): 297-313. Doi: https://doi.org/10.1520/jfs14455j

Suzuki, E. M. (1999b). Infrared spectra of U.S. Automobile original topcoats (1974-1989): VI. Identification and analysis of yellow organic automotive paint pigments - Isoindolinone Yellow 3R, Isoindoline Yellow, Anthrapyrimidine Yellow, and miscellaneous yellows. Journal of Forensic Sciences **44**(6): 1151-1175. Doi: https://doi.org/10.1520/jfs14584j

Suzuki, E. M. (2014a). Infrared Spectra of U.S. Automobile Original Finishes (Post - 1989). VIII: In Situ Identification of Bismuth Vanadate Using Extended Range FT-IR Spectroscopy, Raman Spectroscopy, and X-Ray Fluorescence Spectrometry. Journal of Forensic Sciences **59**(2): 344-363. Doi: https://doi.org/10.1111/1556-4029.12318

Suzuki, E. M. (2014b). Infrared spectra of U.S. automobile original finishes (1998-2000). IX. identification of bismuth oxychloride and silver/white mica pearlescent pigments using extended range FT-IR spectroscopy, XRF spectrometry, and SEM/EDS analysis. Journal of Forensic Sciences **59**(5): 1205-1225. Doi: https://doi.org/10.1111/1556-4029.12414

Suzuki, E. M. ,Carrabba, M. (2001). In situ identification and analysis of automotive paint pigments using line segment excitation raman spectroscopy: I. Inorganic topcoat pigments. Journal of Forensic Sciences **46**(5): 1053-1069. Doi: https://doi.org/10.1520/jfs15099J

Suzuki, E. M. ,Marshall, W. P. (1997). Infrared spectra of U.S. automobile original topcoats (1974-1989): III. In situ identification of some organic pigments used in yellow, orange, red, and brown nonmetallic and brown metallic finishes-benzimidazolones. Journal of Forensic Sciences **42**(4): 619-648. Doi: https://doi.org/10.1520/jfs14174j

Suzuki, E. M. ,Marshall, W. P. (1998). Infrared spectra of U.S. automobile original topcoats (1974-1989): IV. Identification of some organic pigments used in red and brown nonmetallic and metallic monocoats - Quinacridones. Journal of Forensic Sciences **43**(3): 514-542. Doi: https://doi.org/10.1520/jfs16179j

Suzuki, E. M. ,McDermot, M. X. (2006). Infrared spectra of U.S. automobile original finishes. VII. Extended range FT-IR and XRF analyses of inorganic pigments In Situ - Nickel Titanate and Chrome Titanate. Journal of Forensic Sciences **51**(3): 532-547. Doi: https://doi.org/10.1111/j.1556-4029.2006.00126.x

SWGMAT (1999). Forensic paint analysis and comparison. Scientific Working Group for Materials Analysis.

https://www.asteetrace.org/static/images/pdf/01%20Forensic%20Paint%20Analysis%20and%20Comparison%20Guidelines.pdf

SWGMAT (2011). Application of the Daubert Standard to Forensic Paint Examinations, Scientific Working Group for Materials Analysis.https://www.asteetrace.org/static/images/pdf/11%20Paint%20Daubert%20-%20PowerPoint%20Presentations.pdf

Tahmassebi, N., Moradian, S. ,Mirabedini, S. M. (2005). Evaluation of the weathering performance of basecoat/clearcoat automotive paint systems by electrochemical properties measurements. Progress in Organic Coatings **54**(4): 384-389. Doi: https://doi.org/10.1016/j.porgcoat.2005.08.004

Tsuge, S. ,Ohtani, H. (2014). Pyrolysis-Gas Chromatography. In Practical Gas Chromatography: A Comprehensive Reference(eds Dettmer-Wilde, K. and Engewald, W.). Springer**:** 829-847.

Tweed, F. T., Cameron, R., Deak, J. S. ,Rodgers, P. G. (1974). The forensic microanalysis of paints, plastics and other materials by an infrared diamond cell technique. Forensic Science **4**(C): 211-218. Doi: https://doi.org/10.1016/0300-9432(74)90110-1

Vahur, S., Teearu, A. ,Leito, I. (2010). ATR-FT-IR spectroscopy in the region of 550–230cm−1 for identification of inorganic pigments. Spectrochimica Acta Part A: Molecular and Biomolecular Spectroscopy **75**(3): 1061-1072. Doi: https://doi.org/10.1016/j.saa.2009.12.056

Van Der Pal, K. J., Sauzier, G., Maric, M., Van Bronswijk, W., Pitts, K. ,Lewis, S. W. (2016). The effect of environmental degradation on the characterisation of automotive clear coats by infrared spectroscopy. Talanta **148**: 715-720. Doi: https://doi.org/10.1016/j.talanta.2015.08.058

Volpé, G. G., Murphy, K. J., Rioux, J. M. ,Stone, H. S. (1988). Vehicle topcoat colour and manufacturer: Frequency distribution and evidential significance. Journal of the Canadian Society of Forensic Science **21**(1-2): 11-18. Doi: https://doi.org/10.1080/00085030.1988.10756957

Wampler, T. P., Bishea, G. A. ,Simonsick, W. J. (1997). Recent changes in automotive paint formulation using pyrolysis-gas chromatography/mass spectrometry for identification. Journal of Analytical and Applied Pyrolysis **40-41**: 79-89. Doi: https://doi.org/10.1016/S0165-2370(97)00009-0

WANG, C., Lei, L. ,Massonnet, G. (2019). Etude préliminaire des peintures automobiles blanches par spectrométrie Raman. Réunion Microtracs Suiss, Solothurn

Wehrens, R. (2011). Chemometrics with R. Springer.

Wei, H., Brill, M., H. ,Mcnulty, M., S. (2015). System and method for color correction of a microscope image. United States, Datacolor Holding AG.

Wheals, B. B. ,Noble, W. (1974). The Pyrolysis Gas Chromatographic Examination of Car Paint Flakes as an Aid to Vehicle Characterization. Journal of the Forensic Science Society **14**(1): 23-32. Doi: https://doi.org/10.1016/S0015-7368(74)70848-9

Wikipedia. (2023), 22 January 2023. "List of Volkswagen Group factories." from https://en.wikipedia.org/wiki/List_of_Volkswagen_Group_factories#External_links.

Wild, J. K. (2022) Analyse de peintures automobiles blanches par Py GC/MS, University of Lausanne.

Wilke, G. ,Jacob, S. (2008). Coatings for Plastic Parts. In Automotive Paints and Coatings(eds Streitberger, H. J. and Dössel, K. F.)**:** 305-349.

Wright, D. M. (2010). A Make-Model-Year Case Involving Unusual Primer Chemistry and Good Resources. JASTEE **2**(1-2): 137-148. https://astee.s3.amazonaws.com/408855_JASTEE_2010_1-2_Wright.pdf

Wright, D. M. (2012). Sourcing Paint Smears: A Hate Crime Highlights the Utility of the Paint Data Query (PDQ) Database. Canadian Society of Forensic Science Journal **45**(2): 79-88. Doi: https://doi.org/10.1080/00085030.2012.10757185

Wright, D. M., Bradley, M. J. ,Mehltretter, A. H. (2013). Analysis and discrimination of single-layer white architectural paint samples. Journal of Forensic Sciences **58**(2): 358-364. Doi: https://doi.org/10.1111/1556-4029.12074

Wright, D. M., Kirby, D. P. ,Thornton, J. I. (2020). Forensic Paint Examination. In Forensic Science Handbook(eds Saferstein, R. and Hall, A. B.). CRC Press. 1**:** 81-150.

Xinhua, N. A. (2018). "The end of 2017: the number of motor vehicles in China is 310 million(2017 年底：我国机动车保有量 3.10 亿辆, 驾驶人 3.85 亿人)." from http://www.gov.cn/xinwen/2018-01/15/content_5256832.htm.

Yang, S. H., Shen, J. Y., Chang, M. S. ,Wu, G. J. (2015). Differentiation of vehicle top coating paints using pyrolysis-gas chromatography/mass spectrometry and multivariate chemometrics with statistical comparisons. Analytical Methods **7**(4): 1527-1534. Doi: https://doi.org/10.1039/c4ay02730b

Zięba-Palus, J. ,Borusiewicz, R. (2006). Examination of multilayer paint coats by the use of infrared, Raman and XRF spectroscopy for forensic purposes. Journal of Molecular Structure **792-793**: 286-292. Doi: https://doi.org/10.1016/j.molstruc.2006.03.072

Zięba-Palus, J. ,Michalska, A. (2014). Characterization of blue pigments used in automotive paints by raman spectroscopy. Journal of Forensic Sciences **59**(4): 943-949. Doi: https://doi.org/10.1111/1556-4029.12499

Zięba-Palus, J., Michalska, A. ,Wesełucha-Birczyńska, A. (2011). Characterisation of paint samples by infrared and Raman spectroscopy for criminalistic purposes. Journal of Molecular Structure **993**(1-3): 134-141. Doi: https://doi.org/10.1016/j.molstruc.2010.12.016

Zięba-Palus, J., Milczarek, J. M. ,Košcielniak, P. (2008a). Application of infrared spectroscopy and pyrolysis-gas chromatography-mass spectrometry to the analysis of automobile paint samples. Chemia Analityczna **53**(1): 109-121. https://www.scopus.com/inward/record.uri?eid=2-s2.0-41649114548&partnerID=40&md5=fb3aaf644ed261dfb3d75ea5cdbbefd2

Zięba-Palus, J. ,Trzcińska, B. M. (2013). Application of infrared and raman spectroscopy in paint trace examination. Journal of Forensic Sciences **58**(5): 1359-1363. Doi: https://doi.org/10.1111/1556-4029.12183

Zięba-Palus, J., Zadora, G. ,Milczarek, J. M. (2008). Differentiation and evaluation of evidence value of styrene acrylic urethane topcoat car paints analysed by pyrolysis-gas chromatography. Journal of Chromatography A **1179**(1): 47-58. Doi: https://doi.org/10.1016/j.chroma.2007.09.045

Zięba-Palus, J., Zadora, G., Milczarek, J. M. ,Kościelniak, P. (2008b). Pyrolysis-gas chromatography/mass spectrometry analysis as a useful tool in forensic examination of automotive paint traces. Journal of Chromatography A **1179**(1): 41-46. Doi: https://doi.org/10.1016/j.chroma.2007.09.044